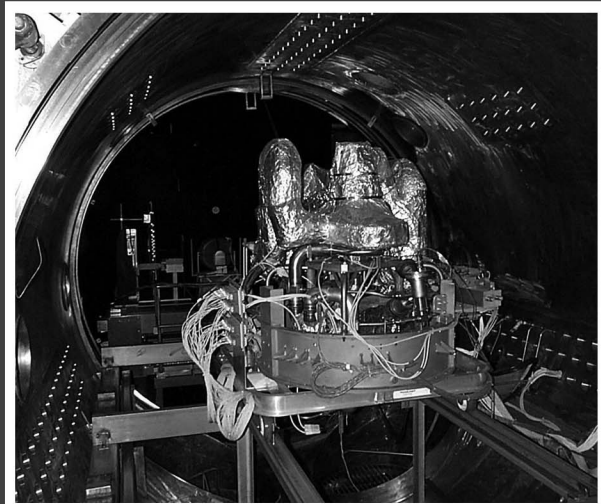


R&T

RESEARCH & TECHNOLOGY 2004
NASA/TM—2005-213419

CLEVELAND • OHIO



GLENN RESEARCH CENTER AT LEWIS FIELD

About the cover:

Top: A closed-Brayton-cycle power-conversion system was tested with the NSTAR thruster at Glenn as part of a nuclear electric propulsion system being developed for an interplanetary spacecraft (pp. 100–101).

Center: Hybrid Power Management Program. A bank of 110 ultracapacitors connected in a series configuration was evaluated for energy storage for the Next Generation Launch Technology Program (pp. 200–201).

Bottom: Parametric Inlet mounted in Glenn's 10- by 10-Foot Supersonic Wind Tunnel. The inlet is an innovative concept for the gas-turbine propulsion system of a supersonic aircraft. It has less mechanical complexity, lower weight, and greater aerodynamic stability and safety than other inlets (pp. 178–179).

Research & Technology 2004



National Aeronautics and
Space Administration

Glenn Research Center
Cleveland, Ohio 44135-3191

NASA/TM—2005-213419

Trade names or manufacturers' names are used in this report for identification only. This usage does not constitute an official endorsement, either expressed or implied, by the National Aeronautics and Space Administration.

Available from

NASA Center for Aerospace Information
7121 Standard Drive
Hanover, MD 21076

National Technical Information Service
5285 Port Royal Road
Springfield, VA 22100

Available electronically at <http://www.grc.nasa.gov/WWW/RT/>

Introduction



The NASA Glenn Research Center at Lewis Field, in partnership with U.S. industries, universities, and other Government institutions, develops critical systems technologies and capabilities that address national priorities. Our world-class research, technology, and capability development efforts are keys to advancing space exploration of our solar system and beyond while maintaining global leadership in aeronautics. Our work is focused on technological advancements in aeropropulsion, space propulsion, power systems, nuclear systems, communications, and human-related systems.

Glenn's activities support all NASA missions and the major programs of our Agency. For example, we support space exploration through our role in developing the propulsion and power systems for an interplanetary, nuclear-based mission. We contribute significantly to economic growth and national security through safe, superior, and environmentally compatible U.S. aircraft propulsion systems. Glenn leads NASA's research in the fields of fluids, combustion, and reacting flow systems, including gravity variation. Glenn also leads in the testing and evaluation of materials and structures for atmospheric and space environ-

ments by utilizing our first-rate facilities. Almost every space shuttle science mission has had an experiment managed by Glenn, and we have conducted a wide array of experiments on the International Space Station.

The Glenn staff consists of over 3200 civil service employees and support service contractor personnel. Scientists and engineers comprise more than half of our workforce, while technical specialists, skilled workers, and an administrative staff support them. We aggressively strive for technical excellence through continuing education, increased diversity in our workforce, and continuous improvement in our management and business practices so that we can expand the boundaries of aeronautics, space, and aerospace technology.

Glenn Research Center is a unique facility located in northern Ohio. The main campus is situated on 350 acres of land adjacent to the Cleveland International Airport, with more than 140 buildings that include 24 major facilities and over 500 specialized research and test facilities. In addition, Plum Brook Station, located 50 miles west of Cleveland, offers four large, world-class facilities for space technology and capability development. All Center capabilities, at both Cleveland and Plum Brook, are available for government and industry programs through Interagency or Space Act Agreements.

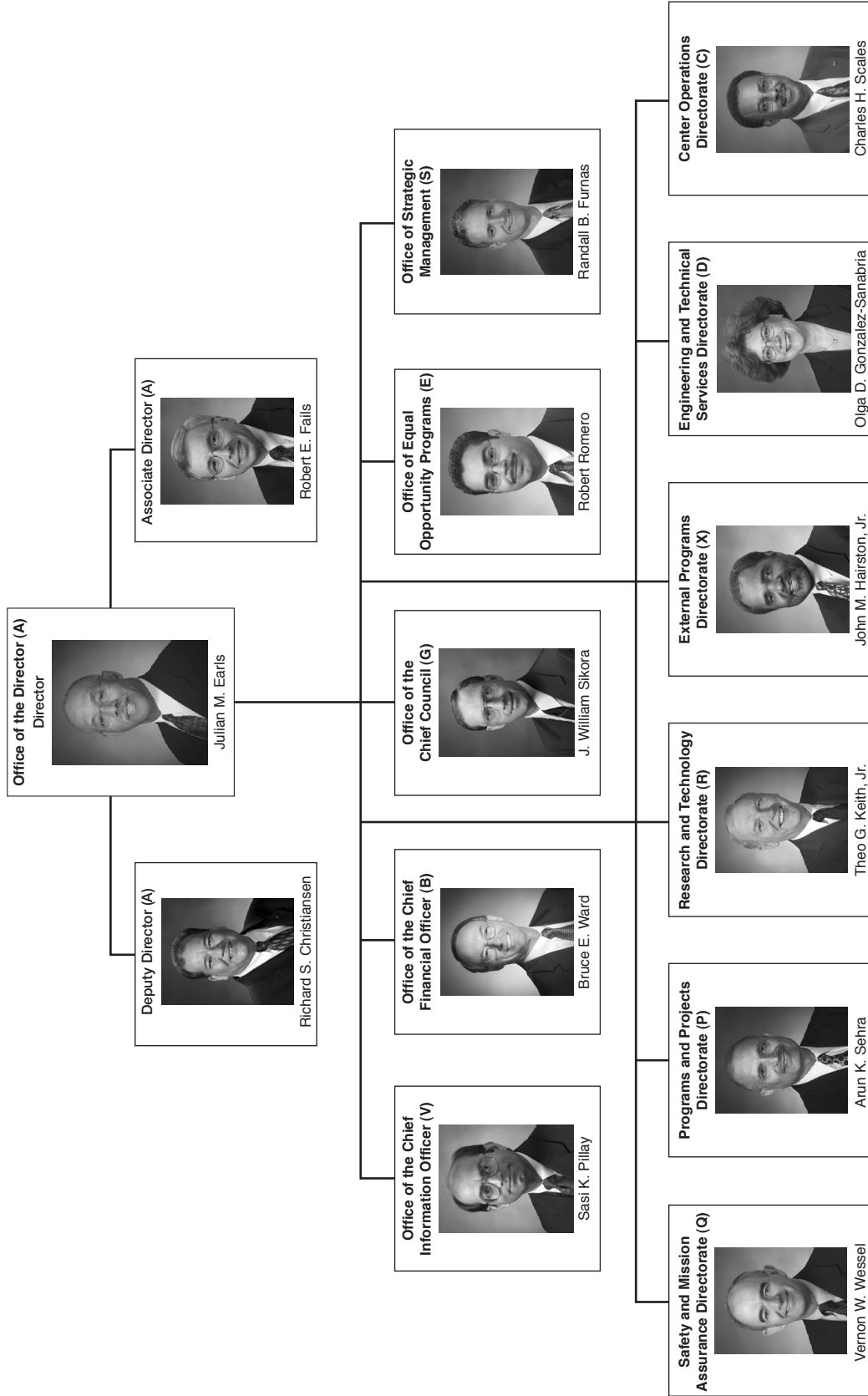
Knowledge is an important product of our activities. Our annual Research & Technology report helps make this knowledge available to potential users in the technical community. This report is organized so that a broad cross section of people can readily use it. Each article begins with a short introductory paragraph and continues with a summary of the progress made during the year in various scientific and technical areas.

We hope that this information is useful to you. If additional information is desired, you are encouraged to contact the researchers identified at the end of each article and to visit Glenn's Web site at <http://www.nasa.gov/glenn/>.

A handwritten signature in black ink that reads "Julian M. Earls". The signature is written in a cursive, flowing style.

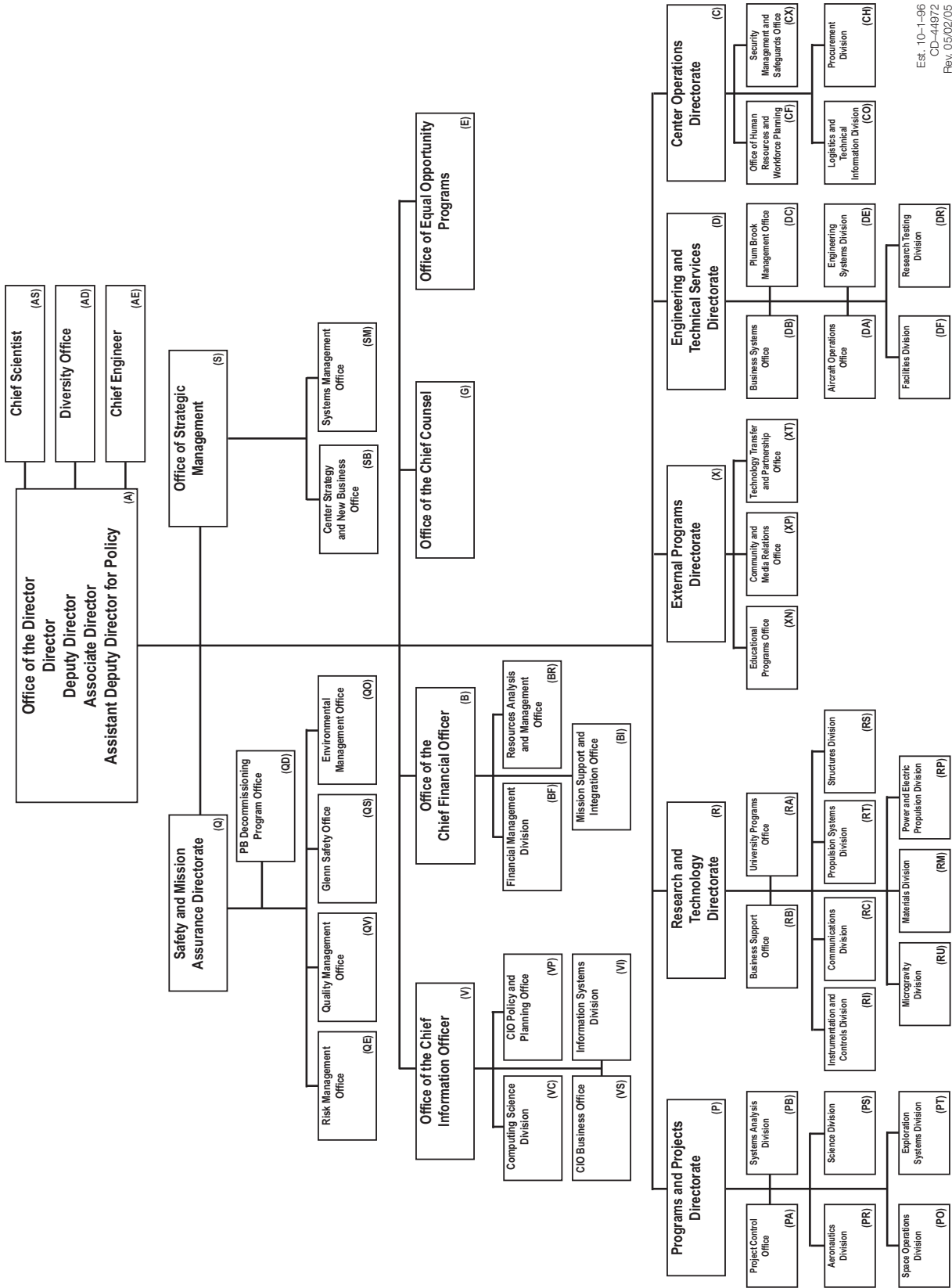
Julian M. Earls
Director

NASA Glenn Research Center Senior Management



CD-48634
December 22, 2004

NASA Glenn Research Center at Lewis Field



Est. 10-1-96
CD-44972
Rev. 05/02/05

Contents

Programs and Projects

Systems Analysis

Bimodal Nuclear Thermal Rocket Propulsion Investigated for Power-Rich, Artificial-Gravity Human Exploration Missions to Mars	2
OTIS 3.2 Software Released	3
Photochemically Etched Construction Technology Developed for Digital Xenon Feed Systems	5
Options Studied for Managing Space Station Solar Array Electrical Hazards for Sequential Shunt Unit Replacement	7
Probabilistic Analysis Techniques Applied to Complex Spacecraft Power System Modeling	9

Exploration Systems

Capillary Flow Experiments Began on the International Space Station	10
Fundamental Research Applied To Enable Hardware Performance in Microgravity	12
Milestones Achieved for the Fluids and Combustion Facility	14
Glenn's Telescience Support Center Provided Around-the-Clock Operations Support for Space Experiments on the International Space Station	15
Flight Hardware Fabricated for Combustion Science in Space	17

Research and Technology

Instrumentation and Controls

Low-Speed Active Flow Control Laboratory Developed	22
Intelligent Life-Extending Controls for Aircraft Engines Studied	23
Enhanced Bank of Kalman Filters Developed and Demonstrated for In-Flight Aircraft Engine Sensor Fault Diagnostics	25
Innovative Adaptive Control Method Demonstrated for Active Suppression of Instabilities in Engine Combustors	26
Discrete Event Supervisory Control Applied to Propulsion Systems	28
Control Algorithms and Simulated Environment Developed and Tested for Multiagent Robotics for Autonomous Inspection of Propulsion Systems	29
Nanorod Material Developed for Use as an Optical Sensor Platform	31
Forward Technology Solar Cell Experiment (FTSCE) for MISSE-5 Verified and Readied for Flight on STS-114	33
Quantum Sensing and Communications Being Developed for Nanotechnology	34
Nondestructive Evaluation Tests Performed on Space Shuttle Leading-Edge Materials Subjected to Impact	36
Molecular Rayleigh Scattering Techniques Developed for Measuring Gas Flow Velocity, Density, Temperature, and Turbulence	37
Megahertz-Frame-Rate Imaging System Developed for Quantitative Velocimetry Measurements in Unsteady High-Speed Flows	38
Ultrasonic Guided-Wave-Scan System Used to Characterize C-Enhanced Silicon Carbide Composite During Creep-Rupture Tests	40
Ability of Impedance-Based Health Monitoring To Detect Structural Damage of Propulsion System Components Assessed	41
Optical Tweezers and Optical Trapping Improved for Future Automated Micromanipulation and Characterization	43

New Deep Reactive Ion Etching Process Developed for the Microfabrication of Silicon Carbide	44
High-Temperature, Thin-Film Ceramic Thermocouples Developed	46
Sonoluminescence: A Galaxy of Nanostars Created in a Beaker	47

Materials

As-Fabricated Reinforced Carbon/Carbon Characterized	49
Followup to Columbia Investigation: Reinforced Carbon/Carbon From the Breach Location in the Wing Leading Edge Studied	50
Flexible Metallic Overwrap Concept Developed for On-Orbit Repair of Space Shuttle Orbiter Leading Edges . . .	51
Glenn Refractory Adhesive for Bonding and Exterior Repair (GRABER) Developed for Repairing Shuttle Damage	53
Properties of PMR Polyimides Improved by Preparation of Polyhedral Oligomeric Silsesquioxane (POSS) Nanocomposites	54
Nonhumidified High-Temperature Membranes Developed for Proton Exchange Membrane Fuel Cells	56
Fluorescent "On-Off" Sensors Studied for Chemical Warfare Agents	57
Mechanical and Electrical Properties of a Polyimide Film Significantly Enhanced by the Addition of Single-Wall Carbon Nanotubes	58
Novel Elastomeric Membranes Developed for Polymer Electrolytes in Lithium Batteries	60
High-Temperature Polymer Composites Tested for Hypersonic Rocket Combustor Backup Structure	61
Mechanically Strong, Lightweight Porous Materials Developed (X-Aerogels)	63
Effects of High-Temperature Exposures on the Fatigue Life of Disk Superalloys Examined	65
Potential High-Temperature Shape-Memory-Alloy Actuator Material Identified	67
Processing of Ni ₃₀ Pt ₂₀ Ti ₅₀ High-Temperature Shape-Memory Alloy Into Thin Rod Demonstrated	68
Candidate Materials Evaluated for a High-Temperature Stirling Convertor Heater Head	69
Full-Scale GRCop-84 Combustion Chamber Liner Preform Fabricated Successfully	71
Quick Access Rocket Exhaust Rig Testing of Coated GRCop-84 Sheets Used to Aid Coating Selection for Reusable Launch Vehicles	73
Thermodynamics of Volatile Species in the Silicon-Oxygen-Hydrogen System Studied	74
Very Tough, Erosion-Resistant Turbine Airfoil Thermal Barrier Coatings Developed	75
Low-Thermal-Conductivity Pyrochlore Oxide Materials Developed for Advanced Thermal Barrier Coatings	77
Strong, Tough Glass Composites Developed for Solid Oxide Fuel Cell Seals	78
Process Developed for Generating Ceramic Interconnects With Low Sintering Temperatures for Solid Oxide Fuel Cells	79
Process Developed for Fabricating Engineered Pore Structures for High-Fuel-Utilization Solid Oxide Fuel Cells	80
Cooled Ceramic Matrix Composite Propulsion Structures Demonstrated	82
Permeability of Candidate Stirling Heater Head Materials Measured	84
SiC/SiC Ceramic Matrix Composites Developed for High-Temperature Space Transportation Applications	85
High-Temperature Piezoelectric Ceramic Developed	86
Structures Self-Assembled Through Directional Solidification	88
High-Temperature Proton-Conducting Ceramics Developed	89

Power and Electrical Propulsion

Proton-Exchange-Membrane Fuel Cell Powerplants Developed and Tested for Exploration Missions	92
Lithium-Ion Batteries Being Evaluated for Low-Earth-Orbit Applications	93
Lithium-Ion Cell Charge-Control Unit Developed	94
Integrated Power and Attitude Control System Demonstrated With Flywheels G2 and D1	95
Testing Done for Lorentz Force Accelerators and Electroless Propulsion Technology Development	96
Advanced Controller Developed for the Free-Piston Stirling Convertor	98
Brayton-Cycle Power-Conversion Unit Tested With Ion Thruster	100

Closed-Cycle Engine Program Used to Study Brayton Power Conversion	101
Stirling Convertor System Dynamic Model Developed	102
Stirling Power Convertors Demonstrated in Extended Operation	104
Reliability of the SRG110 Stirling Convertor Quantified	105
Work Began on Contracts for Radioisotope Power Conversion Technology Research and Development	106
Low-Temperature Chalcopyrite Thin-Film Solar Cells Developed for Space Photovoltaic Applications	108
Ground-Laboratory to In-Space Effective Atomic-Oxygen Fluence Determined for DC 93–500 Silicone	110
Vacuum Ultraviolet Radiation Effects on DC93–500 Silicone Film Studied	112
Conductive Composites Made Less Expensively	113
Concept Developed for an Implanted Stimulated Muscle-Powered Piezoelectric Generator	114
Ozone Exposure System Designed and Used to Test High-Altitude Airship Materials	116
Microsystem Cooler Concept Developed and Being Fabricated	117
Reliability of Electronics for Cryogenic Space Applications Being Assessed	119

Structures

Structural Benchmark Tests of Composite Combustion Chamber Support Completed	120
Benchmark Calibration Tests Completed for Stirling Convertor Heater Head Life Assessment	121
Titanium Aluminide Scramjet Inlet Flap Subelement Benchmark Tested	123
Stainless-Steel-Foam Structures Evaluated for Fan and Rotor Blades	124
Integrity of Polymethylmethacrylate (PMMA) Chemically Welded Joints Examined	126
Life Predicted in a Probabilistic Design Space for Brittle Materials With Transient Loads	127
Liquid-Hydrogen-Cooled 450-hp Electric Motor Test Stand Being Developed	130
Ironless High-Power-Density Permanent Magnet Electric Motors Designed for Emissionless Aircraft Propulsion	131
High-Temperature (1000 °F) Magnetic Thrust Bearing Test Rig Completed and Operational	131
G2 Flywheel Module Operated at 41,000 rpm	132
Fuel-Cell-Powered Electric Motor Drive Analyzed for a Large Airplane	133
Damage-Tolerant, Affordable Composite Engine Cases Designed and Fabricated	135
Prototype Variable-Area Exhaust Nozzle Designed	136
Switched-Reluctance Cryogenic Motor Tested and Upgraded	137
Analytical Micromechanics Modeling Technique Developed for Ceramic Matrix Composites Analysis	139
Design Sensitivity for a Subsonic Aircraft Predicted by Neural Network and Regression Models	140
Advanced Vibration Analysis Tool Developed for Robust Engine Rotor Designs	142
System Developed for Real-Time Blade-Flutter Monitoring in the Wind Tunnel	143
Power Requirements Determined for High-Power-Density Electric Motors for Electric Aircraft Propulsion	144
Flutter Stability Verified for the Trailing Edge Blowing Fan	146
Fundamental Mistuning Model for Probabilistic Analysis Studied Experimentally	147
NESTEM Probabilistic Analysis Used to Study Mistuned Bladed Disks and Blisks With Aerodynamic and Structural Coupling	147
Primal and Dual Integrated Force Methods Used for Stochastic Analysis	148
Spur Gear Wear Investigated in Support of Space Shuttle Return-To-Flight Efforts	149
High-Temperature Knitted Spring Tubes Improved for Structural Seal Applications	151
Advanced Ceramic Wafer Seals Demonstrated at 2000 °F	153
Software Developed for Analyzing High-Speed Rolling-Element Bearings	154
Oxide Ceramic Films Grown on 60 Nitinol for NASA and Department of Defense Applications	156
Ambient Pressure Test Rig Developed for Testing Oil-Free Bearings in Alternate Gases and Variable Pressures	157
Tribological Behavior of Nano-Onions in Krytox 143AB Evaluated	159
Journal Bearing Analysis Suite Released for Planetary Gear System Evaluation	161

Propulsion Systems

Benchmark Problems Used to Assess Computational Aeroacoustics Codes	164
Turbofan Noise Reduction Associated With Increased Bypass Nozzle Flow	166
National Combustion Code Used To Study the Hydrogen Injector Design for Gas Turbines	167
Transferable Calibration Standard Developed for Quantitative Raman Scattering Diagnostics in High-Pressure Flames	170
Emissions Measured in the Exhaust of a CFM-56 Engine on a DC-8	172
Adaptive Technologies Developed and Demonstrated for Extending the Stable Operating Range of Compressors	173
SmagIcE 2D Version 1.8: Software Toolkit Developed for Aerodynamic Simulation Over Iced Airfoils	175
Piloted Flight Simulator Developed for Icing Effects Training	176
Subsonic Scarf Inlets Investigated	177
Parametric Inlet Tested in Glenn's 10- by 10-Foot Supersonic Wind Tunnel	178
Wind-US 1.0 Released by NPARC Alliance	180
Directional Attenuation of Jet Noise With Eccentric Coannular Nozzle Investigated	181
Pressure Control for Low Earth Orbit Investigated	183
Synthetic Vortex Generator Jets Used to Control Separation on Low-Pressure Turbine Airfoils	184
Object-Oriented Version of Glenn-HT Code Released: Glenn-HT2000	187

Microgravity

New Species of Fire Discovered: Fingering Flamelets Form a Dynamic Population	189
Soldering Tested in Reduced Gravity	190
Flow-Boiling Critical Heat Flux Experiments Performed in Reduced Gravity	192
Condensing Heat Exchanger Concept Developed for Space Systems	194
Binary Colloidal Alloy Test-3 (BCAT-3) Tabletop Space Station Experiment Continues	196
Two-Phase Flow Technology Developed and Demonstrated for the Vision for Exploration	197

Engineering and Technical Services

Engineering Development

Hybrid Power Management Program Evaluated Ultracapacitors for the Next Generation Launch Transportation Project	200
System Developed for Bulk Flow Imaging of a Two-Phase Fluid in a Cylindrical Couette	201
Acoustic Liquid Manipulation Used to Enhance Electrochemical Processes	202
Theoretical and Experimental Unsteady Aerodynamics Compared for a Linear Oscillating Cascade With a Supersonic Leading-Edge Locus	203
Model-Based, Multiscale Self-Tuning Controller Developed for Active Combustion Control	205

Appendixes

NASA Headquarters Program Offices	207
Programs and Projects	208
Index of Authors and Contacts	211

2004

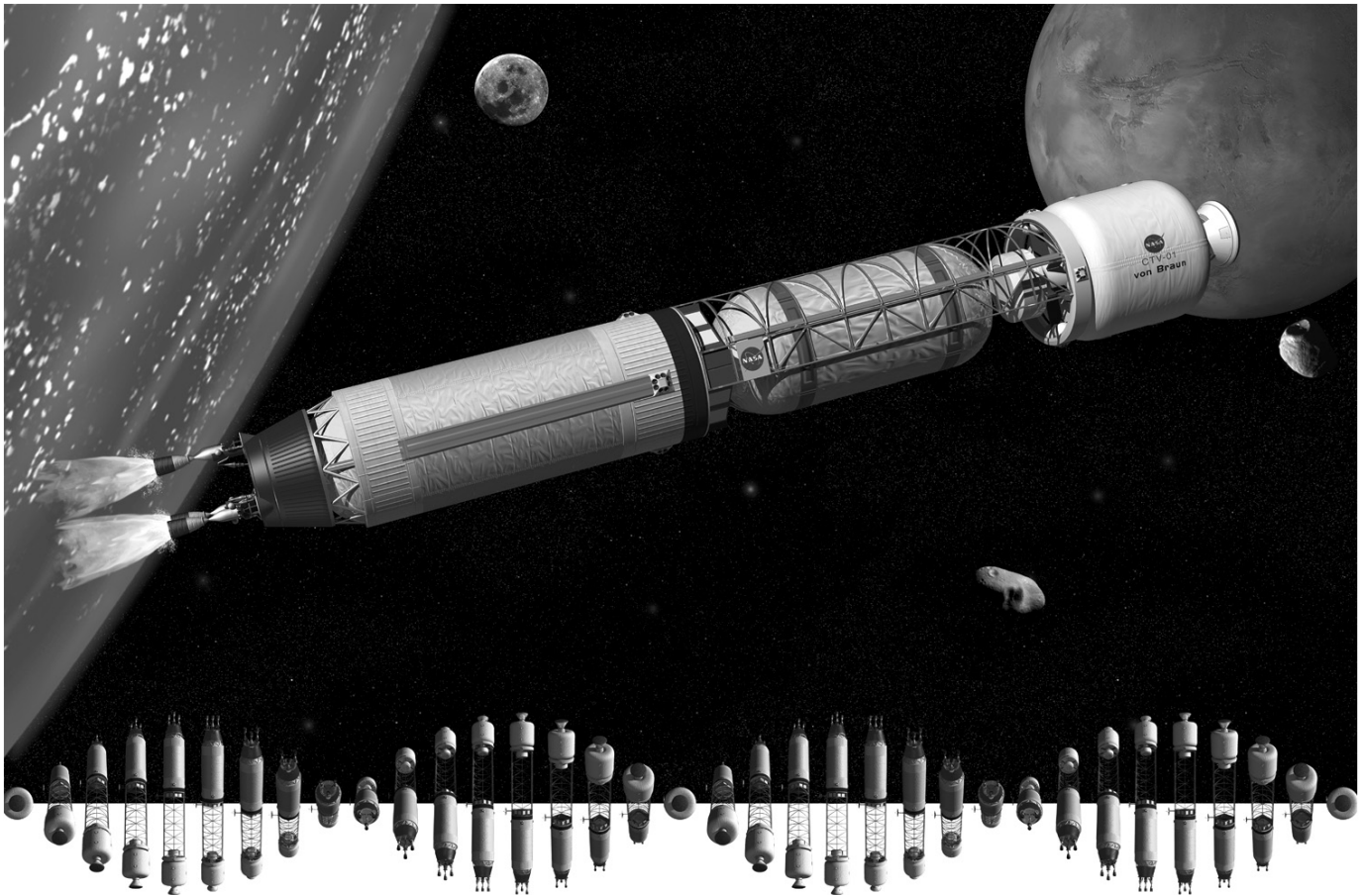
PROGRAMS AND PROJECTS

SYSTEMS ANALYSIS

EXPLORATION SYSTEMS

Systems Analysis

Bimodal Nuclear Thermal Rocket Propulsion Investigated for Power-Rich, Artificial-Gravity Human Exploration Missions to Mars



Artificial-gravity BNTR crew transfer vehicle for Mars.

The NASA Glenn Research Center is involved in systems and mission analysis studies for Prometheus and the President's Vision for Space Exploration. In support of this effort, engineers at Glenn have been studying the application of nuclear thermal rocket (NTR) engines to human missions to Mars.

The NTR is one of the leading propulsion options for future NASA human exploration missions because of its high specific impulse capability (I_{sp} ~875 to 950 sec) and attractive engine thrust-to-weight ratio (>3). Because only a relatively small amount of enriched uranium-235 fuel is consumed in an NTR during the primary propulsion maneuvers of a typical Mars mission, engines configured for both propulsive thrust and modest power generation (referred to as bimodal operation) provide the basis for a robust, power-rich stage with efficient propulsive capture capability.

A family of modular bimodal NTR (BNTR) space-transfer-vehicle concepts has been developed that utilize a common core stage powered by three ~15-klb_f engines that produce 50 kWe of total electrical power for crew life support, high-data-rate communications with Earth, and an active refrigeration system for long-term, zero-boiloff liquid hydrogen (LH₂) storage. Candidate nuclear fuels for BNTR engines include uranium carbide (UC₂) particles with a

chemical-vapor-deposited coating in graphite and uranium-carbide zirconium-carbide (UC-ZrC) in graphite, which were developed during the Nuclear Engine for Rocket Vehicle Application (NERVA) program, as well as uranium oxide (UO₂) in tungsten (W) metal cermet. These fuels, which are listed in order of increasing temperature capability, can produce hot hydrogen exhaust ranging from ~2550 to 2900 K. Each engine has its own closed-cycle Brayton rotating unit, capable of generating up to 25 kWe, that provides an engine-out capability. Under nominal conditions, each Brayton rotating unit would operate at two-thirds of the rated power (~17 kWe).

Compared with other propulsion options currently being studied, Mars mission architectures using BNTR transfer vehicles require fewer transportation system elements. This makes space operations simpler and reduces mission mass and risk.

In addition, artificial gravity capability can be easily integrated into the BNTR vehicle design to ensure crew health and fitness on long-duration missions. On a representative crew transfer vehicle, the bimodal core stage is connected to an inflatable TransHab (transfer habitat) module via an innovative saddle truss that is open underneath to allow the inline LH₂ propellant tank to be easily jettisoned following the trans-Mars injection burn. After the tank is released, the crew transfer vehicle initiates vehicle rotation at ~4 rpm to provide the crew with a Mars gravity environment (~0.38 times Earth gravity, g_E) during the outbound transit. A higher rotation rate of ~6 rpm would provide about 0.8 g_E during the return leg of the mission to help reacclimate the crew to Earth's gravity. A variant of the LH₂ NTR option, known as the LOx-augmented NTR (or LANTR), would add an oxygen afterburner nozzle to the BNTR if variable thrust, variable I_{sp} , or stage volume reduction was needed.

Bibliography

Borowski, S.K.; Dudzinski, L.A.; and McGuire, M.L.: Bimodal Nuclear Thermal Rocket (NTR) Propulsion for Power-Rich, Artificial Gravity Human Exploration Missions to Mars. IAA-01-IAA.13.3.05, 2001.

Borowski, Stanley K.; Dudzinski, Leonard A.; and McGuire, Melissa L.: Artificial Gravity Vehicle Design Option for NASA's Human Mars Mission Using "Bimodal" NTR Propulsion. AIAA Paper 99-2545, 1999.

Find out more about this research:

<http://trajectory.grc.nasa.gov/>

Glenn contacts:

Dr. Stanley K. Borowski, 216-977-7091, Stanley.K.Borowski@nasa.gov; and Melissa L. McGuire, 216-977-7128, Melissa.L.McGuire@nasa.gov

Authors:

Dr. Stanley K. Borowski, Melissa L. McGuire, and Leonard A. Dudzinski

Headquarters program office:

Exploration Systems

Programs/Projects:

Project Prometheus, Exploration Systems

OTIS 3.2 Software Released

Trajectory, mission, and vehicle engineers concern themselves with finding the best way for an object to get from one place to another. These engineers rely upon special software to assist them in this. For a number of years, many engineers have used the OTIS program for this assistance. With OTIS, an engineer can fully optimize trajectories for airplanes, launch vehicles like the space shuttle, interplanetary spacecraft, and orbital transfer vehicles. OTIS provides four modes of operation, with each mode providing successively stronger optimization capability. The most powerful mode uses a mathematical method called implicit integration to solve what engineers and mathematicians call the optimal control problem. OTIS 3.2, which was developed at the NASA Glenn Research Center, is the latest release of this industry workhorse and features new capabilities for parameter optimization and mission design.

OTIS stands for Optimal Control by Implicit Simulation, and it is implicit integration that makes OTIS so powerful at solving trajectory optimization problems. Why is this so important? The optimization process not only determines how to get from point A to point B, but it can also determine how to do this

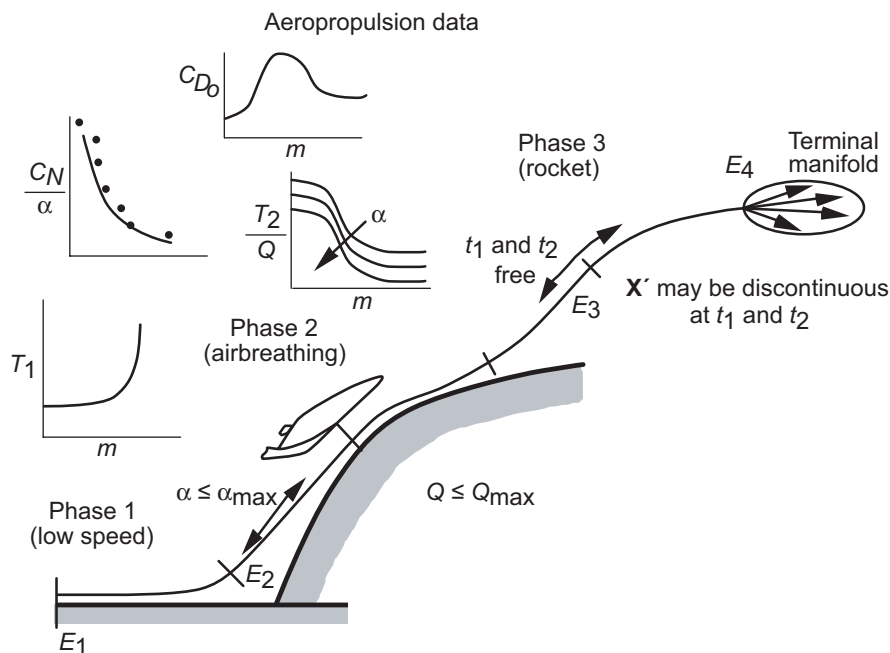
with the least amount of propellant, with the lightest starting weight, or in the fastest time possible while avoiding certain obstacles along the way. There are numerous conditions that engineers can use to define optimal, or best. OTIS provides a framework for defining the starting and ending points of the trajectory (point A and point B), the constraints on the trajectory (requirements like "avoid these regions where obstacles occur"), and what is being optimized (e.g., minimize propellant). The implicit integration method can find solutions to very complicated problems when there is not a lot of information

available about what the optimal trajectory might be. The method was first developed for solving two-point boundary value problems and was adapted for use in OTIS. Implicit integration usually allows OTIS to find solutions to problems much faster than programs that use explicit integration and parametric methods. Consequently, OTIS is best suited to solving very complicated and highly constrained problems.

Typical OTIS input includes a description of the objective function (the thing that is the measure of goodness) and a number of general specifications that describe what the program should output, and how these results should be formatted. Also, OTIS provides input items for modeling vehicles by the stage of operation. This is entirely analogous to the stages of a rocket, where first one stage operates and then another and another. It also has input items for describing phases of operation. Within each phase, the user specifies the stage that is operating, the current constraints on the operation of the vehicle,

the initial and final conditions of the phase, the bounds on the problem, and the control parameters—such as steering angles and engine throttle parameters. See the diagram for a notional representation of the phases and stages.

The Boeing Company wrote the first versions of OTIS for the U.S. Air Force in 1985. Since then, NASA has taken ownership of OTIS and has systematically improved and updated it. OTIS is written in Fortran 77 and uses the SNOPT nonlinear programming package. The OTIS program is restricted to users within the United States who are working for the Federal Government, its entities, contractors, and subcontractors. Eligible users can obtain OTIS from NASA Glenn's Technology Transfer and Partnership Office by following the links at <http://otis.grc.nasa.gov/request.shtml>.



Typical trajectory optimization problem. (Note: C_N , coefficient of normal force; α , angle of attack; C_{D_0} , coefficient of base drag; m , mach number; T_1 , T_2 , temperature during phases 1 and 2; Q , dynamic pressure during phase 2; t_1 , t_2 , initial and final phase times; \mathbf{X}' , state vector dynamics; E_x , phase times in seconds.)

Find out more about this research:

OTIS:
<http://otis.grc.nasa.gov>

Space Propulsion and Mission Analysis Office at Glenn:
<http://trajectory.grc.nasa.gov>

Glenn contacts:
 John P. Riehl, 216-977-7061,
John.P.Riehl@nasa.gov; and
 Waldy K. Sjauw, 216-977-7066,
Waldy.K.Sjauw@nasa.gov

Authors:
 John P. Riehl and Waldy K. Sjauw

Headquarters program office:
 Exploration Systems

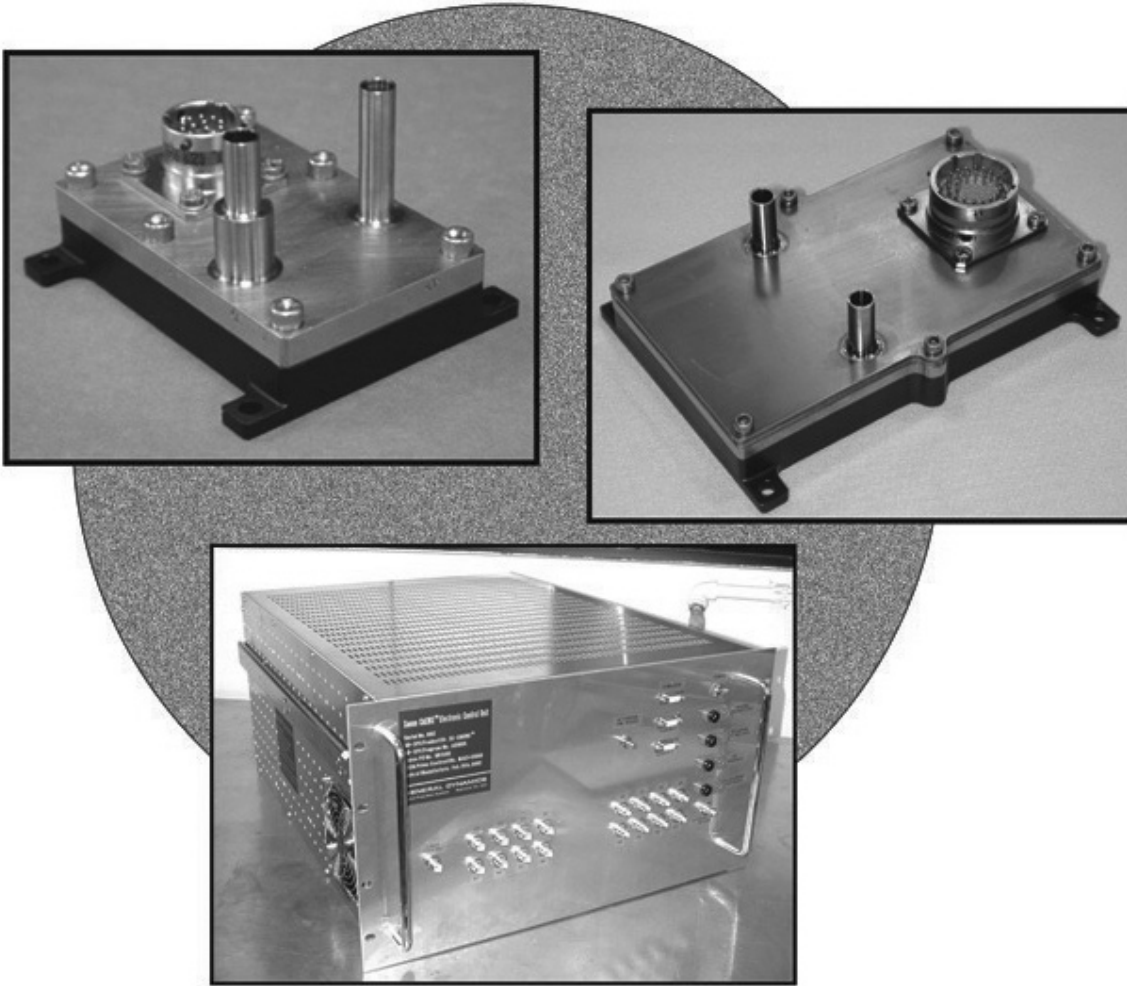
Programs/Projects:
 In-Space Systems

Photochemically Etched Construction Technology Developed for Digital Xenon Feed Systems

Electric propulsion systems are quickly emerging as attractive options for primary propulsion in low Earth orbit, in geosynchronous orbit, and on interplanetary spacecraft. The driving force behind the acceptance of these systems is the substantial reduction in the propellant mass that can be realized. Unfortunately, system designers are often forced to utilize components designed for chemical propellants in their electric systems. Although functionally acceptable, these relatively large, heavy components are designed for the higher pressures and mass flow rates required by chemical systems. To fully realize the benefits of electric propulsion, researchers must develop components that are optimized for the low flow rates, critical leakage needs, low pressures, and limited budgets of these emerging systems.

Starting in 2001, a team led by VACCO Aerospace Products was selected by NASA under an Advanced Cross-Enterprise Technology Development

Program to conduct a project entitled "Photo-Chemically Etched Construction Technology for Digital Xenon Feed Systems." This program consists of application-engineering xenon pressure- and flow-control modules using a proprietary VACCO technology called Chemically Etched Miniature Systems (ChEMS, VACCO Industries, Inc., Space Products, South El Monte, CA), which is based on VACCO's extensive in-house experience in the precision chemical etching of metals and plastics.

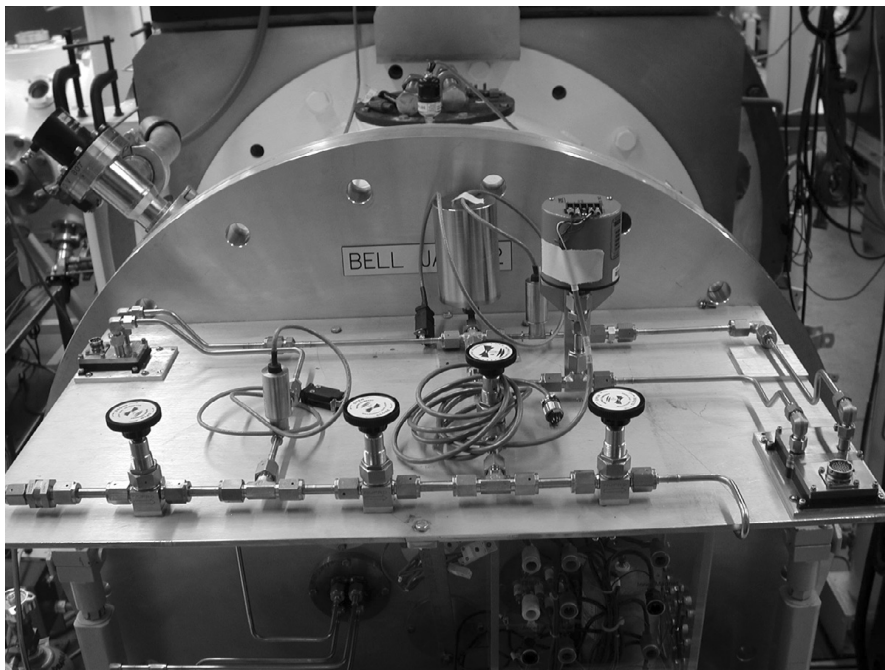


Critical components of a xenon feed system (XFS) developed by VACCO. Top left: Pressure-control module that provided variable-pressure control. Top right: Flow-control module that enabled high-fidelity regulation of the xenon flow to the thruster. Bottom: Electronic-control unit that was the interface to a computer where the XFS control software was operated.

ChEMS modules consist of multiple layers of etched metal or plastic sheets that, when stacked and bonded together, form an assembly of all of the components and their interconnecting flow paths. These modules can alter pressure and flow-rate set points as well as compensate for changing inlet pressure and temperature conditions. The size and mass of complex modules is drastically reduced through the fabrication of components and interconnecting features that are an order of magnitude smaller and lighter than components made using traditional machining techniques.

Several functional features enable the ChEMS-based xenon feed system (XFS) to be ideally suited to the control of xenon to the thrusters in electric propulsion systems. These include

- **Variable set point.**—The XFS mass flow rate and pressure set points are variable and can be changed at the control computer.
- **Pressure and temperature compensation.**—Xenon mass flow can be accurately maintained over a wide band of propellant temperatures and pressures.
- **Reliability.**—The only moving parts in the XFS are the suspended armatures for the 12 valves. The armatures are welded to S-springs that guide them so that they move without sliding against adjacent parts. To preclude failure, researchers designed the S-springs for low stress and high fatigue life.
- **Failure tolerance.**—The XFS can function even after sustaining two isolation valve failures. In addition, failure of one or more of the valves in the digital flow-control array will degrade flow-control accuracy and engine performance, but it will not cause loss of the engine.



Xenon feed system (XFS) assembled with the VACCO-developed components and configured to operate the NASA 120M (2- to 3-kW) Hall thruster.

This 3-year contract led to the successful development of a single-line xenon feed system. The major elements of the feed system, shown in the photograph on the preceding page, include the variable-pressure-control module, the digital flow-control module, and the electronic-control unit (designed and fabricated by Aerojet RRC (Redmond, WA)) to operate these modules, which interfaces the XFS to the control computer. The initial operating targets for the flow- and pressure-control modules were selected in discussions with the NASA Glenn Research Center and the Jet Propulsion Laboratory, at which time it was decided to size the flow control for use with a multikilowatt Hall effect thruster.

Fabrication of the pressure-control module and a first-generation electronic-control unit were completed in 2002. After a series of sealing issues with the flow elements of the flow-control module were resolved via an extensive in-house research and development effort at VACCO, a fully functional unit was completed and tested extensively in 2003, along with a second electronic control unit. The components were integrated into the XFS at Glenn in late 2003. This feed system (shown in the photograph to the left), was successfully used to control the anode flow during testing of a NASA 120M Hall effect thruster.

The final phase of this NASA Research Announcement was to resolve control issues that arose during thruster testing. This work was completed by VACCO and Aerojet RRC in April 2004. The completed hardware, along with the feed system, was delivered to Glenn in May 2004 for completion of this contract.

In conclusion, the ChEMS technology represents an important breakthrough in the size, mass, and cost of miniature fluid systems. The application

of ChEMS technology to xenon flow control has resulted in a module ideally suited for electric propulsion applications. The ChEMS XFS provides system designers with a technology that allows them to realize the full potential of electric propulsion.

Glenn contacts:

Timothy R. Verhey, 216-433-7458, Timothy.R.Verhey@nasa.gov; and David T. Jacobson, 216-433-3691, David.T.Jacobson@nasa.gov

Authors:

Ben Otsap, Joseph Cardin, Timothy R. Verhey, Vincent K. Rawlin, Juergen Mueller, Randall Aadlund, Robert Kay, and Michael Andrews

Headquarters program office:

OAT (Energetics)

Programs/Projects:

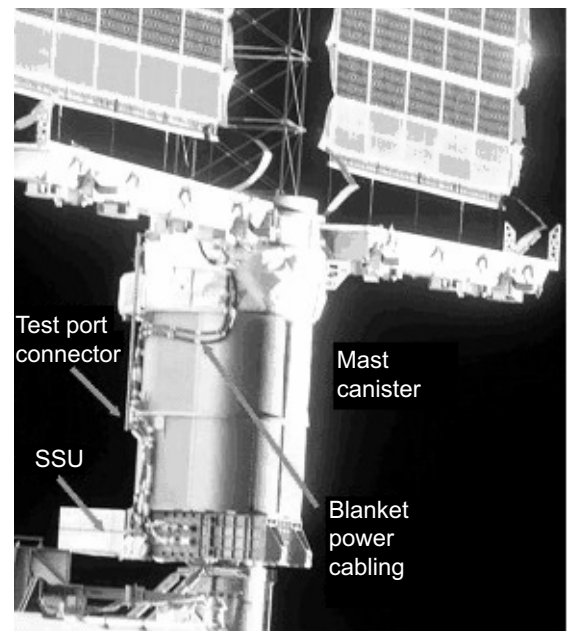
Science Mission, In-Space Technology, Exploration Mission, Project Prometheus

Options Studied for Managing Space Station Solar Array Electrical Hazards for Sequential Shunt Unit Replacement

The U.S. solar array strings on the International Space Station are connected to a sequential shunt unit (SSU). The job of the SSU is to shunt, or short, the excess current from the solar array, such that just enough current is provided downstream to maintain the 160-V bus voltage while meeting the power load demand and recharging the batteries. Should an SSU fail on-orbit, it would be removed and replaced with the on-orbit spare during an astronaut space walk or extravehicular activity (EVA) (see the photograph). However, removing an SSU during an orbit Sun period with input solar array power connectors fully energized could result in substantial hardware damage and/or safety risk to the EVA astronaut. The open-circuit voltage of cold solar-array strings can exceed 320 V, and warm solar-array strings could feed a short circuit with a total current level exceeding 240 A.

Replacing the SSU during eclipse when the array is not in sunlight would seem optimal, except that the maximum eclipse period is only 36 min. This does not provide sufficient time to remove and replace the SSU while allowing for contingencies. Several other options for the SSU remove-and-replace procedure were assessed at the NASA Glenn Research Center, including

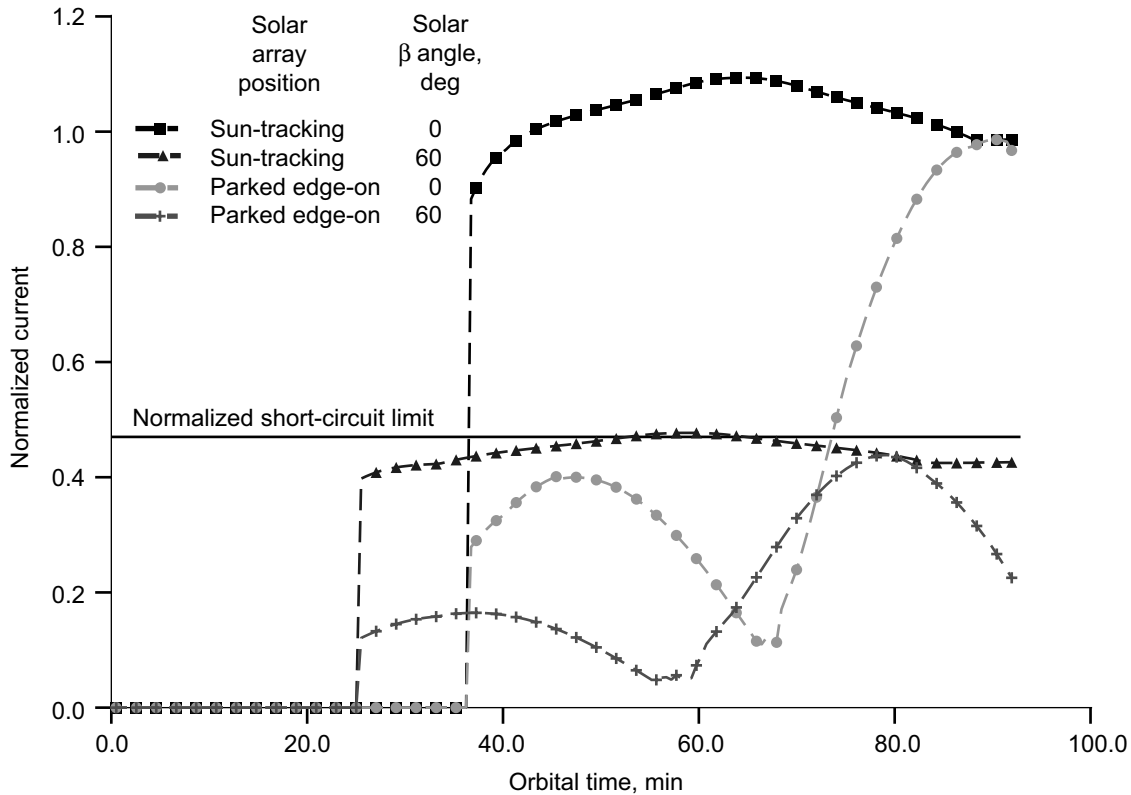
- (1) Leave the failed SSU in place.
- (2) Change-out the SSU during one eclipse period.
- (3) Change-out the SSU during several eclipse periods.
- (4) Retract the solar array; then change-out the SSU during multiple-orbit Sun and eclipse periods.
- (5) Design, build, and install a temporary shunting plug on the solar-array string power connectors, and change-out the SSU during several orbit eclipse periods.
- (6) Design, build, and install a temporary shunting plug on the solar-array-string test-port connectors, and change-out the SSU during several orbit eclipse periods.



Sequential shunt unit (SSU) mounted on the beta gimbal platform (below the mast canister).

From the perspective of defining and managing solar-array-string electrical hazards, this analysis identified option (6), installing a shunt plug on the solar-array-string test-port connectors, as a workable SSU replacement procedure via EVA.

In this option, the test-port-connector shunt plug would collapse the array



Normalized short-circuit current, I_{sc} , versus orbit solar β angle (angle between the orbit plane and the Earth-Sun line). Velocity vector for the International Space Station (ISS) is aligned with the ISS +x-axis in this figure.

string voltage and dissipate string short-circuit current I_{sc} through a low-resistance electrical shunt that is passively cooled. This approach would afford the EVA crew multiple orbits to accomplish the SSU remove-and-replace procedure. Also, this approach would not introduce additional risk for damaging SSU power connectors because shunt plugs would be inserted in the test-port connectors. The test-port connectors are located away from the SSU and, thus, do not impede the SSU remove-and-replace operations.

The only undesirable feature of this option is that there are restrictions on the allowable array string I_{sc} . The normalized string I_{sc} must be 0.47 or lower to maintain an acceptably low temperature in the test-port-connector 22-gauge wire bundles. Operational strategies were devised that maintained the normalized I_{sc} value at acceptably low values for the International Space Station flight in the solar inertial flight mode for a wide range of solar β angles and the preferred solar-array park angle for EVA operations (see the graph). Array string current and voltage capability predictions were generated using the bifacial solar-array model incorporated in Glenn's System Power Analysis for Capability Evaluation (SPACE) electrical-power-system performance code.

Find out more about this research:
<http://space-power.grc.nasa.gov>

Glenn contacts:
 Ann M. Delleur, 216-433-5519,
 Ann.M.Delleur@nasa.gov; and
 Thomas W. Kerslake, 216-433-5373,
 Thomas.W.Kerslake@nasa.gov

Authors:
 Ann M. Delleur, Thomas W. Kerslake,
 and Robert K. Levy

Headquarters program office:
 Exploration Systems

Programs/Projects:
 ISS

Probabilistic Analysis Techniques Applied to Complex Spacecraft Power System Modeling

Electric power system performance predictions are critical to spacecraft, such as the International Space Station (ISS), to ensure that sufficient power is available to support all the spacecraft's power needs. In the case of the ISS power system, analyses to date have been deterministic, meaning that each analysis produces a single-valued result for power capability because of the complexity and large size of the model. As a result, the deterministic ISS analyses did not account for the sensitivity of the power capability to uncertainties in model input variables. Over the last 10 years, the NASA Glenn Research Center has developed advanced, computationally fast, probabilistic analysis techniques and successfully applied them to large (thousands of nodes) complex structural analysis models. These same techniques were recently applied to large, complex ISS power system models. This new application enables probabilistic power analyses that account for input uncertainties and produce results that include variations caused by these uncertainties. Specifically, N&R Engineering, under contract to NASA, integrated these advanced probabilistic techniques with Glenn's internationally recognized ISS power system model, System Power Analysis for Capability Evaluation (SPACE).

An advanced, fast probabilistic integrator (FPI) technique was used in this effort, because the traditional method for performing probabilistic analyses, the Monte Carlo method, is time consuming and computationally prohibitive for large complex models. Monte Carlo techniques involve running thousands of individual analyses, each with a slightly different set of input variables. The results from all those cases are integrated to obtain the sensitivity of the output variable—in this case, power—to those input uncertainties. However, when FPI is used, only a few analyses need to be performed; and FPI then integrates those results to approximate a complete Monte Carlo analysis.

ISS power analyses require thousands of input variables to model all the power system components: solar arrays, which generate power from sunlight; batteries

that are charged during the sunlight and provide power when the solar arrays do not; and a large power distribution network, consisting of cables, circuit breakers, converters, and controllers to route power to various ISS users. To demonstrate SPACE power system probabilistic analysis, researchers at N&R Engineering with assistance from Glenn varied a sample of five input variables, including Earth albedo (sunlight reflected off the Earth), the efficiency of a power-conversion unit, and the attitude of the ISS. Results show that the variation in power capability can now be represented by not just a single value, but rather as a set of probabilities that a certain power level will be achieved.

The results of this project also proved that Glenn's advanced probabilistic analysis techniques (FPI), which were developed for large complex structural analysis models, can be used to assess complex spacecraft power systems. Glenn now has an integrated tool that can be used for probabilistic power system performance assessment. This new capability will allow ISS operators more insight into the performance of the power system and to operate the ISS power system closer to its operating limits with higher confidence.

Glenn contacts:

Jeffrey S. Hojnicky, 216-433-5393,
Jeffrey.S.Hojnicky@nasa.gov; and
Jeffrey J. Rusick, 216-433-5375,
Jeffrey.J.Rusick@nasa.gov

Authors:

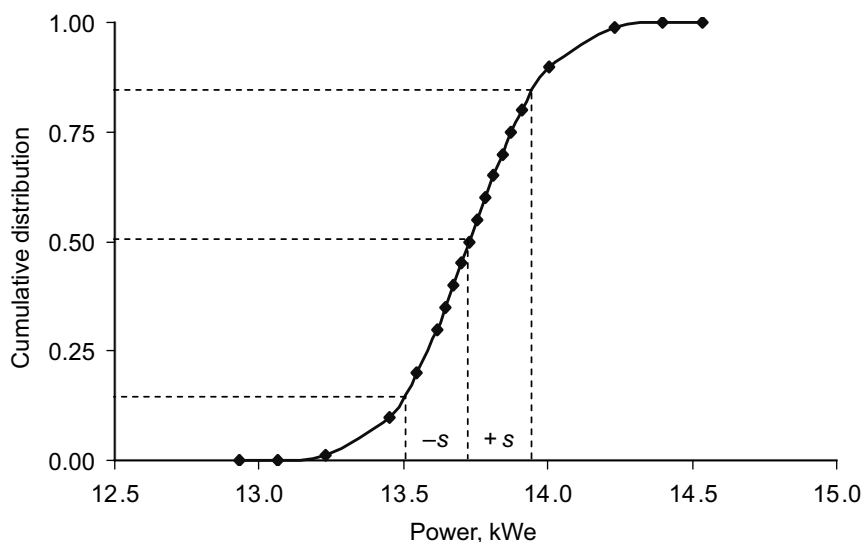
Jeffrey S. Hojnicky and Jeffrey J. Rusick

Headquarters program office:

Aeronautics Research

Programs/Projects:

ISS, Spacecraft Power Systems



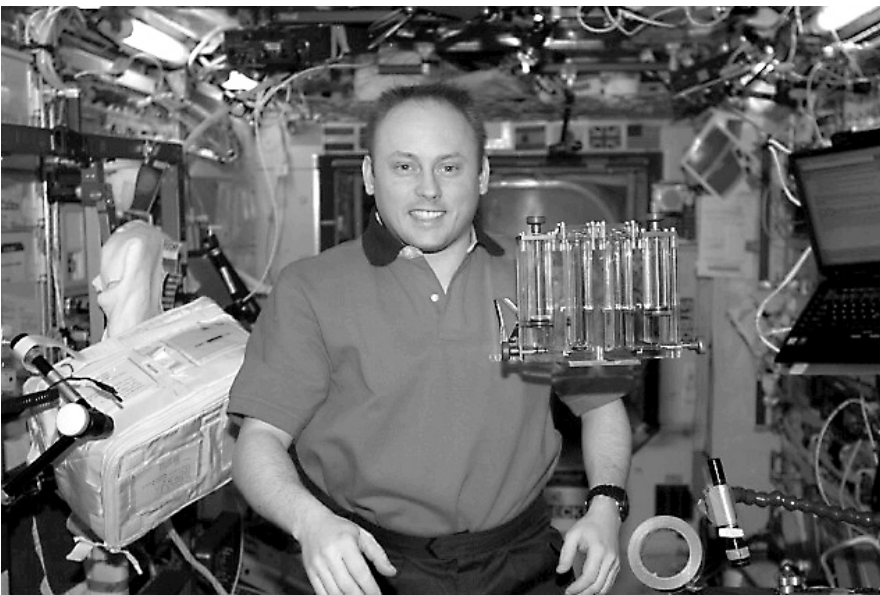
Sample showing the probability of achieving a particular power level on a single ISS power channel. Mean power, 13.7 kWe; standard deviation of power, σ , 0.22.

Exploration Systems

Capillary Flow Experiments Began on the International Space Station

The Capillary Flow Experiments (CFEs) are a suite of fluid physics flight experiments designed to investigate capillary flows and phenomena in low gravity. Data obtained from the CFEs will be crucial to NASA's Space Exploration Initiative, particularly pertaining to fluids management systems such as fuels and cryogen storage systems, thermal control systems (e.g., water recycling), and materials processing in the liquid state. NASA's current plans for exploration missions assume the use of larger liquid propellant masses than have ever flown on interplanetary missions. Under low-gravity conditions, capillary forces can be exploited to control fluid orientation so that such large mission-critical systems perform predictably. The first of the CFE experiments has been conducted on the International Space Station, and the data are being analyzed. The experiment suite is described briefly.

CFE is a simple fundamental scientific study that can yield quantitative results from safe, low-cost, short time-to-flight, hand-held fluids experiments. The experiments aim to provide results of critical interest to the capillary flow community that cannot be achieved in ground-based tests: for example, dynamic effects associated with a moving-contact boundary condition, capillary-driven flow in interior corner networks, and critical wetting phenomena in complex geometries. Specific applications of the results center on particular fluids challenges concerning propellant tanks. The knowledge gained will help spacecraft fluid systems designers increase system reliability, decrease system mass, and reduce overall system complexity.

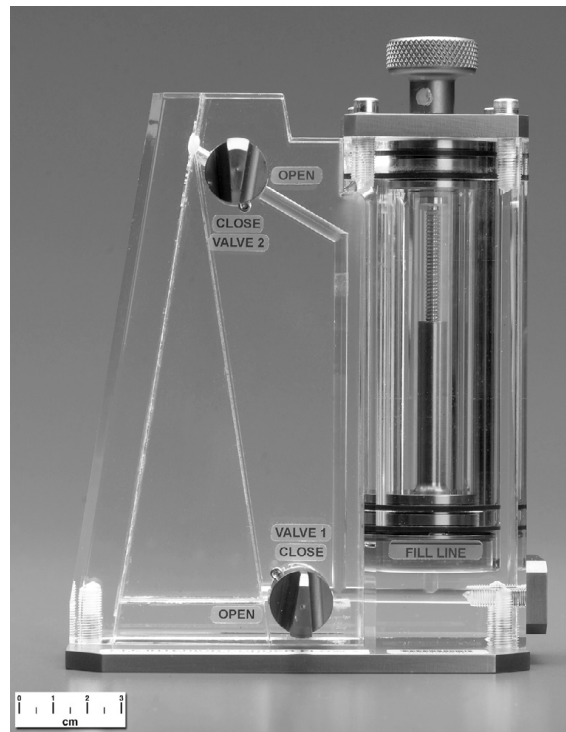
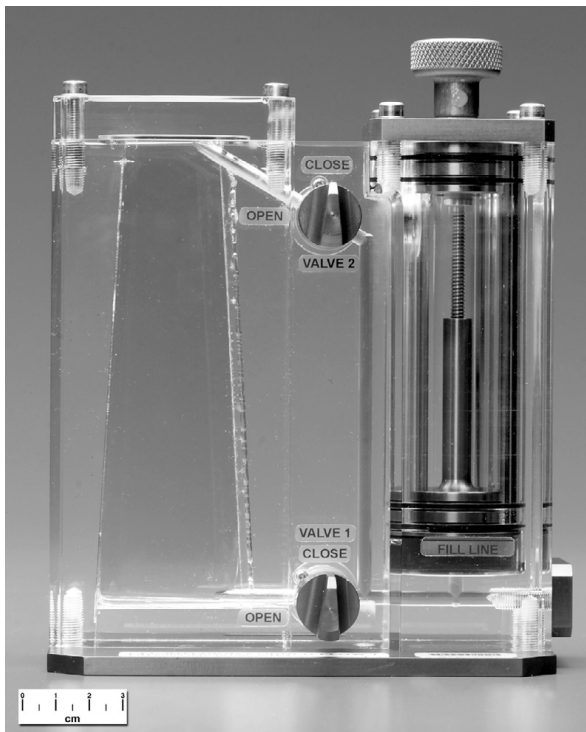


Science Officer Mike Fincke performs the CFE on orbit on Expedition 9 as a part of Saturday Science.

CFE is a NASA Glenn Research Center experiment developed under contract by ZIN Technologies, Inc. Three experiments constitute CFE—the Interior Corner Flow (ICF), the Vane Gap (VG), and the Contact Line (CL) experiments; and each experiment has two unique experimental units. All units use similar fluid-injection hardware, have simple and similarly sized test chambers, and rely solely on video for highly quantitative data. Silicone oil is the fluid used for all the tests, with different viscosities depending on the unit. Differences between units are primarily fluid properties, wetting conditions, and test cell cross section. The experiment procedures are simple and intuitive.

ICF is designed to understand propellant management and passive capillary flow in tapered geometries for which boundary conditions are not well understood or modeled. VG is designed to investigate the critical wetting condition that arises between interior corners that do not actually make contact, in particular, the corner and gap formed by an interior vane and the interior wall of a propellant tank, or between the intersection of vanes in a complex vane network.

The CL experiment is designed to study a fundamental and practical concern for low-gravity fluid phenomena: the impact of the dynamic contact line. The contact line controls the interface shape, stability, and dynamics of capillary systems in low gravity. The CFE–CL experiments will provide a direct measure of the extremes in behavior expected from either a free or pinned contact-line condition. There are two CL units, identical except for



Interior Corner Flow units. Left: ICF-1 has a triangular cross section in the horizontal plane of the test section. Right: ICF-2 is a tapered triangle from the base to the top and has a rectangular cross section in the horizontal plane of the test section.



Vane Gap unit 1. VG-1 and VG-2 are nearly identical, but VG-2 has a coating along the interior surfaces that changes the wetting characteristics of the fluid. VG-2 also has a slightly thicker vane than VG-1. This changes the interaction of the fluid with the vane and the side wall.



Contact Line unit 2. CL-2 flight unit showing pinning edge in right-center fluid chamber.

their respective wetting characteristics. One of the two CL units is shown in the bottom right photograph on the preceding page.

Contact Line unit 1 (CL-1), the ICF units, and VG units are complete and awaiting launch. Contact Line unit 2 (CL-2) was launched to the space station on Progress 13 in January 2004. International Space Station Science Officer Michael Fincke operated CL-2 on August 28 and again on September 18, 2004. He induced a variety of fluid disturbances, including taps, slides, and multiple lateral and axial perturbations. Video data were taken and are being analyzed by Principal Investigator Mark Weislogel at Portland State University under a grant from Glenn.

The following observations have been made. The correct contact-line boundary condition is pivotal to accurate modeling of large-length-scale capillary surface dynamics. Large-amplitude lateral oscillations created an hourglass configuration in the smooth cylinder, but the pinned interface did not de-pin. Under certain conditions, the pinned interface natural frequency was twice that of the smooth cylinder, and flows predominantly parallel to the contact line did not change the frequency or settling times.

Find out more about this research:

Mark Weislogel's Web site:

<http://www.me.pdx.edu/~mmw/>

AIAA paper describing CFE:

<http://www.me.pdx.edu/~mmw/AIAACFE.pdf>

Glenn contacts:

J. Mark Hickman, 216-977-7105, John.M.Hickman@nasa.gov; and Robert. D. Green, 216-433-5402, Robert.D.Green@nasa.gov

Authors:

J. Mark Hickman and Robert D. Green

Headquarters program office:

Exploration Systems

Programs/Projects:

Human System Research and Technology, Life Support & Habitation, Low-Gravity and Exploration Research, Multiphase Flow Technologies

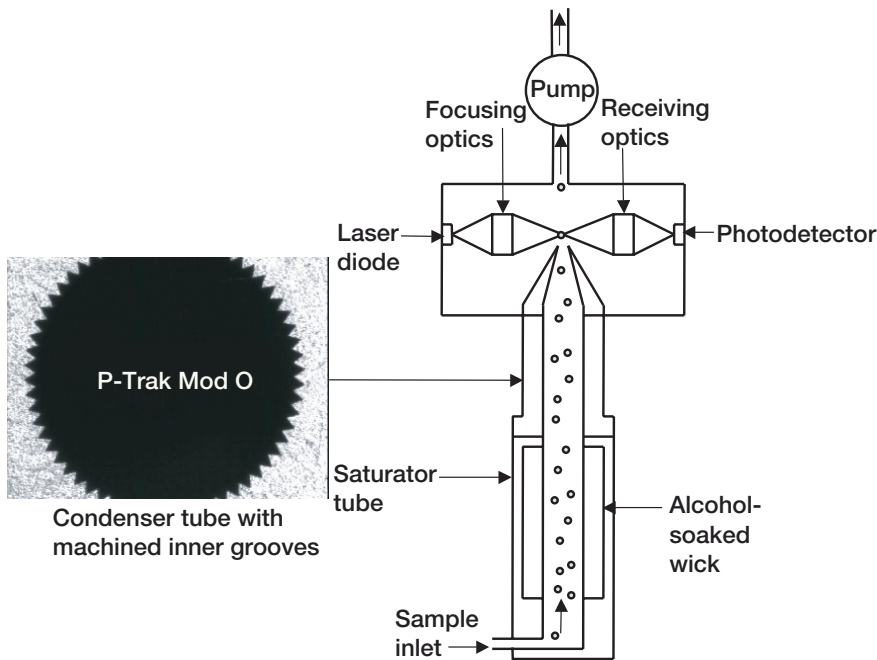
Fundamental Research Applied To Enable Hardware Performance in Microgravity

NASA sponsors microgravity research to generate knowledge in physical sciences. In some cases, that knowledge must be applied to enable future research. This article describes one such example. The Dust and Aerosol measurement Feasibility Test (DAFT) is a risk-mitigation experiment developed at the NASA Glenn Research Center by NASA and ZIN Technologies, Inc., in support of the Smoke Aerosol Measurement Experiment (SAME). SAME is an investigation that is being designed for operation in the Microgravity Science Glovebox aboard the International Space Station (ISS). The purpose of DAFT is to evaluate the performance of P-Trak (TSI Incorporated, Shoreview, MN)—a commercially available condensation nuclei counter and a key SAME diagnostic—in long-duration microgravity because of concerns about its ability to operate properly in that environment. If its microgravity performance is proven, this device will advance the state of the art in particle measurement capabilities for space vehicles and facilities, such as aboard the ISS.

The P-Trak, a hand-held instrument, can count individual particles as small as 20 nm in diameter in an aerosol stream. Particles are drawn into the device by a built-in suction pump. Upon entering the instrument, these particles pass through a saturator tube where they mix with an alcohol vapor (see the figure on the next page). This mixture then flows through a cooled condenser tube where some of the alcohol condenses onto the sample particles, and the droplets grow in a controlled fashion until they are large enough to be counted. These larger droplets pass through an internal nozzle and past a focused laser

beam, producing flashes of light that are sensed by a photodetector and then counted to determine particle number concentration. The operation of the instrument depends on the proper internal flow and recycling of isopropyl alcohol in both the vapor and liquid phases.

As the instrument was originally designed, alcohol that condenses on the inner wall of the condenser drains back down the saturator tube by gravity. The condenser in the unit was modified to promote the capillary flow of liquid alcohol back toward the saturator without depending on gravitational forces. This was accomplished through a series of 60 precisely machined grooves, each 0.009 in. deep, which promote the wicking of the liquid alcohol in the proper direction along the condenser's inner



P-Trak internal components and flow.

wall. This design was developed by fluids physics researchers at Glenn following an analysis to measure the contact angle of isopropyl alcohol on the aluminum surfaces of the condenser. The technique for this analysis is based on the results of fundamental research conducted at Glenn that investigated the wetting properties of liquids on surfaces (ref. 1).

For the DAFT experiment, both a modified and an unmodified version of the P-Trak will be tested in the long-duration microgravity conditions aboard the ISS. In addition to the P-Traks, another commercial instrument, the TSI DustTrak, will be utilized with the experiment. The DustTrak measures particle concentrations and is not sensitive to gravity. For experiment operations, DAFT will be secured to the front of an Expedite the Processing of Experiments to Space Station (EXPRESS) Rack and gaseous nitrogen provided by the rack will be used to fill 15-liter sample bags. These bags also will be loaded with a small quantity of a characterized source of particulates made up of Arizona road dust. One of the P-Traks and the DustTrak will then simultaneously draw samples from these bags while recording measurements of particle counts and mass concentrations, respectively. Prior to the particulate/nitrogen sample entering the instruments, the smallest particles will be removed from the flow stream by a device called the DAFT Impactor, which was designed with the guidance of scientists at the National Institute of Standards and Technology.

The EXPRESS laptop computer will be used to download the recorded measurements from the instruments and downlink them to the ground. There, they will be compared to quantitatively assess the operation of the P-Trak: that is, whether or not the readings of the P-Trak properly correlate to the readings of the DustTrak. These instruments also will take data from samples of the ISS cabin air. Environmental Control and Life Support Systems personnel at the NASA Johnson Space Center and NASA Marshall Space Flight Center have expressed a strong interest in these measurements since they will provide valuable information regarding particulate loading in the ISS cabin atmosphere. The DAFT hardware has been formally turned over to Johnson and awaits shipment to the launch site.

Reference

1. Allen, J.S.: An Analytical Solution for Determination of Small Contact Angles From Sessile Drops of Arbitrary Size. *J. Colloid Interface Sci.*, vol. 261, 2003, pp. 481–489.

Find out more about this research:

http://microgravity.grc.nasa.gov/combustion/daft/daft_index.htm

Glenn contacts:

William A. Sheredy, 216-433-3685, William.A.Sheredy@nasa.gov;
Dr. David L. Urban, 216-433-2835, David.L.Urban@nasa.gov; and
Dr. Gary A. Ruff, 216-433-5697, Gary.A.Ruff@nasa.gov

Author:

William A. Sheredy

Headquarters program office:

Exploration Systems

Programs/Projects:

Life Support & Habitation

Milestones Achieved for the Fluids and Combustion Facility

In 2004, President Bush outlined a new space exploration vision for NASA. The exploration programs will seek profound answers to questions of our origins, whether life exists beyond Earth, and how we could live in other worlds. In response, research projects from NASA's Fluid Physics Research Program were moved into the Exploration Systems Mission Directorate and realigned to support the major milestones of this directorate. A new goal of this research is to obtain an understanding of the physical phenomena that are important in the design of the many space-based and ground-based fluids systems that utilize multiphase flow, such as life support, propulsion, and power systems.

The Fluids and Combustion Facility (FCF) is a payload planned for the International Space Station (ISS) that will support the study of fluid physics and combustion science in a long-duration, microgravity environment. The FCF is a system of on-orbit and ground hardware, software, experiment operations, and planning designed to accommodate a wide variety of investigations. On orbit, it will comprise two powered racks called the Combustion Integrated Rack and the Fluids Integrated Rack (FIR, see the photograph to the right). The FCF is being designed for autonomous and/or remotely controlled operations primarily through the Telescience Support Center at the NASA Glenn Research Center. Experimentation in the FIR will focus on fluids physics phenomena affected by gravity, including the distribution of phases, pressure drops, and heat transfer coefficients (see the following photograph). Knowledge gained of these physical phenomena will enhance the design of space-based and ground-based systems.

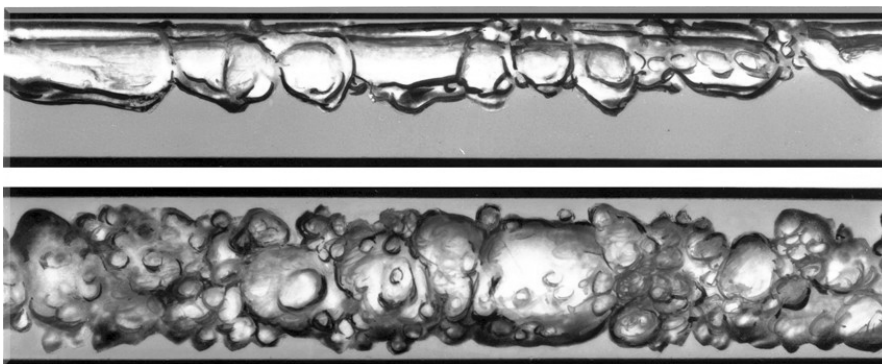
The FIR contains the hardware and software necessary for conducting a wide range of experiments, including experiments supporting NASA's Exploration Systems mission, while meeting ISS requirements and limitations related to safety and valuable resources, such as up/down mass and crew time. It provides many resources and capabilities that can be easily reconfigured for a wide variety of experimentation. The FIR utilizes the Active Rack Isolation System, which improves the microgravity environment for experiments by attenuating on-orbit vibrations transmitted from the Destiny Module to the



Fluids and Combustion Facility—Combustion Integrated Rack and Fluids Integrated Rack.

International Standard Payload Rack. The FIR environmental subsystem will utilize air and water to remove up to 6 kW of heat generated by the FIR and payload hardware. The electrical power control unit will provide 120 and 28 Vdc power, power management and control functions, as well as fault protection. The FIR will provide payloads with access to the ISS gaseous nitrogen and vacuum systems through the gas interface subsystem. The FIR command and data management subsystem will provide command and data handling for both facility and payload hardware. The FIR cameras will provide various cameras and light sources to support imaging needs.

The FCF is being developed at Glenn under a prime contract with Northrop Grumman. Researchers have concluded the project's design phase and are currently assembling and testing flight hardware. In the past year, the FIR team successfully completed several major milestones, including the integration of



Air-water multiphase flow.

the core systems (structural, power, and environmental control) into the FIR; a functional checkout of the core systems; the Active Rack Isolation System functional checkout and interface test; and several key ISS command and data-handling interface verifications. The flight hardware availability date is June 2005, which supports a shuttle launch no earlier than December 2005. There remain several variables that will affect the ultimate FIR launch date such as the shuttle return-to-flight date, the revised ISS assembly sequence, ISS resources available to payloads, and the payload's manifesting priority given its relevance to exploration research.

Find out more about this research:

<http://fcf.grc.nasa.gov/pages/project.html>

Glenn contacts:

Frank G. Gati, 216-433-2655, Frank.Gati@nasa.gov; and Myron E. Hill, 216-433-5279, Myron.E.Hill@nasa.gov

Authors:

Frank G. Gati and Myron E. Hill

Headquarters program office:

Exploration Systems

Programs/Projects:

Microgravity Science

Glenn's Telescience Support Center Provided Around-the-Clock Operations Support for Space Experiments on the International Space Station

NASA Glenn Research Center's Telescience Support Center (TSC) allows researchers on Earth to operate experiments onboard the International Space Station (ISS) and the space shuttles. NASA's continuing investment in the required software, systems, and networks provides distributed ISS ground operations that enable payload developers and scientists to monitor and control their experiments from the Glenn TSC. The quality of scientific and engineering data is enhanced while the long-term operational costs of experiments are reduced because principal investigators and engineering teams can operate their payloads from their home institutions.

Glenn plays a major role in conducting space experiments. In 1993, the TSC began providing ground support for experiments aboard space shuttle flights. During 2000 and 2001, the TSC went through a major renovation and expansion, more than doubling its capacity. The TSC is now a secure, multipurpose facility designed to provide dedicated support for simultaneous training, simulations, and real-time operations of space experiments. The current configuration consists of the Payload Operations Center, the Communication and Network Support Room, the TSC Operations and Support Room, and a visitors viewing area that provides access on a noninterference basis.

Since 2001, the TSC has provided over 26,000 hr of continuous support for diverse microgravity research experiments onboard the ISS, 24 hr a day, 7 days a week, while requiring less than 100 hr of crew intervention. Secure, dedicated audio, video, and data interfaces are provided to payload teams, including a digital stream of two channels of video from the ISS and the ability to



Jack Lekan operates the InSPACE experiment aboard the ISS from the Glenn TSC.

communicate directly with the ISS crew. Hardware and software provide the ability to send commands to payload hardware and to receive feedback via telemetry data and video links.

Pre-mission planning and post-mission debriefing support is provided for all payloads. The TSC staff begins planning for support of a payload up

to 18 months prior to the start of operations, depending on the complexity of the payload's operational requirements. Payload developers plan the operations, such as mission timeline development, resource planning, simulations, and training from the TSC. The TSC staff trains all the payload operations teams prior to mission operations. Training is tailored to each payload and covers all aspects of operations.

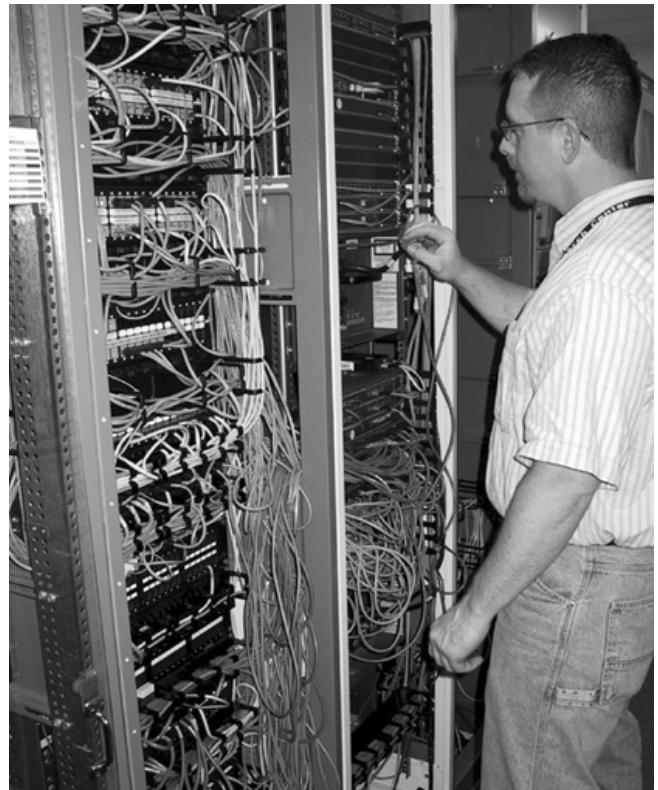
In addition to 5000 ft² for conducting payload operations, the TSC is also a communications and data center. The TSC provides secure digital audio links with the ISS Huntsville Operations Support Center. Audio systems at the TSC provide 45 separate digital channels for payload developers to communicate with the various groups working to support ISS operations. All data, voice, and video resources are available for each payload at its respective console workstation. Workstations and unique audio channels are configured for each payload team according to the team's needs so that the team can receive specific data from their flight hardware on orbit. The TSC provides at least two workstations for each payload and can manage dozens of terabytes of downlinked data from payloads.

Real-time video also is networked to the TSC, allowing payload developers to view ISS video, which displays crew members interacting with their experiments on orbit and can include images of experiment execution. The TSC can receive two of the four ISS video channels simultaneously, and can route video directly to the payload developer's console position, on the basis of the developer's requirements. All systems are monitored by the sustaining engineering staff daily and by automated systems around the clock. Short- and long-term storage of scientific and engineering data and access to a public Web site containing processed data are also provided. Technical support can be provided to operation sites outside Glenn when requested.

In fiscal year 2004, six ISS payload teams (SAMS, MAMS, BCAT-3, CFE, INSPACE, and PIMS) successfully operated their experiments from the Glenn TSC. The TSC upgraded 33 workstations to Windows XP and installed a state-of-the-art hot failover firewall system. Also, in preparation for the launch and subsequent operations of the Fluids and



Voice communications enable researchers to interact with the Payload Operations Integration Center at the NASA Marshall Space Flight Center in Huntsville, Alabama.



The TSC has an elaborate network system to support voice, video, and data distribution within the TSC.



DAFT is operated on the ISS by Glenn engineers.



DAFT operators review data received from their experiment on the ISS.

Combustion Facility (FCF) aboard the ISS, the FCF Central Data System hardware, which provides 29.4 TB of disk storage, was integrated into the TSC network.

Glenn contacts:

Diane C. Malarik, 216-433-3203, Diane.C.Malarik@nasa.gov; and Thomas H. St. Onge, 216-433-3557, Thomas.H.StOnge@nasa.gov

Author:

Diane C. Malarik

Headquarters program office:

Exploration Systems

Programs/Projects:

Microgravity Science

Flight Hardware Fabricated for Combustion Science in Space

In January 2004, President George W. Bush outlined an exciting new space exploration vision. The exploration programs will seek profound answers to questions of our origins, whether life exists beyond Earth, and how we could live in other worlds. In support of this vision, NASA's microgravity combustion research program is being realigned to support major milestones such as a human Moon landing and establishment of a lunar exploration testbed. The design and operation of exploration spacecraft and partial-gravity habitats presents new challenges for fire safety, waste incineration, and power generation. A major goal of NASA's microgravity combustion program is to address these challenges by gaining increased understanding and insight into the behaviors of microgravity and partial-gravity flames.

The Fluids and Combustion Facility, a facility-class payload planned for the International Space Station (ISS), will support the study of fluid physics

and combustion science in a long-duration, microgravity environment (see the photographs on the next page). The facility is a system of on-orbit and ground hardware, software, experiment operations, and planning designed to accommodate a wide variety of investigations. The majority of the on-orbit hardware will remain there and be used by many investigations. Each investigation will customize the facility with a small amount of hardware and software. The facility will be adaptable and

modular so that it can be upgraded with new hardware and software as needed.

The facility comprises two powered racks: the Combustion Integrated Rack (CIR) and the Fluids Integrated Rack. These will be located adjacent to each other in the U.S. Laboratory Module, Destiny. The two racks share common features and perform the functions of structural hardware, power control and distribution, environmental controls, command and data management, communications, and stowage. The facility is being designed to accommodate 5 to 15 experiments during the lifetime of the Fluids and Combustion Facility.

The CIR contains the hardware and software necessary for conducting combustion science experiments. It is designed to accommodate a range of combustion experiments while meeting ISS requirements and limitations such as safety, power and energy, cooling, mass, crew time, stowage, resupply flights, and downlink.

The International Standard Payload Rack provides the supporting and mounting elements for the CIR subsystems and mechanical connections to Destiny. The CIR provides a bifold door with upper and lower halves, and the passive rack isolation system attenuates on-orbit vibrations transmitted from Destiny to the rack.

The optics bench provides structural support, electrical connections, and mounting locations. It spans two-thirds of the rack vertically and can be slid out from the rack and folded down for access to both sides. It contains the wiring and cooling airflow, and diagnostics can be interchanged via a quick-latch mechanism at any of eight universal mounting locations around the chamber.

The combustion chamber has a volume of 100 liters (0.40 m in diameter and 0.90 m in length). The front lid opens for access to the chamber. The experiment mounting structure is mounted on guide rails in the chamber. This structure supports internal components, such as a burner, a sample holder, diagnostic sensors, a flow tunnel, and interface hardware. Electrical, vacuum, gas, and other connections are made through an interface resource ring. The chamber has eight interchangeable windows and a maximum design pressure differential of 827 kPa (120 psig).

The diagnostics measurement systems measure the required and desired combustion phenomena. Many of these are imaging systems that include the imaging device, an illumination source, and an image-processing package. Digital imaging systems are used for data fidelity and ease in data transfer and storage. The diagnostic measurements provided by the CIR include pressure measurements; visible, ultraviolet, and near-infrared imaging; gas composition; and acceleration.

The Fuel/Oxidizer Management Assembly provides gaseous fuels, oxidizers, and diluents to the combustion chamber, sampling and analysis of the chamber



Engineering models of the Fluids and Combustion Facility. The Combustion Integrated Rack (CIR) is shown on the left; the Fluids Integrated Rack is shown on the right.

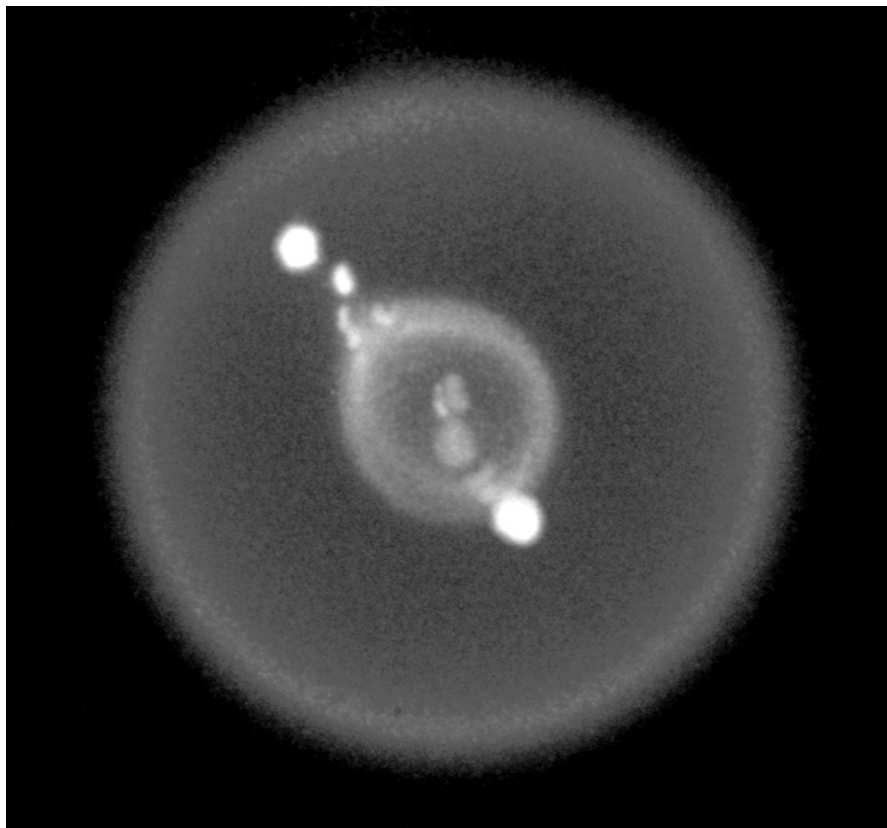
contents, and venting to space through the ISS vacuum exhaust system. It contains gas supply bottles, valves, pressure regulators and switches, and mass flow controllers. The gas bottles may be either 1.0, 2.25, or 3.8 liters and are replaceable by the crew.

The electrical power system performs electrical power distribution, conversion, control, management, and fault protection. The system provides 120 Vdc or converts the ISS 120 Vdc to the 28 Vdc needed for most loads. The environmental control systems remove waste thermal energy, detect smoke and fire, and provide access to the ISS-provided nitrogen and to the vent system.

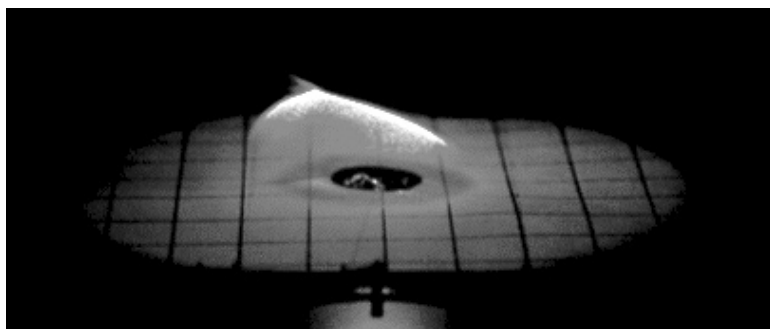
The command and data management system consists of an input-output processor, the Fuel/Oxidizer Management Assembly control unit, a laptop computer, and image-processing packages. The input-output processor provides commanding and controls, data acquisition and processing, data management and checking, and communications to the crew and ground operators.

The combustion areas that can be studied in the CIR include, but are not limited to, fire prevention, detection, and suppression; incineration of solid wastes; power generation; flame spread; soot and polycyclic aromatic hydrocarbons; and materials synthesis. Near-term experiments will support the exploration vision.

When possible, similar investigations will be flown at the same time to increase the use of common hardware and diagnostics. A set of multiuser chamber inserts is being designed to support experiments in droplets, solid fuels, and gaseous fuels. Commercial and international investigations will provide their own chamber inserts or other resources instead of using a NASA insert.



Flame image of an isolated droplet burning in microgravity. This figure is shown in color in the online version of this article (<http://www.grc.nasa.gov/WWW/RT/2004/PT/PTO-omalley.html>).



Flame image of a thin sheet of paper burning in microgravity. This figure is shown in color in the online version of this article (<http://www.grc.nasa.gov/WWW/RT/2004/PT/PTO-omalley.html>).

The candidate initial investigations will study the combustion of small, spherical, individual fuel droplets (see the top figure). They will demonstrate the use of the CIR and will use a common experiment insert and similar measurements. They will determine the flammability of a fuel droplet in limiting atmospheres of oxygen. Solid fuel experiments will focus on the quantification of material flammability in low-pressure, increased-oxygen atmospheres (see the bottom figure). The fuels include wire insulation, advanced composites, packing foam, and materials for inflatable structures. Gaseous fuel experiments will determine the effectiveness of various extinguishing agents.

The Fluids and Combustion Facility is being developed at the NASA Glenn Research Center in Cleveland, Ohio, under a prime contract with Northrop Grumman Information Technology. The overall system has concluded its flight hardware fabrication phase and is moving toward flight hardware testing at the package and system levels. Launch of the CIR is currently scheduled for 2006.

Find out more about this research:

Fluids and Combustion Facility:
<http://fcf.grc.nasa.gov>

Microgravity combustion research at Glenn:
<http://microgravity.grc.nasa.gov/combustion/>

Glenn contacts:
Terence F. O'Malley, 216-433-2960,
Terence.F.OMalley@nasa.gov; and
Dr. Karen J. Weiland, 216-433-3623,
Karen.J.Weiland@nasa.gov

Authors:
Terence F. O'Malley and
Dr. Karen J. Weiland

Headquarters program office:
Exploration Systems

Programs/Projects:
Microgravity Science

2004

RESEARCH AND TECHNOLOGY

INSTRUMENTATION AND CONTROLS

MATERIALS

POWER AND ELECTRICAL PROPULSION

STRUCTURES

PROPULSION SYSTEMS

MICROGRAVITY

Instrumentation and Controls

Low-Speed Active Flow Control Laboratory Developed

The future of aviation propulsion systems is increasingly focused on the application of control technologies to significantly enhance the performance of a new generation of air vehicles. Active flow control refers to a set of technologies that manipulate the flow of air and combustion gases deep within the confines of an engine to dynamically alter its performance during flight. By employing active flow control, designers can create engines that are significantly lighter, are more fuel efficient, and produce lower emissions. In addition, the operating range of an engine can be extended, yielding safer transportation systems. The realization of these future propulsion systems requires the collaborative development of many base technologies to achieve intelligent, embedded control at the engine locations where it will be most effective.

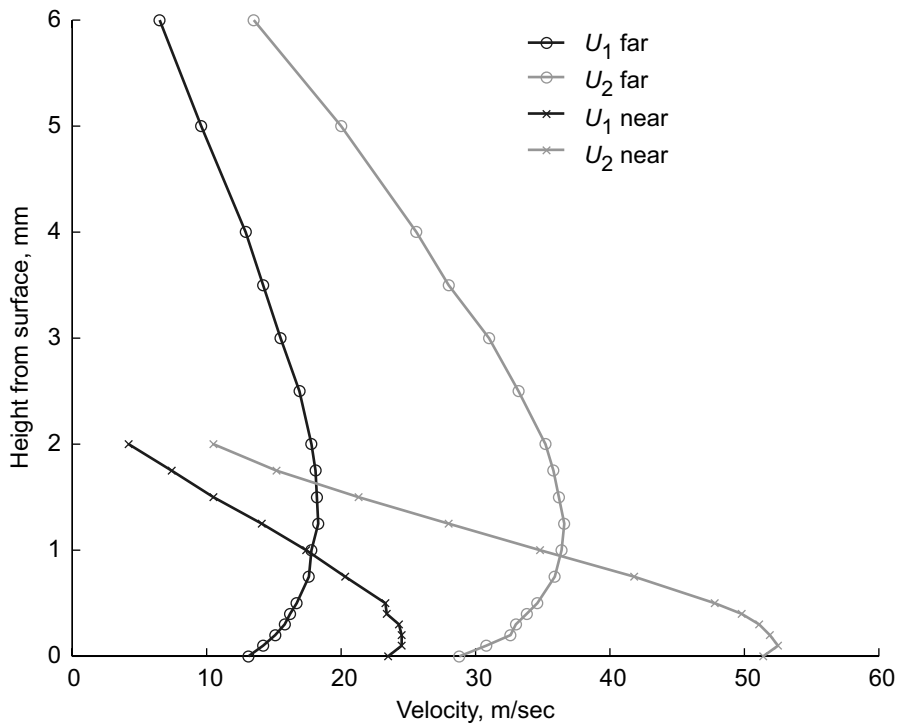
NASA Glenn Research Center's Controls and Dynamics Technology Branch has developed a state-of-the-art low-speed Active Flow Control Laboratory in which emerging technologies can be integrated and explored in a flexible, low-cost environment. The facility allows the most promising developments to be pre-screened and optimized before being tested on higher fidelity platforms, thereby reducing the cost of experimentation and improving research effectiveness.

The laboratory includes a low-speed wind tunnel (shown in the figure to the left), with a calibrated test section that can be used to evaluate advanced flow-control actuators and sensors, and a state-of-the-art real-time control development platform for designing and testing closed-loop algorithms. A variety of precision instrumentation is available for evaluating and quantifying performance metrics. Two-dimensional flow-field visualization is provided by particle imaging velocimetry. A high-speed data-acquisition system and a variety of actuation mechanisms are available for investigating unsteady flow-field phenomena.

This laboratory has been instrumental in developing techniques to quantify the performance and optimize the design of injector configurations for the flow-control technologies currently under development. The graph on the next page shows an example of the characterization of an injector design used in compressor experiments. The objective in this instance was to energize the boundary layer flow by



Active Flow Control Laboratory. The inset shows the test section, which is 12 in. square and supports velocities up to 40 m/sec.



Example of the velocity profile of an injector design for a separation control application in a compressor. Note the identification of the peak velocity in the near and far field and its spread as it propagates downstream. The parameter U_1 is the flow rate of the low-velocity jet, and U_2 is approximately twice the initial velocity. In applications related to turbine film cooling, control mechanisms are being explored that increase the effectiveness of cooling flows while reducing the mass flow requirement, potentially leading to increased operating efficiency.

maintaining a high velocity along the wall yet minimizing jet penetration into the free-stream flow path. The design considers many factors including jet source pressure, injection mass flow requirements, and the complexity of manufacturing the components.

Find out more about this research:
<http://www.grc.nasa.gov/WWW/cdtb/>

Glenn contacts:

Dennis E. Culley, 216-433-3797,
 Dennis.E.Culley@nasa.gov; and
 Dr. Michelle M. Bright, 216-433-2304,
 Michelle.M.Bright@nasa.gov

Authors:

Dennis E. Culley and
 Dr. Michelle M. Bright

Headquarters program office:

Aeronautics Research

Programs/Projects:

PR&T, UEET, IR&D

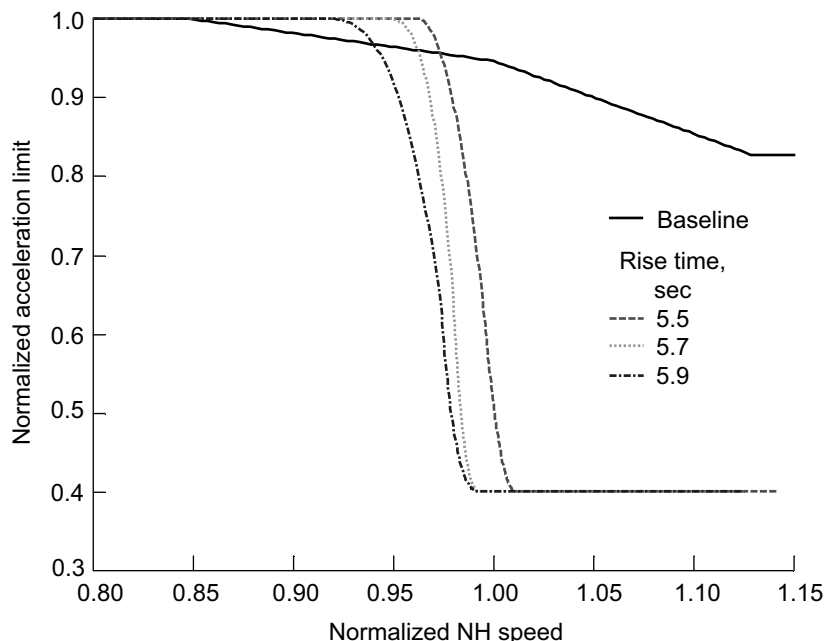
Intelligent Life-Extending Controls for Aircraft Engines Studied

Current aircraft engine controllers are designed and operated to provide desired performance and stability margins. Except for the hard limits for extreme conditions, engine controllers do not usually take engine component life into consideration during the controller design and operation. The end result is that aircraft pilots regularly operate engines under unnecessarily harsh conditions to strive for optimum performance. The NASA Glenn Research Center and its industrial and academic partners have been working together toward an intelligent control concept that will include engine life as part of the controller design criteria. This research includes the study of the relationship between control action and engine component life as well as the design of an intelligent control algorithm to provide proper tradeoffs between performance and engine life. This approach is expected to maintain operating safety while minimizing overall operating costs.

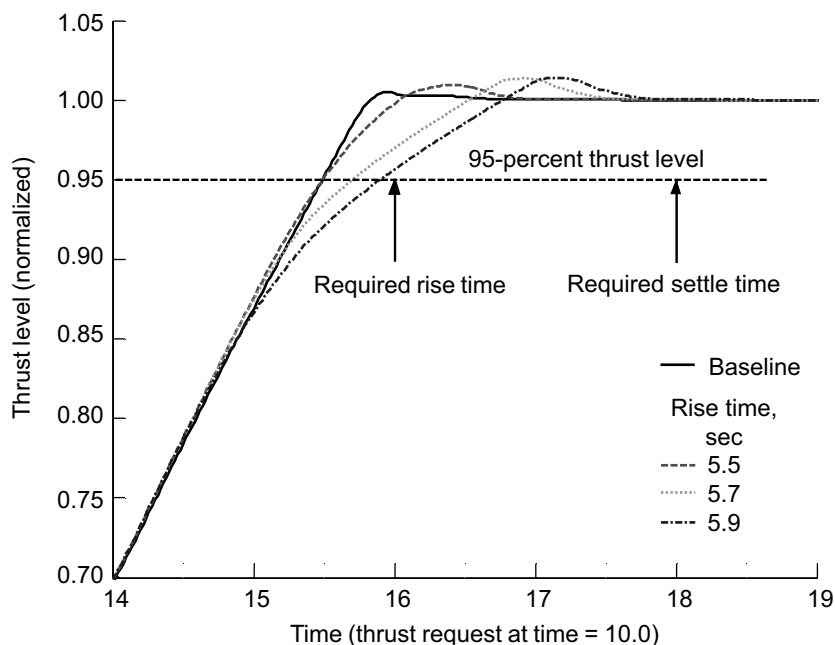
In this study, the thermomechanical fatigue (TMF) of a critical component was selected to demonstrate how an intelligent engine control algorithm can significantly extend engine life with only a very small sacrifice in performance. An intelligent engine control scheme based on modifying the high-pressure spool speed (NH) was proposed to reduce TMF damage from ground idle to takeoff. The NH acceleration schedule was optimized to minimize the TMF damage for a

given rise-time constraint, which represents the performance requirement. The intelligent engine control scheme was used to simulate a commercial short-haul aircraft engine.

The top graph compares the optimum schedules for rise times of 5.5, 5.7, and 5.9 sec with the original schedule. These acceleration schedules provide the best results in minimizing the TMF damage for specified rise time requirements. They suggest that the controller should continue the maximum acceleration of



Optimized acceleration schedule (normalized).



Response curves for different optimized schedules.

NH beyond the designed 85 percent, and take a sharper cut in the acceleration to reduce the maximum strain at the peak temperature. This acceleration schedule strategy will keep the rise time relatively constant while reducing the maximum temperature difference (ΔT) between the airfoil and the stator endwall.

The bottom graph shows the thrust response curves of the selected optimized acceleration schedules during the takeoff acceleration process. It can be seen that the optimized thrust curves are kept at a slower acceleration rate when the full power level is being approached. Although the overshoots are about the same in all cases, the maximum metal temperatures are all reduced in the optimized cases in comparison to the baseline. The slow acceleration helps to reduce the maximum temperature difference between the stator airfoil and the endwall.

The table on the next page shows the simulation results of the optimized schedule in terms of its impact on engine life. The results show that the new control schedules can reduce the maximum metal temperature as well as the difference in temperature between the airfoil and endwall of the cooled stator. In comparison to the baseline case, an optimized acceleration schedule can reduce the TMF damage of the selected component by 34 percent for standard flight conditions while keeping the rise time unchanged. This translates to about 52 percent more flights before the removal of the component from service.

The table shows that the TMF damage can be reduced even more if the engine is allowed to incur a small delay in thrust rise time. The tradeoffs between rise time and TMF damage can be significant. By allowing the rise time to increase from 5.5 to 5.9 sec, the usable engine life can

OPTIMIZED THERMOMECHANICAL FATIGUE DAMAGE VERSUS RISE TIME

Rise time	Maximum metal temperature (difference from baseline), T_{metal} , °F	Maximum change in temperature, (difference from baseline), ΔT_{max} , °F	TMF reduction, percent	Life extension, percent
5.50	Baseline	Baseline	----	----
5.50	-16	-30	34	52
5.60	↓	-44	46	85
5.70		-50	51	104
5.80		-59	56	127
5.90		-65	58	138

be more than doubled with the optimized schedule over that with the nominal schedule. This result is important for engine controller design philosophy because it may prompt the reevaluation of engine performance requirements to account for overall operating costs.

The research results depend heavily on the fidelity of the engine operation model, thermal model, and life model. Further research in these areas is important for successful transition of the intelligent life-extending control approach to operating aircraft engines.

Enhanced Bank of Kalman Filters Developed and Demonstrated for In-Flight Aircraft Engine Sensor Fault Diagnostics

In-flight sensor fault detection and isolation (FDI) is critical to maintaining reliable engine operation during flight. The aircraft engine control system, which computes control commands on the basis of sensor measurements, operates the propulsion systems at the demanded conditions. Any undetected sensor faults, therefore, may cause the control system to drive the engine into an undesirable operating condition. It is critical to detect and isolate failed sensors as soon as possible so that such scenarios can be avoided. A challenging issue in developing reliable sensor FDI systems is to make them robust to changes in engine operating characteristics due to degradation with usage and other faults that can occur during flight. A sensor FDI system that cannot appropriately account for such scenarios may result in false alarms, missed detections, or misclassifications when such faults do occur.

To address this issue, an enhanced bank of Kalman filters was developed, and its performance and robustness were demonstrated in a simulation environment. The bank of filters is composed of $m + 1$ Kalman filters, where m is the number of sensors being used by the control system and, thus, in need of monitoring. Each Kalman filter is designed on the basis of a unique fault hypothesis so that it will be able to maintain its performance if a particular fault scenario, hypothesized by that particular filter, takes place.

Bibliography

Guo, Ten-Huei, Chen, P.: Intelligent Life-Extending Controls for Aircraft Engines. AIAA-2004-6468, 2004.

Guo, T.-H.: A Roadmap for Aircraft Engine Life Extending Control. Proceedings of the 2001 American Control Conference, Arlington, VA, June 2001.

Find out more about this research:

<http://www.grc.nasa.gov/WWW/cdtb/>

Glenn contact:

Dr. Ten-Huei Guo, 216-433-3734,
Ten-Huei.Guo-1@nasa.gov

Author:

Dr. Ten-Huei Guo

Headquarters program office:

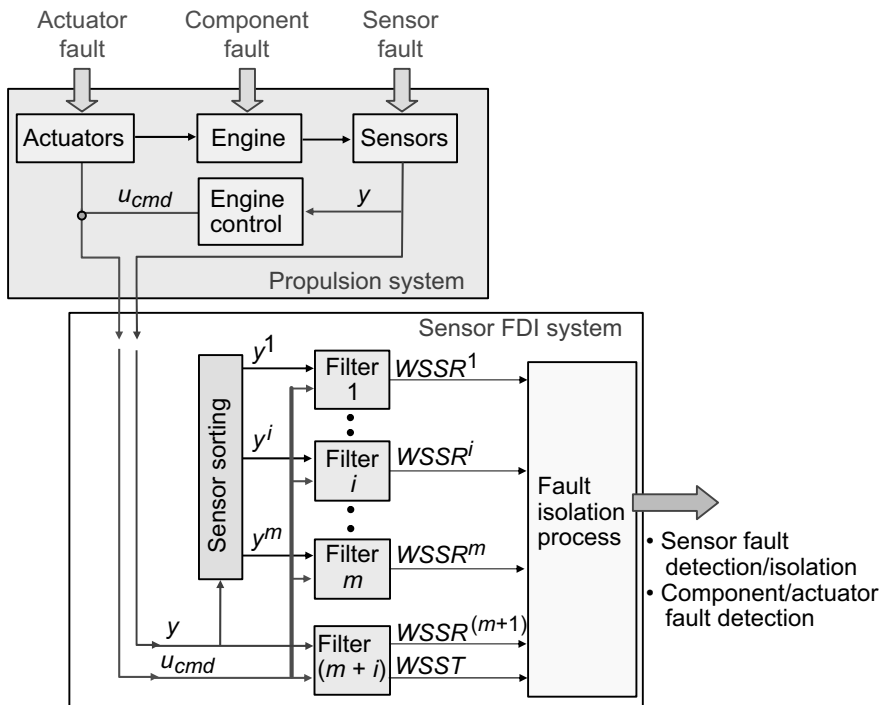
Aeronautics Research

Programs/Projects:

CICT

Each of the m Kalman filters is designed to estimate the engine state variables and a specific set of sensor measurements using $m - 1$ sensors. The sensor that is not used by a particular filter is the one being monitored by that filter for sensor fault detection. One additional Kalman filter, the $(m + 1)^{\text{st}}$, is designed to detect component and actuator faults. This additional filter distinguishes component and actuator faults from sensor faults; therefore, it makes the sensor FDI system robust to component and actuator failure.

With this FDI architecture, where a bank of Kalman filters are running in parallel, each Kalman filter generates a fault indicator signal that indicates



Architecture of the sensor fault detection and isolation (FDI) system, where (u_{cmd} , control commands; y , sensor measurements; y^i , subset of sensor measurements used by filter i ; $WSSR$ (weighted sum of squared residuals) fault indicator signal; $WSSR^i$, fault indicator signal generated by filter i ; $WSST$, fault indicator signal (weighted sum of squared tuners).

the existence of faults in the system being monitored. When a sensor, component, or actuator fails, all the Kalman filters generate large fault indicator signals except for the one that is using the correct hypothesis. Consequently, sensor faults can be detected and isolated, and component and actuator faults can be detected.

This approach was applied to a nonlinear commercial aircraft engine simulation. Its performance was evaluated at multiple power settings during cruise operation with respect to (1) missed detections, (2) false alarms, (3) misclassifications, and (4) robust sensor fault isolation. Among these categories, the most significant result was observed for misclassifications, which are considered to be the worst erroneous diagnosis that the FDI system can generate

during flight. At three different power settings, the sensor FDI system was tested with 1000 different events of component or actuator faults in the simulation environment. The sensor FDI system did not classify any of these component or actuator faults as a sensor fault, thus avoiding any misclassifications. Through extensive evaluation, the enhanced bank of Kalman filters technique demonstrated good performance and robustness, indicating that this technology is promising for improving the safety of aircraft gas turbine engines.

Bibliography

Kobayashi, Takahisa; and Simon, Donald L.: Evaluation of an Enhanced Bank of Kalman Filters for In-Flight Aircraft Engine Sensor Fault Diagnostics. ASME Paper GT2004-53640 (NASA/TM-2004-213203, ARL-TR-3252). <http://gltrs.grc.nasa.gov/cgi-bin/GLTRS/browse.pl?2004/TM-2004-213203.html>

QSS Group, Inc., contact:

Takahisa Kobayashi, 216-433-3739, Takahisa.Kobayashi@grc.nasa.gov

U.S. Army Research Laboratory, Vehicle Technology Directorate at Glenn contact:

Donald L. Simon, 216-433-3740, Donald.L.Simon@grc.nasa.gov

Authors:

Takahisa Kobayashi and Donald L. Simon

Headquarters program office:

Aeronautics Research

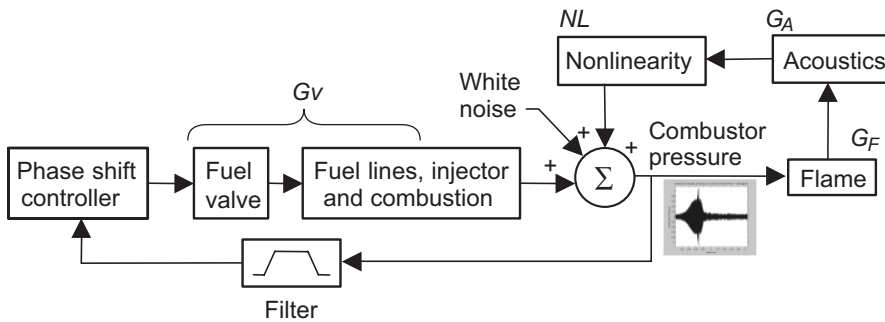
Programs/Projects:

AvSSP

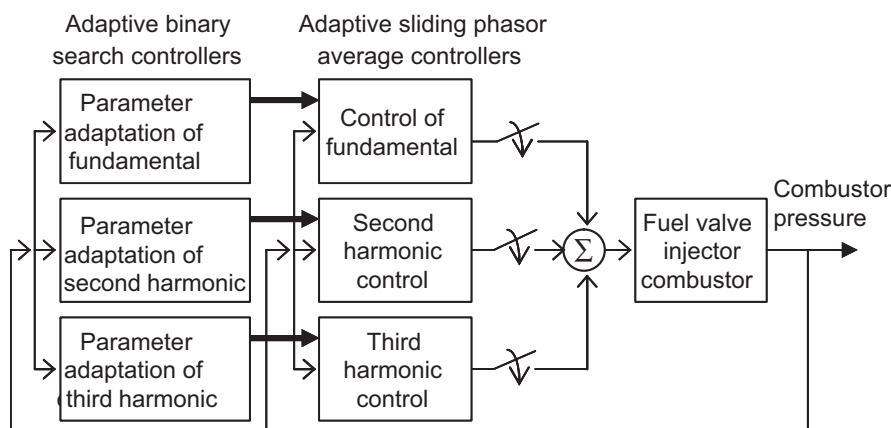
Innovative Adaptive Control Method Demonstrated for Active Suppression of Instabilities in Engine Combustors

This year, an improved adaptive-feedback control method was demonstrated that suppresses thermoacoustic instabilities in a liquid-fueled combustor of a type used in aircraft engines. Extensive research has been done to develop lean-burning (low fuel-to-air ratio) combustors that can reduce emissions throughout the mission cycle to reduce the environmental impact of aerospace propulsion systems. However, these lean-burning combustors are susceptible to thermoacoustic instabilities (high-frequency pressure waves), which can fatigue combustor components and even downstream turbine blades. This

can significantly decrease the safe operating life of the combustor and turbine. Thus, suppressing the thermoacoustic combustor instabilities is an enabling technology for meeting the low-emission goals of the NASA Ultra-Efficient Engine Technology (UEET) Project.



Combustion instability control block diagram (adaptive sliding phasor-average controller); G_v , G_F , and G_A are transfer functions of the associated combustion process reflected in the figure; NL is a damping nonlinearity that restricts the amplitude of the opened-loop self-excited instability.



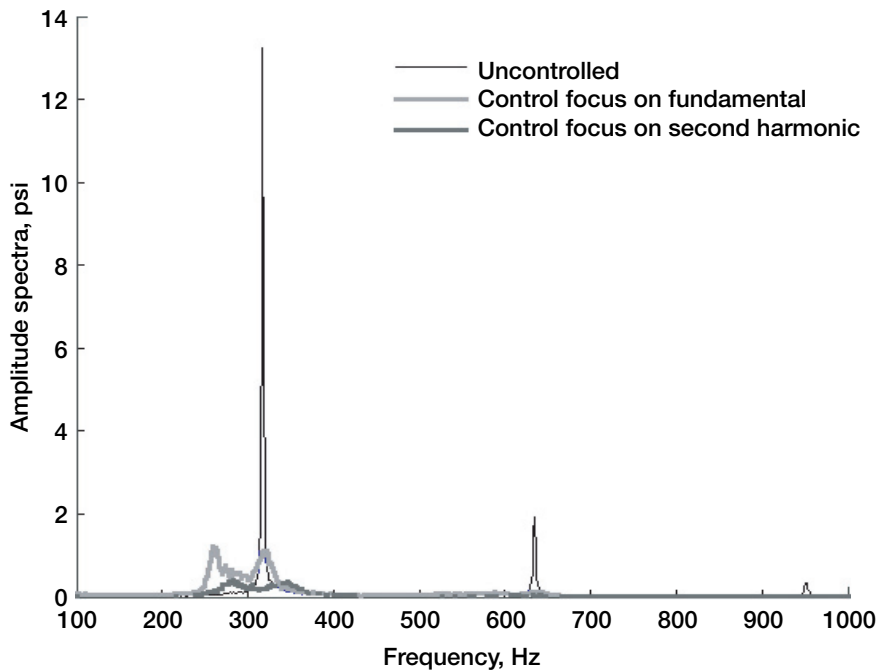
Modified combustion instability control block diagram.

Combustor instability suppression poses a challenging feedback control problem because of unmodeled dynamics, large dead-time phase delays of a few cycles, combustor noise, large amplitude modulations, random phase walks, and a system that continuously transitions through inherently unstable operation at increased suppression levels. To overcome these difficulties, a sophisticated control approach was developed that does not depend on detailed modeling of system dynamics. In this control approach, named “adaptive sliding phasor-averaged control,” the controller phase continuously slides back and forth inside the boundaries of an effective stability region that lies within a restricted control region in a stationary frame of reference. The combustor pressure oscillations are sensed through a band-pass filter to isolate the instability from the noise; the filtered pressure oscillations are continuously phase shifted at a rate of 40 Hz in the direction that suppresses the instability; and the phase-shifted pressure signal is used to command the fuel actuator at a rate of 10 kHz to suppress the instability. In addition, discontinuous exponential gain modulation and control parameter adaptation are employed to accommodate the effects of large dead-time phase delay in this process and also to better tune the controller as the control is applied.

This original combustion instability control method was shown to reduce thermoacoustic-driven combustor pressure oscillations and was demonstrated for a high-frequency (530-Hz) instability on a single-nozzle combustor rig at the

United Technologies Research Center. This rig emulated an actual engine instability experience and has many of the complexities of a real engine combustor (i.e., an actual fuel nozzle and swirler, dilution cooling, etc.). This was the first known successful demonstration of high-frequency combustor instability suppression in a realistic aircraft engine environment.

By analyzing these test results as well as results from an earlier low-frequency (~290-Hz) rig configuration, and from an aeronautics engine under development, we discovered a phenomenon called intraharmonic coupling, which causes energy coupling between the instability harmonics. This phenomenon was exploited in the control design by modifying the control algorithm to focus control selectively on the fundamental instability mode and/or any of its harmonics. The original combustor rig at United Technologies Research Center was transferred and reassembled at Glenn. This rig was configured to simulate a more coherent instability at a lower frequency of approximately 330 Hz. Test results showed that by focusing control action on the second harmonic, both the amplitude spectra and the time-domain pressure oscillations of the instability were substantially reduced (considerably more than when control was focused on the fundamental mode of the instability). The amount of fuel modulation required to achieve this level of suppression was also substantially reduced. In addition, the higher order harmonics were eliminated for all practical purposes. The effects of focusing control action at harmonic frequencies higher than the second harmonic could not be studied in this test because of the limited control bandwidth of the fuel actuator. We plan to investigate this innovative control approach further as part of the low-emission combustor development effort under the UEET Project.



Amplitude spectra density of uncontrolled versus controlled instability for control focusing on the fundamental and the second harmonic.

Bibliography

Kopasakis, George; and DeLaat, John C.: Adaptive Instability Controls in a Liquid-Fueled Combustor. NASA/TM—2002-211805 (AIAA-2002-4075), 2002. <http://gltrs.grc.nasa.gov/cgi-bin/GLTRS/browse.pl?2002/TM-2002-211805.html>

Kopasakis, George: High Frequency Adaptive Instability Controls in a Liquid-Fueled Combustor. NASA/TM—2003-212535 (AIAA-2003-4491), 2003. <http://gltrs.grc.nasa.gov/cgi-bin/GLTRS/browse.pl?2003/TM-2003-212535.html>

Kopasakis, George: Systems Characterization of Combustor Instabilities With Controls Design Emphasis. NASA/TM—2004-212912 (AIAA-2004-0638), 2004. <http://gltrs.grc.nasa.gov/cgi-bin/GLTRS/browse.pl?2004/TM-2004-212912.html>

Kopasakis, G.; DeLaat, J.; and Chang, C.: Validation of an Adaptive Combustion Instability Control Method for Gas-Turbine Engines. AIAA-2004-4028, 2004.

Find out more about Active

Combustion Control:

<http://www.grc.nasa.gov/WWW/cdtb/projects/combustor/>

Glenn contact:

George Kopasakis, 216-433-5327, George.Kopasakis-1@nasa.gov

Author:

George Kopasakis

Headquarters program office:

Aeronautics Research

Programs/Projects:

VSP, UEET

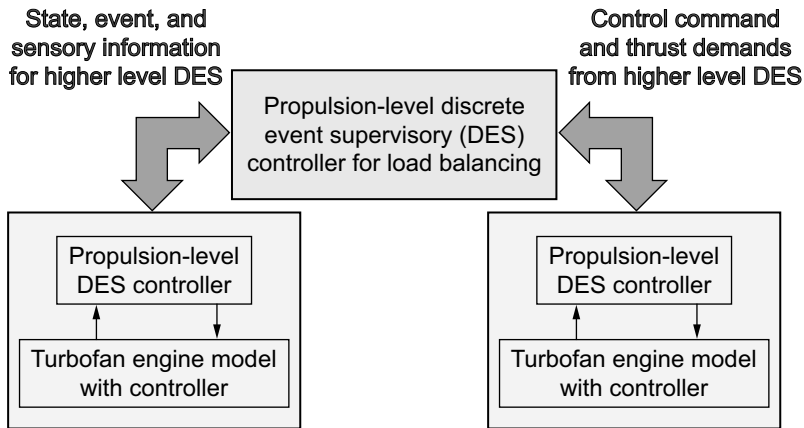
Discrete Event Supervisory Control Applied to Propulsion Systems

The theory of discrete event supervisory (DES) control was applied to the optimal control of a twin-engine aircraft propulsion system and demonstrated in a simulation. The supervisory control, which is implemented as a finite-state automaton, oversees the behavior of a system and manages it in such a way that it maximizes a performance criterion, similar to a traditional optimal control problem. DES controllers can be nested such that a high-level controller supervises multiple lower level controllers. This structure can be expanded to control huge, complex systems, providing optimal performance and increasing autonomy with each additional level.

The DES control strategy for propulsion systems was validated using a distributed testbed consisting of multiple computers—each representing a module of the overall propulsion system—to simulate real-time hardware-in-the-loop testing. In the first experiment, DES control was applied to the operation of a nonlinear simulation of a turbofan engine (running in closed loop using its own feedback controller) to minimize engine structural damage caused by a combination of thermal and structural loads. This enables increased on-wing time for the

engine through better management of the engine-component life usage. Thus, the engine-level DES acts as a life-extending controller through its interaction with and manipulation of the engine's operation.

Next, the DES control strategy was applied to a simulation of a twin engine aircraft's propulsion control system, where each of the engines had its own low-level DES controller as in the first experiment. This higher level propulsion control specifically addressed the issue of load balancing between the engines to maintain overall propulsion performance. The propulsion-level



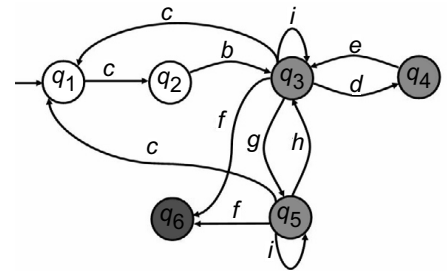
Twin-engine aircraft propulsion system showing the hierarchical propulsion-level DES controller above the two engine-level DES controllers.

DES achieved this by giving the engine that could better handle the load the majority of the burden and giving the engine with more accumulated component damage (less remaining component life) the smaller share of the load. The simulation runs demonstrated that the system with the propulsion-level DES control was able to successfully complete the predefined mission more consistently than the system without the controller.

The experiments demonstrated that hierarchical discrete-event supervisory control could successfully manage the operation of a complex system in an intelligent manner to achieve the goals of the mission. They also demonstrated that as more levels of DES control are implemented, the level of autonomy of the overall system increases. Researchers at the NASA Glenn Research Center have been working with grantees at the Pennsylvania State University to more fully develop the hierarchical DES theory for application to aerospace-related problems.

Bibliography

Fu, Jinbo; Yasar, Murat; and Ray, Asok: Optimal Discrete Event Supervisory Control of Aircraft Gas Turbine Engines. Proceedings of the American Control Conference, Boston, MA, June 2004.



The engine-level DES is a finite-state machine representing the set of states (circles) and events (arrows) that model the operation of the engine.

Yasar, M., et al.: Hierarchical Discrete Event Supervisory Control of Aircraft Propulsion Systems. AIAA-2004-6469, 2004.

U.S. Army Research Laboratory, Vehicle Technology Directorate at Glenn contact:

Jonathan S. Litt, 216-433-3748,
Jonathan.S.Litt@grc.nasa.gov

Glenn contact:

Neerav Shah, 216-433-3502,
Neerav.Shah@nasa.gov

Authors:

Jonathan S. Litt and Neerav Shah

Headquarters program office:

Aeronautics Research

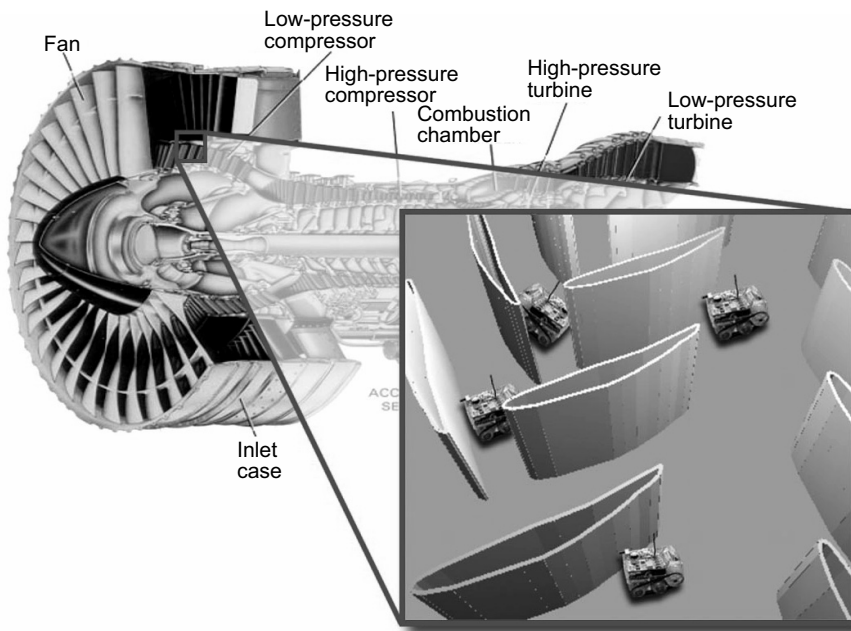
Programs/Projects:

Engineering for Complex Systems

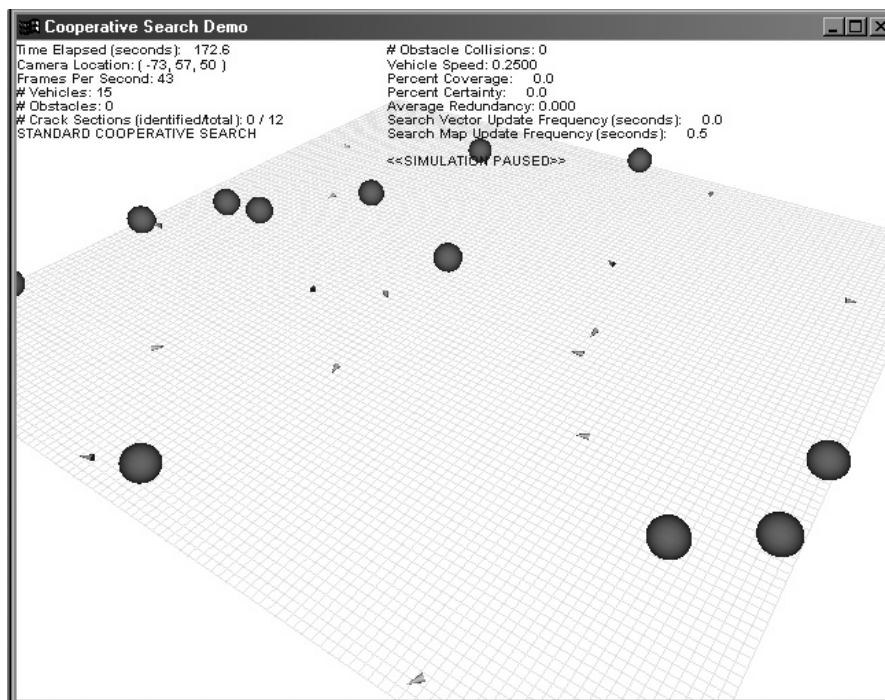
Control Algorithms and Simulated Environment Developed and Tested for Multiagent Robotics for Autonomous Inspection of Propulsion Systems

The NASA Glenn Research Center and academic partners are developing advanced multiagent robotic control algorithms that will enable the autonomous inspection and repair of future propulsion systems. In this application, on-wing engine inspections will be performed autonomously by large groups of cooperative miniature robots that will traverse the surfaces of engine components to search for damage. The eventual goal is to replace manual engine inspections that require expensive and time-consuming full engine teardowns and allow the early detection of problems that would otherwise result in catastrophic component failures. As a preliminary step toward the long-term realization of a practical working system, researchers are developing the technology to implement a proof-of-concept testbed demonstration.

In a multiagent system, the individual agents are generally programmed with relatively simple controllers that define a limited set of behaviors. However, these behaviors are designed in such a way that, through the localized interaction among individual agents and between the agents and the environment, they result in self-organized, emergent group behavior that can solve a given complex problem, such



Conceptual drawing showing a cooperative team of miniature mobile robots autonomously inspecting the interior of an engine for damage.



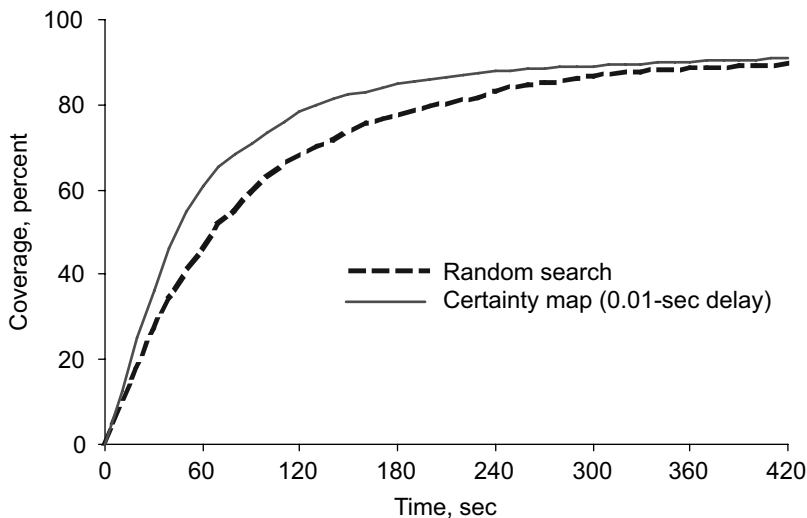
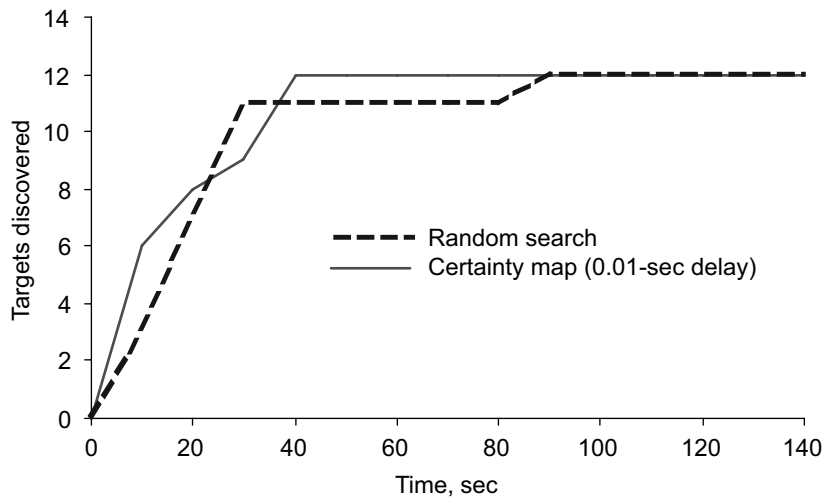
Screen capture of three-dimensional simulation software developed at Glenn to facilitate the testing of multiagent control algorithms.

as cooperative inspection. One advantage to the multiagent approach is that it allows for robustness and fault tolerance through redundancy in task handling. In addition, the relatively simple agent controllers demand minimal computational capability, which in turn allows for greater miniaturization of the robotic agents.

Under this effort, researchers have developed and tested a range of algorithms to address pertinent control objectives such as cooperative search, coverage completeness, and obstacle avoidance. Algorithms range from those that require centralized coordination and communication to those that take a more distributed approach and rely only on indirect interactions. Each approach has strengths and weaknesses. Research is underway to refine these algorithms and to investigate how elements of each approach can be combined to exploit their respective strengths in a practical implementation that best addresses the specific inspection application.

The researchers developed an interactive, three-dimensional graphical simulation environment to facilitate the design and testing of the control algorithms. This virtual testbed software can model a three-dimensional environment that represents the interior of a turbine system, replete with obstacles and barriers. Agents representing inspection robots within this environment are capable of full 6-degree-of-freedom steering. The cooperative actions of the agents are controlled with plug-in control logic modules that allow developers to quickly implement and test various algorithms and to demonstrate the resulting multiagent behavior in real-time, three-dimensional motion graphics.

The final validation of these multiagent algorithms will be performed in a proof-of-concept demonstration in which a team of real demonstration robots will cooperatively search for “damage” targets in a hardware robotic testbed facility that is being constructed at Glenn. This demonstration will validate the feasibility of using cooperative multiagent robotics to perform efficient and effective inspections in applications such as on-wing turbine engine maintenance.



Simulation results showing how search agents can find targets more quickly and cover the environment more efficiently when they use a certainty map-based cooperative search algorithm instead of a random search.

Bibliography

Wong, E.; and Litt, J.: Autonomous Multi-Agent Robotics for Inspection and Repair of Propulsion Systems. AIAA-2004-6364, 2004.

Find out more from the Controls and Dynamics Technology Branch:

<http://www.grc.nasa.gov/www/cdtb/>

Glenn contact:

Edmond Wong, 216-433-8917,
Edmond.Wong-1@nasa.gov

U.S. Army Research Laboratory, Vehicle Technology Directorate at Glenn contact:

Jonathan S. Litt, 216-433-3748,
Jonathan.S.Litt@grc.nasa.gov

Author:

Edmond Wong

Headquarters program office:

Aeronautics Research

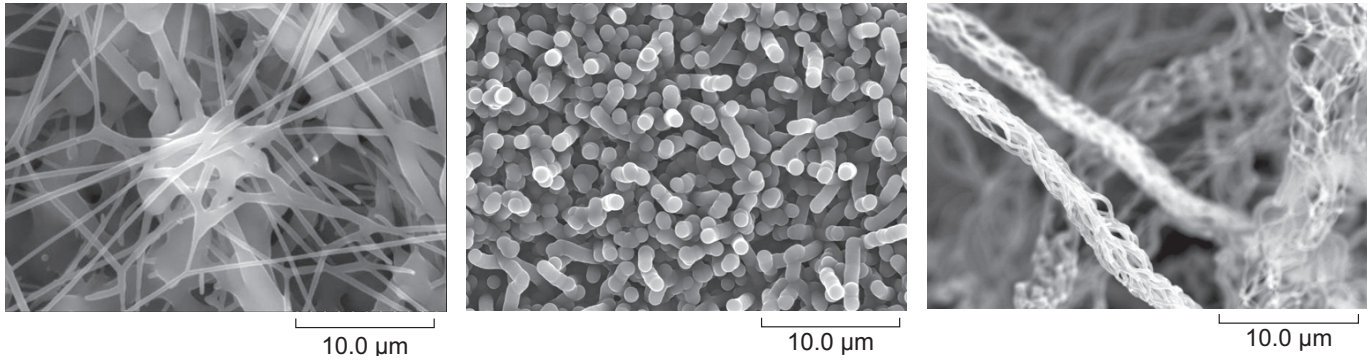
Programs/Projects:

LEAP

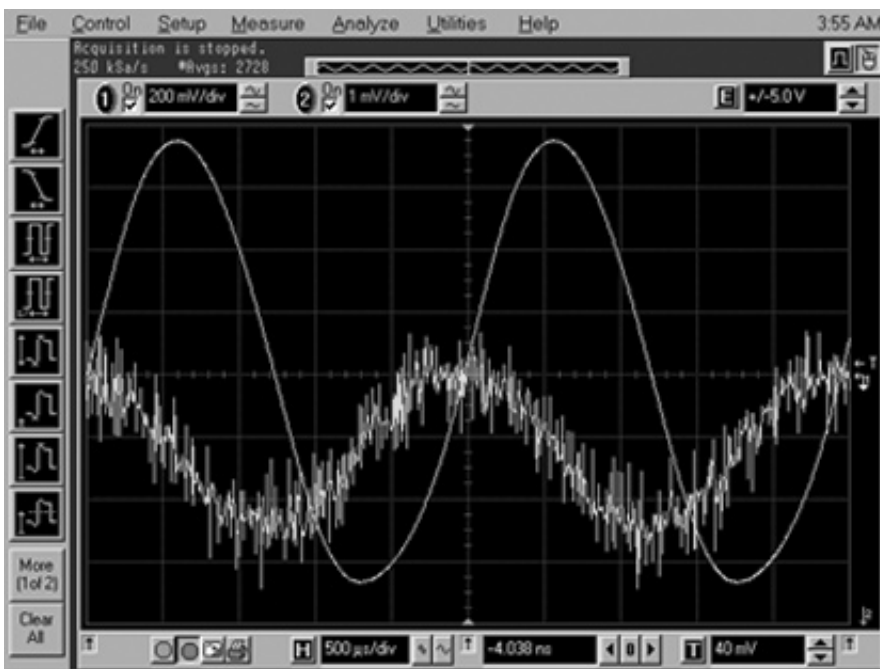
Nanorod Material Developed for Use as an Optical Sensor Platform

Optical sensors are becoming increasingly important in the development of new nonintrusive or embedded sensors. The use of light and material optical properties helps us measure unknown parameters such as temperature, pressure, flow, or chemical species. The focus of this work is to develop new nanostructure platforms upon which optical sensors can be constructed. These nanorods are synthesized oxides that form a base structure to which luminescent sensing dyes or dopants can be attached or embedded. The nanorod structure allows for a much greater open area than closed or polymer-based sensors do, enabling a much faster contact of the measured species with the luminescent sensor and, thus, a potentially faster measurement.

The initial development of the nanorod-based optical sensor has been as a fast-response air-pressure sensor. This concept offers the ultimate in sensor surface area: it maximizes sensor-to-media interaction because it is just above the molecular size scale. The pressure sensing works on the basis of oxygen quenching, or the available oxygen in air. Having a very



Left: Scanning electron microscope image of the tangled-mat optical platform. The weblike structure adds to the platform's overall physical properties. Center: Scanning electron microscope image of the regularly oriented array concept for potential use as an optical sensor. This structure has a grasslike appearance with all individual limbs aligning; this type of platform has potential as an optical flow sensor. Right: Scanning electron microscope image of braided ropelike structures, which have more mechanical strength than the individual strands shown in the center photograph.



Oscilloscope trace showing signals measured from a conventional wired pressure transducer and from the fast-response optical-pressure sensor.

open structure (approximately 100 times more open than similar sensors) on which the dye is attached allows an unimpeded movement of air molecules in and out of the pressure sensor, providing the very fast response. The idea is to have an entire surface area function as a pressure transducer rather than using a single embedded wired sensor. The surface would be probed with a laser to measure the pressure and temperature of the dye, thus providing an unlimited number of measurement locations.

The nanorod structures that have been produced can be classified in two categories, tangled mats and regularly oriented arrays, as illustrated in the microscopic images. Tangled mats are characterized by their random orientation

and cross-connecting, which provide higher strength, high porosity, and large surface area normal to the sensing direction. The regularly oriented arrays can grow in various geometries, often producing round or rectangular cross sections resembling nanoribbons or nanobelts, producing a more delicate, ordered arrangement. Samples of several different materials and shapes have been dyed using a dipping method with no adverse physical changes to the nanostructure. Optical characterization of the pressure sensor for pressure response, photostability, and frequency response is ongoing.

Find out more about this research:
<http://www.grc.nasa.gov/WWW/OptInstr/>

Glenn contacts:

Timothy J. Bencic, 216-433-5690,
 Timothy.J.Bencic@nasa.gov, and
 Dr. Randall L. Vander Wal, 216-433-9065,
 Randall.L.VanderWal@grc.nasa.gov

Author:

Timothy J. Bencic

Programs/Projects:

Glenn IR&D

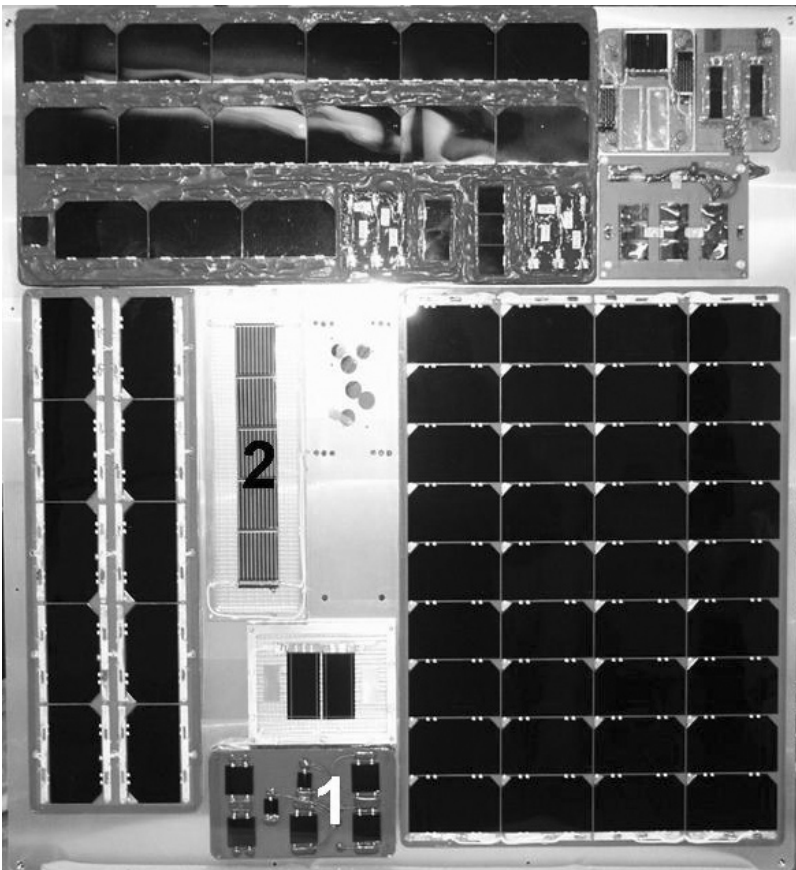
Forward Technology Solar Cell Experiment (FTSCE) for MISSE-5 Verified and Readied for Flight on STS-114

The Forward Technology Solar Cell Experiment (FTSCE) is a space solar cell experiment built as part of the Fifth Materials on the International Space Station Experiment (MISSE-5): Data Acquisition and Control Hardware and Software. It represents a collaborative effort between the NASA Glenn Research Center, the Naval Research Laboratory, and the U.S. Naval Academy. The purpose of this experiment is to place current and future solar cell technologies on orbit where they will be characterized and validated. This is in response to recent on-orbit and ground test results that raised concerns about the in-space survivability of new solar cell technologies and about current ground test methodology. The various components of the FTSCE are assembled into a passive experiment container—a 2- by 2- by 4-in. folding metal container that will be attached by an astronaut to the outer structure of the International Space Station. Data collected by the FTSCE will be relayed to the ground through a transmitter assembled by the U.S. Naval Academy. Data-acquisition electronics and software were designed to be tolerant of the thermal and radiation effects expected on orbit. The experiment has been verified and readied for flight on STS-114.

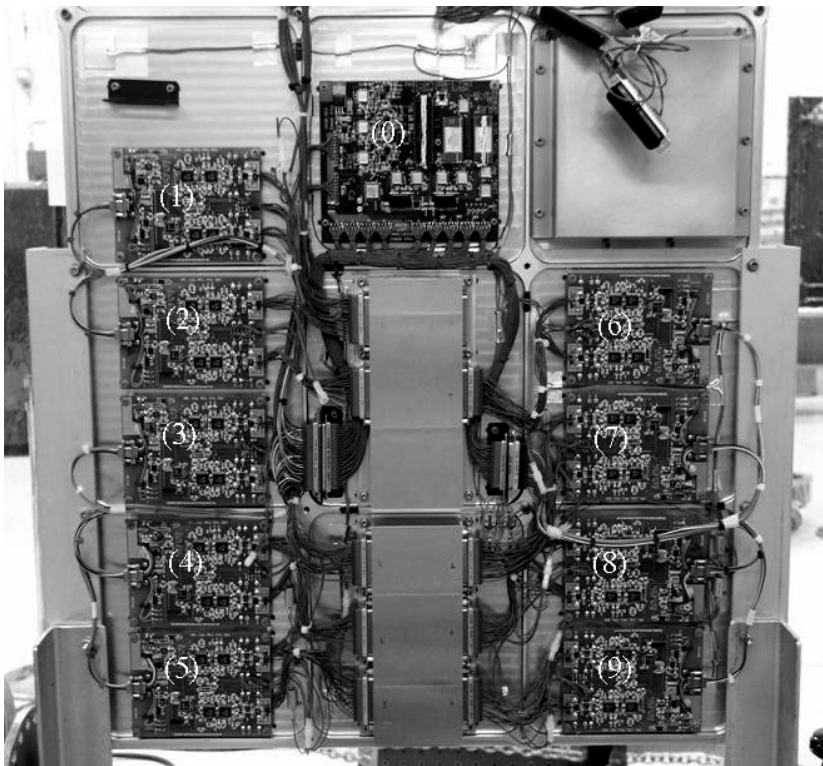
The FTSCE consists of an experiment deck (as shown in the photograph on this page) that contains the various solar cells under test, along with a primary solar panel for experiment power, Sun-position sensors, and temperature sensors.

The data-acquisition electronics designed and built by the Glenn team are shown in the photograph on the next page. The electronics consist of one main microprocessor board and nine data-acquisition boards. The main microprocessor board serves as the command interpreter and controls the data-acquisition boards. The core of this assembly is a radiation-tolerant 80C32E microcontroller, random access memory (RAM), and electrically erasable programmable read-only memory. The main microprocessor board includes flash memory so that data are not only transmitted to the ground, but also archived on orbit.

Each data-acquisition board can measure a 32-point current-versus-voltage (IV) curve on four individual solar cells, making two temperature measurements and taking data from one Sun-angle sensor. Multipoint IV curves are created by using a power metal oxide semiconductor field effect transistor (MOSFET) as a variable resistor. In practice, most solar cell experiments employ a bank of switched load resistors or a programmable, bipolar current source for making the IV measurements. The MOSFET configuration provides a substantial improvement over previous IV measurement technology because it is much lighter and smaller than the aforementioned load resistors and it is safer for the cells than a current source.



FTSCE experiment deck to be placed into the MISSE-5 passive experiment container. Glenn's GaAs/SiGe/Si and CuIn(Ga)Se₂ experiments (labeled 1 and 2, respectively) are shown.



Data-acquisition electronics designed, manufactured, programmed, and tested by engineers and technicians at Glenn. The electronics are mounted on the electronics deck. A single main microprocessor board (labeled 0) controls nine daughter boards (labeled 1 to 9) that measure the current-versus-voltage curve, temperature, and Sun angle.

Bibliography

Walters, Robert J., et al.: Materials on the International Space Station—Forward Technology Solar Cell Experiment. Mater. Sci. Eng. B, vol. 116, 2005, pp. 257–263.

Quantum Sensing and Communications Being Developed for Nanotechnology

An interdisciplinary quantum communications and sensing research effort for application in microdevices has been underway at the NASA Glenn Research Center since 2000. Researchers in Glenn’s Instrumentation and Controls, Communications Technology, and Propulsion and Turbomachinery Divisions have been working together to study and develop techniques that utilize quantum effects for sensing and communications. The emerging technology provides an innovative way to communicate faster and farther using less power and to sense, measure, and image environmental properties in ways that are not possible with existing technology.

Find out more about this research:

Glenn’s Optical Instrumentation Technology Branch:

<http://www.grc.nasa.gov/WWW/OptInstr/OptInstr.html>

Glenn’s Photovoltaic and Space Environments Branch:

<http://powerweb.grc.nasa.gov/pvsee/>

Glenn contacts:

Michael J. Krasowski, 216–433–3729, Michael.J.Krasowski@nasa.gov; Lawrence C. Greer, 216–433–8770, Lawrence.C.Greer@nasa.gov; and David M. Wilt, 216–433–6293, David.M.Wilt@nasa.gov

Ohio Aerospace Institute (OAI) contacts:

Phillip P. Jenkins, 216–433–2233, Phillip.P.Jenkins@grc.nasa.gov; and Joseph M. Flatico, 216–433–5053, Joseph.M.Flatico@grc.nasa.gov

Authors:

Michael J. Krasowski, Phillip P. Jenkins, Lawrence C. Greer, and Joseph M. Flatico

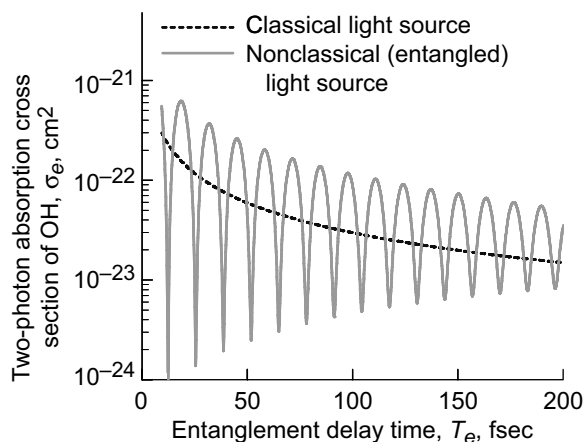
Headquarters program office:

OAT

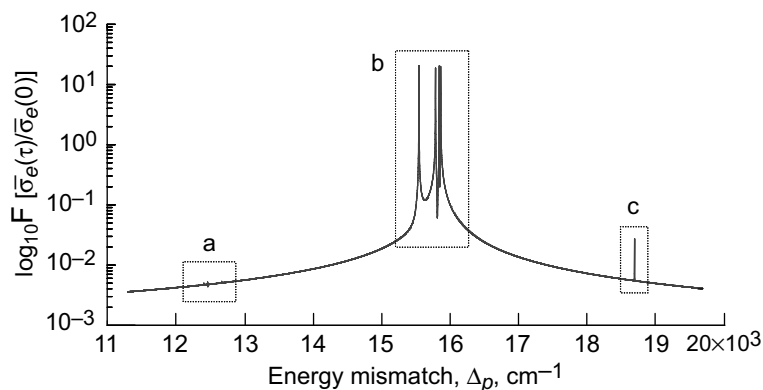
Programs/Projects:

Energetics

The Quantum Sensing and Communications team has completed initial tests of an optical communications system for low-radiated-power communications. Information has been optically transmitted over 1 meter of free space in an optically noisy environment. The information was carried in about 10,000 photons/sec,



Two-photon absorption cross section of OH ($A-X$) as a function of the entanglement delay time (solid line). The classical two-photon cross section (dashed line) exhibits monotonic behavior. The non-monotonic variation in the absorption cross section can be used to extract virtual-state energy-level information.



Fourier transform of the two-photon absorption cross section of OH ($A-X$) reveals the virtual-state energy spectrum. The virtual states can be seen in the peaks highlighted by the three enclosed boxes (labeled a, b, and c). Virtual states of a molecule show the actual transition path taken by the molecule after it has absorbed the first photon, but before it has absorbed the second photon. These virtual states are impossible to observe using conventional, nonentangled photons. $A^2_{\epsilon} + -X^2_{\pi}$; electronic transition of OH.

or about 3 femtowatts (10^{-15} W) of radiated optical power, at a frequency of 1 kHz. This amounts to 3 attowatts (10^{-18} W) of radiated power per bit of information: one of the lowest power tests of information transfer over free space in a noisy environment known. This technology could solve the ongoing problem of how to communicate with, or otherwise extract information from, a nanoscale electromechanical systems (NEMS) device. This testbed will be used in the future to develop optical communications protocols and components applicable for nanorobots.

An example of ongoing quantum sensing work that is part of this project is a theoretical study where entangled photon virtual-state spectroscopy is applied to a molecular system for the first time (ref. 1). Entangled two-photon spectroscopy is a new technique that will permit ultra-high-sensitivity measurements of molecular properties with very little optical power (attowatts). This technique has applications, for example, in two-photon fluorescence confocal microscopy because it greatly reduces the optical power needed to avoid optical damage to the specimen being probed. This work demonstrates that the two-photon absorption cross section of the hydroxyl radical (OH) induced by the entangled photons is non-monotonic as a function of entanglement delay time, as shown in the graph on the left. Taking the Fourier transform of the data in the left graph allows one to probe the virtual-state energy eigenvalues of OH in energy or frequency space, as shown in the graph on the right. Thus, one can use a fixed laser excitation energy to produce an energy spectrum. That is, an energy spectrum can be obtained without scanning the laser wavelength. This analysis reveals fundamental requirements and limitations in this new spectroscopic technique such as the requirement that the relative path delay be varied over a picosecond (10^{-12} sec) range with a femtosecond (10^{-15} sec) resolution.

Reference

1. Kojima, Jun; and Nguyen, Quang-Viet: Entangled Biphoton Virtual State Spectroscopy of the $A^2_{\epsilon} + -X^2_{\pi}$ System of OH. Chem. Phys. Lett., vol. 396, 2004, pp. 323–328.

Glenn contacts:

John D. Lekki, 216–433–5650, John.D.Lekki@nasa.gov;
 Dr. Quang-Viet Nguyen, 216–433–3574, Quang-Viet.Nguyen-1@nasa.gov;
 Binh V. Nguyen, 216–433–8338, Binh.V.Nguyen@nasa.gov;
 Marc A. Seibert, 216–433–3535, Marc.A.Seibert@nasa.gov;
 Terry M. Sanders, 216–433–5849, Terry.M.Sanders@nasa.gov; and
 Kenneth E. Weiland, 216–433–3843, Kenneth.E.Weiland@nasa.gov

Ohio Aerospace Institute (OAI) contact:

Dr. Jun Kojima, 440–962–3095, Jun.Kojima@grc.nasa.gov

Authors:

John D. Lekki and Dr. Quang-Viet Nguyen

Headquarters program office:

OAT

Programs/Projects:

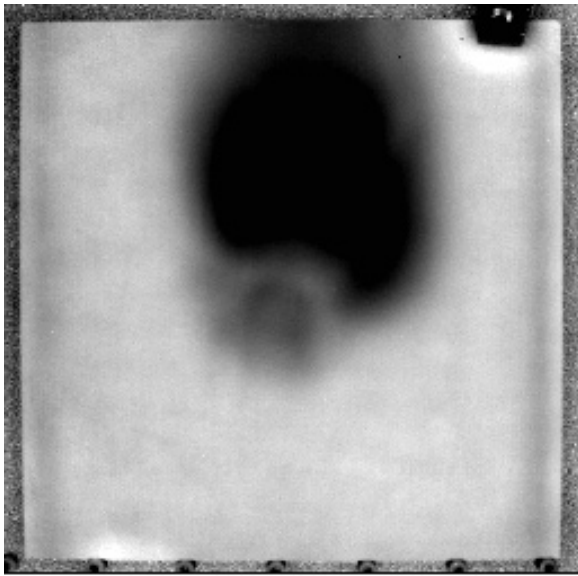
LEAP

Nondestructive Evaluation Tests Performed on Space Shuttle Leading-Edge Materials Subjected to Impact

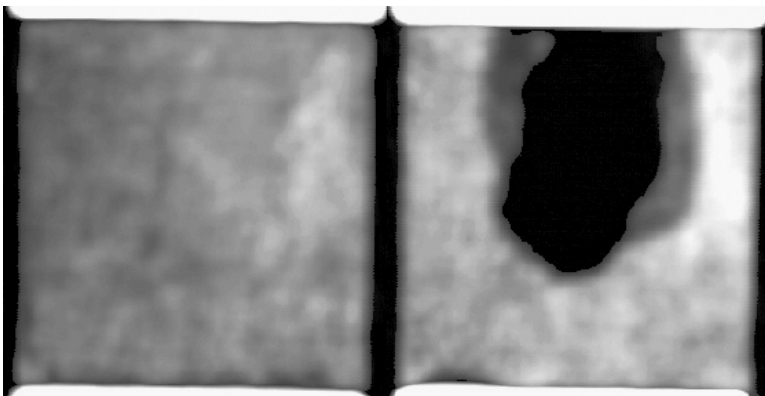
In support of the space shuttle Return To Flight efforts at the NASA Glenn Research Center, a series of nondestructive evaluation (NDE) tests were performed on reinforced carbon/carbon (RCC) composite panels subjected to ballistic foam impact. The impact tests were conducted to refine and verify analytical models of an external tank foam strike on the space shuttle leading edge. The NDE tests were conducted to quantify the size and location of the resulting damage zone as well as to identify hidden damage.

Two primary NDE methods were employed in this effort, pulsed thermography and ultrasonic C-scan. In pulsed thermography, the material under inspection is

excited with a short pulse of heat from high-intensity flash lamps. A series of thermal images is then captured over a period of time. Defect regions are seen as nonuniform surface temperatures, or hot spots, in the images (see the top figure). Advanced processing techniques are used to improve detection capability and image contrast. Ultrasonic C-scan uses a short ultrasonic pulse introduced into a material to identify defect regions. As the ultrasonic wave passes through the material, defects scatter and reflect the wave. This creates lower amplitude signals as measured by a receiving transducer, which are seen as a dark area in the resulting image (see the bottom figure).



Thermography image of reinforced carbon/carbon panel after impact. Dark region indicates extent of subsurface damage.



Before (left) and after (right) ultrasonic C-scan images of impacted reinforced carbon/carbon panel. Darker region indicates reduction or loss of ultrasonic signal due to damage.

This approach was successful in identifying and characterizing damage from foam striking the RCC materials directly and at a 45° angle. The two complementary NDE methods were able to confirm the damage identification and location. Further tests are planned to address damage due to ice and other objects. The NDE research was performed by personnel from Glenn's Optical Instrumentation and NDE branch and Cleveland State University and is supported by the space shuttle Return To Flight program.

Cleveland State University contacts:

Richard E. Martin, 216-433-3684,
Richard.E.Martin@grc.nasa.gov; and
James R. Bodis, 216-433-8376,
James.R.Bodis@grc.nasa.gov

Glenn contact:

Dr. Don J. Roth, 216-433-6017,
Donald.Roth@nasa.gov

Authors:

Richard E. Martin, James R. Bodis, and
Dr. Don J. Roth

Headquarters program office:

OAT

Programs/Projects:

RTF

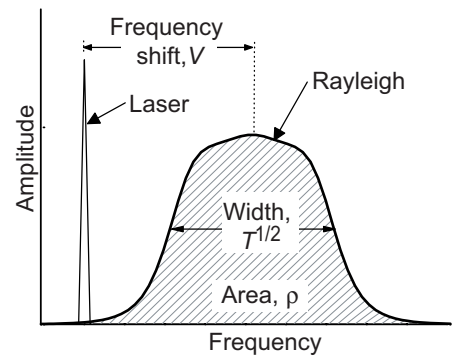
Molecular Rayleigh Scattering Techniques Developed for Measuring Gas Flow Velocity, Density, Temperature, and Turbulence

Nonintrusive optical point-wise measurement techniques utilizing the principles of molecular Rayleigh scattering have been developed at the NASA Glenn Research Center to obtain time-averaged information about gas velocity, density, temperature, and turbulence, or dynamic information about gas velocity and density in unseeded flows. These techniques enable measurements that are necessary for validating computational fluid dynamics (CFD) and computational aeroacoustic (CAA) codes. Dynamic measurements allow the calculation of power spectra for the various flow properties. This type of information is currently being used in jet noise studies, correlating sound pressure fluctuations with velocity and density fluctuations to determine noise sources in jets. These nonintrusive techniques are particularly useful in supersonic flows, where seeding the flow with particles is not an option, and where the environment is too harsh for hot-wire measurements.

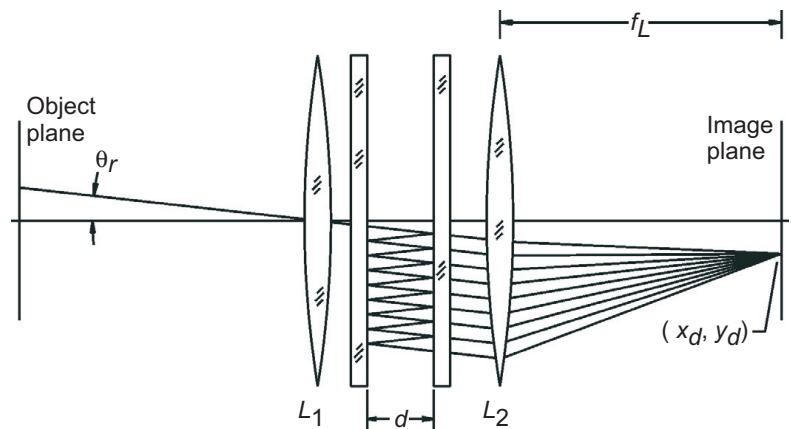
Molecular Rayleigh scattering is the result of elastic light scattering from gas molecules. When light from a single-frequency laser beam passes through a gas, the scattered light is shifted in frequency by the Doppler effect because of the bulk motion of the molecules. The optical frequency spectrum of Rayleigh scattered light contains information about the gas density, bulk velocity, and temperature. The top figure shows a Rayleigh scattering spectrum containing the narrow laser line and the broadened Rayleigh spectral peak. If the gas composition is known, the total intensity of the Rayleigh spectrum is directly proportional to the gas density. The frequency shift between the laser peak and the Rayleigh peak is proportional to the bulk flow velocity. The width of the Rayleigh spectrum is related to the gas temperature.

In both the time-averaged and dynamic measurement techniques, the spectra of the laser light and the Rayleigh scattered light are analyzed with a Fabry-Perot interferometer (see the center figure) operated in the static imaging mode. The resulting circular fringe pattern contains spectral information about the light. The bottom figure shows sample fringe patterns for narrow-line-width laser light (left), and Rayleigh scattered light (right). The Rayleigh fringe is thermally broadened and shifted radially from the laser fringe by an amount proportional to the gas velocity.

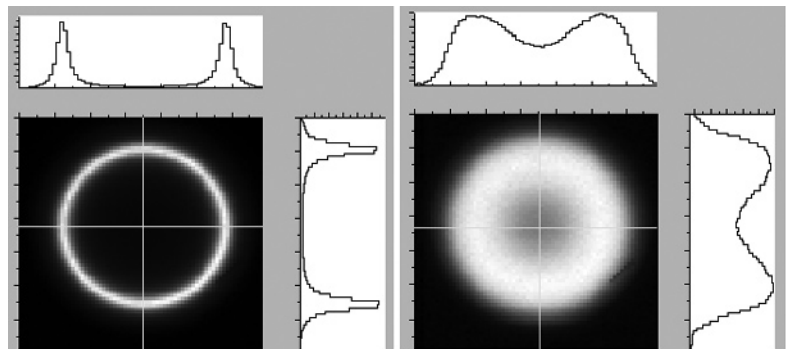
For time-averaged measurements, the resulting fringe pattern is recorded with a low-noise charge-coupled device (CCD) camera. Nonlinear least-squares analysis of the fringe pattern using a kinetic theory model of the Rayleigh scattered light provides estimates of the velocity, density, temperature, and turbulence of the gas flow averaged over the integration time of the camera.



Rayleigh scattering spectrum.



Fabry-Perot interferometer.



Sample fringe patterns. Left: Narrow-line-width laser light. Right: Rayleigh scattered light.

For dynamic measurements, the camera system is replaced by a detection system consisting of three photomultiplier tubes (PMTs) operated in the photon-counting mode and sampled

at rates up to 100 kHz. One PMT measures the total intensity of the collected scattered light to provide dynamic density information. A set of concentric mirrors is used to split the fringe pattern generated from the Rayleigh scattered light passing through the Fabry-Perot interferometer into inner and outer regions. The intensity of the light in the inner and outer regions of the fringe is monitored with the other two PMTs. The ratio of the intensities provides a measure of the flow velocity since the ratio changes as the fringe diameter increases or decreases. We are planning to extend the dynamic technique to allow for temperature measurement by increasing the spatial sampling resolution so that information about the width of the spectrum is available.

Bibliography

Mielke, A.F., et al.: Time-Average Measurement of Velocity, Density, Temperature, and Turbulence Using Molecular Rayleigh Scattering. Proceedings of the 12th International Symposium on Applications of Laser Techniques to Fluid Mechanics, Lisbon, Portugal, 2004.

Mielke, A.F., et al.: Time-Average Molecular Rayleigh Scattering Technique for Measurement of Velocity, Density, Temperature, and Turbulence Intensity in High Speed Nozzle Flows. AIAA-2004-0706, 2004.

Panda, J., et al.: Time-Averaged Velocity, Temperature and Density Surveys of Supersonic Free Jets. HT-FED-2004-56856, 2004.

Panda, J, et al.: Effect of Heating on Turbulent Density Fluctuations and Noise Generation From High Speed Jets. AIAA-2004-3016, 2004.

Panda, J.; and Seasholtz, R.G.: Experimental Investigation of Density Fluctuations in High-Speed Jets and Correlation With Generated Noise. J. Fluid Mech., vol. 450, 2002, pp. 97-130.

Seasholtz, R.G.; Panda, J.; and Elam, K.A.: Rayleigh Scattering Diagnostic for Measurement of Velocity and Density Fluctuation Spectra. AIAA-2002-0827, 2002.

Panda, J.; Seasholtz, R.G.; and Elam, K.: Further Progress in Noise Source Identification in High Speed Jets Via Causality Principle. AIAA-2003-3126, 2003.

Find out more about this research:

<http://www.grc.nasa.gov/WWW/OptInstr/>

Glenn contact:

Amy F. Mielke, 216-433-6757,
Amy.F.Mielke@nasa.gov

Authors:

Amy F. Mielke, Dr. Richard G. Seasholtz, Kristie A. Elam, and Dr. Jayanta Panda

Headquarters program office:

OAT

Programs/Projects:

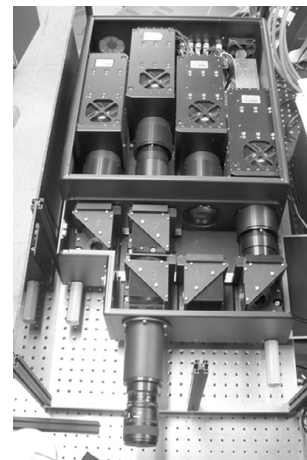
QAT, UEET, IR&D

Special recognition:

NASA Glenn Best Paper Award in 2003 for Panda and Seasholtz (2002)

Megahertz-Frame-Rate Imaging System Developed for Quantitative Velocimetry Measurements in Unsteady High-Speed Flows

The ability to capture the unsteady dynamics of high-speed compressible flows requires the use of ultrafast imaging diagnostics. Application of particulate-based scattering techniques to these types of flows also requires the use of high-power, pulsed illumination sources such as Nd:YAG solid-state lasers. High-accuracy flow-field measurements having both high spatial and temporal bandwidth have not been previously available because of the combined constraints imposed by the limited frame rate of high-sensitivity digital image sensors and the limited pulse repetition rates of commercially available solid-state lasers. To address this shortcoming and the need for a flow diagnostic system that satisfies the requirements mentioned, researchers at the NASA Glenn Research Center developed a



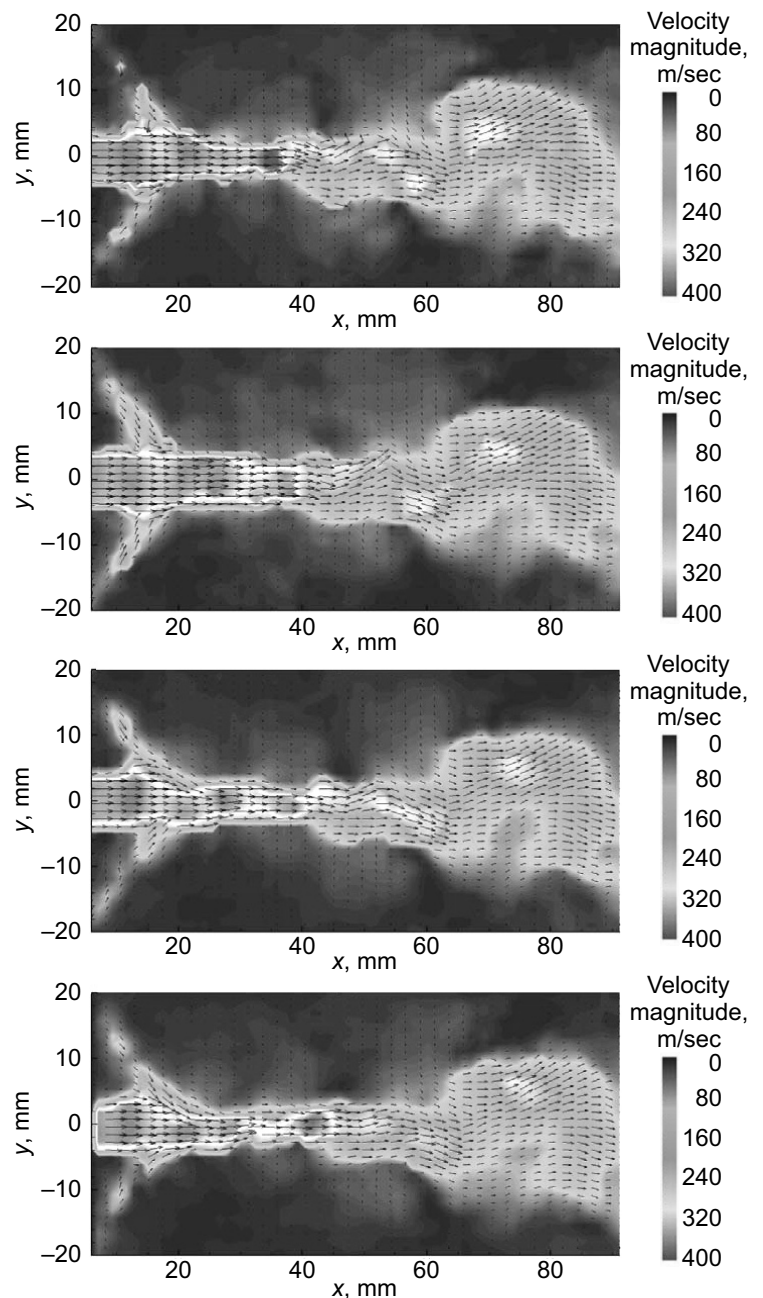
Left: MHz-repetition-rate pulse-burst-mode laser. Right: MHz-frame-rate camera.

high-resolution, high-framing-rate quantitative flow-measurement imaging system.

The imaging system is composed of a megahertz- (MHz-) repetition-rate pulse-burst-mode laser (built in-house) and a commercial MHz-framing-rate charge-coupled device (CCD) camera. The laser and camera are shown in the left and right photographs (preceding page), respectively. The laser contains six flashlamp-pumped Nd:YAG amplifier stages and can produce a burst train of high-energy pulses (on the order of 10) during each flashlamp discharge period, with individual pulse energies exceeding 75 mJ at 532 nm. Novel features of the laser include the use of fast-acting Pockels cells for pulse-train generation and a phase-conjugate mirror for removing parasitic background light in the pulse train. The camera, having a single optical input, comprises an internal image splitter unit and four individual intensified, frame-straddling, high-resolution 1280- by 1024-pixel CCD camera modules. The intensifiers allow for a sequence of eight full-resolution frames to be acquired in rapid succession. The combined laser and camera system provides imaging frame rates ranging from 50 kHz to 2 MHz, suitable for use in high-speed, unsteady, light-scattering-based velocimetry measurement techniques.

The new imaging system was used to obtain, for the first time, MHz-repetition-rate digital particle image velocimetry (DPIV) data from a supersonic nozzle flow with pulsed microjet actuation. The pulsed train from the laser was formed into a sheet, which was used to illuminate the particulate seeded nozzle flow. The high-speed imaging camera was used to record the positions of the particles at each pulse in the illumination train. The acquired image data were cross-correlation processed to obtain the velocity fields. The resulting sequence of velocity vector maps for the pulsed nozzle flow is shown in the figure to the right, where a high-speed fluid packet is ejected from the nozzle core flow.

Ongoing work to extend the capabilities of the imaging system includes making planar Doppler velocimetry measurements by replacing the existing camera optics with nonpolarizing optical components, reducing the laser head form factor to improve portability, and enhancing the temperature stabilization of thermally sensitive laser components to improve ruggedness in harsh testing environments.



Sequence of velocity vector maps of supersonic nozzle flow with pulsed microjet excitation obtained via MHz-frame-rate DPIV. This figure is shown in color in the online version of this article (<http://www.grc.nasa.gov/WWW/RT/2004/RI/RIO-opalski.html>).

Bibliography

Wernet, M.; and Opalski, A.: Development and Application of a MHz Frame Rate Digital Particle Image Velocimetry System. AIAA-2004-2184, 2004.

Find out more about this research:
<http://www.grc.nasa.gov/WWW/OptInstr/>

QSS Group, Inc., contact:
Dr. Anthony B. Opalski, 216-433-3908, Anthony.B.Opalski@grc.nasa.gov

Glenn contact:
Dr. Mark P. Wernet, 216-433-3752, Mark.P.Wernet@nasa.gov

Authors:
Dr. Anthony B. Opalski and
Dr. Mark P. Wernet

Headquarters program office:
OAT

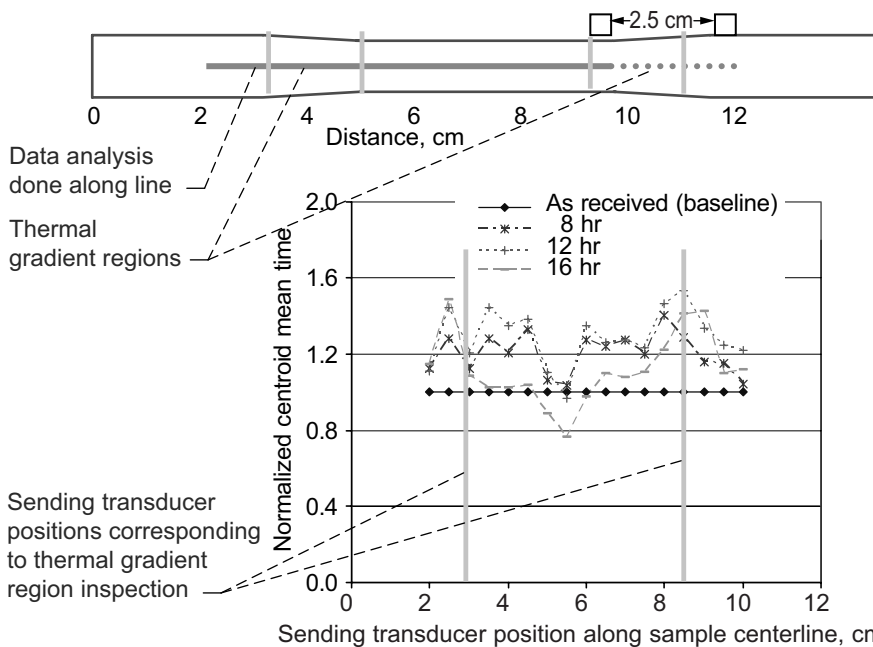
Programs/Projects:
NGLT

Ultrasonic Guided-Wave-Scan System Used to Characterize C-Enhanced Silicon Carbide Composite During Creep-Rupture Tests

Ceramic matrix composites (CMCs) are being developed for advanced aerospace propulsion applications in order to save weight, improve reuse capability, and increase performance. However, mechanical and environmental loads applied to CMCs can cause degradation in the form of discrete flaws and distributed microdamage that can play a significant role in reducing desirable physical properties. Categories of microdamage include fiber/matrix debonding (interface failure), matrix microcracking, fiber fracture and buckling, oxidation, and second-phase formation. Distributed microdamage in CMCs has proven difficult to characterize nondestructively because of the complex microstructure and macrostructure of these materials, and a recent study regarding the durability of a ceramic matrix composite discussed the requirement for improved nondestructive evaluation (NDE) methods for monitoring degradation in these materials.

This year, an ultrasonic guided-wave-scan system developed at the NASA Glenn Research Center was used to nondestructively characterize damage in C/SiC

(carbon fiber in silicon carbide matrix) ceramic matrix composite samples that underwent high-temperature creep-rupture testing. The samples were creep tested to failure at 1200 °C in air at a stress of 69 MPa (10 ksi). The creep tests were interrupted for ultrasonic guided-wave evaluation every 2 hr until the material samples failed. The damage was expected to be primarily of the oxidation type, which results in the carbon fibers literally disappearing. Since ultrasonic testing has proven sensitive to characterizing voids in ceramics, the use of the ultrasonic guided-wave-scan system was explored for (1) mapping evolving oxidation profiles along the sample length (as manifested by evolving voids) and (2) predicting ultimate failure location.

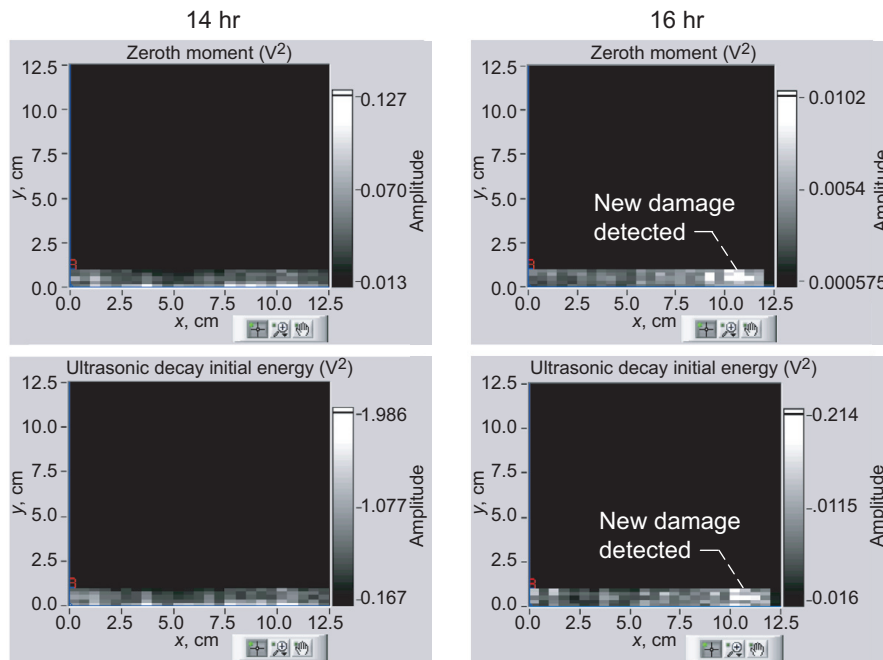


The ultrasonic guided-wave method used at Glenn results in complicated, multimode signals. These signals undergo specialized signal processing routines to extract parameters of the time and frequency domain. These parameters have proven to be sensitive to changes in microstructural conditions and to the presence of defects. In this study, one of the calculated parameters, centroid mean time, appeared to exhibit an evolving spatial trend that would be consistent with the nonuniform oxidation damage across the sample that has been reported previously. Specifically, normalized centroid mean time line profiles from 8 to 16 hr showed

approximately 20- to 40-percent lower values at the center versus the thermal gradient regions in a creep-rupture-tested sample, possibly indicating a difference in porosity between these areas. In addition, initial energy images showed that two other calculated parameters, zeroth moment and ultrasonic decay, were clearly indicated at the eventual failure location for the sample 1.5 hr prior to failure. This is a highly significant result since other nondestructive evaluation methods did not reveal these indications.

The graph on the preceding page shows the normalized centroid mean time as a function of creep hours and locations along the centerline of the sample. This parameter, computed from the raw time domain ultrasonic signal, appears to

resolve differences between oxidation behavior at the center versus the thermal gradient regions of the sample. The figure on this page shows the zeroth moment and ultrasonic decay initial energy images for the C/SiC sample after 14 hr and after 16 hr of creep tensile testing. Note the white indication in both 16-hr images at $x = 10$ to 11 cm. This was the eventual failure location, and it was not apparent after only 14 hr of testing.



Zeroth moment and ultrasonic decay initial energy images for C/SiC sample after 14 hr and after 16 hr of creep tensile testing.

Bibliography

Roth, Don, et al.: Characterization of C/Enhanced SiC Composite During Creep-Rupture Tests Using an Ultrasonic Guided Wave Scan System. NASA/TM—2004-213055, 2004. <http://gltrs.grc.nasa.gov/cgi-bin/GLTRS/browse.pl?2004/TM-2004-213055.html>

Glenn contact:

Dr. Don Roth, 216-433-6017,
Donald.J.Roth@nasa.gov

Authors:

Dr. Don J. Roth, Laura M. Cosgriff,
Richard E. Martin, and Michael J. Verrilli

Headquarters program office:

OAT

Programs/Projects:

UEET, RTF

Ability of Impedance-Based Health Monitoring To Detect Structural Damage of Propulsion System Components Assessed

Impedance-based structural-health-monitoring uses piezoelectric (PZT) patches that are bonded onto or embedded in a structure. Each individual patch behaves as both an actuator of the surrounding structural area as well as a sensor of the structural response. The size of the excited area varies with the geometry and material composition of the structure, and an active patch is driven by a sinusoidal voltage sweep. When a PZT patch is subjected to an electric field, it produces a mechanical strain; and when it is stressed, it produces an electric charge. Since the patch is bonded to the structure, driving a patch deforms and vibrates the structure. The structure then produces a localized dynamic response. This structural system response is transferred back to the PZT patch, which in turn produces an electrical response. The electromechanical impedance method is based on the principle of electromechanical coupling

between the active sensor and the structure, which allows researchers to assess local structural dynamics directly by interrogating a distributed sensor array. Because of mechanical coupling between the sensor and the host structure, this mechanical effect is picked up by the sensor and, through electromechanical coupling inside the active element, is reflected in electrical impedance measured at the sensor's terminals.

Experiments on simple-geometry specimens (thin-gauge aluminum square plates) were conducted to assess the potential of the electromechanical impedance method for detecting structural damage. Plate specimens (100 by 100 by 1.53162 mm) were made from 6061-T6 aluminum alloy sheet. Each plate was instrumented with one 10- by 10-mm PZT patch (0.1905-mm-thick PSI-5A4E material) purposely located at a location sensitive to vibration. This location was determined by conducting a finite-element analysis focusing on the modal response of the plate. Researchers used 10-mm straight electrical-discharge-machining notches to simulate cracks.

Multiple scenarios were addressed. A single notch was placed at three different locations with increasing distance from the patch as shown in the top figure. Multiple plates were used, with each plate having only a single notch at one of the three locations. Electromechanical impedance data were obtained with an HP 4194A impedance analyzer (Hewlett Packard, Palo Alto, CA). During the experiments, the specimens were supported on foam to provide an unconstrained support condition.

A series of 15 experiments were conducted over the frequency band 20 to 40 kHz, which was selected on the basis of repeatability results. The data were processed to consider the real part of the electromechanical impedance spectrum. The change induced in the spectrum by the presence of damage, for the notch located closest to the PZT sensor, is shown in the bottom figure. The presence of the notch significantly modified the frequency response function. This was indicated by shifting of the resonant frequencies and by the appearance of new resonances. The calculated correlation coefficient for this case was 0.497.

Glenn contact:

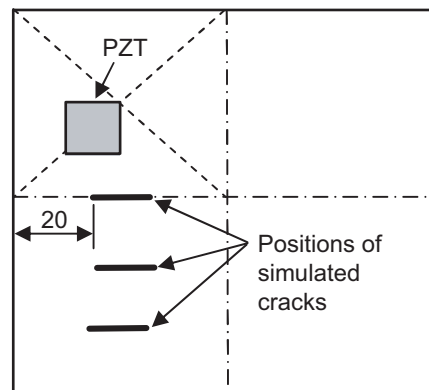
Dr. George Y. Baaklini, 216-433-6016,
George.Y.Baaklini@nasa.gov

Cleveland State University contact:

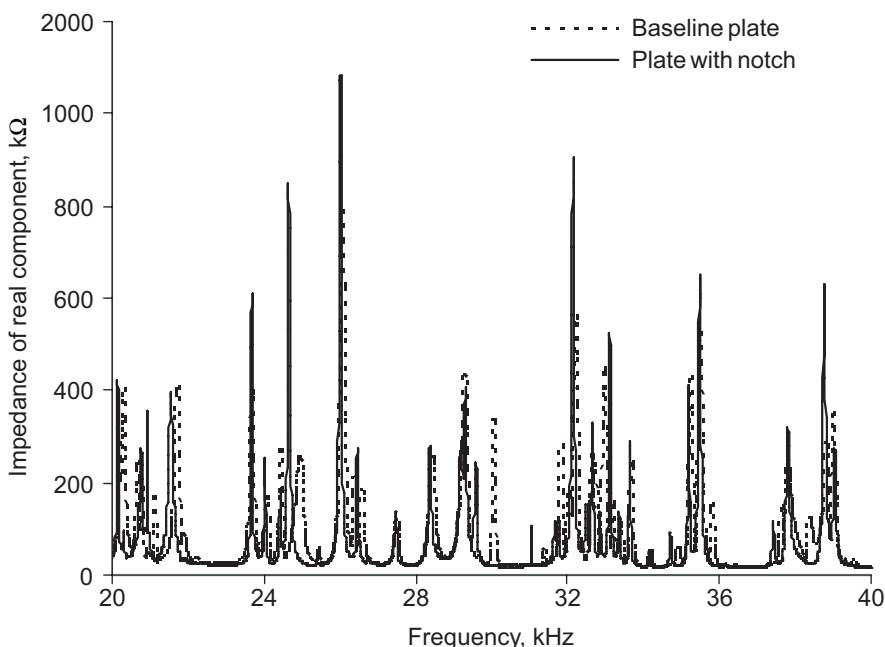
Richard E. Martin, 216-433-3684,
Richard.E.Martin@grc.nasa.gov

Authors:

Richard E. Martin, Dr. Andrew L. Gyekenyesi, and Prof. Jerzy T. Sawicki



Progression of specimen geometries with simulated cracks at various distances from the PZT sensor.



Averaged electromechanical impedance results for a plate with and without a notch.

Headquarters program office:

OAT

Programs/Projects:

AvSSP

Optical Tweezers and Optical Trapping Improved for Future Automated Micromanipulation and Characterization

Optical trap arrays are being developed at the NASA Glenn Research Center for holding, manipulating, and optically interrogating arrays of nanotube sensors. The trap arrays, for example, might be used to arrange arrays of chemical sensors for insertion onto a chip in liquid, air, and vacuum environments. Neural-network-controlled spatial light modulators (SLMs) are to generate and control the trap positions and trap profiles in three dimensions.

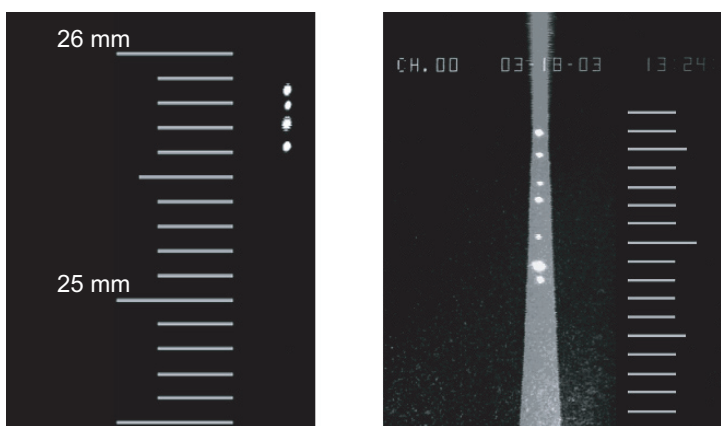
Glenn researchers have optically levitated glass and polystyrene microspheres in air. The following figure shows examples of microparticles optically trapped in air at Glenn. Typical object-to-lens distances for conventional microscope optical tweezers systems, where particles are confined to a liquid environment, are less than 5 mm. Previous maximum trapping distances from the focusing lens were 5 cm for levitated particles in air. Recently, Glenn researchers used a 135-mm-focal-length lens to levitate groups of test particles more than 25 mm above a glass plate, and more than 13 cm from the focusing lens. Groups of levitated particles can be raised and lowered by changing the height of the beam focus. In addition, levitated particles can be translated horizontally by changing the horizontal position of the beam focus.

SLM-generated traps are used to position and rotate nanotube clusters in liquid. The SLM can be used to alter a trap profile to exert torque on a nanotube as well as to change its position. The figure to the top right shows Laguerre-Gaussian (doughnut-mode) trap profiles exerting torques on nanotube clusters that are optically trapped in liquid.

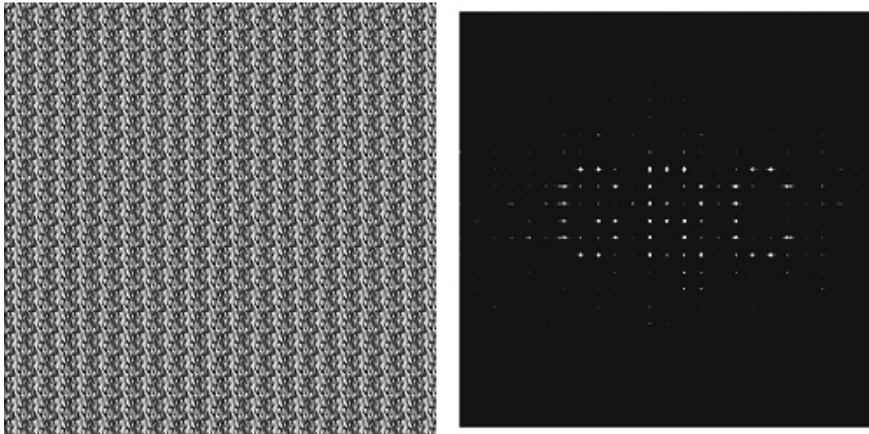


Cluster of rotating silicon-carbide nanotubes trapped in a Laguerre-Gaussian optical trap. The rotation in this instance was counterclockwise.

Glenn also has developed techniques for matching the limited processing capability of neural-network software to the full 480-by-480-pixel resolution of the SLMs. One technique is called tiling. In tiling, the 480-by-480-pixel scattered-light image from the trap array is scaled down to fewer than 10,000 pixels. Neural-network software can then easily be trained to generate a hologram of fewer than 10,000 pixels from the scaled image. The hologram might be intended to move a trap to a new position, for example. The reduced-size hologram is replicated, and the replicas are stacked or tiled to cover the full 480 by 480 pixels of the spatial light modulator. The left side of the figure on the next page shows an array of 48-by-48-pixel holograms that were stacked to cover the full 480 by 480 pixels of the SLM and to generate the 480-by-480-pixel trap array shown on the right. Other stages of neural-network processing can be used to increase resolution and to perform sophisticated detection of scattered light profiles. A neural network can be trained



Left: Four 100- μ m-diameter glass particles optically levitated to a height of over 25 mm. Right: Composite photograph illustrating the particle positions of optically levitated glass microspheres in the focused beam. The small scale divisions shown are in millimeters.



Neural networks can easily generate smaller holograms. These can be tiled to control an SLM to generate the 480- by 480-pixel array of traps. Left: Array of 48- by 48-pixel holograms. Right: Corresponding array of optical traps.

to generate a hologram to move a trap to a particular location within an image tile. The hologram is scaled and added to a tiled hologram to move traps to anywhere in a 480 by 480 array of locations. A third class of networks can be used to detect slight changes in the axial-location-dependent light-scattering profiles from a sensor. This network can be used to control the third dimension of the sensor location.

New Deep Reactive Ion Etching Process Developed for the Microfabrication of Silicon Carbide

Silicon carbide (SiC) is a promising material for harsh environment sensors and electronics because it can enable such devices to withstand high temperatures and corrosive environments. Microfabrication techniques have been studied extensively in an effort to obtain the same flexibility of machining SiC that is possible for the fabrication of silicon devices. Bulk micromachining using deep reactive ion etching (DRIE) is attractive because it allows the fabrication of microstructures with high aspect ratios (etch depth divided by lateral feature size) in single-crystal or polycrystalline wafers. Previously, the Sensors and Electronics Branch of the NASA Glenn Research Center developed a DRIE process for SiC using the etchant gases sulfur hexafluoride (SF_6) and argon (Ar) (ref. 1). This process provides an adequate etch rate of 0.2 $\mu\text{m}/\text{min}$ and yields a smooth surface at the etch bottom. However, the etch sidewalls are rougher than desired, as shown in the top photomicrograph on the next page. Furthermore, the resulting structures have sides that slope inwards, rather than being precisely vertical. A new DRIE process for SiC was developed at Glenn that produces smooth, vertical sidewalls, while maintaining an adequately high etch rate.

Bibliography

Decker, Arthur J., et al.: Neural Network for Image-to-Image Control of Optical Tweezers. Proceedings of SPIE, vol. 5514 (NASA/TM—2004-213201), 2004.

Wrbanek, Susan Y.; and Weiland, Kenneth E.: Optical Levitation of Micro-Scale Particles in Air. NASA/TM—2004-212889, 2004. <http://gltrs.grc.nasa.gov/cgi-bin/GLTRS/browse.pl?2004/TM-2004-212889.html>

Find out more about this research:

<http://www.grc.nasa.gov/WWW/OptInstr/OptInstr.html>

Glenn contact:

Susan Y. Wrbanek, 216-433-2006, Susan.Y.Wrbanek@nasa.gov

Authors:

Susan Y. Wrbanek and
Dr. Arthur J. Decker

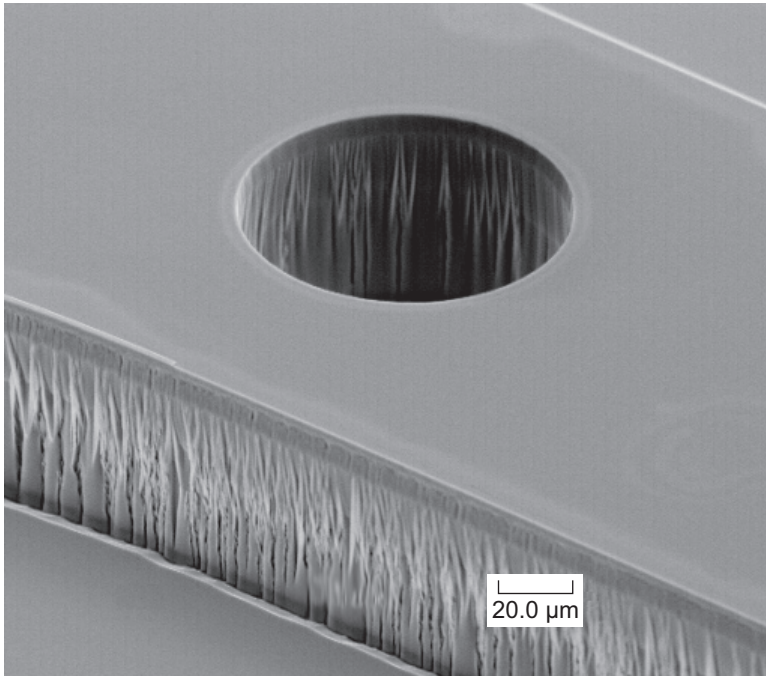
Headquarters program office:

OAT

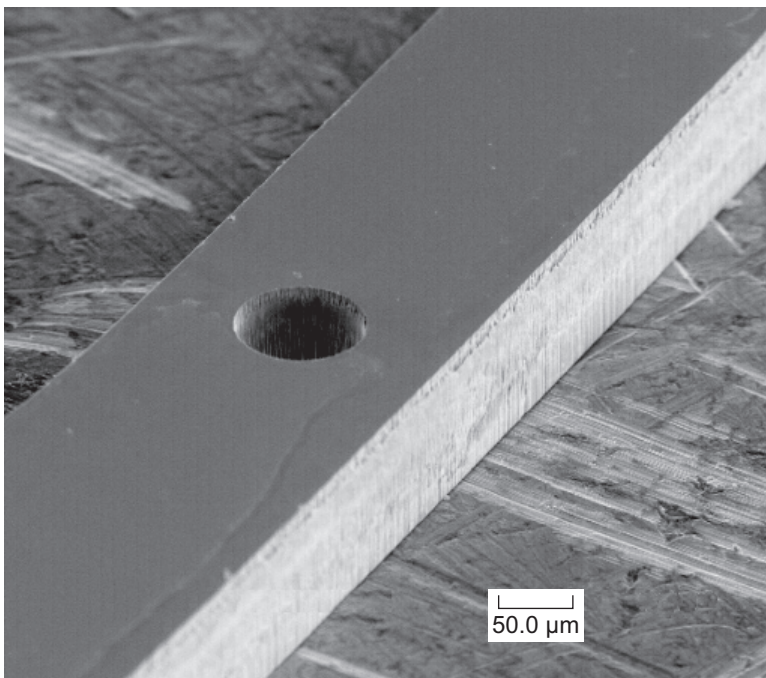
Programs/Projects:

LEAP

A time-multiplexed etch-passivate (TMEP) process is widely used in the DRIE of silicon in forming structures with aspect ratios greater than 30. This technique alternates fluorine-plasma etching of the substrate with the deposition of a passivating polymer layer to produce an anisotropic profile (i.e., vertical sidewalls). Without TMEP, high rates of lateral etching occur because of the high reactivity of silicon with fluorine radicals, which causes the etch mask to be undercut and reduces the aspect ratio attainable. On the other hand, SiC is relatively inert, and appreciable etch rates using a fluorine plasma are



SEM image of a microscale tensile test specimen in the process of fabrication using SF_6 and Ar plasma. Single-crystal SiC has been etched to a depth of 80 μm .



SEM image of a microscale tensile test specimen fabricated using a TMEP process. A single-crystal SiC wafer with a thickness of 135 μm has been etched entirely through.

obtained only when the SiC surface is subjected to ion bombardment. Since the ions are well collimated and strike only the horizontal surfaces of the substrate, the SiC etch process is inherently anisotropic. The lateral etch rate, however, while small, is not zero, which roughens the sidewalls.

By utilizing a TMEP process, Glenn researchers have been able to control the roughness and slope of the sides of etched SiC features. An etch mask of electroplated nickel is used to selectively protect areas of the wafer. SF_6 is used as the etching gas, and octafluorocyclobutane (C_4F_8) is used to deposit a fluorocarbon polymer film that protects the sidewalls from lateral etching. Scanning electron microscope (SEM) images of patterned features demonstrate smooth, vertical sidewalls (see the bottom photomicrograph). Depths of 150 μm have been achieved with dimensions as low as 50 μm . Further development of the process is expected to enable the fabrication of high-aspect-ratio structures in SiC with smooth sidewalls.

Reference

1. Beheim, Glenn M.: Deep Reactive Ion Etching for Bulk Micromachining of Silicon Carbide. The MEMS Handbook, Mohamed Gad-el-Hak, ed., CRC Press LLC, Boca Raton, FL, 2002, pp. 21-1 to 21-12.

Find out more about this research:

<http://www.grc.nasa.gov/WWW/SiC/SiC.html>

Glenn contacts:

Laura Evans, 216-433-9845,
 Laura.J.Evans@nasa.gov; and
 Dr. Glenn Beheim, 216-433-3847,
 Glenn.M.Beheim@grc.nasa.gov

Authors:

Laura J. Evans and
 Dr. Glenn M. Beheim

Headquarters program office:

OAT

Programs/Projects:

AEFT

High-Temperature, Thin-Film Ceramic Thermocouples Developed

To enable long-duration, more distant human and robotic missions for the Vision for Space Exploration, as well as safer, lighter, quieter, and more fuel efficient vehicles for aeronautics and space transportation, NASA is developing instrumentation and material technologies. The high-temperature capabilities of thin-film ceramic thermocouples are being explored at the NASA Glenn Research Center by the Sensors and Electronics Branch and the Ceramics Branch in partnership with Case Western Reserve University (CWRU). Glenn's Sensors and Electronics Branch is developing thin-film sensors for surface measurement of strain, temperature, heat flux, and surface flow in propulsion system research. Glenn's Ceramics Branch, in conjunction with CWRU, is developing structural and functional ceramic technology for aeropropulsion and space propulsion.

Ceramic-based thermocouples are known for their high stability and robustness at high temperatures in environments where metals could not survive, but typically, they are found in the form of rods or probes. Ceramics also have a substantial cost advantage. At present, sensors intended for use at high temperatures are made of platinum and other noble metals. The current price of platinum exceeds

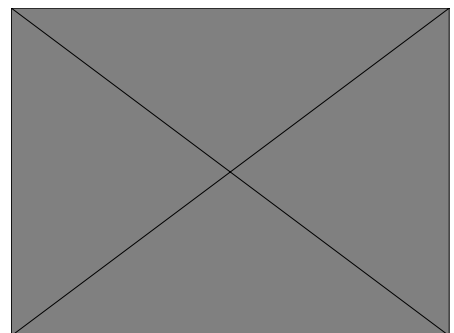
\$900 per troy ounce, more than 50,000 times the cost of the basic material cost of ceramics.

Glenn and CWRU have joined forces to investigate the feasibility of using ceramics as thin-film thermocouples for extremely high temperature applications, thus taking advantage of both the stability and robustness of ceramics and the nonintrusiveness of thin films.

Thermocouple samples for testing are fabricated from high-purity sputtering targets in Glenn's Microsystems Fabrication Laboratory. Thermoelectric data on thin-film chromium silicide (CrSi) and tantalum carbide (TaC) were measured for temperatures up to 650 °C for CrSi and to 450 °C for TaC. The thermoelectric voltage output of a thin-film CrSi versus TaC thermocouple was found to be at least 10 times that of the standard type R (platinum-rhodium vs. platinum) thermocouple, producing 59 mV with a 600 °C temperature gradient. The photograph on the left shows the CrSi-TaC thermocouple in a test fixture at Glenn, and the resulting output signal is compared with a type R thermocouple output in the graph below. The temperature differential across the sample, from the



Test fixture in Glenn's Thin Film Sensors Laboratory with the CrSi-TaC test sample in place.



Relative thermoelectric voltage output of the CrSi-TaC thermocouple compared with the standard type R thermocouple on the test sample.

center of the sample inside the oven to the sample mount outside the oven, is measured using a type R thermocouple on the sample.

Because of the low oxidation temperatures of these thin-film thermocouple elements, additional research needs to be conducted into protective overcoats for the films if they are to be practical in oxidizing environments. Also, thin-film ceramic thermocouples must be tested in an inert atmosphere or vacuum to gain an understanding of their performance and applicability in space-relevant environments.

This merging of the high-temperature capabilities of ceramics with the non-intrusiveness of thin films is ongoing. It appears that a new class of ceramic thin films can be used as high-temperature thermocouples, and this technology is believed to have applications as resistive temperature and strain sensors as well. This research advances the effort to develop a complete sensor package using ceramics as thin-film sensors in environments where standard metal sensors would not survive.

Bibliography

Wrbanek, John D., et al.: Development of Thin Film Ceramic Thermocouples for High Temperature Environments. NASA/TM—2004-213211 (AIAA-2004-3549), 2004. <http://gltrs.grc.nasa.gov/cgi-bin/GLTRS/browse.pl?2004/TM-2004-213211.html>

Find out more about this research:
<http://www.grc.nasa.gov/WWW/sensors/>

Glenn contacts:

John D. Wrbanek, 216-433-2077, John.D.Wrbanek@nasa.gov;
Gus C. Fralick, 216-433-3645, Gustave.C.Fralick@nasa.gov; and
Dr. Serene C. Farmer, 216-433-3289, Serene.C.Farmer@nasa.gov

Case Western Reserve University contact:

Dr. Ali Sayir, 216-433-6254, Ali.Sayir@grc.nasa.gov

Authors:

John D. Wrbanek, Gustave C. Fralick, Dr. Serene C. Farmer, Dr. Ali Sayir, Charles A. Blaha, and José M. Gonzalez

Headquarters program office:

Aeronautics Research

Programs/Projects:

PR&T

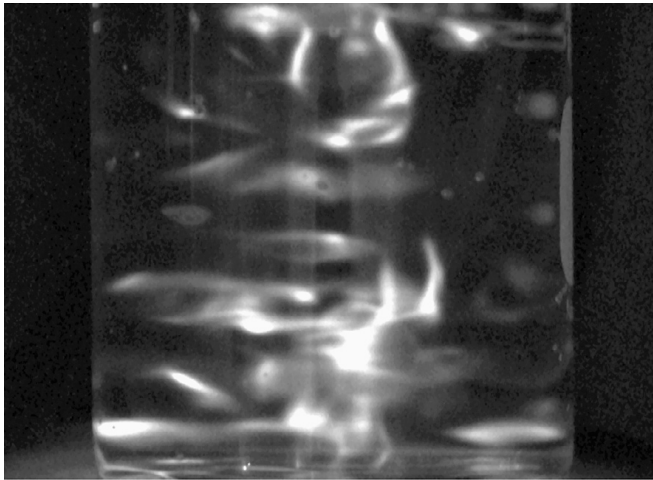
Sonoluminescence: A Galaxy of Nanostars Created in a Beaker

As part of basic and applied research on advanced instrumentation technologies, the NASA Glenn Research Center is examining applications for sonoluminescence: ultrasonically produced glowing bubbles that are hotter than the Sun. In the last decade, those outside of the ultrasonic community have become interested in understanding sonoluminescence and in using some of its more interesting properties. First discovered in the 1930s as a byproduct of early work on sonar, the phenomenon is defined as the generation of light energy from sound waves. This glow, which was originally thought to be a form of static electricity, was found to be generated in flashes of much less than a billionth of a second that result when microscopic bubbles of air collapse. The temperature generated in the collapsing bubbles is at least 4 times that of the surface of the Sun.

Theories for the cause of the glow from a collapsing bubble range from black-body radiation, plasma ionization, quantum vacuum fluctuations, or coherent optical lasing. Even as these theories are being explored, applications for the effect are taking shape, from fusion containment to thin-film deposition systems. Glenn has begun an in-house examination of sonoluminescence to develop instrumentation and measurement techniques that could ultimately use the phenomenon to enable safer, lighter, quieter, and more fuel efficient

vehicles for aeronautics and space transportation and exploration.

In Glenn's dark-room apparatus, an amplified sinusoidal signal was used to drive a high-intensity ultrasonic transducer horn probe inserted into the open top of separate glass containers filled with 50, 100, and 250 ml of distilled water. At specific input frequencies, multibubble sonoluminescence (MBSL) was generated and then photographed in preparation for the examination of the effect by Glenn's state-of-the-art fiber-optic and thin-film sensors. The submicroscopic glowing bubbles are not visible as distinct points, but rather as a collection of corkscrew filaments, or a "galaxy" of "nanostars," in the containers.

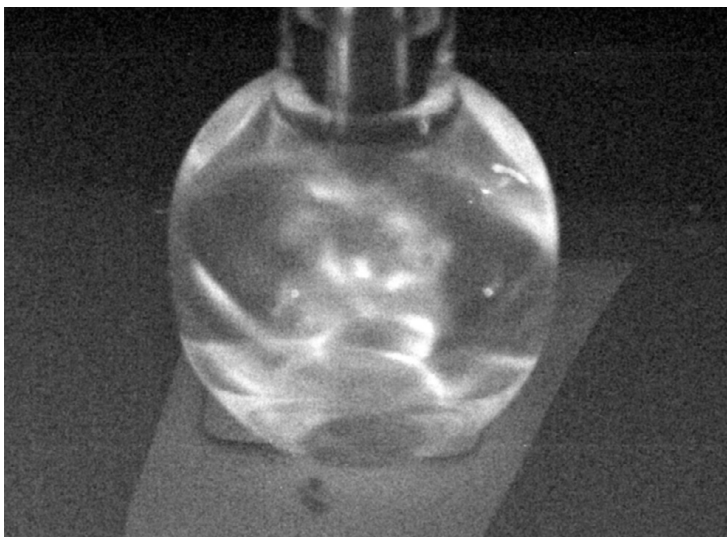


*Left: Enhanced image of MBSL at 109 kHz in a 100-ml beaker. Exposure time, 2 min at f/2.8; field of view, 6.6 by 5.1 cm.
Right: Enhanced image of MBSL at 107 kHz in a 50-ml flask. Exposure time, 3 min at f/2.8; field of view, 7.1 by 5.4 cm.*

The images above were produced with very little processing other than a brightness- or contrast-level enhancement. Resolutions of the MBSL filaments of approximately 100 μm per pixel were achieved. Longer exposure times could brighten an image, but they also blurred the image because the positions of the filaments varied irregularly around the local pressure maximums. A 3-min exposure recorded approximately 18 million cycles of the bubbles flashing. An image of the 50-ml flask, which was produced with a

color charge-coupled device (CCD) imager calibrated to a standard color-rendition chart, is shown in the final figure.

The chaotic MBSL filament structure can be observed in relation to the testing cell walls to a submillimeter resolution integrated over a long time frame (millions of cycles). This fine resolution will guide instrumentation and measurement technique development so that we can ultimately formulate an application of the effect.



Enhanced image of MBSL at 106 kHz in a 50-ml flask. Exposure time, 5 min at f/2.8; field of view, 9.5 by 6.8 cm. This image is shown in color in the online version of this article (<http://www.grc.nasa.gov/WWW/RT/2004/RI/RIS-Jwrbanek2.html>). The colors were calibrated by a color standard.

Find out more about this research:
<http://www.grc.nasa.gov/WWW/sensors/>

Glenn contacts:

Gus C. Fralick, 216-433-3645,
Gustave.C.Fralick@nasa.gov;
John D. Wrbanek, 216-433-2077,
John.D.Wrbanek@nasa.gov; and
Susan Y. Wrbanek, 216-433-2006,
Susan.Y.Wrbanek@nasa.gov

Authors:

John D. Wrbanek, Gustave C. Fralick,
Susan Y. Wrbanek, and Kenneth E. Weiland

Headquarters program office:

Aeronautics Research

Programs/Projects:

LEAP, AEFT, BPP

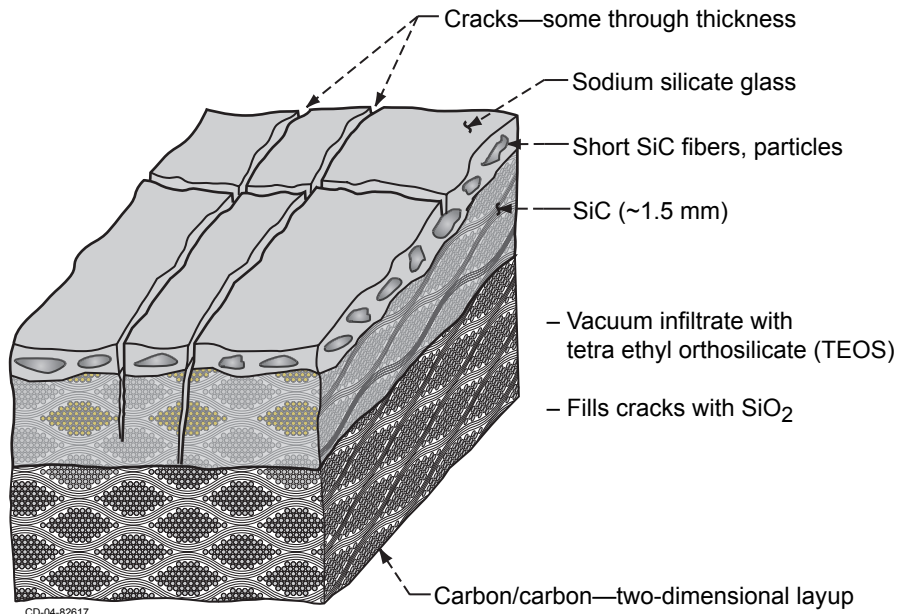
Materials

As-Fabricated Reinforced Carbon/Carbon Characterized

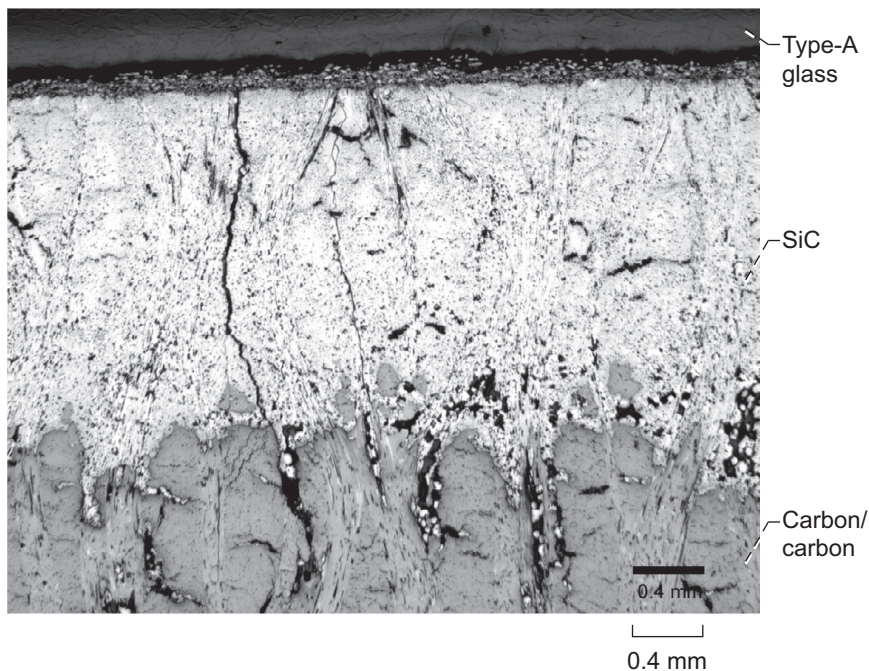
Reinforced carbon/carbon (RCC) is a critical material for the space shuttle orbiter. It is used on the wing leading edge and the nose cap, where maximum temperatures are reached on reentry. The existing leading-edge system is a single-plate RCC composite construction with a wall thickness of approximately

1/4 in., making it a prime reliant protection scheme for vehicle operation.

The schematic to the left illustrates the RCC material. The RCC material and the leading-edge design were developed concurrently in the 1970s utilizing existing state-of-the-art technologies. For safe operation, the hottest leading-edge panels are currently limited to 50 missions because of the oxidation of the carbon composite substrate. This limit was established through empirical correlations of calculated mass loss with strength reduction. Extensive testing and flight qualification have been done on this material, and it is an integral part of the orbiter. The Columbia accident was caused by damaged RCC on the wing leading edge that was unable to provide the proper protection for the wing components.



RCC material used for the shuttle orbiter.

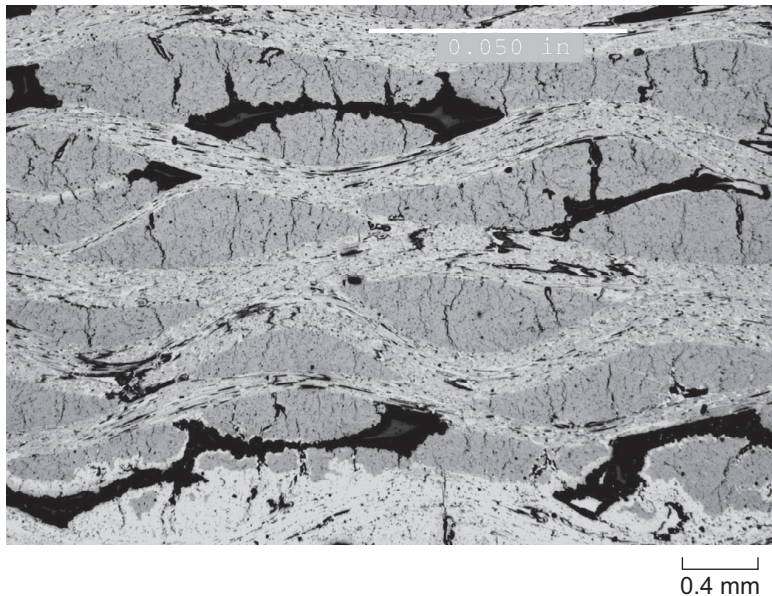


Polished cross section showing outer layers.

As part of the Return To Flight efforts, an RCC aging team composed of members at the NASA Glenn Research Center, NASA Marshall Space Flight Center, NASA Johnson Space Center, NASA Langley Research Center, and Argonne National Laboratory was established to examine RCC in the as-fabricated, flown, and furnace-oxidized state. Leading-edge material with actual exposures of up to 30 missions is now available to assess the severity of actual strength reduction through testing with current analytical techniques. Characterization is done with nondestructive evaluation, microstructural examination, and mechanical testing. A detailed microstructural examination of as-fabricated RCC is an essential part of this task so that we can understand the baseline material. Samples were obtained in various stages of the process and examined with optical and electron optical techniques. Surfaces and

mounted, polished cross sections were examined. Quantitative image analysis was used to determine porosity in the polished cross sections, and gas adsorption techniques were used to measure internal surface areas.

The microstructure of the as-fabricated material had large variations in a variety of areas including the porosity, coating morphology, and crack density. The photomicrograph on the preceding page shows the Type-A glass, the silicon carbon (SiC) layer, and the carbon/carbon substrate. The following photomicrograph shows a region of the carbon/carbon substrate. The origin of these pores can be traced to processing steps. Many of the voids are due



Polished cross section showing pores in substrate.

to shrinkage of the resin material during pyrolysis.

Establishing a well-documented database for the as-fabricated material in combination with existing databases will assist in assessing aging effects from high-temperature and environmental exposure of the flown and furnace- or arc-jet-conditioned material.

Find out more about this research:

<http://www.grc.nasa.gov/WWW/EDB/>

Glenn contacts:

Dr. Nathan S. Jacobson, 216-433-5498, Nathan.S.Jacobson@nasa.gov; and Dr. Anthony M. Calomino, 216-433-3311, Anthony.M.Calomino@nasa.gov

Lockheed Martin Missiles and Fire Control contact:

Neal Webster, 972-603-9448, Neal.Webster@lmco.com

Authors:

Dr. Nathan S. Jacobson, Dr. Anthony M. Calomino, and Neal Webster

Headquarters program office:

Space Operations Mission Directorate

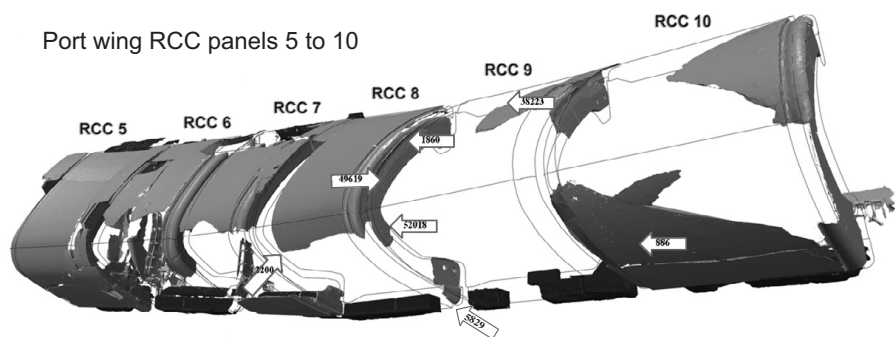
Programs/Projects:

RTF

Followup to Columbia Investigation: Reinforced Carbon/Carbon From the Breach Location in the Wing Leading Edge Studied

Initial estimates on the temperature and conditions of the breach in the Space Shuttle Columbia's wing focused on analyses of the slag deposits. These deposits are complex mixtures of the reinforced carbon/carbon (RCC) constituents, insulation material, and wing structural materials.

Identification of melted/solidified Cerachrome insulation (Thermal Ceramics, Inc., Augusta, GA) indicated that the temperatures at the breach had exceeded 1760 °C.



Sample locations in recovered RCC.

For the present study, a series of samples were removed from the RCC at the breach location of the recovered Columbia wing leading edge, as shown in the illustration to the left. Some knife-edge surfaces of the RCC exposed relatively clean carbon/carbon. From these surfaces, further information on the conditions of the accident could be extracted.

Microscopy at the NASA Glenn Research Center revealed the mode of attack of the hot oxidizing gases. This photomicrograph illustrates the “pointed” morphology characteristic of the oxidation of carbon fibers.

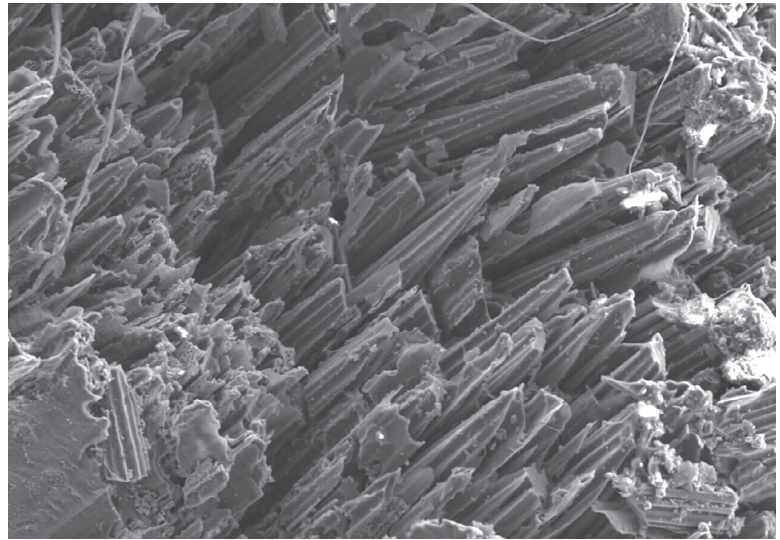
A second set of samples was studied at Sandia National Laboratories. Sandia has developed a novel technique to look at carbon chars and determine temperatures from Raman spectroscopy. The Raman spectra consist of two characteristic peaks at 1350 and 1600 cm^{-1} . The magnitude and peak shape correlate with the size of the crystalline domains in the carbon chars. These, in turn, correlate with exposure temperatures in standards. Lower exposure temperatures yield nanocrystalline graphite, whereas higher temperatures yield larger graphite crystals. Comparison with standards indicates that the temperatures on some of the recovered RCC fragments may have been greater than 2700 °C. These results provide new evidence of the upper temperature limits experienced at the breached wing leading edge of Columbia.

Find out more about this research:

<http://www.grc.nasa.gov/WWW/EDB/>

Glenn contacts:

Dr. Nathan S. Jacobson, 216-433-5498, Nathan.S.Jacobson@nasa.gov; and
Dr. Elizabeth J. Opila, 216-433-8904, Elizabeth.J.Opila@nasa.gov



50.0 μm

Electron micrograph of carbon/carbon taken near the breach showing an oxidation pattern.

Sandia National Laboratories contact:

David Tallant, 505-844-3629,
drtalla@sandia.gov

Authors:

Dr. Nathan S. Jacobson,
Dr. Elizabeth J. Opila, and David Tallant

Headquarters program office:

Space Operations Mission Directorate

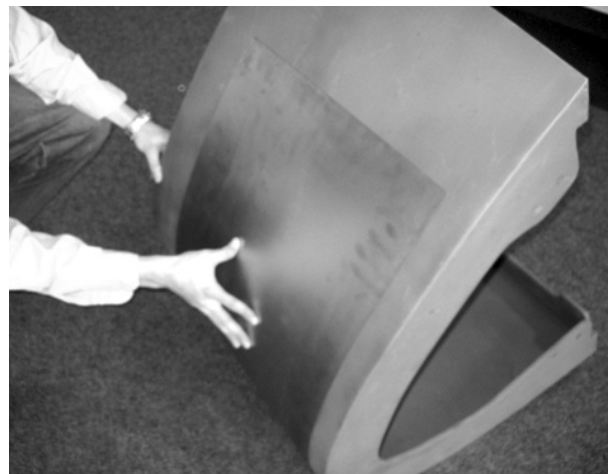
Programs/Projects:

RTF

Flexible Metallic Overwrap Concept Developed for On-Orbit Repair of Space Shuttle Orbiter Leading Edges

The Columbia accident has focused attention on the critical need for on-orbit repair concepts for leading edges in the event that damage is incurred during space shuttle orbiter flight. Damage that is considered as potentially catastrophic for orbiter leading edges ranges from simple cracks to holes as large as 16 in. in diameter. NASA is particularly interested in examining potential solutions for areas of larger damage since such a problem was identified as the cause for the Columbia disaster.

One possible idea for the on-orbit repair of the reinforced carbon/carbon (RCC) leading edges is an overwrap concept that would use a metallic sheet flexible enough to conform to the contours of the orbiter and robust enough to protect any problem area from catastrophic failure during reentry. The photograph to the right shows a simplified view of the application of a refractory metal sheet over a mockup of

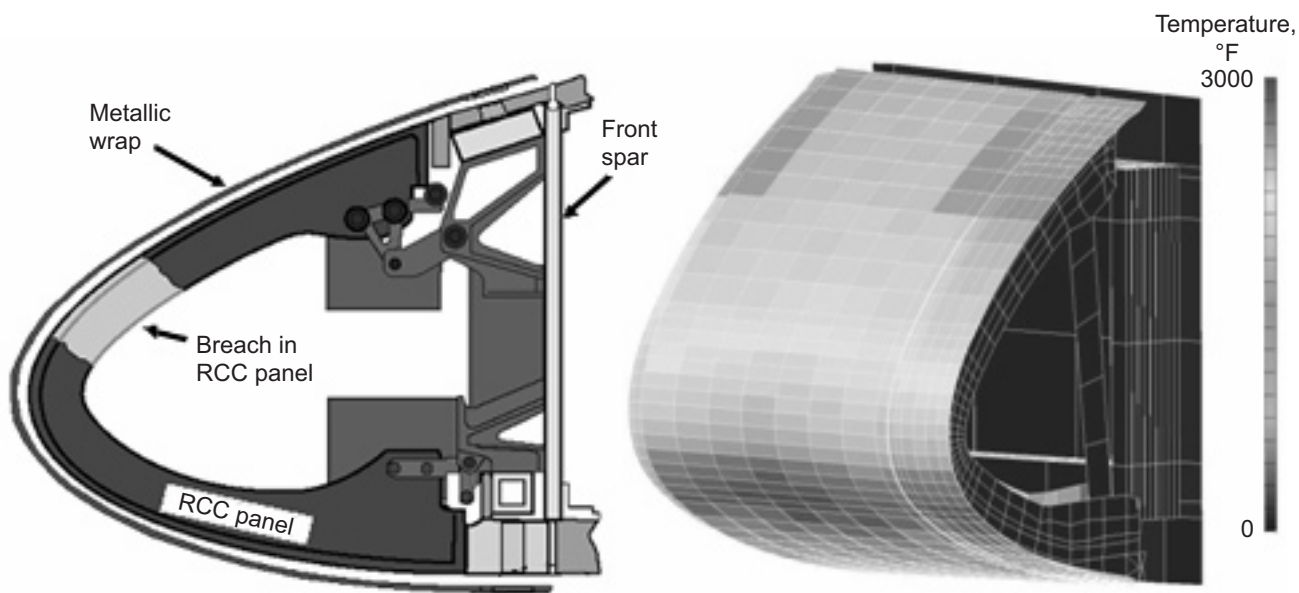


Representation of concept for a refractory metal overwrap. Mockup of the space shuttle orbiter RCC panel 9.

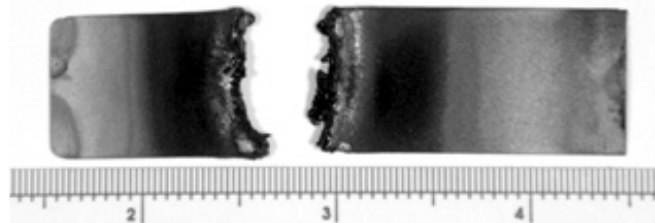
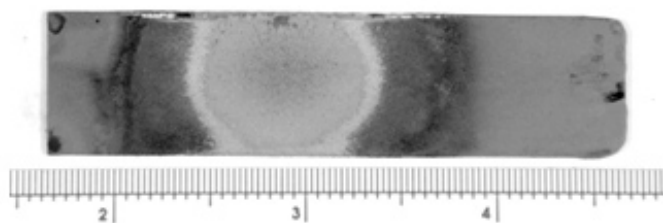
shuttle orbiter panel 9, which experiences the highest temperatures on the shuttle during reentry. The metallic overwrap concept is attractive because of its versatility as well as the ease with which it can be included in an onboard "repair kit."

Reentry of the orbiter into Earth's atmosphere imposes extreme requirements on repair materials. Temperatures can exceed 1650 °C for up to 15 min in the presence of an extremely oxidizing plasma environment. Several other factors are critical, including catalysity, emissivity, and vibrational and aerodynamic

loads. Materials chosen for this application will need to be evaluated with respect to high-temperature capability, resistance to oxidation, strength, coefficient of thermal expansion, and thermal conductivity. The top figure shows the temperature profile across panel 9 during reentry as well as a schematic of the overwrap concept itself.



Overwrap concept for leading-edge wing repair and a corresponding temperature profile for panel 9. This figure is shown in color in the online version of this article (<http://www.grc.nasa.gov/WWW/RT/2004/RM/RM03M-ritzert.html>).



Screening of a candidate overwrap material using an oxygen-propane torch at Glenn. Photographs show examples of successful and failed torch screening. This figure is shown in color in the online version of this article (<http://www.grc.nasa.gov/WWW/RT/2004/RM/RM03M-ritzert.html>).

Refractory metals, which by definition have a melting temperature greater than 2000 °C, are candidates for a flexible overwrap repair concept. This class of metals exhibits high strengths and can withstand extreme temperatures. The significant problem with these materials, however, is their high propensity for oxidation. Coatings are critical for the success of a refractory metal leading-edge repair. Silicide coating can be applied to the metallic materials to improve the chances of survival through the oxidizing reentry environment. These coatings, however, are inherently brittle and crack as the overwrap is conformed to the leading edges. Processes are being investigated to mitigate oxidation through cracks in the coating either through introducing an oxidation-resistant underlayer or by introducing a crack-healing overlayer such as a type-A coating (e.g., sodium silicate).

Several refractory metal candidates were screened at the NASA Glenn Research Center as potential overwrap candidates. Alloys of niobium, tantalum, molybdenum, and rhenium were coated with an R512E silicide and were evaluated by a torch that simulates the temperature profile during a 15-min reentry. Although a few of the candidates showed potential for successful application, the rhenium sample was clearly the most promising. The bottom figure on the preceding page shows the torch setup used. Work is continuing with the development of an iridium underlayer that will mitigate oxidation attack of the rhenium in the event that cracks form in the silicide coating.

Several design issues remain before a metallic overwrap can be considered as a reliable repair concept. Expansion differences with the RCC and attachment

of the overwrap to the shuttle panels are two of the hurdles yet to be evaluated. The promising results gathered for rhenium and other refractory metal candidates have made this a primary concept for the repair of large damaged areas.

Find out more about this research:

NASA Glenn Research Center:

<http://www.nasa.gov/glenn/>

Advanced Metallics Branch:

<http://www.grc.nasa.gov/WWW/AdvMet/webpage/>

Glenn contacts:

Frank J. Ritzert, 216-433-8199,
Frank.J.Ritzert@nasa.gov; and
Dr. James A. Nesbitt, 216-433-3275,
James.A.Nesbitt@nasa.gov

Author:

Frank J. Ritzert

Headquarters program office:

OSF

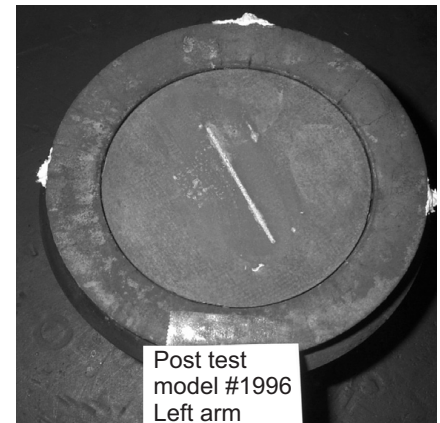
Programs/Projects:

Space Shuttle, RTF

Glenn Refractory Adhesive for Bonding and Exterior Repair (GRABER) Developed for Repairing Shuttle Damage

Advanced in-space repair technologies for reinforced carbon/carbon composite (RCC) thermal protection system (TPS) structures are critically needed for the space shuttle Return To Flight (RTF) efforts. These technologies are also critical for the repair and refurbishment of thermal protection system structures of future Crew Exploration Vehicles of space exploration programs. The Glenn Refractory Adhesive for Bonding and Exterior Repair (GRABER) material developed at the NASA Glenn Research Center has demonstrated capabilities for repair of small cracks and damage in RCC leading-edge material. The concept consists of preparing an adhesive paste of desired ceramic in a polymer/phenolic resin matrix with appropriate additives, such as surfactants, and then applying the paste into the damaged or cracked area of the RCC composite components with caulking guns. The adhesive paste cures at 100 to 120 °C and transforms into a high-temperature ceramic during simulated vehicle reentry testing conditions.

A number of plasma torch and arc-jet tests were carried out to evaluate the crack repair capability of GRABER materials for RCC composites. Cracks were introduced in RCC specimens by machining slots and filling them with GRABER repair compound. Six RCC specimens with 0.035- and 0.064-in. machined slots were repaired with GRABER, and the repaired specimens were tested in the arc-jet facilities at the NASA Johnson Space Center and the NASA Ames Research Center for approximately 15 min. All six samples



GRABER-repaired RCC specimen after arc-jet testing. The crack was 1.5 in. long and 0.035 in. wide. The specimen survived simulated reentry testing.

survived the tests without any burn through. This photograph shows the front view of a crack-repaired RCC specimen after arc-jet testing. The

GRABER-based repair materials stopped the plasma flow through the specimen and prevented any damage. It is important to point out that unrepaired RCC specimens with a similar type of damage will have significant burn through because of plasma oxidation, which transforms the small crack region into a large hole, leading to catastrophic damage.

GRABER-based materials have multifunctionality and versatility for a wide variety of repair applications. They have been used as adhesives and sealants in the patch/plug concept and have performed exceptionally well in plasma-torch and arc-jet testing. These materials have also shown exceptional plasma performance as inner-to-outer mold line materials for a filled-wing concept. The materials are being used to prepare adhesive patches and flexible ceramic prepreps using different types of fabrics to repair large damaged areas. Further development and testing are underway to optimize the materials' properties and extend the application temperatures.

Find out more about this research:

Materials Division highlights, 2004:

<http://www.grc.nasa.gov/WWW/MDWeb/hilights/HCY2004.html>

Materials Division highlights, July 2004:

<http://www.grc.nasa.gov/WWW/MDWeb/hilights/Cy2004/H072004.html>

On-orbit shuttle repair takes shape:
<http://www.aiaa.org/aerospace/images/articleimages/pdf/lannottaugust04.pdf>

Making the Space Shuttles Safer: Return To Flight Efforts at Glenn:
http://www.nasa.gov/centers/glenn/projects/RTF_summary.html

QSS Group, Inc., contact:
 Dr. Mrityunjay Singh, 216-433-8883,
 Mrityunjay.Singh@grc.nasa.gov

Glenn contact:
 Dr. Andrew J. Eckel, 216-433-8185,
 Andrew.J.Eckel@nasa.gov

Authors:
 Dr. Mrityunjay Singh and
 Tarah P. Shpargel

Headquarters program office:
 Space Operations Mission Directorate

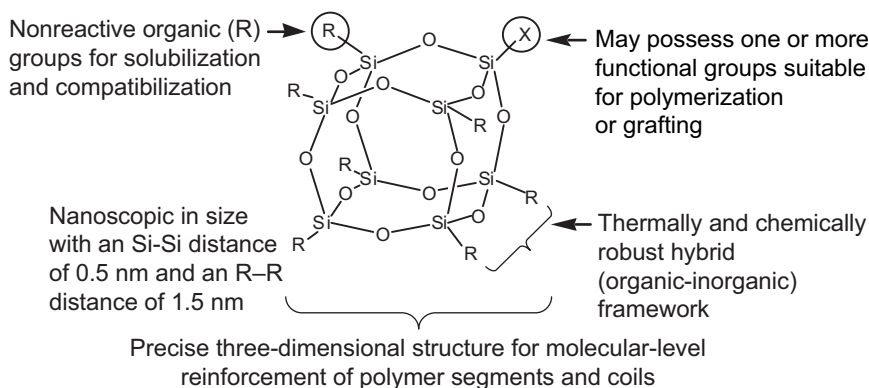
Programs/Projects:
 Space Shuttle, RTF

Properties of PMR Polyimides Improved by Preparation of Polyhedral Oligomeric Silsesquioxane (POSS) Nanocomposites

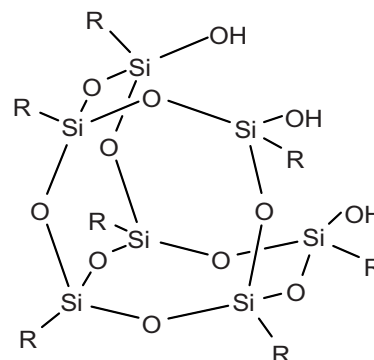
The field of hybrid organic-inorganic materials has grown drastically over the last several years. This interest stems from our ever-increasing ability to custom-build and control molecular structure at several length scales. This ability to control both the composition and structure of hybrid materials is sometimes broadly referred to as nanocomposite systems. One class of hybrid (organic-inorganic) nanostructured material is polyhedral oligomeric silsesquioxane (POSS), shown in the diagram on the left. The hybrid composition gives POSS materials dramatically enhanced properties relative to traditional hydrocarbons and inorganics. An important benefit of this technology is that it makes possible the formulations of nanostructured chemicals with excellent thermal

and oxidative stability. This is largely due to the inorganic component.

Researchers at the NASA Glenn Research Center investigated adding two different functional POSS triols (R: ethyl and phenyl) to improve the properties of a polymerization of monomeric reactants (PMR) resin (see the diagram on the right). Both



Anatomy of a POSS chemical.



Chemical structures of POSS triol.

of these POSS-triol monomers are easily dissolved in methanol, which makes them well suited for typical PMR formulation approaches.

The PMR polyimide resin (HFPE-II-52, a NASA second-generation polyimide resin) was prepared with different amounts of POSS triol. Both neat resins and carbon-fiber-reinforced polymer matrix composites were processed using the currently optimized HFPE-II-52 processing cycle. Physical and mechanical characterization—differential scanning calorimetry, thermogravimetric analysis (TGA), and dynamical mechanical analysis (DMA)—of resins with POSS incorporation were performed and compared with the control.

Initial experiments were performed to analyze any influence the addition of POSS to HFPE may have on the chemistry of the system. Differential scanning

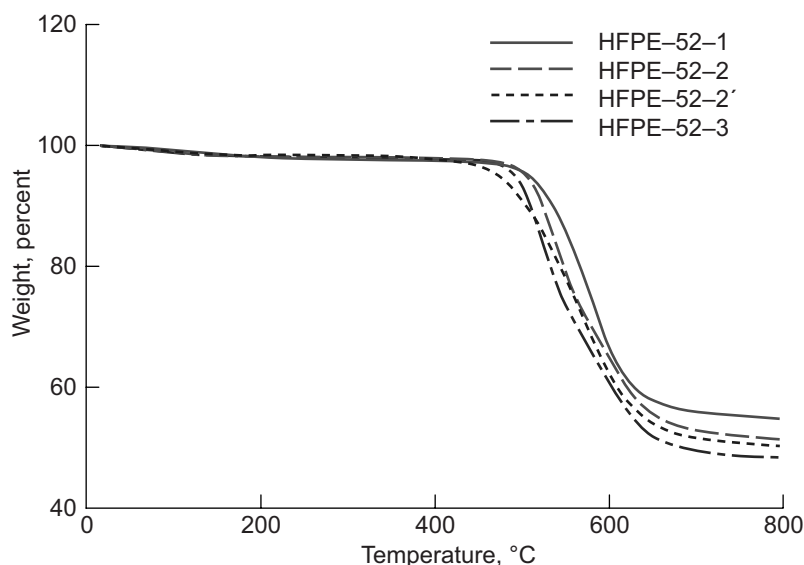
calorimetry results indicated that the addition of POSS did not affect the cross-linking reaction of the endcaps. In addition, Fourier transform infrared microscopy analysis showed no effect on imidization.

A critical issue with aerospace resins is the high-temperature stability of the material. The top graph shows the TGA traces of HFPE-II-52 with POSS triols added and compared with the control sample.

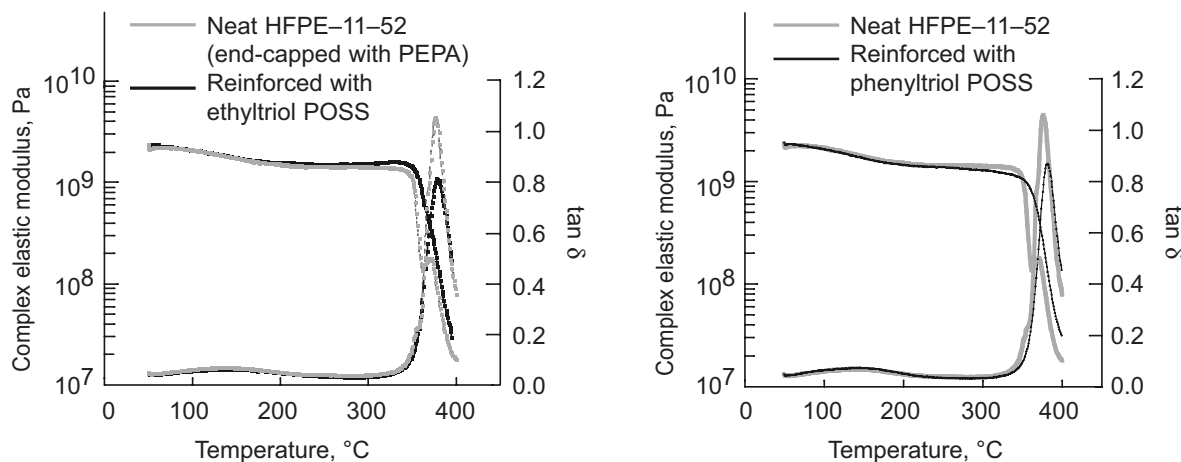
By TGA, HFPE-II-52 with POSS inclusions showed an enhanced thermal stability in a nitrogen (N_2) environment. These experiments will be repeated in normal air and oxygen (O_2) environments to examine the oxidative stability.

DMA was performed to examine the thermomechanical properties of these hybrid organic-inorganic polyimides. The bottom graphs show that samples reinforced with POSS triol exhibit an improved high-temperature dimensional stability in comparison to the control HFPE-II-52.

In summary, it has been demonstrated that nanostructured chemicals such as POSS can be incorporated into high-performance resins using the standard PMR approach. The



TGA traces of HFPE-II-52 containing 15 wt% of two moieties of POSS triol. This figure is shown in color in the online version of this article (<http://www.grc.nasa.gov/WWW/RT/2004/RM/RM05P-campbell.html>).



Left: DMA of neat HFPE-II-52 and HFPE-II-52 reinforced with 15 wt% of ethyltriol POSS. Right: DMA of neat HFPE-II-52 and HFPE-II-52 reinforced with 15 wt% of phenyltriol POSS, where $\tan \delta$ is the (loss modulus)/(storage modulus): that is, (energy lost as heat)/(energy stored elastically). This figure is shown in color in the online version of this article (<http://www.grc.nasa.gov/WWW/RT/2004/RM/RM05P-campbell.html>).

incorporation of these hybrid nanostructured chemicals will improve the thermal and dimensional stability of high-temperature thermoset polyimides.

This work was performed at the NASA Glenn Research Center by Professor Andre Lee from Michigan State University. Professor Lee worked at Glenn through the NASA Faculty Fellowship Program.

Find out more about this research:

<http://www.grc.nasa.gov/WWW/MDWeb/5150/Polymers.html>

Glenn contact:

Sandi G. Campbell, 216-433-8489, Sandi.G.Campbell@nasa.gov

Michigan State University contact:

Prof. Andre Lee, 517-355-5112, leea@msu.edu

Authors:

Sandi G. Campbell and Prof. Andre Lee

Headquarters program office:

Aeronautics Research

Programs/Projects:

VSP, UEET

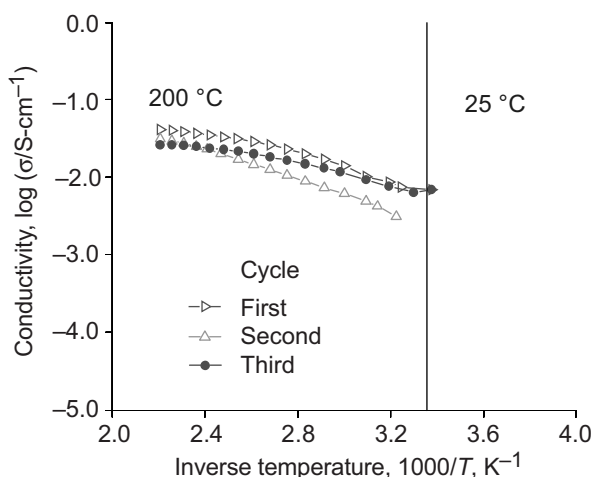
Nonhumidified High-Temperature Membranes Developed for Proton Exchange Membrane Fuel Cells

Fuel cells are being considered for a wide variety of aerospace applications. One of the most versatile types of fuel cells is the proton-exchange-membrane (PEM) fuel cell. PEM fuel cells can be easily scaled to meet the power and space requirements of a specific application. For example, small 100-W PEM fuel cells are being considered for personal power for extravehicular activity suit applications, whereas larger PEM fuel cells are being designed for primary power in airplanes and in uninhabited air vehicles.

Typically, PEM fuel cells operate at temperatures up to 80 °C. To increase the efficiency and power density of the fuel cell system, researchers are pursuing methods to extend the operating temperature of the PEM fuel cell to 180 °C. The most widely used membranes in PEM fuel cells are Nafion 112 and Nafion 117—sulfonated perfluorinated polyethers that were developed by DuPont. In addition to their relatively high cost, the properties of these membranes limit their use in a PEM fuel cell to around 80 °C. The proton conductivity of Nafion membranes significantly decreases above 80 °C because the membrane dehydrates. The useful operating range of Nafion-based PEM fuel cells can be extended to over 100 °C if ancillary equipment, such as compressors and humidifiers, is added to maintain moisture levels within the membrane. However, the addition of these components reduces the power density and increases the complexity of the fuel cell system.

Researchers at the NASA Glenn Research Center have developed a new type of membrane material (GRC AeroM) for use in PEM fuel cells that has excellent proton conductivity at temperatures as high as 180 °C. The unique feature of these membranes is that they do not require any external

humidification to operate. The membranes were designed to take advantage of novel microencapsulation methods and advanced membrane designs being pursued by Glenn's Polymer Branch. The resulting membranes have demonstrated excellent reproducible and stable ionic conductivity even after 24 hr of cycling the membrane temperature from 23 to 180 °C (see the graph on the preceding



Conductivity data for GRC AeroM as function of temperature. Multiple temperature cycles shown.

page). Plans for future work focus on constructing membrane electrode assemblies with these materials and testing them in a single-cell hydrogen-air fuel cell.

Find out more about this research:

<http://www.grc.nasa.gov/WWW/MDWeb/5150/Polymers.html>

Glenn contacts:

Dr. James D. Kinder, 216-433-3149, James.D.Kinder@nasa.gov; and
Dr. Michael A. Meador, 216-433-9518, Michael.A.Meador@nasa.gov

Author:

Dr. James D. Kinder

Headquarters program office:

Aeronautics Research

Programs/Projects:

VSP, LEAP

Fluorescent “On-Off” Sensors Studied for Chemical Warfare Agents

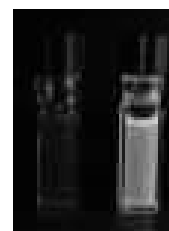
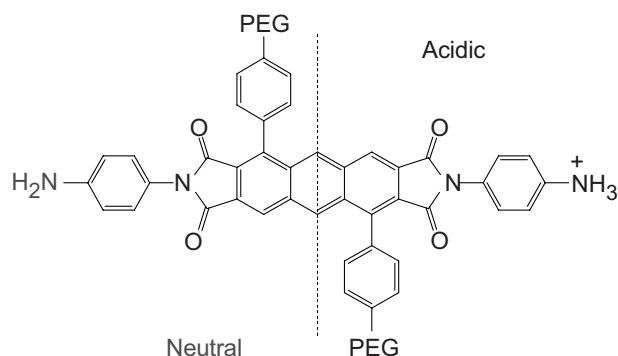
Sensing of chemical warfare agents is a topic of current and growing interest. Chemical agents can be detected or signaled by changes in photoinduced properties, such as absorption (color), emission intensity (brightness), and luminescence wavelength (color of emission). Quenching of photoluminescence intensity is of particular interest since sensitivity is inherently enhanced because of a distinct contrast between signaling events (i.e., luminescent and nonluminescent states). Researchers have utilized photoinduced electron transfer (PET), energy transfer, and other methods to produce on/off sensors based on aromatic and polycyclic aromatic hydrocarbons, aromatic heterocycles, and transition metal complexes. Each approach targets specific sensing applications and maintains distinct advantages and disadvantages that warrant continued investigations.

At the NASA Glenn Research Center, our approach to chemical sensors is based on creating new luminescent species that can be adapted to respond to generic or specific target molecules. Specifically, an aminofunctionalized anthracene bisimide (ABI-NH₂) (ref. 1) was synthesized and evaluated as a sensory material for highly reactive chemical species. Anthracene was utilized as the luminescent core because of its relative abundance (i.e., low cost) and depth of synthetic manipulation. Anthracene also possesses favorable photophysical properties, such as strong absorption and high quantum yield. Limitations include photoinduced cycloaddition reactions, including dimerization under concentrated conditions and formation of peroxides in the presence of oxygen.

ABI-NH₂ was prepared using standard and advanced synthetic methodology, and its chemosensory behavior was studied (ref. 2). Photophysical evaluation of ABI-NO₂, the precursor and model for ABI-NH₂, in N, N-dimethylformamide (DMF) revealed unique properties, in comparison to anthracene, including visible absorption, green fluorescence, and photostability in the presence of

oxygen. Unlike the nitrosubstituted compound, emission from ABI-NH₂ was quenched via efficient intramolecular photoinduced electron transfer (PET) from the amine substituents.

Reaction of ABI-NH₂ with common acid halides, such as thionyl chloride and acetyl chloride, resulted in dramatic fluorescence enhancement.



Representation of sensing behavior. Top: ABI-NH₂ in neutral and acidic environments. PEG, polyethylene glycol. Bottom: Off-on luminescence sensing.

Acids, such as hydrochloric acid or trifluoroacetic acid, also turned “on” the luminescence of ABI-NH₂ by a reversible dequenching process. In addition, acid halides of organophosphates, such as methylphosphonic dichloride and dimethylphosphinic chloride, initiated the luminescence of ABI-NH₂. These analytes were chosen to mimic the reactivity of organophosphate-based nerve gases (e.g., sarin gas). These data suggest that ABI-NH₂ could be applied for the early detection of toxic chemicals.

References

1. Morris, J.L., et al.: Synthesis of Extended Linear Aromatics Using Tandem Diels-Alder Aromatization Reactions. *J. Org. Chem.*, vol. 59, no. 21, 1994, pp. 6484–6486.
2. Ilhan, F.; Tyson, D.S.; and Meador, M.A.: Synthesis and Chemosensory Behavior of Anthracene Bisimide Derivatives. *Chem. Mater.*, vol. 16, 2004, pp. 2978–2980.

Glenn contact:

Dr. Michael A. Meador, 216–433–9518,
Michael.A.Meador@nasa.gov

Ohio Aerospace Institute (OAI) contacts:

Dr. Daniel S. Tyson, 216–433–3188,
Daniel.S.Tyson@grc.nasa.gov; and
Dr. Faysal Ilhan, 216–433–6094,
Ulvi.F.Ilhan@grc.nasa.gov

Authors:

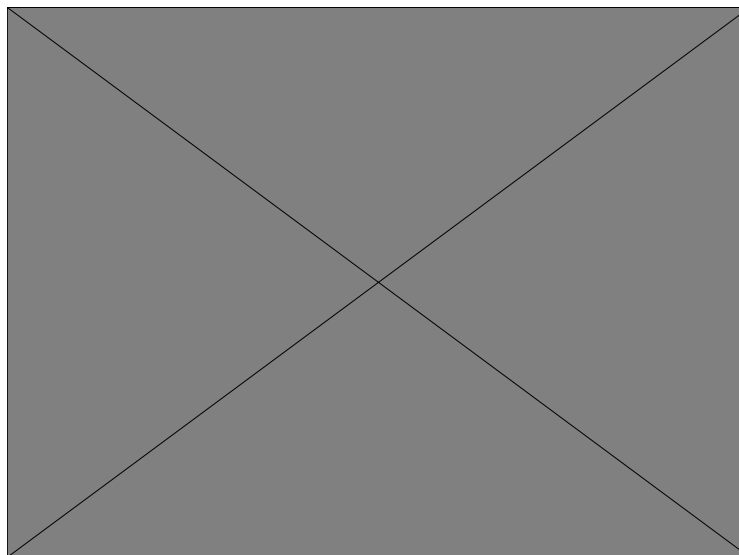
Dr. Daniel S. Tyson, Dr. Faysal Ilhan, and
Dr. Michael A. Meador

Headquarters program office:

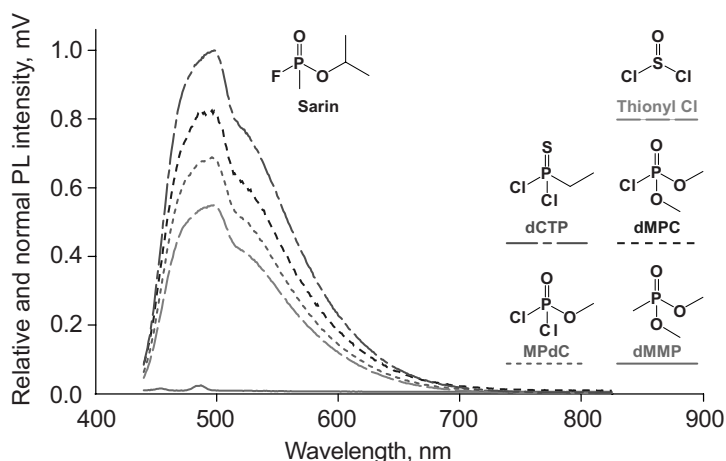
Aeronautics Research

Programs/Projects:

VSP, LEAP, AEFT, Glenn IR&D



Titration data. The complete curve represents three independent thionyl chloride experiments with varying initial concentrations of thionyl chloride. Inset: Selected emission spectra recorded with 425-nm excitation. This figure is shown in color in the online version of this article (<http://www.grc.nasa.gov/WWW/RT/2004/RM/RM07P-meador.html>).



Emission spectra. ABI-NH₂ in the presence of organophosphate-based substances similar to nerve gases. PL, photoluminescence.

Mechanical and Electrical Properties of a Polyimide Film Significantly Enhanced by the Addition of Single-Wall Carbon Nanotubes

Single-wall carbon nanotubes have been shown to possess a combination of outstanding mechanical, electrical, and thermal properties. The use of carbon nanotubes as an additive to improve the mechanical properties of polymers and/or enhance their thermal and electrical conductivity has been a topic of

intense interest. Nanotube-modified polymeric materials could find a variety of applications in NASA missions including large-area antennas, solar

arrays, and solar sails; radiation shielding materials for vehicles, habitats, and extravehicular activity suits; and multifunctional materials for vehicle structures and habitats. Use of these revolutionary materials could reduce vehicle weight significantly and improve vehicle performance and capabilities.

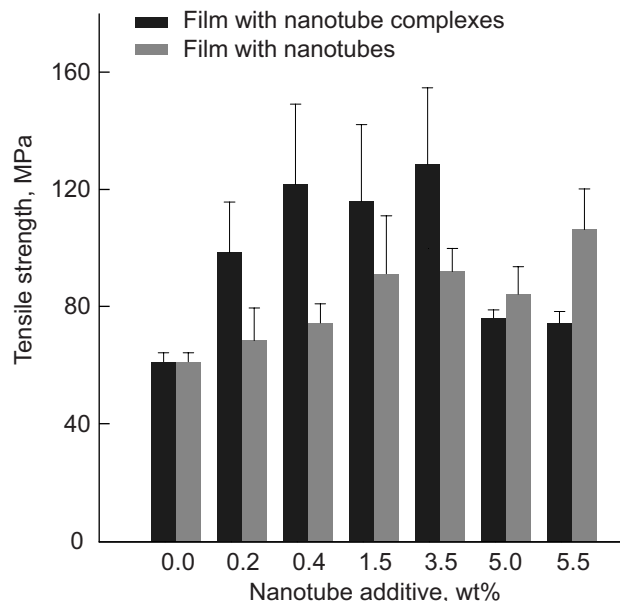
However, many of these applications may not be realized unless there are reliable methods to disperse nanotubes into the polymer matrix. By themselves, carbon nanotubes do not dissolve in most solvents, and they tend to agglomerate because of electrostatic (van der Waal's) interactions. Recent work at the NASA Glenn Research Center has focused on the development of molecular complexes between carbon nanotubes and large aromatic hydrocarbons to enhance the solubility of carbon nanotubes without adversely affecting their desirable properties. This work has led to new nanotube complexes that form colloidal dispersions in organic solvents. These suspensions are stable for days at room temperature and can be easily used in the fabrication of nanotube-reinforced polymer films.

A recent study compared the effect of adding varying amounts of nanotubes and nanotube complexes on the tensile strength and electrical conductivity of a polyimide film. The bar chart shows the results.

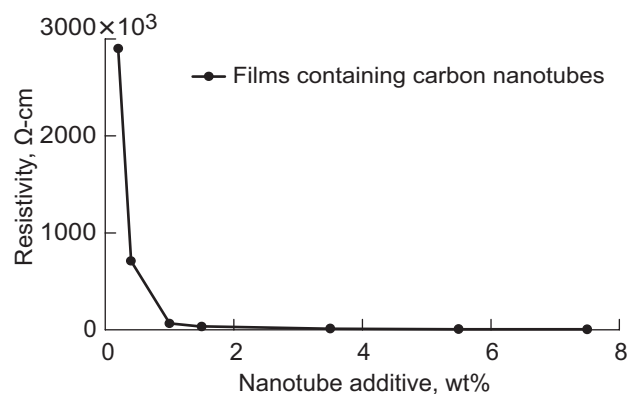
Addition of either nanotubes or nanotube complexes increased the tensile strength of the polyimide film. However, at low loading levels (below 3.5 wt%), addition of the nanotube complexes had a larger effect on tensile strength than the addition of the neat nanotubes did. Overall, addition of these complexes as much as doubled the tensile strength of the polyimide film.

The effect of added single-wall nanotubes on the resistivity of the same polyimide film is shown in the line graph. Addition of single-wall nanotubes resulted in as much as a 1000-fold decrease in film resistivity (this translates into 1000 times higher electrical conductivity). The effects of adding nanotube complexes on the resistivity of the polyimide are currently being measured.

These results demonstrate that mechanical properties and electrical conductivity of polymers can be altered significantly by the addition of small amounts (less than 10 wt%) of single-wall carbon nanotubes. Molecular complexes prepared with these nanotubes produce larger effects on mechanical property enhancement than do the neat nanotubes. Although the resistivities of films prepared with these complexes have not been measured, we anticipate that they will follow the same trends seen for the mechanical properties. This work suggests that nanotube-doped polymers could be used as multifunctional materials in future NASA missions.



Effect of addition of single-wall carbon nanotubes or nanotube complexes on the tensile strength of a polyimide film.



Effect of added single-wall carbon nanotubes on the resistivity of a polyimide film.

Glenn contacts:

Marisabel Lebron, 216-433-2292,
Marisabel.Lebron-Colon-1@nasa.gov;
and Dr. Michael A. Meador, 216-433-9518,
Michael.A.Meador@nasa.gov

Author:

Dr. Michael A. Meador

Headquarters program office:

Aeronautics Research

Programs/Projects:

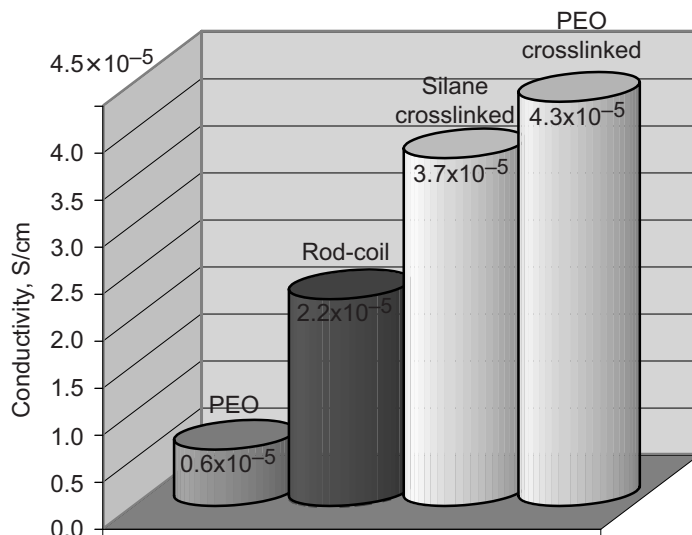
VSP, LEAP, AEFT

Novel Elastomeric Membranes Developed for Polymer Electrolytes in Lithium Batteries

Lithium-based polymer batteries for aerospace applications need to be highly conductive from -70 to 70 °C. State-of-the-art polymer electrolytes are based on polyethylene oxide (PEO) because of the ability of its ether linkages to solvate lithium ions. Unfortunately, PEO has a tendency to form crystalline regions below 60 °C, dramatically lowering conductivity below this temperature. PEO has acceptable ionic conductivities (10^{-4} to 10^{-3} S/cm) above 60 °C, but it is not mechanically strong. The room-temperature conductivity of PEO can be increased by adding solvent or plasticizers, but this comes at the expense of thermal and mechanical stability. One of NASA Glenn Research Center's objectives in the Polymer Rechargeable System program (PERS) is to develop novel polymer electrolytes that are highly conductive at and below room temperature without added solvents or plasticizers.

Glenn previously produced a series of rod-coil block copolymers made from polyimide rods alternating with short PEO segments. When doped with lithium salts, these polymers were strong, flexible, thermally and mechanically stable up to high temperatures, and completely amorphous over the required temperature range. Furthermore, these polymers demonstrated room-temperature conductivities as high as 2.3×10^{-5} S/cm, in comparison to 6.0×10^{-6} S/cm for state-of-the-art PEO measured in-house.

Recently, Glenn researchers made new block copolymers that improve upon the conductivity of the rod-coil polymer systems while maintaining dimensional stability. In the new systems, the polyimide segment is replaced by a triazine molecule with three reactive sites toward primary amines. The third reactive position provides a site for both branching to increase conductivity and cross-linking to provide mechanical strength. Films have been cross-linked by silicon-oxygen bridges to provide a partial inorganic network. The most conductive films in this series have a room-temperature conductivity of 3.7×10^{-5} S/cm when doped with lithium salts. Films also have been cross-linked with PEO



Room-temperature conductivity of state-of-the-art PEO and previous rod-coil polyimides compared with new elastomeric polymers.

molecules that are terminated with primary amines at both ends. The highest conductivity obtained so far for these films is 4.3×10^{-5} S/cm. These new polymers are readily cast into rubbery freestanding films when cured at 160 °C. The polymer films are stable to over 300 °C and can be stretched to over 7 times their original length.

Find out more about this research:
<http://www.grc.nasa.gov/WWW/MDWeb/5150/Polymers.html>

Ohio Aerospace Institute (OAI) contact:

Dr. Dean M. Tigelaar, 216-433-3667,
 Dean.M.Tigelaar@grc.nasa.gov

Glenn contact:

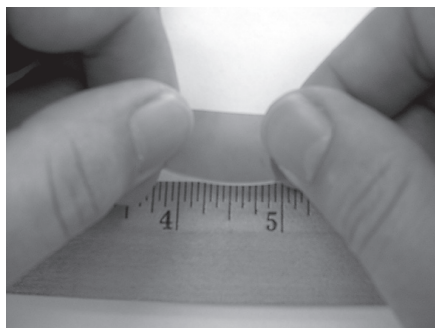
Dr. Maryann B. Meador, 216-433-3221,
 Maryann.Meador-1@nasa.gov

Authors:

Dr. Dean M. Tigelaar,
 Dr. Maryann B. Meador,
 Dr. James D. Kinder, and
 William R. Bennett

Headquarters program office:
 Exploration Systems

Programs/Projects:
 Energetics, PERS



Silane cross-linked elastomer before and after stretching.

High-Temperature Polymer Composites Tested for Hypersonic Rocket Combustor Backup Structure

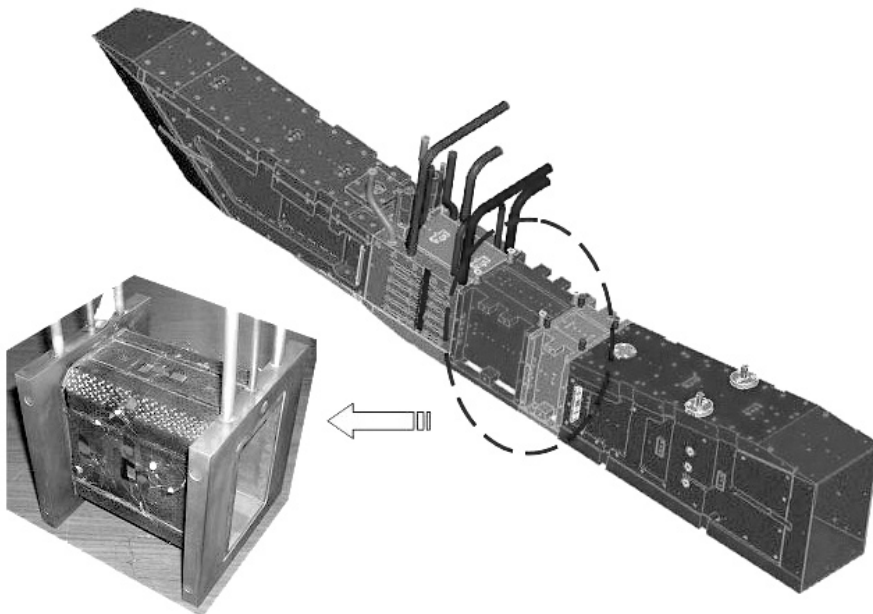
Significant component weight reductions are required to achieve the aggressive thrust-to-weight goals for the Rocket Based Combined Cycle (RBCC) third-generation, reusable liquid propellant rocket engine, which is one possible engine for a future single-stage-to-orbit vehicle. A collaboration between the NASA Glenn Research Center and Boeing Rocketdyne was formed under the Higher Operating Temperature Propulsion Components (HOTPC) program and, currently, the Ultra-Efficient Engine Technology (UEET) Project to develop carbon-fiber-reinforced high-temperature polymer matrix composites (HTPMCs). This program focused primarily on the combustor backup structure to replace all metallic support components with a much lighter polymer-matrix-composite- (PMC-) titanium honeycomb sandwich structure (refs. 1 to 3).

On the basis of literature and database analyses and scouting feasibility studies, a Glenn-developed second-generation polymerization of monomeric reactants (PMR) polyimide resin (PMR-II-50) composite reinforced with a carbon fiber (M40J) was considered for the high-temperature facesheet of the sandwich structure that required substantial stiffness to contain deflections in the combustor. Challenges were raised because of the severe rocket engine environments—including the extremely high power density, temperature extremes (up to 600 °F), high thermal gradients, severe thermal shock under humid conditions (maximum heat-up rate ~250 °F/sec), extreme fluid flow rates and pressure changes (from 0 to 100 psi over approximately 100 sec), reactive propellants and complex dynamics, and geometric restriction of the rectangular combustion chamber design. Finally, the significant mismatch of the thermal

expansion between the combustor inner metal jacket and PMC facesheet was another challenge to the design and manufacturing of this sandwich structure.

A multiteam collaboration was established to validate and optimize the use of the dissimilar materials. The tasks performed in this validation included evaluating the PMC structure-process-property relations, understanding the performance durability for both coupons and subcomponents, applying high-temperature adhesive bonding and surface treatments, performing finite element modeling for various component configurations as a function of thermal- and pressure-loading conditions, optimizing the design and manufacturing of the subscale and full-scale structures, and conducting a full-scale engine simulation of the complete combustor. This building-block approach was adopted for a successful integration of all these materials into the PMC combustor support structure. Risks were minimized through extensive design analysis, testing of the PMC panels and Pathfinder sandwich panels, and fabricating demonstrators.

During the design of the lightweight support structure (see the illustration to the left), PMC corner clips were added to stabilize combustor wall deflections. The combination of thicker adhesive layers and optimized posture conditions improved bond strength, which significantly reduced the thermal expansion mismatch and the components' residual stresses. The hot-fire testing of the HTPMC combustor support structure for the RBCC engine was successfully conducted at ATK-General Applied Science Laboratory (GASL) (see the photograph on the next page).



Artist's rendering of typical all-metal A5 RBCC engine and photograph of the PMC-supported combustor.

This testing concluded a 3-year collaboration between Glenn and Boeing.

The support structure successfully survived a total of eight hot-fire test runs: that is, it met the design specifications by withstanding up to 50-psig chamber pressure at 285 °F PMC temperature under 4000 °F combustion gas with 10 ft/sec and 1450-psia water cooling for durations of 40 to 60 sec. The Computer Aided Tap Tester nondestructive evaluation verified the structural integrity of the PMC facesheets, core, and bondlines before and after each hot-fire test. Significant weight reductions were achieved. A Boeing Company tradeoff study indicated that replacing the all-metal support structure with the PMC-titanium honeycomb structure afforded a weight savings of up to 77 percent and an overall combustor weight savings of ~25 percent.

In addition to satisfying an important technical milestone, this activity is noteworthy because it constitutes a number of firsts. This was the first application for Rocketdyne of an HTPMC in a space propulsion component. Successful completion of this test will enable Rocketdyne to explore other applications for HTPMCs in their engines. It was also the first time that a full-scale PMC structure had been tested at GASL. Experience gained from this testing will enable GASL to more easily test similar structures.

This research was supported by the (HOTPC) Program managed by Carol Ginty. We would like to express our gratitude to the following groups for their collaboration on this project: Ohio Aerospace Institute (OAI), Air Force Research Laboratory (AFRL–MLBC and AFRL–MLS), University of Denver, Adherent Technologies, Gougeon Brothers, Inc., SRI, Maverick Corp., YLA, Inc., Intec, Inc., Boeing-Long Beach, Boeing Phantom Works—Seattle, Canyon Composites, Inc., Fiber Innovation, Inc., and Innovative Ind.

Bibliography

Sutter, J.K.: High-Temperature Polymers in Aerospace Applications. Proceedings of the 14th International Conference on Composite Materials (ICCM–14), session 219, Paper ID no. 1684, San Diego, CA, 2003.

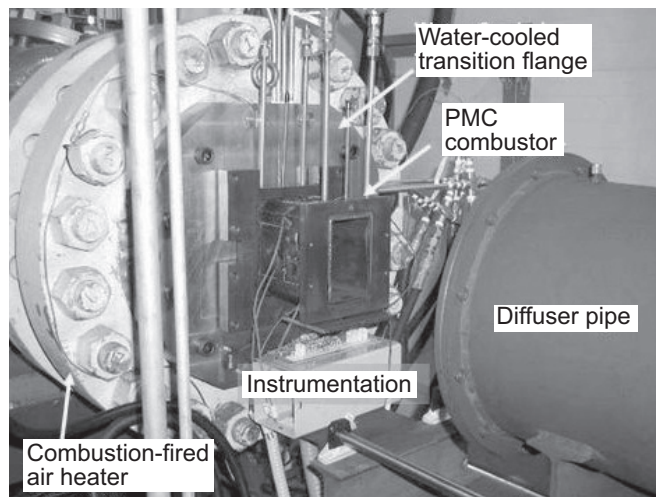
Shin, E. Eugene, et al.: Design and Fabrication Issues of High Temperature PMCs for Aerospace Propulsion Applications. SAMPE 2002, Long Beach, CA, 2002, pp. 341–355.

Thesken, John C., et al.: High-Temperature Polymer Composites Studied for Space Propulsion Applications. Research & Technology 2002. NASA/TM—2003-211990, 2003, pp. 31–32. <http://www.grc.nasa.gov/WWW/RT2002/5000/5150sutter.html>

Find out more about this research:

NASA Glenn Research Center:

<http://www.nasa.gov/glenn/>



Hot-fire test setup of the PMC-supported combustor at GASL.

Polymers Branch:

<http://www.grc.nasa.gov/WWW/MDWeb/5150/Polymers.html>

Life Prediction Branch:

<http://www.grc.nasa.gov/WWW/LPB/>

Boeing-Rocketdyne:

<http://www.boeing.com/space/rdyne/>

Glenn contact:

Dr. James K. Sutter, 216–433–3226, James.K.Sutter@nasa.gov

Ohio Aerospace Institute (OAI) contacts:

Dr. E. Eugene Shin, 216–433–2544, E.Eugene.Shin@grc.nasa.gov; and Dr. John C. Thesken, 216–433–3012, John.C.Thesken@grc.nasa.gov

Boeing-Rocketdyne Division contact:

Jeffrey E. Fink, 818–586–7253, Jeffrey.E.Fink@Boeing.com

Authors:

Dr. E. Eugene Shin, Dr. James K. Sutter, Dr. John C. Thesken, and Jeffrey E. Fink

Headquarters program office:

Aeronautics Research

Programs/Projects:

VSP, HOTPC, UEET/HLLWCT

Mechanically Strong, Lightweight Porous Materials Developed (X-Aerogels)

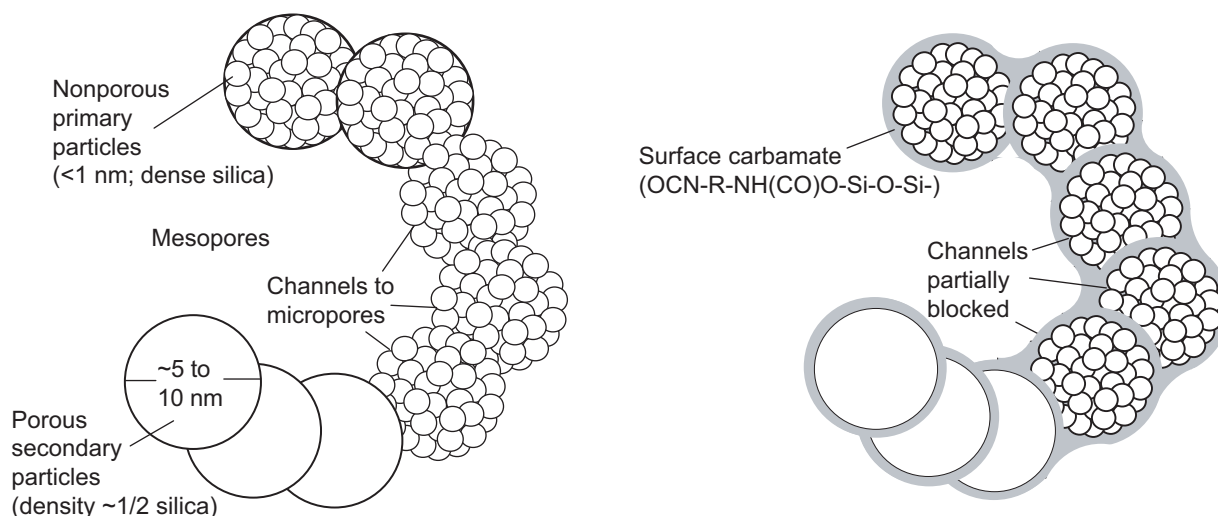
Aerogels are attractive materials for a variety of NASA missions because they are ultralightweight, have low thermal conductivity and low-dielectric constants, and can be readily doped with other materials. Potential NASA applications for these materials include lightweight insulation for spacecraft, habitats, and extravehicular activity (EVA) suits; catalyst supports for fuel cell and in situ resource utilization; and sensors for air- and water-quality monitoring for vehicles, habitats, and EVA suits. Conventional aerogels are extremely fragile and require processing via supercritical fluid extraction, which adds cost to the production of an aerogel and limits the sizes and geometries of samples that can be produced from these materials. These issues have severely hampered the application of aerogels in NASA missions.

Researchers at the NASA Glenn Research Center have developed a new class of strong lightweight materials, named X-Aerogels. These materials are produced by reacting the internal (mesoporous) surfaces of porous networks of inorganic nanoparticles with polymeric crosslinking agents. The following illustration shows a schematic of the microstructure of a typical aerogel before and after modification with an isocyanate. Reaction of the aerogel with an isocyanate monomer results in the formation of conformal polyurethane/polyurea coating around the nanoparticles.

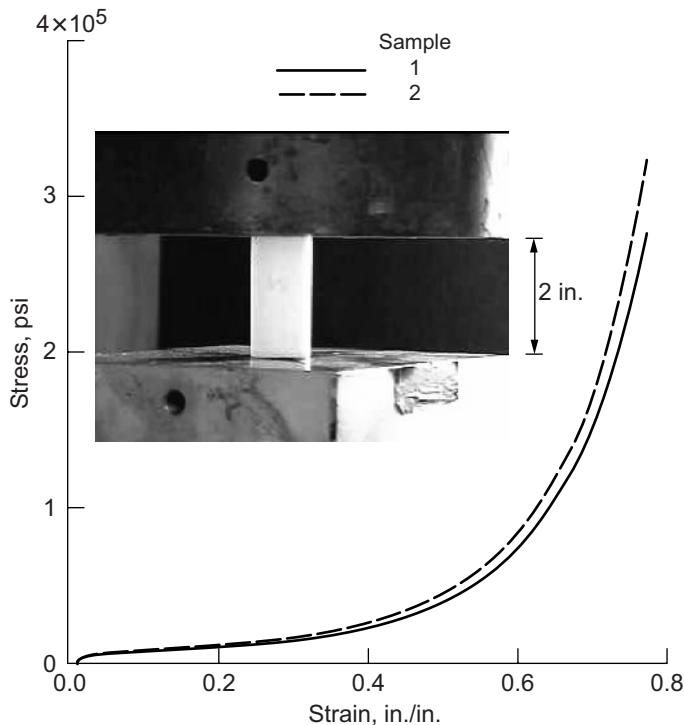
The most striking feature of these novel aerogels is that, for a nominal increase (no more than threefold) in density, their mechanical strength can be increased by up to 300 times that of the unmodified, conventional aerogel. In addition, the specific compressive strength of these materials is ~10 times that of steel. The graph on the next page shows the stress-strain curve of a typical X-Aerogel monolith under a compressive load. Under compression, these aerogels fail

at a load of about 30,000 psi, where the sample has been compressed to ~80 percent of its original length with no buckling and only a minimal "swelling" (~20 percent). This occurs mostly during the last stages of compression. The thermal conductivity of these new aerogels is in the range of only 20 to 40 mW/mK, about 3 to 6 times that of a conventional aerogel. Ongoing research with these materials is focused on reducing their density and thermal conductivity while maintaining acceptable mechanical properties.

Other Glenn research is focused on extending this approach to the development of other aerogel materials. Two parallel approaches are being explored—(1) developing aerogels from other inorganic materials besides silica and (2) utilizing other polymer cross-linkers besides diisocyanates. Along these lines, this chemistry has been successfully demonstrated with more than 35 different



Microstructure of a silica aerogel cross-linked with polyurethane/polyurea (X-Aerogel).

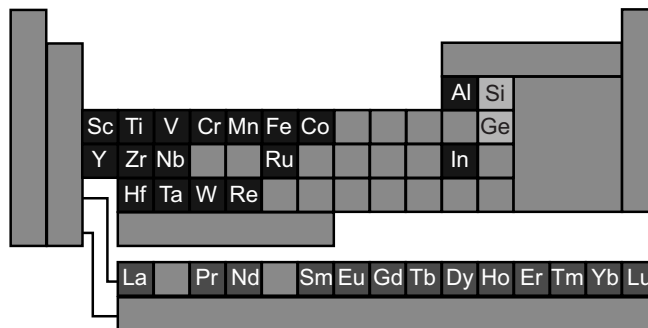


Stress-strain curves from a compressive strength test of an isocyanate cross-linked X-Aerogel monolith ($\sim 0.45 \text{ g/cm}^3$, 0.7 in. diam, 1.5 in. long). (Data obtained by Prof. Samit Roy of Oklahoma State University).

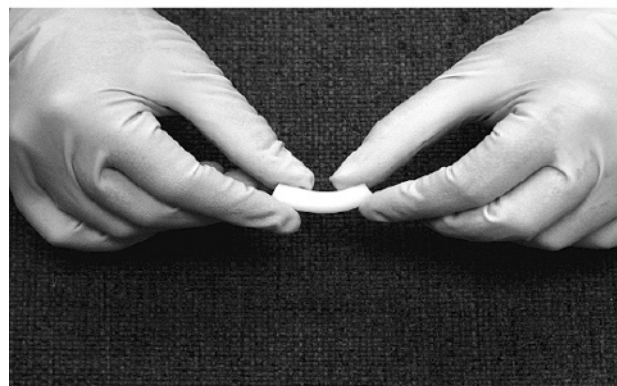
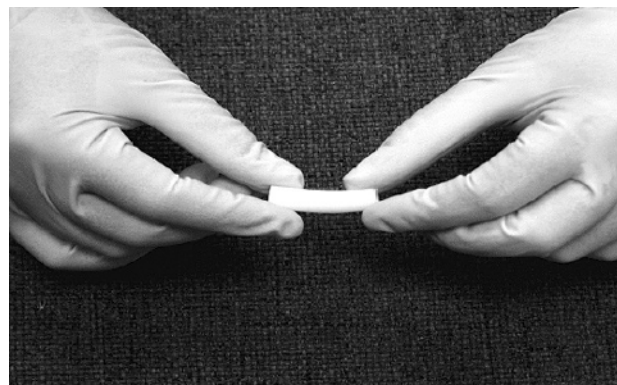
metal and semimetal oxide aerogels utilizing isocyanates as the cross-linking agent (see the periodic table). Many of these new aerogel materials may have unique optical, magnetic, or electrical properties.

In addition, the surfaces of the silica aerogels have been modified with (1) amines that have then been cross-linked with epoxies and (2) olefins, such as polystyrene. Polystyrene, because of its high hydrogen content, has been shown to be an effective radiation shielding material. The radiation shielding capabilities of polystyrene cross-linked aerogels are currently under investigation. It may be possible that these new aerogels could afford both radiation protection and thermal insulation to astronauts on future exploration missions. Silica-based X-Aerogel chemistry has also been modified to produce flexible systems (see the photographs). These new aerogel compositions could be used as EVA suit insulation, where conventional aerogels cannot be used because they are too rigid and fragile.

In addition to the NASA mission applications discussed above, X-Aerogels could find use in a variety of nonaerospace applications, including catalyst supports for automotive and industrial applications, thermal and acoustic insulation materials for construction, optoelectronic devices, and packaging of sensitive electronic devices.



Periodic table showing elements that have been made into aerogels and have been successfully cross-linked into X-Aerogels.



Flexible, low-density ($\sim 50 \text{ mg/cm}^3$) isocyanate cross-linked X-Aerogel.

Bibliography

Zhang, Guohui., et al.: Isocyanate Cross-Linked Silica Aerogel Monoliths: Preparation and Characterization. *J. Non-Cryst. Solids*, vol. 350, 2004, pp. 152–164.

Bertino, M.F., et al.: Room Temperature Synthesis of Noble Metal Clusters in the Mesopores of Mechanically Strong Silica-Polymer Aerogel Composites. *J. Sol-Gel Sci. Tech.*, vol. 30, no. 1, 2004, pp. 43–48.

Leventis, Nicholas, et al.: Synthesis and Characterization of Ru(II) Tris(1,10-Phenanthroline)-Electron Acceptor Dyads Incorporating the 4-Benzoyl-N-Methylpyridinium Cation or N-Benzyl-N'-Methyl-Viologen. Improving the Dynamic Range, Sensitivity, and Response Time of Sol-Gel-Based Optical Oxygen Sensors. *Chem. Mater.*, vol. 16, 2004, pp. 1493–1506.

Bertino, M.F., et al.: High Resolution Patterning of Silica Aerogels. *J. Non-Cryst. Solids*, vol. 333, 2004, pp. 108–110.

Zhang, G., et al.: Isocyanate Cross-Linked Silica: Structurally Strong Aerogels. *Polymer Preprints*, vol. 44, no. 1, 2003, pp. 35–36.

Find out more about NASA Glenn:

<http://www.nasa.gov/glenn/>

Glenn contact:

Dr. Nicholas Leventis, 216–433–3202,
Nicholas.Leventis-1@nasa.gov

Author:

Dr. Nicholas Leventis

Headquarters program office:

Aeronautics Research

Programs/Projects:

IR&D

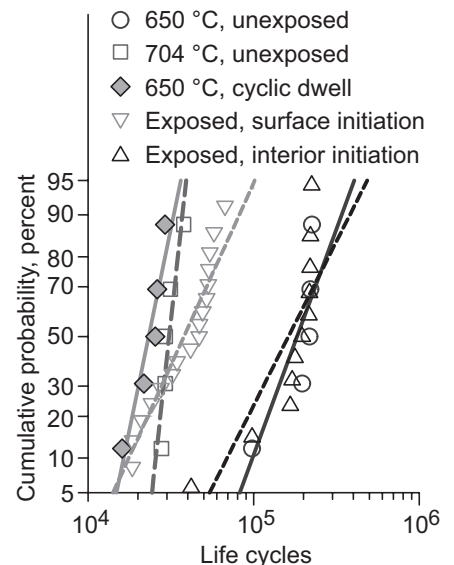
Effects of High-Temperature Exposures on the Fatigue Life of Disk Superalloys Examined

Tests used to characterize the low-cycle-fatigue resistance of disk superalloys are usually performed at cyclic frequencies of 0.33 Hz or faster. However, service conditions for disks in some aerospace and land-based gas turbine engines can produce major cycle periods extending from minutes to hours and days.

Over a service life, this can produce total service times near the maximum temperature that exceed 100 hr for aerospace applications and 100,000 hr for land-based applications. Such time-dependent effects of realistic mission cycles on fatigue resistance can be significant in superalloy disks, and need to be considered for accurate disk life prediction.

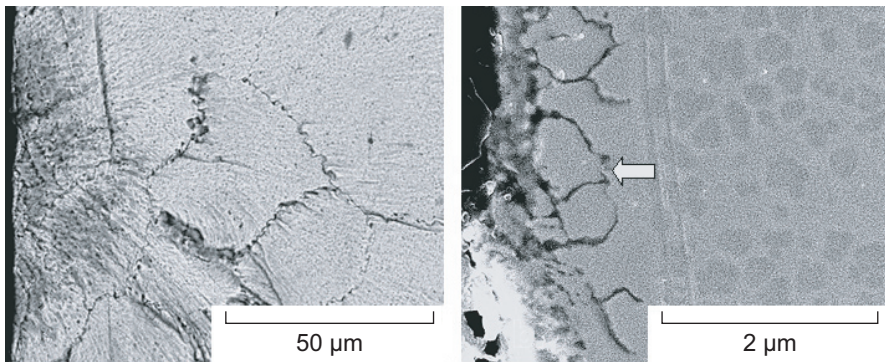
The purpose of this study at the NASA Glenn Research Center was to examine the effects of extended exposures and extended cycle periods on the fatigue resistance of two disk superalloys. Current alloy Udimet 720 (Special Metals Corporation, Huntington, WV) disk material was provided by Solar Turbines/Caterpillar Co., and advanced alloy ME3 was provided by the NASA Ultra-Efficient Engine Technologies (UEET) Project, in powder-metallurgy-processed, supersolvus heat-treated form. Fatigue specimens were fully machined and exposed in air at temperatures of 650 to 704 °C for extended times. Then, they were tested using conventional fatigue tests with a total strain range of 0.70 percent and a minimum-to-maximum strain ratio of zero to determine the effects of prior exposure on fatigue resistance. Subsequent tests with extended dwells at minimum strain in each fatigue cycle were performed to determine cyclic exposure effects.

The effects of various prior exposures at 650 to 704 °C for 100 to 1029 hr were first evaluated on Udimet 720 fatigue life and failure modes. Resulting Udimet 720 fatigue lives at 650 °C, including prior exposed and unexposed lives, could be generally grouped according to failure-initiation sites (see the graph on this page). Specimens failing from surface-oxide-initiated cracks had about 80-percent lower lives than those failing from internal cracks at inclusions or grain facets.



Udimet 720 fatigue lives for 0.70-percent strain range at 650 °C—including prior exposed, unexposed, and cyclic dwell lives—could be generally grouped by failure initiation sites.

Cyclic dwell tests at 650 °C were then performed with a dwell time based on the longest prior exposure time at 650 °C divided by the subsequent log mean cyclic life. These tests reduced mean lives by about 90 percent from unexposed, conventional test lives,

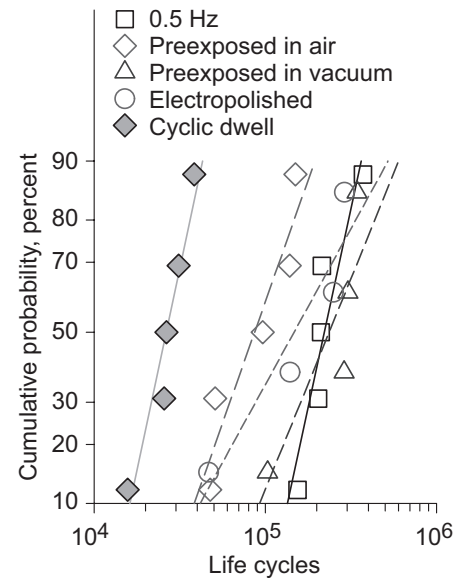


Fractured surfaces (left) and metallographic sections (right) showed failures initiated at surface oxidation for many exposed and all cyclic dwell specimens of Udimet 720 and ME3.

and specimens invariably failed from surface-oxide-initiated cracks (see the photomicrographs above). Cyclic dwell lives were lower than the preexposed lives, suggesting that the damage produced by each fatigue cycle and a dwell exposure can interact.

Further discriminating evaluations were performed using disk alloy ME3 with a constant total exposure time. Cyclic dwell tests were first performed on ME3 to get a log mean cyclic life of 26,362 cycles and test duration of 439 hr at the same strain conditions as before (see the graph on this page). This test duration time was then used as the prior exposure condition. The contribution of environmental attack was isolated by comparing prior exposures of 704 °C/439 hr in air versus vacuum. Prior exposure in air reduced fatigue life about 50 percent from unexposed levels, and induced surface-oxide-initiated failures. Prior exposures in vacuum did not significantly reduce subsequent mean fatigue life from unexposed levels, and did not induce surface failures. This indicated that the air environment was strongly contributing to the damage. Long exposures could also be detrimental by reducing the beneficial compressive residual stresses produced near the specimen surface during machining. These effects were evaluated by electropolishing away the surface layer on several specimens before conventional fatigue testing. The fatigue lives of these specimens showed more scatter than for the unpolished specimens, but fatigue life was not consistently reduced by the electropolishing. This indicated that the relaxation of beneficial compressive residual stresses was not strongly driving the life reductions due to exposure. Cyclic dwell testing was again most damaging, reducing mean fatigue life about 90 percent in comparison to unexposed, conventional fatigue test life.

It was concluded that exposure effects can significantly influence disk superalloy fatigue lives by shifting the failure initiation sites from internal defects to environment-affected surface layers. Prior exposures of specimens can be used to help approximate some aspects of the exposure effects that may



Controlled experiments on ME3 for 0.70-percent strain range at 704 °C indicated that mixed cycling and exposure in air is life limiting.

occur during service by activating, to some degree, a fatigue cracking mechanism at surface oxidation. However, more realistic cyclic dwell tests produced the lowest lives here, and these can give more accurate indications of the effect of cumulative exposure on service lives.

Glenn contacts:

Tim Gabb, 216-433-3272, Timothy.P.Gabb@nasa.gov; and Jack Telesman, 216-433-3310, Ignacy.Telesman-1@nasa.gov

Ohio Aerospace Institute (OAI) contact:

Pete T. Kantzos, 216-433-5202, Pete.T.Kantzoz@grc.nasa.gov

Authors:

Dr. Tim P. Gabb, Dr. Jack Telesman, Dr. Pete T. Kantzos, and James W. Smith

Headquarters program office:

Aeronautics Research

Programs/Projects:

AvSSP, Ultra Safe, UEET

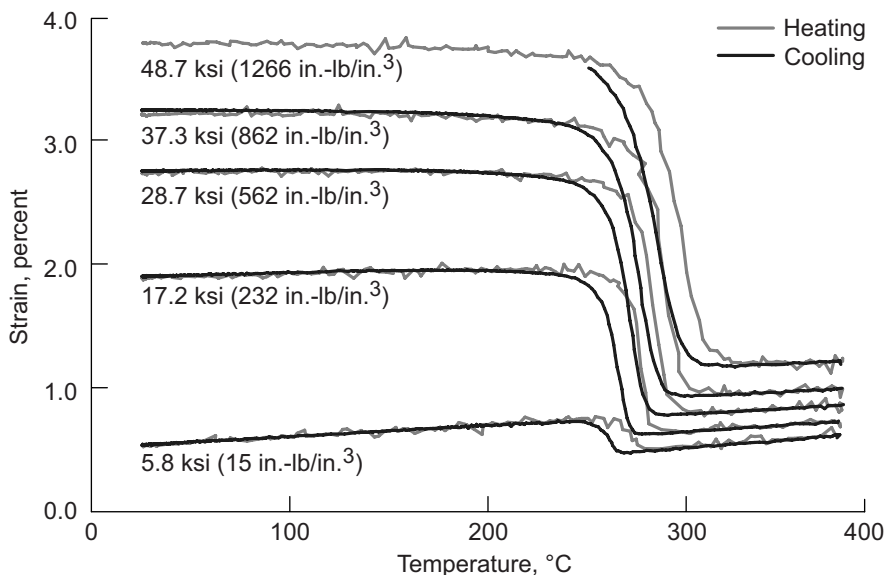
Potential High-Temperature Shape-Memory-Alloy Actuator Material Identified

Shape-memory alloys are unique “smart materials” that can be used in a wide variety of adaptive or “intelligent” components. Because of a martensitic solid-state phase transformation in these materials, they can display rather unusual mechanical properties including shape-memory behavior. This phenomenon occurs when the material is deformed at low temperatures (below the martensite finish temperature, M_f) and then heated through the martensite-to-austenite phase transformation. As the material is heated to the austenite finish temperature A_f , it is able to recover its predeformed shape. If a bias is applied to the material as it tries to recover its original shape, work can be extracted from the shape-memory alloy as it transforms. Therefore, shape-memory alloys are being considered for compact solid-state actuation devices to replace hydraulic, pneumatic, or motor-driven systems.

Currently available shape-memory alloys have a temperature limit of about 70 °C, and thus their use in turbine engines is quite restricted. The NASA Glenn Research Center has been investigating the properties of various ternary NiTi-X alloys to look for compositions that could be utilized as high-temperature shape-memory alloys for high-force actuator applications. Although many ternary NiTi-based alloys have high transformation temperatures, there are insufficient data to make a definitive determination of the suitability of these alloys as high-temperature actuator materials (ref. 1). We have determined that some alloys previously identified as promising candidates on the basis of their

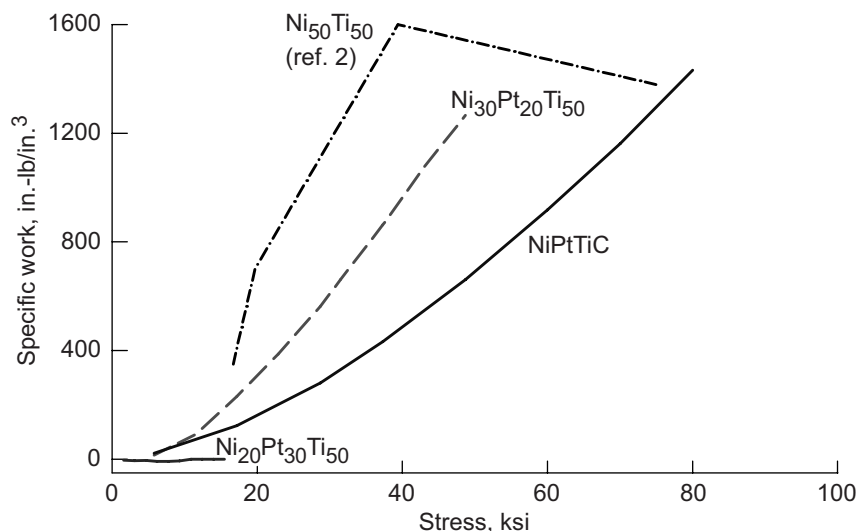
transformation temperature alone do not exhibit sufficient mechanical properties to be used in such applications (e.g., Ni₂₀Pt₃₀Ti₅₀). However, we have identified a baseline alloy, Ni₃₀Pt₂₀Ti₅₀ (at.%) and derivative compositions that look exceptionally promising.

The baseline Ni₂₀Pt₃₀Ti₅₀ alloy has transformation temperatures of M_s , 270 °C; M_f , 245 °C; A_s , 260 °C; and A_f , 275 °C, permitting this alloy to be used at sustained temperatures of about 240 °C, over 3 times the temperature capability of commercial alloys. In simple extruded form, the material has a tensile ductility of about 5 percent at room temperature and is capable of 100-percent strain recovery (elastic + shape memory) when deformed up to its fracture limit. However, previous experience has shown that recovery under stress-free conditions is not an adequate assessment of the material's potential to perform work. Consequently, strain-temperature cycles were performed under varying constant applied stress levels. The work performed by the martensite-to-austenite transformation was determined by multiplying the transformation strain during heating by the applied stress level (see the graph on this page). The work capability of the material measured from these curves was over 1200 in.-lb/in.³ and appeared to be limited only by the tensile ductility of the alloy, which can be increased significantly through proper thermomechanical treatment. This work level is comparable to those of typical binary NiTi alloys (ref. 2).



Set of strain-temperature curves for Ni₂₀Pt₃₀Ti₅₀ measured under various constant-stress conditions. The light and dark curves show the alloy response during heating and cooling, respectively.

Although the results are preliminary, it would appear that Ni₂₀Pt₃₀Ti₅₀ is an attractive material for use in



Comparison of the amount of work performed by the martensitic transformation as a function of applied stress level for various NiTiPt alloys and binary NiTi. The 20 Pt-containing alloys can perform work similar to that of binary NiTi.

high-temperature actuator applications. Continuum Dynamics, Inc., a leading designer of smart components for various propulsion systems, has reviewed these properties and has chosen this alloy for possible incorporation into the design of an adaptive supersonic inlet.

Processing of Ni₃₀Pt₂₀Ti₅₀ High-Temperature Shape-Memory Alloy Into Thin Rod Demonstrated

High-temperature shape-memory alloys (HTSMAs) based on nickel-titanium (NiTi) with significant ternary additions of palladium (Pd), platinum (Pt), gold (Au), or hafnium (Hf) have been identified as potential high-temperature actuator materials for use up to 500 °C. These materials provide an enabling technology for the development of “smart structures” used to control the noise, emissions, or efficiency of gas turbine engines. The demand for these high-temperature versions of conventional shape-memory alloys also has been growing in the automotive, process control, and energy industries. However

References

1. Noebe, R.D.; Biles, T.; and Padula II, S.A.: NiTi-Based High-Temperature Shape-Memory Alloys: Properties, Prospects, and Potential Applications. NASA/TM—2005-213104, 2005.
2. Cross, W.B.; Kariotis, A.H.; and Stimlet, F.J.: Nitinol Characterization Study. NASA CR-1433, 1969.

Glenn contact:

Dr. Ronald D. Noebe, 216-433-2093, Ronald.D.Noebe@nasa.gov

Ohio Aerospace Institute (OAI)

contact:

Darrell J. Gaydosh, 216-433-5809, Darrell.J.Gaydosh@grc.nasa.gov

Authors:

Dr. Ronald D. Noebe, Darrell J. Gaydosh, Tiffany A. Biles, and Dr. Anita Garg

Headquarters program office:

Aeronautics Research

Programs/Projects:

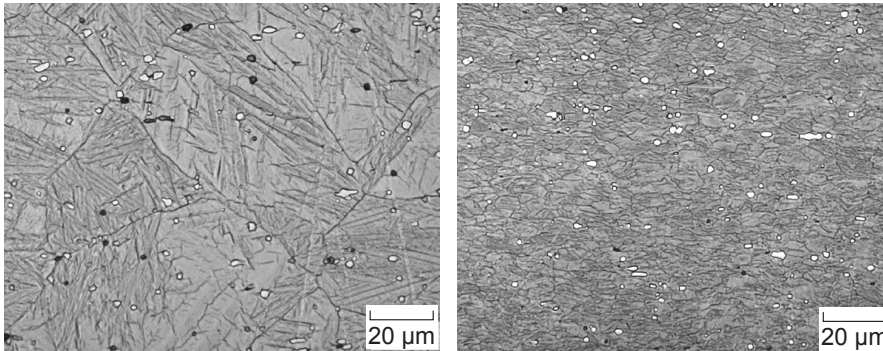
UEET, IPSFT

these materials, including the NiPtTi alloys being developed at the NASA Glenn Research Center, will never find widespread acceptance unless they can be readily processed into useable forms.

Consequently, Glenn researchers have been working with various metal fabricators in the processing of HTSMA, mapping successful processing conditions for the extrusion and forging of wrought material. In addition, one of the necessary steps in the eventual maturation of these alloys is the ability to produce the material into thin rod or wire form. Therefore, we recently demonstrated successful processing conditions for the fabrication of HTSMA thin rod by



Piece of Ni₃₀Pt₂₀Ti₅₀ 0.056-in.-diameter rod processed by high-temperature swaging.



Left: Microstructure of as-extruded alloy before swaging. Right: Microstructure of the final 0.056-in.-diameter $Ni_{30}Pt_{20}Ti_{50}$ rod, resulting in at least an order-of-magnitude reduction in grain size.

high-temperature swaging in conjunction with Rhenium Alloys, Inc. (see the photograph on the preceding page).

Thermomechanical processing of a $Ni_{30}Pt_{20}Ti_{50}$ alloy into fine-diameter rod form results in at least an order-of-magnitude reduction in grain size in comparison to the starting grain size of the as-extruded material (as seen in the photomicrographs above). We anticipate that this modification to the

microstructure of the NiPtTi will significantly improve the mechanical properties of the alloy. Therefore, plans call for future efforts to characterize the mechanical properties of the HTSMA rod and to further develop processing conditions for the eventual fabrication of fine-diameter wire.

Glenn contact:

Dr. Ronald D. Noebe, 216-433-2093,
Ronald.D.Noebe@nasa.gov

Rhenium Alloys, Inc., contact:

Todd Leonhardt, 440-365-7388,
Todd.Leonhardt@rhenium.com

Authors:

Dr. Ronald D. Noebe, Susan L. Draper,
Tiffany A. Biles, and Todd Leonhardt

Headquarters program office:

Aeronautics Research

Programs/Projects:

QAT

Candidate Materials Evaluated for a High-Temperature Stirling Convertor Heater Head

The Department of Energy and NASA have identified Stirling Radioisotope Generators (SRGs) as a candidate power system for use on long-duration, deep-space science missions and Mars rovers (ref. 1).

One of the developments planned for an upgraded version of the current SRG design is to achieve higher efficiency by increasing the overall operating temperature of the system. Currently, the SRG operates with a heater head temperature of 650 °C and is fabricated from the nickel-base superalloy 718. The current operating temperature is at the limit of alloy 718's capability, and any planned increase in temperature will be contingent on identifying a more capable material from which to fabricate the heater head. To this end, personnel at the NASA Glenn Research Center are evaluating advanced materials for a high-temperature heater head to allow a higher convertor temperature ratio and, thus, increase the system efficiency (ref. 2). A generic list of properties that were used to screen the candidate materials follows: (1) creep, (2) fabricability, (3) helium gas containment, (4) long-term stability and compatibility, (5) ability to form a hermetical closeout seal, and (6) ductility and toughness.

For the lower end of the advanced heater head operating temperature range, superalloys are an obvious choice. To identify potential candidates, Glenn researchers screened essentially all commercially available superalloys on the

basis of their published properties to the criteria just listed. From this initial screening, five candidate superalloys were chosen for detailed testing: MarM-247, Udimet 720, IN738LC, IN939, and MA754. A 50-lb heat of each material was then obtained, and creep testing was performed at various stress/temperature combinations. After 1 year of creep testing and microstructural characterization, we decided that MarM-247 was the most promising candidate. Additional heats of MarM-247 were then obtained, with various grain sizes in order to determine the optimum grain size for maximizing creep resistance in the thin, 1-mm-thick heater heads.

Screening criteria similar to those used for the superalloys were used to

screen the refractory alloys. ASTAR-811C (tantalum alloy) and rhenium were chosen for in-depth study. ASTAR-811C is promising for high-temperature applications because of its high melting temperature, high strength, and good weldability, fabricability, and ductility. Rhenium was included as a refractory metal candidate for high-temperature space power applications because of its excellent high-temperature strength, low-temperature ductility, good weldability, and good fabricability. Long-term creep testing of these alloys is currently underway.

Because of the high cost of rhenium, machining a heater head from a solid ingot would be extremely expensive since a large amount of material is wasted. It was, therefore, important to demonstrate near-net-shape (NNS) processing of a rhenium heater head. The figure shows the result of this development effort.

With NNS feasibility now demonstrated, plans for future work focus on creep property optimization. Numerous vacuum creep frames have been refurbished, and we plan to use these extensively in determining the vacuum creep resistance of these alloys.

References

1. Thieme, Lanny G.; and Schreiber, Jeffrey G.: Supporting Development for the Stirling Radioisotope Generator and Advanced Stirling Technology Development at NASA GRC. NASA/TM-2005-213409 (AIP Conf. Proc., vol. 746, 2005, pp. 674-681), 2005. <http://gltrs.grc.nasa.gov/cgi-bin/GLTRS/browse.pl?2005/TM-2005-213409.html>
2. Bowman, Randy; Ritzert, Frank; and Freedman, Marc: Evaluation of Candidate Materials for a High-Temperature Stirling Converter Heater Head. Space Technology and Applications International Forum—STAIF 2004, Mohamed S. El-Genk, ed., AIP Conference Proceedings, vol. 699, 2004, pp. 821-828.

Find out more about this research:

NASA Glenn Research Center:

<http://www.nasa.gov/glenn/>

Glenn's Thermo-Mechanical Systems Branch:

<http://www.grc.nasa.gov/WWW/tmsb/>

Glenn's Power and Propulsion Office:

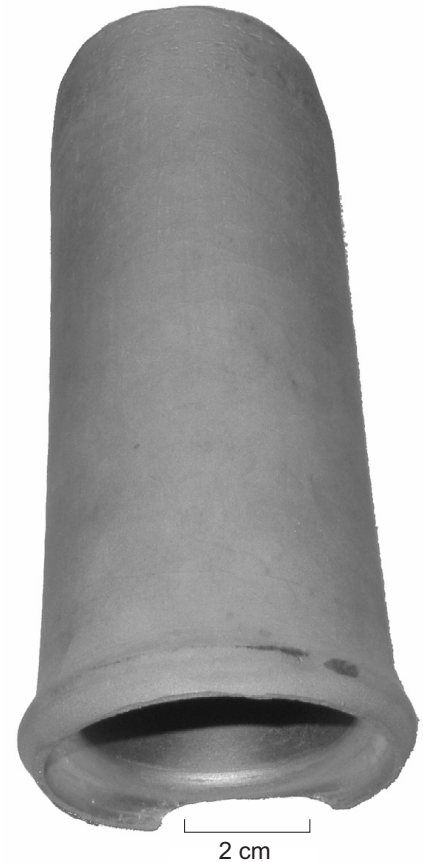
<http://space-power.grc.nasa.gov/ppo/>

Glenn's Advanced Metallics Branch:

<http://www.grc.nasa.gov/WWW/AdvMet/webpage/>

Glenn contacts:

Dr. Randy R. Bowman, 216-433-3205, Randy.R.Bowman@nasa.gov; and Frank J. Ritzert, 216-433-8199, Frank.J.Ritzert@nasa.gov



NNS forming of a rhenium heater head.

Authors:

Dr. Randy R. Bowman and Frank J. Ritzert

Headquarters program office:

Space Science

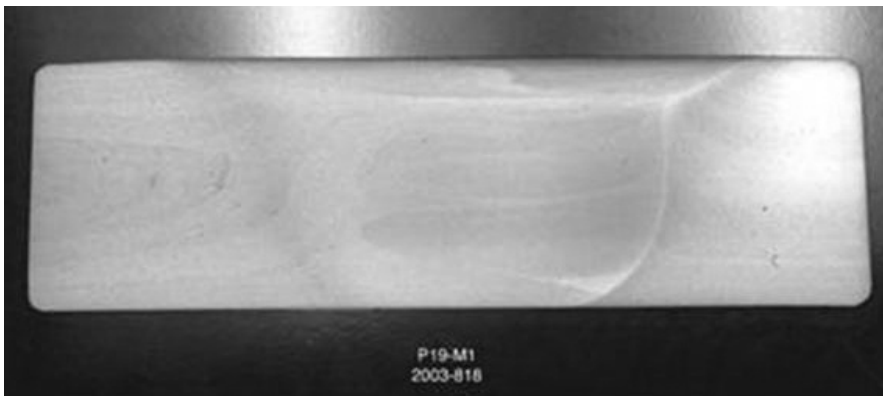
Programs/Projects:

Project Prometheus, SRG110

Full-Scale GRCop-84 Combustion Chamber Liner Preform Fabricated Successfully

GRCop-84 (Cu-8 at.% Cr-4 at.% Nb) has been under development at the NASA Glenn Research Center for several years. The alloy possesses a unique combination of good thermal conductivity, high elevated temperature strength, long creep life, and long low-cycle-fatigue. The alloy is also more oxidation resistant than pure copper and most competitive alloys. The combination of properties has attracted attention from major rocket engine manufacturers who are interested in the alloy for the combustion chamber liner in their next generation of regeneratively cooled engines. Before GRCop-84 can be used in a main combustion chamber application, it must be demonstrated that the alloy can be made successfully to the large sizes and proper shape needed and that it retain useful properties. Recent efforts have successfully demonstrated the ability to fabricate a liner preform via metal spinning that retains the alloy's strength even in the welded sections.

GRCop-84 is a powder metallurgy alloy. Powder is canned and extruded to make a solid rectangular billet. Once consolidated into a solid, GRCop-84 can be processed like most copper-based alloys using conventional techniques. To make these liners, the billet was warm rolled into 1.27-cm (0.5-in.) plates approximately 47 cm wide by 127 cm long (18.5 by 50 in.). The plates were cut to size and formed into half cylinders. The edges of the half cylinders were machined to provide a tight, uniform joint at the mating surfaces between the two pieces.



Cross section of an FSW showing the complete penetration and excellent joining of two 1.27-cm (0.5-in.) plates with a butt joint.

The half cylinders were joined at the NASA Marshall Space Flight Center. Friction stir welding (FSW) was selected to join the alloy because of past experience with aluminum-based alloys and technical considerations that indicated that FSW would not significantly degrade properties in the weld zone. Efforts at Marshall demonstrated that GRCop-84 has a very wide processing window and could be easily welded using FSW. A typical weld cross section is shown in the photograph on this page, and the table lists the strength of welds done on several plates.

The GRCop-84 cylinders were metal spun at Spin Tech in Paso Robles, California, to a size equivalent to that of a 40,000-lb-thrust rocket engine. The metal spinning was done in two steps. The first step rough sized the cylinders, and the second step produced the final hourglass shape with the proper envelope dimensions. The top photograph on the next page shows the cylinder undergoing final metal spinning into the hourglass shape, and the final photograph compares a cylinder not yet metal spun and the finished main combustion chamber liner preform. The weld is clearly visible on the surface of the cylinder but is difficult to distinguish in the metal-spun preform.

ROOM-TEMPERATURE TENSILE STRENGTH OF FSW JOINTS

Material	0.2-percent offset yield strength		Ultimate tensile strength		Elongation, percent	Reduction in area, percent
	MPa	ksi	MPa	ksi		
1.27-cm plate—round samples (average of three welds, six tests)	203.6	29.5	403.4	58.5	18.0	20.3
1.27-cm plate—full-thickness samples (average of two welds, eight tests)	203.7	29.5	404.6	58.6	17.8	Not applicable
As-extruded GRCop-84 bar	225.6	32.7	403.1	58.4	21.4	45.1
FSW properties as percent of baseline properties	90.3		100.2		83.6	45.0



Metal spinning of GRCop-84 into the final hourglass-shaped liner preform.



A comparison of a welded cylinder and a liner preform after completion of metal spinning. The cylinder is 18 in. tall.

Inspection using visual and non-destructive evaluation methods did not reveal any failures or defects developing in the welds. One preform was destructively tensile tested to determine the strength of the weld joints. The results in the following table show that the welds were as strong as the annealed plate used as starting stock and actually stronger than the starting stock at 538 °C.

Although additional testing including an eventual hot fire testing of a liner is needed, results so far show that GRCop-84 liners can be produced easily with conventional fabrication methods and that the alloy retains all of its properties even in the weld joint of a metal-spun preform. This makes GRCop-84 an extremely attractive material for regeneratively cooled rocket engine main combustion chamber liners and other high-temperature, high-heat-flux heat exchanger applications.

Glenn contact:

Dr. David L. Ellis, 216-433-8736,
David.L.Ellis@nasa.gov

NASA Marshall contact:

Carolyn K. Russell, 256-544-2705,
Carolyn.K.Russell@nasa.gov

Spin Tech contact:

Rick Goudy, 805-237-4994,
rick.goudy@tcsn.net

Authors:

Dr. David L. Ellis, Carolyn K. Russell,
and Rick Goudy

Headquarters program office:

Exploration Systems

Programs/Projects:

Space Launch Initiative, Propulsion
Technology and Integration

Special recognition:

Turning Goals Into Reality Award 2003

**TENSILE STRENGTH OF METAL-SPUN GRCOP-84 LINER PREFORMS
IN THE WELD REGION**

Material	0.2-percent offset yield strength		Ultimate tensile strength	
	MPa	ksi	MPa	ksi
FSW and metal spun; room temperature	246.3	35.7	419.5	60.8
FSW and metal spun; 538 °C (1000 °F)	157.3	22.8	176.6	25.6
As-extruded GRCop-84 bar; room temperature	225.6	32.7	403.1	58.4
As-extruded GRCop-84 bar; 538 °C (1000 °F)	107.8	15.6	138.9	20.1

Quick Access Rocket Exhaust Rig Testing of Coated GRCop-84 Sheets Used to Aid Coating Selection for Reusable Launch Vehicles

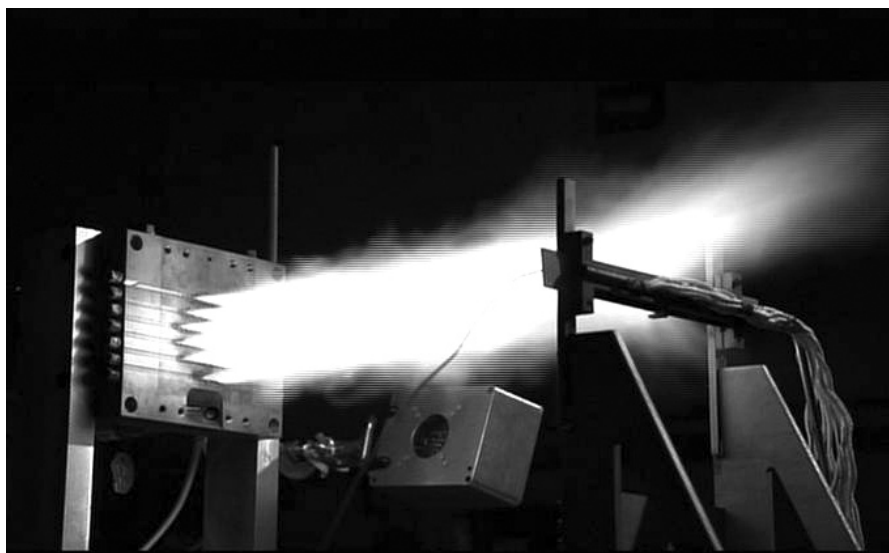
The design of the next generation of reusable launch vehicles calls for using GRCop-84 copper alloy liners based on a composition¹ invented at the NASA Glenn Research Center: Cu-8(at.%)Cr-4%Nb. Many of the properties of this alloy have been shown to be far superior to those of other conventional copper alloys, such as NARloy-Z (ref. 1). Despite this considerable advantage, it is expected that GRCop-84 will suffer from some type of environmental degradation depending on the type of rocket fuel utilized. In a liquid hydrogen (LH₂), liquid oxygen (LO₂) booster engine, copper alloys undergo repeated cycles of oxidation of the copper matrix and subsequent reduction of the copper oxide, a process termed "blanching" (ref. 2). Blanching results in increased surface roughness and poor heat-transfer capabilities, local hot spots, decreased engine performance, and premature failure of the liner material. This environmental degradation coupled with the effects of thermomechanical stresses, creep, and high thermal gradients can distort the cooling channel severely, ultimately leading to its failure (ref. 3).

The application of protective coatings on a GRCop-84 substrate can minimize or eliminate many of these problems and extend the operational life of the combustion liner (ref. 3). Such coatings may increase component reliability, shorten depot maintenance turnaround time, and lower operational costs. Therefore, Glenn is actively pursuing the development of advanced overlay coatings technology for GRCop-84 liners. This research effort encompasses the development of technology in four major areas: (1) new metallic coating compositions, (2) application techniques, (3) test methods, and (4) life-prediction design methodology using finite element analysis. This report discusses the results of a specific

test method involving the exposures of coated GRCop-84 sheets to a H₂/O₂ combustion flame in Glenn's Quick Access Rocket Exhaust (QARE) rig.

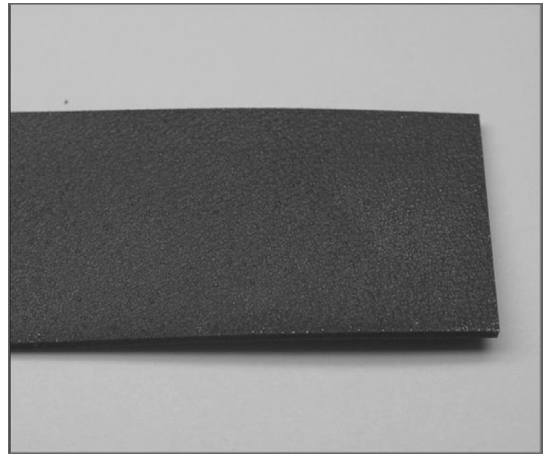
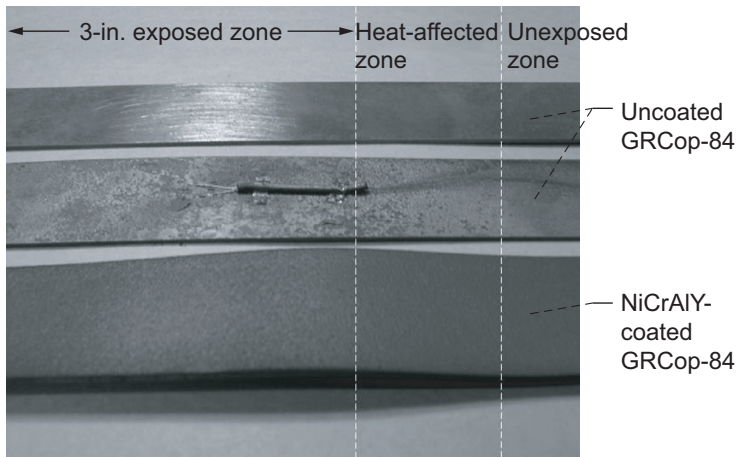
Both faces of several 1-mm-thick GRCop-84 sheets, having a cross-sectional area of about 305 by 305 mm², were vacuum plasma sprayed with the desired coating. The coatings selected for these evaluation studies were Cu-26Cr, NiAl, and NiCrAlY. The sheets were observed to have distorted during the spraying process. Test specimens were machined from these coated sheets, where each specimen was about 305 mm long and 25.4 mm wide. Both coated and uncoated specimens were subjected to an intense H₂/O₂ combustion flame using a mixture ratio of about 6, where the specimens either were cycled between room temperature and approximately 700 °C for 20 cycles or were subjected to a constant flame exposure for a cumulative time of about 10 min (see the photograph to the left). The specimens were held in a specially designed fixture and subjected to backside air and conductive cooling. Prior to the exposure tests, a superalloy sheet specimen was instrumented with five thermocouples to calibrate the rig. In a typical cycle, the specimen reached a temperature of about 700 °C within 20 sec, whereas the cool down to room temperature occurred in 300 sec.

A visual examination of the exposed specimens revealed that uncoated GRCop-84 specimens undergo severe environmental degradation that results in oxide spall and surface roughness (see the photograph to the left). In actual applications, this surface condition is unacceptable because of the reduced heat transfer



QARE rig testing of a coated GRCop-84 sheet.

¹Cu, copper; Cr, chromium; Nb, niobium.



Left: Comparison of NiCrAlY-coated and uncoated GRCop-84 before and after exposure to a H_2/O_2 combustion flame. Right: Unexposed NiCrAlY-coated GRCop-84 sheet.

capability of the liner, associated hot spots, and the potential risk for the liner material to fail. Similarly, specimens coated with Cu-26Cr did not perform well in these tests. These coatings formed blisters, indicating localized failure due to debonding with the substrate. In contrast, specimens coated with NiAl and NiCrAlY performed very well, with no visual distinction between the exposed and unexposed regions of the specimens. For example, the photograph on the left shows the exposed NiCrAlY-coated specimen, whereas the photograph on the right shows the unexposed NiCrAlY-coated specimen.

References

1. Ellis, David L.; and Michal, Gary M.: Mechanical and Thermal Properties of Two Cu-Cr-Nb Alloys and NARloy-Z. NASA CR-198529, 1996.
2. Morgan, Deena B.; and Kobayashi, A.C.: Main Chamber Combustion and Cooling Technology Study; Final Report. NASA CR-184345, 1989.
3. Quentmeyer, R.J.: Experimental Fatigue Life Investigation of Cylindrical Thrust Chambers. NASA TM X-73665, 1977.

Find out more about this research:
<http://www.grc.nasa.gov/WWW/EDB/>

Glenn contact:
 Dr. Sai V. Raj, 216-433-8195,
 Sai.V.Raj@nasa.gov

Authors:
 Dr. Sai V. Raj, Raymond C. Robinson,
 and Dr. Louis J. Ghosn

Headquarters program office:
 Space Exploration

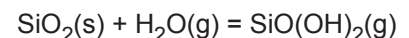
Programs/Projects:
 NGLT, PR&T

Thermodynamics of Volatile Species in the Silicon-Oxygen-Hydrogen System Studied

The volatilization of silica (SiO_2) to silicon hydroxides and oxyhydroxides because of reaction with water vapor is important in a variety of high-temperature corrosion processes. For example, the lifetimes of silicon carbide (SiC) and silicon nitride (Si_3N_4)-based components in combustion environments are limited by silica volatility. To understand and model this process, it is essential to have accurate thermodynamic data for the formation of volatile silicon hydroxides and oxyhydroxides.

This reaction was studied at the NASA Glenn Research Center with a transpiration apparatus, illustrated in the figure on the next page. A silica sample was reacted with gas streams containing controlled amounts of water vapor, and the resultant silicon-oxygen-hydrogen (Si-O-H) vapor species

condensed downstream. From the amount of condensate, accurate vapor pressures could be determined. The vapor pressure as a function of pressure indicated that the following two reactions are likely:



We found that the first reaction was significant over the whole temperature range studied (1073 to 1728 K), whereas the second reaction became important at the highest temperatures (1673 to 1728 K).

Temperature-dependent vapor pressure measurements lead to thermodynamic data. Second law measurements lead to a heat of formation $\Delta_f H^\circ(1200) = -1354 \pm 2.7$ kJ/mol and entropy $S^\circ(1200) = 544.4 \pm 2.1$ kJ/mol-K. Third law measurements lead to $\Delta_f H^\circ(298) = -1344.3 \pm 1.2$ kJ/mol. These are in very good agreement with previous measurements and previous ab initio calculations. A third law analysis of the high-temperature data led to a $\Delta_f H^\circ(298)$ for $\text{SiO}(\text{OH})_2(\text{g})$ of -831 ± 5 kJ/mol. This value is also consistent with previous experiments.

Find out more about this research:

<http://www.grc.nasa.gov/WWW/EDB/>

Glenn contacts:

Dr. Nathan S. Jacobson, 216-433-5498, Nathan.S.Jacobson@nasa.gov; and Dr. Elizabeth J. Opila, 216-433-8904, Elizabeth.J.Opila@nasa.gov

East Central University contact:

Dwight Myers, 580-310-5389, dmyers@mailclerk.ecok.edu

Authors:

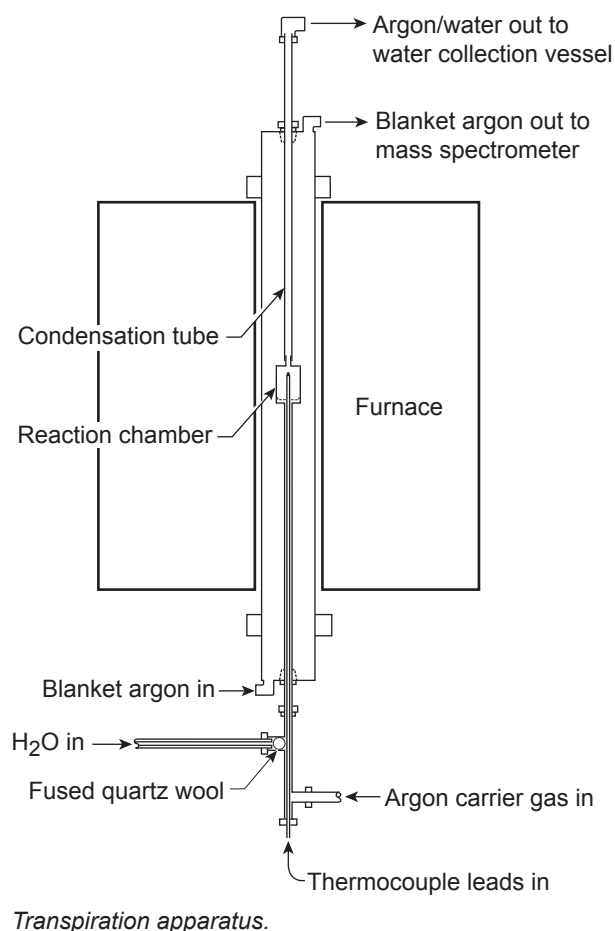
Dr. Nathan S. Jacobson, Dr. Elizabeth J. Opila, Dr. Evan H. Copland, and Dr. Dwight Myers

Headquarters program office:

Aeronautics Research

Programs/Projects:

VSP, UEET

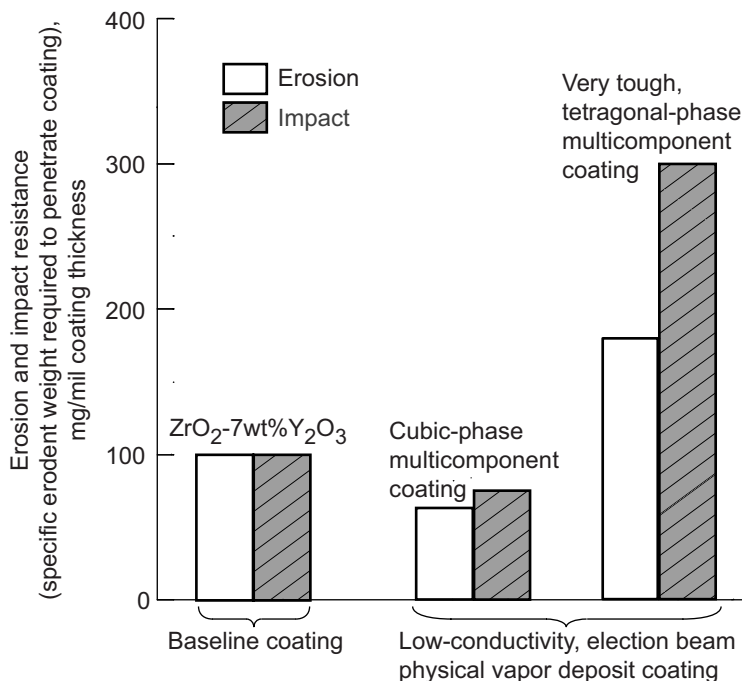


Very Tough, Erosion-Resistant Turbine Airfoil Thermal Barrier Coatings Developed

Ceramic thermal barrier coatings (TBCs) are receiving increased attention for advanced gas turbine engine applications. These coatings are considered to be technologically important because of their ability to further increase engine operating temperatures and reduce cooling requirements, thus achieving higher engine efficiency, lower emissions, and increased performance goals. To take full advantage of the capabilities of these coatings, researchers need to use an aggressive design approach whenever possible—one that allows greater temperature reductions through the coating systems and less cooling air to the components.

Advanced TBCs that have significantly lower thermal conductivity and better thermal stability than current coatings have been developed for future ultra-efficient, low-emission engine systems (refs. 1 and 2). Multicomponent-doped, defect-clustered TBCs have been shown to offer the low conductivity and high stability required for future high-temperature engine applications (refs. 1 and 2).

For TBCs designed for turbine airfoil applications, good erosion and impact resistance, in addition to low thermal conductivity and high stability, are crucial in order to effectively protect the components under high heat flux, high velocity flow, and particulate erosion and impact conditions. In this study at the NASA Glenn Research Center, advanced low-conductivity coatings, possessing the partially stabilized nontransformable tetragonal t' structure, were designed and optimized for high erosion and impact performance. The NASA Ultra-Efficient Engine Technology (UEET)



Erosion and impact testing results of a multicomponent, partially stabilized, nontransformable tetragonal *t'* coating ZrO₂-(Y,Gd,Yb)₂O₃ coating system, showing improved performance in comparison to the baseline ZrO₂-7wt%Y₂O₃ and cubic-phased low-conductivity coatings.

Project low-conductivity coating systems were processed by electron-beam physical-vapor-deposit techniques at GE Aircraft Engines (Cincinnati, OH) and Howmet Coatings Corporation (Whitehall, MI) using prefabricated evaporation ingots that were made of the carefully designed compositions.

Considerable thermal conductivity reductions were observed in comparison to the state-of-the-art baseline ZrO₂-7wt%Y₂O₃ coatings after high-temperature sintering for the multicomponent, partially stabilized nontransformable tetragonal *t'* coating systems (ref. 3). The 2200 °F burner rig erosion and impact testing results indicated that the composition optimizations significantly improved the toughness and erosion/impact resistance of the low-conductivity coating systems.

References

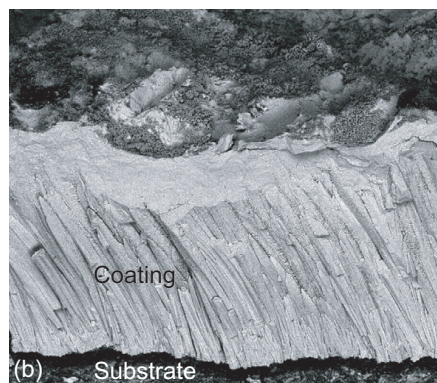
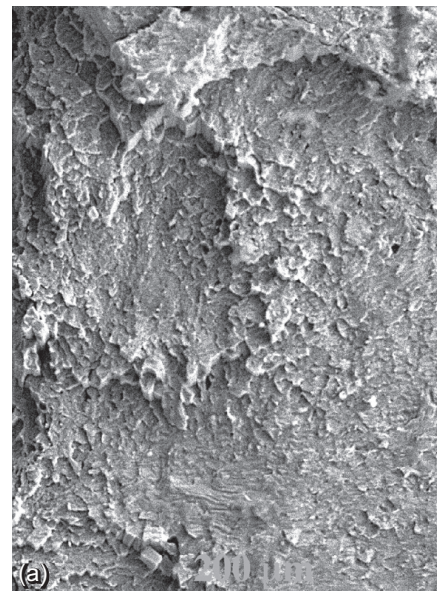
1. Zhu, Dongming; and Miller, Robert A.: Thermal Conductivity and Sintering Behavior of Advanced Thermal Barrier Coatings. *Ceramic Eng. Sci. Proc.*, vol. 23, no. 4, 2002, pp. 457–468.
2. Zhu, Dongming; and Miller, Robert A.: Development of Advanced Low Conductivity Thermal Barrier Coatings. *Int. J. Appl. Ceramic Technol.*, vol. 1, no. 1, 2004, pp. 86–94.
3. Zhu, Dongming; and Miller, Robert A.: Thermal and Environmental Barrier Coatings for Advanced Propulsion Engine Systems. NASA/TM—2004-213129, 2004. <http://gltrs.grc.nasa.gov/cgi-bin/GLTRS/browse.pl?2004/TM-2004-213129.html>

Find out more about this research: <http://www.grc.nasa.gov/WWW/EDB/>

U.S. Army Research Laboratory, Vehicle Technology Directorate at

Glenn, contact:

Dr. Dongming Zhu, 216–433–5422; Dongming.Zhu@grc.nasa.gov



Thermal barrier coating showing very tough impacting fracture surface after 1200-cycle burner rig impact testing at 2200 °F. (a) Surface morphologies. (b) Cross-section micrograph.

Glenn contact:

Dr. Robert A. Miller, 216–433–3298; Robert.A.Miller@nasa.gov

Authors:

Dr. Dongming Zhu and Dr. Robert A. Miller

Headquarters program office:

Aeronautics Research

Programs/Projects:

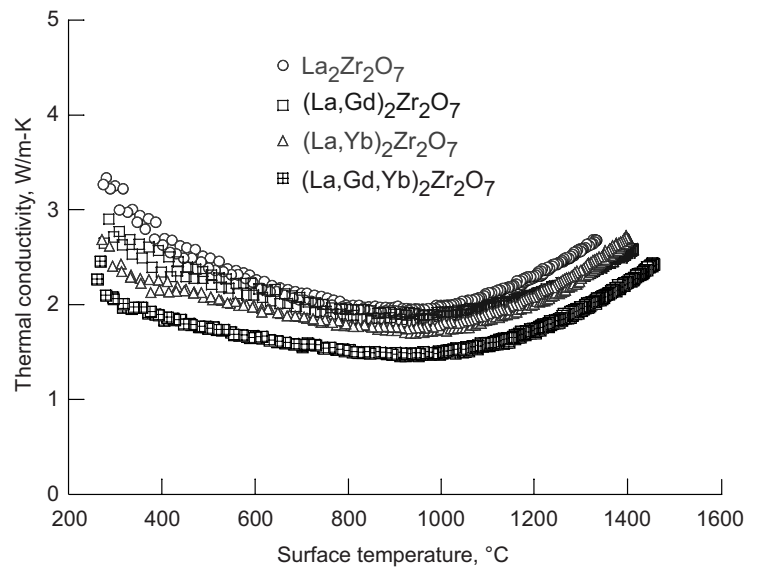
VSP, UEET

Low-Thermal-Conductivity Pyrochlore Oxide Materials Developed for Advanced Thermal Barrier Coatings

When turbine engines operate at higher temperatures, they consume less fuel, have higher efficiencies, and have lower emissions. The upper-use temperatures of the base materials (superalloys, silicon-based ceramics, etc.) used for the hot-section components of turbine engines are limited by the physical, mechanical, and corrosion characteristics of these materials. Thermal barrier coatings (TBCs) are applied as thin layers on the surfaces of these materials to further increase the operating temperatures. The current state-of-the-art TBC material in commercial use is partially yttria-stabilized zirconia (YSZ), which is applied on engine components by plasma spraying or by electron-beam physical vapor deposition. At temperatures higher than 1000 °C, YSZ layers are prone to sintering, which increases thermal conductivity and makes them less effective. The sintered and densified coatings can also reduce thermal stress and strain tolerance, which can reduce the coating's durability significantly. Alternate TBC materials with lower thermal conductivity and better sintering resistance are needed to further increase the operating temperature of turbine engines.

Under NASA's Ultra Efficient Engine Technology (UEET) Project, advanced TBCs are being developed to provide vital thermal protection for turbine engine hot-section components, such as combustor liners, turbine blades, and turbine vanes at gas temperatures exceeding 1650 °C (3000 °F) in harsh combustion environments. The new TBCs must have significantly increased phase stability, lower lattice and radiation thermal conductivity, and improved sintering and thermal stress resistance under the engine high-heat-flux and severe thermal cycling conditions. Pyrochlore oxides of general composition, $A_2B_2O_7$, where A is a 3+ cation (lanthanum to lutetium) and B is a 4+ cation (zirconium, hafnium, titanium, etc.), are one such class of ceramic materials. These oxides have a high melting point, a relatively high coefficient of thermal expansion, and low thermal conductivity, which make them suitable for applications as high-temperature thermal barrier coatings. The primary objective of this study at the NASA Glenn Research Center was to devise approaches to further lower the thermal conductivity of pyrochlore oxide compounds. An oxide-doping approach was used where part of cation A was substituted by other cations (e.g., $A_{1-x}M_xB_2O_7$, where $x = 0 - 0.5$ and M = rare earth or other cations) in the pyrochlore materials.

Powders of various compositions were synthesized by the sol-gel method and hot pressed into dense 1-in.-diameter disks. The thermal conductivity of these disks was measured at temperatures up to 1550 °C using a steady-state



Thermal conductivity as a function of surface test temperature of hot-pressed doped and undoped $La_2Zr_2O_7$. The rare-earth-doped and codoped pyrochlore oxides showed lower thermal conductivity than the undoped $La_2Zr_2O_7$.

laser-heat-flux technique. As an example, results for $La_{2-x}M_xZr_2O_7$ systems (where M = gadolinium (Gd), ytterbium (Yb), or Gd + Yb) are shown in the graph. The rare-earth-oxide-doped pyrochlores ($(La,Gd)_2Zr_2O_7$, $(La,Yb)_2Zr_2O_7$, and $(La,Gd,Yb)_2Zr_2O_7$) have lower thermal conductivity than the undoped $La_2Zr_2O_7$. The thermal conductivity of material codoped with Gd + Yb is ~30 percent lower than that of the undoped oxide. These results clearly demonstrate that the thermal conductivity of pyrochlore oxides can be reduced greatly by doping, especially through codoping with other cations.

Thus, doping or codoping with one or more cations at the A sites in $A_2B_2O_7$ pyrochlores, such as $La_2Zr_2O_7$, results in lower thermal conductivity. These

ceramic materials have great potential as TBCs at much higher temperatures than with the state-of-the-art YSZ zirconia. These new TBCs would greatly reduce the temperature across the coating, which would translate to turbine engines with higher operating temperatures, lower fuel consumption, higher efficiency, and lower emissions.

Bibliography

Zhu, Dongming; Bansal, Narottam P.; and Miller, Robert A.: Thermal Conductivity and Stability of $\text{HfO}_2\text{-Y}_2\text{O}_3$ and $\text{La}_2\text{Zr}_2\text{O}_7$ Evaluated for 1650 °C Thermal/Environmental Barrier Coating Applications. *Ceram. Trns.*, vol. 153, 2004, pp. 331–343.

Zhu, D., et al.: Thermal Conductivity of Ceramic Coating Materials Determined by a Laser Heat Flux Technique. *High Temperature Ceramic Matrix Composites*, W. Krenkel, R. Naslain, and H. Schneider, eds., Wiley-VCH, Weinheim, Germany, 2001, pp. 262–267.

Glenn contact:

Dr. Narottam P. Bansal, 216–433–3855,
Narottam.P.Bansal@nasa.gov

U.S. Army Research Laboratory, Vehicle Technology Directorate at Glenn, contact:

Dr. Dongming Zhu, 216–433–5422,
Dongming.Zhu@grc.nasa.gov

Authors:

Dr. Narottam P. Bansal and
Dr. Dongming Zhu

Headquarters program office:

Aeronautics Research

Programs/Projects:

VSP, UEET

Strong, Tough Glass Composites Developed for Solid Oxide Fuel Cell Seals

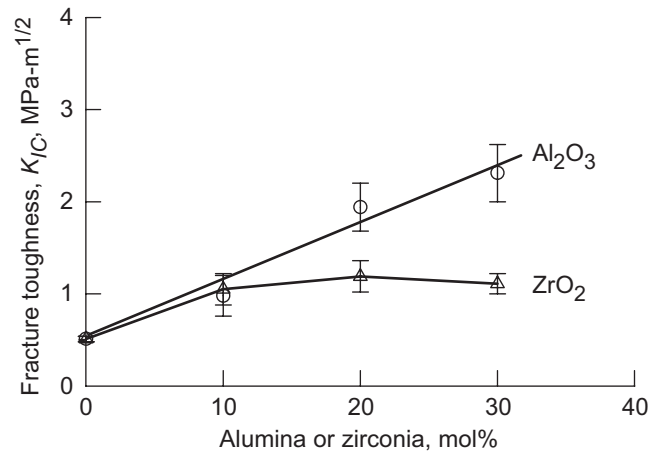
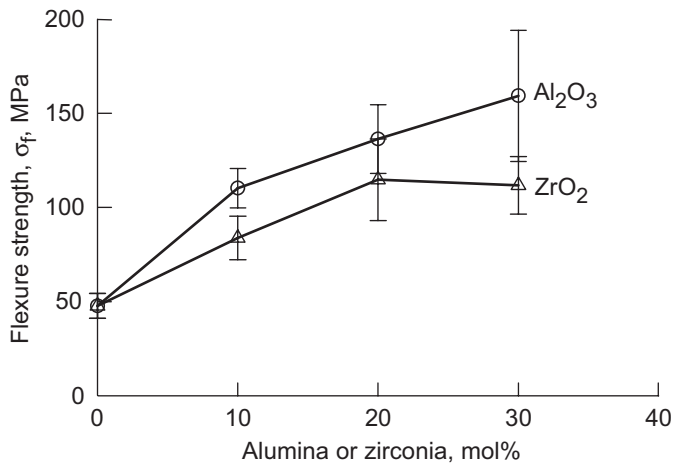
A fuel cell is an electrochemical device that continuously converts the chemical energy of a fuel directly into electrical energy. It consists of an electrolyte, an anode, and a cathode. Various types of fuel cells are available, such as direct methanol fuel cells, alkaline fuel cells, proton-exchange-membrane fuel cells, phosphoric acid fuel cells, molten carbonate fuel cells, and solid oxide fuel cells (SOFCs). The salient features of an SOFC are all solid construction and high-temperature electrochemical-reaction-based operation, resulting in clean, efficient power generation from a variety of fuels. SOFCs are being developed for a broad range of applications, such as portable electronic devices, automobiles, power generation, and aeronautics.

SOFCs of two different designs, tubular and planar, are currently under development. Planar SOFCs offer several advantages, such as simple manufacturing and a relatively short current path, resulting in higher power density and efficiency than for the tubular design. However, planar SOFCs require hermetic seals to separate and contain the fuel and oxidant within the cell and to bond cell components together. The requirements for SOFC sealing materials are severe since the cells will operate at 600 to 1000 °C for thousands of hours, with sealing materials exposed to both oxidizing and reducing conditions. The seals must be chemically and mechanically compatible with different oxide and metallic cell components and should be electrically insulating. Also, they must survive cycling between room and operational temperatures.

Various glass and glass-ceramics based on borate, phosphates, and silicates are being examined for SOFC seals. Silicate glasses are expected to perform better than borate and phosphate glasses. A barium calcium aluminosilicate (BCAS) glass of composition (mol%) $35\text{BaO-15CaO-5Al}_2\text{O}_3\text{-10B}_2\text{O}_3\text{-35SiO}_2$ has been developed by the Department of Energy's Pacific Northwest National Laboratory (PNNL) for use as sealing material for planar SOFCs.

During thermal cycling of SOFC, the glass seal is prone to cracking. To alleviate this problem, PNNL asked for the help of researchers at the NASA Glenn Research Center in improving the strength and fracture toughness of this glass. To achieve this goal, we reinforced the glass with alumina platelets or 3 mol% yttria-stabilized zirconia (3YSZ) particulates. Panels of glass containing 0 to 30 mol% of the ceramic reinforcements were hot pressed and machined into test bars. Mechanical and physical properties, including four-point flexure strength, fracture toughness, elastic modulus, and density of the glass composites, were determined at room temperature.

Flexure strength (see the graph on the left, next page) increased with an increase in alumina or 3YSZ content. For the same ceramic content, composites containing alumina platelets showed much higher strength than those with 3YSZ. Fracture toughness (see the graph on the right, next page), measured by the single-edge



Left: Flexure strength of BCAS glass composites containing various mole percent of alumina platelets or 3YSZ particulates.

Right: Fracture toughness of BCAS glass composites containing various mole percent of alumina platelets or 3YSZ particulates.

v-notched beam method, showed similar large improvements. The increase in fracture toughness was much more significant for composites reinforced with alumina platelets than for those containing 3YSZ. Fracture toughness of the glass improved by 350 and 120 percent for composites containing 30 mol% of alumina and 3YSZ, respectively. Elastic modulus also increased with an increasing amount of reinforcement. The increase in elastic modulus was more predominant for composites reinforced with alumina than with 3YSZ. The addition of alumina did not have much effect on the glass density, whereas the composite density increased linearly with increasing 3YSZ content.

Thus, it has been demonstrated that reinforcing with alumina platelets can improve the strength of barium calcium aluminosilicate glass by as much as 250 percent and fracture toughness by as much as 350 percent. Leak tests for these glass composite seals are planned to be carried out at PNNL and should result in much improved seals for SOFCs.

This research was done under a Space Act Agreement between the NASA Glenn Research Center and the Department of Energy's Pacific Northwest National Laboratory.

Glenn contact:

Dr. Narottam P. Bansal, 216-433-3855,
Narottam.P.Bansal@nasa.gov

University of Toledo contact:

Dr. Sung R. Choi, 216-433-8366,
Sung.R.Choi@grc.nasa.gov

Authors:

Dr. Narottam P. Bansal and
Dr. Sung R. Choi

Headquarters program office:

Aeronautics Research

Programs/Projects:

VSP, LEAP

Process Developed for Generating Ceramic Interconnects With Low Sintering Temperatures for Solid Oxide Fuel Cells

Solid oxide fuel cells (SOFCs) have been considered as premium future power-generation devices because they have demonstrated high energy-conversion efficiency, high power density, and extremely low pollution, and have the flexibility of using hydrocarbon fuel. The Solid-State Energy Conversion Alliance (SECA) initiative, supported by the U.S. Department of Energy and private industries, is leading the development and commercialization of SOFCs for low-cost stationary and automotive markets. The targeted power density for the initiative is rather low, so that the SECA SOFC can be operated at

a relatively low temperature (~700 °C) and inexpensive metallic interconnects can be utilized in the SOFC stack.

As only NASA can, the agency is investigating SOFCs for aerospace applications. Considerable high power

density is required for the applications. As a result, the NASA SOFC will be operated at a high temperature (~900 °C) and ceramic interconnects will be employed. Lanthanum chromite-based materials have emerged as a leading candidate for the ceramic interconnects. The interconnects are expected to co-sinter with zirconia electrolyte to mitigate the interface electric resistance and to simplify the processing procedure. Lanthanum chromites made by the traditional method are sintered at 1500 °C or above. They react with zirconia electrolytes (which typically sinter between 1300 and 1400 °C) at the sintering temperature of lanthanum chromites. It has been envisioned that lanthanum chromites with lower sintering temperatures can be co-fired with zirconia electrolyte. Nonstoichiometric lanthanum chromites can be sintered at lower temperatures, but they are unstable and react with zirconia electrolyte during co-sintering.

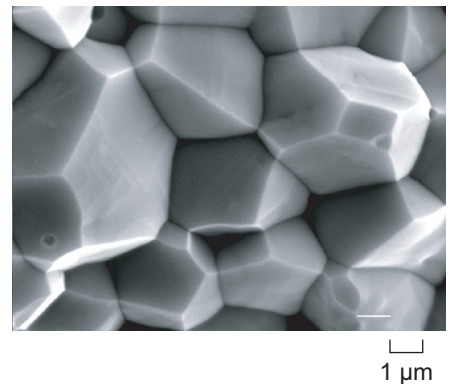
NASA Glenn Research Center's Ceramics Branch investigated a glycine nitrate process to generate fine powder of the lanthanum-chromite-based materials. By simultaneously doping calcium on the lanthanum site, and cobalt and aluminum on the chromium site, we could sinter the materials below 1400 °C. The doping concentrations were adjusted so that the thermal expansion coefficient matched that of the zirconia electrolyte. Also, the investigation was focused on stoichiometric compositions so that the materials would have better stability.

Co-sintering and chemical compatibility with zirconia electrolyte were examined by x-ray diffraction, scanning electron microscopy, and energy dispersive spectroscopy (line scanning and dot map). The results showed that the materials bond well, but do not react, with zirconia electrolyte. The electric conductivity of the materials measured at 900 °C in air was about 20 S/cm.

Bibliography

Deshpande, Kishori; Mukssyan, Alexander; and Varma, Arvind: Aqueous Combustion Synthesis of Strontium-Doped Lanthanum Chromite Ceramics. *J. Am. Ceram. Soc.*, vol. 86, no. 7, 2003, pp. 1149–1154.

Sakai, Natsuko, et al.: Lanthanum Chromite-Based Interconnects as Key Materials for SOFC Stack Development. *Int. J. Appl. Ceram. Technol.*, vol. 1, no. 1, 2004, pp. 23–30.



Sintering results: fractured surface of the ceramic interconnect after sintering at 1400 °C for 2 hr.

Find out more about this research:

<http://www.grc.nasa.gov/WWW/MDWeb/>

Glenn contact:

Dr. Jon C. Goldsby, 216–433–8250,
Jon.C.Goldsby@nasa.gov

QSS Group, Inc., contact:

Zhimin Zhong, 216–433–6494,
Zhimin.Zhong@grc.nasa.gov

Authors:

Zhimin Zhong and Dr. Jon C. Goldsby

Headquarters program office:

OAT

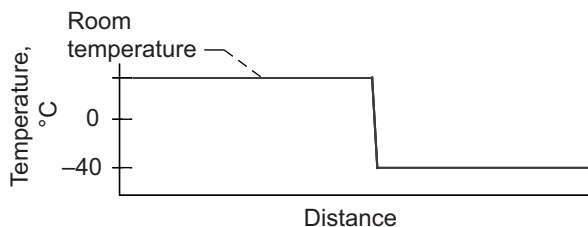
Programs/Projects:

VSP, LEAP

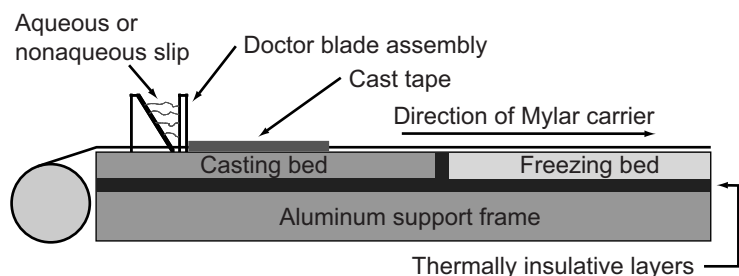
Process Developed for Fabricating Engineered Pore Structures for High-Fuel-Utilization Solid Oxide Fuel Cells

Solid oxide fuel cells (SOFCs) have tremendous commercial potential because of their high efficiency, high energy density, and flexible fuel capability (ability to use fossil fuels). The drive for high-power-utilizing, ultrathin electrolytes (<10 μm), has placed an increased demand on the anode to provide structural support, yet allow sufficient fuel entry for sustained power generation. Concentration polarization, a condition where the fuel demand exceeds the supply, is evident in all commercial-based anode-supported cells, and it presents a significant roadblock to SOFC commercialization.

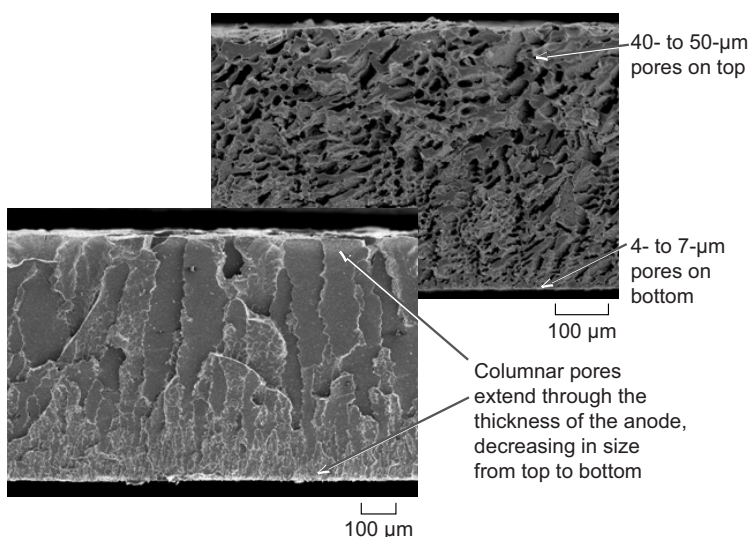
Recently, a novel tape casting process (see the top figure on the next page) was developed at the NASA Glenn Research Center that allows for the fabrication, in a single processing step, of graded columnar pore structures in a wide variety of materials, including all common SOFC anodes,



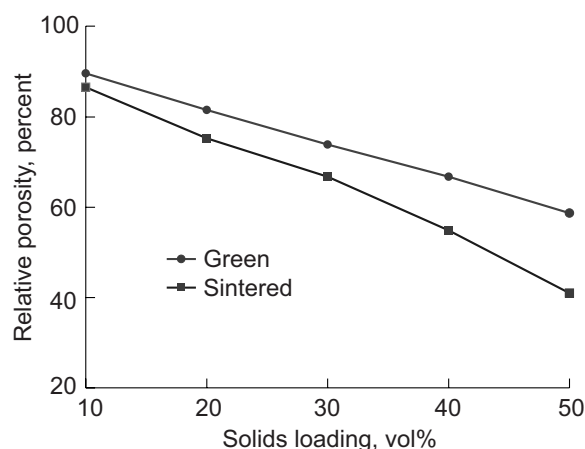
Temperature profile at 40 °C processing.



Freeze-casting apparatus.



Microstructures showing the various morphologies and magnitudes of scale for the porous engineered membranes.



Influence of slurry solids loading on the as-processed (green) density and the heat-treated (sintered) density.

cathodes, and cermets. This new process, called freeze-tape casting, is based on existing tape casting platforms and can yield continuous large-area membranes. The process uses environmentally friendly water-based slurries to directionally solidify the solvent, thus creating a unique pore structure. The freezing pattern of the ice is realized microstructurally in the form of graded porosity and columnar porosity, depending on the processing parameters. As seen in the micrographs, an order of magnitude difference in pore diameters can be created that span the entire thickness of the samples. Freeze-tape casting further allows for the tailoring of pore structures by controlling slurry solids loading and/or the freezing rate, allowing for easy modification of the final porosity and morphology. The effects of solids loading are shown in the final graph.

Although this technology has potential for a growing number of applications—including catalyst supports, osmotic membranes, and particulate/liquid filtration—it was developed for enhanced SOFCs. As can be seen in the micrographs of the anode-electrolyte coupling, SOFCs based on this casting technology have the potential for increased fuel utilization (improved gas delivery), increased

power density, and decreased weight. Extensive efforts in establishing processing-properties relationships in conjunction with cell fabrication will culminate in electrochemical and mechanical properties testing.

Glenn contact:

Dr. Serene C. Farmer, 216-433-3289,
Serene.C.Farmer@nasa.gov

Authors:

Dr. Stephen W. Sofie,
Dr. Thomas L. Cable, and
Dr. Sam M. Salamone

Headquarters program office:

Aeronautics Research

Programs/Projects:

VSP, LEAP

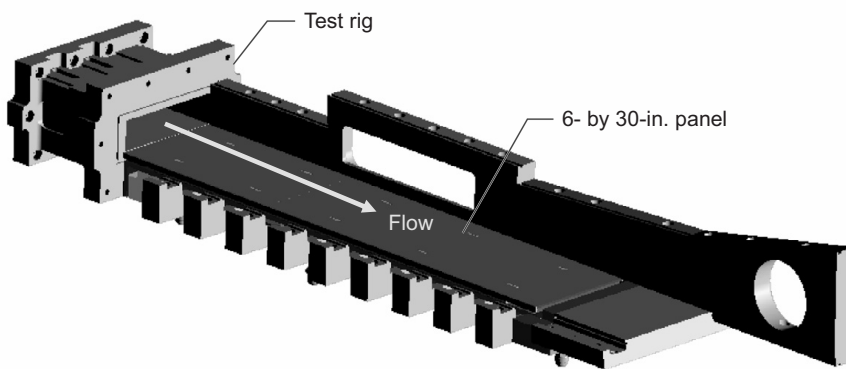
Cooled Ceramic Matrix Composite Propulsion Structures Demonstrated

NASA's Next Generation Launch Technology (NGLT) Program has successfully demonstrated cooled ceramic matrix composite (CMC) technology in a scramjet engine test. This demonstration represented the world's largest cooled nonmetallic matrix composite panel fabricated for a scramjet engine and the first cooled nonmetallic composite to be tested in a scramjet facility.

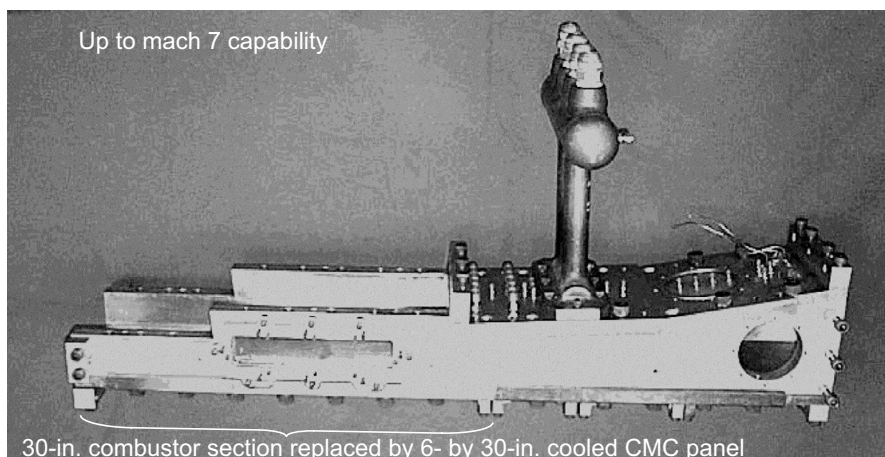
Lightweight, high-temperature, actively cooled structures have been identified as a key technology for enabling reliable and low-cost space access. Tradeoff studies have shown this to be the case for a variety of launch platforms, including rockets and hypersonic cruise vehicles. Actively cooled carbon and CMC structures may meet high-performance goals at significantly lower weight, while improving safety by operating with a higher margin between the design temperature and material upper-use temperature. Studies have shown that using actively cooled CMCs can reduce the weight of the cooled flow-path component from 4.5 to 1.6 lb/ft² and the weight of the propulsion system's cooled surface area by more than 50 percent. This weight savings enables

advanced concepts, increased payload, and increased range. The ability of the cooled CMC flow-path components to operate over 1000 °F hotter than the state-of-the-art metallic concept adds system design flexibility to space-access vehicle concepts. Other potential system-level benefits include smaller fuel pumps, lower part count, lower cost, and increased operating margin.

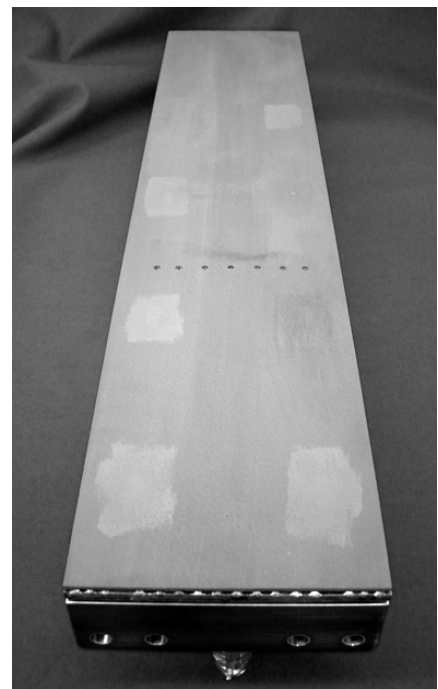
An innovative, cooled CMC design concept was developed in which a CMC hot surface panel was mechanically joined to a metallic coolant containment system by means of high-temperature CMC fasteners. This concept has the advantages of both low-cost manufacture and repairability, and its aggressive development schedule was met by an integrated design and fabrication approach. Initial test results of conceptual designs for cooled 1-by-6-in. coupons

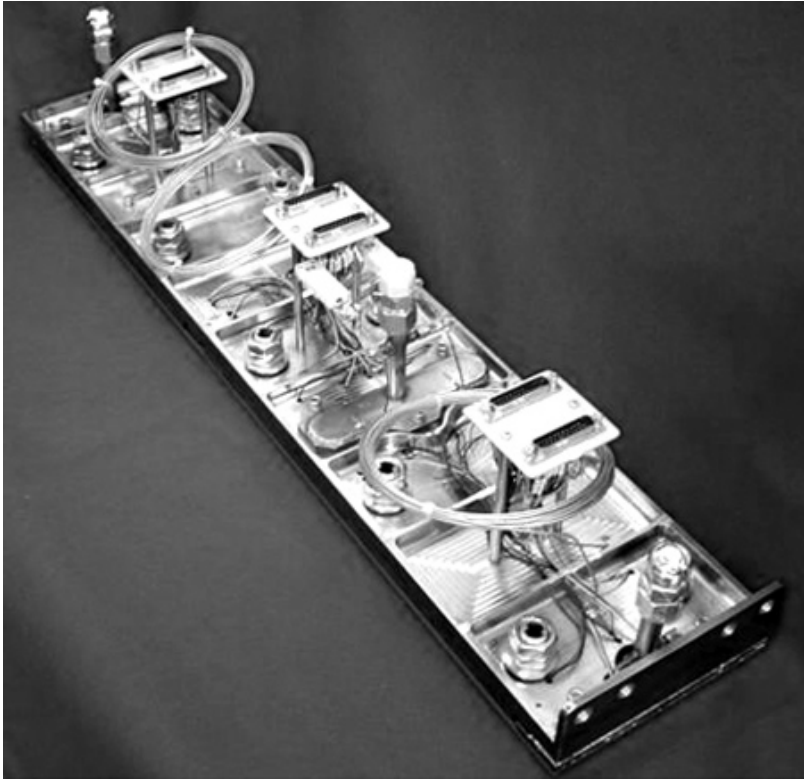


United Technologies scramjet facility with near sidewall and top panel omitted.



Left: United Technologies scramjet engine displaying section of combustor replaced by cooled CMC panel. Right: As-fabricated CMC panel assembly.





Fully instrumented CMC panel before testing in scramjet rig at United Technologies.

evaluated in a quartz lamp rig at United Technologies Research Center were used to validate the basic CMC heat exchanger concept by verifying cooling effectiveness. In the second testing phase, at the NASA Glenn Research Center, rocket engine tests on 2.5- by 10-in. panels were used to optimize the heat exchanger design by identifying critical issues and refining various design variables before scaling up to the scramjet-engine-scale component. The rocket engine tests evaluated the cooling effectiveness and structural integrity of various design concepts, resulting in planned material downselects and design concept refinement.

After successful tests with 2.5- by 10-in. panels, the fabrication process was scaled up to produce 6- by 30-in. panels, the largest cooled CMC panels ever fabricated. These panels were successfully tested in a United Technologies scramjet engine, demonstrating the performance benefits of cooled CMCs in a scramjet engine for the first time. This lightweight, high-temperature, and high-heat-flux component and the technology's adaptability to complex shapes may enable safe, affordable, and reliable future space transportation systems.

This project is a collaborative effort between multiple NASA centers, the Air Force Research Laboratory, and industry, from planning through execution. Actively cooled composites were identified as a key technology for the Venture-Star aerospike engine, for various hypersonic vehicle propulsion systems, and for meeting Integrated High Payoff Rocket Propulsion Technology goals. Specific applications have targeted various technical performance metrics, and competitive selections have invoked a broad range of industrial partners.

Throughout development, a dedicated core group of researchers from Glenn, the NASA Langley Research Center, and the NASA Marshall Space Flight Center has advocated, sustained, and transferred the technology by holding workshops and focusing efforts on specific, measurable, progressive developmental steps. Contract partners have included Pratt & Whitney, Boeing-Rocketdyne, Rockwell Science Center, Snecma (France), GE Power Systems Composites, Goodrich Corporation, Refractory Composites, Inc., and HITCO Carbon Composites, Inc. The concept demonstration by Pratt & Whitney in the Air Force's HySet engine at United Technologies represents a milestone critical to utilizing this technology for low-cost space access.

Bibliography

Jaskowiak, Martha H.; Dickens, Kevin W.; and Lawrence, Timothy W.: Light-Weight CMC Heat Exchanger Panels for Combined Cycle Propulsion Systems. Proceedings of the JANNAF 27th Airbreathing Propulsion Subcommittee Meeting, CPIA-JSC-CD-24, 2003. Available from Chemical Propulsion Information Agency (CPIA).

Jaskowiak, Martha H.; Dickens, Kevin W.; and Lawrence, Timothy W.: Actively Cooled Ceramic Matrix Composite Panels for Aerospace Applications. National Space & Missile Materials Symposium, June 23-27, 2003, San Diego, CA.

Glenn contact:

Martha H. Jaskowiak, 216-433-5515, Martha.H.Jaskowiak@nasa.gov

ZIN Technologies contact:

Kevin W. Dickens, 216-433-6491, Kevin.W.Dickens@grc.nasa.gov

Authors:

Martha H. Jaskowiak and Kevin W. Dickens

Headquarters program office:

Aeronautics Research

Programs/Projects:

NGLT

Special recognition:

Turning Goals Into Reality Award 2004

Permeability of Candidate Stirling Heater Head Materials Measured

Researchers at the NASA Glenn Research Center are evaluating high-temperature materials for Stirling heater heads for second- and third-generation Stirling radioisotope power systems that would help to increase the system efficiency to 30 to 35 percent and the system specific power to 8 to 10+ W/kg. Ceramic materials could make it possible for the convertor hot-end temperature to be increased to 1050 to 1200 °C, in comparison to the current 650 °C with an Inconel 718 heater head. A hermetically sealed Stirling heater head must retain a constant internal pressure of nearly 400-psi helium (He) throughout its useful life (120,000 hr) at the design operating temperature. Therefore, He permeability was measured for eight potential materials and compared with the permeability of the current heater head material, Inconel 718.

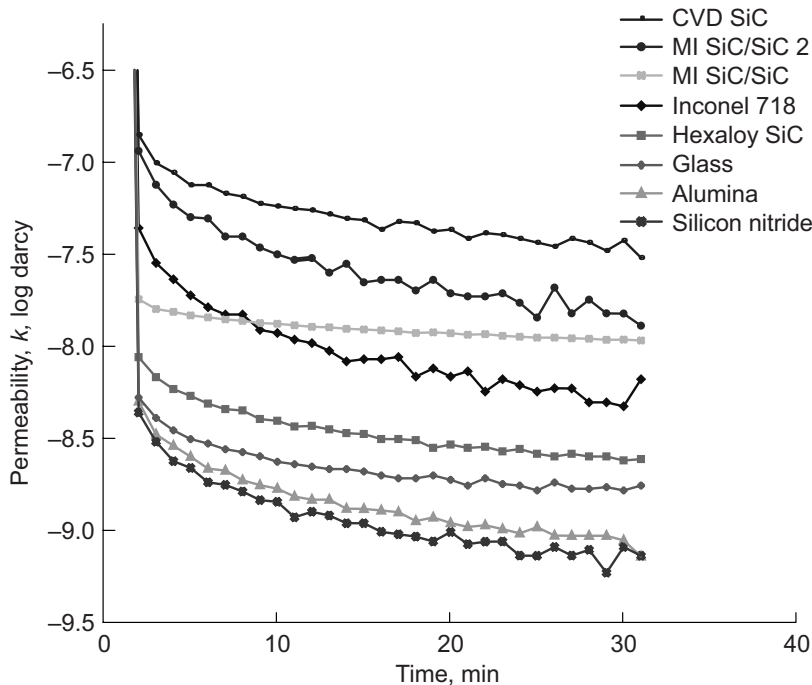
The eight materials included silicon nitride (Si_3N_4), silicon dioxide (SiO_2), both sintered and chemical vapor deposited (CVD) silicon carbide (SiC), alumina (Al_2O_3), two types of melt-infiltrated (MI) SiC/SiC composites, and a carbon/SiC composite (C/SiC). Glenn submitted samples of each material to Porous Materials, Inc., Ithaca, New York, for permeability analysis. At room temperature and 30-psi He, four materials— Si_3N_4 , Al_2O_3 , SiO_2 , and sintered SiC—demonstrated lower permeability than Inconel 718. The CVD SiC and all the composite materials were significantly more permeable to He than the baseline material.

These initial results show that ceramic materials are feasible replacements for the baseline Inconel 718. Glenn purchased from Porous Materials, Inc., a newly designed diffusion permeameter that is able to measure permeability at temperatures up to 1000 °C, and pressures up to 400 psi He. This will enable

Material	Darcian permeability, ^a $K,^b \text{ m}^2$
Si_3N_4	7.15×10^{-22}
Al_2O_3	7.09×10^{-22}
SiO_2	1.70×10^{-21}
Sintered SiC	2.48×10^{-21}
Inconel 718	6.51×10^{-21}
MI SiC/SiC #2	1.27×10^{-20}
CVD SiC	2.97×10^{-20}
MI SiC/SiC #1	1.06×10^{-20}
C/SiC	8.84×10^{-16}

^aAll materials were tested at room temperature and 30-psi He in the Porous Materials, Inc., diffusion permeameter, with two exceptions. The CVD SiC was tested at 20-psi He (leakage occurred at higher pressure), and the CVD C/SiC was measured in the gas permeameter with air as the fluid because of the much higher flow rate through the material.

^bPermeability was reported by Porous Materials, Inc., in darcy. (One darcy = 10^{-8} m^2 .) Permeability coefficients K_{He} were calculated from reported values by the relationship $K_{\text{He}} = (P_d/P_u)(D/A)S_{\text{eff}}$, where P_d is the pressure in the down tube, P_u is the pressure in the up tube, D is the specimen thickness, A is the specimen area, and S_{eff} is the effective pumping rate.



Permeability coefficient, K_{He} , in log darcy versus time in minutes. Smaller negative numbers indicate greater permeability. For example, silicon nitride and silica are less permeable to He than Inconel 718 is.

additional in-house permeability testing at temperatures and pressures relevant to the Stirling heater head. These measurements are necessary to select the best ceramic material for use at the higher temperatures.

Glenn contact:

Marc R. Freedman, 216-433-3284,
Marc.R.Freedman@nasa.gov

QSS Group, Inc., contact:

Dr. Mrityunjay Singh, 216-433-8883,
Mrityunjay.Singh@grc.nasa.gov

Authors:

Marc R. Freedman and Mrityunjay Singh

Headquarters program office:

Exploration Systems

Programs/Projects:

Project Prometheus, Advanced Stirling Technology

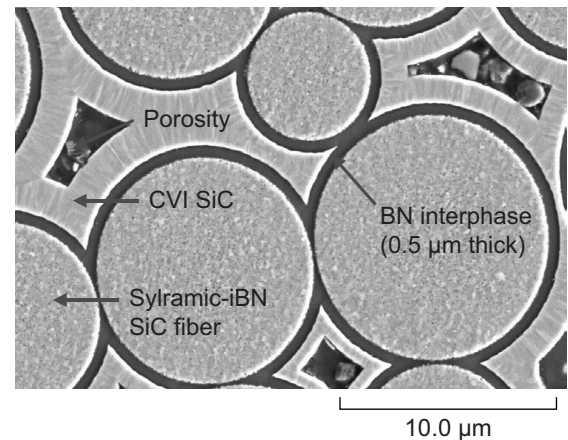
SiC/SiC Ceramic Matrix Composites Developed for High-Temperature Space Transportation Applications

Researchers at the NASA Glenn Research Center have been developing durable, high-temperature ceramic matrix composites (CMCs) with silicon carbide (SiC) matrices and SiC or carbon fibers for use in advanced reusable launch vehicle propulsion and airframe applications in the Next Generation Launch Technology (NGLT) Program (ref. 1). These CMCs weigh less and are more durable than competing metallic alloys, and they are tougher than silicon-based monolithic ceramics (refs. 1 to 3). Because of their high specific strength and durability at high temperatures, CMCs such as C/SiC (carbon-fiber-reinforced silicon carbide) and SiC/SiC (silicon-carbide-fiber-reinforced silicon carbide) may increase vehicle performance and safety significantly and reduce the cost of transporting payloads to orbit.

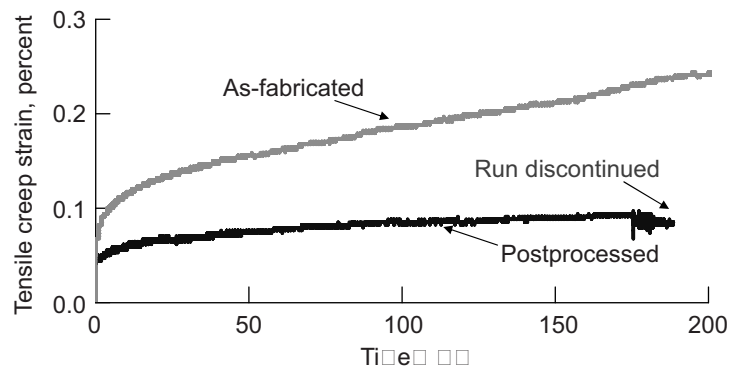
The composite components of primary interest in the NGLT Propulsion Research and Technology Project were cooled CMC heat exchanger panels (ref. 4) and inserted uncooled CMC turbine blades. Our materials development task initially focused on C/SiC, which has typically been the primary CMC system of interest for reusable launch vehicle airframe and propulsion component applications. However, these components were expected to perform for at least 100 hot hours of operation at peak temperatures in the range of 1427 to 1650 °C (2600 to 3000 °F) in air or combustion gases under mechanical and thermal stresses. Because required material properties and characteristics included low permeability, oxidation and creep resistance, and the ability to withstand extreme thermal transients, we initiated the development of a high-temperature SiC/SiC CMC to take advantage of (1) the uncracked matrix of SiC/SiC (as-processed C/SiC has cracks in the matrix and fiber tows), (2) the superior oxidation resistance of SiC fibers, and (3) the use of a boron nitride (BN) interphase, which is more oxidatively stable than the C interphase used in C/SiC.

SiC/SiC composites developed in the past for aeronautics applications were clearly unsuitable for long-term application at 1450 °C because SiC fibers with inadequate creep resistance were used and/or melt-infiltrated (MI) SiC matrices (ref. 5) were used that had significant amounts of free silicon, which limits the maximum use temperature. In this study, full chemical vapor infiltrated (CVI) SiC/SiC CMCs containing state-of-the-art SiC fibers (Sylramic-iBN) and interphases (silicon-doped BN) were developed (see the photomicrograph). These CVI SiC/SiC CMCs have survived over 500 hr of creep-rupture testing at 1450 °C in air under an applied stress of 69 MPa (ref. 1). In comparison, MI SiC/SiC developed in the NASA Ultra-Efficient Engine Technology Project ("1/01 Material") experienced excessive specimen

deformation and failed after approximately 50 hr under the same conditions. The improved durability of the CVI SiC/SiC is attributed to its more refractory matrix (unlike in MI SiC/SiC CMCs, the matrix does not incorporate free silicon, which becomes molten at temperatures >1410 °C). A postprocessing heat treatment (ref. 3) of the CVI SiC/SiC further improved the creep resistance and thermal



Microstructure of a Sylramic-iBN SiC-fiber-reinforced CVI SiC CMC, showing the center of a fiber tow in the center of the specimen.



Creep-rupture of as-fabricated (creep rate, $1.7 \times 10^{-9} \text{ sec}^{-1}$) and postprocessed (creep rate, $2.5 \times 10^{-10} \text{ sec}^{-1}$) CVI SiC/SiC CMCs in air at 1450 °C (2642 °F), under 69-MPa (10-ksi) loading.

conductivity of the material (see the graph on the preceding page). Eliminating the porosity that is inherent in CMCs densified via CVI through additional processing to densify the matrix could improve durability, and alternate processing routes are currently being evaluated at Glenn through Independent Research & Development funding.

NGLT SiC/SiC development ended in September 2004 because the program was cancelled. However, this material development effort indicated that CVI SiC/SiC is a viable candidate for high-temperature applications, including inserted CMC turbine blades, cooled CMC panels, and reusable space vehicle airframe applications. Recently initiated development at Glenn of MI and CVI SiC/SiC CMCs with higher proportional limits (through Independent Research & Development funding) is further improving material durability and providing materials that can be used in the new space exploration initiatives.

References

1. Kiser, J.D., et al.: Durable High Temperature Ceramic Matrix Composites for Next Generation Launch Technology Propulsion Applications. Proceedings of the JANNAF 27th Airbreathing Propulsion Subcommittee Meeting, CPIA-JSC-CD-24, 2003. Available from Chemical Propulsion Information Agency (CPIA).
2. Kiser, J.D., et al.: Ceramic Matrix Composites for Reusable Launch Vehicle Propulsion Applications: A Comparison of C/SiC and SiC/SiC. Proceedings of the National Space and Missile Materials Symposium, Monterey, CA, June 24–28, 2001. Available from Anteon Corporation, NSMMS Coordinator.
3. Bhatt, R.T.; and DiCarlo, J.A.: Method Developed for Improving the Thermomechanical Properties of Silicon Carbide Matrix Composites. Research & Technology 2003, NASA/TM—2004-212729, 2004, pp. 20–21. <http://www.grc.nasa.gov/WWW/RT/2003/5000/5130bhatt.html>
4. Jaskowiak, M.H.: Research & Technology 2004, NASA/TM—2005-213419, 2005, pp. 82–83. <http://www.grc.nasa.gov/WWW/RT/2004/RM/RM24C-jaskowiak.html>

5. DiCarlo, J.A., et al.: High-Performance SiC/SiC Ceramic Composite Systems Developed for 1315 °C (2400 °F) Engine Components. Research & Technology 2003, NASA/TM—2004-212729, 2004, pp. 12–13. <http://www.grc.nasa.gov/WWW/RT/2003/5000/5100dicarlo.html>

Glenn contact:

J. Douglas Kiser, 216–433–3247,
James.D.Kiser@nasa.gov

U.S. Army Research Laboratory contact:

Dr. Ramakrishna T. Bhatt, 216–433–5513;
Ramakrishna.T.Bhatt@grc.nasa.gov

Authors:

J. Douglas Kiser,
Dr. Ramakrishna T. Bhatt,
Dr. Gregory N. Morscher,
Dr. Hee Mann Yun,
Dr. James A. DiCarlo, and
Jeanne F. Petko

Headquarters program office:

NGLT

Programs/Projects:

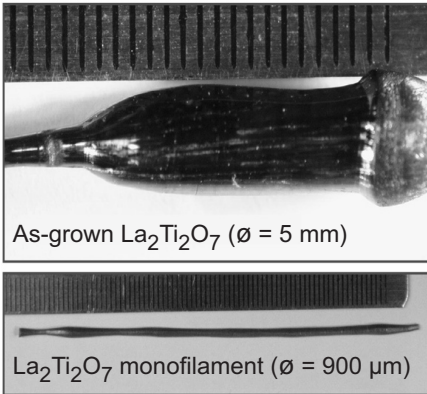
NGLT, Propulsion Research and Technology, Glenn IR&D (emphasis on improving resistance to matrix cracking), Exploration Systems (vehicle airframe or propulsion applications)

High-Temperature Piezoelectric Ceramic Developed

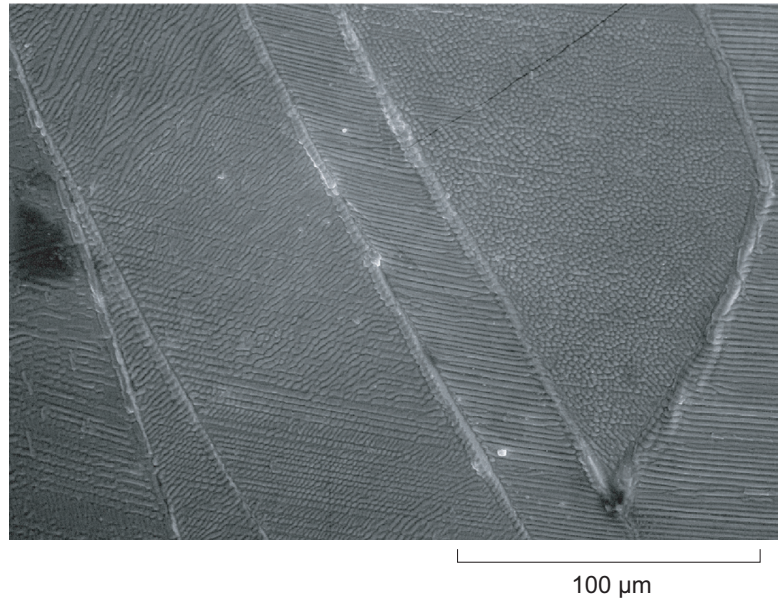
Active combustion control of spatial and temporal variations in the local fuel-to-air ratio is of considerable interest for suppressing combustion instabilities in lean gas turbine combustors and, thereby, achieving lower NO_x levels. The actuator for fuel modulation in gas turbine combustors must meet several requirements: (1) bandwidth capability of 1000 Hz, (2) operating temperature compatible with the fuel temperature, which is in the vicinity of 400 °F, (3) stroke of ~4 mils (100 μm), and (4) force of 300 lb-force. Piezoelectric actuators offer the fastest response time (microsecond time constants) and can generate forces in excess of 2000 lb-force. The state-of-the-art piezoceramic material in industry today is Pb(Zr,Ti)O₃, called PZT. This class of piezoelectric ceramic is currently used in diesel fuel injectors and in the development of high-response fuel-modulation valves. PZT materials are generally limited to operating temperatures of 250 °F, which is 150 °F lower than the desired operating temperature for gas turbine combustor fuel-modulation injection valves. Thus, there is a

clear need to increase the operating temperature range of piezoceramic devices for active combustion control in gas turbine engines.

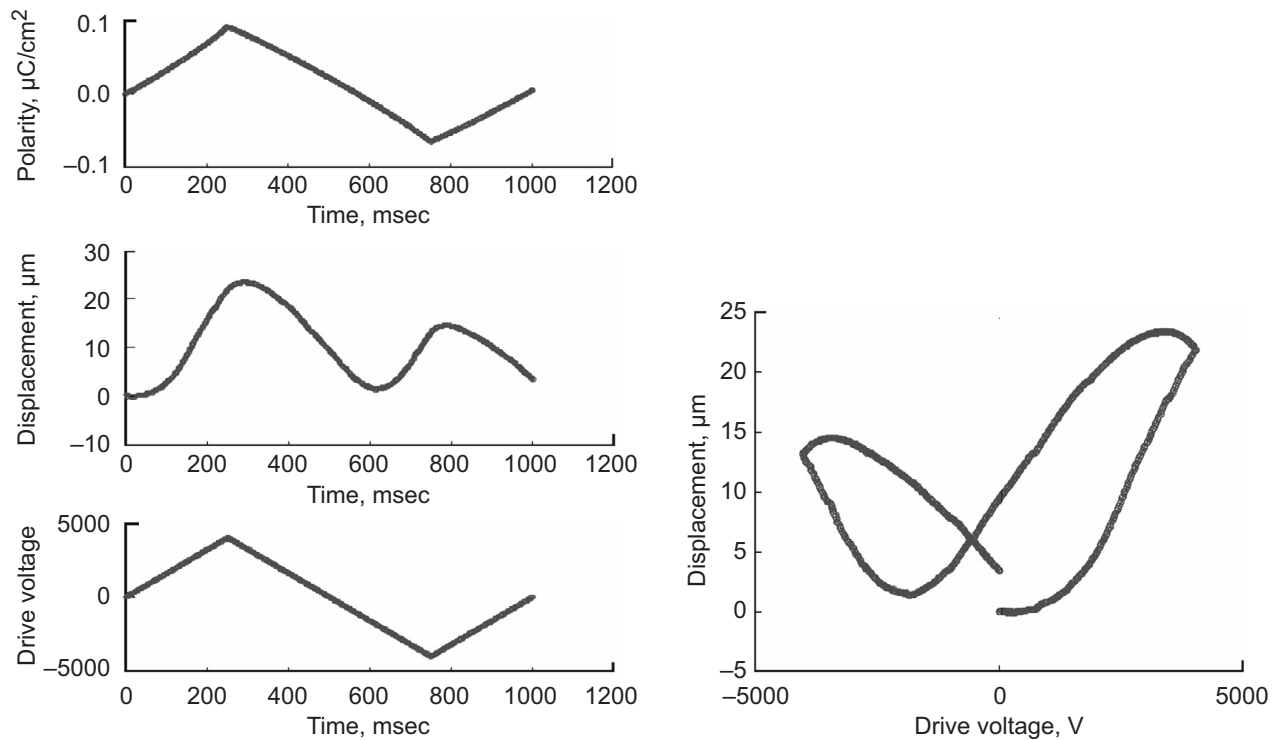
Over the past year, substantial progress was made at the NASA Glenn Research Center in demonstrating the feasibility of high-temperature piezoelectric materials. A novel laser-melt process was developed for growing single-crystal fibers and rods of lanthanum-titanate (see the top left photograph on the next page),



Different diameter high-temperature piezoelectric $\text{La}_2\text{Ti}_2\text{O}_7$ single crystals are grown. $\text{La}_2\text{Ti}_2\text{O}_7$ crystals in monofilament form are used for high-temperature composite fabrication. Larger diameter single crystals are used to produce textured bulk piezoelectric specimens. \varnothing = diameter.



Textured high-temperature piezoelectric $\text{La}_2\text{Ti}_2\text{O}_7$ successfully grown. Crystal habit is $\sim 12^\circ$ off $[110]$ as determined by x-ray (not shown).



High-temperature piezoelectric $\text{La}_2\text{Ti}_2\text{O}_7$. Left: Time-dependent response of the drive voltage, displacement, and polarity. Right: Corresponding elongation and contraction of the 1-mm-thick ceramic element (± 4 kV, 10 sec).

and lanthanum titanate ($\text{La}_2\text{Ti}_2\text{O}_7$) was demonstrated to produce electrically actuated displacements one-quarter that of commercial lead-based piezoelectrics. However, with a high-curie-temperature material (2600 °F), lanthanum titanate has the potential for displacement at temperatures where commercial PZT fails. In addition, we are developing a lower-cost method for texturing the polycrystalline material. (This yields about 80 percent of the single-crystal

displacement but is much more amenable to commercial production.) This processing technique produces fully dense textured ceramics (see the photomicrograph at the top right), eliminates grain boundary phases,

and produces oriented low-energy interfaces. The textured piezoelectric ceramic structures ensure a high level of strain capability and a high degree of electromechanical coupling. Texture achieves much of the property benefits of single crystals, including greater success in polarization (domain alignment through application of high voltage, which enhances performance). This is of paramount importance with additional high-temperature piezoelectric ceramics systems of interest, such as bismuth perovskite and other systems of low crystal symmetry. Low crystal symmetry greatly increases the difficulty of polarization. The results shown in the graphs on the preceding page are for an initial chemical formulation; refinements in composition and processing are expected to increase both the displacement and temperature capability. This work is an enabling technology for adaptive flow and combustion control concepts for intelligent propulsion systems.

Case Western Reserve University contact:

Dr. Ali Sayir, 216-433-6254, Ali.Sayir@grc.nasa.gov

Glenn contacts:

Dr. Serene C. Farmer, 216-433-3289, Serene.C.Farmer@nasa.gov; and Dr. Frederick W. Dynys, 216-433-2404, Frederick.W.Dynys@nasa.gov

Authors:

Dr. Ali Sayir, Dr. Serene C. Farmer, and Dr. Frederick W. Dynys

Headquarters program office:

Aeronautics Research

Programs/Projects:

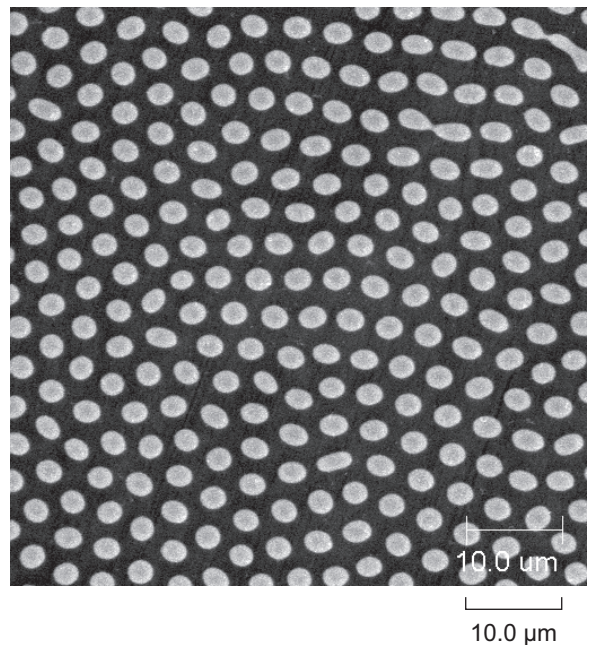
VSP, Intelligent Engines Foundation Technology, UEET

Structures Self-Assembled Through Directional Solidification

Nanotechnology has created a demand for new fabrication methods with an emphasis on simple, low-cost techniques. Directional solidification of eutectics (DSE) is an unconventional approach in comparison to low-temperature biomimetic approaches. A technical challenge for DSE is producing microstructural architectures on the nanometer scale. In both processes, the driving force is the minimization of Gibb's free energy. Self-assembly by biomimetic approaches depends on weak interaction forces between organic molecules to define the architectural structure. The architectural structure for solidification depends on strong chemical bonding between atoms. Constituents partition into atomic-level arrangements at the liquid-solid interface to form polyphase structures, and this atomic-level arrangement at the liquid-solid interface is controlled by atomic diffusion and total undercooling due to composition (diffusion), kinetics, and curvature of the boundary phases. Judicious selection of the materials system and control of the total undercooling are the keys to producing structures on the nanometer scale.

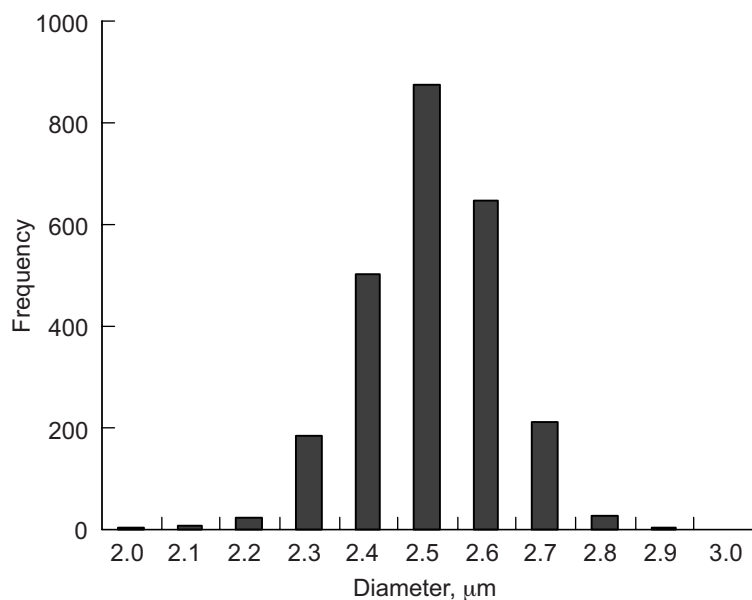
The silicon-titanium silicide (Si-TiSi_2) eutectic forms a rod structure under isothermal cooling conditions. At the NASA Glenn Research Center, directional solidification was employed along with a thermal gradient to promote uniform rods oriented with the thermal gradient. This photomicrograph shows the typical transverse microstructure of a solidified Si-TiSi_2 eutectic composition. The dark and light gray regions are Si and TiSi_2 , respectively. Preferred rod orientation along the thermal gradient was poor. The ordered TiSi_2 rods have a narrow distribution in diameter of 2 to 3 μm , as shown in the graph on the next page. The rod diameter showed a weak dependence on process conditions.

Anisotropic etch behavior between different phases provides the opportunity to fabricate structures with high aspect ratios. The photomicrographs on the

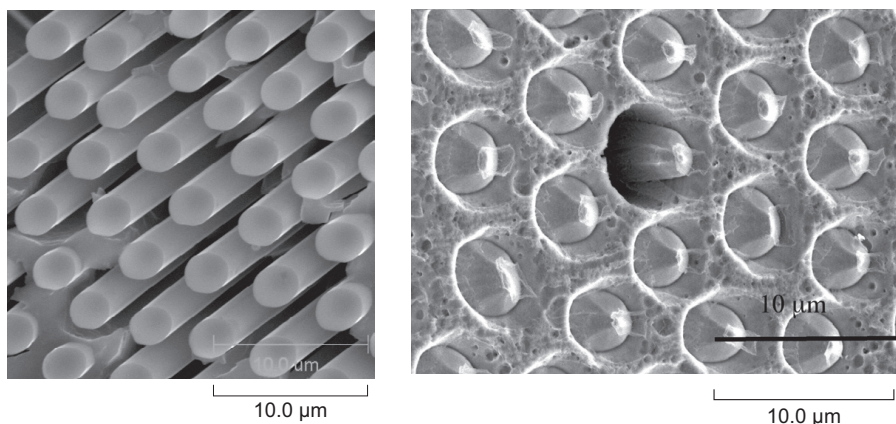


TiSi₂ rods in a Si matrix.

next page show the resulting microstructure after a wet chemical etch and a dry plasma etch. The wet chemical etches the silicon away, exposing the TiSi_2 rods, whereas plasma etching preferentially etches the Si-TiSi_2 interface to form a crater. The porous architectures are applicable to fabricating microdevices or creating templates for part fabrication. The



Diameter distribution of TiS₂ rods.



Left: Potassium-hydroxide- (KOH)- etched DSE Si-TiS₂. Right: Plasma-etched Si-TiS₂ microstructure.

porous rod structure can serve as a platform for fabricating microplasma devices for propulsion or microheat exchangers and for fabricating microfilters for miniaturized chemical reactors. Although more work is required, self-assembly from DSE can have a role in microdevice fabrication.

Currently, aspect ratios are limited in semiconducting materials because the anisotropic etch properties are controlled by crystallography. Additional benefits of DSE include fabrication simplicity, process control of microstructure, and stability of the structure at high temperatures. Like other bottomup methods, DSE is not suitable for making complex or interconnected patterns.

Glenn contact:

Dr. Frederick W. Dynys, 216-433-2404,
Frederick.W.Dynys@nasa.gov

Case Western Reserve University contact:

Dr. Ali Sayir, 216-433-6254,
Ali.Sayir@grc.nasa.gov

Authors:

Dr. Frederick W. Dynys and Dr. Ali Sayir

Headquarters program office:

Aeronautics Research

Programs/Projects:

Aerospace and Power Base
Nanotechnology

High-Temperature Proton-Conducting Ceramics Developed

High-temperature protonic conductors (HTPC) are needed for hydrogen separation, hydrogen sensors, fuel cells, and hydrogen production from fossil fuels. The HTPC materials for hydrogen separation at high temperatures are foreseen to be metal oxides with the perovskite structure $A^{2+}B^{4+}O_3^{2-}$ and with the trivalent cation (M^{3+}) substitution at the B^{4+} -site to introduce oxygen vacancies. The high affinity for hydrogen ions (H^+) is advantageous for protonic transport, but it increases the reactivity toward water (H_2O) and carbon

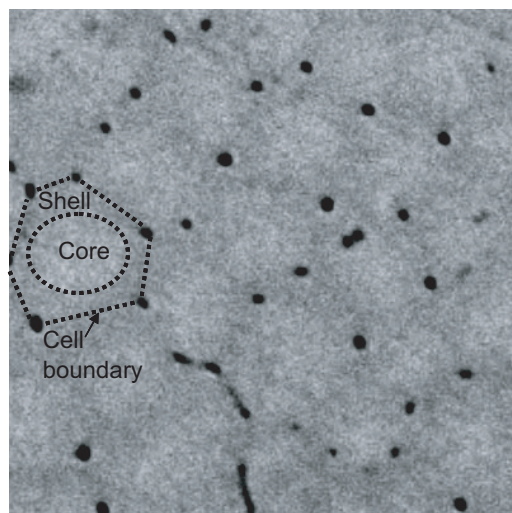
dioxide (CO_2), which can lead to premature membrane failure. In addition, there are considerable technological challenges related to the processing of HTPC materials. The high melting point and multi-cation chemistry of HTPC materials creates difficulties in

in achieving high-density, single-phase membranes by solid-state sintering. The presence of secondary phases and grain-boundary interfaces are detrimental to the protonic conduction and environmental stability of polycrystalline HTPC materials.

This investigation at the NASA Glenn Research Center explored the prospect of improving the protonic conductance and chemical stability concurrently by producing high-density structures by melt processing. Melt processing of ceramics is being developed to produce engineered microstructures to enhance material properties. The investigation focused on simple ABO_3 and complex $A_3(B'_{1+x}B''_{2-x})O_{9-\delta}$ perovskite structures using chemical compositions of $SrCe_{1-x}Y_xO_{3-\delta}$ and $Sr_3(Ca_{1+x}Nb_{2-x})O_{9-\delta}$. The advantages of melt processing over solid-state sintering are (1) high-density materials approaching 100 percent are achievable by pore coalescence in the melt; (2) secondary grain boundary phases are eliminated, and coherent low-energy interfaces are formed; and (3) self-assembly produced ordered microstructures at the nanoscale. Melt-processed materials demonstrate stability in high-temperature environments containing high concentrations of water vapor (4 to 6 months).

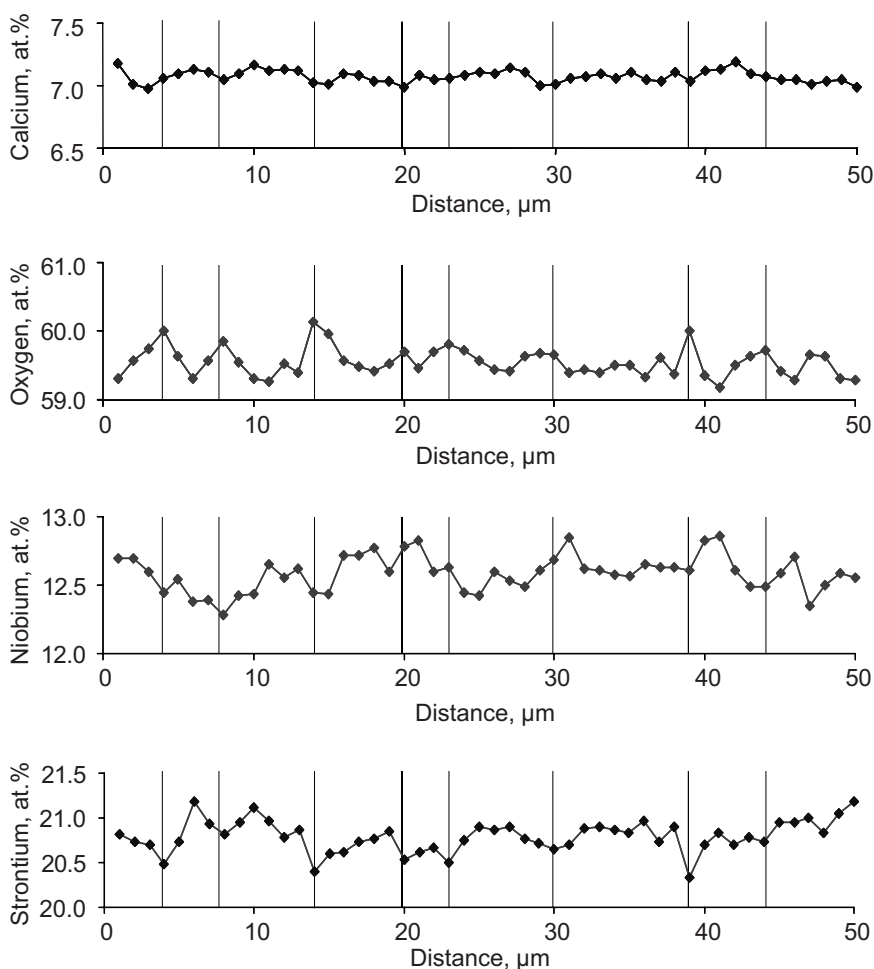
The backscattered-electron scanning electron micrograph image shown here, along with the superimposed schematic drawing, illustrates a compositional segregation (core-shell) produced by the melt process for $Sr_3(Ca_{1+x}Nb_{2-x})O_{9-\delta}$. The core of the cells is richer in calcium and strontium, whereas the shell of the cells is richer in oxygen and niobium, as revealed by the wavelength-dispersive x-ray chemical mappings shown in the graphs on this page. Determined by impedance spectroscopy, the shell regions act as resistive barriers for protonic conduction, whereas the core region exhibits higher protonic conduction for $Sr_3(Ca_{1+x}Nb_{2-x})O_{9-\delta}$.

Transmission electron microscopy (TEM) examination of melt-processed HTPC materials revealed fabricated nanoscale architectures that cannot be achieved by solid-state sintering. The next two figures show dark-field images of nanoscale architectures in $SrCe_{0.9}Y_{0.1}O_{3-\delta}$ (left) and $Sr_3(Ca_{1+x}Nb_{2-x})O_{9-\delta}$ (right). Selected area diffraction and high-resolution TEM analysis reveal that the domains in $SrCe_{0.9}Y_{0.1}O_{3-\delta}$ consist of a phase where the oxygen octahedras are tilted. This tilting is believed to reduce the rotation angle for the diffusing

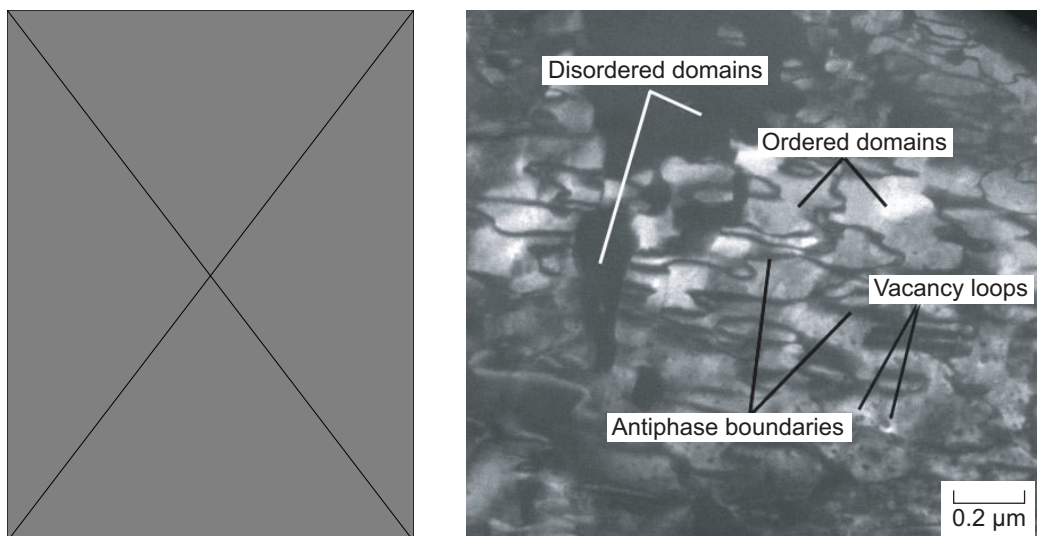


20 μm

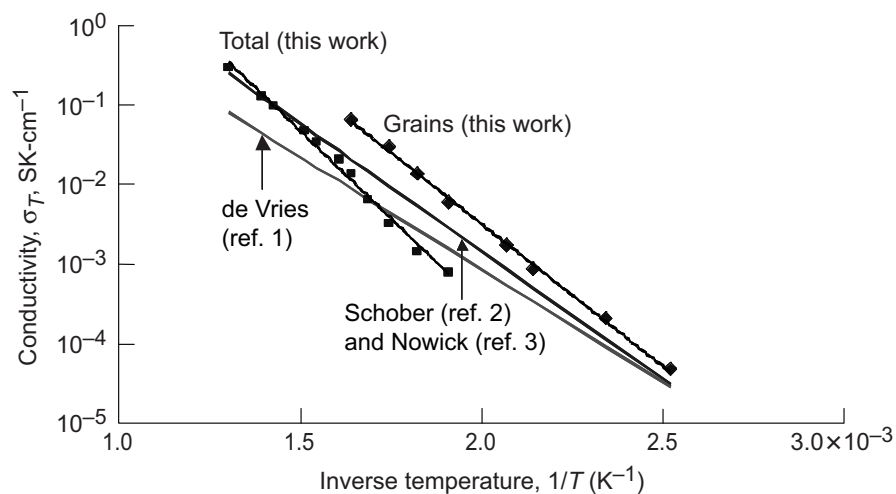
Scanning electron microscope photograph of a cross section of $Sr_3(Ca_{1+x}Nb_{2-x})O_{9-\delta}$ imaged by backscattered electrons. Superimposed illustration shows the core, shell, and cellular boundary.



Chemical concentration profiles across several cells (vertical lines indicate cell boundaries) of a $Sr_3(Ca_{1+x}Nb_{2-x})O_{9-\delta}$ sample. Oxygen-rich boundaries are revealed.



Left: Nanodomain formation in melt-processed $\text{SrCe}_{1-x}\text{Y}_x\text{O}_{3-\delta}$. Boundaries indicate the oxygen cage tilting mode; arrows show the domain boundaries. Right: TEM image of $\text{Sr}_3(\text{Ca}_{1+x}\text{Nb}_{2-x})\text{O}_{9-\delta}$ showing a complex nanodomain structure. Nanodomains exist as ordered and disordered regions. Ordered domains are separated by antiphase boundaries.



Grain conductivity and total conductivity of melt-processed $\text{SrCe}_{1-x}\text{Y}_x\text{O}_{3-\delta}$ in comparison to literature values. Impedance spectroscopy measurements show a high intragrain conductance. Poor conduction of the grain boundary reduces the total conductance.

H^+ ion, enhancing the transfer rate from one oxygen octahedron to the next octahedron. This interpretation has been supported by the superior conductivity data shown in the final graph. The impedance analysis shows that the intragrain has superior conductance that can be associated with nanodomain formation. Engineering the microstructure, down to the nanoscale (as shown in the dark-field image on the left) is continuing, and our current research is focused on assembling these nanodomains on a macroscale to enhance the H_2 permeability rate. The conductivity data shown in the final graph has a strong merit for hydrogen-generation technology in the temperature region of 400 to 600 °C. Applications could be in hydrogen production and separation, using

small reformers and electrolyzers, or in a high-temperature hydrogen sensor for aerospace applications.

References

1. de Vries, K.J.: Electrical and Mechanical Properties of Proton Conducting $\text{SrCe}_{0.95}\text{Yb}_{0.05}\text{O}_{3-\alpha}$. SSIOD, vol. 100, nos. 3–4, 1997, pp. 193–200.
2. Schober, T.: Water Vapor Solubility and Impedance of High Temperature Proton Conductor $\text{SrZr}_{0.9}\text{Y}_{0.1}\text{O}_{2.95}$. SSIOD, vol. 145, nos. 1–4, 2001, pp. 319–324.
3. Nowick, A.S.; and Du, Yang: High-Temperature Protonic Conductors With Perovskite-Related Structures. SSIOD, vol. 77, 1995, pp. 137–146.

Case Western Reserve University contact:

Dr. Ali Sayir, 216–433–6254,
Ali.Sayir@grc.nasa.gov

Glenn contact:

Dr. Frederick W. Dynys, 216–433–2404,
Frederick.W.Dynys@nasa.gov

Authors:

Dr. Ali Sayir, Dr. Frederick W. Dynys,
and Dr. M.H. Berger

Headquarters program office:

Aeronautics Research

Programs/Projects:

IR&D

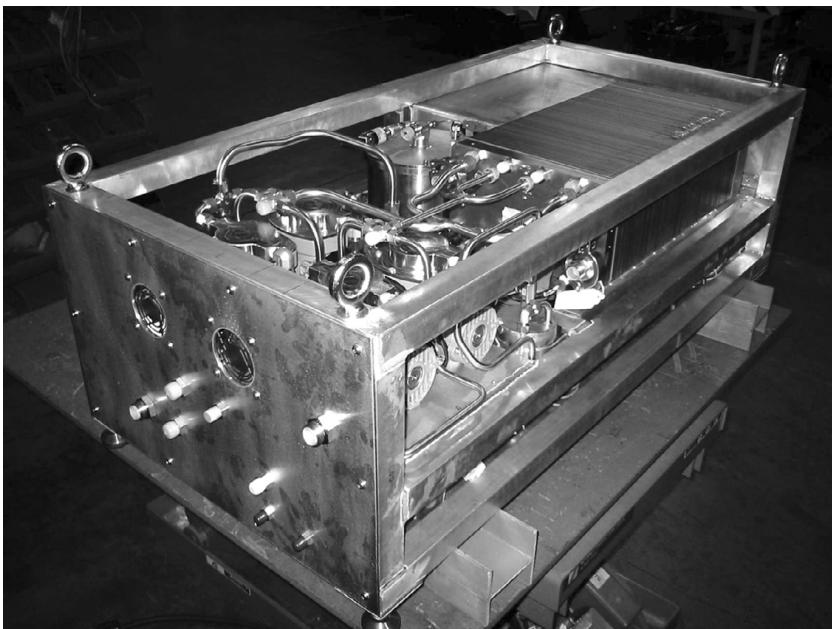
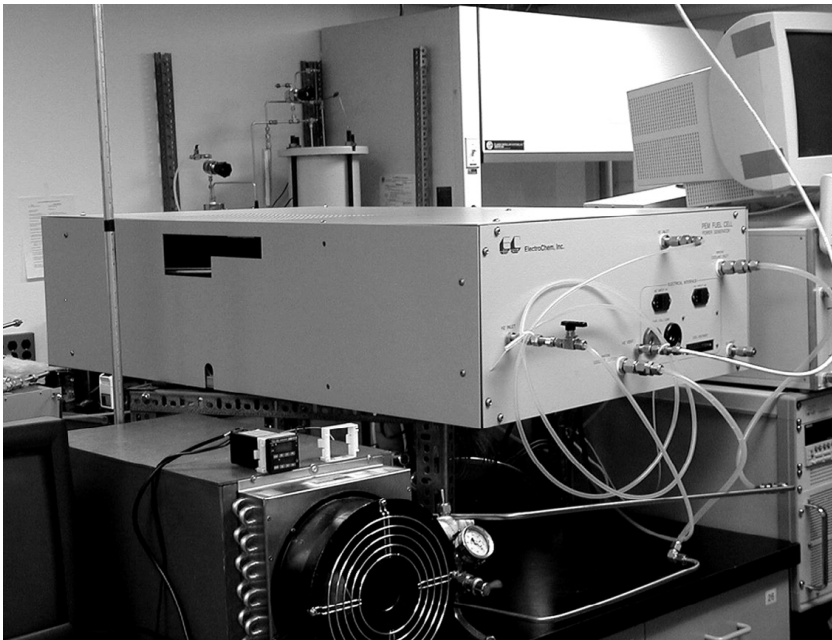
Power and Electrical Propulsion

Proton-Exchange-Membrane Fuel Cell Powerplants Developed and Tested for Exploration Missions

Proton-exchange-membrane fuel cell (PEMFC) technology has received major attention for terrestrial applications, such as the automotive and residential markets, for the past 20 years. This attention has significantly advanced the maturity of the technology, resulting in ever more compact, efficient, reliable,

and inexpensive PEMFC designs. In comparison to the terrestrial operating environment, the space operating environment is much more demanding. Microgravity to high-gravity loads and the need to use pure oxygen (rather than air) as the fuel cell oxidizer place more stringent demands on PEMFC technology. NASA and its partners from industry are leveraging terrestrial PEMFC advancements by conducting parallel space technology development for future exploration missions.

A team from the NASA Glenn Research Center, NASA Johnson Space Center, and NASA Kennedy Space Center recently completed the first phase of a PEMFC powerplant development effort for exploration missions. The industry partners for this phase of the development effort were ElectroChem, Inc., and Teledyne Energy Systems, Inc. Under contract to Glenn, both of these industry partners successfully designed, fabricated, and tested a breadboard PEMFC powerplant in the 1- to 5-kW power range (see the photographs). These powerplants were based on existing company-proprietary fuel cell stack designs, combined with off-the-shelf components, which formed the balance of the powerplant design. Subsequent to the contractor development efforts, both powerplants were independently tested at Johnson to verify operational and performance characteristics, and to determine suitability for further technology development in the second phase of the NASA-led effort. Following the independent NASA testing, Teledyne Energy Systems, Inc., was selected to develop an engineering model PEMFC powerplant.



Top: ElectroChem breadboard. Bottom: Teledyne breadboard.

COMPARISON OF BREADBOARD PEMFC
POWERPLANT CHARACTERISTICS

Vendor	ElectroChem	Teledyne
Nominal power, kW	1.0	5.0
Number of cells	45	82
Cell active area, cm ²	232	302
Nominal current density, mA/cm ²	110	270
Peak power capability (peak/nominal)	6:1	>6:1
Reactant recirculation approach	Passive (ejectors)	Active (pumps)

This effort was initiated by the 2nd Generation Reusable Launch Vehicle (RLV) Program Office in 2001; it transitioned to the Next Generation Launch Technologies (NGLT) Program Office in 2003. The effort is now being funded by the Exploration Program Office. We plan to summarize the results from the

ongoing engineering model PEMFC powerplant development in a future Research & Technology article.

Glenn contacts:

Mark A. Hoberecht, 216-433-5362,
Mark.A.Hoberecht@nasa.gov; and
Nang T. Pham, 216-433-6165,
Nang.T.Pham@nasa.gov

Authors:

Mark A. Hoberecht and Nang T. Pham

Headquarters program office:

Exploration Systems

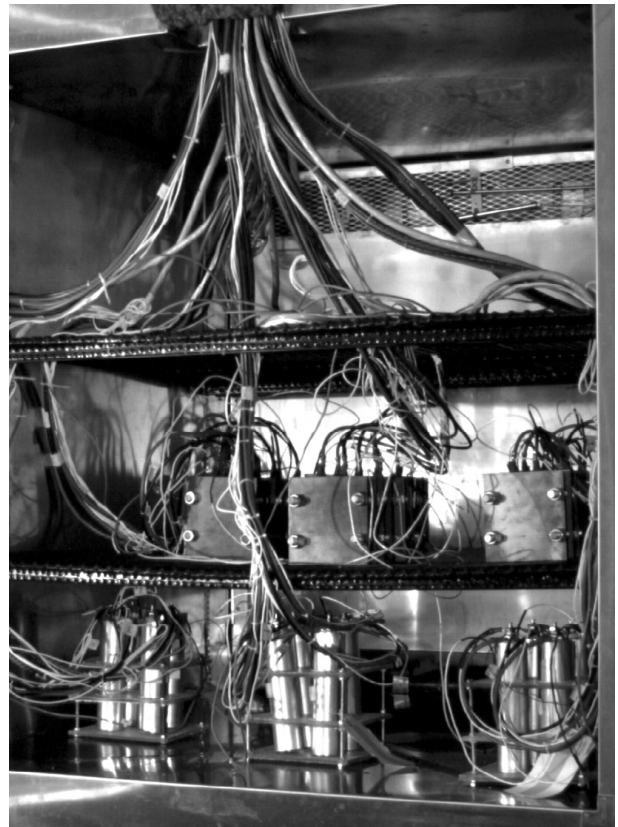
Programs/Projects:

Exploration Systems, Space Power
Systems R&T

Lithium-Ion Batteries Being Evaluated for Low-Earth-Orbit Applications

The performance characteristics and long-term cycle life of aerospace lithium-ion (Li-ion) batteries in low-Earth-orbit applications are being investigated. A statistically designed test using Li-ion cells from various manufacturers began in September 2004 to study the effects of temperature, end-of-charge voltage, and depth-of-discharge operating conditions on the cycle life and performance of these cells. Performance degradation with cycling is being evaluated, and performance characteristics and failure modes are being modeled statistically. As technology improvements are incorporated into aerospace Li-ion cells, these new designs can be added to the test to evaluate the effect of the design changes on performance and life.

Cells from Lithion and Saft have achieved over 2000 cycles under 10 different test condition combinations and are being evaluated. Cells from Mine Safety Appliances (MSA) and modules made up of commercial-off-the-shelf 18650 Li-ion cells connected in series/parallel combinations are scheduled to be added in the summer of 2005. The test conditions include temperatures of 10, 20, and 30 °C, end-of-charge voltages of 3.85, 3.95, and 4.05 V, and depth-of-discharges from 20 to 40 percent. The low-Earth-orbit regime consists of a 55-min charge, at a constant-current rate that is 110 percent of the current required to fully recharge the cells in 55 min until the charge voltage limit is reached, and then at a constant voltage for the remaining charge time. Cells are discharged for 35 min at the current required for their particular depth-of-discharge condition.



Lithium-ion cells from Saft and Lithion installed in a test chamber.

Cells are being evaluated in four-cell series strings with charge voltage limits being applied to individual cells by the use of charge-control units designed and produced at the NASA Glenn Research Center (ref. 1). These charge-control units clamp the individual cell voltages as each cell reaches its end-of-charge voltage limit, and they bypass the excess current from that cell, while allowing the full current flow to the remaining cells in the pack.

The goal of this evaluation is to identify conditions and cell designs for Li-ion technology that can achieve more than 30,000 low-Earth-orbit cycles. Testing is being performed at the Naval Surface Warfare Center, Crane Division, in Crane, Indiana.

Reference

1. Reid, Concha M., et al.: Lithium-Ion Cell Charge-Control Unit Developed, Research & Technology 2004, NASA/TM—2005-213419, 2005, pp. 94–95. <http://www.grc.nasa.gov/WWW/RT/2004/RP/RPC-reid.html>

Find out more about this research:
<http://www.grc.nasa.gov/WWW/Electrochemistry/>

Glenn contacts:

Barbara I. McKissock, 216–433–6102, Barbara.I.McKissock@nasa.gov; and Thomas B. Miller, 216–433–6300, Thomas.B.Miller@nasa.gov

Author:

Barbara I. McKissock

Headquarters program office:

Exploration Systems

Programs/Projects:

Power Systems R&T, Science and Exploration Orbiters, ISS

Lithium-Ion Cell Charge-Control Unit Developed

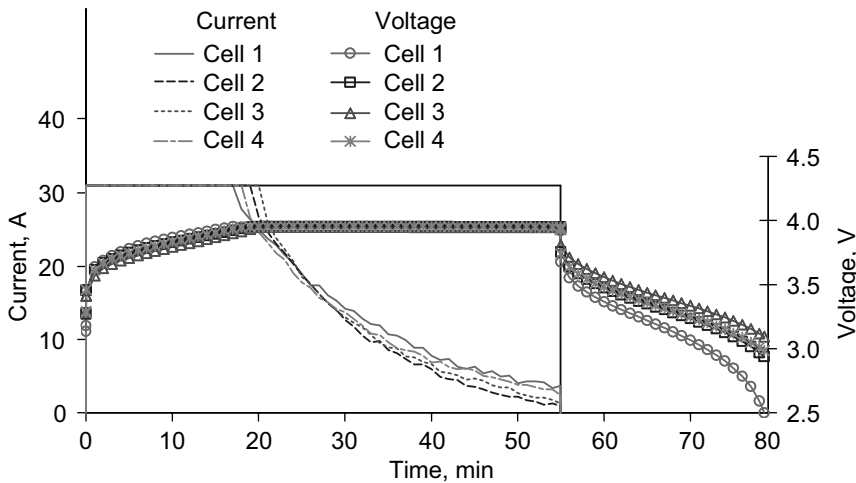
A lithium-ion (Li-ion) cell charge-control unit was developed as part of a Li-ion cell verification program (ref. 1). This unit manages the complex charging scheme that is required when Li-ion cells are charged in series. It enables researchers to test cells together as a pack, while allowing each cell to charge individually. This allows the inherent cell-to-cell variations to be addressed on a series string of cells and reduces test costs substantially in comparison to individual cell testing.

Life-test data of Li-ion cells is critical in order to establish their performance capabilities for NASA missions and exploration goals. NASA missions that fly in low Earth orbit require more than 30,000 cycles to meet many mission requirements, and Li-ion batteries are relatively new to this type of application. They require a more complex charging scheme than is typically required of the alkaline cells that they may replace, and they require that strict voltage cutoff levels be established and followed to ensure safe, long operation.

So that this requirement could be addressed on the laboratory test level, a method was needed to manage the current through each cell once it reached its cutoff voltage limit. In response to these requirements, a team of researchers at the NASA Glenn Research Center developed a Li-ion cell charge-control unit. The unit allows multiple Li-ion battery cells in a series-connected pack to charge independently of each other when they are being charged from a single current source. The unit serves the dual purpose of (1) ensuring that individual

cells are charged at full current up to their voltage limit and are then held at that voltage while allowing the current to taper so that the cell can continue to gain additional capacity without becoming overcharged and (2) allowing cells that are at lower states of charge to continue to be charged at full current until they reach their voltage limit.

The unit consists of electronic circuits and thermal management devices housed in a common package. It also contains isolated annunciators to signal when each cell is actively being bypassed. These annunciators can be used by external charge managers or can be connected in series to signal that all cells have reached maximum charge. The charge-control circuitry is self-powered by each of the battery cells being regulated, eliminating the



Charge control of four Li-ion cells during low-Earth-orbit cycling.

need for an external power source or controller to drive the circuitry. A 110-V alternating-current source of electricity is required to power the thermal management portion of the system, and a small direct-current voltage source is needed to activate the annunciator signal, if desired.

The Li-ion cell charge-control unit can address the unique charging requirements of Li-ion cells on an individual cell basis while reducing the number of channels required to test the cells, resulting in substantial cost savings to the testing program. The charge-control unit was coinvented at Glenn by NASA and QSS Group, Inc., researchers, and the work was performed under

the NASA Aerospace Flight Battery Systems program funded through the Energetics Project of NASA's Office of Aerospace Technology.

Reference

1. McKissock, Barbara I.: Lithium-Ion Batteries Being Evaluated for Low-Earth-Orbit Applications. Research & Technology 2004, NASA/TM—2005-213419, 2005, pp. 93–94. <http://www.grc.nasa.gov/WWW/RT/2004/RP/ RPC-mckissock.html>

Find out more about this research:

<http://www.grc.nasa.gov/WWW/Electrochemistry/>

Glenn contacts:

Concha M. Reid, 216-433-8943, Concha.M.Reid@nasa.gov; and Michelle A. Manzo, 216-433-5261, Michelle.A.Manzo@nasa.gov

Authors:

Concha M. Reid, Michelle A. Manzo, Robert M. Button, and Russel Gemeiner

Headquarters program office:

OAT

Programs/Projects:

NASA Aerospace Battery Systems

Integrated Power and Attitude Control System Demonstrated With Flywheels G2 and D1

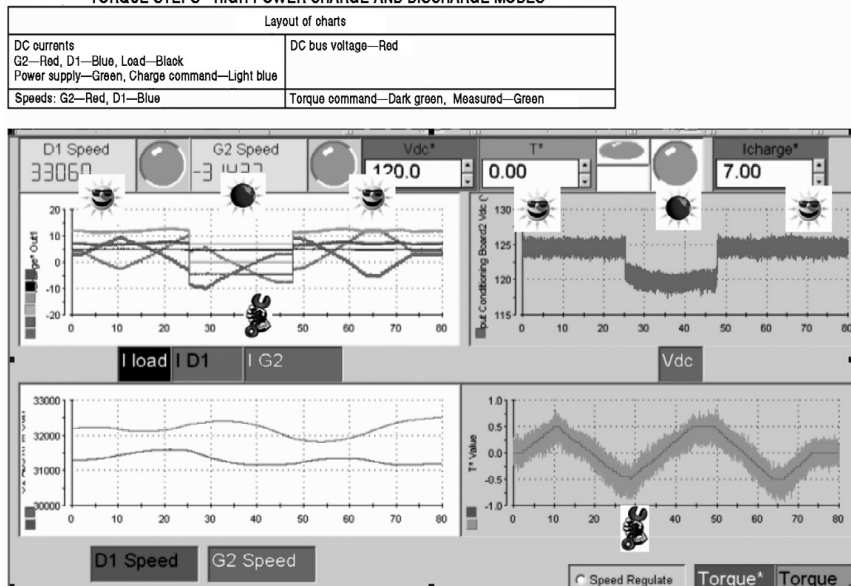
On September 14, 2004, NASA Glenn Research Center's Flywheel Development Team experimentally demonstrated a full-power, high-speed, two-flywheel system, simultaneously regulating a power bus and providing a commanded output torque. Operation- and power-mode transitions were demonstrated up to 2000 W in charge and 1100 W in discharge, while the output torque was simultaneously regulated between ± 0.8 N-m.

The G2 and D1 flywheels—magnetically levitated carbon-fiber wheels with permanent magnet motors—were used for the experiment. The units were mounted on an air bearing table in Glenn's High Energy Flywheel Facility. The operational speed range for these tests was between 20,000 and 60,000 rpm. The bus voltage was regulated at 125 V during charge and discharge, and charge-discharge and discharge-charge transitions were demonstrated by



Test hardware for Integrated Power and Attitude Control System.

TORQUE STEPS—HIGH-POWER CHARGE AND DISCHARGE MODES



IPACS power and torque profile. This figure is shown in color in the online version of this article (<http://www.grc.nasa.gov/WWW/RT/2004/RP/RPE-jansen.html>).

changing the amount of power that the power supply provided between 300 and 0 W. In a satellite system, this would be the equivalent of changing the amount of energy that the solar array provides to the spacecraft. In addition to regulating the bus voltage, we simultaneously controlled the net torque produced by the two flywheel modules. Both modules were mounted on an air table that was restrained by a load cell. The load cell measured the force on the table, and the torque produced by the two flywheels on the table

could be calculated from that measurement. This method was used to measure the torque produced by the modules, yielding net torques from -0.8 to 0.8 N-m. This was the first Glenn demonstration of the Integrated Power and Attitude Control System (IPACS) at high power levels and speeds.

Find out more about this research:

Aerospace Flywheel Development:
<http://space-power.grc.nasa.gov/ppo/projects/flywheel/>

Glenn's Structural Mechanics & Dynamics Branch:
<http://structures.grc.nasa.gov/5930/>

Glenn contacts:
 Raymond F. Beach, 216-433-5320, Raymond.F.Beach@nasa.gov; and
 James F. Soeder, 216-433-5328, James.F.Soeder@nasa.gov

University of Toledo contact:
 Ralph H. Jansen, 216-433-6038, Ralph.H.Jansen@grc.nasa.gov

Author:
 Ralph H. Jansen

Headquarters program office:
 Exploration Systems

Programs/Projects:
 Energetics

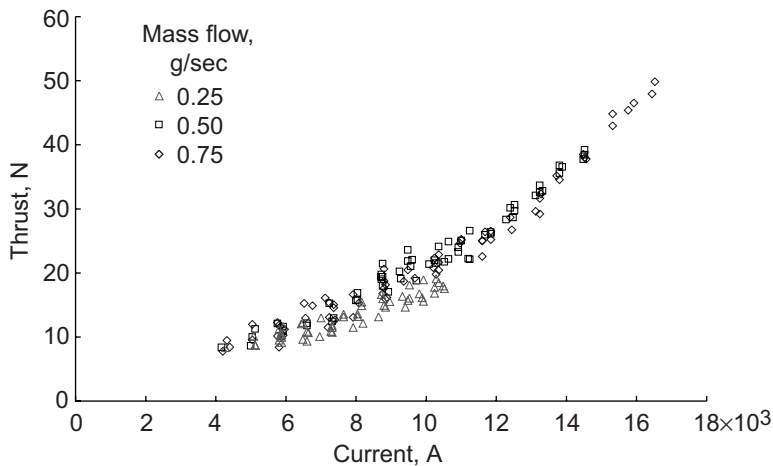
Testing Done for Lorentz Force Accelerators and Electrodeless Propulsion Technology Development

The NASA Glenn Research Center is developing Lorentz force accelerators and electrodeless plasma propulsion for a wide variety of space applications. These applications range from precision control of formation-flying spacecraft to primary propulsion for very high power interplanetary spacecraft. The specific thruster technologies being addressed are pulsed plasma thrusters, magnetoplasmadynamic thrusters, and helicon-electron cyclotron resonance acceleration thrusters.

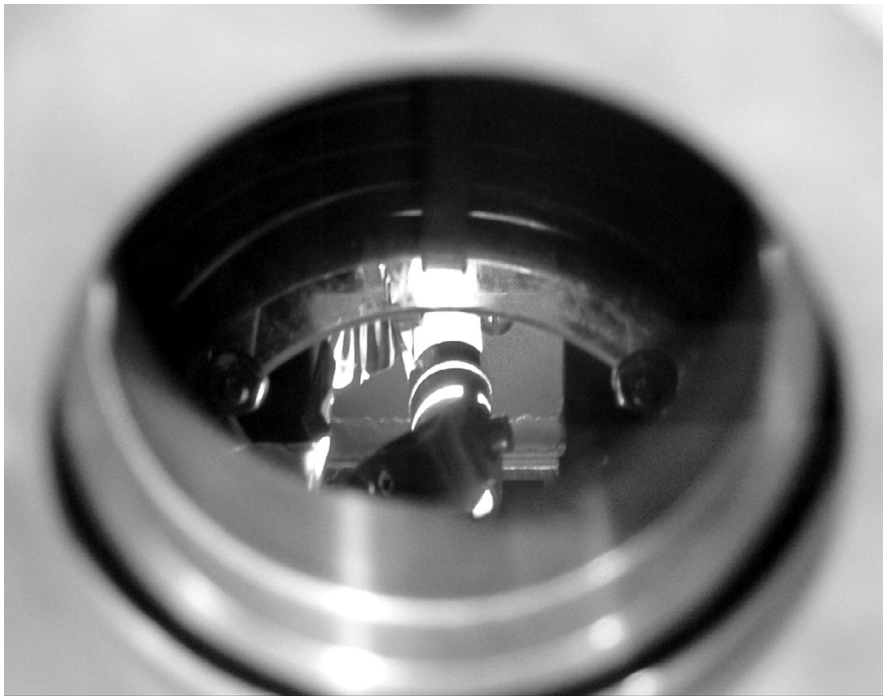
The pulsed plasma thruster mounted on the Earth Observing-1 spacecraft was operated successfully in orbit in 2002. The two-axis thruster system is fully incorporated in the attitude determination and control system and is being used to automatically counteract disturbances in the pitch axis of the spacecraft. Recent on-orbit operations have focused on extended operations

to add flight operation time to the total accumulated thruster life. The results of the experiments pave the way for electric propulsion applications on future Earth-imaging satellites.

Future pulsed plasma thrusters will include longer-life, higher-precision, multi-axis thruster configurations for applications such as three-axis attitude control systems or high-precision, formation-flying systems. Advanced components, such as a



Magnetoplasmadynamic thruster performance mapped over a range of currents and flow rates.



Helicon source operating in inductive mode inside the vacuum chamber.

mica-foil capacitor, a wear-resistant spark plug, and a multichannel power-processing unit were developed under NASA contract with Unison Industries, General Dynamics, and C.U. Aerospace. A life test has demonstrated over 39 million pulses on these components, which approaches the near-term life requirements for deep-space interferometry demonstrator missions. The spark plug life is less than expected. Excessive spark plug electrode wear is being addressed by incorporating novel wear-resistant metals. The improved design is currently under evaluation. In addition, a three-axis pulsed-plasma thruster demonstration module, which examines thruster packaging

issues, was fabricated and was operated successfully in a functionality test.

High-power steady-state Lorentz force accelerators are being considered as primary propulsion options for robotic and piloted interplanetary and deep-space missions. The Lorentz force accelerator team is developing megawatt-class magnetoplasmadynamic thrusters to meet these demanding future mission requirements. The self-field baseline magnetoplasmadynamic thruster has been tested with argon propellant at power levels up to approximately 5 MW. Thruster performance was accurately measured using a thrust stand and calibrated mass flow and power measurements. The thrust reached values up to 50 N at 16,000 A, for mass flow rates ranging from 0.25 to 0.75 g/sec, with thruster operation at higher currents limited by the onset of voltage oscillations. The thrust values display the expected quadratic increase in thrust with discharge current characteristic of these devices. The use of an additional applied magnetic field and the use of hydrogen propellant are the next steps in improving thruster performance.

Electric propulsion thrusters either currently in use or near realization share the need for electrodes in direct contact with the plasma they generate. The elimination of the electrode-plasma interaction could either increase lifetime with high-performance propellants or allow the use of in situ propellants such as lunar oxygen. In recognition of the potential advantages offered by electrodeless propulsion, Glenn has begun to investigate helicon wave sources both as possible replacements to existing thruster components and as the basis for future advanced in-space propulsion systems. The initial research effort has been to

determine the feasibility of a short, narrow helicon source and to find the proper magnetic field strengths, radiofrequency power levels, and flow rates for effective plasma ionization. The first operation of the helicon source to generate plasma was achieved as shown in the photograph on the preceding page.

Find out more about this research:

Earth Observing-1 PPT experiment:

<http://space-power.grc.nasa.gov/ppo/projects/eo1/>

Earth Observing-1:

<http://eo1.gsfc.nasa.gov/>

Lorentz Force Accelerator research at Glenn:

<http://www.grc.nasa.gov/WWW/lfa/>

Glenn contact:

Eric J. Pencil, 216-977-7463, Eric.J.Pencil@nasa.gov

Ohio Aerospace Institute (OAI)

contact:

James H. Gilland, 216-433-6192,
James.H.Gilland@grc.nasa.gov

Authors:

Eric J. Pencil, James H. Gilland,
Lynn A. Arrington, and Dr. Hani Kamhawi

Headquarters program offices:

Science, Exploration Systems, Earth
Science, Space Science, Space Flight,
Aerospace Technology

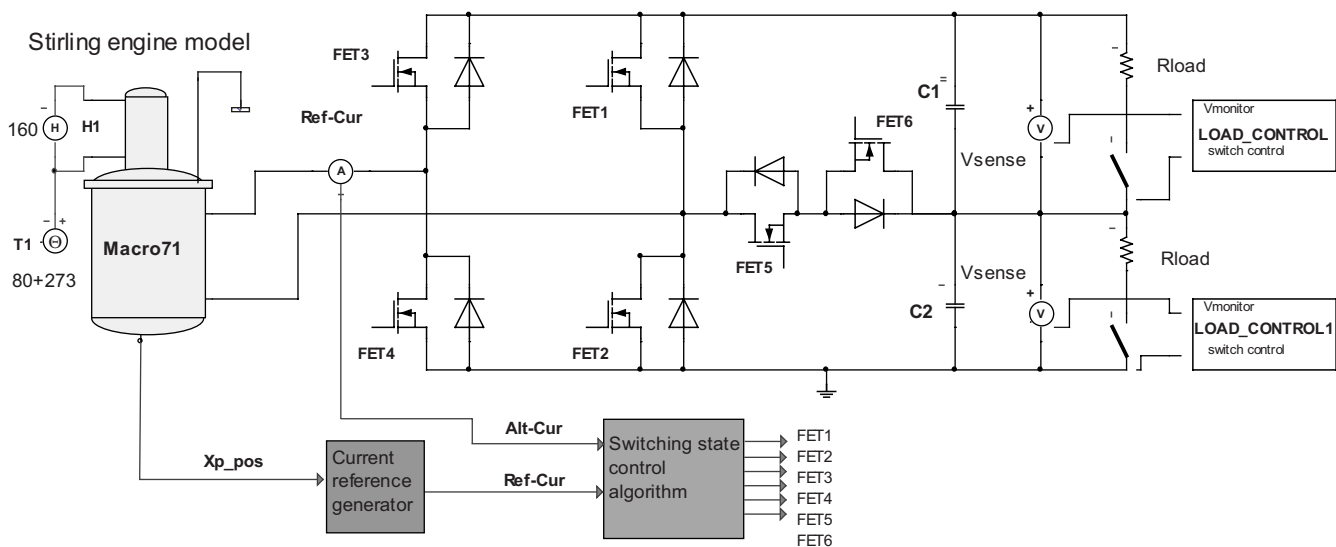
Programs/Projects:

Energetics, Project Prometheus

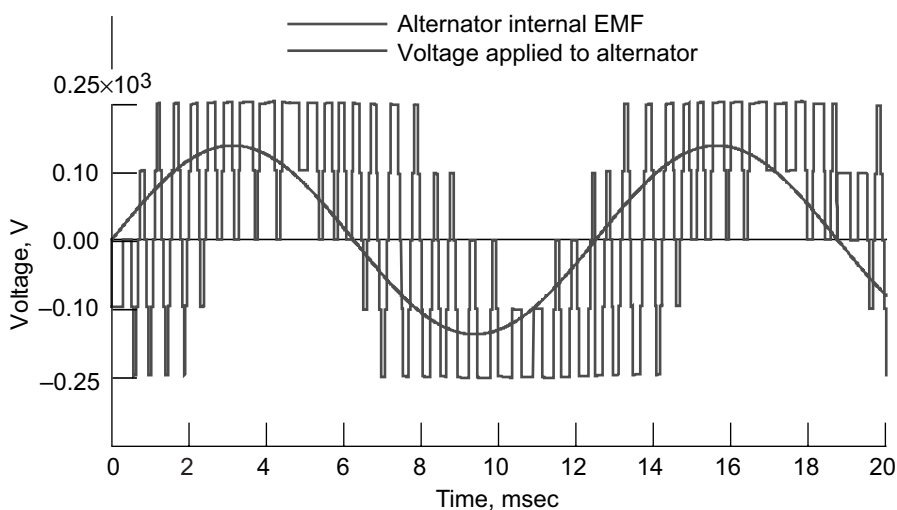
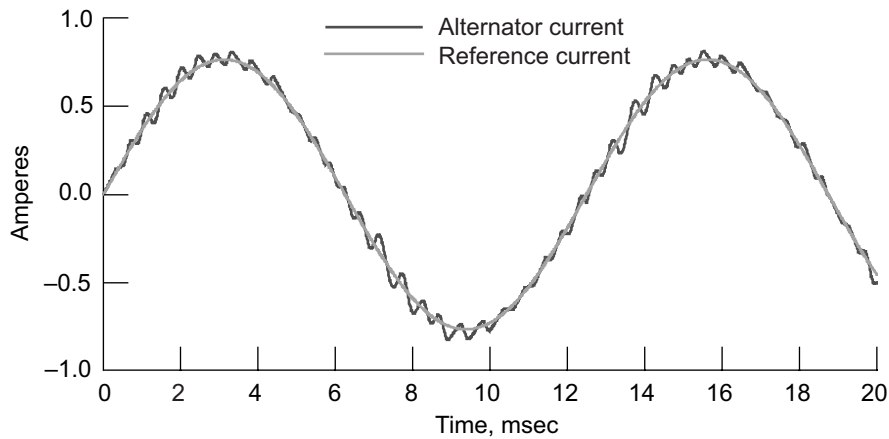
Advanced Controller Developed for the Free-Piston Stirling Convertor

A free-piston Stirling power convertor is being considered as an advanced power-conversion technology for future NASA deep-space missions requiring long-life radioisotope power systems. The NASA Glenn Research Center has identified key areas where advanced technologies can enhance the capability

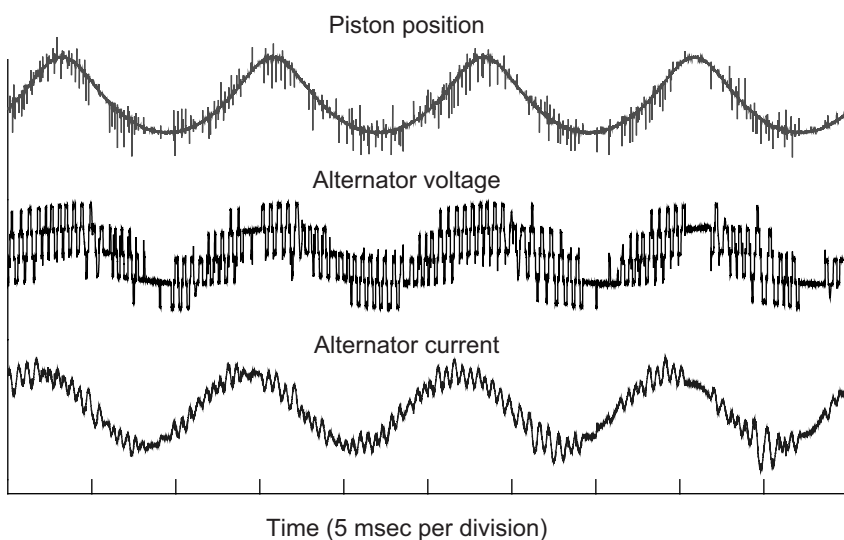
of Stirling energy-conversion systems. One of these is power electronic controls. Current power-conversion technology for Glenn-tested Stirling



Active Power Factor Controller (APFC) and the Technology Demonstration Convertor's system dynamic model (ref. 1). *Alt-Cur*, alternator current; *C1* and *C2*, capacitors 1 and 2; *FET1* to *FET6*, MOSFET (metal oxide semiconductor field effect transistor) control signal 1 to 6; *H1*, hot-end temperature; *Ref-Cur*, reference current signal; *Rload*, load resistor; *T1*, cold-end temperature; *Vsense*, load voltage; *Xp_pos*, piston position.



Simplorer simulations of the APFC.



APFC operation with dual-opposed Stirling Technology Demonstration Convertors. This graph is shown in color in the online version of this article (<http://www.grc.nasa.gov/WWW/RT/2004/RP/RPT-gerber.html>).

systems consists of an engine-driven linear alternator generating an alternating-current voltage controlled by a tuning-capacitor-based alternating-current peak voltage load controller. The tuning capacitor keeps the internal alternator electromotive force (EMF) in phase with its respective current (i.e., passive power factor correction). The alternator EMF is related to the piston velocity, which must be kept in phase with the alternator current in order to achieve stable operation. This tuning capacitor, which adds volume and mass to the overall Stirling convertor, can be eliminated if the controller can actively drive the magnitude and phase of the alternator current.

To support the state-of-the-art development activity, the Active Power Factor Controller (APFC) has been developed. This controller utilizes active power factor correction electronics and microcontroller-based controls. The selected power-stage topology for the APFC is based on a three-level full-bridge circuit (ref. 2). This circuit, which was modeled in Simplorer (Ansoft Corporation, Pittsburgh, PA), as shown in the diagram on the preceding page, is similar to a standard full-bridge circuit, except that it can provide five voltage levels for positive current control and five voltage levels for negative current control. The full-bridge topology can provide only two voltage levels for each current polarity. The top and center graphs show Simplorer simulations of the alternator current, the reference current, the alternator internal EMF, and the voltage applied to the alternator by the power stage.

Abreadboard version of the controller has been designed, fabricated, and tested successfully with dual-opposed Stirling convertors at light loads as shown in the bottom graph. Future plans are to continue the development process and to test at the full rated convertor power.

References

1. Regan, Timothy F.; Gerber, Scott S.; and Roth, Mary Ellen: Development of a Dynamic, End-to-End Free Piston Stirling Converter Model. NASA/TM—2004-212941, 2004. <http://gltrs.grc.nasa.gov/cgi-bin/GLTRS/browse.pl?2003/TM-2004-212941.html>
2. Bor-Ren Lin; and Zong-Liang Hung: A Single-Phase Bidirectional Rectifier With Power Factor Correction. Proceedings of IEEE Region 10 International Conference on Electrical and Electronic Technology, IEEE Catalogue No. 01CH37239, vol. 2, 2001, pp. 601–605.

Find out more about this research:

<http://www.grc.nasa.gov/WWW/tmsb/>

ZIN Technologies, Inc., contacts:

Scott S. Gerber, 216–433–5226, scott.gerber@zin-tech.com; and
Mike Jamison, 216–433–2588, mike.jamison@zin-tech.com

Glenn contact:

Mary Ellen Roth, 216–433–6288,
MaryEllen.Roth-1@nasa.gov

Author:

Scott S. Gerber

Headquarters program office:

Science

Programs/Projects:

Project Prometheus

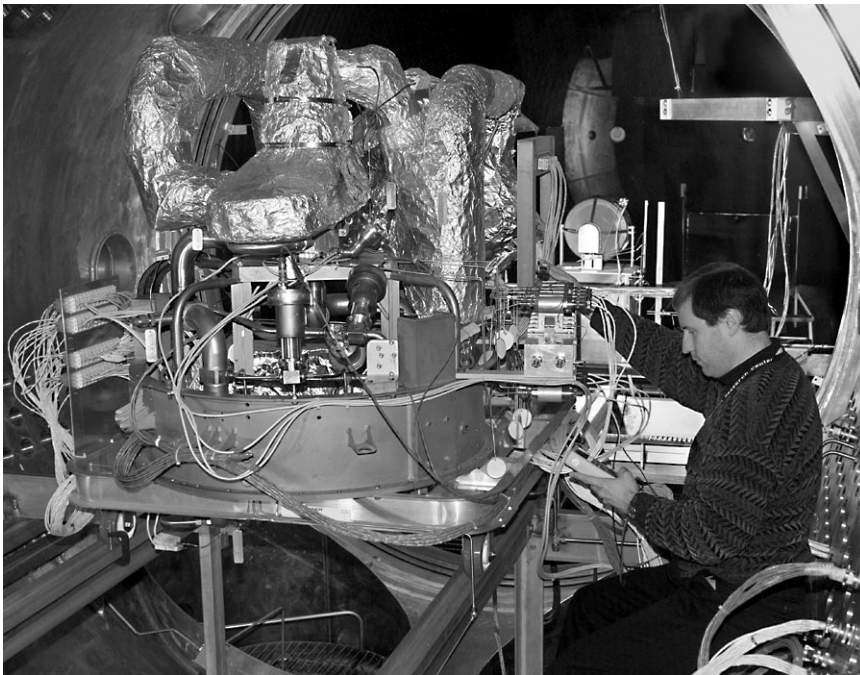
Brayton-Cycle Power-Conversion Unit Tested With Ion Thruster

Nuclear electric propulsion has been identified as an enabling technology for future NASA space science missions, such as the Jupiter Icy Moons Orbiter (JIMO) now under study. An important element of the nuclear electric propulsion spacecraft is the power-conversion system, which converts the reactor heat to electrical power for use by the ion propulsion system and other spacecraft loads. The electrical integration of the power converter and ion thruster

represents a key technical challenge in making nuclear electric propulsion technology possible.

This technical hurdle was addressed extensively on December 1, 2003, when a closed-Brayton-cycle power-conversion unit was tested with a gridded ion thruster at the NASA Glenn Research Center. The test demonstrated end-to-end power throughput and marked the first-ever coupling of a Brayton turboalternator and a gridded ion thruster, both of which are candidates for use on JIMO-type missions. The testing was conducted at Glenn's Vacuum Facility 6, where the Brayton unit was installed in the 3-m-diameter vacuum test port and the ion thruster was installed in the 7.6-m-diameter main chamber.

The Brayton test unit was a fully integrated power-conversion system including a turboalternator, recuperator, and gas cooler with helium-xenon working fluid designed for operation up to 2 kW. The heat source used in the test was a series of silicon-carbide electrical resistance heaters



Closed-Brayton-cycle and NSTAR thruster installed in Glenn's Vacuum Facility 6.

contained in a shell and tube heat exchanger that heated the helium-xenon gas to over 1000 K, simulating a fission reactor source. A commercial chiller with a pumped ethylene glycol cooling loop provided waste heat rejection, simulating a space radiator system.

The ion thruster used in the test was an engineering model of the NASA Solar Electric Propulsion Technology Application Readiness (NSTAR) gridded ion thruster used successfully as the main propulsion system on the NASA Deep Space 1 Mission in 1998. The NSTAR thruster is rated for operation up to 2.3 kW, providing 92-mN thrust and 3100-sec specific impulse using xenon propellant. The similar power rating of the Brayton-cycle power-conversion unit and the NSTAR made for a natural pairing.

The Brayton alternator power was routed through a fully representative power management and distribution (PMAD) system, designed and built in-house at Glenn. The PMAD converted the 55-V (root mean square, line-to-neutral), three-phase alternating-current (ac) alternator output to 1100 direct-current volts (Vdc) for use by the thruster beam supply. A transformer-rectifier-filter approach was used for the ac-to-dc conversion.

The PMAD system also provided Brayton speed and voltage control via a parasitic load radiator designed to maintain a constant load on the alternator regardless of thruster demand. High-speed load transfer between the parasitic load radiator and the thruster beam supply provided fault protection during thruster recycles. Recycles are intermittent and unpredictable electrical transients that occur with ion thrusters, resulting in a momentary short-circuit

condition. If not properly managed, thruster recycles could harm the thruster grids, the PMAD, or the Brayton rotating equipment. The testing verified that a recycle could be detected, the power switched from the beam supply within several milliseconds, and the power switched back to the beam supply in less than a second, all while maintaining the thruster in operating mode.

Find out more about this research:

<http://www.grc.nasa.gov/WWW/tmsb/>

Glenn contact:

Lee S. Mason, 216-977-7106,
Lee.S.Mason@nasa.gov

Analex Corporation contact:

David S. Hervol, 216-433-9624,
David.S.Hervol@grc.nasa.gov

Author:

David S. Hervol

Headquarters program office:

Exploration Systems

Programs/Projects:

Project Prometheus

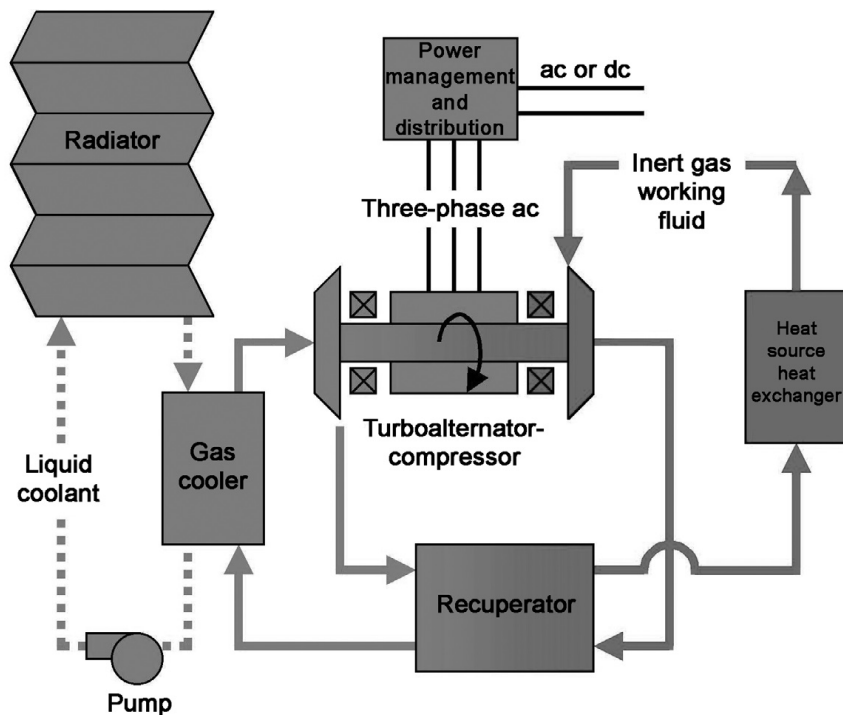
Closed-Cycle Engine Program Used to Study Brayton Power Conversion

One form of power conversion under consideration in NASA Glenn Research Center's Thermal Energy Conversion Branch is the closed-Brayton-cycle engine. In the tens-of-kilowatts to multimewatt class, the Brayton engine lends itself to potential space nuclear power applications such as electric propulsion or surface power. The Thermal Energy Conversion Branch has most recently concentrated its Brayton studies on electric propulsion for Prometheus. One piece of software used for evaluating such designs over a limited tradeoff space has been the Closed Cycle Engine Program (CCEP).

The CCEP originated in the mid-1980s from a Fortran aircraft engine code known as the Navy/NASA Engine Program (NNEP). Components such as a solar collector, heat exchangers, ducting, a pumped-loop radiator, a nuclear heat source, and radial turbomachinery were added to NNEP, transforming it into a

high-fidelity design and performance tool for closed-Brayton-cycle power conversion and heat rejection. CCEP was used in the 1990s in conjunction with the Solar Dynamic Ground Test Demonstration conducted at Glenn.

Over the past year, updates were made to CCEP to adapt it for an electric propulsion application. The pumped-loop radiator coolant can now be n-heptane, water, or sodium-potassium (NaK); liquid-metal pump



Recuperated closed-Brayton-cycle power-conversion system with heat rejection.

design tables were added to accommodate the NaK fluid. For the reactor and shield, a user can now elect to calculate a higher fidelity mass estimate. In addition, helium-xenon working-fluid properties were recalculated and updated.

CCEP allows researchers to design a closed-Brayton-cycle power-conversion system and then evaluate the system's off-design performance. Design trade-off studies conducted with CCEP included varying alternator power output, system peak pressure, turbomachinery shaft speed, helium-xenon molecular weight, and compressor pressure ratio. Design point calculations of interest were the system total mass, radiator area, and heat input required. Steady-state off-design performance studies included reducing the shaft speed, bypassing the recuperator, and reducing the turbine inlet temperature to see how the change in operating conditions affected the heat input required, the alternator power output, and the potential for the radiator fluid to freeze. Transient analysis in CCEP is being used in more extensive off-design performance analysis.

CCEP contains enough flexibility to make it useful for a variety of closed-Brayton-cycle configurations. Whether future CCEP versions are maintained in the Fortran format or the methods and equations are transported to a new platform, CCEP will continue its legacy as a powerful closed-Brayton-cycle design and analysis tool.

Bibliography

Ensworth, Clint B., III; and McKissock, David B.: Closed Cycle Engine Program Used in Solar Dynamic Power Testing Effort. Research & Technology 1997, NASA/TM—1998-206312, 1998, pp. 139–140. <http://www.grc.nasa.gov/WWW/RT1997/6000/6920ensworth.htm>

Mason, Lee S.: Power-Conversion Concept Designed for the Jupiter Icy Moons Orbiter. Research & Technology 2003, NASA/TM—2004-212729, 2004, p. 76. <http://www.grc.nasa.gov/WWW/RT/2003/5000/5490mason.html>

Find out more about this research:

<http://www.grc.nasa.gov/WWW/tmsb/>

Glenn contact:

Michael J. Barrett, 216-433-5424, Michael.J.Barrett@nasa.gov

Analex Corporation contact:

Paul K. Johnson, 216-433-3814, Paul.K.Johnson@grc.nasa.gov

Author:

Paul K. Johnson

Headquarters program office:

Exploration Systems

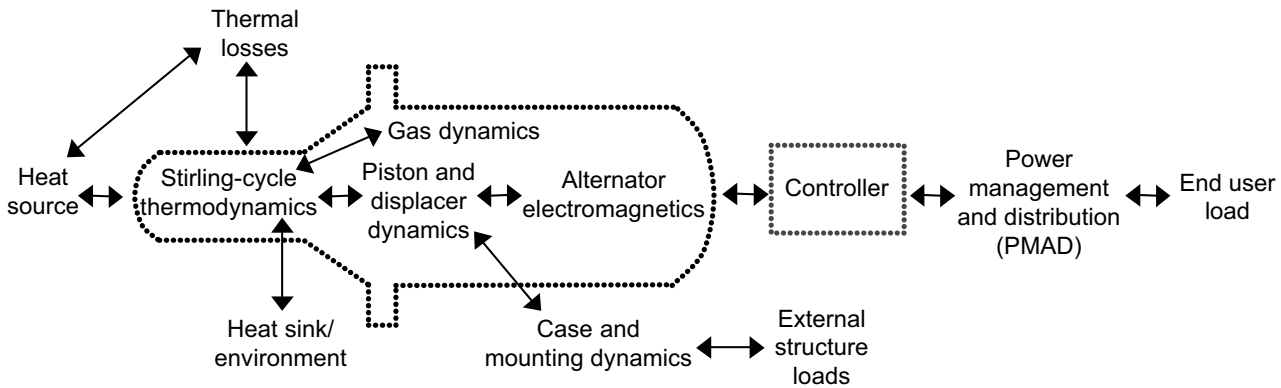
Programs/Projects:

Project Prometheus

Stirling Converter System Dynamic Model Developed

Free-piston Stirling converters are being developed for potential use on NASA exploration missions. In support of this effort, the NASA Glenn Research Center has developed the Stirling converter System Dynamic Model (SDM). The SDM models the Stirling cycle thermodynamics; heat flow; gas, mechanical, and mounting dynamics; the linear alternator; and the controller. The SDM's scope extends from the thermal energy input to thermal, mechanical, and

electrical energy output, allowing one to study complex system interactions among subsystems. Thermal, mechanical, fluid, magnetic, and electrical subsystems can be studied in one model. The SDM is a



Scope of the Stirling convertor SDM within the domain of the entire spacecraft power system.

nonlinear time-domain model containing subcycle dynamics, which simulates transient and dynamic phenomena that other models cannot. The entire range of convertor operation is modeled, from startup to full-power conditions.

The SDM has been developed as a “bottom-up” model based on first principles. Components are modeled separately, then combined into subsystems. The SDM can be set up to include multiple convertors in various mechanical and electrical configurations, including dual-opposed, parallel-electrical, and series-electrical configurations. It is being used to model free-piston convertors from less than 100 W to over 10 kW.

In modeling the Stirling cycle thermodynamics, the SDM assumes the isothermal Stirling cycle of the Schmidt model. It considers pumping losses through the heat exchangers and internal gas flows through the clearance seals. It includes the piston and displacer masses, along with case masses. The SDM models the piston offset due to the so-called seal pumping effect, and it connects the case mass to a ground through a compliant damped linkage. The temperature-dependent alternator model includes the output current, voltage, and electromagnetic force. A library of various controller models has been created.

The 55-We Technology Demonstration Convertor hardware and data available at Glenn are being used to validate the SDM empirically. The available data include test results documenting steady-state normal operation as well as test results that explore the robustness of the system. These include three different tests in which the power factor of the load circuit was varied by varying the value of a capacitor in series with the load. The tests covered different system configurations and different power levels. SDM simulations were performed that duplicated the test conditions for each of these tests. The results were compiled and used in the SDM validation. The model is also useful in the design of controllers and in the study of various systems issues.

The Glenn SDM uses the Ansoft Simplorer 7.0 platform. It is now being linked with Sage (Stirling cycle simulation software) to provide enhanced thermodynamic capability. The Sage thermodynamics option will be used in simulations where the isothermal Stirling cycle is not sufficiently accurate.

Bibliography

Lewandowski, Edward J.; and Regan, Timothy F.: Overview of the GRC Stirling Convertor System Dynamic Model. AIAA-2004-5671, 2004.

Regan, Timothy F.; and Lewandowski, Edward J.: Application of the GRC Stirling Convertor System Dynamic Model. AIAA-2004-5672, 2004.

Find out more about this research:

<http://www.grc.nasa.gov/WWW/tmsb/>

Sest, Inc., contacts:

Edward J. Lewandowski, 216-433-5525, Edward.J.Lewandowski@grc.nasa.gov; and Timothy F. Regan, 216-433-2086, Timothy.F.Regan@grc.nasa.gov

Glenn contact:

Jeffrey G. Schreiber, 216-433-6144, Jeffrey.G.Schreiber@nasa.gov

Authors:

Edward J. Lewandowski and Timothy F. Regan

Headquarters program office:

Science

Programs/Projects:

Project Prometheus

Stirling Power Convertors Demonstrated in Extended Operation

A 110-W Stirling Radioisotope Generator (SRG110) is being developed by Lockheed Martin Astronautics of Valley Forge, Pennsylvania, under contract to the Department of Energy of Germantown, Maryland. The generator will be a high-efficiency electric power source for NASA space exploration missions that can operate in the vacuum of deep space or in a gaseous atmosphere, such as on the surface of Mars. The generator converts heat supplied by the decay of a plutonium heat source into electric power for the spacecraft. In support of the SRG110 project, the NASA Glenn Research Center has established a technology effort that will provide some of the key data to ensure a successful transition to flight for what will be the first dynamic power system to be used in space. High system efficiency is obtained through the use of free-piston Stirling power-conversion technology. Glenn tasks include in-house testing of Stirling convertors and controllers, materials evaluation and heater head life assessment, structural dynamics, evaluation of electromagnetic interference, assessment of organics, and reliability analysis. There is also an advanced technology effort that is complementary to the near-term technology effort, intended to reduce the mass of the Stirling convertor and increase efficiency.

To demonstrate the capability for long life, Glenn has been tasked with extended operation of a pair of flight prototype Stirling power convertors—Technology Demonstration Convertors (TDCs) #13 and #14. The TDCs were developed by the Stirling Technology Company of Kennewick, Washington. TDCs #13

and #14 recently surpassed 1 year of operation and now have over 9850 hr of extended operation. The power output and efficiency have remained nearly constant throughout this test. TDCs #15 and #16 are scheduled to begin extended operation at Glenn later this year following a vibration test that will simulate the dynamics of launch, and TDCs #5 and #6 will begin extended operation in a thermal vacuum environment intended to simulate operation in deep space. Extended operation of all convertors will continue in support of Lockheed Martin and the SRG110 project.

Bibliography

Thieme, Lanny G.; and Schreiber, Jeffrey G.: Supporting Development for the Stirling Radioisotope Generator and Advanced Stirling Technology Development at NASA GRC. NASA/TM—2005-213409 (AIP Conf. Proc., vol. 746, 2005, pp. 674–681), 2005. <http://gltrs.grc.nasa.gov/cgi-bin/GLTRS/browse.pl?2005/TM-2005-213409.html>

Schreiber, Jeffrey G.; and Thieme, Lanny T.: Accomplishments of the NASA GRC Stirling Technology Development Project. AIAA–2004–5517, 2004.

Find out more about this research:
<http://www.grc.nasa.gov/WWW/tmsb/>

Glenn contact:

Jeffrey G. Schreiber, 216–433–6144,
Jeffrey.G.Schreiber@nasa.gov

Author:

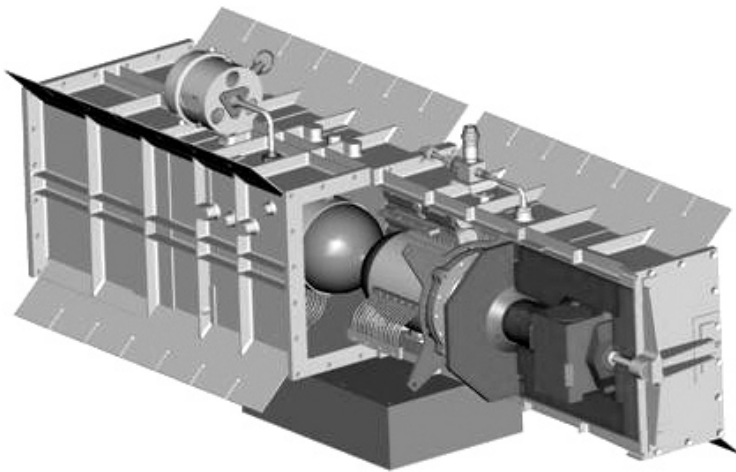
Jeffrey G. Schreiber

Headquarters program office:

Science

Programs/Projects:

Project Prometheus



TDCs #13 and #14 on an extended operation test at Glenn.

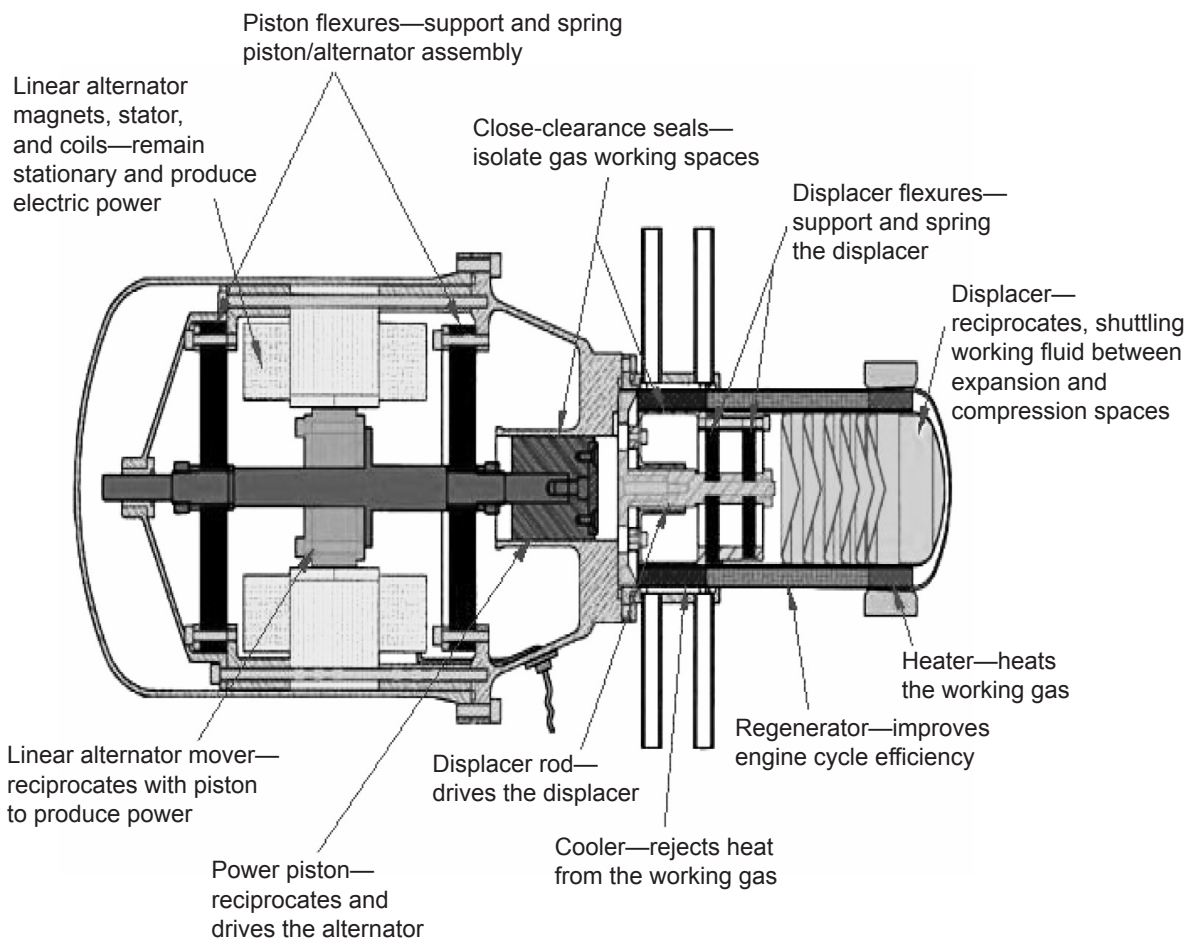
Reliability of the SRG110 Stirling Converter Quantified

The NASA Glenn Research Center has been involved in the development of Stirling power-conversion technology and is currently providing technical support to the Department of Energy and Lockheed Martin, of Valley Forge, Pennsylvania, their system integration contractor, for the 110-W Stirling Radioisotope Generator (SRG110). Stirling radioisotope power-conversion technology is a potential candidate for future deep-space science and exploration missions. The SRG110 has a multifold increase in efficiency and would reduce the inventory of the radioisotope fuel by a factor of 4 in comparison to systems used to power past missions.

The SRG110 is a new radioisotope power system that will have to perform efficiently for up to 14 years; therefore, high reliability is of paramount importance. The SRG110 has five major subsystems: the heat source, the Stirling Converter Assembly (SCA), the structure, the radiator, and the controller. The SCA is a free-piston device consisting of many components, materials,

electronics, and heat exchangers, and it involves multiple disciplines. Critical components governing the performance and reliability of the SCA are the heater head, regenerator, displacer, flexures, fasteners, clearance seals, cooler, linear alternator (magnets, stators, and coils), and heat exchangers.

The design variables of different SCA components inherit uncertainties from the material behavior, the loads, the manufacturing and fabrication processes, component integration



110-W Stirling Radioisotope Generator (SRG110).

and the interfaces of components, and human factors. Conventional design approaches based on factors of safety (which do not quantify the reliability) have resulted in highly conservative, expensive designs. Glenn has pursued a more rational reliability approach: quantifying SCA reliability while meeting key mission objectives, such as flight qualification, certification, and mission success.

These efforts have addressed reliability of the heater head, the flexures, the linear alternator magnets, and the fasteners. Heater head reliability for long-term durability under sustained high-temperature loads and rare thermal excursions has been quantified and verified with the accelerated test data. Analysis has shown that the reliability is most sensitive to uncertainties in the creep behavior of the material. In addition, the reliability of the flexures for a fatigue life of 35 billion cycles during a mission has been evaluated, and the test data are being verified. Initial evaluation showed that the reliability of the flexures is most sensitive to variations in the piston stroke. Evaluation of the linear alternator magnets showed that the reliability of the generated voltage is most sensitive to uncertainties in the gap between the mover and the stator and to the magnetization properties of magnets. Sensitivity evaluation provides guidelines to improve reliability by identifying the variables to control during operation as well as tests to be performed for verification.

Evaluation of the reliability of other SCA components, as well as testing to provide quantification, is in process. We also plan to integrate the results of the SCA component reliability to quantify the reliability of the overall SCA, and to verify them with the test data that are being collected from the extended operation of the Stirling convertors.

Bibliography

Shah, Ashwin R., and Schreiber, Jeffrey G.: Reliability Issues in Stirling Radioisotope Power Systems. NASA/TM—2004-213428 (AIAA-2004-5506), 2004. <http://gltrs.grc.nasa.gov/cgi-bin/GLTRS/browse.pl?2004/TM-2004-213248.html>

Shah, Ashwin R., et al.: Reliability Based Life Assessment of Stirling Converter Heater Head. Presented at the Space Technology and Applications International Forum (STAIF-2004), AIAA, Albuquerque, NM, 2004.

Find out more about this research:

<http://www.grc.nasa.gov/WWW/tmsb/>

Sest, Inc., contact:

Ashwin R. Shah, 440-234-9173,
Ashwin.Shah@SestInc.com or
Ashwin.R.Shah@grc.nasa.gov

Glenn contact:

Jeffrey G. Schreiber, 216-433-6144,
Jeffrey.G.Schreiber@nasa.gov

Authors:

Ashwin R. Shah and Jeffrey G. Schreiber

Headquarters program office:

Science

Programs/Projects:

Project Prometheus

Work Began on Contracts for Radioisotope Power Conversion Technology Research and Development

NASA has had a history of successful space flight missions that depended on radioisotope-fueled power systems. These Radioisotope Power Systems (RPSs) converted the heat generated from the decay of radioisotope material into useful electrical power. An RPS is most attractive in applications where photovoltaics are not optimal, such as deep-space applications where the solar flux is too low or extended applications on planets such as Mars where the day/night cycle, settling of dust, and life requirements limit the usefulness of photovoltaics. NASA's Radioisotope Power Conversion Technology (RPCT) Program is developing next-generation power-conversion technologies that will enable future missions that have requirements that cannot be met by the two RPS flight systems currently being developed by the Department of Energy

for NASA: the Multi-Mission Radioisotope Thermoelectric Generator and the Stirling Radioisotope Generator (SRG).

RPCT performance goals include improvement over the state-of-practice General Purpose Heat Source/Radioisotope Thermoelectric Generator (GPHS-RTG, 7-percent efficiency and 5 W/kg at the beginning

of the mission) by providing significantly higher efficiency to reduce the number of radioisotope fuel modules and to increase specific power (watts/kilogram). Other general RPCT goals include safety, long-life (14 years, with well-understood degradation), reliability, scalability, multimission capability (in vacuum and atmosphere), resistance to radiation (from the GPHS-RTG or potential mission environments), and minimal interference with the scientific payload.

The RPCT Program has awarded five development contracts using more mature technologies (technology readiness levels (TRLs) 3 to 5) and five research contracts using less mature technologies (TRLs 1 to 3). The selections include a broad range of conversion technologies including dynamic technologies (free-piston Stirling and turbo-Brayton), and static technologies (thermoelectric and thermophotovoltaic). Most of the contracts are developing

technologies applicable to a nominal 100-W-class RPS, but two of the research contracts using thermoelectrics are specific to a low-power RPS (milliwatt to multiwatt class). Each contract has a performance period of 3 years and will be divided into three 1-year phases, with options to continue the following phase after the conclusion of each phase.

A Government-led Advanced RPS Systems Assessment Team was formed, with members from the NASA

The five higher TRL development contracts, along with the contractor's performance estimates at the end of phase I, are shown in the following table:

Company	Technology	Direct-current power, We	Efficiency, percent	Specific power, W/kg
Creare, Inc.	Precision fabricated miniature-rotor turbo-Brayton power converter	60	25	9
Creare, Inc.	Thermophotovoltaic converter using InGaAs cells ^a	85	>15	10
Edtek, Inc.	Thermophotovoltaic converter using GaSb cells ^b	80	16	14
Sunpower, Inc.	Advanced free-piston Stirling convertor	82	37	10
Teledyne Energy Systems, Inc.	Segmented thermoelectrics using Bi-Te with PbTe, and PbSnTe/TAGS ^c	24	10	3.2

^aInGaAs, indium gallium arsenide.

^bGaSb, gallium antimony.

^cBi-Te, bismuth-tellurium; PbTe, lead-tellurium; PbSnTe/TAGS, lead-tin-tellurium/tellurium-antimony-germanium-silver.

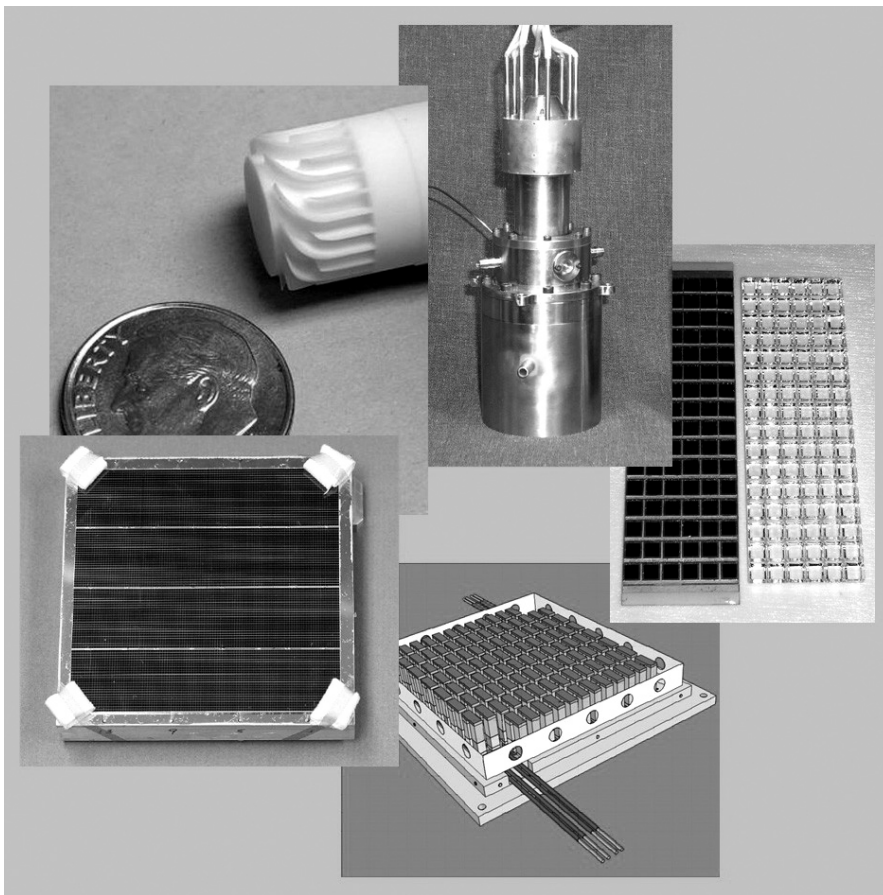
The five lower TRL research contracts, which may only deal with components, are summarized in the final table:

Company	Technology	Power	Efficiency, percent
Cleveland State University	Microfabrication Stirling regenerator	6- to 9-percent gain for Stirling convertor	-----
Essential Research, Inc.	Dot-junction InGaAs-on-InP cell for thermophotovoltaics ^a	-----	30
Hi-Z, Inc.	Multiwatt quantum well Si-Ge thermoelectrics ^b	-----	30
Massachusetts Institute of Technology	Nanostructure Si-Ge thermoelectrics ^b	-----	12 to 14
Teledyne Energy Systems, Inc.	Cascaded superlattice PbTe/TAGS BiTe Thermoelectric ^c	50- to 100-mW module	>8

^aInGaAs-on-InP, indium gallium arsenide on indium phosphide.

^bSiGe, silicon germanium.

^cPbTe/TAGS, lead tellurium/tellurium-antimony-germanium-silver; BiTe, bismuth tellurium.



Collage of hardware and designs developed during the RPCT phase-I development contracts, representing Brayton, Stirling, thermoelectric, and thermophotovoltaic technology.

Glenn Research Center (lead), the Jet Propulsion Laboratory, the Department of Energy, and Orbital Sciences Corporation. The team's function is to review the technologies being developed under the 10 RPCT contracts, assess their relevance to NASA's future missions, and provide recommendations to the RPS program with regard to status of the technology, technology development options, phase-to-phase funding, and potential down-selection. The team also is responsible for using the RPCT technologies to develop conceptual RPS designs and for projecting system-level performance.

Find out more about this research:
<http://www.grc.nasa.gov/WWW/tmsb/>

Glenn contact:
 Wayne A. Wong, 216-433-6318,
 Wayne.A.Wong@nasa.gov

Author:
 Wayne A. Wong

Headquarters program office:
 Science

Programs/Projects:
 Project Prometheus

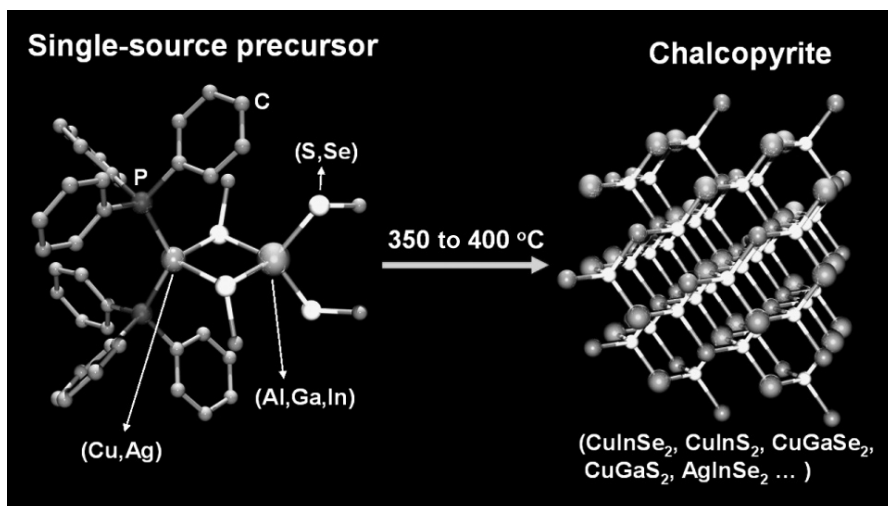
Low-Temperature Chalcopyrite Thin-Film Solar Cells Developed for Space Photovoltaic Applications

The NASA Glenn Research Center is researching low-cost, highly efficient chalcopyrite thin-film solar cells on lightweight polymer substrates that will ultimately lower the mass-specific power (watts/kilograms) of the cells, allowing extra payload for missions in space as well as cost reduction. In addition, thin-film cells are anticipated to have greater resistance to radiation damage in space, enabling their use in a wide range of orbits and prolonging their lifetime. The flexibility of the substrate has the added benefit of enabling roll-to-roll processing.

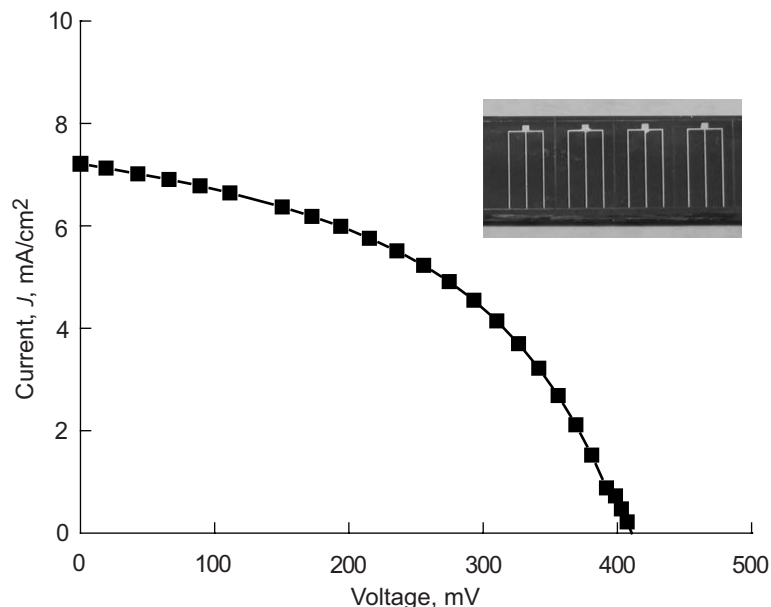
Current methods for depositing ternary chalcopyrite (I-III-VI₂) thin-film compounds often require multisource inorganic/organometallic precursors and high-temperature (>500 °C) processes, including toxic sulfurization or selenization steps. The high-temperature requirements are incompatible with existing space-grade polymer substrates, and the use of toxic gases is not

environmentally friendly. To overcome these obstacles, Glenn and the Ohio Aerospace Institute (OAI) have developed single-source precursors for the thin-film deposition of chalcopyrite materials (ref. 1). The precursors have "built-in" I-III-VI stoichiometry with desirable thermophysical properties for low-temperature deposition.

Aerosol-assisted chemical vapor deposition (AACVD) can easily be adapted to use liquid precursors in



Decomposition of single-source precursor to yield chalcopyrite compounds.



Light current-voltage characteristics of a chalcopyrite thin-film solar cell (Al/Ni/ITO/i-ZnO/CuInS₂/CdS/Mo/glass) fabricated with CuInS₂ deposited by AACVD using a single-source precursor.

the deposition of large-area thin films. Single-source precursors have enabled the AACVD of single-phase (112)-oriented copper indium sulfide (CuInS₂) thin films on glass substrates at under 400 °C and have showed promising potential for polymer substrates (refs. 2 and 3).

The entire fabrication process for the chalcopyrite photovoltaic device was established at Glenn, and the CuInS₂ thin-film solar cells on glass were constructed at Glenn, Oberlin College, and the Institute of Energy Conversion

at the University of Delaware (ref. 3). The light current-voltage characteristics of the solar cell showed an open-circuit voltage over 400 mV and a short-circuit current over 7 mA/cm²; that is comparable to other AACVD-made, chalcopyrite thin-film solar cells using more than one source. The single-source precursors can provide a simple novel fabrication process for multijunction solar cells composed of several chalcopyrite compounds with different bandgaps.

References

1. Banger, Kulbinder K., et al.: A New Facile Route for the Preparation of Single-Source Precursors for Bulk, Thin-Film and Nanocrystallite I-III-VI Semiconductors. *Inorg. Chem.*, vol. 42, issue 24, 2003, pp. 7713-7715.
2. Jin, Michael H., et al.: The Effect of Film Composition on the Texture and Grain Size of CuInS₂ Prepared by Spray Pyrolysis. *Proceedings of the 3rd World Conference on Photovoltaic Energy Conversion*, vol. A, 2003, pp. 430-433.
3. Jin, Michael H., et al.: Solar Cells Fabricated with CuInS₂ Films Deposited Using Single-Source Precursors. *Proceedings of the 19th European Photovoltaic Solar Energy Conference*, 4AV.1.71, 2004.

Find out more about this research:
<http://powerweb.grc.nasa.gov/pvsee/>

Glenn contact:

Dr. Aloysius F. Hepp, 216-433-3835,
 Aloysius.F.Hepp@nasa.gov

Ohio Aerospace Institute (OAI) contact:

Dr. Michael H.-C. Jin, 216-433-3540,
 Michael.H.Jin@grc.nasa.gov

Authors:

Dr. Michael H.-C. Jin,
 Dr. Kulbinder K. Banger,
 Jeremiah S. McNatt,
 Dr. John E. Dickman, and
 Dr. Aloysius F. Hepp

Headquarters program office:

Exploration Systems

Programs/Projects:

ESR&T

Ground-Laboratory to In-Space Effective Atomic-Oxygen Fluence Determined for DC 93–500 Silicone

Surfaces on the leading edge of spacecraft in low Earth orbit (e.g., surfaces facing the velocity direction), such as on the International Space Station, are subject to atomic oxygen attack, and certain materials are susceptible to erosion. Therefore, ground-based laboratory testing of the atomic oxygen durability of spacecraft materials is necessary for durability assessment when flight data are not available. For accurate space simulation, the facility is commonly calibrated on the basis of the mass loss of Kapton (DuPont, Wilmington, DE) as a control sample for effective fluence determination. This is because Kapton has a well-characterized atomic oxygen erosion yield (E_y , in cubic centimeters per atom) in the low Earth orbit (LEO) environment.

Silicones, a family of commonly used spacecraft materials, do not chemically erode away with atomic oxygen attack like other organic materials that have volatile oxidation products. Instead, silicones react with atomic oxygen and form an oxidized hardened silicate surface layer. Often the loss of methyl groups causes shrinkage of the surface skin and “mud-tile” crazing degradation. But silicones often do not lose mass, and some silicones actually gain mass during atomic oxygen exposure. Therefore, the effective atomic oxygen fluence for silicones in a ground-test facility should not be determined on the basis of traditional mass-loss measurements, as it is with polymers that erode. Another method for determining effective fluence needs to be employed for silicones.

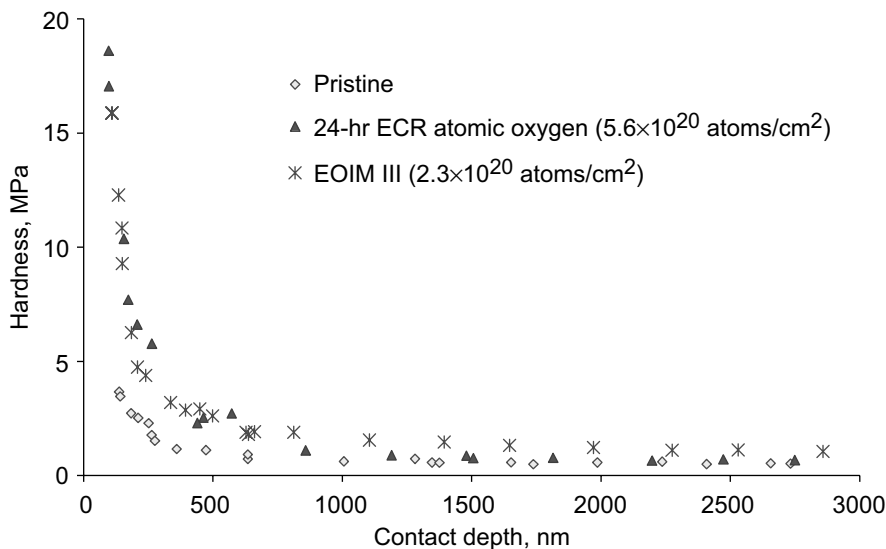
A new technique has been developed at the NASA Glenn Research Center for determining the effective atomic oxygen fluence for silicones in ground-test facilities. This technique determines the equivalent amount of atomic oxygen oxidation on the basis of changes in the surface-oxide hardness. The specific approach developed was to compare changes in the surface hardness of ground-laboratory-exposed DC93–500 silicone with DC93–500 exposed to LEO atomic oxygen as part of a shuttle flight experiment. The on-the-ground to in-space effective atomic oxygen fluence was determined on the basis of the Kapton effective fluence in the ground-laboratory facility that produced the same hardness for the fluence in space.

Because microhardness measurements need to be obtained on the very surface layer of a rubber substrate (with primarily elastic deformation), traditional techniques for microhardness characterization, which apply relatively large forces and characterize hardness on the basis of plastic deformation, could not be used. Therefore, nanomechanical testing, using ultralight load indentations and continuous load-displacement monitoring, was used to determine the surface hardness of the silicones. Hardness versus contact depth were obtained for five DC93–500 samples exposed to atomic oxygen in an electron cyclotron resonance (ECR) thermal energy source facility (exposed for 18 to 40 hr, corresponding to Kapton mass-loss effective fluences of 4.2×10^{20} to 9.4×10^{20} atoms/cm², respectively) and for a space-exposed DC93–500. The

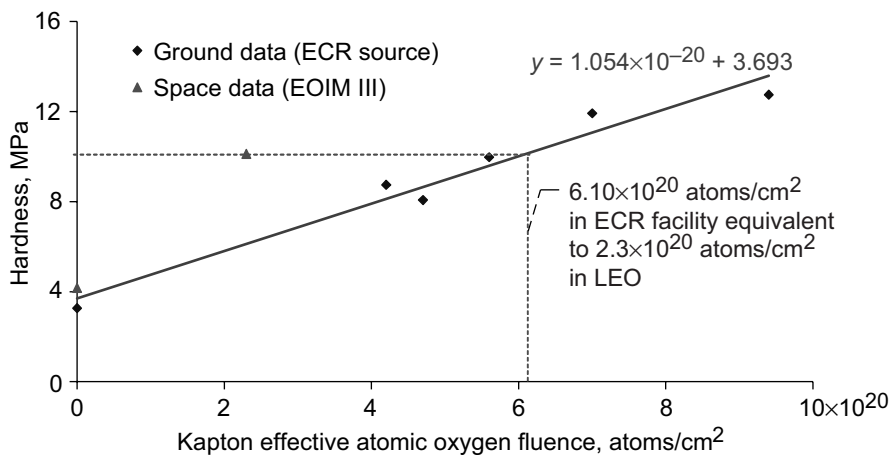
in-space exposed DC93–500 sample was exposed to LEO atomic oxygen as part of the Evaluation of Oxygen Interactions With Materials III (EOIM III) shuttle flight experiment flown on STS–46. This sample was exposed to directed ram atomic oxygen from within the shuttle bay and received a LEO atomic oxygen fluence of $2.3 \pm 0.3 \times 10^{20}$ atoms/cm². Pristine controls for the ECR tests and for the EOIM III flight sample were also measured. The top graph on the next page provides the hardness versus contact depth for pristine DC93–500, the EOIM–III flight sample, and DC93–500 exposed to the ECR atomic-oxygen source for 24 hr.

Values obtained from the curve-fit equations for each data set of hardness versus contact depth were used to produce plots of hardness versus Kapton effective atomic oxygen fluence at contact depths of 150, 200, 250, and 300 nm. These depths represent the “near surface” data. The 150-nm contact depth plot is provided in the bottom graph on the next page.

The ECR Kapton effective fluences that provided the same hardness as for the EOIM III sample for depths of 150, 200, 250, and 350 nm were determined to be 6.10, 6.00, 6.04, and 6.16×10^{20} atoms/cm², respectively. Averaging these values provides 6.08×10^{20} atoms/cm²; therefore, the Kapton effective atomic oxygen fluence in the ECR facility needs to be 2.64 times higher than in LEO to produce exposure damage in the ground test silicone equivalent to what occurred in the space-exposed silicone.



Hardness versus contact depth for pristine, 24-hr ECR-exposed, and LEO space-exposed DC93-500 silicone.



Hardness versus Kapton atomic oxygen effective fluence at a contact depth of 150 nm.

This technique has been directly correlated with silicone pressure-sensitive adhesive (PSA) samples that have been ECR exposed for International Space Station solar-array diode tape blocking assessment. The DC93-500 samples were ECR exposed simultaneously with silicone PSA samples. On-orbit, the silicone PSA surface will eventually convert to a hardened silicate glass layer, changing from a sticky surface to a glassy nonblock surface. By using the correlation of ground and space DC93-500 data, one can deduce the ground-test effective fluence of the silicone PSA and can more accurately determine the degree of blocking versus atomic oxygen exposure that can be expected on-orbit for the space station diode tape.

Glenn contacts:

Kim K. de Groh, 216-433-2297, Kim.K.deGroh@nasa.gov; and Bruce A. Banks, 216-433-2308, Bruce.A.Banks@nasa.gov

Authors:

Kim K. de Groh, Bruce A. Banks, and David Ma

Headquarters program office:

OAT, Energetics

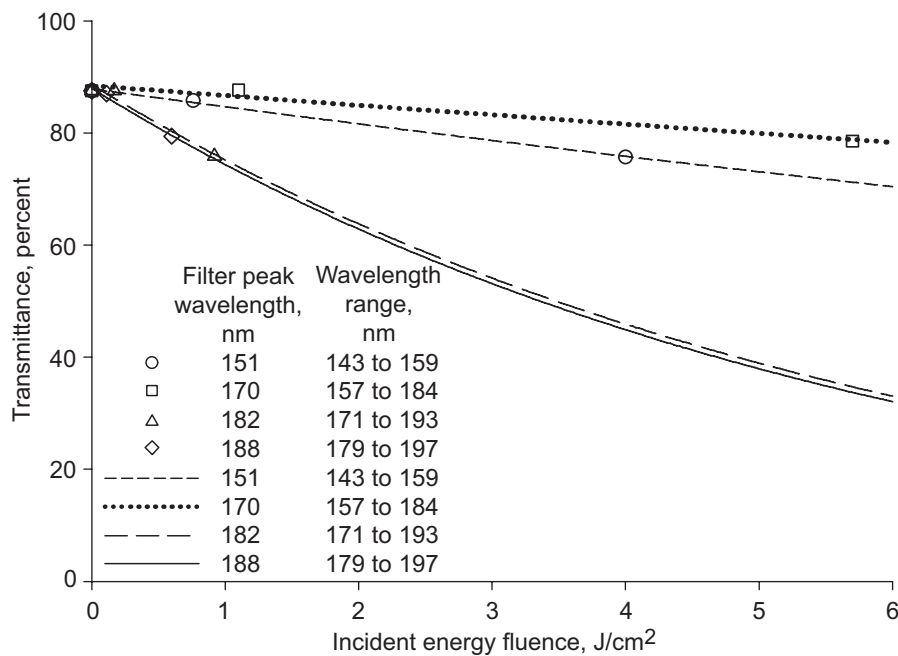
Programs/Projects:

Environmentally durable spacecraft such as ISS, EOS, and future spacecraft

Vacuum Ultraviolet Radiation Effects on DC93–500 Silicone Film Studied

A space-qualified silicone polymer, DC93–500 (Dow Corning, Midland, MI), has been used as a spacecraft solar cell adhesive and has been proposed for use in a Fresnel lens solar concentrator for space power applications. Applications of DC93–500 for exterior space system surfaces require an understanding of its overall space environmental durability. Vacuum ultraviolet (VUV) radiation is among the space environment elements that can be hazardous to the properties of DC93–500, causing degradation in optical and mechanical properties. For materials or components that have not been tested previously for long-duration performance in space, such as DC93–500 in freestanding film form, ground laboratory testing is an important tool for assuring durability. However, differences between the space environment and ground laboratory testing environments lead to complexities in interpreting the ground test results. Two important differences between space and laboratory vacuum ultraviolet exposure conditions are irradiance spectra and light intensity. These important differences were the basis for laboratory experiments conducted to examine VUV wavelength dependence and VUV intensity dependence of DC93–500 degradation. Testing conducted at the NASA Glenn Research Center along with additional data provided through a grant with the University of Nebraska-Lincoln, has advanced the understanding of VUV effects on DC93–500 and has provided important conclusions regarding the use of ground laboratory VUV testing to predict the space environment performance of DC93–500.

In one set of experiments, transmittance degradation of DC93–500 was examined as a function of exposure to narrow wavelength bands (~20-nm bandwidth) of VUV in the 140- to 200-nm-wavelength range. The graph on this page plots the transmittance of DC93–500 at 250 nm, a wavelength where significant degradation was evident, versus the incident VUV energy fluence. It is evident from this figure that VUV exposure through filters that transmit longer wavelengths caused a higher rate of transmittance degradation than VUV exposure through filters that transmit shorter wavelengths. The most likely explanation for this is that the longer wavelengths penetrate more deeply into DC93–500 and, therefore, affect more of the bulk of the material. This theory was validated through ellipsometric measurements, which determined VUV penetration into DC93–500 as a function of wavelength.



Transmittance of 152-µm DC93–500 silicone film at 250 nm as a function of incident VUV energy fluence provided by exposure to various wavelength ranges through narrow bandpass filters.

In another set of experiments, broad-spectrum VUV exposures (to wavelengths greater than 115 nm) were used to examine the effects of VUV intensity on the degradation rates of optical and mechanical properties. The graph on the next page shows elongation at failure for 152-µm-thick DC93–500 silicone films as a function of exposure given in equivalent space solar exposure hours (ESH) for intensities of 1.5, 3.0, and 5.5 times the solar VUV intensity (i.e., number of “suns”). Ultimate tensile strength, elongation at failure, and transmittance were found to decrease with increasing exposure, and the rate of degradation was found to be independent of intensity. Mechanical properties and optical properties decreased, approaching asymptotic values near the 2000–ESH exposure level. This work is part of ongoing research to

support the development of long-duration, durable space power system materials and surfaces.

Find out more about this research:

<http://www.grc.nasa.gov/WWW/epbranch/>

Glenn contacts:

Joyce A. Dever, 216-433-6294, Joyce.A.Dever@nasa.gov; and Bruce A. Banks, 216-433-2308, Bruce.A.Banks@nasa.gov

Authors:

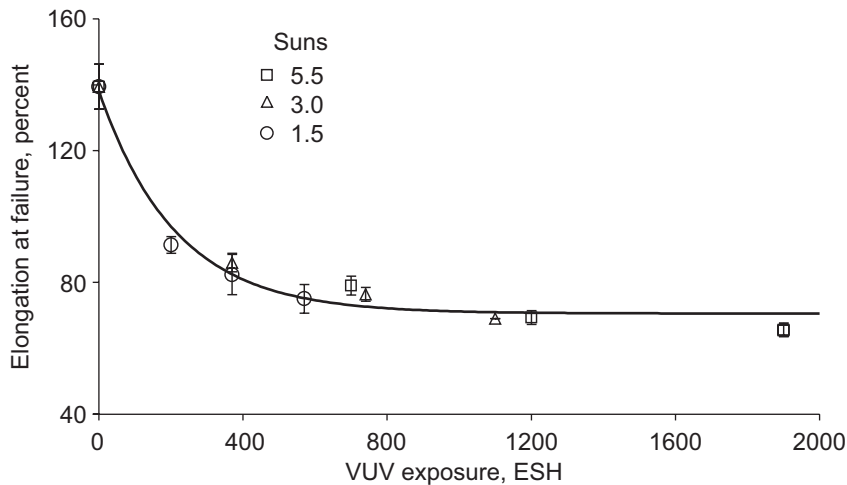
Joyce A. Dever, Bruce A. Banks, and Li Yan

Headquarters program office:

Exploration Systems

Programs/Projects:

ESR&T

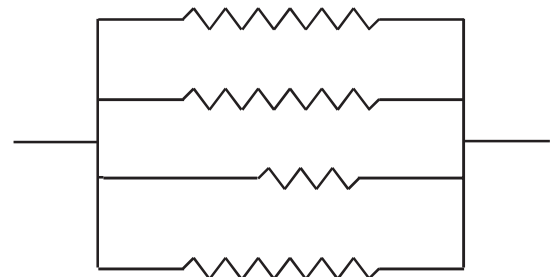


Elongation at failure for 152- μ m DC93-500 silicone as a function of VUV exposure equivalent sun hours.

Conductive Composites Made Less Expensively

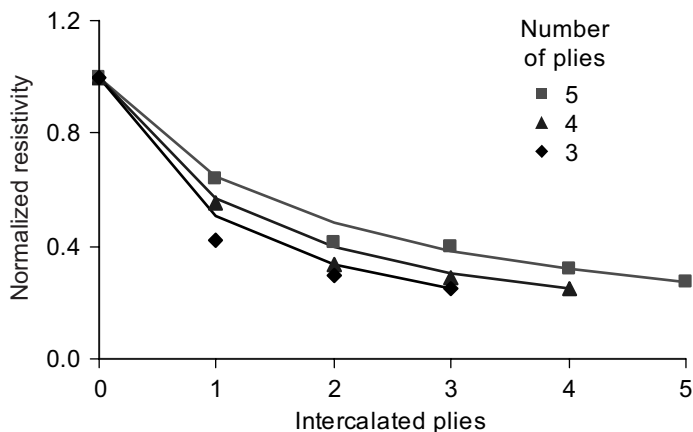
The use of electrically conductive composite structures for electrostatic dissipation, electromagnetic interference shielding, and ground return planes could save between 30 and 90 percent of the mass of the structure, in comparison to aluminum (ref. 1). One strategy that has been shown to make conducting composites effectively uses intercalated graphite fiber as the reinforcement. Intercalation—the insertion of guest atoms or molecules between the graphene planes—can lower the electrical resistivity of graphite fibers by as much as a factor of 10, without sacrificing mechanical or thermal properties.

But what can you do if your requirements call for a material with a higher conductivity than that of graphite epoxy composite, and intercalated graphite composite exceeds your budget? A cost-effective alternative might be a laminar composite in which just some of the graphite fiber plies are intercalated. Scientists at the NASA Glenn Research Center have found that constructing laminar composites with just one ply of intercalated graphite fibers combined with three plies of pristine graphite fibers results in a composite resistivity that is one-half that of the fully pristine composite.



A simple four-resistor parallel circuit is electrically equivalent to a four-ply composite. In this figure, the short resistor represents a layer of lower resistance (i.e., intercalated) fibers.

Through constructing many different laminar composites using woven graphite fiber fabrics with a different resistivity in each layer, it was found that the resistivity of laminar



Points represent the experimentally measured (resistivity/resistivity of pristine fiber composite) of three-, four-, and five-ply graphite fiber-epoxy composites as a function of the number of plies intercalated with bromine, with the remaining plies pristine. The lines show the results from the parallel resistor model.

composites follows a parallel-circuit model (see the sketch on the preceding page). Since bromine intercalation lowers the fiber resistivity by a factor of 5, one ply of bromine-intercalated Thornel (Cytex Engineered Materials, Tempe, AZ) P-100 graphite fiber ($50\text{-}\mu\Omega\text{-cm}$) combined with three plies of pristine P-100 graphite fiber ($250\text{-}\mu\Omega\text{-cm}$) results in a composite resistance half that of a composite made solely from the pristine fibers. This very simple model does not take into account such factors as the variation in the volume fraction of the fiber, which can be very important. But even at that, the data were found to be a very close fit for three-, four-, and five-ply composites (see the graph). The

results were the same whether the intercalated fibers were in surface layers or buried layers.

The implication of this work is that the most cost-effective solutions to filling the needs of specific applications may involve composites in which a single layer carries most of the electrical load, while all the layers share the mechanical load.

Reference

1. Gaier, J.R.: Intercalated Graphite Fiber Composites as EMI Shields in Aerospace Structures. IEEE Trans. Electromag. Compat., vol. 34, issue 3, 1992, pp. 351–356.

Glenn contact:

Dr. James R. Gaier, 216-433-6686, James.R.Gaier@nasa.gov

Author:

Dr. James R. Gaier

Headquarters program office:

OAT

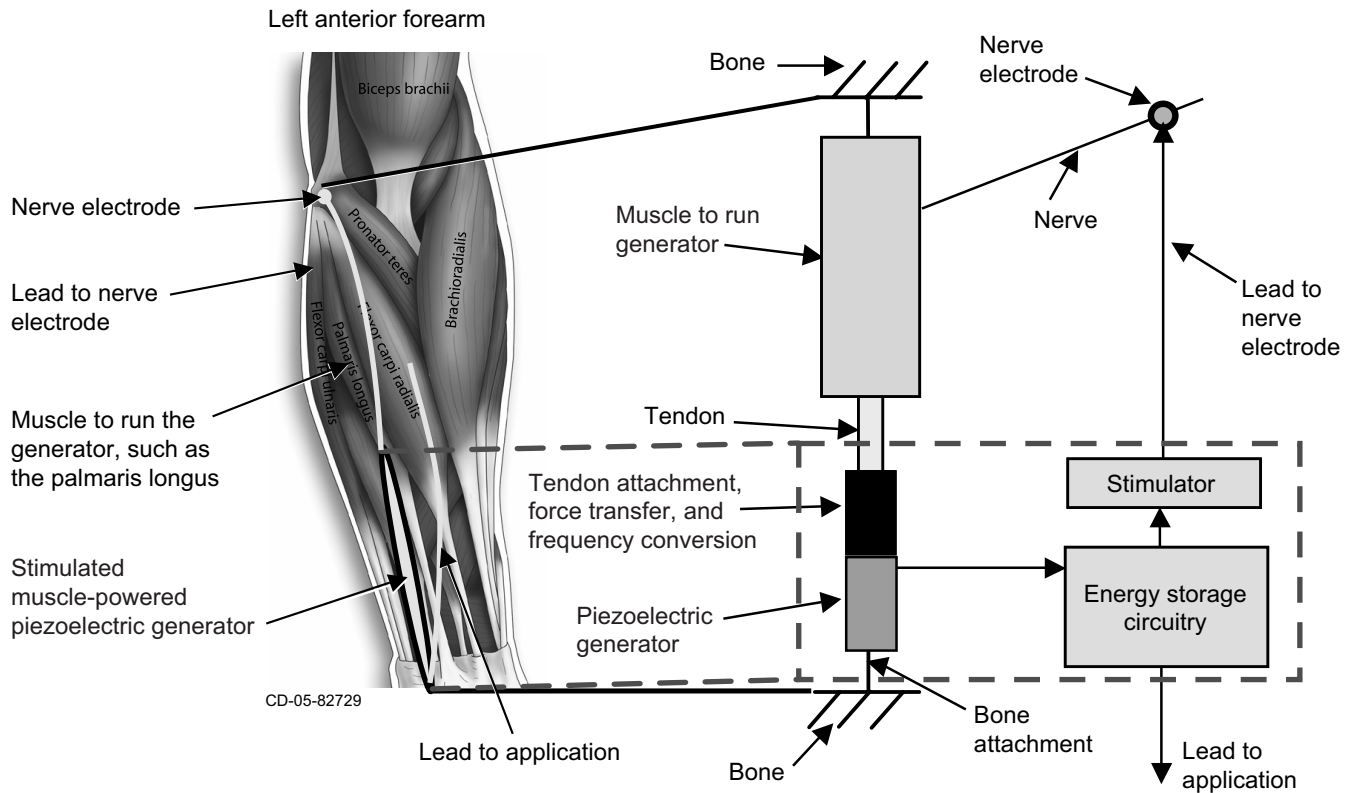
Programs/Projects:

High-conductivity, low-weight applications such as electromagnetic shielding enclosures and ground planes

Concept Developed for an Implanted Stimulated Muscle-Powered Piezoelectric Generator

Implanted electronic devices are typically powered by batteries or transcutaneous power transmission. Batteries must be replaced or recharged, and transcutaneous power sources burden the patient or subject with external equipment prone to failure. A completely self-sustaining implanted power source would alleviate these limitations. Skeletal muscle provides an available autologous power source containing native chemical energy that produces power in excess of the requirements for muscle activation by motor nerve stimulation.

A concept has been developed to convert stimulated skeletal muscle power into electrical energy (see the illustration on the next page). We propose to connect a piezoelectric generator between a muscle tendon and bone. Electrically stimulated



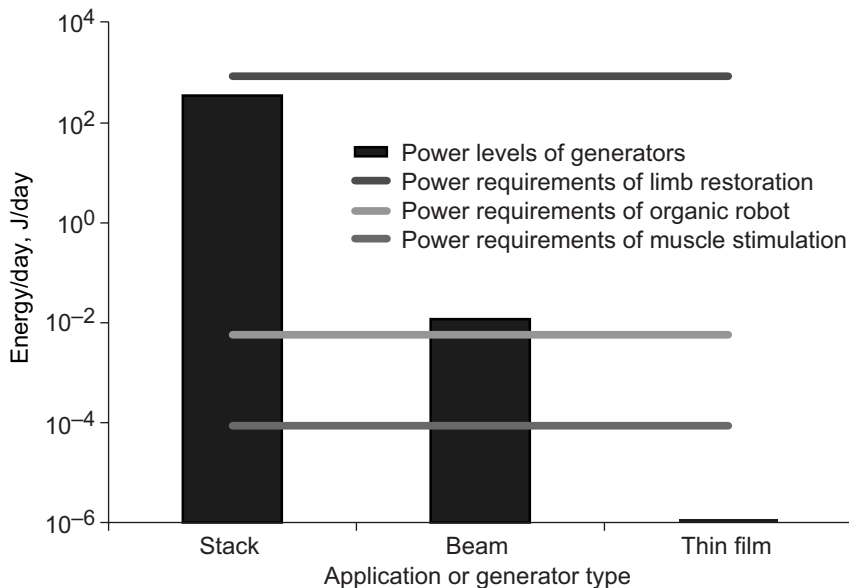
Concept for an implanted, stimulated muscle-powered generator. The tendon of a muscle, such as the palmaris longus, is detached from its distal bone. Piezoelectric material is attached in series between the tendon and bone. Electrically stimulated muscle contractions exert force on the piezoelectric material, producing a charge across the material. The generated energy is stored in a battery or capacitor and used to power the stimulator and other loads.

muscle contractions would exert force on the piezoelectric generator, charging a storage circuit that would be used to power the stimulator and other devices.

Software circuit models are being used to evaluate the fundamental design considerations for the muscle-powered piezoelectric generator. We are evaluating the most effective size, shape, and material for the piezoelectric generator, given the physiological constraints imposed by the biological system. Piezoelectric generator shapes include stacks, beams, and thin film; and piezoelectric materials include ceramics and polymers. A piezoelectric generator can be electrically represented as a voltage source in series with a capacitor. The voltage depends on the magnitude, frequency, and direction of the force application; the piezoelectric constant; and the dimensions of the material. The capacitance depends on the dielectric constant and the dimensions of the material. The input to the piezoelectric generator is the tension developed by the muscle. For simulation purposes, this input was modeled as a 10-N, 1-Hz sinusoid.

Piezoelectric stack generators were found to produce more power than beam or thin-film generators for this application. These stacks are composed of many layers of thin lead zirconate titanate plates. The most sensitive parameter to output power generation was the overall thickness, indicating that the number of layers should be maximized. Increasing the number of layers increases the capacitance of the generator, allowing impedance matching with a higher capacity capacitor in the storage circuit.

The theoretical output power of the piezoelectric stack generator was



Summary of the power-generation levels of the three generators compared with the power-consumption levels of two applications and the power-consumption level of the muscle stimulator required to run the generator. The stack generator theoretically produces more power than is needed to power the organic robot; therefore, a self-supporting system may be feasible.

significantly higher than the anticipated power requirements for muscle stimulation or organic robot operation, indicating that a stimulated muscle-powered generator may be feasible (see the preceding bar chart). The generator may be feasible for totally powering some applications and for augmenting external power sources or implanted, limited-life power sources of high-power-consuming applications. Additional modifications, such as frequency tuning and optimization of the system, may be required to increase the output power of the generator enough to power applications such as neuroprostheses for restoring limb function. The results support the continued development

of an implanted, stimulated muscle-powered piezoelectric generator.

This project is funded by NASA Glenn Research Center's Alternate Energy Foundational Technologies Project, which is part of the NASA Vehicle System Program of the Aeronautics Research Enterprise. The project is a collaboration between investigators at NASA, Case Western Reserve University, and MetroHealth Medical Center.

Find out more about this research:
<http://www.grc.nasa.gov/WWW/AERO/base/rac.htm>

Glenn contacts:
 Beth Lewandowski, 216-433-8873, Beth.E.Lewandowski@nasa.gov; and
 David Ercegovic, 216-977-7009, David.B.Ercegovic@nasa.gov

Case Western Reserve University contacts:
 Kevin Kilgore, 216-778-3801, klk4@po.cwru.edu; and
 Kenneth Gustafson, 216-368-8626, kjg@po.cwru.edu

Authors:
 Beth Lewandowski, Kevin Kilgore, David Ercegovic, and Kenneth Gustafson

Headquarters program office:
 Aeronautics Research

Programs/Projects:
 VSP, AEFT

Ozone Exposure System Designed and Used to Test High-Altitude Airship Materials

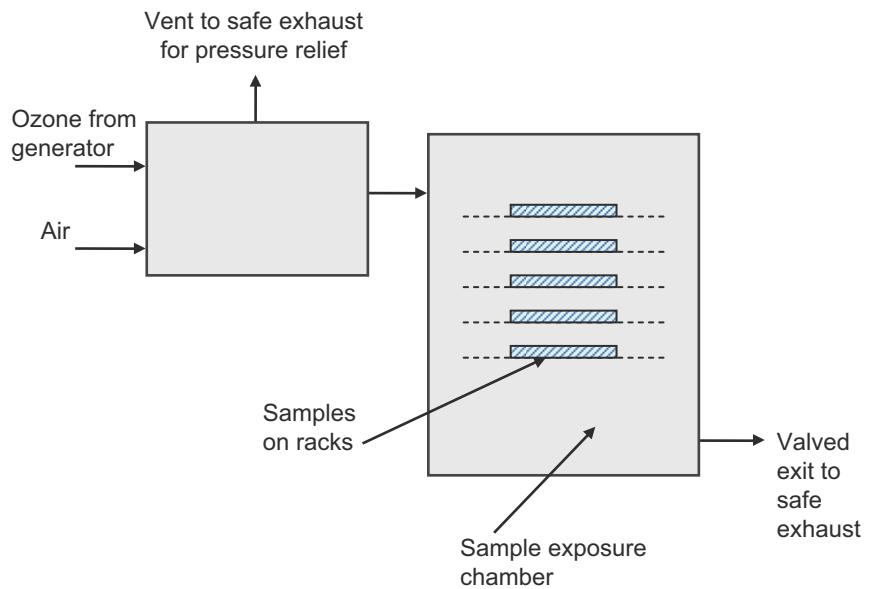
High-altitude airships can receive high doses of ozone over short mission durations. For example, in 1 year at an altitude of 70,000 ft, the ozone fluence (number arriving per unit area) can be as high as 1.2×10^{24} molecules/cm². Ozone exposure at these levels can embrittle materials or change the performance of solar cells. It is important to expose components and materials to the expected ozone dosage to determine if the ozone exposure could cause any mission-critical failures.

A system was designed and used at the NASA Glenn Research Center to expose small materials and components to the desired dosage of ozone. Commercial ozone generators typically produce higher concentrations of ozone than are needed to simulate

the Earth's upper atmosphere, so the output of a commercial generator was diluted in a mixing chamber with air. The output from the mixing chamber was then allowed to flow into an exposure chamber where the ozone concentration was monitored. The concentration needed to simulate the upper atmosphere was higher than the range of the ozone detector, however. To determine the concentration of ozone in the chamber, we conducted several tests—stopping the ozone flow altogether and watching the concentration of ozone in the exposure chamber as a function of time for different airflow rates. Initially, the detector was pegged off scale, but then it dropped to levels that the detector could read, and we generated a family of curves at different airflow rates by plotting the ozone concentration as a function of the time that the ozone was turned off. The data fit followed a simple exponential decay model, so this could then be used to determine the airflow rate that was needed to produce the desired concentration of ozone for the exposure duration needed. The flux (number per unit area per time) of ozone arriving at a surface in the Earth's upper atmosphere for test concentration and duration determination can be estimated by using standard gas laws giving the flux:

$$\text{flux} = 1/4 \times \text{density of ozone} \times \text{average velocity of ozone molecule}$$

By using this technique, we could achieve full mission fluences in a few hours of exposure in the laboratory. The data generated by testing exposed materials and components can give great insight into mission performance and can alert designers to potential critical failures.



Ozone-exposure system.

Find out more about this research:

<http://www.grc.nasa.gov/WWW/epbranch/>

Glenn contacts:

Sharon K. Miller, 216-433-2219, Sharon.K.Miller@nasa.gov; and Bruce A. Banks, 216-433-2308, Bruce.A.Banks@nasa.gov

Author:

Sharon K. Miller

Headquarters Program Office:

TTPO

Programs/Projects:

Exposure of components and materials for durability testing for high-altitude airship applications

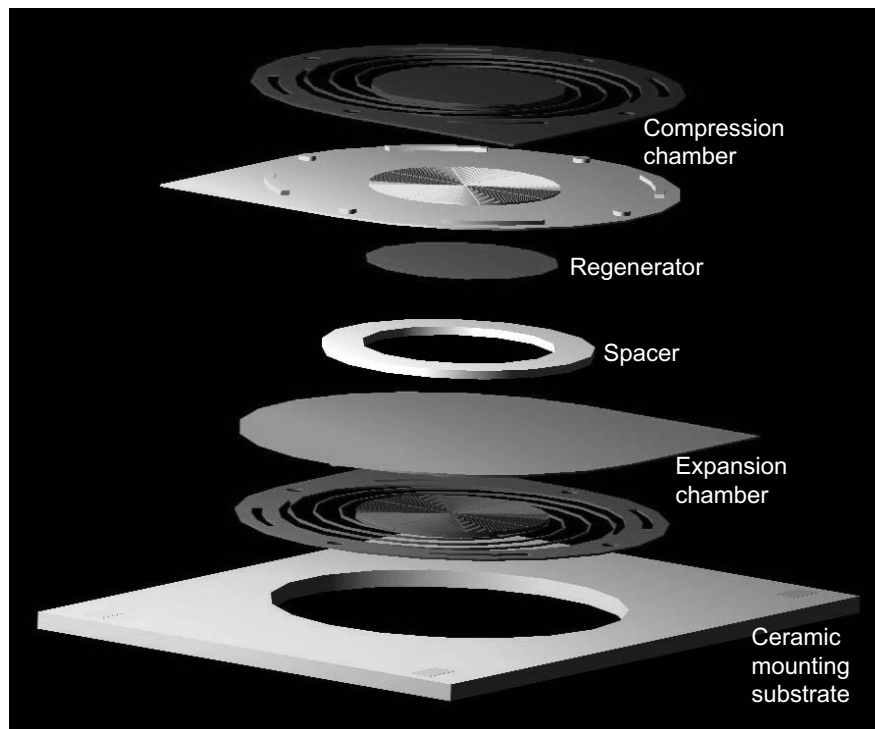
Microsystem Cooler Concept Developed and Being Fabricated

A patented microsystem cooler concept has been developed by the NASA Glenn Research Center. It incorporates diaphragm actuators to produce the Stirling refrigeration cycle within a planar configuration compatible with the thermal management of electronics, sensors, optical and radiofrequency systems, microarrays, and other microsystems. The microsystem cooler is most suited to volume-limited applications that require cooling below the ambient or sink temperature. Johns Hopkins University Applied Physics Laboratory is

conducting development testing and fabrication of a prototype under a grant from Glenn.

Primary components of the planar device include two diaphragm actuators that replace the pistons

found in traditional-scale Stirling machines, and a microregenerator that stores and releases thermal energy to the working gas during the Stirling cycle. The use of diaphragms eliminates the frictional losses and bypass leakage associated with pistons while permitting reversal of the hot and cold sides of the device during operation to allow precise temperature control. The concept has evolved into a design incorporating deep-reactive ion-etching fabrication to produce electrostatically driven comb-drive diaphragms with a spiral spring mounting for maximum deflection. A prototype device based on this design (see the following illustration) is being fabricated.



Prototype microsystem cooler design.

The regenerator part of the micro-system cooler is critical to the feasibility and performance of the device. A piezoelectric-actuated test apparatus was constructed to characterize this critical component, and several regenerator candidates were fabricated and tested. Johns Hopkins custom fabricated two of the regenerators of porous ceramic, and Polar Thermal Technologies constructed one regenerator of multiple layers of nickel and photoresist in an offset grating pattern. An additional regenerator composed of random stainless-steel fiber matrix commonly used in existing traditional-scale Stirling machines was prepared for comparison to the custom-fabricated regenerators.

Test results indicate that each regenerator exhibits a unique system resonant frequency where the greatest membrane deflection occurs, and hence the greatest swept volume (see the table). These data will be used to select the regenerator with the best combination of high resonant frequency and maximum membrane deflection for the prototype device.

Bibliography

Moran, Matthew E.: Microsystem Cooler Development. NASA/TM—2004-213307 (AIAA–2004–5611), 2004. <http://gltrs.grc.nasa.gov/cgi-bin/GLTRS/browse.pl?2004/TM-2004-213307.html>

Glenn contact:

Matthew E. Moran, 216–433–8324, Matthew.E.Moran@nasa.gov

Author:

Matthew E. Moran

Headquarters program office:

Exploration Systems

Programs/Projects:

Enabling Concepts & Technologies, Energetics

SUMMARY OF PASSIVE MEMBRANE DISPLACEMENT FOR EACH REGENERATOR AT 400-V INPUT

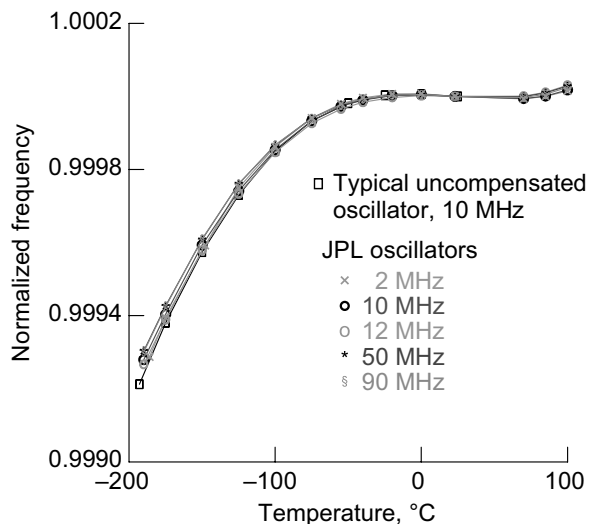
Regenerator	Resonant frequency, Hz	Displacement at resonance, μm	Displacement at 1000 Hz, μm
Layered nickel-photoresist	500 \pm 100	98	55
Large-grain porous ceramic	800 \pm 100	104	36
Small-grain porous ceramic	800 \pm 100	108	31
Random stainless-steel fiber	1500 \pm 100	50	50

Reliability of Electronics for Cryogenic Space Applications Being Assessed

Many future NASA missions will require electronic parts and circuits that can operate reliably and efficiently in extreme temperature environments below typical device specification temperatures. These missions include the Mars Exploration Laboratory, the James Webb Space Telescope, the Europa Orbiter, surface rovers, and deep-space probes. In addition to NASA, the aerospace and commercial sectors require cryogenic electronics in applications that include advanced satellites, military hardware, medical instrumentation, magnetic levitation, superconducting energy management and distribution, particle confinement and acceleration, and arctic missions. Besides surviving hostile space environments, electronics capable of low-temperature operation would enhance circuit performance, improve system reliability, extend lifetime, and reduce development and launch costs. In addition, cryogenic electronics are expected to result in more efficient systems than those at room temperature.

Presently, electronic parts suppliers rate their commercial-off-the-shelf components for operation between 0 and 70 °C. These parts have limitations in extended temperature ranges because of the materials used, device design and packaging, and manufacturing processes. Military-grade devices are rated at -55 to 125 °C, and use different processes. Limited information is available on the performance of components and circuits outside of these temperature ranges. In addition, little is known about the effects of the thermal cycling that is typical of most space missions. Understanding the effects of extreme temperatures on electronics and determining their performance reliability are critical elements for aiding mission planners in the design of spacecraft power systems, as well as in establishing associated risk factors.

There are ongoing efforts at the NASA Glenn Research Center to establish a database on the reliability of electronic devices under extreme low-temperature operation for space applications. These efforts are performed under NASA's Low-Temperature Electronics Program with emphasis on device and circuit characterization at cryogenic temperatures and under long-term, wide-temperature thermal cycling. The results of these investigations will be used to establish safe operating areas and to identify degradation mechanisms and failure modes. This body of knowledge will be disseminated to mission planners and system designers in order to optimize design and mitigate risks. Electronics investigated in this work include passive and active components, digital and analog transducers, direct-current to direct-current converters, sensors, logic and control circuits, operational amplifiers, and semiconductor switches. The graph, for example, shows the normalized output frequency of five programmable oscillators along with that of a typical uncompensated 10-MHz oscillator as a function of temperature between 100 and -195 °C. It can be clearly seen that the curves for the five Jet Propulsion Laboratory (JPL) programmable oscillators were virtually identical to each other and to that of the crystal oscillator, and that the frequency of all the devices began to drop as the temperature approached around -40 °C. This decrease in frequency became steeper as temperature was reduced further.



Normalized output frequency of six oscillators versus temperature. Frequency normalized to frequency at 23 °C. This figure is shown in color in the online version of this document (<http://www.grc.nasa.gov/WWW/RT/2004/RP/RPY-patterson.html>).

These research efforts are being performed by support from the NASA Electronic Parts and Packaging (NEPP) Program and through collaboration with other Government agencies, industrial and aerospace companies, and academia. The program supports missions as well as technology development efforts at the NASA Goddard Space Flight Center, the NASA Langley Research Center, and JPL.

Find out more about this research:

<http://www.grc.nasa.gov/WWW/epbranch/ephome.htm>

Glenn contact:

Richard L. Patterson, 216-433-8166,
Richard.L.Patterson@nasa.gov

QSS Group, Inc., contact:

Ahmad Hammoud, 216-433-8511,
Ahmad.Hammoud@grc.nasa.gov

Authors:

Richard L. Patterson and
Ahmad Hammoud

Headquarters program office:

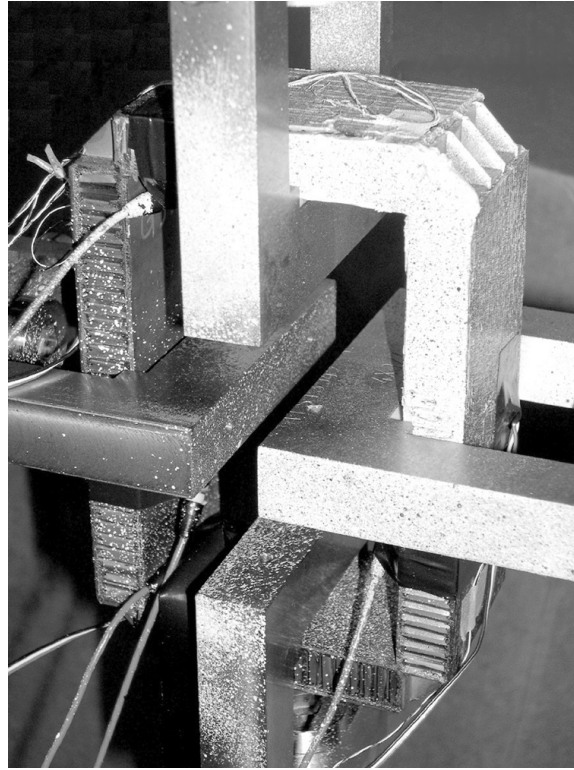
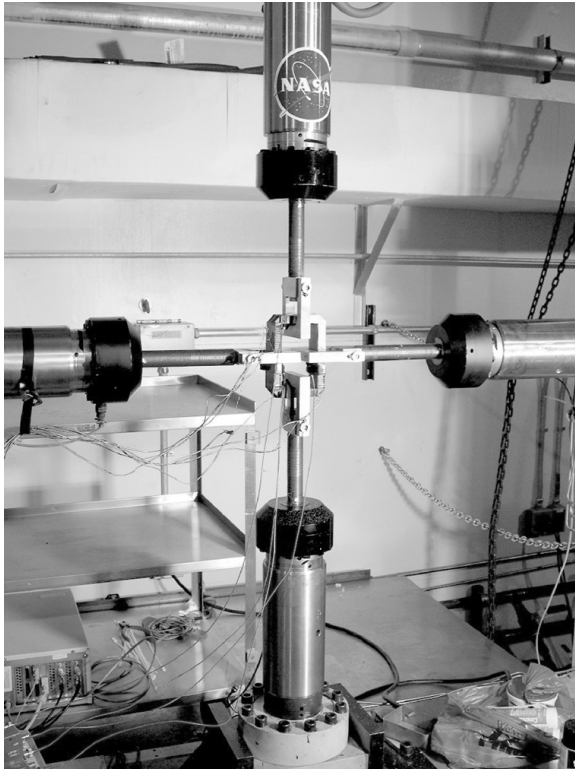
OSS

Programs/Projects:

NEPP, NEPAG, JWST, Mars 07,
JIMO, Europa Lander

Structures

Structural Benchmark Tests of Composite Combustion Chamber Support Completed



Left: Benchmark test configuration for simulated pressure loading of a combustion-chamber support test article.

Right: Test-article honeycomb core with face sheets (speckle pattern applied for photographic strain correlation).

A series of mechanical load tests was completed on several novel design concepts for extremely lightweight combustion chamber support structures at the NASA Glenn Research Center (<http://www.nasa.gov/glenn/>). The tests included compliance evaluation, preliminary proof loadings, high-strain cyclic testing, and finally residual strength testing of each design (see the photograph on the left). Loads were applied with single rollers (see the photograph on the right) or pressure plates (not shown) located midspan on each side to minimize the influence of contact stresses on corner deformation measurements. Where rollers alone were used, a more severe structural loading was produced than the corresponding equal-force pressure loading: the maximum transverse shear force existed over the entire length of each side, and the corner bending moments were greater than for a distributed (pressure) loading. Failure modes initiating at the corner only provided a qualitative indication of the performance limitations since the stress state was not identical to internal pressure. Configurations were tested at both room and elevated temperatures. Experimental results were used to evaluate analytical prediction tools and finite-element methodologies for future work, and they were essential to provide insight into the deformation at the corners. The tests also were used to assess fabrication and bonding details for the complicated structures. They will

be used to further optimize the design of the support structures for weight performance and the efficacy of corner reinforcement.

The test articles were fabricated using sandwich construction technology to provide high specific structural efficiency (refs. 1 to 4). Inner stainless steel face sheets supported a flexible, rectangular, thin-walled, cooled combustion chamber (chamber not included in the benchmark test pieces), and a titanium foil honeycomb core tied this to the outer polyimide-carbon-fiber polymer-matrix-composite face sheets. Some designs included exterior polymer-matrix-composite reinforcements across the four corners.

All components were bonded together with high-temperature adhesive and were cured at the design operating temperature. The chamber support designs were developed for use in a hypersonic air-breathing rocket-based combined-cycle propulsion system. The rectangular cross section was a function of the combustion process as well as the vehicle-engine aerodynamics. The composite combustion chamber support was a collaborative effort between NASA and Rocketdyne Propulsion & Power of the Boeing Company (<http://www.boeing.com/space/rdyne/flash.html>).

These ongoing tests were conducted at Glenn's Structural Benchmark Test Facility by the Polymers Branch (<http://www.grc.nasa.gov/WWW/MDWeb/5150/Polymers.html>) in collaboration with the Life Prediction Branch (<http://www.grc.nasa.gov/WWW/LPB/>). They used a large 500-kN (110,000-lb)-capacity in-plane biaxial load frame to simulate pressure loading through four hydraulic actuators applying scaled loads to the test articles' inner surfaces. The load frame included a fully digital data acquisition and control system. A hot-air furnace provided uniform specimen temperatures for the isothermal elevated-temperature tests. A four-sensor acoustic emissions system monitored crack initiation, adhesive debonds, and other anomalies. Real-time strains were measured with eight strain gauges, and full-field two- and three-dimensional surface strain plots were produced post test through correlation with high-resolution digital images of random speckle patterns applied to the specimens. Digital-format video recordings were made of the residual strength tests. Elevated- and room-temperature tests of alternative designs are expected to be completed in fiscal year 2005.

References

1. Shin, E. Eugene, et al.: Design and Fabrication Issues of High Temperature PMCs for Aerospace Propulsion Applications. Presented at SAMPE 2002, Long Beach, CA, May 2002.
2. Stokes, Eric H.; Shin, E. Eugene; and Sutter, James K.: Mechanical Testing of PMCs Under Simulated Rapid Heat-Up Propulsion Environments. Presented at SAMPE 2002, Long Beach, CA, May 2002.
3. Thesken, J.C., et al.: Thermomechanical Fatigue of Polyimide Composites in Reusable Propulsion Systems. Presented at SAMPE 2004, Long Beach, CA, May 2004.
4. Thesken, J.C., et al.: Design Analysis of a Composite Combustion Chamber Support. Presented at SAMPE 2004 (<http://www.sampe.org>), Long Beach, CA, May 2004.

Find out more about this research:

NASA Glenn Research Center:
<http://www.nasa.gov/glenn/>

Polymers Branch:
<http://www.grc.nasa.gov/WWW/MDWeb/5150/Polymers.html>

Life Prediction Branch:
<http://www.grc.nasa.gov/WWW/LPB/>

Boeing-Rocketdyne:
<http://www.boeing.com/space/rdyne/flash.html>

Glenn contacts:
David L. Krause, 216-433-5465,
David.L.Krause@nasa.gov; and
Dr. James K. Sutter, 216-433-3226,
James.K.Sutter@nasa.gov

Ohio Aerospace Institute (OAI) contacts:
Dr. John C. Thesken, 216-433-3012,
John.C.Thesken@grc.nasa.gov; and
Dr. E. Eugene Shin, 216-433-2544,
Euy-sik.E.Shin@grc.nasa.gov

Authors:
David L. Krause, Dr. John C. Thesken,
Dr. E. Eugene Shin, and
Dr. James K. Sutter

Headquarters program office:
OAT

Programs/Projects:
HOTPC, Access to Space

Benchmark Calibration Tests Completed for Stirling Converter Heater Head Life Assessment

A major phase of benchmark testing has been completed at the NASA Glenn Research Center (<http://www.nasa.gov/glenn/>), where a critical component of the Stirling Radioisotope Generator (SRG) is undergoing extensive experimentation to aid the development of an analytical life-prediction methodology (ref. 1). Two special-purpose test rigs subjected SRG heater-head pressure-vessel test articles to accelerated creep conditions, using the standard design

temperatures to stay within the wall material's operating creep-response regime, but increasing wall stresses up to 7 times over the design point. This resulted in well-controlled "ballooning" of the heater-head hot end.

The test plan was developed to provide critical input to analytical parameters in a reasonable period of time.

The SRG is being developed for multimission use, including the electric power supply for long-duration deep-space missions (ref. 2). For this application, the heater head must endure high temperatures at low stress levels for a long time. These conditions impose an operation-limiting mechanism of material creep—a slow, gradual increase in the pressure-vessel diameter that reduces system performance because of internal dimensional tolerances. Because the SRG must operate for more than 10 years, testing the heater head at the low design-wall stress alone would likely cause high scatter of the very small magnitude creep strains in the short term. This would be of limited value in providing a robust life-prediction tool. Therefore, the test articles' stress levels were raised by increasing test pressures to accelerate the creep results. In addition, although creep-limited components have been designed satisfactorily using material properties generated from traditional uniaxial tests, the heater head is subjected to a highly biaxial state of stress. To supplement the ongoing uniaxial creep tests on flight heat Inconel 718 material (ref. 3), researchers designed the benchmark test program to experimentally evaluate the response to this specific biaxial stress condition.

The completed calibration testing included three shorter term, high-stress benchmark tests conducted on geometrically simplified test vessels fabricated from a heat of flight material: the test conditions caused rapidly increasing creep strains in 1 to 3 months (see the photograph). A fourth test was performed on a flight prototype design test article; this extended the test duration to 6 months. Glenn researchers plan to conduct two additional tests of test articles fabricated to flight prototype specifications at design operating pressure for 1 year or more. One of these tests will be with a “full-up” specimen with structurally significant attachments. It will be conducted with additional externally applied axial stress to duplicate actual flight loading.

The test facility is located at Glenn's Life Prediction Branch's (<http://www.grc.nasa.gov/WWW/LPB/>) Structural Benchmark Test Facility. The test stand includes two independently operated test rigs with argon-pressurization systems capable of 3000 psig. Two 3-kW induction power supplies provide even heating and temperature profiling. A custom data acquisition and control system is employed to safely conduct tests and record results.

The benchmark testing was performed for Glenn's Thermal Energy Conversion Branch (<http://www.grc.nasa.gov/WWW/tmsb/>) and Power and Propulsion Office (<http://space-power.grc.nasa.gov/ppo/>) as part of an in-house project supporting the development of the SRG. NASA's Office of Space Science provided funding for this effort. Lockheed Martin and Stirling Technology Company are developing the SRG110 for the Department of Energy, which is managing the overall SRG project.



Three-month test of IN 718 heater head at 650 °C (1200 °F) with induction heater coils and diametral extensometer quartz glass probes.

References

1. Halford, Gary R., et al.: Structural Analysis of Stirling Power Converter Heater Head for Long-Term Reliability, Durability, and Performance. NASA/TM—2002-211327, 2002. <http://gltrs.grc.nasa.gov/cgi-bin/GLTRS/browse.pl?2002/TM-2002-211327.html>
2. Schreiber, Jeffrey G.; and Thieme, Lanny G.: Overview of NASA GRC Stirling Technology Development. NASA/TM—2004-212969 (AIAA-2003-6093), 2003. <http://gltrs.grc.nasa.gov/cgi-bin/GLTRS/browse.pl?2004/TM-2004-212969.html>
3. Bowman, Randy R.: Long-Term Creep Assessment of a Thin-Walled Inconel 718 Stirling Power-Converter Heater Head. Proceedings of the 36th Intersociety Energy Conversion Engineering Conference, vol. 1, 2001, pp. 435–440.

Find out more about this research:**Thermal Energy Conversion Branch:**<http://www.grc.nasa.gov/WWW/tmsb/>**Power and Propulsion Office:**<http://space-power.grc.nasa.gov/ppo/>**NASA Glenn Research Center:**<http://www.nasa.gov/glenn/>**Life Prediction Branch:**<http://www.grc.nasa.gov/WWW/LPB/>**Glenn contacts:**

David L. Krause, 216-433-5465, David.L.Krause@nasa.gov;
 Dr. Gary R. Halford, 216-433-3265, Gary.R.Halford@nasa.gov; and
 Dr. Randy R. Bowman, 216-433-3205, Randy.R.Bowman@nasa.gov

Authors:

David L. Krause, Dr. Gary R. Halford,
 and Dr. Randy R. Bowman

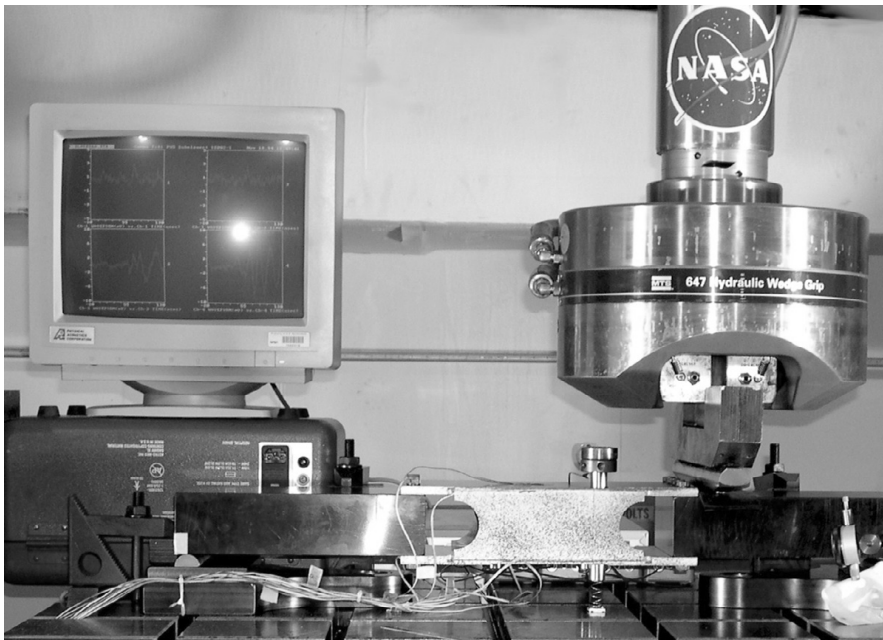
Headquarters program office:

OSS

Programs/Projects:

Project Prometheus, SRG110

Titanium Aluminide Scramjet Inlet Flap Subelement Benchmark Tested



Benchmark test configuration for inlet flap subelement (object painted white with black speckles).

A subelement-level ultimate strength test was completed successfully at the NASA Glenn Research Center (<http://www.nasa.gov/glenn/>) on a large gamma titanium aluminide (TiAl) inlet flap demonstration piece. The test subjected the part to prototypical stress conditions by using unique fixtures that allowed both loading and support points to be located remote to the part itself (see the photograph). The resulting configuration produced shear,

moment, and the consequent stress topology proportional to the design point. The test was conducted at room temperature, a harsh condition for the material because of reduced available ductility. Still, the peak experimental load-carrying capability exceeded original predictions.

The lightweight TiAl subelement was designed with several complicated features and fabrication technologies to demonstrate full-scale manufacturing capability as a potential backstructure material for maintainable composite panel heat exchangers in the inlet, combustor, and nozzle section of a turbine-based combined-cycle propulsion system (refs. 1 and 2). The achievement of aggressive thrust-to-weight and long-life goals requires advanced materials such as TiAl for next-generation launch vehicles. This subelement was constructed with the high-strength, high-temperature alloy Gamma MET PX,¹ with a weight-reduction potential of approximately 40 percent in comparison to a baseline Inconel 718 configuration (ref. 2). It was a collaborative effort

¹ Gamma MET PX is a trademark of PLANSEE AG, Austria. Alloy composition is based on TNB alloys developed by GKSS Research Center, Germany.

between NASA, Pratt & Whitney (<http://www.pratt-whitney.com>), Engineering Evaluation & Design (<http://www.eeandd.com>), PLANSEE AG (<http://www.plansee.com>), and the Austrian Space Agency (<http://www.asaspace.at>).

The TiAl inlet flap was designed to satisfy many functional objectives. Structurally, it avoided complicated shapes, minimized the number of stress concentrations, and used one-pass brazing for sheet construction and local reinforcement at high-stress locations. During the benchmark test, sensors detected early cracking at less than the predicted failure load; it was theorized that a face-sheet-to-web braze began to peel at this level. The local separations resulting from the braze peeling allowed load shedding to stiffer adjacent regions of the structure. The loading ramp progressed with quite linear structural response and with continued crack detection until a peak load approximately 10-percent higher than predicted was reached, when the subelement fractured completely. This high load-carrying capacity demonstrated a significant TiAl material success.

The test was completed in-house at Glenn's Life Prediction Branch's (<http://www.grc.nasa.gov/WWW/LPB/>) Structural Benchmark Test Facility. It utilized a large 500-kN (110,000-lb) load frame with a fully digital data acquisition and control system. A four-sensor acoustic emissions system monitored crack detection and growth. Real-time strains were measured with eight strain gauges, and digital images of a random speckle pattern applied to the subelement were correlated after testing to produce full-field, through-the-thickness surface strain plots. Glenn's Advanced Metallics Branch (<http://www.grc.nasa.gov/WWW/AdvMet/webpage/>) personnel performed related sheet tensile, fatigue, and creep tests, and a number of realistic feature tests, including bond shear, stepped tensile, bolted clevis, and braze peel tests.

References

1. Draper, S.L., et al.: Advanced Metallic Materials for Turbine Based Combined Cycle Propulsion Systems. Presented at the JANNAF 39th Combustion Subcommittee, 27th Airbreathing Propulsion, 21st Propulsion Systems Hazards Committee, and 3rd Modeling and Simulation Subcommittee Joint Meeting, Dec. 2003. Available from Chemical Propulsion Information Agency (CPIA).

2. Doehnert, B., et al.: Final report for NASA Contract No. NAS3-01138 Task Order 11, FR-26186-1, Pratt & Whitney Space Propulsion, West Palm Beach, FL, Apr. 2004.

Find out more about this research:

NASA Glenn Research Center:
<http://www.nasa.gov/glenn/>

Advanced Metallics Branch:
<http://www.grc.nasa.gov/WWW/AdvMet/webpage/>

Life Prediction Branch:
<http://www.grc.nasa.gov/WWW/LPB/>

Pratt & Whitney:
<http://www.pratt-whitney.com>

Engineering Evaluation & Design:
<http://www.eeandd.com>

Glenn contacts:
David L. Krause, 216-433-5465,
David.L.Krause@nasa.gov; and
Susan L. Draper, 216-433-3257,
Susan.L.Draper@nasa.gov

Authors:
David L. Krause and Susan L. Draper

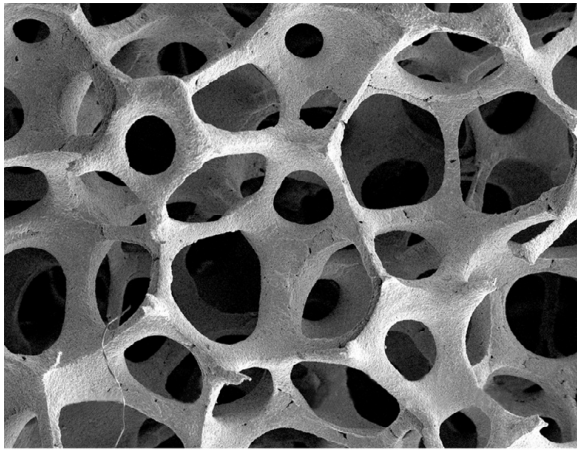
Headquarters program office:
OAT

Programs/Projects:
NGLT, RTA, TBCC

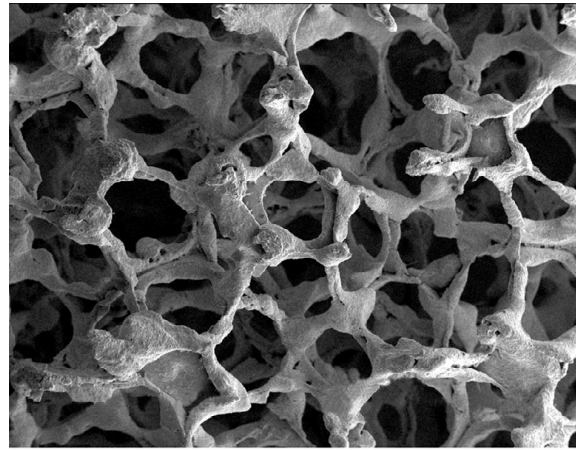
Stainless-Steel-Foam Structures Evaluated for Fan and Rotor Blades

The goal of this project is to use a sandwich structure design, consisting of two stainless-steel face sheets and a stainless-steel-foam core, to fabricate engine fan and propeller blades. Current fan blades are constructed either of polymer matrix composites (PMCs) or hollow titanium alloys. The PMC blades are expensive and have poor impact resistance on their leading edges, thereby requiring a metallic leading edge to satisfy the Federal Aviation Administration's impact requirements relating to bird strikes. Hollow titanium blades cost more to fabricate because of the intrinsically difficult fabrication issues associated with titanium alloys. However, both these current concepts produce acceptable lightweight fan blades.

The NASA Glenn Research Center is studying a possible low-cost alternative to the current technologies: a stainless-steel sandwich structure encasing a stainless-steel-foam core. The face sheets provide structural strength and resistance for the blade, whereas the foam core decreases the overall density, increases vibrational and acoustic damping, maintains face



1 mm



1 mm

Structures of 17-4 PH foams. Left: Good structure with clean, smooth ligaments. Right: Poor structure with broken, knobby ligaments.

sheet separation, and enhances stiffness (ref. 1). The use of a commercially available aerospace stainless steel and commercial manufacturing methods is expected to produce fan, propeller, and rotor blades that can be manufactured at low cost yet have mechanical properties and densities equivalent to those of currently used designs. Thus, the new design approach could yield a new generation of low-cost, low-density fan blades with performance equal to or better than that of blades produced by conventional manufacturing processes.

Recent work at Glenn has focused on aerospace grade 17-4 PH stainless-steel sandwich panels for these applications. This material is corrosion resistant; possesses excellent impact, high strength, and fatigue properties; and is commercially available, inexpensive, and easy to fabricate. Sandwich foam panels were produced by a commercial vendor using a proprietary powder-metallurgy process. The panels were evaluated nondestructively, then shear and bend tests were conducted. The foam cores were tested in compression. It was observed that the mechanical properties of the foam core were not as good as the predicted values. This was attributed to shrinkage porosity in the ligaments of the foam core formed during the manufacturing process. Foam cores with better integrity were fabricated with further optimization of the manufacturing process. These improvements are depicted in the scanning electron microscope (SEM) photographs, showing a superior quality foam core (left photograph) and a poor-quality foam core (right photograph). The compressive strength of the good-quality foam core was observed to be nearly 3 times that of the poor-quality foam core. Another critical issue for these structures is the quality of the brazed joint between the face sheets and the foam. The brazed joint was studied in detail using destructive and nondestructive methods (ref. 2). Improvement of the brazed joint greatly increased the shear strength of the sandwiched panel.

With the recently improved properties, a series of experimental and theoretical optimization studies can be performed to investigate foam characteristics, such as the number of cells per unit length, the density (i.e., the thickness of the ligaments on the cell edges), and the face-sheet thickness. A range of material requirements will ultimately be defined that will allow the sandwich

structure to be utilized in a fan-blade application. Finally, a contoured fan blade will be manufactured to demonstrate the viability of the manufacturing process.

References

1. Min, James B., et al.: Analysis of Stainless Steel Sandwich Panels With a Metal Foam Core for Lightweight Fan Blade Design, AIAA-2004-1836, 2004.
2. Cosgriff, Laura M., et al.: Ultrasonic Spectroscopy of Stainless Steel Sandwich Panels. Presented at the 35th International SAMPE Conference, Dayton, OH, Dec. 2003.

Find out more about the research of Glenn's Life Prediction Branch:

<http://www.grc.nasa.gov/WWW/LPB/>

Glenn contacts:

Dr. Bradley A. Lerch, 216-433-5522, Bradley.A.Lerch@nasa.gov; and Dr. Sai V. Raj, 216-433-8195, Sai.V.Raj@nasa.gov

Authors:

Dr. Bradley A. Lerch, Dr. Sai V. Raj, Dr. Louis J. Ghosn, Dr. Mohan G. Hebsur, Laura M. Cosgriff, Dr. James B. Min, and Frederic A. Holland, Jr.

Headquarters program office:

OAT

Programs/Projects:

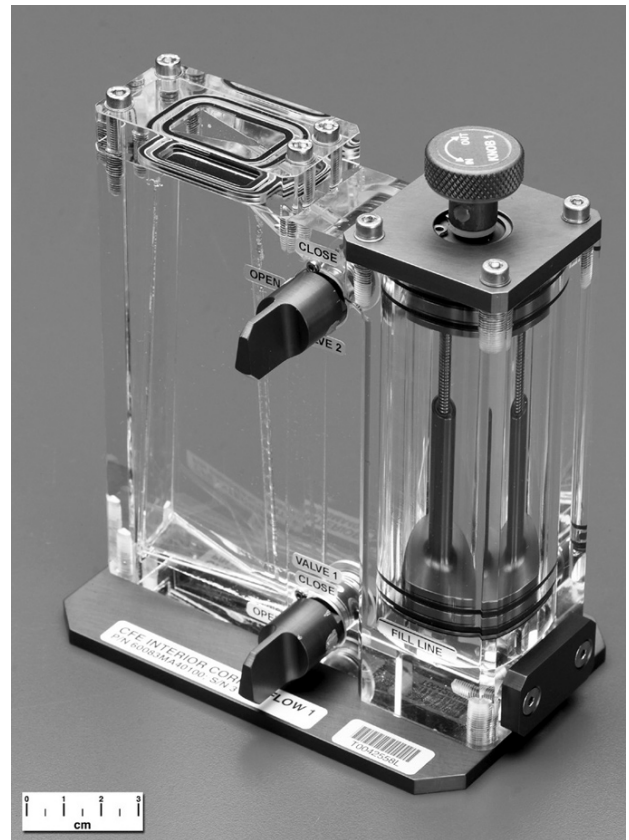
Ultra Safe

Integrity of Polymethylmethacrylate (PMMA) Chemically Welded Joints Examined

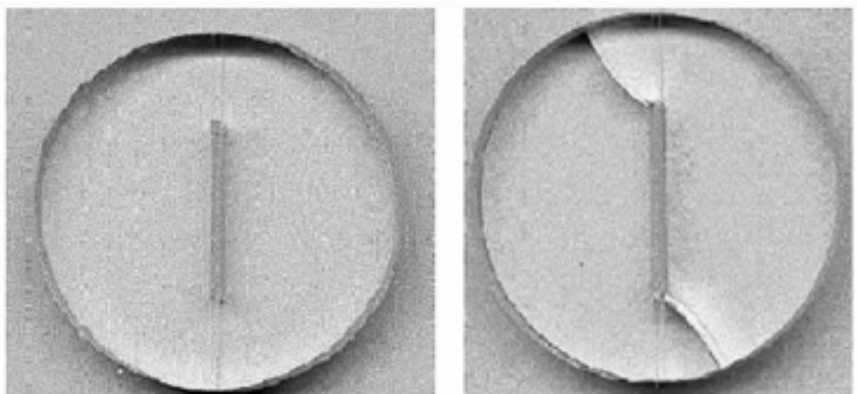
NASA Glenn Research Center's Capillary Flow Experiments (CFE) program is developing experiment payloads to explore fluid interfaces in microgravity on the International Space Station. The information to be gained from the CFE is relevant to the design of fluid-bearing systems in which capillary forces predominate, for example in the passive positioning of liquids in spacecraft fuel tanks. To achieve the science goals of CFE, Glenn researchers constructed several types of experiment vessels (ref. 1). One type of vessel, known as the interior corner flow (ICF), will be used to determine important transients for low-gravity liquid management in a two-phase system. Each vessel has a cylindrical fluid reservoir connected to each end of the test chamber by internal transport tubes, each with a quarter-turn shutoff valve (see the top photograph). These multipiece vessels are made from polymethylmethacrylate (PMMA) because of its excellent optical properties (i.e., the fluids can be observed easily in the vessel). Because of the complexity of certain vessels, the test chamber had to be manufactured in pieces and welded chemically. Some past experience with adhesive bonded plastic showed that the experiment fluid degraded the adhesive to the point of failure. Therefore, it was necessary to see if the fluid also degraded the chemically welded PMMA joints.

In response to these concerns, a joint CFE-Glenn program was conducted to investigate the effect of silicone oil on the strength of the bonded PMMA. A number of different tests were conducted to assess the joint strength. These included tests on the PMMA parent material, tests on welded PMMA, and notched samples of both welded and unwelded PMMA. In addition, samples were aged in either air or silicone oil for up to 8 weeks to investigate any potential deleterious effects of the environment.

The results showed that neither parent material nor welded structures were degraded by long-term exposures in air or silicone oil. Notched samples lowered the strength and failure strain of the materials, and these decreases were predictable from fracture mechanics. Also, biaxial stress states from the



Interior corner flow vessel for CFE experiment.



Brazilian-disk, welded samples. Left: Weld line in the pretest state. Right: Kinked crack from a mode-II test.

notch did not adversely affect the weld joint. This was verified by using Brazilian disks to examine both mode-I and mode-II cracks (see the bottom photograph on the preceding page). These tests indicated that the crack prefers to follow a mode-I type path rather than following the weld, suggesting that the weld has nearly parent material properties. A fracture analysis was performed on the ICF vessel using the actual dimensions and proof pressure. This analysis showed that there was a factor of 3 margin of safety for the worse-case conditions.

Reference

1. Weislogel, M., et al.: The Capillary Flow Experiments: Handheld Fluids Experiments for International Space Station. AIAA-2004-1148, 2004.

Find out more about the research of Glenn's Life Prediction Branch:

<http://www.grc.nasa.gov/WWW/LPB/>

Glenn contact:

Dr. Bradley A. Lerch, 216-433-5522,
Bradley.A.Lerch@nasa.gov

OAI contact:

Dr. John C. Thesken, 216-433-3012,
John.C.Thesken@grc.nasa.gov

Authors:

Dr. Bradley A. Lerch,
Dr. John C. Thesken, Charles T. Bunnell,
Carol E. Kurta, and Mike Sydenstricker

Headquarters program office:

Life Support & Habitation,
Exploration Systems

Programs/Projects:

Exploration Systems

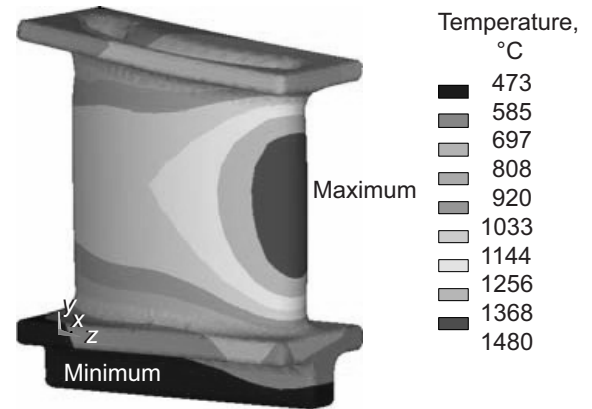
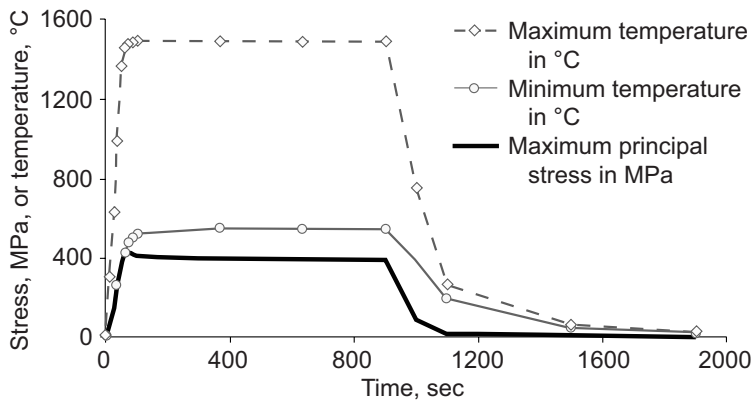
Life Predicted in a Probabilistic Design Space for Brittle Materials With Transient Loads

Analytical techniques have progressively become more sophisticated, and now we can consider the probabilistic nature of the entire space of random input variables on the lifetime reliability of brittle structures. This was demonstrated with NASA's CARES/*Life* (Ceramic Analysis and Reliability Evaluation of Structures/*Life*) code combined with the commercially available ANSYS/Probabilistic Design System (ANSYS/PDS), a probabilistic analysis tool that is an integral part of the ANSYS finite-element analysis program. ANSYS/PDS allows probabilistic loads, component geometry, and material properties to be considered in the finite-element analysis. CARES/*Life* predicts the time-dependent probability of failure of brittle material structures under generalized thermomechanical loading—such as that found in a turbine engine hot-section. Glenn researchers coupled ANSYS/PDS with CARES/*Life* to assess the effects of the stochastic variables of component geometry, loading, and material properties on the predicted life of the component for fully transient thermomechanical loading and cyclic loading.

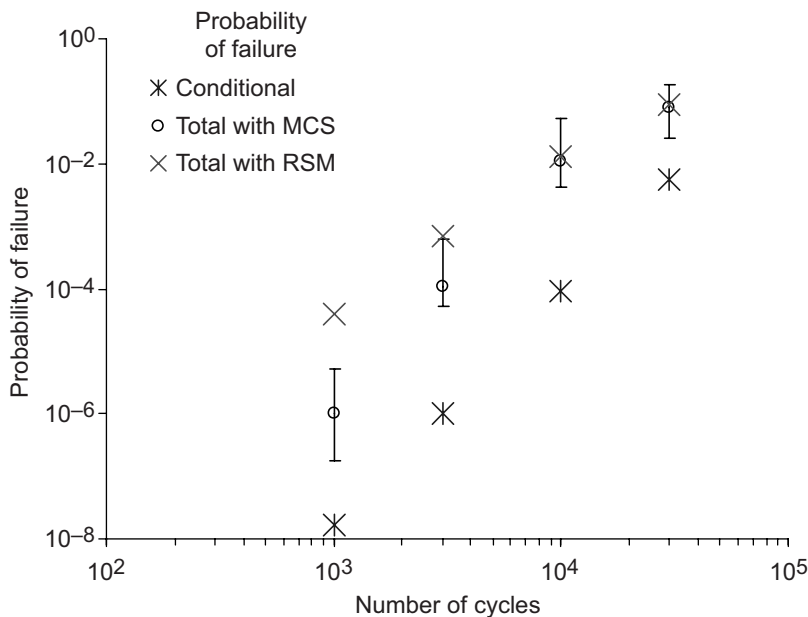
In this implementation, the material parameters associated with reliability analysis—the Weibull and fatigue parameters—can themselves be made stochastic. This simulates batch-to-batch variations in the material reliability response or, alternately, the statistical uncertainty of the estimated parameters

from the true parameters derived from experimental rupture data. It enables a more realistic assessment of brittle material component integrity. This capability will be useful in the design of ceramic turbine blades and vanes, thermal protection system parts, dental prosthetics, solid oxide fuel cells, and microelectromechanical systems (MEMS), as well as other applications that employ brittle materials.

A simplified turbine vane model simulating engine startup and shutdown follows, with details given in reference 1. The stator vane was assumed to be composed of a typical silicon nitride. The effects of a probabilistic engine startup/shutdown load profile and of probabilistic Weibull and fatigue



Left: Maximum temperatures and stresses versus time for a simulated startup/shutdown cycle of a ceramic turbine vane. Right: Finite-element model results showing the stator vane temperature profile at 75 sec—the moment of highest loading. Maximum and minimum temperatures, 1480 and 473 °C; time step, 75 sec.



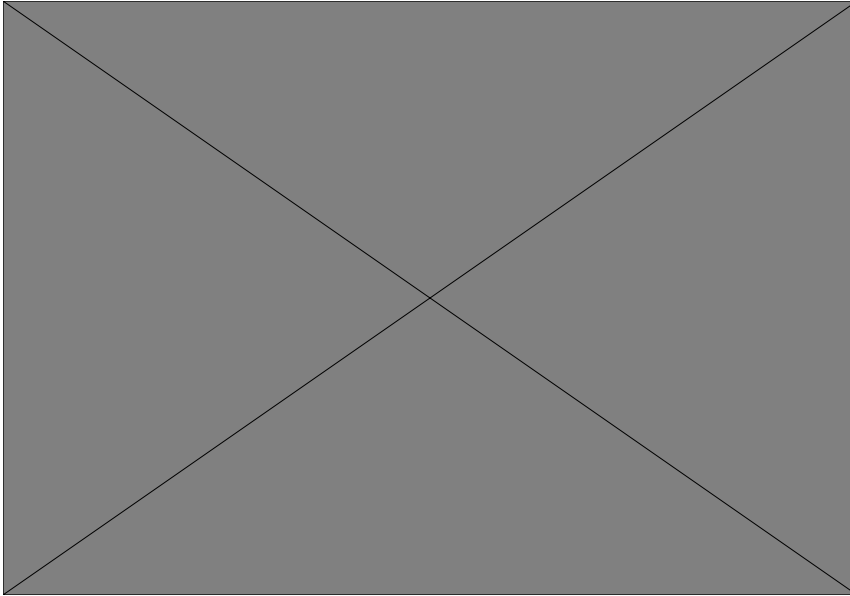
Results for conditional (deterministic) and total probability from the PDS using Monte-Carlo simulation (MCS) and the response-surface method (RSM).

parameters on the predicted integrity for a given number of startup/shutdown engine cycles were examined.

For the probabilistic analysis, 11 input parameters were identified as random quantities and were assigned a statistical distribution function to quantify their randomness. The random input variables impacting the finite-element analysis

included material properties, thermal boundary conditions, and the startup time of the load cycle. The heat-transfer coefficient was assumed to be a coupled random value dependent on the variability of the heat-transfer mechanism coupled with the randomness of the mass flow. The random input variables affecting only the CARES/*Life* part of the analysis included the brittle material Weibull and fatigue parameters. The distribution types as well as the distribution parameters, although not based on measured data, nevertheless represented very realistic values.

The transient operation was characterized by four phases. Phase 1, startup, lasted 50 sec. This was followed by phase 2—850 sec of hold time. Phase 3 was a 200-sec shutdown, and phase 4 was an 800-sec hold time for cooling down. The top left figure illustrates this transient profile for one loading cycle. The top right figure shows the stator vane thermal profile at 75 sec—the moment of maximum transient loading.



Sensitivity of conditional failure probability at 1000 load cycles with Monte-Carlo simulation.

The bottom graph on the preceding page shows the average predicted failure probability (the so-called total probability) versus loading cycles for two probability methods—the Monte-Carlo simulation and the response-surface method—as well as a conditional (deterministic) finite-element analysis using averaged properties. This “total probability” is just the average of all the individual simulation trials. The differences between the deterministic and probabilistic analyses were due to highly nonlinear and skewed probability distributions. These results show that not taking stochastic response into account can lead to a nonconservative design. Correlation between the Monte-Carlo simulation and the response-surface method would improve as the number of simulations increased. In this case, we used 400 simulations for the Monte-Carlo simulation.

The pie chart shows the sensitivity analysis results reported by ANSYS/PDS. Most of the input variables that significantly impact the failure probability either influence the temperature results or the stresses of the finite-element analysis. All of these input variables have a strongly nonlinear influence on the conditional failure probability.

The significant difference between the conditional failure probability and the total failure probability indicates that ignoring the random influences outlined previously may lead to a nonconservative design. The conditional failure probability itself may be acceptably low, but the total failure probability could

be, as in this example, two orders of magnitudes higher, which might not be considered safe enough.

We have demonstrated that a probabilistic life-prediction methodology for transient loading can be combined with a generalized probabilistic finite-element analysis program. This useful combination can be applied to other interesting problems, such as the effect of the reentry envelope on the reliability of certain passive ultra-high-temperature thermal protections systems or, for dental prosthetics, the effect on reliability of random loading direction and loading magnitude over time. It also would be useful in determining MEMS lifetime where tolerances on dimensions are a significant fraction of the overall part size.

Reference

1. Reh, Stefan; Palfi, Tamas; and Nemeth, Noel N.: Probabilistic Analysis Techniques Applied to Lifetime Reliability Estimation of Ceramics. Presented at the JANNAF 39th Combustion Subcommittee, 27th Airbreathing Propulsion, 21st Propulsion Systems Hazards Committee, and 3rd Modeling and Simulation Subcommittee Joint Meeting, Dec. 2003. Available from Chemical Propulsion Information Agency (CPIA).

Glenn contact:

Noel N. Nemeth, 216-433-3215,
Noel.N.Nemeth@nasa.gov

Authors:

Noel N. Nemeth, Tamas Palfi, and Stefan Reh

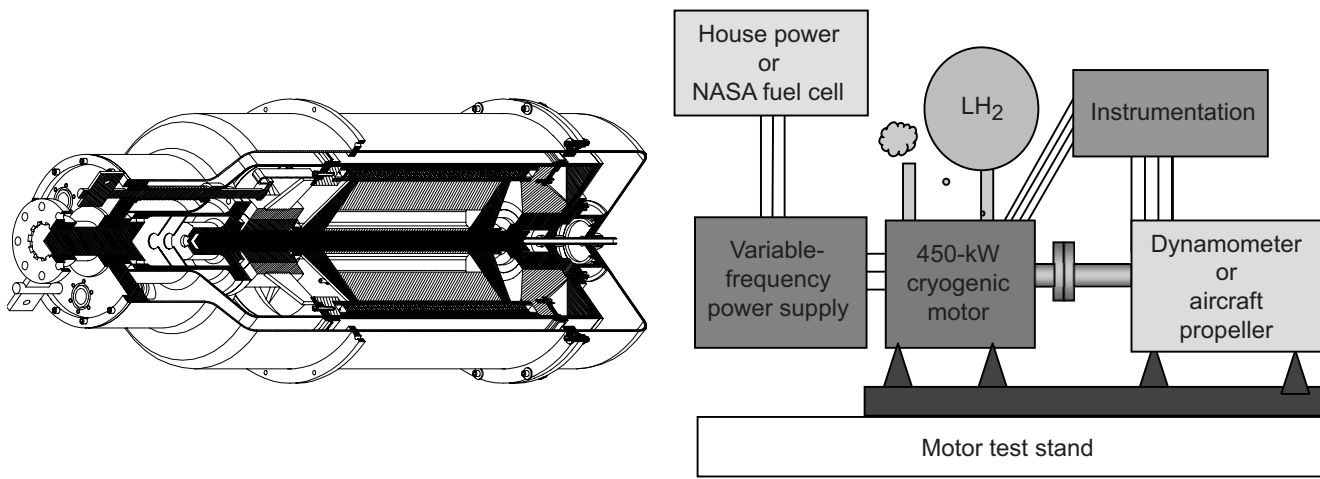
Headquarters program office:

Vehicle Systems

Programs/Projects:

UEET

Liquid-Hydrogen-Cooled 450-hp Electric Motor Test Stand Being Developed



Cryogenic motor/generator and motor test stand. Anticipated motor parameters: length, 35 in.; diameter, 16 in.; weight, 279 lb; power, 450 hp; speed, 6000 rpm; 480 V; three phases.

With growing concerns about global warming, there is a need to develop pollution-free aircraft. One approach is to use hydrogen-fueled aircraft that use fuel cells or turbogenerators to produce electric power to drive the electric motors that turn the aircraft's propulsive fans. Hydrogen fuel would be carried as a liquid, stored at its boiling point of 20.5 K (−422.5 °F). Conventional electric motors, however, are too heavy for aircraft propulsion. We need to develop high-power, lightweight electric motors (high-power-density motors).

One approach is to increase the conductivity of the wires by cooling them with liquid hydrogen (LH₂). This would allow superconducting rotors with an ironless core. In addition, the motor could use very pure aluminum or copper, substances that have low resistances at cryogenic temperatures. A preliminary design of a 450-hp LH₂-cooled electric motor was completed and is being manufactured by a contractor. This motor will be tested at the NASA Glenn Research Center and will be used to test different superconducting materials such as magnesium diboride (MgB₂). The motor will be able to operate at speeds of up to 6000 rpm.

This motor will serve as a realistically sized prototype that will be representative of motors used in general-aviation and transport-sized aircraft. In addition, it will be able to be integrated into ground-based propulsion system demonstrators being developed at NASA and to serve as either a motor or as a generator, powered by either hydrogen-burning turbines or fuel cells. This

work was supported by the Alternate Energy Foundation Technologies (AEFT) Project.

**U.S. Army Research Laboratory,
Vehicle Technology Directorate at
Glenn contact:**

Albert F. Kascak, 216-433-6024,
Albert.F.Kascak@grc.nasa.gov

Glenn contacts:

Dr. Gerald V. Brown, 216-433-6047,
Gerald.V.Brown@nasa.gov; and
Jeffrey J. Trudell, 216-433-5303,
Jeffrey.J.Trudell@nasa.gov

Authors:

Albert F. Kascak, Jeffrey J. Trudell, and
Dr. Gerald V. Brown

Headquarters program office:

OAT

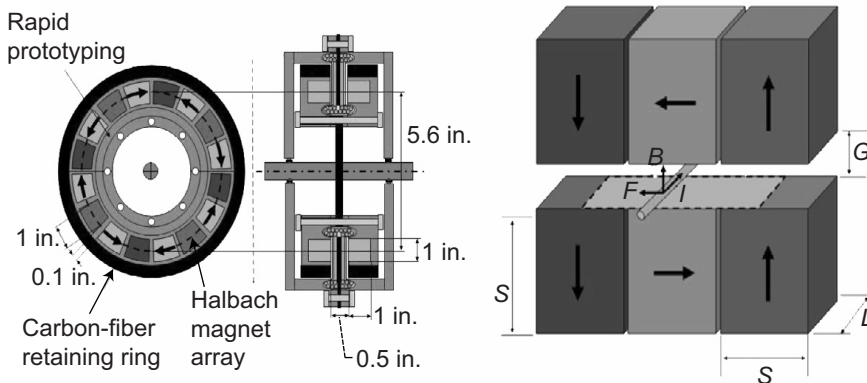
Programs/Projects:

AEFT

Ironless High-Power-Density Permanent Magnet Electric Motors Designed for Emissionless Aircraft Propulsion

With growing concerns about global warming, there is a need to develop pollution-free aircraft. One approach is to use hydrogen-fueled aircraft that use fuel cells or turbogenerators to produce electric power to drive the electric motors that turn the aircraft's propulsive fans. Hydrogen fuel would be carried as a liquid, stored at its boiling point of 20.5 K (−422.5 °F). Conventional electric motors, however, are too heavy to use on an aircraft. We need to develop high-power, lightweight electric motors (high-power-density motors).

At the NASA Glenn Research Center, our approach is first to improve the heat removal from the stator, by using forced-convection heat transfer, and second to improve the magnetic flux circuit with a Halbach Array. This will eliminate the need for an iron core. The last improvement will be to increase the speed of the motor while containing the permanent magnets with a carbon fiber ring.



Left: Ironless permanent magnet brushless direct-current motor. Right: Halbach magnet array.

An ironless motor was designed to have a 5.6-in.-mean-diameter cylindrical Halbach Array with nominally 1 in.³ permanent magnets. It is brushless and can run at speeds up to 15,000 rpm. The motor is being manufactured and will be used to test different stator designs. The stators use vacuum-potted, epoxied Litz wire, with molded cooling channels. This work was supported by the Alternate Energy Foundation Technologies (AEFT) Project.

U.S. Army Research Laboratory, Vehicle Technology Directorate at Glenn contact:

Albert F. Kascak, 216-433-6024,
Albert.F.Kascak@grc.nasa.gov

Glenn contacts:

Dr. Gerald V. Brown, 216-433-6047,
Gerald.V.Brown@nasa.gov; and
Jeffrey J. Trudell, 216-433-5303,
Jeffrey.J.Trudell@nasa.gov

Authors:

Albert F. Kascak, Jeffrey J. Trudell, and
Dr. Gerald V. Brown

Headquarters program office:

OAT

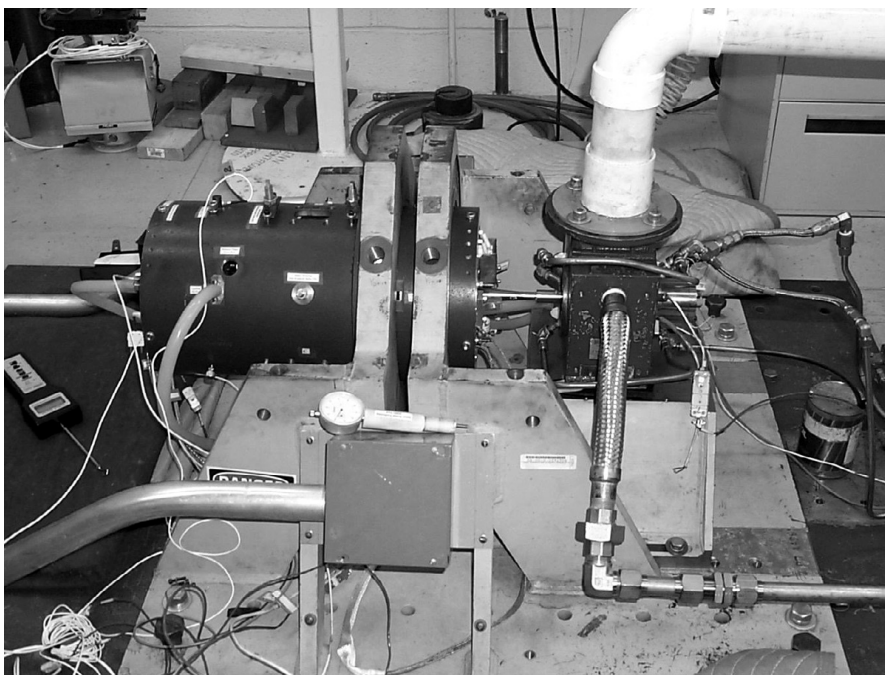
Programs/Projects:

AEFT

High-Temperature (1000 °F) Magnetic Thrust Bearing Test Rig Completed and Operational

Large axial loads are induced on the rolling element bearings of a gas turbine. To extend bearing life, designers use pneumatic balance pistons to reduce the axial load on the bearings. A magnetic thrust bearing could replace the balance pistons to further reduce the axial load. To investigate this option, the U.S. Army Research Laboratory, the NASA Glenn Research Center, and Texas A&M University designed and fabricated a 7-in.-diameter magnetic

thrust bearing to operate at 1000 °F and 30,000 rpm, with a 1000-lb load capacity. This research was funded through a NASA Space Technology Transfer Act with Allison Advance Development Company under the



High-speed, 1000 °F magnetic thrust test facility.

Ultra-Efficient Engine Technology (UEET) Intelligent Propulsion Systems Foundation Technology project.

The test rig was commissioned at Glenn in July 2004. Technical barriers that were addressed included designing a thrust disk design that can withstand high stresses at high speeds and temperatures, designing a disk attachment to the

rotor, developing high-temperature coils, compensating for thermal expansion, developing a way to measure axial load at high speeds and temperatures, and developing cold and hot alignment procedures.

The test facility is operational, and a LabVIEW (National Instruments Corporation, Austin, TX) data-acquisition system is being used to collect test results. High-temperature and high-speed tests are in progress and are scheduled to be completed by the second quarter of 2005.

**U.S. Army Research Laboratory,
Vehicle Technology Directorate at
Glenn contact:**

Gerald T. Montague, 216-433-6252,
Gerald.T.Montague@grc.nasa.gov

Glenn contact:

Andrew J. Provenza, 216-433-6025,
Andrew.J.Provenza@nasa.gov

Author:

Gerald T. Montague

Headquarters program office:

OAT

Programs/Projects:

UEET

G2 Flywheel Module Operated at 41,000 rpm

NASA Glenn Research Center's Flywheel Development Team designed, built, and successfully operated the new G2 flywheel to 41,000 rpm on September 2, 2004. This work was supported by the Aerospace Flywheel Technology Program—a NASA Office of Aerospace Technology ETC Program funded by the Energetics Project. The work was performed by a team of civil servants, contractors, and grantees managed by Glenn's Electrical Systems Development Branch, Structural Mechanics and Dynamics Branch, and Space Power & Propulsion Test Engineering Branch. The G2 flywheel was designed to be a low-cost modular testbed for flywheel system integration and component demonstrations.

This is the first module designed by Glenn, and it reached rated speed in a fraction of the time required for all the previous modules. New redundant magnetic bearings designed by Texas A&M University were used to levitate the rotor, and a new type of resolver conceived at Glenn was used for angle feedback.

The design was supported by analytical work in magnetic bearing control and motor control that reduced the time from final assembly to full-speed demonstration to 1 month—a factor of 4 faster than the time for the previous module. More careful attention to the vacuum system resulted in better operating pressures. New electrical connectors were used that are more reliable, meet military standards, and are easier to work with. The G2 spin losses were 30-percent lower than those for the D1 flywheel, and the rotor temperatures rose only 10 °F in

9 hr of testing. Total spin losses were measured by disconnecting the motor and recording the speed versus time as the flywheel spun down because of losses. It took about 5.5 hr to spin down from 41,000 to 12,000 rpm. The reduced spin losses are a result of the Texas A&M bearing design and the improved vacuum. The low rotor temperature indicates that the split between the rotor and stator losses has shifted mostly to the stator. This is exactly what we are aiming for because the stator can be conductivity-cooled, whereas the rotor is only radiatively cooled. We plan to use the G2 flywheel in conjunction with the D1 flywheel to demonstrate full-power integrated power and attitude control.

Find out more about this research:

<http://space-power.grc.nasa.gov/ppo/projects/flywheel/>

Glenn contact:

James F. Soeder, 216-433-5328,
James.F.Soeder@nasa.gov

University of Toledo contact:

Ralph H. Jansen, 216-433-6038,
Ralph.H.Jansen@grc.nasa.gov

Authors:

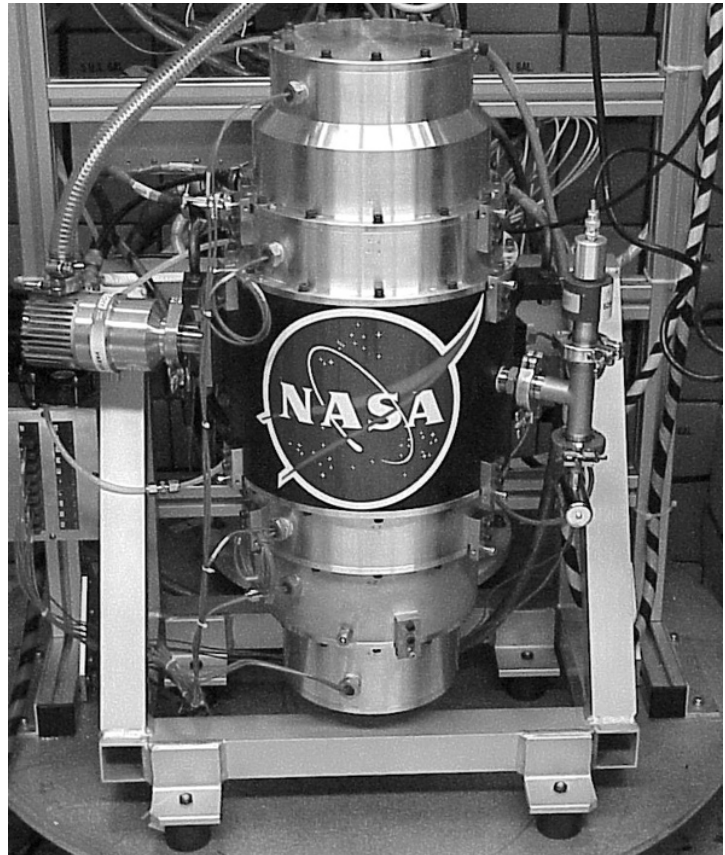
Ralph H. Jansen and Kerry L. McLallin

Headquarters program office:

Exploration Systems

Programs/Projects:

Human & Robotic Technology, CEV, Human Lunar Return, Earth and Space Science

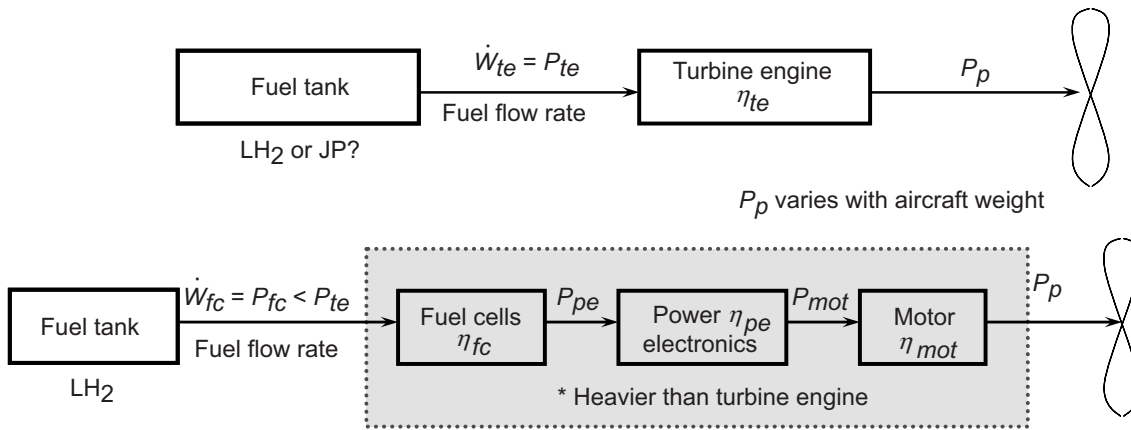


NASA G2 flywheel module.

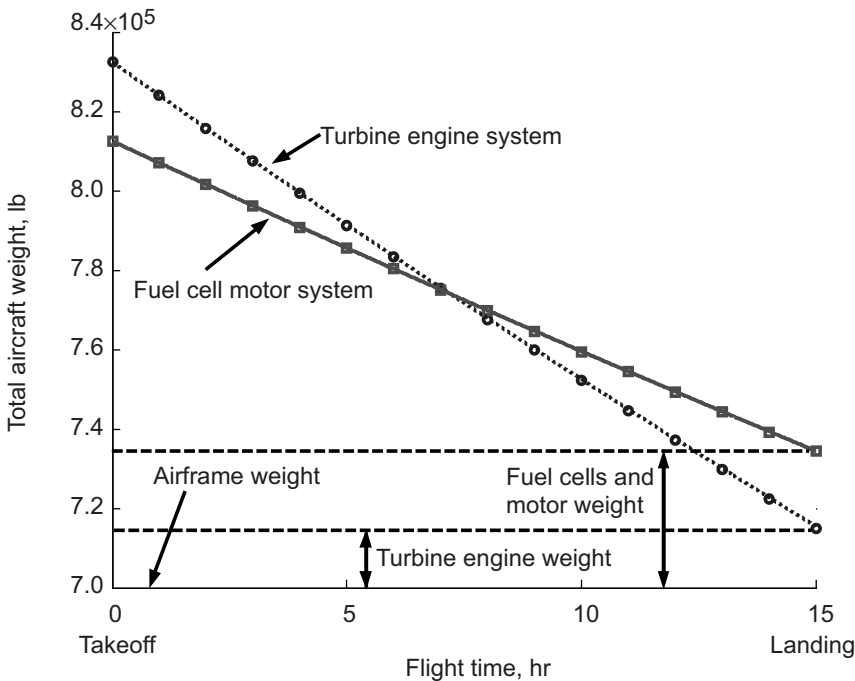
Fuel-Cell-Powered Electric Motor Drive Analyzed for a Large Airplane

Because of its high efficiency, fuel cell technology may be used to launch a new generation of more-electric aeropropulsion and power systems for future aircraft. Electric-motor-driven airplanes using fuel-cell powerplants would be beneficial to the environment because of fuel savings, low noise, and zero carbon-dioxide emissions. In spite of the fuel cell's efficiency benefit, to produce the same shaft drive power, a fuel-cell-powered electric-drive system must be definitely heavier than a turbine-drive system. However, the fuel-cell system's overall efficiency from fuel-to-shaft power is higher than for a turbine-drive system. This means that the fuel consumption rate could be lower than for a conventional system. For heavier, fuel-laden planes for longer flights, we might achieve substantial fuel savings. In the airplane industry, in fact, an efficiency gain of even a few percentage points can make a major economic difference in operating costs.

This article presents a preliminary analysis, showing how much extra propulsion system weight can be justified by a given increase in efficiency. Our simulation model, which consists of takeoff, climb, cruise, descent, and landing modules, was developed at the NASA Glenn Research Center using specifications and characteristics obtained from aircraft and engine manufacturers, Internet Web sites, and other published sources. For a comparative study, we assumed that



Top: Turbine-drive system. Bottom: Fuel-cell-powered electric motor drive system. JP, jet fuel; P_{fc} , input power of fuel cell; P_{mot} , input power of motor; P_p , shaft drive power; P_{pe} , input power of power electronics; P_{te} , input power of turbine engine; \dot{W}_{fc} , fuel flow rate for fuel cell; \dot{W}_{te} , fuel flow rate for turbine engine; η_{fc} , efficiency of fuel cell; η_{mot} , efficiency of motor; η_{pe} , efficiency of power electronics; η_{te} , efficiency of turbine engine.



Total aircraft weight as a function of time for the two systems from takeoff to landing during a 15-hr flight.

both powerplants were fueled by liquid hydrogen (LH_2), and the Boeing 747-400 airframe with four GE CF6-80C2 engines (GE Aircraft Engines) and their characteristics were used for both systems, except that the fuselage volume change associated with most hydrogen-fueled systems was neglected.

The top figure shows a turbine-drive system and a fuel-cell-powered electric motor drive system. The turbine engine system directly drives the propulsor, whereas the electric motor requires fuel cells and power electronics. We first characterized each component by simple specific-power coefficients (horsepower per pound) based on the literature survey and then calculated fuel flow

rate using the combustion specific energy of LH_2 for the same power to the propulsor from the two systems.

The bottom figure shows the simulation results for total aircraft weight as a function of time for the two systems from takeoff to landing during a 15-hr flight. Notice that the fuel cell aircraft takes off lighter (less fuel load) but lands heavier (heavier powerplant).

This analysis can be applied to other candidate systems to drive the propulsor, as long as each component can be approximately characterized by a simple specific power coefficient and a power efficiency from input to output. This work was supported by the Alternate Fuel Propulsion System Tech Development program.

Glenn contacts:

Dr. Benjamin B. Choi, 216-433-6040, Benjamin.B.Choi@nasa.gov; and Dr. Gerald V. Brown, 216-433-6047, Gerald.V.Brown@nasa.gov

Authors:

Dr. Benjamin B. Choi and Dr. Gerald V. Brown

Headquarters program office:

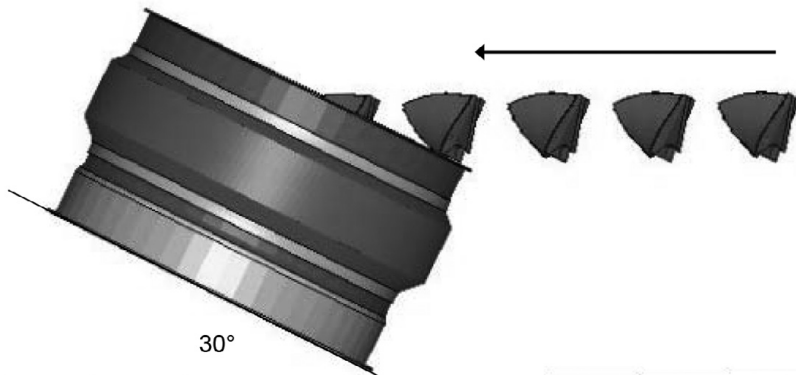
Aeronautics Research

Programs/Projects:

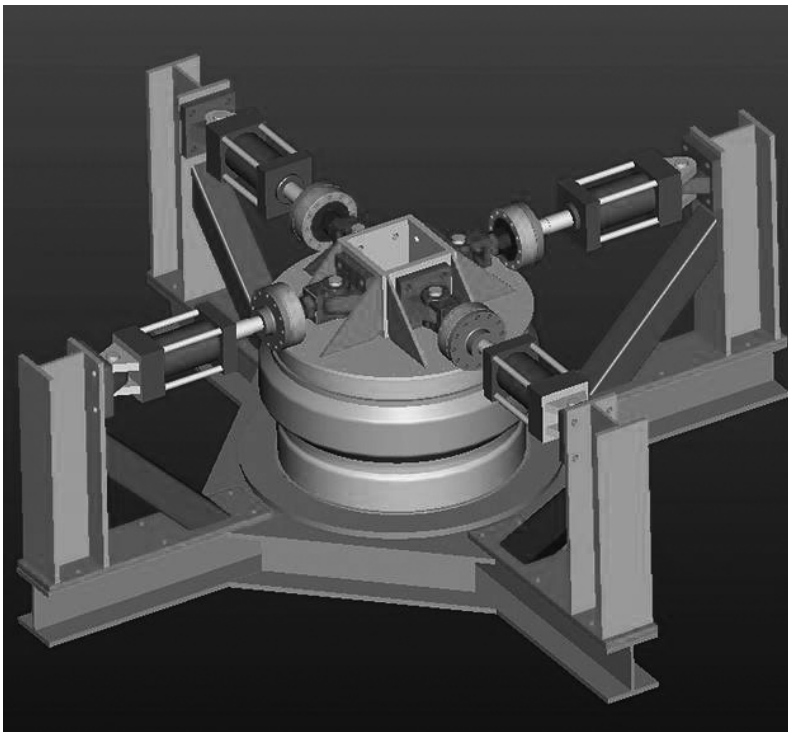
Alternate Fuel Propulsion System Tech Development Program

Damage-Tolerant, Affordable Composite Engine Cases Designed and Fabricated

An integrated team of NASA personnel, Government contractors, industry partners, and university staff have developed an innovative new technology for commercial fan cases that will substantially influence the safety and efficiency of future turbine engines. This effective team, under the direction of the NASA Glenn Research Center and with the support of the Federal Aviation Administration, has matured a new class of carbon/polymer composites and demonstrated a 30- to 50-percent improvement in specific containment



Ballistic impact test configuration for full-scale composite case determined by computer simulation. Blade angle, impact location, and case inclination angle were selected to simulate blade dynamics in an engine blade-out test.



Test cell for postimpact damage tolerance testing of engine fan cases and a production-quality metal/softwall case provided by an engine company.

capacity (blade fragment kinetic energy/containment system weight). As the heaviest engine component, the engine case/containment system greatly affects both the safety and efficiency of aircraft engines. The ballistic impact research team has developed unique test facilities and methods for screening numerous candidate material systems to replace the traditional heavy, metallic engine cases. This research has culminated in the selection of a polymer matrix composite reinforced with triaxially braided carbon fibers and technology demonstration through the fabrication of prototype engine cases for three major commercial engine manufacturing companies.

Affordable composite fan cases have been designed and fabricated for both hardwall and softwall containment strategies through sustained NASA Aviation Safety Program investment, leveraged Space Act Agreements and Small Business Innovation Research, and committed partnerships. In the hardwall design, the fan case must be thick enough to prevent penetration of blade fragments. In the softwall design, the inner layer of the fan case is penetrated and the blade fragments are caught by a layer of high-strength fabric, such as Kevlar (DuPont). In both designs, the engine case must maintain structural integrity after impact and withstand the rigorous loads imposed by an out-of-balance rotor. Sub-component-level tests of the prototype engine cases are planned by Glenn and the engine companies to assess both the impact response and the postimpact structural integrity. Evaluations are currently underway for side-by-side comparisons of full-scale prototype composite containment systems to conventional containment systems of existing engine products contributed

by General Electric, Honeywell, and Williams International. Company projections show weight reductions of up to 50 percent with comparable or lower manufacturing costs.

The research at Glenn has been a multidisciplinary effort with personnel from Glenn's Structural Mechanics and Dynamics, Polymers, Structural Analysis, Life Prediction, and Advanced Metallics branches. Other key partners in this program are General Electric, Honeywell, Williams International, A&P Technology, North Coast Tool & Machine, North Coast Composites, Cincinnati Testing Laboratory, the Ohio State University, the University of Akron, Ohio Aerospace Institute, and the Federal Aviation Administration. This research was part of the Jet Engine Containment Concepts and Blade-Out Simulation Team recognized with a 2004 NASA Turning Goals Into Reality Award.

Glenn contacts:

Dale A. Hopkins, 216-433-3260, Dale.A.Hopkins@nasa.gov; and
Dr. Gary D. Roberts, 216-433-3244, Gary.D.Roberts@nasa.gov

Authors:

Dale A. Hopkins, Dr. Gary D. Roberts,
Dr. J. Michael Pereira, and
Dr. Cheryl L. Bowman

Headquarters program office:

OAT

Programs/Projects:

Aerospace Propulsion & Power R&T
Base, Ultra Safe, AvSSP (Single Air-
craft Accident Prevention, Propulsion
System Safety Technologies), UEET

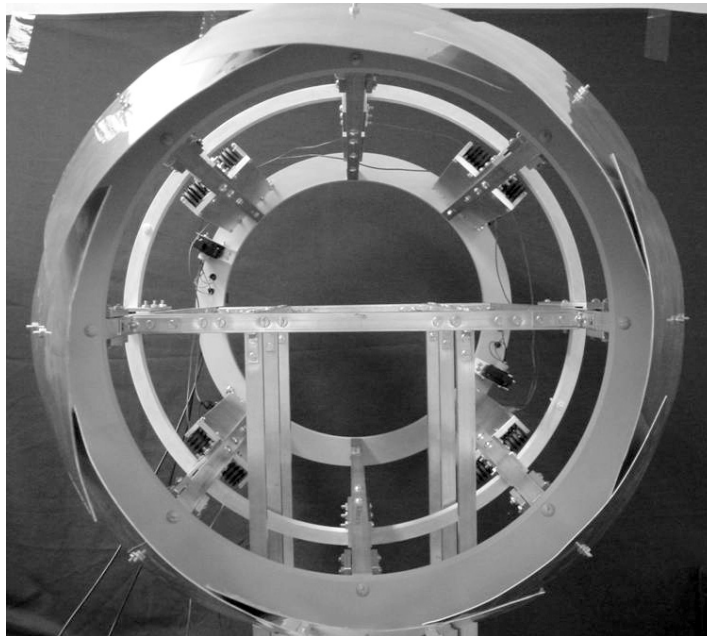
Special recognition:

Turning Goals Into Reality Award 2004

Prototype Variable-Area Exhaust Nozzle Designed

Ongoing research in NASA Glenn Research Center's Structural Mechanics and Dynamics Branch to develop smart materials technologies for adaptive aeropropulsion components has resulted in the design of a prototype variable-area exhaust nozzle (see the photograph to the right). The novel design exploits the potential of smart materials to improve the performance of existing fixed-area exhaust nozzles by introducing new capabilities for adaptive shape control, vibration damping, and flow manipulation. The design utilizes two different smart materials: shape memory alloy wires as actuators and magnetorheological fluids as damper locks.

The prototype of the variable-area exhaust nozzle consists of an assembly of eight overlapping leaves, four shape-memory-alloy wire actuators, and four magnetorheological fluid damper locks. Electrical heating is used to actuate the shape-memory-alloy wires from the fully open position shown in the photograph to the right to the 40-percent reduced-area position depicted in the photograph on the next page. The magnetorheological damper locks are subsequently used to hold the



Prototype of a variable-area exhaust nozzle utilizing shape-memory-alloy wire actuators and magnetorheological fluid damper locks in a fully open configuration.

exhaust nozzle in the reduced-area configuration. Constant-force springs return the shape-memory-alloy wires to their original length once the electrical heating is removed. A computerized data acquisition and real-time control system has been implemented using a sliding-mode-based robust controller to operate the system.

This design represents a novel approach to using adaptive shape-control research to achieve performance benefits from smart materials. This research was conducted under a grant by the University of Houston in collaboration with Glenn researchers and was supported by the Ultra-Efficient Engine Technology (UEET) Project.

Glenn contact:

Dr. Ho-Jun Lee, 216-433-3316,
Ho-Jun.Lee-1@nasa.gov

Authors:

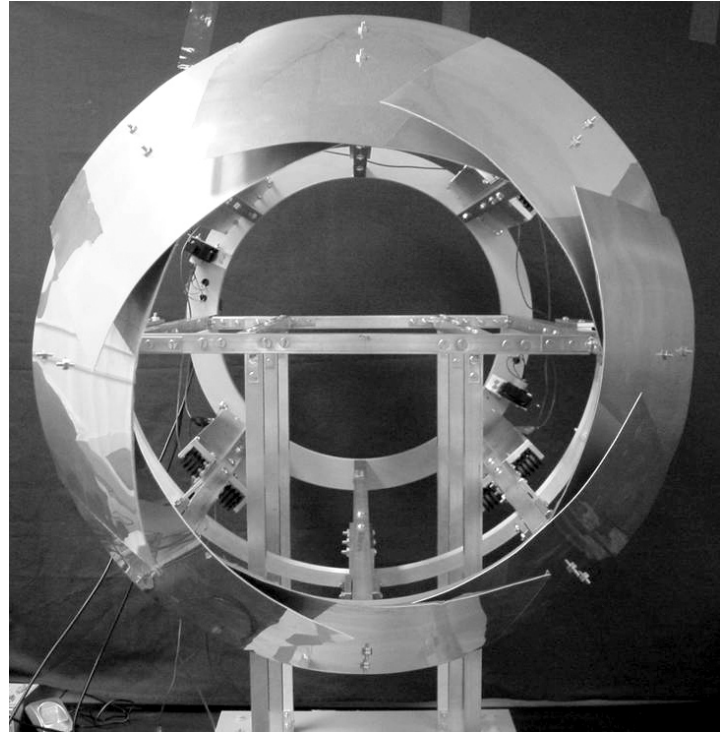
Dr. Ho-Jun Lee and Prof. Gangbing Song

Headquarters program office:

OAT

Programs/Projects:

UEET



Reduced-area configuration of the variable-area exhaust nozzle after the shape-memory-alloy wires are electrically heated.

Switched-Reluctance Cryogenic Motor Tested and Upgraded

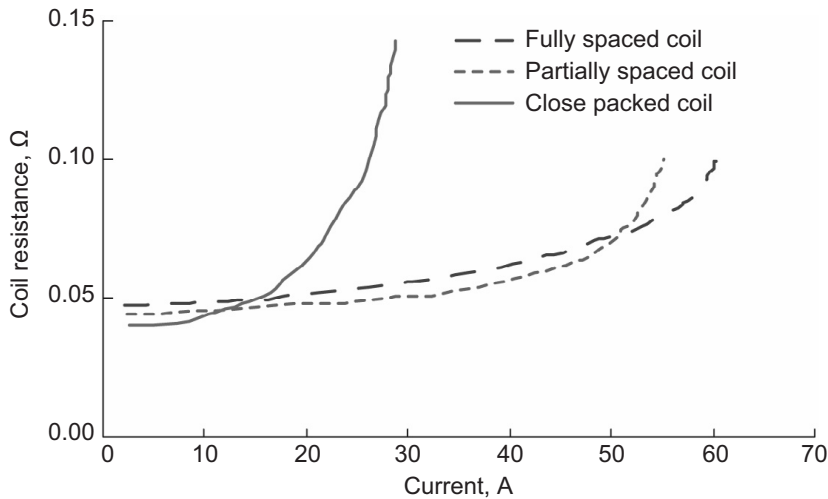
Pollution-free flight is one of NASA's goals for the 21st century. One method of approaching that goal is to use hydrogen-fueled aircraft that use fuel cells or turbogenerators to produce electric power to drive electric motors that turn the aircraft's propulsive fans or propellers. Hydrogen fuel would likely be carried as a liquid, stored in tanks at hydrogen's boiling point of 20.5 K (-422.5 °F). The liquid hydrogen could provide essentially free refrigeration to cool electric motor windings before being used as fuel. Either superconductivity or the low resistance of pure copper or aluminum in liquid hydrogen could be applied to greatly increase electric current density and motor power density.

At the NASA Glenn Research Center, a testbed motor with copper windings was operated in liquid nitrogen at current densities and torque densities that would not be possible at room temperature. Coil current capacity measurements and locked-rotor torque measurements were made to guide planned upgrades in coil geometry and power electronics and to validate analysis methods that can be extended to liquid-hydrogen-cooled motors.

In early operation (ref. 1), the motor produced 10.6 kW (14.2 hp) in liquid nitrogen. In the first phase of upgrading, we doubled the drive voltage per pole in the motor by splitting each coil in half and driving each half with the same type of power amplifier that had been used for the whole coil. Because the phases (and even "half phases") in a switched reluctance motor operate virtually independently of each other, we could excite the windings on just one pole pair and then project the measured results to full-motor performance by multiplying the torque and power produced by 6. This yielded a projected power of 15.0 kW (20.1 hp).

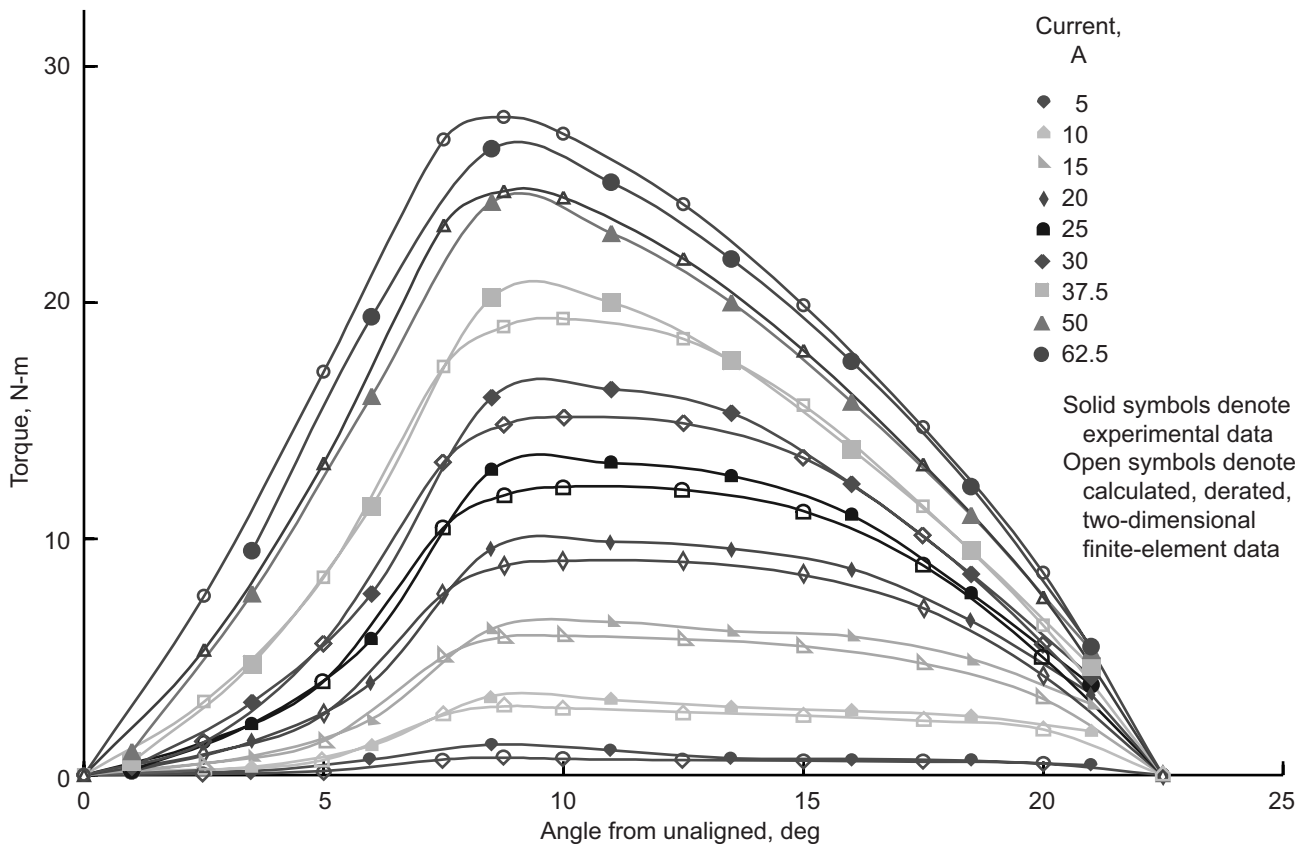
The current-carrying capacities of three types of coils installed in the switched-reluctance motor were measured. The close-packed coil had no spacing between the layers of wire on the coil end turns. The partially spaced coil had no gap between the two inner layers but spaces between the other layers, and the fully spaced coil had gaps between each pair of layers of wire. The

coil resistance in the motor in liquid nitrogen as a function of current is shown in the top graph. The close-packed coil can carry less than 30 A, whereas the two coils that have spacing on the end turns can carry more than 53 A each. The current density corresponding to the latter current is 5300 A/cm².



Coil resistance in switched-reluctance motor in liquid nitrogen versus current for three types of coils.

Locked rotor torque measurements were made as a function of rotor position and of current up to 62.5 A in liquid nitrogen and compared with torques from a two-dimensional finite-element calculation. The results are shown in the top graph, where the finite element torques were multiplied by a derating factor of 89 percent. The factor, selected to produce a reasonable fit between experiment and calculation over the range of the angular and current variables, is needed to correct for axial fringing, which the



Comparison of 11-percent derated two-dimensional finite-element and experimental torques as a function of current and angle.

two-dimensional finite-element method cannot calculate. The current capacity and torque measurements indicate that substantial improvements in motor power density should be possible with appropriate improvements in coil geometry and power conditioning.

Reference

1. Brown, Gerald V.: Cryogenic Electric Motor Tested. Research & Technology 2003, NASA/TM—2004-212729, 2004, pp. 162–163. <http://www.grc.nasa.gov/WWW/RT/2003/5000/5930brown.html>

Glenn contact:

Dr. Gerald V. Brown, 216–433–6047, Gerald.V.Brown@nasa.gov

University of Toledo contact:
Mark W. Siebert, 216–433–6012,
Mark.W.Siebert@grc.nasa.gov

Authors:

Dr. Gerald V. Brown and
Mark W. Siebert

Headquarters program office:

OAT

Programs/Projects:

Propulsion and Power, VSP, RAC, AEFT

Analytical Micromechanics Modeling Technique Developed for Ceramic Matrix Composites Analysis

Ceramic matrix composites (CMCs) promise many advantages for next-generation aerospace propulsion systems. Specifically, carbon-reinforced silicon carbide (C/SiC) CMCs enable higher operational temperatures and provide potential component weight savings by virtue of their high specific strength. These attributes may provide system-wide benefits. Higher operating temperatures lessen or eliminate the need for cooling, thereby reducing both fuel consumption and the complex hardware and plumbing required for heat management. This, in turn, lowers system weight, size, and complexity, while improving efficiency, reliability, and service life, resulting in overall lower operating costs (refs. 1 and 2).

However, the fiber architectures of C/SiC CMCs are more complex because of the weaving, braiding, and knitting of fiber yarns over tape laminates. Thus, along with the development of fabrication processes and test methodologies, the development of analytical models to predict the mechanical properties and strength of textile composites is of increasing importance.

The micromechanics computer program for textile composites (MicroTex) analysis was developed at the NASA Glenn Research Center to provide a user-friendly tool for analyzing a wide variety of multilayered, oriented, fabric-reinforced woven and braided composites and laminated composites. Improved from a prior code (TEXCAD, refs. 3 and 4), MicroTex can calculate overall thermal and mechanical properties and make engineering estimates of damage progression and strength. This code discretely models the yarn centerline paths within the textile repeating unit cell by assuming sinusoidal

undulations at yarn cross-over points, and it uses a yarn discretization scheme (which subdivides each yarn into smaller, piecewise straight yarn slices) together with either a three-dimensional strain-averaging procedure or a thin composite plate theory to calculate overall thermal and mechanical properties, stress distributions, and layer average strains (refs. 3 and 4).

For the failure analysis, the textile composite failure is defined as the loss of the loading capability of the repeating unit cell, which depends on the stiffness reduction due to material slice failure and nonlinear material properties. Two models, a fracture model and a continuum model, are employed for the failure analysis of material slices (matrix and yarn slices). In addition to the maximum strain and maximum stress criteria of TEXCAD (ref. 5), a statistical criterion

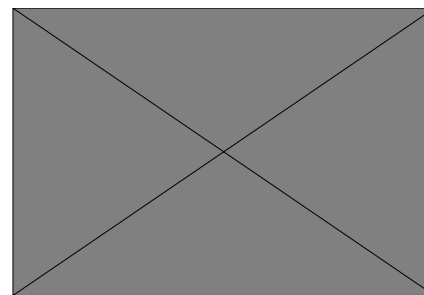
based on the shear-lag model, fracture mechanics, and statistical principles is used to predict the tensile failure of yarn slices (ref. 6). Although the technique is applicable to any kind of composite material, it is particularly focused on CMCs in this article. A fatigue analysis modeling capability was also incorporated into this computer program to predict the fatigue life of the structural components on the basis of the overall stiffness reduction and the material (matrix and yarn) strengths decreasing with cyclic loads.

An experimental investigation was performed to determine the fatigue and static behavior of fiber architectures of $[0^\circ/90^\circ]$ two-dimensional-layup C/SiC CMC specimens and to verify the analytical models through experiments. The specimens were loaded in static tension and in tension-tension fatigue under isothermal fixed-frequency conditions. Two temperature levels and a range of stress levels for fatigue were used to assess performance. The tests were conducted at 23 and 1000 °C. Modulus and cycles to failure were measured several times during the test.

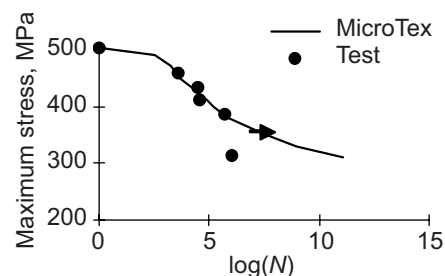
The graphs present the methodologies and capabilities of the computer program by giving sample problems with comparisons to experimental data. This work was supported by the Ultra-Efficient Engine Technology (UEET) Project.

References

1. Herbell, T.P.; Eckel, A.J.; and Brockmeyer, J.W.: Composites in High Speed Turbines for Rocket Engines. High Temperature High Performance Materials for Rocket Engines and Space Applications, Kamleshwar Upadhaya, ed., The Mineral, Metals, and Materials Society, Warrendale, PA, 1994, pp. 13–20.
2. Brockmeyer, Jerry W.: Fiber-Reinforced Ceramic Matrix Composites for Earth-to-Orbit Rocket Engine Turbines; Final Report, NASA CR–198526, 1996. Available from NASA Center for Aerospace Information.
3. Naik, Rajiv A.: TEXCAD—Textile Composite Analysis for Design. Version 1.0: User's Manual; Final Report. NASA CR–4639, 1994.
4. Naik, Rajiv A.: Analysis of Woven and Braided Fabric Reinforced Composites. NASA CR–194930, 1994.
5. Naik, Rajiv A.: Failure Analysis of Woven and Braided Fabric Reinforced Composites. NASA CR–194981, 1994.
6. Min, J.; Shi, Y.; and Card, M.: Progressive Failure Analysis Modeling Techniques for Ceramic Matrix Textile Composites. AIAA–2002–1400, 2002.



Stiffness reduction for $[0^\circ/90^\circ]$ plain weave for maximum stress at 410.60 MPa.



S–N curve for $[0^\circ/90^\circ]$ C/SiC plain-weave composite.

Glenn contact:

Dr. James B. Min, 216–433–2587,
James.B.Min@nasa.gov

Author:

Dr. James B. Min

Headquarters program office:

OAT

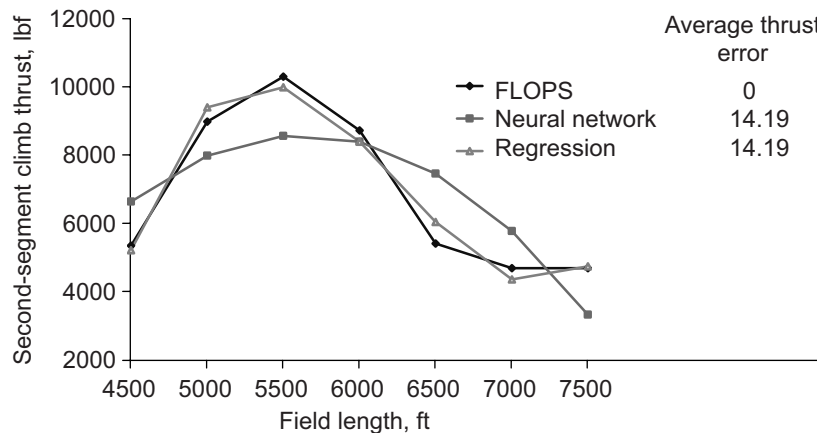
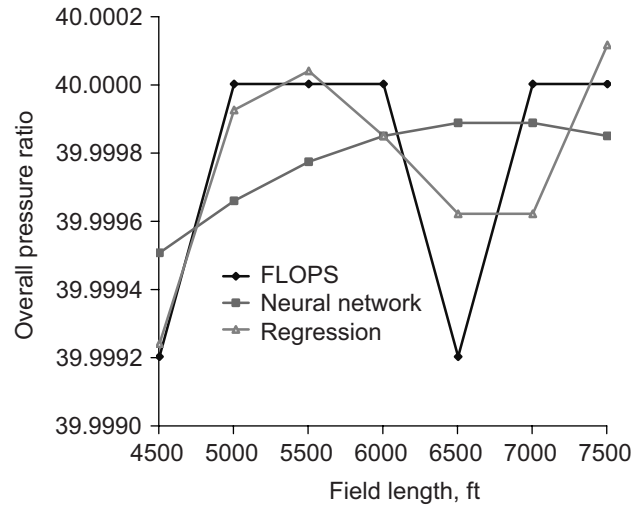
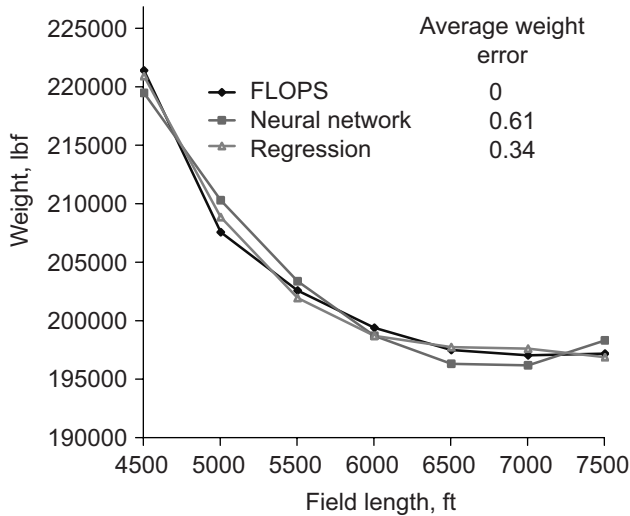
Programs/Projects:

UEET

Design Sensitivity for a Subsonic Aircraft Predicted by Neural Network and Regression Models

A preliminary methodology was obtained for the design optimization of a subsonic aircraft by coupling NASA Langley Research Center's Flight Optimization System (FLOPS) with NASA Glenn Research Center's design optimization testbed (COMETBOARDS with regression and neural network analysis approximators). The aircraft modeled can carry 200 passengers at a cruise speed of Mach 0.85 over a range of 2500 n mi and can operate on standard

6000-ft takeoff and landing runways. The design simulation was extended to evaluate the optimal airframe and engine parameters for the subsonic aircraft to operate on nonstandard runways. Regression and neural



Top left: Gross aircraft weight in pounds force. Top right: Overall pressure ratio. Average error, 0. Scale magnified. Bottom: Second-segment climb thrust.

network approximators were used to examine aircraft operation on runways ranging in length from 4500 to 7500 ft.

The graphs depict typical solutions: aircraft weight versus the field length (top left), overall pressure ratio (top right), and second-segment climb thrust (bottom). Optimum aircraft weight increased for the shorter field length and decreased for the longer length, as expected. The overall pressure ratio exhibited a discontinuity at a field length of 6500 ft. The neural network model negotiated the discontinuity by following a mean path (top right graph). The regression approximation had a tendency to hug the data. The behavior of the second-segment climb thrust (bottom graph), is similar to that of the overall pressure ratio. The error in the neural network and regression models was in the range of 1 to 5 percent. The time needed to generate one set of optimum solutions was about 1/2 hr when the FLOPS code was used. It was reduced to about 1 min with the neural network method and to 1 sec with the regression method. The performance of the neural network and regression methods is considered satisfactory for the design sensitivity of the subsonic aircraft.

Bibliography

Patnaik, S.N., et al.: A Subsonic Aircraft Design Optimization With Neural Network and Regression Approximators. NASA/TM—2004-213059 (AIAA–2004–4606), 2004. <http://gltrs.grc.nasa.gov/cgi-bin/GLTRS/browse.pl?2004/TM-2004-213059.html>

Glenn contact:

Dale A. Hopkins, 216–433–3260,
Dale.A.Hopkins@nasa.gov

Authors:

Dr. Surya N. Patnaik and Dale A. Hopkins

Headquarters program office:

OAT

Programs/Projects:

Ultra Safe, UEET, HSR

Advanced Vibration Analysis Tool Developed for Robust Engine Rotor Designs

The primary objective of this research program is to develop vibration analysis tools, design tools, and design strategies to significantly improve the safety and robustness of turbine engine rotors. Bladed disks in turbine engines always feature small, random blade-to-blade differences, or mistuning. Mistuning can lead to a dramatic increase in blade forced-response amplitudes and stresses. Ultimately, this results in high-cycle fatigue, which is a major safety and cost concern. In this research program, the necessary steps will be taken to transform a state-of-the-art vibration analysis tool, the Turbo-Reduce forced-response prediction code, into an effective design tool by enhancing and extending the underlying modeling and analysis methods. Furthermore, novel techniques will be developed to assess the safety of a given design. In particular, a procedure will be established for using natural-frequency curve veerings to identify ranges of operating conditions (rotational speeds and engine orders) in which there is a great risk that the rotor blades will suffer high stresses. This work also will aid statistical studies of the forced response by reducing the necessary number of simulations. Finally, new strategies for improving the design of rotors will be pursued.

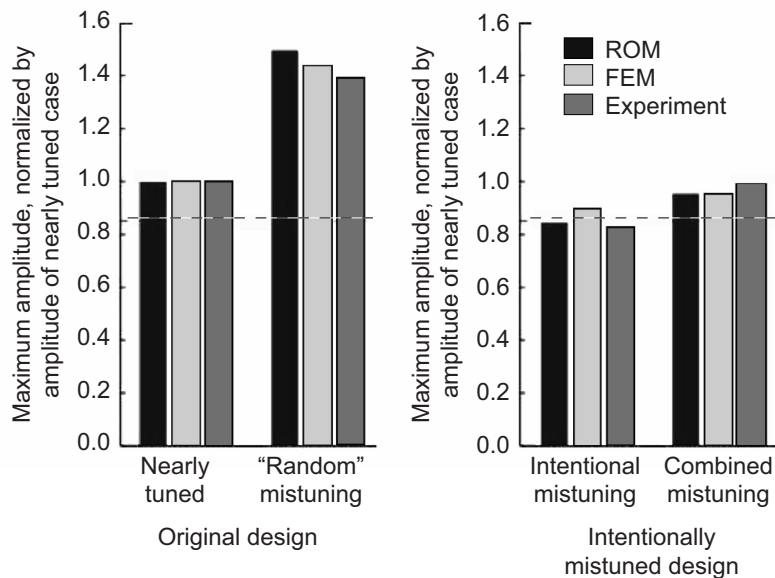
Several methods have been investigated, including the use of intentional mistuning patterns to mitigate the harmful effects of random mistuning, and the modification of disk stiffness to avoid reaching critical values of interblade coupling in the desired operating range. In the short term, the computational tools, analysis methods, and design assessment techniques will allow engineers to evaluate and improve rotor designs in the early design stages. In the long term, the new design strategies will help pave the way for eliminating high-cycle fatigue in turbine engines.

Research activities for this project have focused on the following three areas:

- (1) Development of methods for analyzing curve veerings and identifying critical regions in a natural-frequency versus engine-order map
- (2) Investigation of strategies for intentional mistuning pattern selection, with an emphasis on efficiently reducing the design space
- (3) Approximation of mistuned amplitude bounds and estimation of blade stress increases due to mistuning.

The research projects described here were performed under a NASA Glenn Research Center grant by University of Michigan researchers in collaboration with Glenn researchers. Details are given in references 1 to 4. This work was supported by the Ultra-Efficient Engine Technology (UEET) Project.

Two different blade types



Experimental study validated finite-element model and reduced-order model predictions for a test case.

References

1. Castanier, Mathew P.; and Pierre, Christophe: Using Intentional Mistuning in the Design of Turbomachinery Rotors. *AIAA J.*, vol. 40, no. 10, 2002, pp. 2077–2086.
2. Castanier, M.P.; Pierre, C.; and Bladh, R.: Investigation Into Using Tuned Free Response Information to Predict Mistuned Forced Response of Bladed Disks. Proceedings of the 7th National Turbine Engine High Cycle Fatigue Conference, Palm Beach Gardens, FL, May 2002.
3. Bladh, R.; Castanier, M.P.; and Pierre, C.: Effects of Multistage Coupling and Disk Flexibility on Mistuned Bladed Disk Dynamics. *J. Eng. Gas Turbines Power*, vol. 125, no. 1, 2003, pp. 121–130.
4. Lim, Sang-Ho, et al.: A Compact, Generalized Component Mode Mistuning Representation for Modeling Bladed Disk Vibration. AIAA–2003–1545, 2003.

Glenn contact:

Dr. James B. Min, 216–433–2587,
James.B.Min@nasa.gov

Author:

Dr. James B. Min

Headquarters program office:

OAT

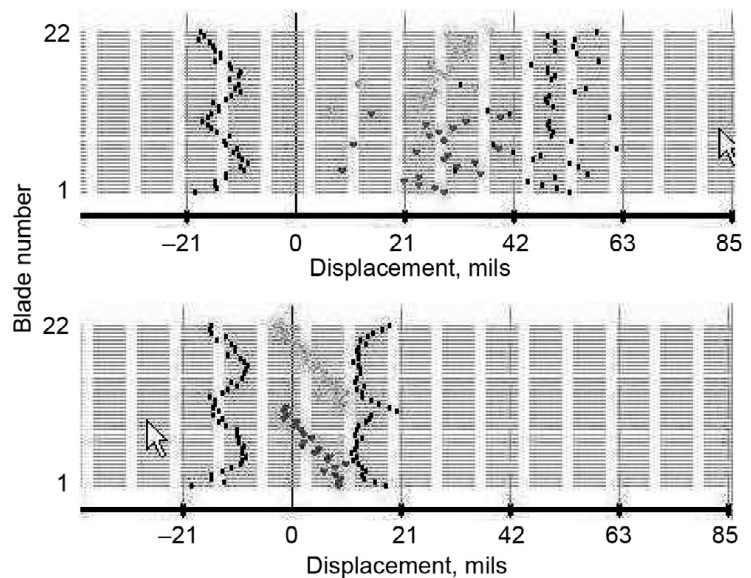
Programs/Projects:

UEET

System Developed for Real-Time Blade-Flutter Monitoring in the Wind Tunnel

Areal-time system has been developed to monitor flutter vibrations in turbomachinery. The system is designed for continuous processing of blade tip timing data at a rate of 10 MB/sec. A USB 2.0 interface provides uninterrupted real-time processing of the data, and the blade-tip arrival times are measured with a 50-MHz oscillator and a 24-bit pipelined architecture counter. The input stage includes a glitch catcher, which reduces the probability of detecting a ghost blade to negligible levels. A graphical user interface provides online interrogation of any blade tip from any light probe sensor. Alternatively, data from all blades and all sensors can be superimposed into a single composite scatter plot displaying the vibration amplitude of each blade.

The graphs illustrate a typical screen display during flutter monitoring. The lower trace was obtained just prior to flutter, and the upper trace was obtained during flutter. There are data



Scatter plot display prior to and during flutter. This figure is shown in color in the online version of this article (<http://www.grc.nasa.gov/WWW/RT/2004/RS/RS18S-kurkov.html>).

from two sensors, green (lightest dots) and red (medium dots). The darkest symbols represent the maximum excursion of each blade since the beginning of recording. There are 22 blades and, consequently, 22 dots for each sensor. Ideally, the dots from each sensor in the lower part should line up on a vertical line; however, because of the slight change in the operating conditions since the reference data were collected, the blades are displayed on a sloping line. The upper flutter plot is clearly distinguishable from the steady-state display. Each blade is instantaneously depicted at a particular point in the nonsynchronous vibration cycle.

Bibliography

Radzikowski, Marc, et al.: Real Time Monitoring Systems for Turbomachinery. ASME Paper GT2004-53992, 2004.

Glenn contact:

Dr. Anatole P. Kurkov, 216-433-5695, Anatole.P.Kurkov@nasa.gov

Authors:

Harbans S. Dhadwal, Mark Radzikowski, Dmitri Strukov, and Dr. Anatole P. Kurkov

Headquarters program office:

OAT

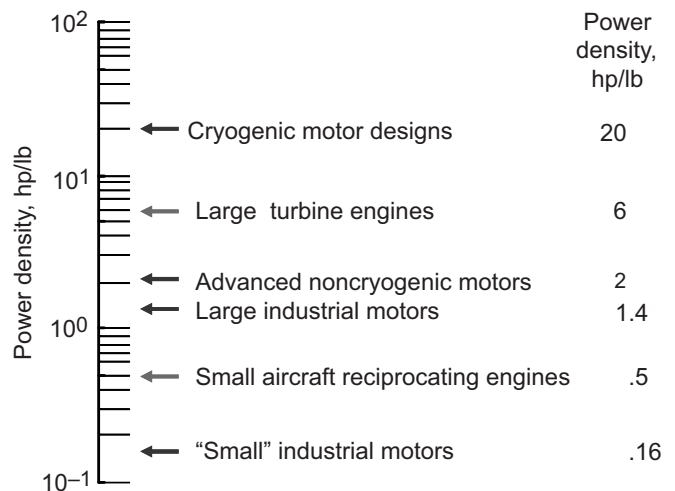
Programs/Projects:

QAT, UEET

Power Requirements Determined for High-Power-Density Electric Motors for Electric Aircraft Propulsion

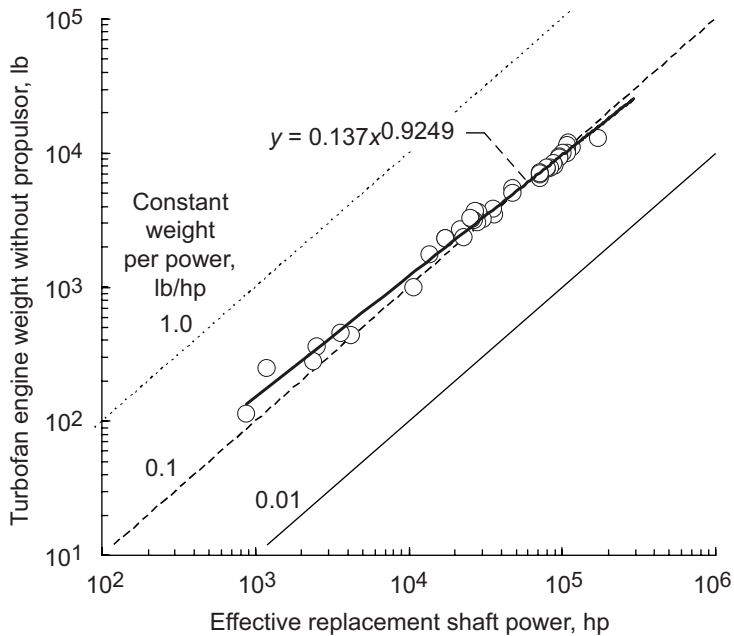
Future advanced aircraft fueled by hydrogen are being developed to use electric drive systems instead of gas turbine engines for propulsion. Current conventional electric motor power densities cannot match those of today’s gas turbine aircraft engines. However, if significant technological advances could be made in high-power-density motor development, the benefits of an electric propulsion system, such as the reduction of harmful emissions, could be realized.

In evaluating the power requirements for replacing gas turbine engines with electric motors, it is important to compare their relative current and potential power densities (see the graph on this page). Comparing a turbofan engine with an electric-motor-driven-fan system requires some decisions on how much power the motor must produce, as well as how much of the turbine engine is actually replaced. This comparison is not a straightforward “apples to apples” comparison, and great attention must be made when converting power and weight variables into equivalent power-density terms. Consequently, researchers at the NASA Glenn Research Center addressed several issues relating to this comparison.



Power-density comparison of engines and motors.

The first issue was that the published weights of turbine engines usually include the propulsor, that is, the propulsive fan and related components,



Turbofan engine weights (without the propulsor weight) as a function of effective replacement shaft power.

such as the fan frame, brackets, supports, exit guide vanes, and containment. These propulsor components would all be required with an electric motor drive. Our first step in making an appropriate comparison of motors and turbofan engines, therefore, is to subtract the propulsor weight from the total weight of a turbofan engine. From some proprietary data we have for actual propulsor weights for large turbofan engines, the average fraction of total engine weight represented by the propulsor components is 30 percent. This factor was used to estimate the propulsor weight for all the midrange engines in our survey, even though the actual propulsor weight would vary with bypass ratio and other variables. Actual values were used for the large engines for which we had data.

A second issue was that the power delivered to the propulsive fan, which a motor would have to supply, is not typically published. Instead, the total turbofan engine thrust T_{tot} (sea-level static takeoff thrust) is published. This total thrust is the sum of the thrust from the fan and the thrust from the jet. From some proprietary data, we derived a typical relation. For engines between 15,000- and 100,000-lb thrust, the power P_{fan} (in horsepower) delivered to the fan through the fan shaft is 1.25 times the total engine static sea-level takeoff thrust in pounds.

The remaining issue was how to deal with the jet thrust of a turbine engine, which does not exist for an electric-motor-driven fan. If an electric motor were

to drive the fan used in a particular turbofan engine (at the same speed and with the same torque), the resulting thrust would be lower than the total thrust of the turbofan engine including its jet. We chose a factor of 0.8 to estimate the fan thrust T_{fan} from the total turbofan engine thrust T_{tot} : that is, $T_{fan} = 0.8 T_{tot}$.

Although this factor would be expected to vary from 0.8 with the bypass ratio and other variables, we used it for all the engines in our survey. Hence, we consider a replacement effective power output of the turbofan engine to be 1.25 times the fan horsepower. This power reasonably represents the power that an electric motor would have to produce to give the same thrust as a turbine engine. This would be accomplished with a somewhat larger fan than for a comparable one used in a turbofan engine.

The resulting replacement power per weight, or power density, requirements for the electric propulsion system is thus obtained (see the graph on this page) when all of the factors above are applied to an engine, or engine class, of interest. This power and weight relationship can be expressed as $weight = 0.137(power)^{0.9249}$.

Glenn contacts:

Dr. Dexter Johnson, 216-433-6046, Dexter.Johnson@nasa.gov; and Dr. Gerald V. Brown, 216-433-6047, Gerald.V.Brown@nasa.gov

Authors:

Dr. Dexter Johnson and Dr. Gerald V. Brown

Headquarters program office:

Aeronautics Mission

Programs/Projects:

VSP, LEAP, RAC

Flutter Stability Verified for the Trailing Edge Blowing Fan

The TURBO-AE aeroelastic code has been used to verify the flutter stability of the trailing edge blowing (TEB) fan, which is a unique technology demonstrator being designed and fabricated at the NASA Glenn Research Center for testing in Glenn's 9- by 15-Foot Low-Speed Wind Tunnel. Air can be blown out of slots near the trailing edges of the TEB fan blades to fill in the wakes downstream of the rotating blades, which reduces the rotor-stator interaction (tone) noise caused by the interaction of wakes with the downstream stators. The TEB fan will demonstrate a 1.6-EPNdB reduction in tone noise through wake filling. Furthermore, the reduced blade-row interaction will decrease the possibility of forced-response vibrations and enable closer spacing of blade rows, thus reducing engine length and weight. The detailed aeroelastic analysis capability of the three-dimensional Navier-Stokes TURBO-AE code was used to check the TEB fan rotor blades for flutter stability. Flutter calculations were first performed with no TEB flow; then select calculations were repeated with TEB flow turned on.

The TEB flow, prescribed as a spanwise variation of flow properties at the trailing edge of the blade, was interpolated onto the TURBO-AE grid. Then, a special-purpose preprocessor was used to convert the flow to source terms. A steady flowfield was computed with TEB flow, using the steady flowfield without TEB flow as the initial guess. A comparison of the flowfields with and without TEB flow showed, as expected, significant differences in the wake region downstream of the trailing edge. With TEB flow, the velocity magnitude was significantly increased in the wake region and the angle of the flow was moderately changed. There was no significant change in either magnitude or flow direction upstream of the trailing edge of the blade.

The blade vibration modeling capability of the TURBO-AE code was used to carry out unsteady flow computations with TEB flow, starting from the steady flowfield calculated as described previously. The aerodynamic damping was calculated when the unsteady flowfield converged to periodicity in time. The graph shows the aerodynamic damping calculated for the two-nodal-diameter pattern bending vibration mode at the takeoff condition. The aerodynamic damping shows a modest increase with TEB flow turned on. The aerodynamic damping is larger than 0.4 percent and shows an increasing trend as the stall line is approached. Thus, for the analyzed takeoff condition and vibration mode, flutter would not be expected. More importantly, the influence of TEB flow on aerodynamic damping and flutter stability was found to be small and stabilizing. Additional flutter calculations need to be carried out to verify that the flutter characteristics are not adversely affected when the TEB flow is turned on for other nodal diameter patterns, vibration modes, and part speed conditions.

The aeroelastic calculations described here were performed under NASA contract NAS3-01116 (issued by NASA Glenn) by Dr. Rakesh Srivastava (University of Toledo) in collaboration with Glenn researchers. This work was supported by the Quiet Aircraft Technology (QAT) Project.

Glenn contact:

Dr. Milind A. Bakhle, 216-433-6037,
Milind.A.Bakhle@nasa.gov

Authors:

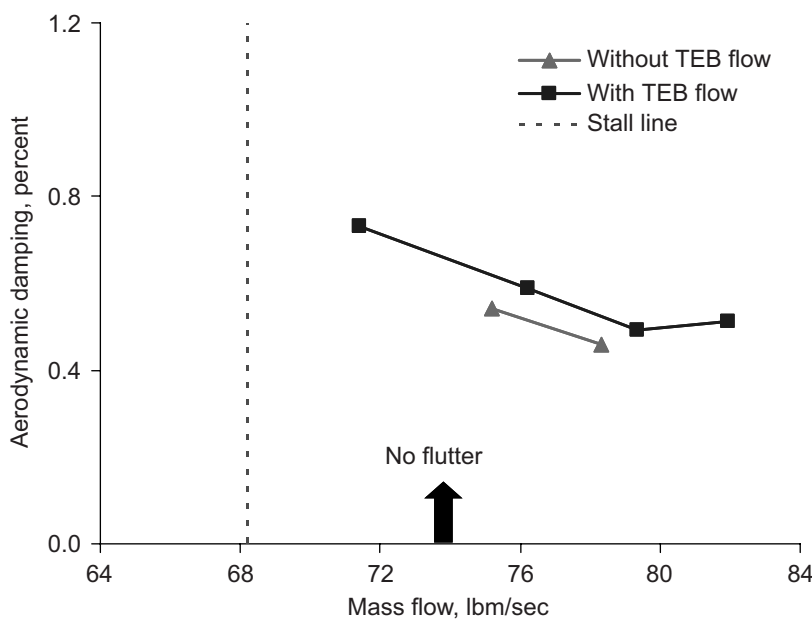
Dr. Milind A. Bakhle and
Dr. Rakesh Srivastava

Headquarters program office:

OAT

Programs/Projects:

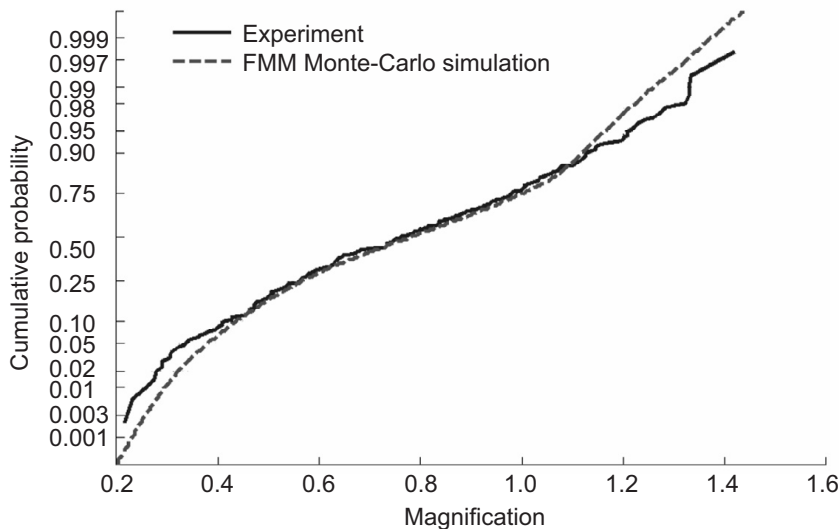
QAT



Aerodynamic damping for the trailing edge blowing (TEB) fan calculated with the TURBO-AE aeroelastic analysis code.

Fundamental Mistuning Model for Probabilistic Analysis Studied Experimentally

The Fundamental Mistuning Model (FMM) is a reduced-order model for efficiently calculating the forced response of a mistuned bladed disk. FMM ID is a companion program that determines the mistuning in a particular rotor. Together, these methods provide a way to acquire mistuning data in a population of bladed disks and then simulate the forced response of the fleet.



Comparison between the cumulative distribution function of simulated blade amplitudes and laboratory measurements.

This process was tested experimentally at the NASA Glenn Research Center, and the simulated results were compared with laboratory measurements of a "fleet" of test rotors. The method was shown to work quite well. It was found that the accuracy of the results depends on two factors: (1) the quality of the statistical model used to characterize mistuning and (2) how sensitive the system is to errors in the statistical modeling.

Glenn contact:

Dr. Shantaram S. Pai, 216-433-3255,
Shantaram.S.Pai@nasa.gov

Carnegie Mellon University contact:

Dr. Jerry H. Griffin, 412-268-3860,
jg9h@andreqw.cmu.edu

Author:

Dr. Jerry H. Griffin

Headquarters program office:

OAT

Programs/Projects:

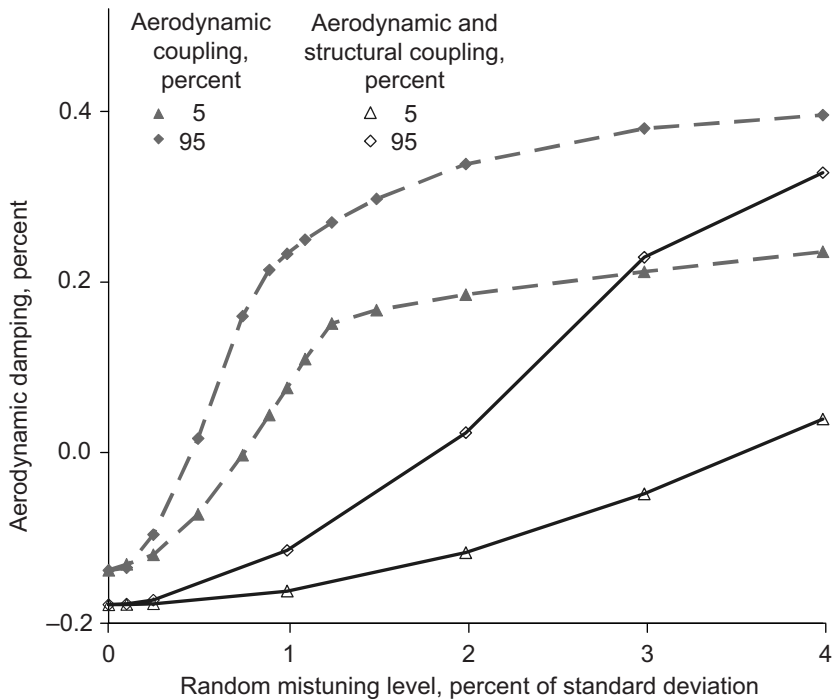
Ultra Safe, UEET

NESTEM Probabilistic Analysis Used to Study Mistuned Bladed Disks and Blisks With Aerodynamic and Structural Coupling

This document summarizes the initial results from a research effort at the NASA Glenn Research Center on blisk and bladed disk mistuning, including both structural and aerodynamic coupling. The structural coupling model is based on the Fundamental Mistuning Model (FMM, developed by Feiner and Griffin). This effort extends the FMM technique to accept aerodynamic coupling coefficients from computational fluid dynamic codes. The model was applied to a representative modern front compressor stage. Flutter stability and forced response were determined with structural coupling only, with aerodynamic coupling only, and with both structural and aerodynamic coupling.

Tuned, randomly mistuned, and near alternately mistuned rotors were considered.

The results show that, although structural coupling does not affect the stability of a tuned system significantly, it plays a key role in the stability of the mistuned system.



Effect of random mistuning on flutter.

In the test case considered, the beneficial effect of mistuning on flutter stability was greatly inhibited by the addition of structural coupling. The graph presents Monte-Carlo simulation results of a randomly mistuned bladed disk. The system is unstable in the tuned state. The figure shows the 5th and 95th percentile aerodynamic damping values as a function of the standard deviation in blade frequency. As is well known, mistuning is

stabilizing. However, the mistuning level required to stabilize the system with structural and aerodynamic coupling is approximately 4 times larger than when aerodynamic coupling is used alone. In addition, the mode shapes were found to differ significantly. For the forced-response case, the inclusion of aerodynamic coupling had a relatively small effect on the global and local response levels. Additional studies are needed to generalize these conclusions for other blade types and cases. In addition, future studies are planned to develop a model that considers multiple, interacting families of modes. This work was performed under NASA Grant NAG3-2928.

Glenn contact:

Dr. Shantaram S. Pai, 216-433-3255, Shantaram.S.Pai@nasa.gov

Duke University contact:

Dr. Robert E. Kielb, 919-660-5327, rkielb@duke.edu

Author:

Dr. Robert E. Kielb

Headquarters program office:

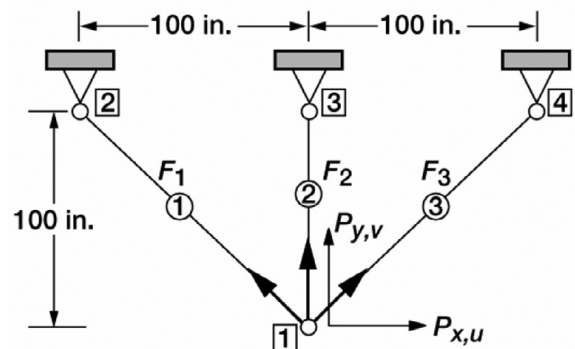
OAT

Programs/Projects:

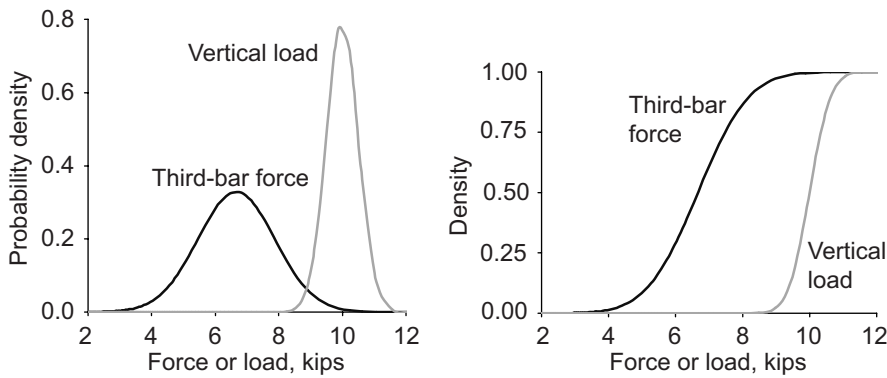
Base R&T

Primal and Dual Integrated Force Methods Used for Stochastic Analysis

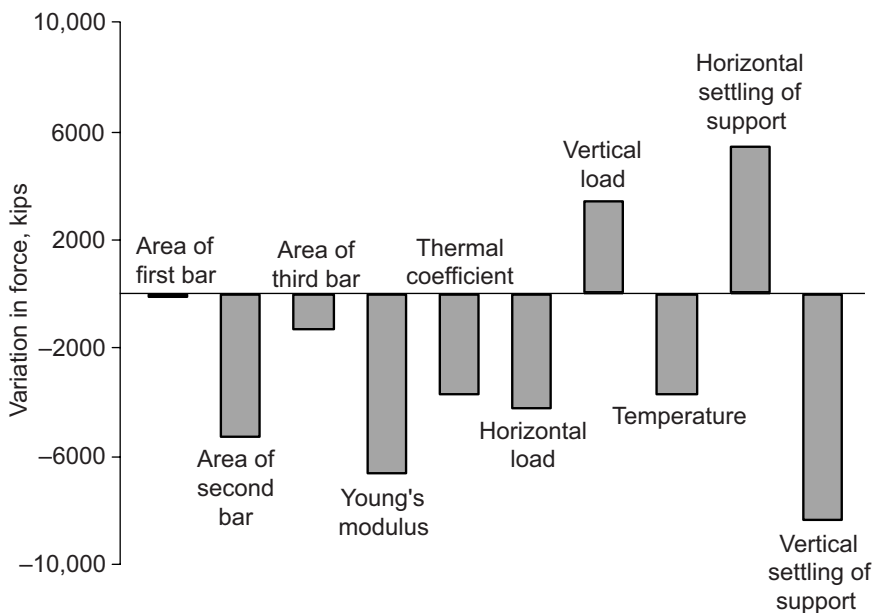
At the NASA Glenn Research Center, the primal and dual integrated force methods are being extended for the stochastic analysis of structures. The stochastic simulation can be used to quantify the consequence of scatter in stress and displacement response because of a specified variation in input parameters such as load (mechanical, thermal, and support settling loads), material properties (strength, modulus, density, etc.), and sizing design variables (depth, thickness, etc.). All the parameters are modeled as random variables with given probability distributions, means, and covariances. The stochastic response is formulated through a quadratic perturbation theory, and it is verified through a Monte Carlo simulation.



Three-bar truss.



Left: Probability distribution function for the third bar force. Right: Cumulative distribution function for the third bar force.



Sensitivities for the third-bar force.

The figure on the preceding page illustrates the stochastic response analysis for a three-bar truss subjected to mechanical, thermal, and support settling loads. The probability and cumulative distribution functions are shown in the left and right graphs, respectively, for the third bar force. The bar force has a much wider variation than the mechanical load. The bar chart shows the sensitivity of the third bar force for a set of 10 primitive variables: three bar areas, the Young's modulus, the coefficient of expansion, two-component mechanical load, temperature variation, and two-component support settling. The sensitivity of the bar force with respect to the Young's modulus is significant because of the presence of temperature and support settling loads. The bar force is most sensitive to the vertical component of support settling.

Glenn contact:

Dr. Shantaram S. Pai, 216-433-3255,
Shantaram.S.Pai@nasa.gov

Ohio Aerospace Institute (OAI) contact:

Dr. Surya N. Patnaik, 216-433-5916,
Surya.N.Patnaik@grc.nasa.gov

Author:

Dr. Surya N. Patnaik

Headquarters program office:

OAT

Programs/Projects:

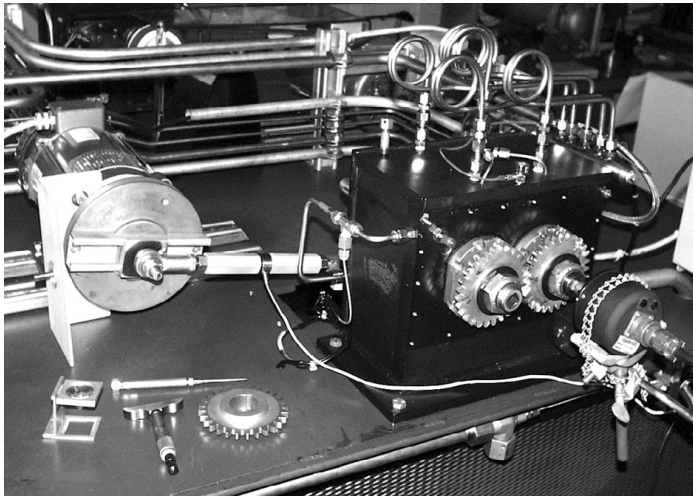
Ultra Safe, UEET

Spur Gear Wear Investigated in Support of Space Shuttle Return-To-Flight Efforts

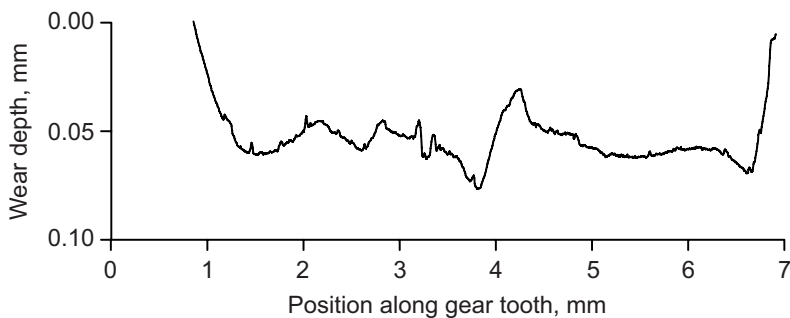
As part of NASA's Return-To-Flight efforts, the Space Operations Program investigated the condition of actuators for the orbiter's rudder speed brake. The actuators control the position of the rudder panels located in the tail of the orbiter, providing both steering control and braking during reentry, approach, and landing. Inspections of flight hardware revealed fretting and wear damage to the critical working surfaces of the actuator gears. To best understand the root cause of the observed damage and to help establish an appropriate reuse

and maintenance plan for these safety critical parts, researchers completed a set of gear wear experiments at the NASA Glenn Research Center.

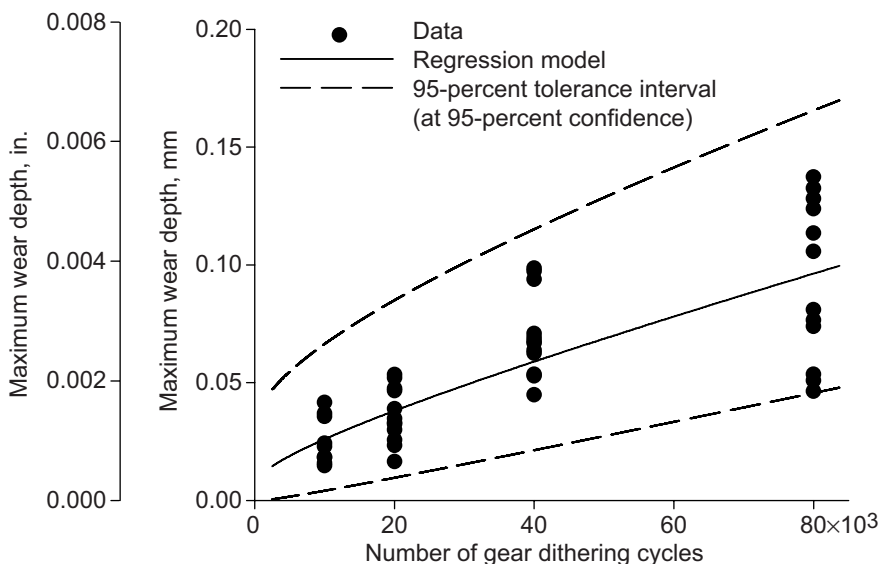
Wear of sufficient magnitude can weaken the strength of a gear tooth,



Glenn's Spur Gear Test Rig setup for gear wear experiments.



Typical gear wear trends and depths for gear tooth positions from low on the tooth (1-mm position) to high along the tooth (7-mm position). The wear shown occurred after 80,000 gear dithering cycles and torque producing a 1.1-GPa (160-ksi) hertzian contact pressure at the pitch-line position on the gear.



Test results for spur gear wear, including regression model and statistically based tolerance interval.

particularly if the hardened surface layer is worn thin. Furthermore, gear tooth wear can accelerate other modes of failure, such as surface pitting fatigue. In addition, wear and pitting debris can be detrimental to the proper operation of bearings within the gearbox. An assessment of technical literature reveals that accurate predictions of gear wear require dedicated laboratory experiments that closely duplicate the gear tooth loads, motions, material, surface topography, and lubrication method for the particular application. A set of gear wear experiments were performed to support the assessment of space shuttle rudder speed-brake gearing. The experiments were completed using Glenn's spur gear test rigs. In the past, these rigs were used to study the performance of high-speed, oil-lubricated gears. The rigs were modified to provide grease lubrication, low-speed operations, and direction reversal (dithering motions), like that which occurs within the orbiter's rudder speed-brake actuators (see the photograph).

Gear wear was measured with high accuracy by employing a stylus profilometer using a specially devised fixture that allowed accurate mounting and orientation of the gear on the measuring machine. In this manner, profile traces of new and worn gear teeth were compared and processed using a computer algorithm to determine wear amounts. A plot of typical wear data (see the top graph) shows how the wear depth varies along the tooth profile. One important measure of the severity of gear wear is the maximum wear depth. The bottom graph summarizes the measured maximum wear depths as a function of gear operating cycles.

The data were modeled to provide intervals to capture the likely range of wear amounts that can be anticipated for a large population of parts operated in identical fashion. The data

show an approximately linear trend for the range of cycles and wear depths investigated, an important finding that will provide confidence in projecting wear rates for gears that are proposed for inspection, assessment, and potential reuse on space shuttle orbiters. This work was completed as part of the NASA Engineering Safety Center's Independent Technical Assessment of Orbiter Rudder Speed Brake Gear Margins.

Find out more about this research:

<http://www.grc.nasa.gov/WWW/5900/5950/>

U.S. Army Research Laboratory, Vehicle Technology Directorate at

Glenn contact:

Dr. Timothy L. Krantz, 216-433-3580, Timothy.L.Krantz@grc.nasa.gov

Glenn contact:

Fred B. Oswald, 216-433-3957,
Fred.B.Oswald@nasa.gov

Authors:

Dr. Timothy L. Krantz and Fred B. Oswald

Headquarters Program Office:

OSF, NESC

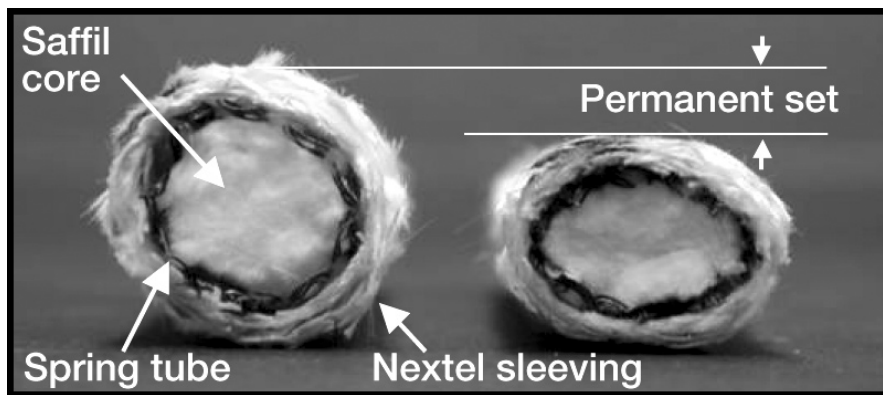
Programs/Projects:

Space Operations, NESC

High-Temperature Knitted Spring Tubes Improved for Structural Seal Applications

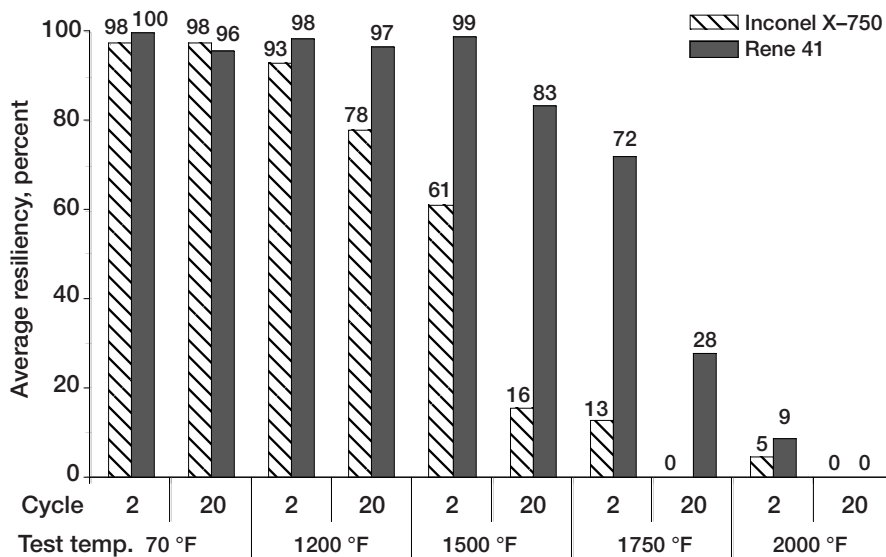
To meet the needs of current and future space vehicles, the NASA Glenn Research Center is developing advanced control surface seals. These seals are used to fill the gaps surrounding actuated structures, such as rudders and body flaps, to shield underlying lower temperature structures, such as mechanical actuators, from the hot gases encountered during atmospheric reentry. During previous testing, the current baseline seal design, which is used on the space shuttle as a thermal barrier and was selected as the rudder-fin seal on the X-38 crew return vehicle, exhibited significant permanent set following compression at 1900 °F (see the following photograph). Decreased resiliency (springback) could prevent the seal from contacting both of the opposing sealing surfaces and allow the ingestion of damaging hot gases during reentry, which could have detrimental effects on vehicle subsystems.

As illustrated in this photograph, the baseline control surface seal comprises three main components. The primary source of resiliency in the seal is an Inconel X-750 (Special Metals Corporation, New Hartford, NY) knitted wire spring tube. The passage of hot gases through the seal is limited by stuffing the spring tube with Saffil batting (Saffil Ltd., Cheshire, UK) and then overbraiding the tube with two layers of Nextel 312 ceramic fabric (3M, St. Paul, MN). The Nextel fabric acts as a thermal barrier, provides a uniform sealing surface, and prevents the loss of Saffil batting through the spring tube walls.

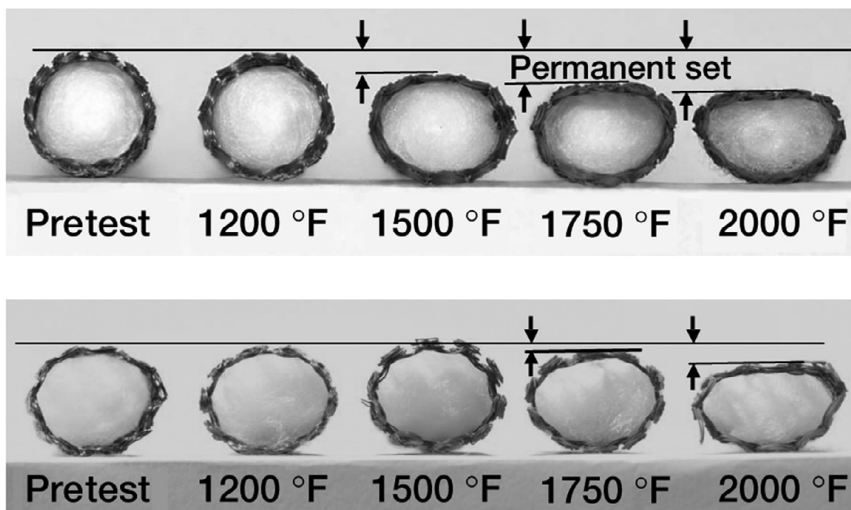


Current baseline control surface seal before (left) and after (right) compression during 1900 °F exposure, showing loss of seal resiliency. Initial seal diameter was approximately 0.62 in.

The loss of resiliency in the current seal design has been attributed to the limited high-temperature strength of the Inconel X-750 spring tube. Hot compression testing at Glenn of the spring tube alone showed significant resiliency degradation at temperatures as low as 1200 °F, which is much lower than the target temperature range of 1800 to 2200 °F for future seal designs. For this reason, the Glenn seals team worked to enhance the performance



Comparison of spring tube resiliency at the start of compression cycles 2 and 20 for heat-treated samples of Inconel X-750 and Rene 41 using the baseline knit geometry at multiple test temperatures.



Post-test photographs showing permanent set in spring tubes at multiple test temperatures after 20 compression cycles (20-percent compression). Top: Heat-treated Inconel X-750. Bottom: Heat-treated Rene 41.

of the baseline control surface seal design by improving the spring tube component. To accomplish this task, a material with high-temperature strength properties superior to Inconel X-750 was required. Following an exhaustive materials database search, Rene 41 (Allvac, Monroe, NC) was selected to replace the Inconel X-750 wire material. Spring tubes were knitted of Rene 41 wire using the baseline spring tube geometry. These samples were then evaluated through a series of cyclic compression tests conducted at multiple temperatures using a state-of-the-art test rig.

As shown in the bar chart, substitution of heat-treated Rene 41 alloy for heat-treated Inconel X-750 improved resiliency significantly. Rene 41 spring tubes maintained greater than 95-percent resiliency through 20 compression

cycles at 1200 °F, whereas Inconel spring tube resiliency dropped as low as 78 percent at cycle 20. At the start of compression cycle 20 at 1500 °F, Rene 41 spring tubes exhibited a 5.2 times resiliency improvement over the baseline design. Rene 41 spring tubes maintained reasonable resiliency up to 1750 °F.

For a sustained resiliency of 75 percent, Rene 41 samples showed a temperature improvement of approximately 275 °F over Inconel X-750 specimens. Resiliency improvements due to material substitution were visually confirmed during post-test spring tube inspection as illustrated in the photographs on this page. Permanent set in the Inconel X-750 spring tubes was clearly evident at 1500 °F, whereas permanent deformation in the Rene 41 samples was nearly undetectable until 1750 °F.

The improvements in spring tube performance achieved by substituting Rene 41 for Inconel X-750 in the baseline knit geometry can be directly applied to current seal applications. By replacing existing Inconel X-750 spring tubes with new Rene 41 spring tubes, the benefits of more resilient control surface seals can be realized immediately. Technical specialists within the space shuttle program have expressed interest in possibly applying this advancement to the shuttle main landing-gear door thermal barriers to provide a greater temperature margin over the baseline design.

Bibliography

DeMange, J.J.; Dunlap, P.H.; and Steinetz, B.M.: Advanced Control Surface Seal Development for Future Space Vehicles. NASA/TM-2004-212898, 2004. <http://gltrs.grc.nasa.gov/cgi-bin/GLTRS/browse.pl?2004/TM-2004-212898.html>

Dunlap, Patrick H.; Steinetz, Bruce M.; and Curry, Donald M.: Rudder/Fin Seal Investigations for the X-38 Re-Entry Vehicle. NASA/TM-2000-210338/REV1 (AIAA-2000-3508), 2000. <http://gltrs.grc.nasa.gov/cgi-bin/GLTRS/browse.pl?2000/TM-2000-210338-REV1.html>

Dunlap, Patrick H., et al.: Further Investigations of Control Surface Seals for the X-38 Re-Entry Vehicle. NASA/TM—2001-210980 (AIAA-2001-3628), 2001. <http://gltrs.grc.nasa.gov/cgi-bin/GLTRS/browse.pl?2001/TM-2001-210980.html>

Dunlap, Patrick H., Jr., et al.: Investigations of Control Surface Seals for Re-Entry Vehicles. NASA/TM—2002-211708, 2002. <http://gltrs.grc.nasa.gov/cgi-bin/GLTRS/browse.pl?2002/TM-2002-211708.html>

Dunlap, P. and Steinetz, B.: Toward an Improved Hypersonic Engine Seal. NASA/TM—2003-212531 (AIAA-2003-4834), 2003. <http://gltrs.grc.nasa.gov/cgi-bin/GLTRS/browse.pl?2003/TM-2003-212531.html>

Taylor, Shawn C., et al.: Evaluation of High Temperature Knitted Spring Tubes for Structural Seal Applications. NASA/TM—2004-213183 (AIAA-2004-3890), 2004. <http://gltrs.grc.nasa.gov/cgi-bin/GLTRS/browse.pl?2004/TM-2004-213183.html>

Find out more about this research:

Structural seals and thermal barriers:

<http://www.grc.nasa.gov/WWW/structuralseal/>

Glenn's Mechanical Components Branch:

<http://www.grc.nasa.gov/WWW/5900/5950/>

Case Western Reserve University

contact:

Shawn Taylor, 216-433-3166,
Shawn.C.Taylor@grc.nasa.gov

University of Toledo contact:

Jeffrey J. DeMange, 216-433-3568,
Jeffrey.J.DeMange@grc.nasa.gov

Glenn contacts:

Patrick H. Dunlap, Jr., 216-433-3017,
Patrick.H.Dunlap@nasa.gov; and
Dr. Bruce M. Steinetz, 216-433-3302,
Bruce.M.Steinetz@nasa.gov

Authors:

Shawn C. Taylor, Jeffrey J. DeMange,
Patrick H. Dunlap, Jr., and
Dr. Bruce M. Steinetz

Headquarters program office:

Exploration Systems

Programs/Projects:

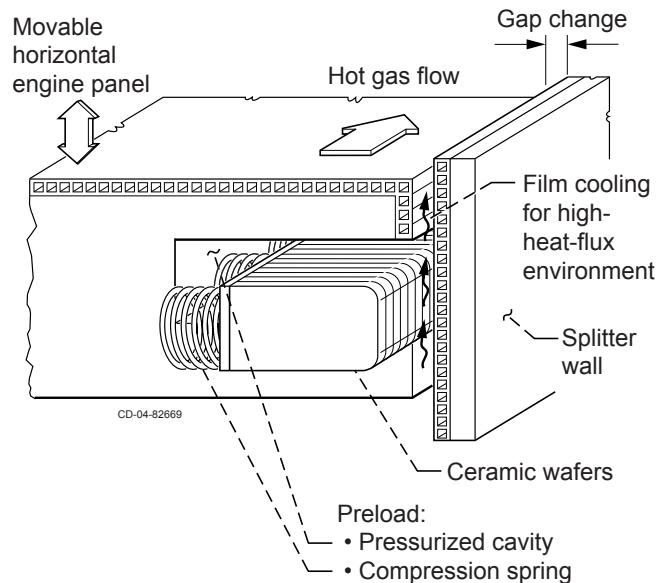
NGLT

Advanced Ceramic Wafer Seals Demonstrated at 2000 °F

Durable, high-temperature sliding seals are required in advanced hypersonic engines and around movable control surfaces on future vehicles. These seals must operate at temperatures of 2000 to 2500 °F, limit hot gas flow, remain resilient for multiple cycles, and resist scrubbing damage against rough surfaces. Current seal designs do not meet these demanding requirements, so the NASA Glenn Research Center is developing advanced seals and preload devices to overcome these shortfalls. An advanced ceramic wafer seal design and two silicon nitride compression spring designs were evaluated in a series of compression, scrub, and flow tests.

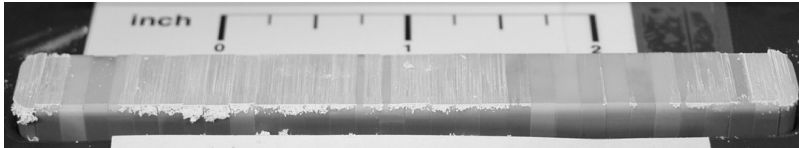
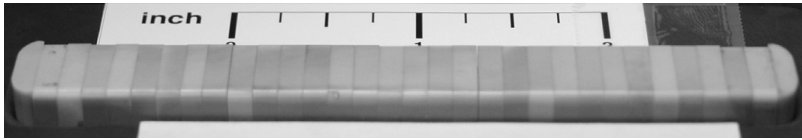
The seals evaluated in this study, which were originally developed during the National Aerospace Plane program, are composed of a series of thin ceramic wafers installed in a channel on a movable panel and preloaded from behind to keep them in contact with the opposing sealing surface (see the figure to the right). The wafers were made of monolithic silicon nitride (Honeywell AS800, Honeywell International, Morris Township, NJ) and were 0.5 in. wide, 0.92 in. tall, and 0.125 in. thick. Commercially available silicon nitride compression springs were evaluated as preload devices to ensure sealing contact with the opposing sealing surfaces.

The silicon nitride wafer seals were proven to be quite robust and wear-resistant. They survived 2000 in. (50.8 m) of scrubbing at 2000 °F against a silicon carbide



Ceramic wafer seal with compression springs as preload devices.

rub surface with no chips or signs of damage (see the photographs on the next page). None of the wafers were chipped or broken, and the weight of each wafer set was almost identical



Silicon nitride wafer seals. Top: Before 2000 °F scrub test. Bottom: After 2000 °F scrub test.

before and after testing. The wafer seals were excellent at blocking flow even after 1000 scrub cycles at 2000 °F. Flow rates measured for the wafers before and after scrubbing were almost identical and were up to 32 times lower than those recorded for the best braided-rope-seal flow blockers.

Silicon nitride compression springs showed promise conceptually as seal preload devices to help maintain seal resiliency. After repeated loading at temperatures up to 2200 °F, the springs showed excellent resiliency and little hysteresis.

This study demonstrated the excellent performance of a new, advanced ceramic wafer seal design at 2000 °F. Additional development is planned to demonstrate the performance of this seal design at temperatures greater than 2500 °F.

Software Developed for Analyzing High-Speed Rolling-Element Bearings

COBRA-AHS (Computer Optimized Ball & Roller Bearing Analysis—Advanced High Speed, J.V. Poplawski & Associates, Bethlehem, PA) is used for the design and analysis of rolling element bearings operating at high speeds under complex mechanical and thermal loading. The code estimates bearing fatigue life by calculating three-dimensional subsurface stress fields developed within the bearing raceways. It provides a state-of-the-art interactive design environment for bearing engineers within a single easy-to-use design-analysis package. The code analyzes flexible or rigid shaft systems containing up to five bearings acted upon by radial, thrust, and moment loads in 5 degrees of freedom. Bearing types include high-speed ball, cylindrical roller, and tapered roller bearings.

COBRA-AHS is the first major upgrade in 30 years of such commercially available bearing software. The upgrade was developed under a Small Business

Bibliography

Dunlap, Patrick H.; Steinetz, Bruce M.; and DeMange, Jeffrey J.: Further Investigations of Hypersonic Engine Seals. NASA/TM—2004-213188 (AIAA-2004-3887), 2004. <http://gltrs.grc.nasa.gov/cgi-bin/GLTRS/browse.pl?2004/TM-2004-213188.html>

Find out more about this research:

Structural seals and thermal barriers:

<http://www.grc.nasa.gov/WWW/structuralseal/>

Glenn's Mechanical Components

Branch:

<http://www.grc.nasa.gov/WWW/5900/5950/>

Glenn contacts:

Patrick H. Dunlap, Jr., 216-433-3017, Patrick.H.Dunlap@nasa.gov; and Dr. Bruce M. Steinetz, 216-433-3302, Bruce.M.Steinetz@nasa.gov

Authors:

Patrick H. Dunlap, Jr., Dr. Bruce M. Steinetz, and Jeffrey J. DeMange

Headquarters program office:

Exploration Systems

Programs/Projects:

NGLT

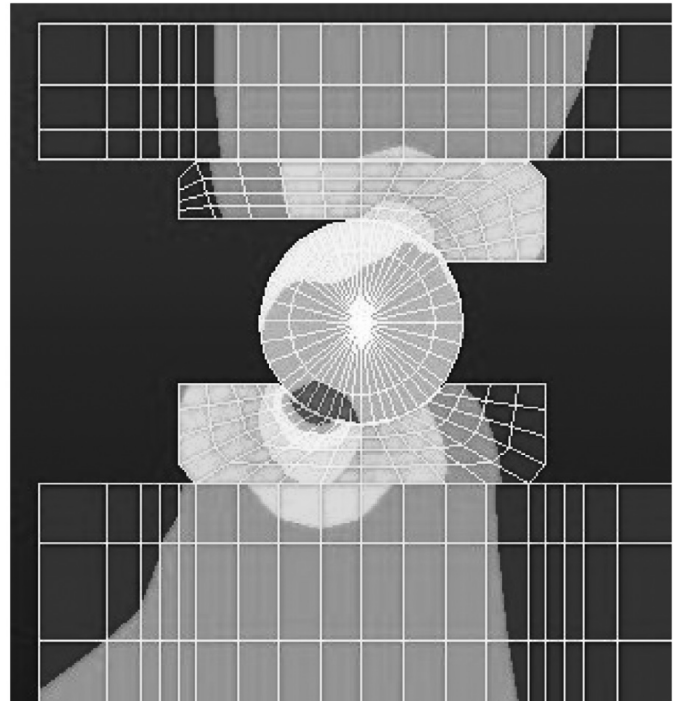
Innovation Research contract from the NASA Glenn Research Center, and incorporates the results of 30 years of NASA and industry bearing research and technology.

Output generated by COBRA-AHS includes bearing deflection due to the imposed loads, contact stresses between the elements and races, heat generation, and bearing fatigue life. The program has a modern menu-driven Windows interface, allowing users to interactively change input

data and quickly see the effect on bearing performance. It also interacts automatically with the widely used ANSYS finite-element analysis program to generate finite-element models of the bearing locations. These models are used for estimating the level and distribution of temperatures within the bearing rings, balls, shaft, and housing sections (see the figure to the right), as well as temperature-induced changes in dimensions. This iterative thermal and dimensional interactive analysis is thereby able to track changes in clearance within the bearing and forecast potential thermal lockup of the bearing.

Much of the code output is graphical for easy interpretation. The figure below shows example output for a cylindrical roller bearing. The left side of the figure is a section through the bearing, and the right side shows the contact stress pattern between the roller and raceway. Notice that this particular case results in high stress at the ends of the roller, a condition that can lead to premature fatigue of the bearing in that region. To reduce this high stress, designers reduce the roller diameter slightly near its ends, a technique called crowning. With COBRA-AHS, a designer can manipulate the various roller crown parameters interactively, getting an immediate update of the contact stress map, in an attempt to achieve a uniform stress at the contact surface.

The principal use of COBRA-AHS is the design and analysis of rolling-element bearings for high-speed rotating machinery, such as jet engines, pumps, turbocompressors, and dental drills. On the basis of its advanced capabilities, the code is being selected as the replacement for the previous



Temperature distribution within the high-speed ball bearing.

industry-standard high-speed bearing program. COBRA-AHS is currently being used by NASA to perform a design audit and analyses on the bearing system for the proposed International Space Station centrifuge.

Find out more about this research:

<http://www.grc.nasa.gov/WWW/5900/5950/>

Glenn contact:

Dr. David P. Fleming, 216-433-6013,
David.P.Fleming@nasa.gov

J.V. Poplawski and Associates contact:

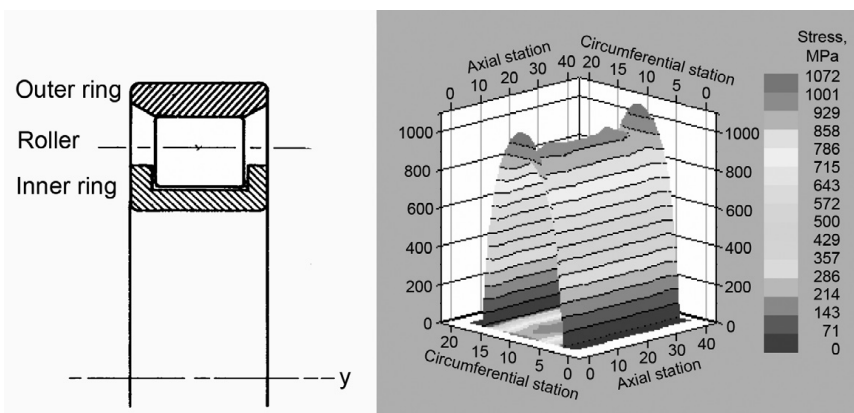
J.V. Poplawski, 610-758-9601,
Jvpoplawski@aol.com

Author:

Dr. David P. Fleming

Headquarters program office:
Aeronautics Research

Programs/Projects:
Propulsion Systems R&T, UEET,
AvSSP, RLV, Microgravity Science



Left: Cylindrical roller bearing. Right: Example of stress between the roller and raceway. This figure is shown in color in the online version of this article (<http://www.grc.nasa.gov/WWW/RT/2004/RS/RS27M-fleming.html>).

Oxide Ceramic Films Grown on 60 Nitinol for NASA and Department of Defense Applications

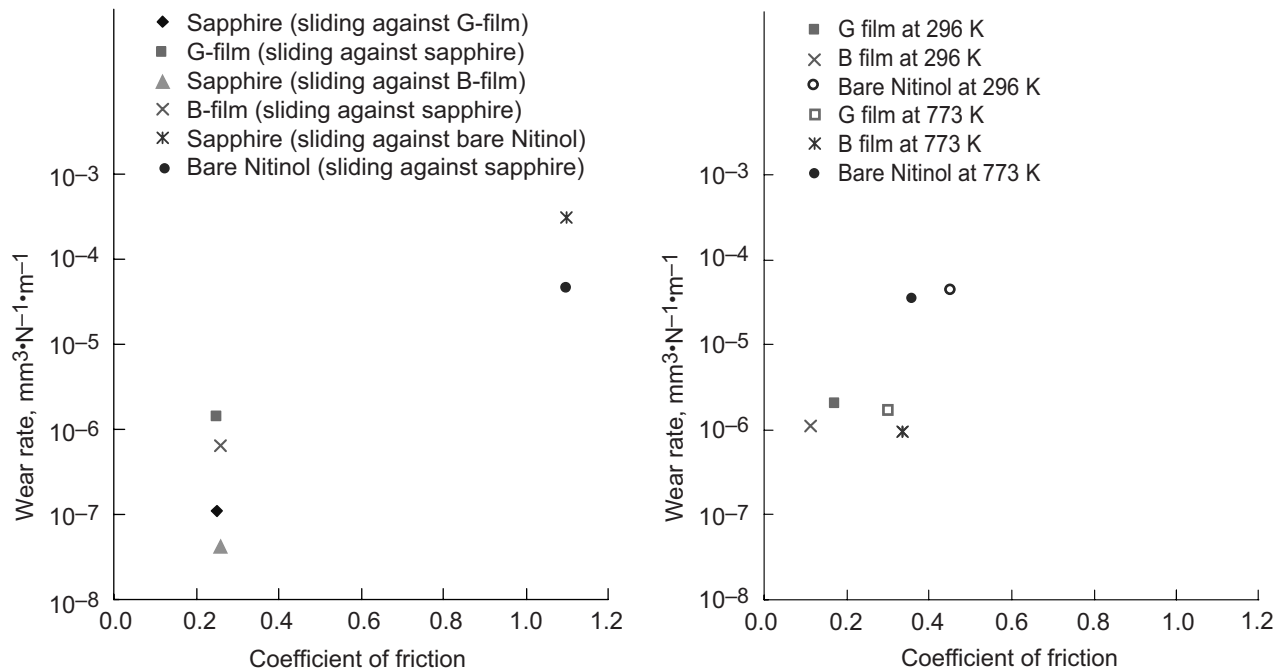
Both the NASA Glenn Research Center and the U.S. Army Research Laboratory, Development and Engineering Center (ARDEC) have worked to develop oxide ceramic films grown on 60 nitinol (60-wt% nickel and 40-wt% titanium) to decrease friction and increase wear resistance under unlubricated conditions. In general, oxide and nonoxide ceramic films have unique capabilities as mechanical-, chemical-, and thermal-barrier materials in diverse applications, including high-temperature bearings and gas bearings requiring low friction, wear resistance, and chemical stability (ref. 1). All oxide ceramic films grown on 60 nitinol were furnished by ARDEC, and materials and surface characterization and tribological experiments were conducted at Glenn.

Titanium oxide, TiO_2 , was formed on 60 nitinol (B film) using a patented oxide treatment (ref. 2). Another TiO_2 with additional metallic species (G film) was formed on 60 nitinol by heating the specimen manually in methylacetylene-propadiene in a liquefied propane flame (ref. 2).

The tribological characteristics of 60 nitinol were improved by both films. In the graph on the left, the films decreased the friction by a factor of 4 and increased the wear resistance by a two-figure factor for sliding in unlubricated conditions, although the wear resistance and endurance life of the B film were superior to those of the G film. In the graph on the right, the B film increased

the wear resistance by factors of 50 and 40 at 296 and 773 K, respectively. Thus, TiO_2 films grown on nitinol can greatly improve the wear resistance while providing low friction.

The development of commercial applications of nitinol is continuing. For example, nitinol has found application as the race in rolling-element bearing assemblies (see the photograph on the next page). To meet the more stringent thrust-to-weight goals of today's high-performance engines, rolling-element bearings must operate at speeds exceeding 2.4 million DN (the product of the inner race bore in millimeters and the speed in revolutions per minute) and at temperatures up to 478 K using lubricating oil or grease. This temperature



Guideline map of coefficients of friction versus dimensional wear coefficients (specific wear rate) for TiO_2 grown on 60 nitinol in sliding contact with sapphire balls in air at 296 and 773 K. Left: Data obtained from unidirectional, pin-on-disk sliding friction experiments conducted at 296 K. Right: Data obtained from reciprocating, pin-on-flat sliding friction experiments conducted at 296 and 773 K.

limit is imposed primarily by the lubricant (ref. 3). Fatigue is considered to be the life-limiting factor for these bearings, although fewer than 10 percent of the failures are fatigue related. Most failures are due to the lubricant, such as lubricant starvation, contamination, and deterioration (ref. 3). In addition, there are significant adhesion, friction, and wear issues that affect the performance and lifetime of the bearing assembly. The promising results of friction and wear properties obtained in this investigation may fit design needs for high-temperature applications because oxide films may be preferred to oil or grease lubrication. At temperatures above 478 K, oil and grease decompose. Nitinol with oxide surfaces can extend operating temperatures while maintaining low friction and high wear resistance.

References

1. Miyoshi, Kazuhisa: Solid Lubrication Fundamentals and Applications. Marcel Dekker, New York, NY, 2003.
2. Miyoshi, Kazuhisa; Lukco, Dorothy; and Cytron, Sheldon J.: Oxide Ceramic Films Grown on 55Ni-45Ti for NASA and Department of Defense Applications: Unidirectional Sliding Friction and Wear Evaluation. NASA/TM—2004-212979, 2004. <http://gltrs.grc.nasa.gov/cgi-bin/GLTRS/browse.pl?2004/TM-2004-212979.html>
3. Zaretsky, Erwin V.: Life Factors for Rolling Bearings. STLE SP-34, 1987.

Glenn contacts:

Dr. Kazuhisa Miyoshi, 216-433-8758, Kazuhisa.Miyoshi-1@nasa.gov; and
Dr. Kenneth W. Street, 216-433-5032, Kenneth.W.Street@nasa.gov

U.S. Army Research Laboratory, Development and Engineering Center contact:

Dr. Sheldon J. Cytron, 973-724-3368, sheldon.cytron@us.army.mil

QSS Group, Inc., contact:

Dr. Dorothy Lukco, 216-433-3741, Dorothy.Lukco@grc.nasa.gov



Nitinol rolling-element bearing assembly.

Authors:

Dr. Kazuhisa Miyoshi,
Dr. Kenneth W. Street,
Dr. Dorothy Lukco, and
Dr. Sheldon J. Cytron

Headquarters program office:

Aeronautics Research

Programs/Projects:

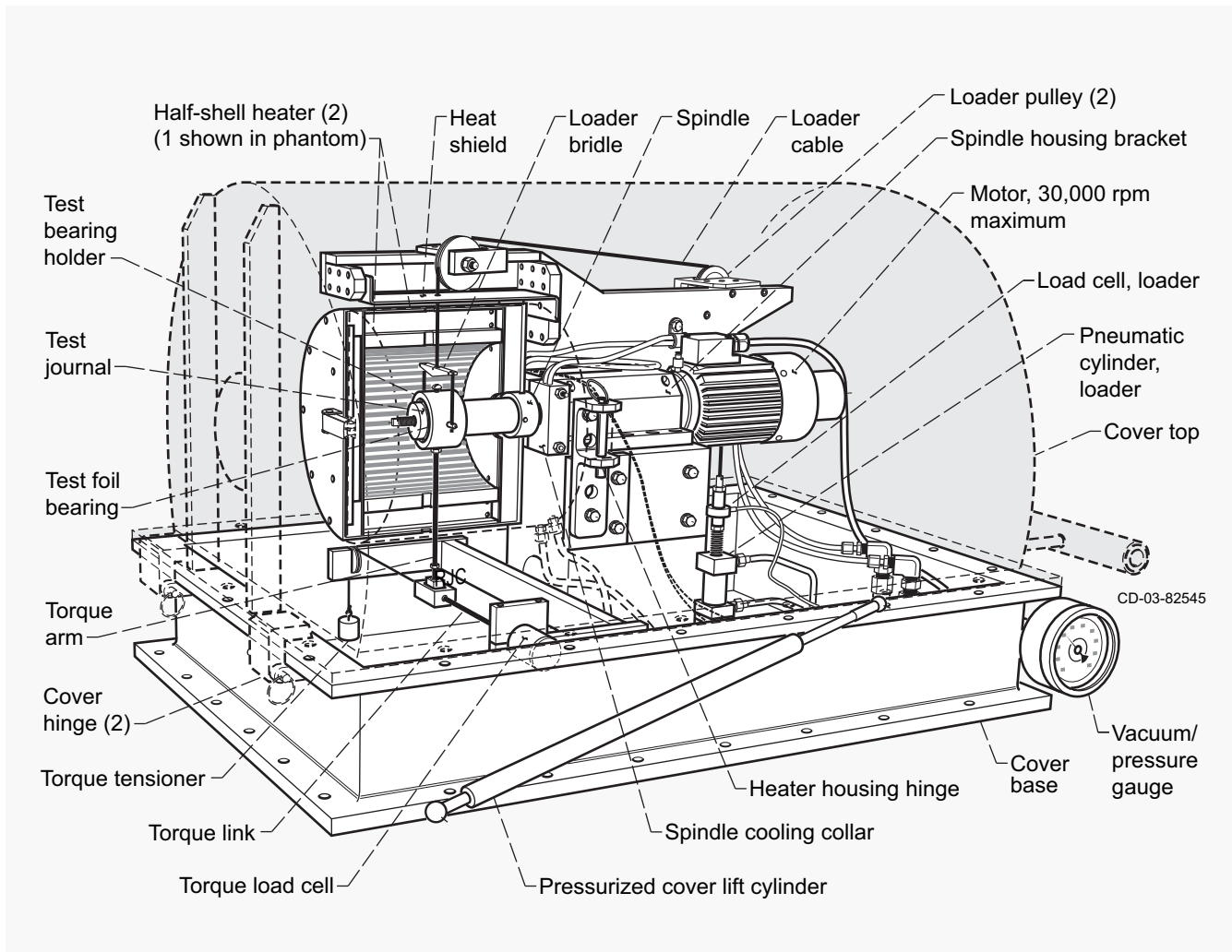
LEAP, VSP, AFFT

Ambient Pressure Test Rig Developed for Testing Oil-Free Bearings in Alternate Gases and Variable Pressures

The Oil-Free Turbomachinery research team at the NASA Glenn Research Center is conducting research to develop turbomachinery systems that utilize high-speed, high-temperature foil (air) bearings that do not require an oil lubrication system. Such systems combine the most advanced foil bearings from industry with NASA-developed high-temperature solid-lubricant technology. New applications are being pursued, such as Oil-Free turbochargers, auxiliary power units, and turbine propulsion systems for aircraft. An Oil-Free business jet engine, for example, would be simpler, lighter, more reliable, and less costly to purchase and maintain than current engines. Another application is

NASA's Prometheus mission, where gas bearings will be required for the closed-cycle turbine-based power-conversion system of a nuclear power generator for deep space.

To support these applications, Glenn's Oil-Free Turbomachinery research team developed the Ambient



Ambient pressure Oil-Free bearing test rig illustration.

Pressure Test Rig. Using this facility, researchers can load and heat a bearing and evaluate its performance with reduced air pressure to simulate high-altitude conditions. For the nuclear application, the test chamber can be purged with gases such as helium to study foil gas bearing operation in working fluids other than air.

During testing, a variable-speed (30,000-rpm maximum) electric motor with an integral precision spindle bearing spins the test journal over which the test foil bearing runs (see the illustration). The test bearing is mounted in a bearing holder that is constrained from turning by a torque arm from which reactionary torque is measured. This is the most important measurement to determine the health and capability of the bearing because the torque from a healthy bearing running on a film of gas is very low, whereas an increase in torque is a sign of sliding frictional contact. Load is applied to the bearing by a bridle (see the inset in the photograph on the next page) that is pulled by a cable that is

routed to a pneumatic cylinder that can apply up to 100 lb. The test bearing can be heated up to 650 °C with two ceramic electric heaters in insulated half shells that form an enclosure around the bearing. Multiple sensors register the temperature and other rig health parameters during the test. All are displayed on a programmable logic controller touch-screen controller (top right of the photograph on the next page), and some are used to trip alarms or shutdowns. All these components can be sealed in by closing the cover. Air or any alternate gas



Ambient pressure test rig in NASA Glenn's Engine Research Building.

can be selected, and a vacuum pump can remove most of the gas, down to 0.1 atm, which corresponds to a 53,000-ft altitude, or gas can be added for pressures up to 2.5 atm.

As a direct result of data collected from this rig, small aircraft turbine engines may be revolutionized by using oil-free bearings that will forever eliminate the

complication, weight, and expense of an oil lubrication system. Furthermore, data from alternate gas operation experiments are imperative for developing safe, compact, and efficient nuclear electrical generators vital for NASA to conduct deep-space exploration and have a manned presence on the Moon and Mars, as directed by the President.

Find out more about this research:

Oil-Free Turbomachinery researchers:
<http://www.grc.nasa.gov/WWW/Oilfree/team.htm>

Oil-Free Turbomachinery Program:
<http://www.grc.nasa.gov/WWW/Oilfree/>

Prometheus:
<http://www.jpl.nasa.gov/jimo/>

Glenn contacts:
 Steven W. Bauman, 216-433-3826,
Steven.W.Bauman@nasa.grc; and
 Dr. Christopher DellaCorte, 216-433-6056,
Christopher.DellaCorte-1@nasa.gov,
 Oil-Free Turbomachinery technical leader

Author:
 Steven W. Bauman

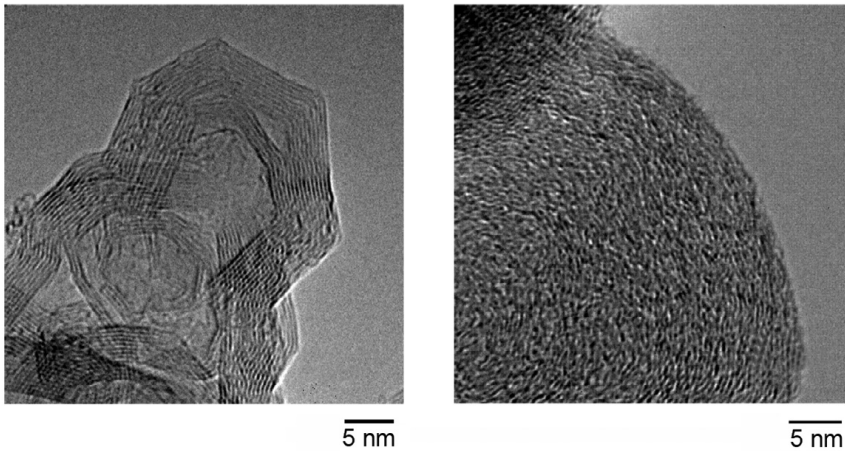
Headquarters program office:
 Space Science, Aeronautics Research

Programs/Projects:
 JIMO, UEET, Project Prometheus

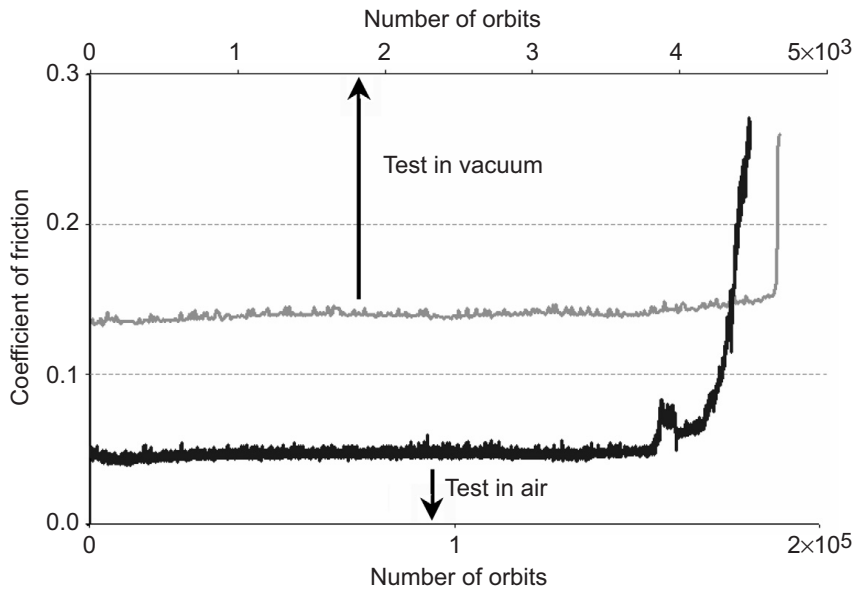
Tribological Behavior of Nano-Onions in Krytox 143AB Evaluated

Nanoparticles have been developed over the past 10 years and have found several applications. This work presents the use of carbon nano-onions as a potential oil additive for aerospace applications. Researchers at the NASA Glenn Research Center tested lubricant lifetimes in ambient air and ultrahigh vacuum and characterized the breakdown products of the friction and wear. These carbon nanoparticles can provide adequate lubrication very similar to that of graphitic material when run in air.

Soot represents one of the very first nanostructured materials, although it has rarely been considered as such. Changes in the carbon nanostructure, resulting in increased graphitic layer plane length, correlate with reactivity loss. Upon heating spherically shaped



Transmission electron microscope pictures. Left: Nano-onion. Right: Carbon black.



Friction coefficient for tests run in vacuum (upper scale) and in air (lower scale).

nanometer-sized carbon black in the absence of oxidant, graphene sheets form, and the initial soot particle templates the growth of a graphitic particle into what is best described as a “sphere” with many flat sides having a hollow interior. Because there are no edge sites, these polygonal graphitic particles, or “nano-onions,” are relatively resistant to oxidation.

Graphite is used as a solid lubricant because of its stability at moderately high temperatures. However, the temperature at which graphite oxidizes rapidly is strongly influenced by surface area. With the size of particles typically employed in lubrication, a great amount of thermal stability is lost because of size reduction either during preparation or during lubrication of contacting

NORMALIZED LIFETIMES OF KRYTOX 143AB WITH NANO-ONIONS FOR DIFFERENCE CONDITIONS

Tribological conditions	Normalized lifetime, orbits/ μg
Vacuum	55
Ambient air	3830

parts. Therefore, we have undertaken a study of the lubricating ability of graphitic nano-onions (ref. 1).

A spiral orbit tribometer (ref. 2) simulates an angular contact bearing. Lubricant allows the system to operate in the boundary lubrication regime. The ball rolls and pivots in a spiral and is maintained in orbit by a guide plate. The force the ball exerts on the guide plate is used to determine the friction coefficient. A suspension of nano-onions in Krytox oil was evaluated at room temperature under ultrahigh vacuum or in air at Glenn as part of our ongoing efforts in aeronautics research.

High-resolution transmission electron microscope images of the nano-onions (see the left photograph) and carbon black (see the right photograph) indicate that the structure of the material changed significantly upon graphitization. In these images, the dark lines indicate the graphene sheets of carbon atoms and the white lines are the spacing between sheets. The analyses of both the nano-onions and carbon black in air indicate high-purity materials.

Raman spectroscopy is often used to characterize graphite and graphitic materials (ref. 3). The spectra obtained from the nano-onions indicate a highly ordered material considerably different from the starting carbon black. The Raman spectrum

of the degradation products resembles the starting carbon black, indicating that the nano-onions are consumed during use.

For tests conducted in ultrahigh vacuum at room temperature, the nano-onions do not improve the lifetime, or change the friction coefficient, of this perfluoropolyether (PFPE) oil. The normalized lifetime (number of orbits performed before failure per microgram of lubricant employed) was calculated. Tests conducted in ambient conditions; however, showed a very low friction coefficient with a long lifetime. Furthermore, the failure was more “progressive” than the one observed in vacuum. Examples of friction traces and the lifetimes obtained are given in the graph and table on the preceding page.

Acknowledgments

The authors gratefully acknowledge Gordon M. Berger (National Center for Space Exploration Research) for assistance with the experiments and Dr. Y.L. Chen (QSS Group, Inc.) and David R. Hull (NASA Glenn) for the transmission electron microscope imaging.

References

1. Street, Kenneth W., et al.: Evaluation of the Tribological Behavior of Krytox 143AB With Nano-Onions. *Tribology Letters* (NASA/TM—2003-212301), vol. 16, nos. 1–2, 2004, pp. 143–149, 2003. <http://gltrs.grc.nasa.gov/cgi-bin/GLTRS/browse.pl?2003/TM-2003-212301.html>
2. Pepper, Stephen V.; and Kingsbury, Edward P.: Spiral Orbit Tribometry—Part I: Description of the Tribometer. *Tribol. Trans.*, vol. 46, no. 1, 2003, p. 57–64.

3. Vander Wal, Randy L., et al.: Carbon Nanostructure Examined by Lattice Fringe Analysis of High-Resolution Transmission Electron Microscopy Images. *Appl. Spectrosc.* (NASA/TM—2003-212214), vol. 58, no. 2, 2004, pp. 230–237, 2003. <http://gltrs.grc.nasa.gov/cgi-bin/GLTRS/browse.pl?2003/TM-2003-212214.html>

Glenn contact:

Dr. Kenneth W. Street, 216–433–5032, Kenneth.W.Street@nasa.gov

National Center for Space

Exploration Research contact:

Dr. Randy L. Vander Wal, 216–433–9065, Randall.L.VanderWal@grc.nasa.gov

Authors:

Dr. Kenneth W. Street, Mario Marchetti, Dr. Randall L. Vander Wal, and Aaron J. Tomasek

Headquarters program office:

Aeronautics Research

Programs/Projects:

AEFT

Journal Bearing Analysis Suite Released for Planetary Gear System Evaluation

Planetary gear systems are an efficient means of achieving high reduction ratios with minimum space and weight. They are used in helicopter, aerospace, automobile, and many industrial applications. High-speed planetary gear systems will have significant dynamic loading and high heat generation. Hence, they need jet lubrication and associated cooling systems. For units operating in critical applications that necessitate high reliability and long life, that have very large torque loading, and that have downtime costs that are significantly greater than the initial cost, hydrodynamic journal bearings are a must.

Computational and analytical tools are needed for sufficiently accurate modeling to facilitate optimal design of these systems. Sufficient physics is needed in

the model to facilitate parametric studies of design conditions that enable optimal designs.

The first transient journal bearing code to implement the Jacobsson-Floberg-Olsson boundary conditions, using a mass-conserving algorithm devised by Professor Emeritus Harold Elrod of Columbia University, was written by David E. Brewé of the U.S. Army



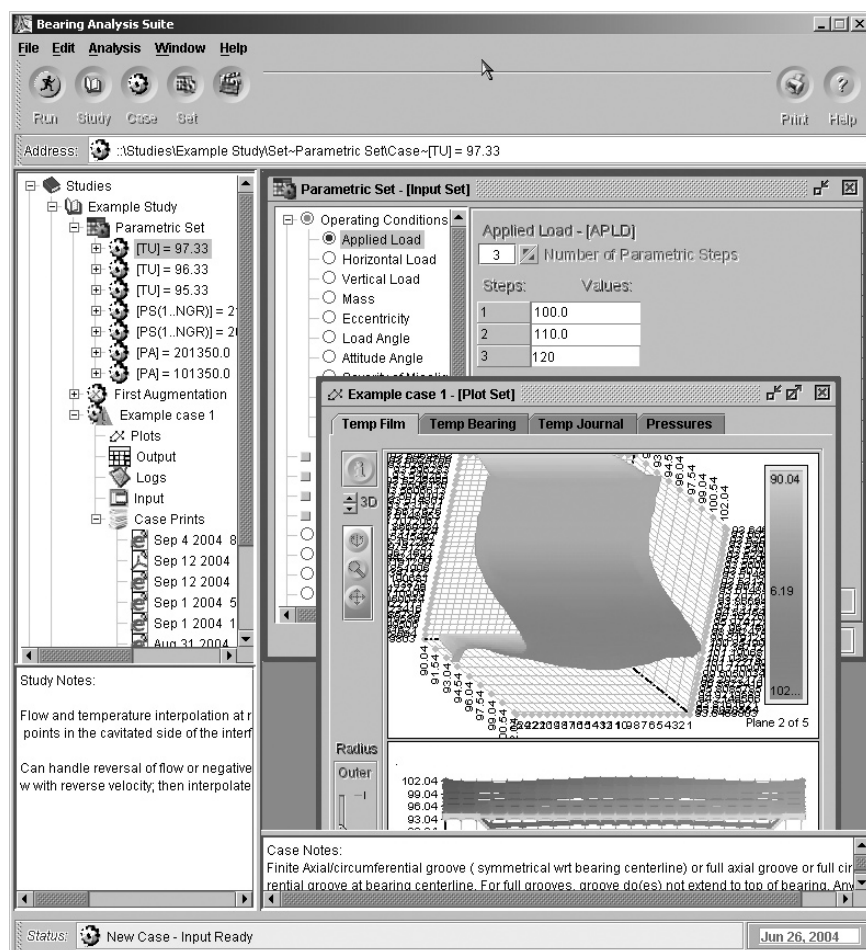
Planetary gear system.

at the NASA Lewis Research Center¹ in 1983. Since then, new features and improved modifications have been built into the code by several contributors supported through Army and NASA funding via cooperative agreements with the University of Toledo (Professor Ted Keith, Jr., and Dr. Desikakary Vijayaraghavan) and National Research Council Programs (Dr. Vijayaraghavan). All this was conducted with the close consultation of Professor Elrod and the project management of David Brewe.

This version uses collocation across the film thickness at Lobatto points and Legendre polynomials to perform a thermohydrodynamic analysis of fluid-film journal bearings. The procedure is based on the development and program of Professor Elrod, and the code was developed by Dr. Vijayaraghavan at NASA Lewis with U.S. Army Research Laboratory, Vehicle Technology Directorate funding.

The latest features now include viscosity variation through the film due to shear heating and pressure viscosity effects. The program also can handle (1) aligned and misaligned bearings, (2) heat conduction through the bearing (stationary surface) and net heat flux through the journal (rotating surface) while considering free convection to the bearing outside and end surfaces, (3) a wide variety of groove designs for several grooves, (4) groove mixing temperature of hot oil carryover with supply, (5) transient or steady-state analysis, (6) rotating or dynamic loading, and (7) the rotation of either surface (i.e., journal or bearing).

In addition, a modern graphical user interface was added to facilitate sim-



User interface of Bearing Analysis Suite Version 1.0.

¹Renamed the NASA Glenn Research Center at Lewis Field in 1999.

ple, intuitive case studies for nonexperienced users. The package is presented as the Bearing Analysis Suite.

Special features of the user interface include the

- Study Manager—Enables the easy generation of parametric sets of cases
- Notes Manager—Provides an intuitive note-taking interface
- Plot Viewer—Shows two- and three-dimensional output plots
- Log Viewer—Gives convergence histograms and three-dimensional convergence plots
- Web Printer—Publishes output to portable document format (PDF) or hypertext markup language (HTML)

Find out more about this research:

Glenn's Tribology & Surface Science Branch:

<http://www.grc.nasa.gov/WWW/SurfSci/>

Bearing Analysis Suite:
<http://www.grc.nasa.gov/WWW/SurfSci/JournalBearings>

Glenn contact:

Dr. Phillip B. Abel, 216-433-6063,
Phillip.B.Abel@nasa.gov

Authors:

David E. Brewe (retired) and
David A. Clark

Programs/Projects:

U.S. Army Research Laboratory,
Vehicle Technology Directorate

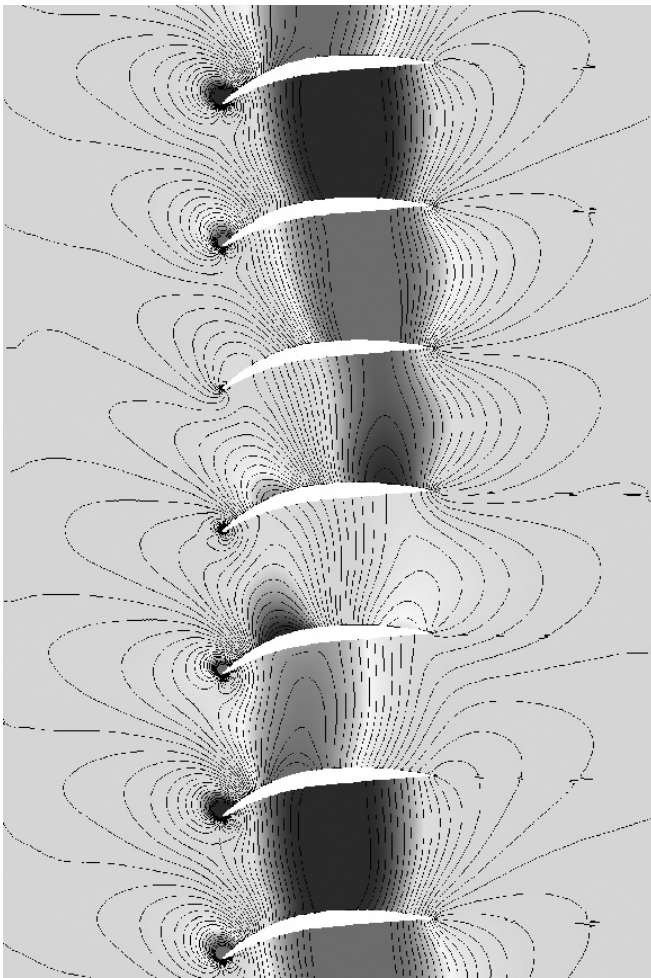
Propulsion Systems

Benchmark Problems Used to Assess Computational Aeroacoustics Codes

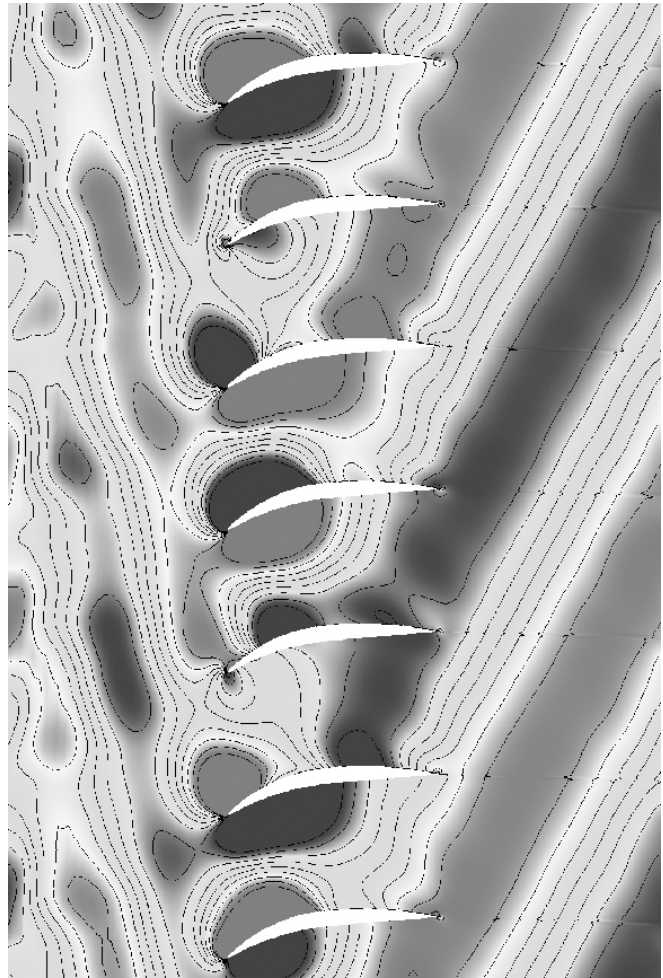
The field of computational aeroacoustics (CAA) encompasses numerical techniques for calculating all aspects of sound generation and propagation in air directly from fundamental governing equations. Aeroacoustic problems typically involve flow-generated noise, with and without the presence of a solid surface, and the propagation of the sound to a receiver far away from the noise source. It is a challenge to obtain accurate numerical solutions to these problems.

The NASA Glenn Research Center has been at the forefront in developing and promoting the development of CAA techniques and methodologies for computing the noise generated by aircraft propulsion systems. To assess the

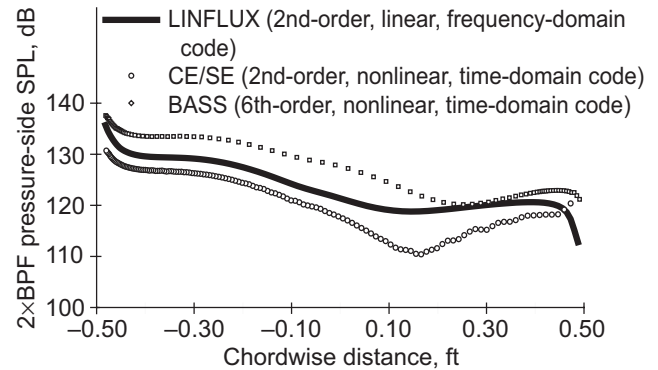
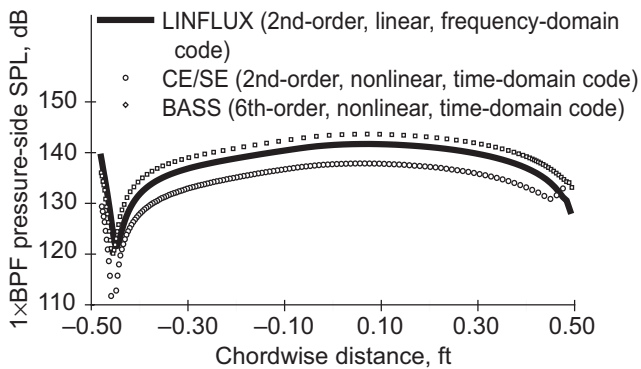
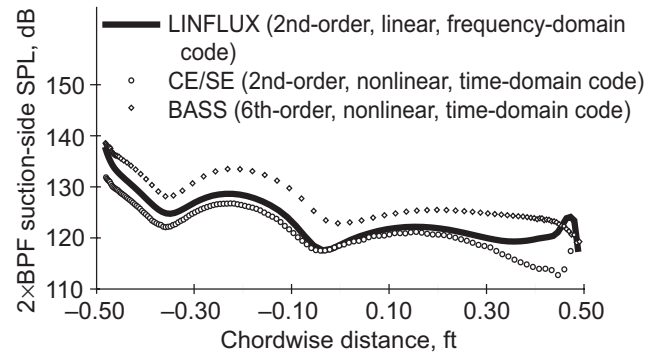
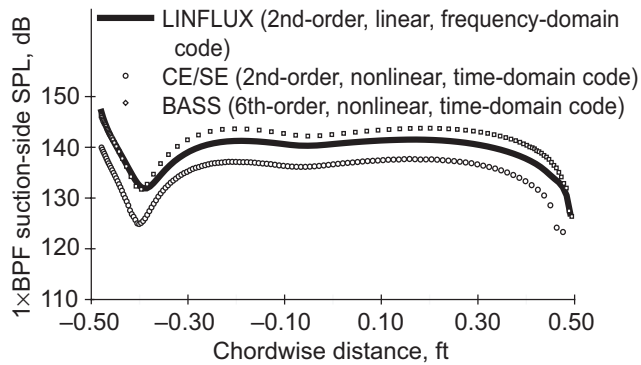
technological advancement of CAA, Glenn, in cooperation with the Ohio Aerospace Institute and the Aero-Acoustics Research Consortium, organized and hosted the Fourth CAA Workshop on Benchmark Problems. Participants from industry and academia from both the United States and abroad joined to present and discuss solutions to benchmark problems. These demonstrated technical



Computed pressure perturbation response to a gust at the primary frequency. This contour plot shows that the perturbations oscillate within the passages between the stator vanes and decay rapidly away from the vanes.



Computed pressure perturbation response to a gust at twice the primary frequency. This contour plot shows that the perturbations are propagating away from the stator vanes in both the upstream and downstream directions.



Computed time-averaged pressure perturbation amplitude on each surface of a typical stator vane at the primary frequency of the gust. This plot compares results from three different codes, with the LINFLUX code representing the benchmark case. BPF, blade passing frequency; SPL, sound pressure level.

Computed time-averaged pressure perturbation amplitude on each surface of a typical stator vane at twice the primary frequency of the gust. This plot compares results from three different codes, with the LINFLUX code representing the benchmark case. BPF, blade passing frequency; SPL, sound pressure level.

progress ranging from the basic challenges to accurate CAA calculations to the solution of CAA problems of increasing complexity and difficulty. The results are documented in the proceedings of the workshop (ref. 1).

Problems were solved in five categories. In three of the five categories, exact solutions were available for comparison with CAA results. A fourth category of problems representing sound generation from either a single airfoil or a blade row interacting with a gust (i.e., problems relevant to fan noise) had approximate analytical or completely numerical solutions. The fifth category of problems involved sound generation in a viscous flow. In this case, the CAA results were compared with experimental data.

A sample result from the workshop is shown here for the case of sound generated by a gust interacting with a cascade of realistic stator vanes. This problem represents a principal source of fan noise in aircraft engines called the rotor-stator interaction noise, which is produced by the impingement of the fan rotor wakes on the fan exit guide vanes. A code called LINFLUX, which was developed at the United Technologies Research Center under Glenn funding, can be used to predict this source in realistic three-dimensional geometries. LINFLUX was used to compute the standard, or benchmark, solution to this problem. The contour plots show the computed pressure perturbations at one and two times the primary gust frequency, which for the specified operating conditions result in decaying (or evanescent) and propagating acoustic fields, respectively. The line plots show detailed pressure perturbation solutions on

a typical vane. Good agreement is shown between the LINFLUX solution and two other codes being developed under Glenn sponsorship. Further comparisons for this problem and results for other problems are found in the proceedings (ref. 1).

Reference

1. Dahl, Milo D., ed., Fourth Computational Aeroacoustics (CAA) Workshop on Benchmark Problems. NASA/CP—2004-212954, 2004. <http://gltrs.grc.nasa.gov/cgi-bin/GLTRS/browse.pl?2004/CP-2004-212954.html>

Glenn contact:

Dr. Milo D. Dahl, 216-433-3578,
Milo.D.Dahl@nasa.gov

Authors:

Dr. Milo D. Dahl and Dr. Edmane Envia

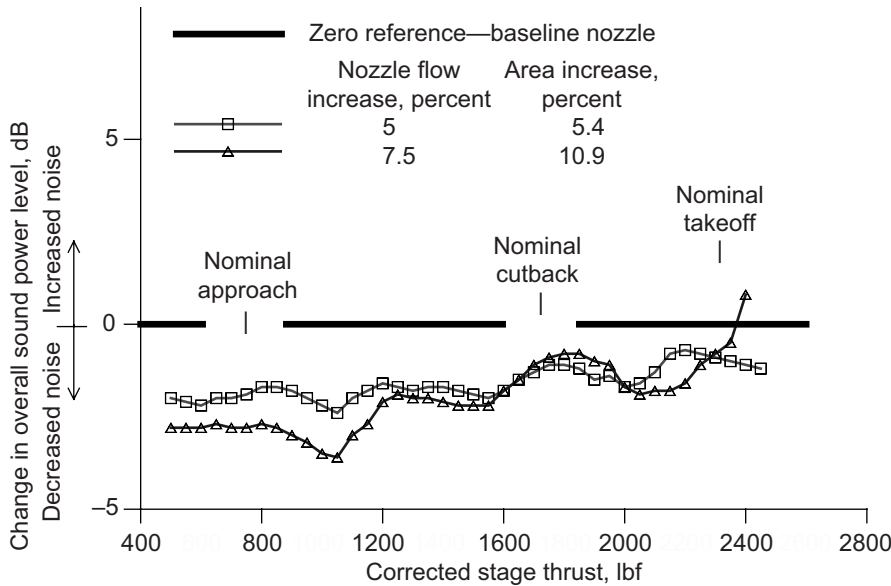
Headquarters program office:

Aeronautics Research

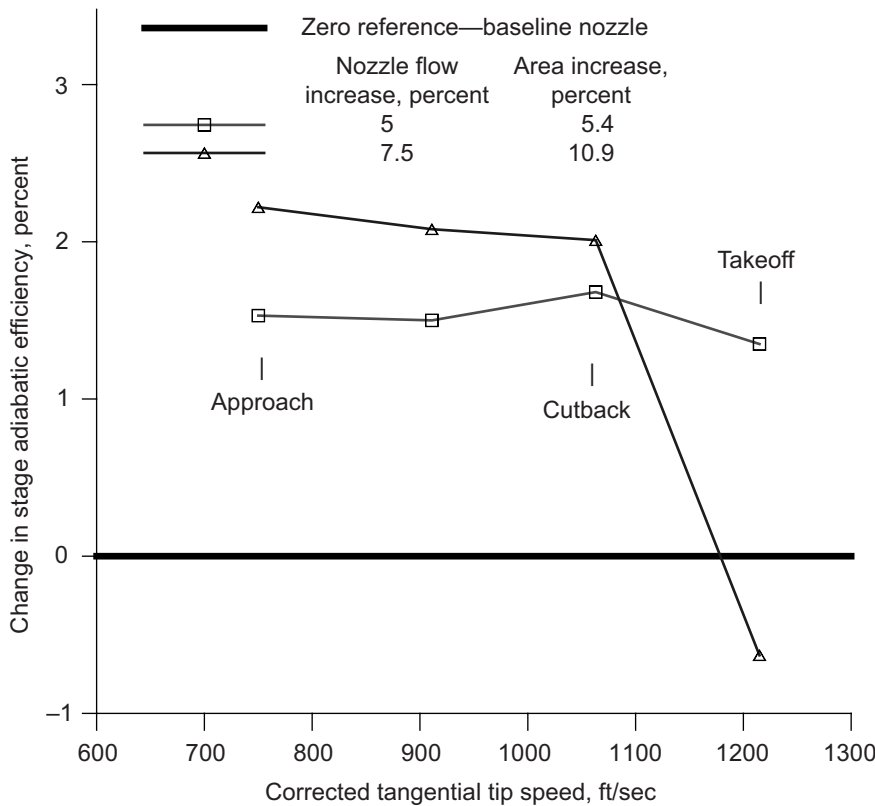
Programs/Projects:

QAT

Turbofan Noise Reduction Associated With Increased Bypass Nozzle Flow



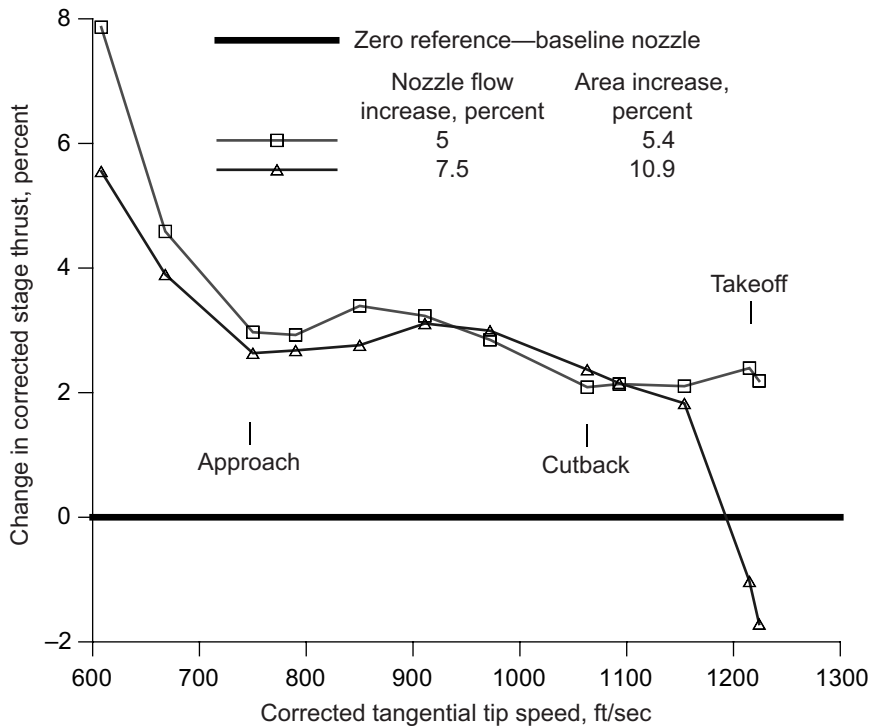
Reduction in overall sound power level with increased nozzle flow as a function of corrected stage thrust.



Change in fan stage adiabatic efficiency with increased nozzle flow as a function of corrected rotor tip speed.

An advanced 22-in. scale model turbofan, typical of a current-generation aircraft engine design by GE Aircraft Engines, was tested in NASA Glenn Research Center's 9-by 15-Foot Low-Speed Wind Tunnel to explore the far-field acoustic effects of an increased bypass nozzle area at simulated aircraft speeds of takeoff, approach, and landing. The wind-tunnel-scale model consisted of the bypass stage fan, stators, and nacelle (including the fan exit nozzle) of a typical turbofan. This fan-stage test was part of the NASA Glenn Fan Broadband Source Diagnostic Test, second entry, which acquired aeroacoustic results over a range of test conditions. A baseline nozzle was selected, and the nozzle area was chosen for maximum performance at sea-level conditions. Two additional nozzles were also tested—one with a 5.4-percent increase in nozzle area over the baseline nozzle (sized for design point conditions), corresponding to a 5-percent increase in fan weight flow, and another nozzle with a 10.9-percent increase in nozzle area over the baseline nozzle (sized for maximum weight flow at sea-level conditions), corresponding to a 7.5-percent increase in fan weight flow. Measured acoustic benefits with increased nozzle area were very encouraging, showing overall sound power level reductions of 2 dB or more (top graph) while the stage adiabatic efficiency (bottom graph) and thrust (graph on the next page) actually increased by several percentage points. These noise-reduction benefits were seen to include both rotor-interaction tones and broadband noise, and were evident throughout the range of measured sideline angles.

These results suggest that, for a typical turbofan engine, a variable-area



Percent change in stage thrust with increased bypass nozzle flow as a function of rotor tip speed.

bypass exhaust nozzle may be an effective way to decrease engine fan-stage noise while increasing aerodynamic performance in terms of adiabatic efficiency and thrust. The baseline fixed-area bypass nozzle in this test was sized for maximum stage performance at sea-level conditions. However, turbofan engine bypass exhaust nozzles are normally sized for maximum

performance at that portion of the aircraft flight profile where most of the flight time is spent—typically at the cruise condition. Increasing the nozzle flow reduced the fan stage noise in this scale model test. Thus, it may be desirable to employ a variable-area engine bypass exhaust nozzle to reduce fan-stage noise levels and optimize performance at all rotor operating speeds. Even the addition of a limited-position variable-area bypass nozzle, to reduce the mechanical complexity and added engine weight of a continuously variable nozzle design, might be an effective retrofit to existing turbofan engines to control fan-stage noise without sacrificing aerodynamic performance.

Glenn contacts:

Richard P. Woodward, 216-433-3923, Richard.P.Woodward@nasa.gov; and Christopher E. Hughes, 216-433-3924, Christopher.E.Hughes@nasa.gov

Authors:

Richard P. Woodward and Christopher E. Hughes

Headquarters program office:

Aeronautics Research

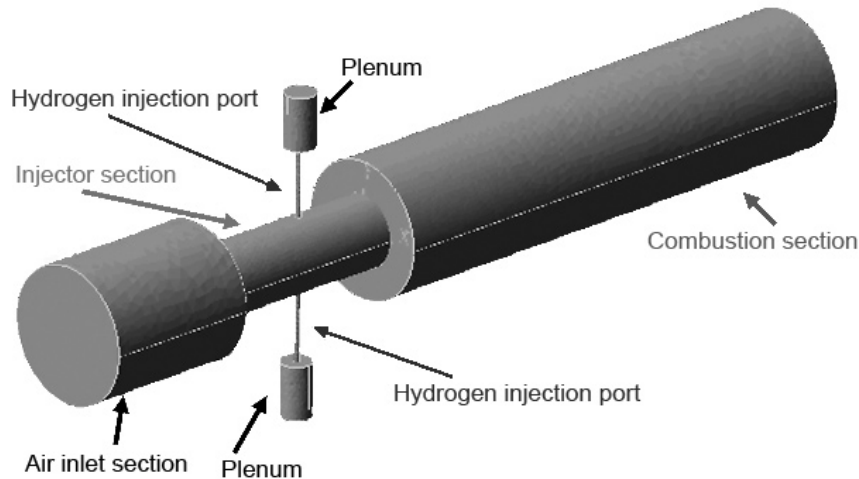
Programs/Projects:

QAT

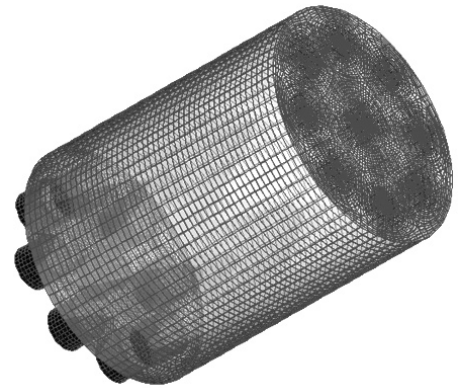
National Combustion Code Used To Study the Hydrogen Injector Design for Gas Turbines

Hydrogen, in the gas state, has been proposed to replace Jet-A (the fuel used for commercial jet engines) as a fuel for gas turbine combustion. For the combustion of hydrogen and oxygen only, water is the only product and the main greenhouse gas, carbon dioxide, is not produced. This is an obvious benefit of using hydrogen as a fuel. The situation is not as simple when air replaces oxygen in the combustion process. (Air is mainly a mixture of oxygen, nitrogen, and argon. Other components comprise a very small part of air and will not be mentioned.) At the high temperatures found in the combustion process,

oxygen reacts with nitrogen, and this produces nitrogen oxide compounds, or NO_x —the main component of atmospheric smog. The production of NO_x depends mainly on two variables: the temperature at which combustion occurs, and the length of time that the products of combustion



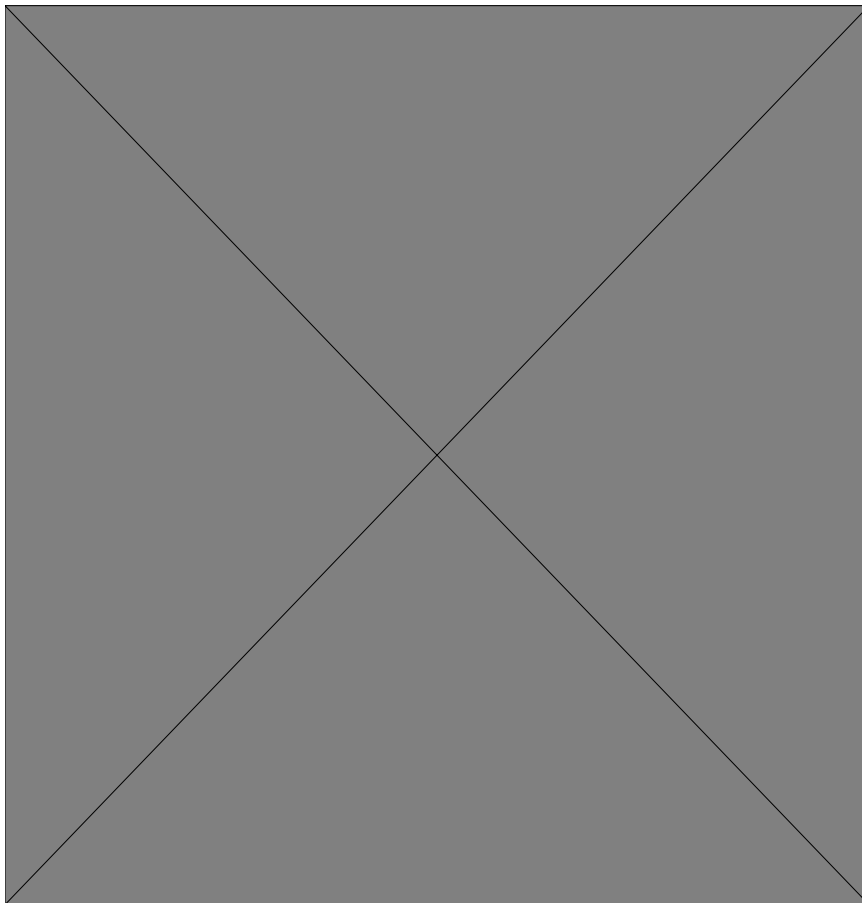
Simplified computational model of a single hydrogen injector used with the NCC.



Computational grid of the multi-injector model used with the NCC. This figure is shown in color in the online version of this article (<http://www.grc.nasa.gov/WWW/RT/2004/RT/RTB-iannetti.html>).

stay, or reside, in the combustor. Starting from a lean (excess air) air-to-fuel ratio, the goal of this research was to minimize hot zones caused by incomplete premixing and to keep the residence time short while producing a stable flame. The minimization of these two parameters will result in low- NO_x hydrogen combustion.

The hardware that actually creates the low- NO_x combustion process is the injector. The National Combustion Code (NCC, ref. 1) was used to conduct numerical studies of hydrogen combustion. The code was enhanced to include a generalized wall function (ref. 2), which represented the underlying injector flow physics better than the original wall function. This research was conducted in three stages: a validation stage (ref. 3), a detailed study of the mixing inside a single injector element (ref. 4), and the study of an array of injector elements. Detailed results were presented about the mixing of fuel and air, flame structures, and combustion species. This numerical information has assisted an ongoing experimental study of hydrogen/air injection concepts. This research effort was an in-house



Temperature contours of the single injector model computed with the NCC. Top: Symmetry plane x. Bottom: Symmetry plane y. This figure is shown in color in the online version of this article (<http://www.grc.nasa.gov/WWW/RT/2004/RT/RTB-iannetti.html>).

effort of NASA Glenn Research Center's Combustion Branch and the Ohio Aerospace Institute (OAI).

References

1. Stubbs, Robert M.; and Liu, Nan-Suey: Preview of the National Combustion Code. AIAA-1997-3114, 1997.
2. Shih, Tsan-Hsing, et al.: Generalized Wall Function for Complex Turbulent Flows. NASA/TM-2000-209936, 2000.
3. Shih, T.-H., et al.: A Study of Hydrogen/Air Combustor Using NCC. AIAA-2001-0808, 2001.
4. Shih, T.-H., et al.: Numerical Study of a Single Hydrogen/Air Gas Turbine Fuel Nozzle. AIAA-2003-4249, 2003.

Find out more about this research:

<http://www.grc.nasa.gov/WWW/combustion/>

Glenn contact:

Anthony C. Iannetti, 216-433-5586,
Anthony.C.Iannetti@nasa.gov

Ohio Aerospace Institute (OAI)

contact:

Andrew T. Norris, 440-962-3071,
Andrew.T.Norris@grc.nasa.gov

Authors:

Anthony C. Iannetti, Tsan-Hsing Shih,
and Andrew T. Norris

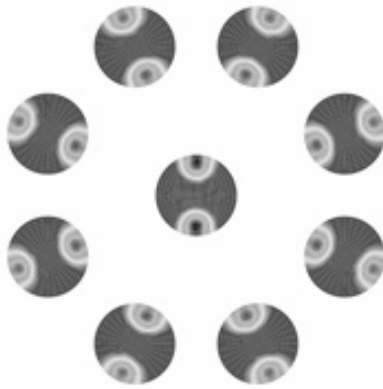
Headquarters program office:

Aeronautics Research

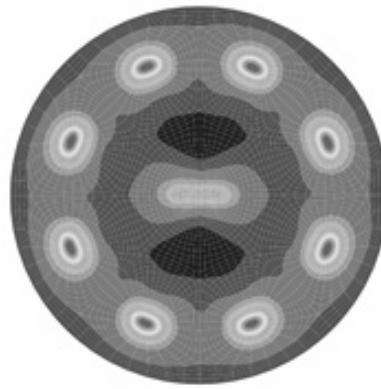
Programs/Projects:

LEAP

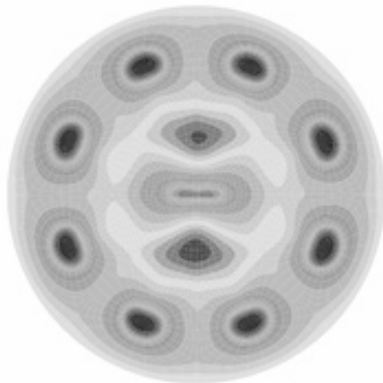
Density (in kg/m³) at inlet



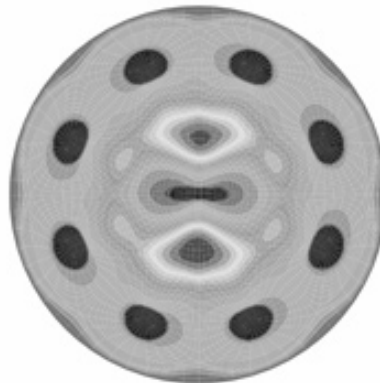
Density (in kg/m³) in combustor



Temperature (in K) at exit



NO_x mass fraction at exit

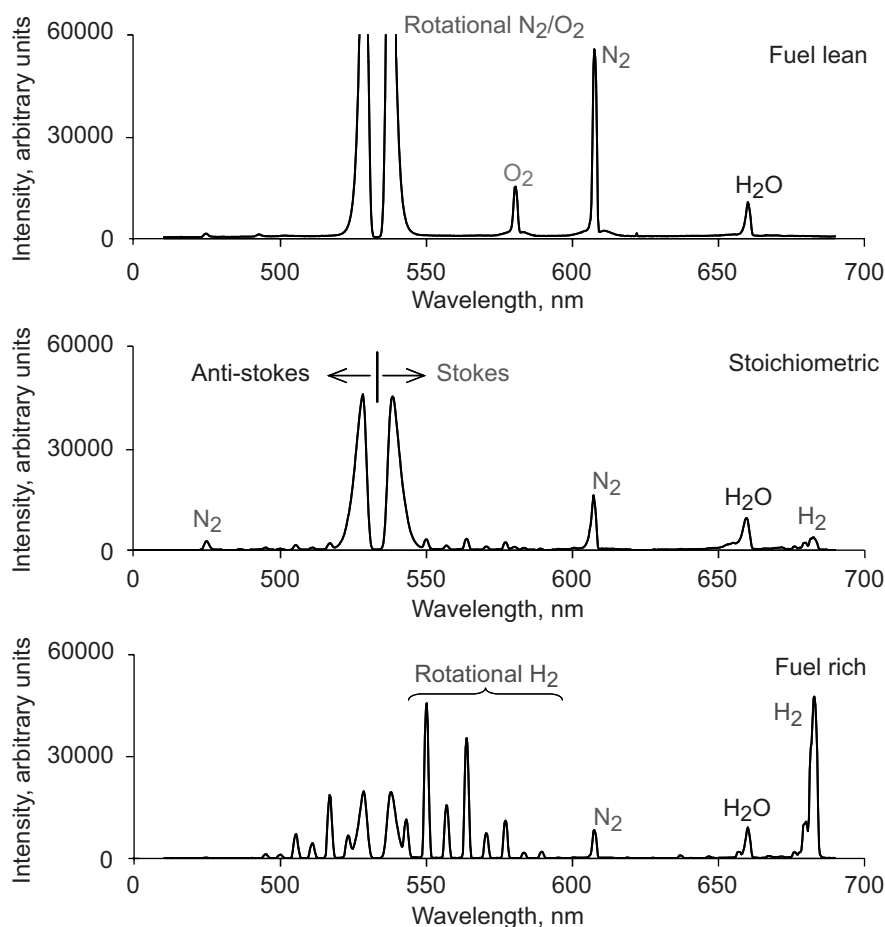


Temperature and NO_x contours computed with the NCC. This figure is shown in color in the online version of this article (<http://www.grc.nasa.gov/WWW/RT/2004/RT/RTB-iannetti.html>).

Transferable Calibration Standard Developed for Quantitative Raman Scattering Diagnostics in High-Pressure Flames

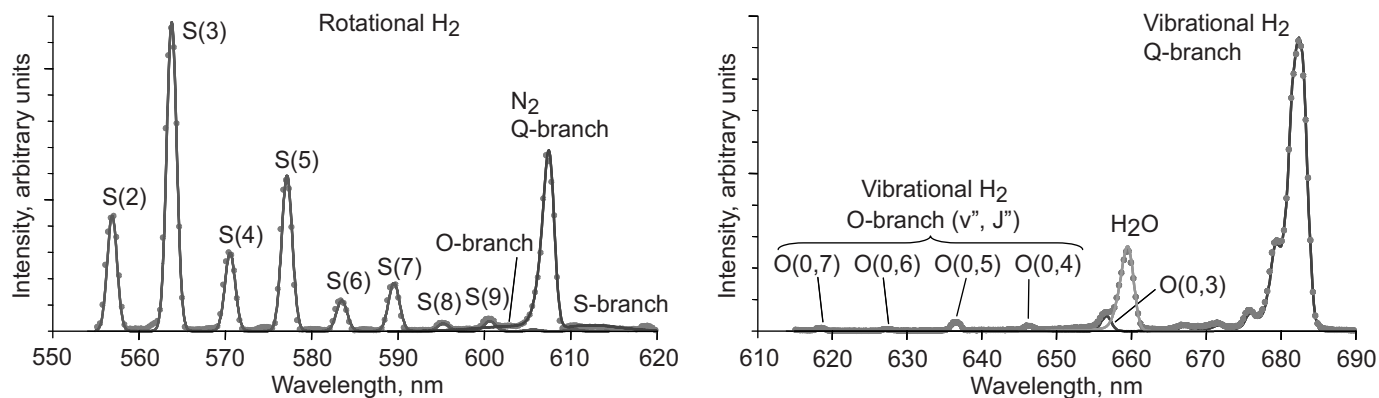
Researchers from NASA Glenn Research Center's Combustion Branch and the Ohio Aerospace Institute (OAI) have developed a transferable calibration standard for an optical technique called spontaneous Raman scattering (SRS) in high-pressure flames. SRS is perhaps the only technique that provides spatially and temporally resolved, simultaneous multiscalar measurements in turbulent flames. Such measurements are critical for the validation of numerical models of combustion. This study has been a combined experimental and theoretical effort to develop a spectral calibration database for multiscalar diagnostics using SRS in high-pressure flames. However, in the

past such measurements have used a one-of-a-kind experimental setup and a setup-dependent calibration procedure to empirically account for spectral interferences, or crosstalk, among the major species of interest. Such calibration procedures, being nontransferable, are prohibitively expensive to duplicate. A goal of this effort is to provide an SRS calibration database using transferable standards that can be implemented widely by other researchers for both atmospheric-pressure and high-pressure (<30 atm) SRS studies. A secondary goal of this effort is to provide quantitative multiscalar diagnostics in high-pressure environments to validate computational combustion codes.

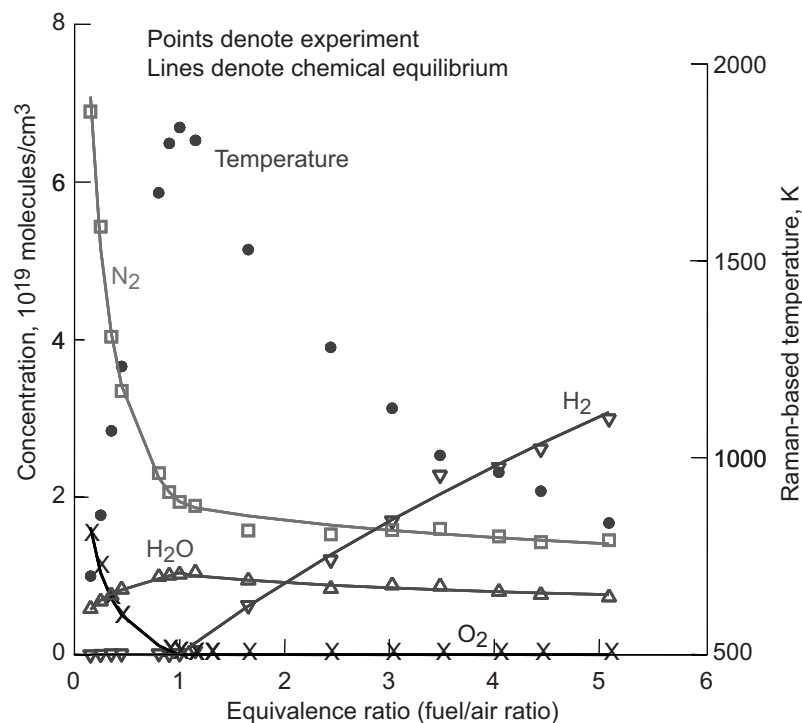


Typical Raman spectra from a 10-atm premixed H₂-air flame at three different equivalence ratios, Φ (from fuel lean, $\Phi = 0.16$, to fuel rich, $\Phi = 4.90$). Note that there is O₂ in the fuel lean data, but not in the fuel rich data, where H₂ appears in large quantities. Data were averaged over 200 laser shots.

To provide quantitative measurements of major species concentration and temperature in high-pressure flames using SRS, researchers must compensate for the spectral interferences, or crosstalk, between different molecular species by using a temperature-dependent calibration matrix. We implement the spectral calibration by using a high-pressure combustion facility that utilizes a specially designed fully premixed gaseous multifuel burner mounted inside a 60-atm pressure vessel that provides optical access for the SRS measurement (refs. 1 to 3). By collecting SRS spectra (400 to 700 nm, with a 0.3-nm resolution) from a variety of high-pressure (10 to 30 atm) hydrogen-fueled flames operating over a wide range of equivalence ratios (see the graphs on this page), we can correlate the pixel-integrated spectral response



Quantitative species concentration and temperature data from a high-pressure (10-atm) hydrogen-air calibration flame obtained using spontaneous Raman scattering. The calibration burner, a novel fully premixed design, was developed especially to provide hot products of combustion that are at chemical equilibrium. The points represent the Raman scattering measurements, and the lines represent the values predicted by chemical equilibrium at the Raman-measured temperature, and are not fits to the data points. These results represent the first use of the newly Glenn-developed transferable standard for Raman scattering in high-pressure flames. This database is unique in its ability to allow other research groups to use Raman scattering as a tool for quantitative measurements in combustion systems.



Comparison of predicted Raman spectra and measurements for a 10-atm ($\Phi = 2.04$) H_2 -air flame. A temperature of 1425 K (obtained from the rotational Raman measurement of H_2) was used for the simulation. Excellent agreement is shown even though no adjustable fitting parameters were used.

from the SRS process to the molecular species densities calculated from the chemical equilibrium. The chemical equilibrium calculations are based on precisely measured (0.5-percent accuracy) fuel-oxidizer flow rates at an assigned temperature and pressure. Since the temperature is measured spectroscopically with an accuracy of better than 10 K, we do not require the assumption of adiabatic equilibrium. The excellent agreement between the data and chemical equilibrium calculations is shown in the top graphs on this page. In addition to the experimental SRS calibration process, we also theoretically model the Raman scattering to quantitatively analyze the spectral interferences (ref. 4). The bottom graph on this page compares the model and experimental data, showing excellent agreement. The spectral modeling aids the development of the calibration matrix functional form, and ultimately, improves the calibration accuracy.

Initially, spectrally simple hydrogen-air flames were used to provide hot combustion products such as nitrogen (N₂), oxygen (O₂), water (H₂O), and hydrogen (H₂) over a wide temperature range. We then moved progressively to more spectrally complicated carbon-containing fuels to include the SRS signals from carbon monoxide and carbon dioxide. Using a technique that we developed previously for the analysis of Raman spectra at high pressures, we determined accurate thermodynamic temperatures and Raman signal intensities for each molecular scattering species in fuel-lean and fuel-rich regions. These intensities were then used to generate the calibration matrix database for all major species and their associated spectral crosstalk effects as a function of temperature (ref. 5). Using this calibration matrix, we could then demonstrate, for the first time, quantitative multispectral measurements of species concentration and temperature in premixed H₂-air flames at 10 atm by using spontaneous Raman scattering in conjunction with a transferable standards calibration database.

References

1. Kojima, Jun; and Nguyen, Quang-Viet: Development of a High-Pressure Gaseous Burner for Calibrating Optical Diagnostic Techniques. NASA/TM—2003-212738, 2003. <http://gltrs.grc.nasa.gov/cgi-bin/GLTRS/browse.pl?2003/TM-2003-212738.html>
2. Kojima, Jun; and Nguyen, Quang-Viet: Measurement and Simulation of Spontaneous Raman Scattering in High-Pressure Fuel-Rich H₂-Air Flames. *Meas. Sci. Tech.*, vol. 15, 2004, pp. 565–580.
3. Nguyen, Q.V.: Disclosure of New Invention and Technology, Fully-Premixed Low-Emissions High-Pressure Multi-Fuel Burner. LEW-17786-1, 2004.
4. Kojima, Jun; and Nguyen, Quang-Viet: Quantitative Analysis of Spectral Interference of Spontaneous Raman Scattering in High-Pressure Fuel-Rich H₂-Air Combustion. *J. Quant. Spectrosc. Radiat. Transfer*, vol. 94, 2005, pp. 439–466.
5. Kojima, J.; and Nguyen, Q.V.: Disclosure of New Invention and Technology (Software), Laser-Raman Spectral Analysis Software for Combustion Diagnostics. LEW-17769-1, 2004.

Glenn contact:

Dr. Quang-Viet Nguyen, 216-433-3574,
Quang-Viet.Nguyen-1@nasa.gov

Ohio Aerospace Institute (OAI) contact:

Dr. Jun Kojima, 440-962-3095,
Jun.Kojima@grc.nasa.gov

Authors:

Dr. Quang-Viet Nguyen and
Dr. Jun Kojima

Headquarters program office:

Aeronautics Research

Programs/Projects:

UEET

Special recognition:

New software technology (LEW-17769-1) developed under this project for the analysis and spectral modeling of Raman scattering received a Software Release Award.

Emissions Measured in the Exhaust of a CFM-56 Engine on a DC-8

A very extensive set of gaseous- and particulate-emissions data from an in-service commercial aircraft engine was obtained by a team of researchers from NASA, the Environmental Protection Agency, and the Department of Defense. The program was led and organized by Dr. Chowen Wey of the UEET Project Office at the NASA Glenn Research Center and was dubbed the Aircraft Particle Emissions eXperiment (APEX). Testing was done at the NASA Dryden Flight Research Center. The main object of APEX was to identify particulate emissions from commercial-aircraft engines.

Measurements were made in the exhaust of a CFM-56 engine on the Dryden DC-8. Two engines were run on three different fuels: (1) JP-8 as the baseline, (2) JP-8 doped for high-sulfur content, and (3) a fuel having relatively high aromatic content. The engines were run over a full range of power settings—including takeoff, climb-out, approach, idle, and several simulated cruise conditions. Two of the four inboard engines were used to maintain torque balance on the aircraft. Two of Glenn's instrument rakes were installed on stands specifically designed for this test and located about 1 and 10 m from the engine-exhaust plane. The 1-m station is shown in the photograph. Each instrument rake

had six particle probes, with probe-tip dilution built in, and six gaseous-sampling probes. The 1-m rake had three additional gas-sampling probes added to either side.

The Glenn contingent measured gaseous emissions by two different methods. The primary gaseous system had standard analyzers, as recommended by the International Commercial Aviation Organization (ICAO) and the Society of Automotive Engineers (SAE). The results from these measurements were used to check engine performance and provided the basis for reducing all the other test data. The other Glenn



Instrument rakes behind the DC-8 engine.

system was composed of a multigas analyzer that is based on the Fourier transform infrared spectroscopy (FTIR) method. This analyzer is being evaluated as a possible alternate method for gaseous-emission measurements. Both analyzer systems were fed the exhaust extracted from gas-sample probes from each stand location.

The gaseous emissions measured in this test compared well with the certification data for the CFM-56. Particulate measurements, taken by two other research groups, contained both volatile and nonvolatile particles. The nonvolatile particles consisted primarily of solid carbon. The volatile particles included sulfur compounds and various organics from the fuel-combustion

process. The volatiles were usually in the vapor state at the engine exhaust plane and tended to condense onto the solid particles in the plume. Other researchers in the test project measured and tracked this process.

This test represents the most thorough exhaust sampling ever conducted, especially for particulate measurements. When this article was written, the data were still being analyzed. Results were reported at the APEX Conference held in Cleveland, Ohio, November 8 to 10, 2004 (ref. 1).

Reference

1. Chwen C. Wey, ed.: Aviation Particle Emissions Workshop. NASA/CP-2004-213398, 2004. <http://gltrs.grc.nasa.gov/cgi-bin/GLTRS/browse.pl?2004/CP-2004-213398.html>

QSS Group, Inc., contact:

Changlie Wey, 216-433-5379,
Changlie.Wey@grc.nasa.gov

Authors:

Paul F. Penko and Changlie Wey

Headquarters program office:

Aeronautics Research

Programs/Projects:

UEET

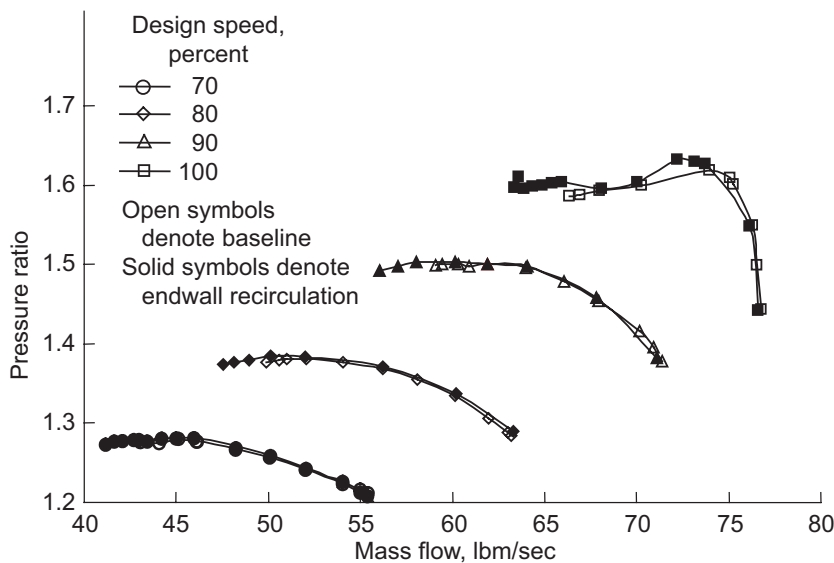
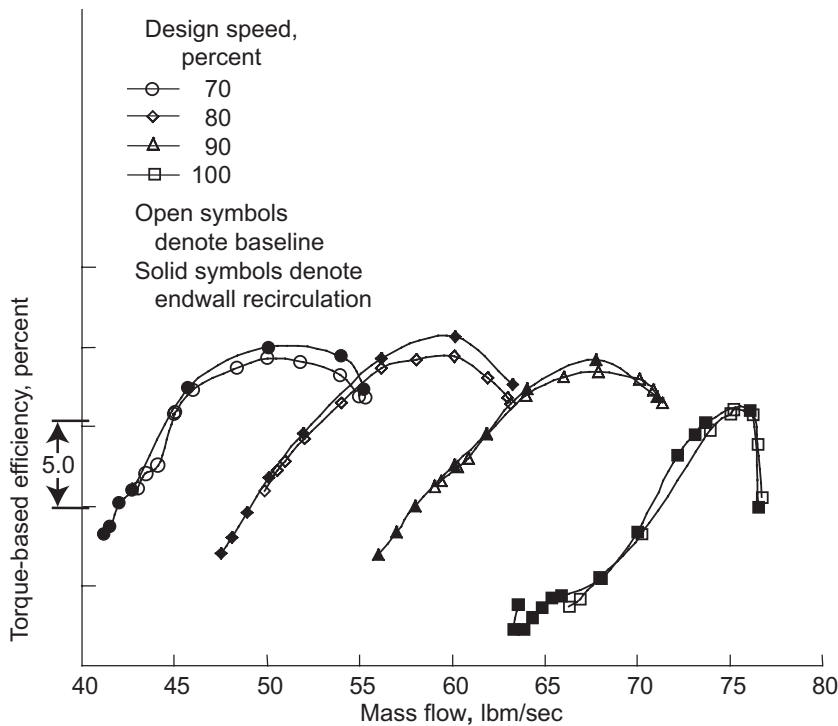
Adaptive Technologies Developed and Demonstrated for Extending the Stable Operating Range of Compressors

The operational envelope of gas turbine engines is constrained by the stability limit of the compression system. The dangers of exceeding this limit are severe, with the potential for engine failure and loss of the aircraft. To avoid such failures, compressor designers provide an adequate stability (stall) margin in the compressor design to account for inlet distortions, degradation due to wear, throttle transients, and other factors that reduce compressor stability from the original design intent. In some cases, the required stall margin results in the compressor operating line being below the

maximum efficiency potential of the compression system. Current approaches to increasing stability tend to decrease the efficiency of the compressor. The focus of this work is to increase the stall margin of compressors without decreasing their efficiency.

Researchers at the NASA Glenn Research Center and the U.S. Army Research Laboratory, Vehicle Technology Directorate, have developed compressor stall-control technologies that have been demonstrated successfully in compressor component tests. These stall-control devices rely on the inherent energy

rise that is imparted by a compressor rotor to recirculate higher energy fluid back to the front of the rotor, thus energizing the low-momentum flow in the rotor casing endwall region that typically sets the stability limits of the compressor. The new concepts have been developed through parametric experimental and computational studies. The technology requires no moving parts and is adaptive because the amount of recirculation depends on the pressure rise across the recirculation path, which is automatically regulated by the rotor work input. Thus, as the compressor is throttled toward stall, the pressure rise across the rotor increases, increasing the driving force across the recirculation path and, thus, the effectiveness of the recirculation in extending the stable operating range of the compressor. The figure compares the pressure-rise characteristics of a transonic fan stage with and without recirculation, showing that the compressor stage operates safely at lower mass flows when recirculation is used. This gain in stable operating range is achieved with no loss in efficiency and by recirculating less than 0.5 percent of the compressor throughflow.



Performance map of NASA Stage 67 showing the extended operating range provided by endwall recirculation stall-control technology.

**U.S. Army Research Laboratory,
Vehicle Technology Directorate at
Glenn contact:**

Dr. Michael D. Hathaway, 216-433-6250,
Michael.D.Hathaway@nasa.gov

Glenn contact:

Dr. Anthony J. Strazisar, 216-433-5881,
Anthony.J.Strazisar@nasa.gov

Authors:

Dr. Michael D. Hathaway and
Dr. Anthony J. Strazisar

Headquarters program office:
Aeronautics Research

Programs/Projects:
UEET, PR&T

Smagglce 2D Version 1.8: Software Toolkit Developed for Aerodynamic Simulation Over Iced Airfoils

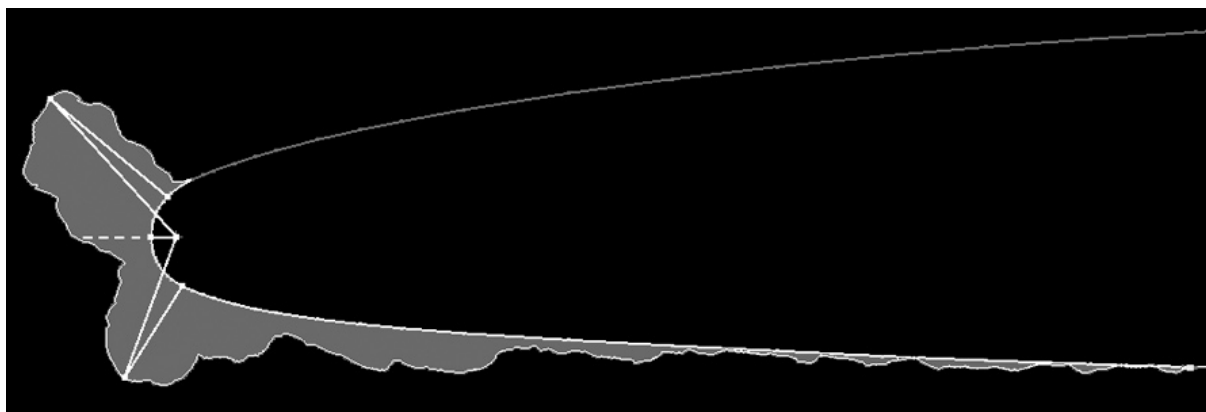
Smagglce 2D version 1.8 is a software toolkit developed at the NASA Glenn Research Center that consists of tools for modeling the geometry of and generating the grids for clean and iced airfoils. Plans call for the completed Smagglce 2D version 2.0 to streamline the entire aerodynamic simulation process—the characterization and modeling of ice shapes, grid generation, and flow simulation—and to be closely coupled with the public-domain application flow solver, WIND. Grid generated using version 1.8, however, can be used by other flow solvers. Smagglce 2D will help researchers and engineers study the effects of ice accretion on airfoil performance, which is difficult to do with existing software tools because of complex ice shapes. Using Smagglce 2D, when fully developed, to simulate flow over an iced airfoil will help to reduce the cost of performing flight and wind-tunnel tests for certifying aircraft in natural and simulated icing conditions.

The following figure shows a sample glaze ice accreted on a business jet airfoil. Smagglce version 1.8 provides tools that (1) examine input data for possible errors (such as tangling introduced during data acquisition), (2) allow users to smooth ice shapes to the level that they desire for their computational fluid dynamics analysis, and (3) control the point density and point distribution over the iced airfoil for grid generation. Ice shapes are numerous, and they affect airfoil performance. Version 1.8 provides tools that measure ice-shape characteristics—such as horn height, angle, and location, and integrated ice area—allowing researchers to examine their effect on aerodynamic performance. Smagglce also allows users to specify the size and location of simple, primitive ice shapes for parametric study.

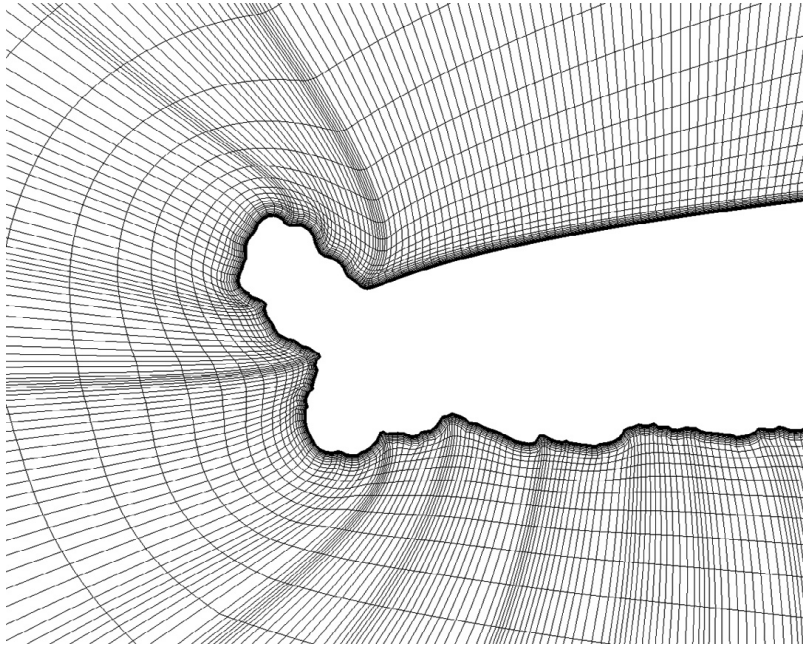
Ice shapes pose difficulty in generating the good-quality grids that are essential for predicting ice-induced complex flow. Version 1.8 provides the tools needed to create high-quality grids. Many tools are uniquely tailored for ice, including

dividing the flow domain into blocks to set up the grid structure prior to grid generation, making changes to the grid-density distribution, and merging and smoothing multiblock grids. The use of a thin, tightly controlled block that wraps around the iced airfoil is an example of a unique feature available for handling difficult ice geometries. The shapes of block edges can be changed with control points by representing the edges as NURBS (Nonuniform Rational B-Splines) curves. The figure on the next page shows a sample grid generated by prerelease Smagglce version 1.8.

To streamline the icing aerodynamic simulation process, developers plan to tie version 2.0 closely to WIND so that users can not only proceed easily from grid generation to flow simulation, but also can graphically overlay the grid on the solution to more effectively modify the grid on the basis of the solution. Details of Smagglce 2D version 1.8 and plans for version 2.0 are reported in reference 1.



Iced airfoil showing ice characteristics: integrated ice area, horn height, and horn angle.



Grid over iced airfoil.

Reference

1. Vickerman, M., et al.: SmagIce: Further Progress in Software for Gridding 2D Iced Airfoils. AIAA-2005-1369, 2005.

Find out more about this research:

<http://icebox-esn.grc.nasa.gov/ext/design/smaggice.html>

Glenn contact:

Mary B. Vickerman, 216-433-5067,
Mary.B.Vickerman@nasa.gov

Authors:

Dr. Yung K. Choo and
Mary B. Vickerman

Headquarters program:

Aeronautics Research

Programs/Projects:

AvSSP

Piloted Flight Simulator Developed for Icing Effects Training

In an effort to expand pilot training methods to avoid icing-related accidents, the NASA Glenn Research Center and Bihle Applied Research Inc. have developed the Ice Contamination Effects Flight Training Device (ICEFTD). ICEFTD simulates the flight characteristics of the NASA Twin Otter Icing Research Aircraft in a no-ice baseline and in two ice configurations simulating ice-protection-system failures. Key features of the training device are the force feedback in the yoke, the instrument panel and out-the-window graphics, the instructor's workstation, and the portability of the unit.

A training curriculum has been developed to familiarize training pilots with the basic flight characteristics of the Twin Otter in no-ice and fully iced configurations so that pilots can compare and contrast the changes in stall and handling characteristics. In addition, a scenario-based lesson is used to demonstrate icing effects during the approach-to-landing segment of a flight. This device

will be used in pilot workshops to demonstrate cues for recognizing iced-airplane handling qualities and the recovery techniques, should a handling anomaly occur.

The ICEFTD demonstrator is the result of 5 years of research and development that (1) explored iced aerodynamic scaling to develop representative aerodynamics at low Reynolds numbers through a series of wind tunnel tests on several scale models of a tailplane airfoil, (2) developed

icing-effects flight-simulation models by conducting wind tunnel tests on a 6.5-percent-scale complete aircraft model, and (3) verified flight-simulation modeling through flight tests of the NASA Twin Otter with simulated ice shapes installed on the wing and tail surfaces. The test techniques and engineering methodology explored in this effort are beneficial to many segments of the aviation industry, from airplane manufacturers to airline operations to pilots who may encounter hazardous icing.

Find out more about this research:

<http://icebox-esn.grc.nasa.gov>

Glenn contacts:

Thomas P. Ratvasky, 216-433-3905,
 Thomas.P.Ratvasky@nasa.gov; and
 Thomas H. Bond, 216-433-3900,
 Thomas.H.Bond@nasa.gov

Author:

Thomas P. Ratvasky

Headquarters program office:

Aeronautics Research

Programs/Projects:

AvSSP, System Wide Accident
 Prevention Project



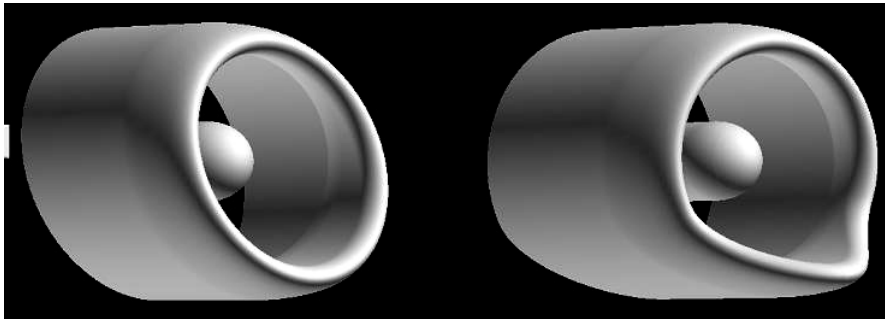
Pilot performing an approach to landing using the Ice Contamination Effects Flight Training Device, with instructor observing pilot reactions.

Subsonic Scarf Inlets Investigated

A computational investigation is underway at the NASA Glenn Research Center to determine the aerodynamic performance of subsonic scarf inlets. These inlets are characterized as being longer over the lower portion of the inlet, as shown in the figure on the next page. One of the key variables being investigated in the research is the circumferential extent of the longer portion of the inlet. The figure shows two specific geometries that are being examined: one in which the length of the inlet transitions from long-to-short over the full 180° from bottom to top, and a second in which the length transitions over 67.5°.

Subsonic scarf inlets are of interest for several reasons. First, extending the lower portion of the inlet has a positive effect on the directional characteristics of the inlet-radiated engine noise. Because of both the geometric barrier of the extension and the resulting internal flow-velocity gradients, the forward-radiating noise

is directed upward and away from the ground, thereby reducing the inlet-radiated flyover noise. In addition, because a scarf inlet draws in more of its air from above than below, the aircraft engine is less likely to ingest any debris that may be present on the runway during takeoff and landing. Finally, the tendency to draw in more airflow from above than below leads to a higher angle-of-attack capability. This characteristic offers the potential for achieving a given angle-of-attack requirement by extending the lower



Subsonic scarf-inlet designs with inlet length transition angles of 180° and 67.5°.

portion of the inlet to form a scarf inlet, rather than by using the traditional approach of increasing inlet thickness.

There are challenges to scarf-inlet design and operation as well. These are most notably obtaining acceptable performance at static conditions, during engine-out climb, and at cruise. These challenges are related to the skewed nature of the incoming airflow and to the “corner” that forms when the length transition angle is less than 180°. This is apparent in the figure for the 67.5° scarf inlet.

Thus far, Glenn researchers have used the three-dimensional WIND computational code described in reference 1 to examine the aerodynamic performance at static, takeoff, and cruise conditions for a whole range of scarf-inlet designs. Scarf-inlet geometric variables that have been investigated include the length of the extension of the lower portion of the inlet, the circumferential extent over which the extension transitions back to the shorter length, and the inlet thickness. Results of the research are given in references 2 and 3 in the form of scarf-inlet performance maps. Additional work is planned

for assessing the limitations of engine-out climb performance and expanding the range of scarf-inlet geometric variables. Computing the acoustic performance of scarf inlets and assessing the tradeoffs between acoustic and aerodynamic performance are long-term goals.

References

1. Bush, R.H.; Power, G.D.; and Towne, C.E.: WIND: The Production Flow Solver of the NPARC Alliance. AIAA-1998-0935, 1998.
2. Abbott, John M.: and Slater, John W.: Computational Study of the Aerodynamic Performance of Three-Dimensional Subsonic Inlets. AIAA-2001-3886, 2001.
3. Abbott, J.: Computational Study of the Aerodynamic Performance of Subsonic Scarf Inlets. AIAA-2004-3406, 2004.

Glenn contact:

John.M. Abbott, 216-433-3607,
John.M.Abbott@nasa.gov

Author:

John M. Abbott

Headquarters program office:

Aeronautics Research

Programs/Projects:

OAT

Parametric Inlet Tested in Glenn’s 10- by 10-Foot Supersonic Wind Tunnel

The Parametric Inlet is an innovative concept for the inlet of a gas-turbine propulsion system for supersonic aircraft. The concept approaches the performance of past inlet concepts, but with less mechanical complexity, lower weight, and greater aerodynamic stability and safety. Potential applications include supersonic cruise aircraft and missiles.

The Parametric Inlet uses tailored surfaces to turn the incoming supersonic flow inward toward an axis of symmetry. The terminal shock spans the opening of the subsonic diffuser leading to the engine. The external cowl area is

smaller, which reduces cowl drag. The use of only external supersonic compression avoids inlet unstart—an unsafe shock instability present in previous inlet designs that use internal supersonic compression. This eliminates the need for complex mechanical systems to control unstart, which reduces weight.



Parametric Inlet mounted in Glenn's 10- by 10-Foot Supersonic Wind Tunnel.

The conceptual design was conceived by TechLand Research, Inc. (North Olmsted, OH), which received funding through NASA's Small-Business Innovation Research program. The Boeing Company (Seattle, WA) also participated in the conceptual design. The NASA Glenn Research Center became involved starting with the preliminary design of a model for testing in Glenn's 10- by 10-Foot Supersonic Wind Tunnel (10x10 SWT). The inlet was sized for a speed of Mach 2.35 while matching requirements of an existing cold pipe used in previous inlet tests. The parametric aspects of the model included interchangeable components for different cowl lip, throat slot, and sidewall leading-edge shapes and different vortex generator configurations. Glenn researchers used computational fluid dynamics (CFD) tools for three-dimensional, turbulent flow analysis to further refine the aerodynamic design.

The mechanical design focused on four key requirements: (1) adhere to the flow-path shape, (2) provide variable geometry for off-design conditions, (3) allow parametric components, and (4) allow rapid changeover of components. These competing requirements led to an unconventional open-top "hull" design. The inlet was split between a top portion containing the motion assembly with moveable ramps and a bottom portion, or hull, consisting of the sidewalls and cowl. This approach allowed the top part to lift off the hull via jackscrews, which exposed components for changeover.

There were eight metered bleed compartments in the region of the inlet throat. To avoid crosstalk between compartments, a custom curtain seal was used.

This seal accommodated the large range of motion of the ramps, whereas the stroke of the inflatable seal edges accommodated the shape change at off-design positions.

The inlet model was fabricated using NASA's Aerospace Test Article Development Cooperative, which split fabrication across five NASA centers. Final assembly and instrumentation were done at Glenn.

The Parametric Inlet underwent 75 hr of testing in Glenn's 10x10 SWT, covering design and off-design conditions. Parameters were varied to reduce spillage and improve performance. A performance level of 92-percent total pressure recovery at a mass-flow ratio of 92 percent was achieved, demonstrating that the concept is a viable alternative to a mixed-compression inlet design. The experimental data are being used to examine the validity of the CFD methods. This will assist in the development of CFD tools for future supersonic inlet design.

Find out more about this research:

Glenn's Inlet Branch:

<http://www.grc.nasa.gov/WWW/Inlet/>

Glenn's Mechanical and Rotating Systems Branch:

<http://www.grc.nasa.gov/WWW/7725/>

Glenn contacts:

Dr. John W. Slater, 216-433-8513, John.W.Slater@nasa.gov;
Dr. David O. Davis, 216-433-8116, David.O.Davis@nasa.gov; and
Paul A. Solano, 216-433-6518, Paul.A.Solano@nasa.gov

Authors:

Dr. John W. Slater, Dr. David O. Davis, and Paul A. Solano

Headquarters program office:

Aeronautics Research

Programs/Projects:

UEET

Special recognition:

Glenn Group Achievement Award,
Glenn Craftsmanship Award

Wind-US 1.0 Released by NPARC Alliance

The NPARC (National Project for Application-oriented Research in CFD) Alliance has released Version 1.0 of Wind-US, the latest in its line of general-purpose, multizone, compressible-flow Navier-Stokes solvers. The NPARC Alliance is a formal partnership between the NASA Glenn Research Center and the Air Force Arnold Engineering Development Center, with additional significant involvement by the Boeing Company's Phantom Works Group, whose mission is to provide an applications-oriented computational fluid dynamics (CFD) system primarily for aerospace flow simulation. The alliance is committed to the long-range maintenance and improvement of this capability, with teams focused on user support, code development, and validation.

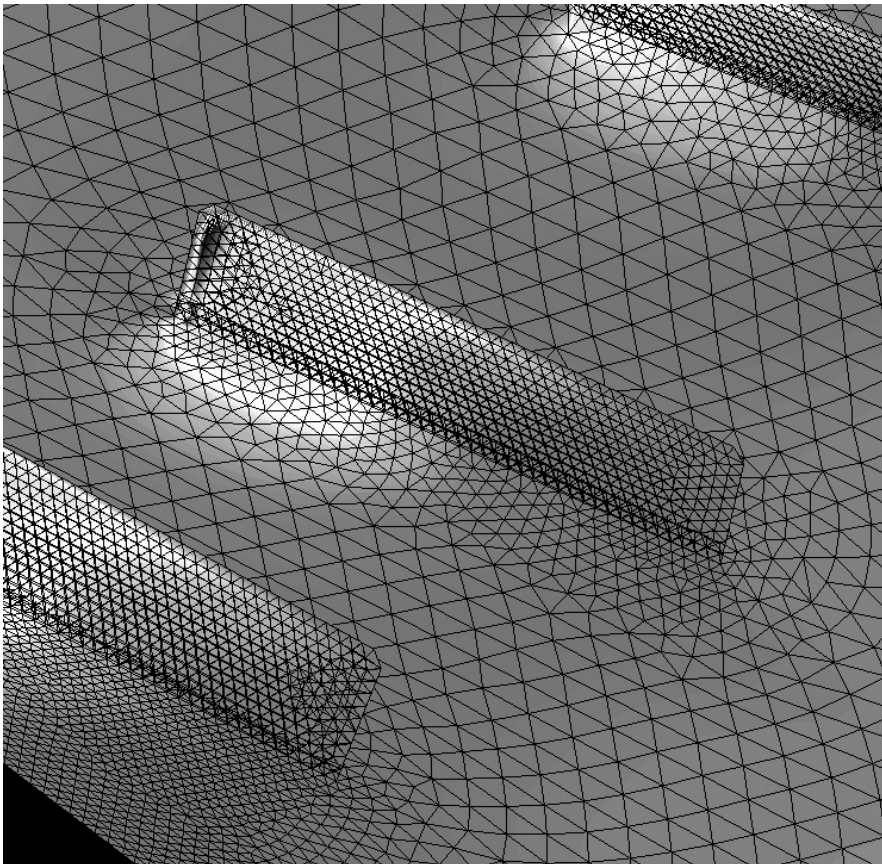
Wind-US now supports unstructured and hybrid structured-unstructured grids, in addition to the widely used structured grid capability in previous Wind versions. The addition of the unstructured and hybrid grid capabilities significantly decreases the time required for surface and volume grid generation, especially for complex geometric configurations.

Wind-US can be used to analyze steady or unsteady flow for a wide range of geometric configurations and over a wide range of flow conditions. A variety of gas models are available, allowing computation of flows with nonperfect gases and chemical reactions. Several turbulence models are available for

Reynolds-averaged Navier-Stokes (RANS) calculations, and a hybrid RANS/LES (large eddy simulation) capability was recently added. Wind-US can be run in serial mode or in a fault-tolerant parallel-processing mode on a multiprocessing system or heterogeneous workstation cluster. In addition to Wind-US itself, a variety of preprocessing and postprocessing tools are included for setting boundary conditions, examining computed results, and other tasks. Computational platforms supported include HP (Hewlett-Packard Company, Palo Alto, CA), SGI (Silicon Graphics, Inc., Mountain View, CA), Sun (Sun Microsystems, Inc., Santa Clara, CA), and Linux.

Extensive Web sites are maintained by the NPARC Alliance, providing code documentation and validation data. The documentation includes user-level manuals describing the operation and use of Wind-US and its associated utilities, and developer-level reference material intended for those interested in modifying or extending the code. The validation site, which contains detailed examples showing the use of Wind-US for a variety of flows and geometries, serves as an archive of analytical, experimental, and computational data suitable for CFD code validation.

All NPARC Alliance software is available free to U.S.-owned companies, public and private universities, and government agencies, for use by U.S. citizens and resident aliens. Instructions for obtaining the code are available at the NPARC Alliance homepage, or from the NPARC Alliance User Support team. Since its initial release in 1998, the Wind code has been acquired by over 300 different organizations, making it one of the most widely used aerospace flow-simulation packages in the United States.



Wind-US unstructured grid computation of surface static pressure in the vicinity of vane effectors in a diffusing S-duct.

Find out more about this research:**NPARC Alliance:**

<http://www.arnold.af.mil/nparc/>

Wind-US documentation:

<http://www.grc.nasa.gov/WWW/winddocs/>

NPARC's CFD Verification & Validation site:

<http://www.grc.nasa.gov/WWW/wind/valid/>

Glenn contacts:

Dr. Charles E. Towne, 216-433-5851, Charles.E.Towne@nasa.gov; and
Dr. Nicholas J. Georgiadis, 216-433-3958, Nicholas.J.Georgiadis@nasa.gov

Author:

Dr. Charles E. Towne

Headquarters program office:

Aeronautics Research

Programs/Projects:

UEET, HPCCP, PR&T

Special recognition:

1999 NASA Software of the Year,
Honorable Mention; 2004 NASA
Software Release Award

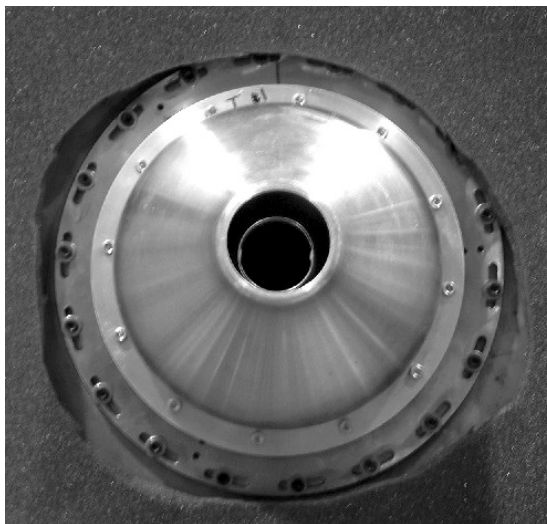
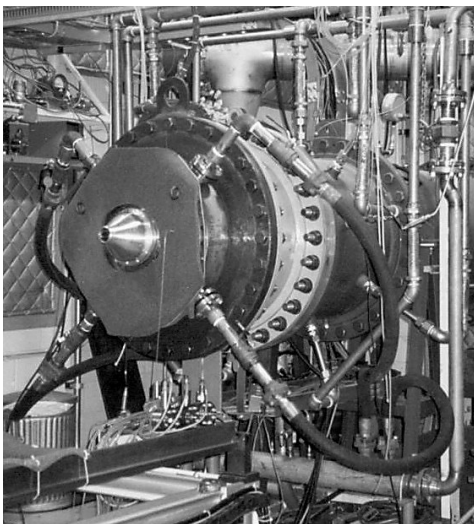
Directional Attenuation of Jet Noise With Eccentric Coannular Nozzle Investigated

Jet noise and flow field were measured to follow up on observations made by Professor D. Papamoschou of the University of California at Irvine (NASA Grant NAG3-2345). When a dual-stream coannular nozzle was arranged nonconcentrically, noise was attenuated significantly on the side where the annulus was thicker (ref. 1). A similar observation was also made in reference 2. The practical significance is obvious. If the bypass flow of a jet exhaust in flight could be diverted to form a thicker layer underneath, then less noise would be heard by an observer on the ground. In view of the current emphasis on jet noise abatement, researchers felt that the effect deserved further attention. This prompted an experiment to confirm the phenomenon in a larger facility and to obtain flow-field data to advance understanding of the mechanism.

The experiment was conducted in an open-jet facility at the NASA Glenn Research Center, shown in the following photographs. The photograph on the right shows a closeup view of the nozzles in the eccentric configuration. The

eccentricity was achieved by placing a beveled gasket at the junction of the outer nozzle and the plenum chamber. The outer nozzle nearly touched the inner nozzle on the narrow side, and the axis of the outer nozzle tilted approximately 2.6° with respect to the axis of the inner nozzle.

Three primary (inner) nozzles were used: one convergent nozzle and two convergent-divergent nozzles with design Mach numbers of 1.3 and 1.5. Each had an exit diameter D_j of 1.485 in. and a lip thickness of



Left: Coannular jet facility. Right: Closeup view of nozzle.

0.030 in. The outer nozzle had an exit diameter D_o of 2.1 in. Thus, the ratio of the primary-to-annular exit area was about 0.92. The annular outer passage was convergent. All data were taken for “cold” flow; that is, the total temperature was constant throughout and equal to that of the ambient temperature. Noise was measured with a microphone located at a distance of about $40 D_j$.

Sound-pressure-level spectra, measured at 25° relative to the downstream jet axis, are compared in this figure for the thicker annulus side of the eccentric configuration and the corresponding concentric configuration. There are data for three inner-jet Mach numbers M_{ji} , as indicated. All data are for an outer-to-inner jet Mach number ratio of approximately 0.5. Clear noise attenuation is observed. The overall sound pressure level dropped by 1.3, 2.0, and 4.9 dB at $M_{ji} = 0.94, 1.3,$ and $1.5,$ respectively. This confirmed the noise attenuation and also the trend that the attenuation increased with increasing jet Mach number. The effect was found to be most pronounced in the direction of peak noise radiation: that is, at shallow angles relative to the jet axis. Further measurements indicated insignificant change in the noise on the thinner annulus side as well as at 90° relative to the jet axis.

Details of the flow field were obtained by pitot-probe and hot-wire surveys. These data showed that the low-speed annular fluid congregated on the thicker annulus side, where a pair of streamwise vortices formed. The flow on that side was also characterized by remarkably low turbulence intensities, commensurate with the observed attenuation in the radiated noise. Further details of this work are provided in reference 3.

References

1. Papamoschou, Dimitri; and Debiasi, M.: Directional Suppression of Noise From a High-Speed Jet. *AIAA J.*, vol. 39, no. 3, 2001, pp. 380–387.
2. Harper-Bourne, Marcus: Physics of Jet Noise Suppression. Proceedings of Jet Noise Workshop, NASA/CP—2001-211152, 2001, pp. 701–719. <http://gltrs.grc.nasa.gov/cgi-bin/GLTRS/browse.pl?2001/CP-2001-211152.html>
3. Zaman, K.: Noise- and Flow-Field of Jets From an Eccentric Coannular Nozzle. AIAA–2004-0005, 2004.

Glenn contacts:

Dr. Khairul B. Zaman, 216–433–5888, Khairul.B.Zaman@nasa.gov; and Dr. James E. Bridges, 216–433–2693, James.E.Bridges@nasa.gov

Author:

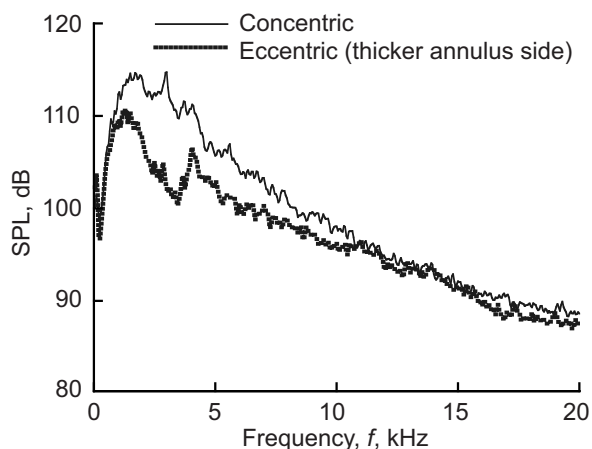
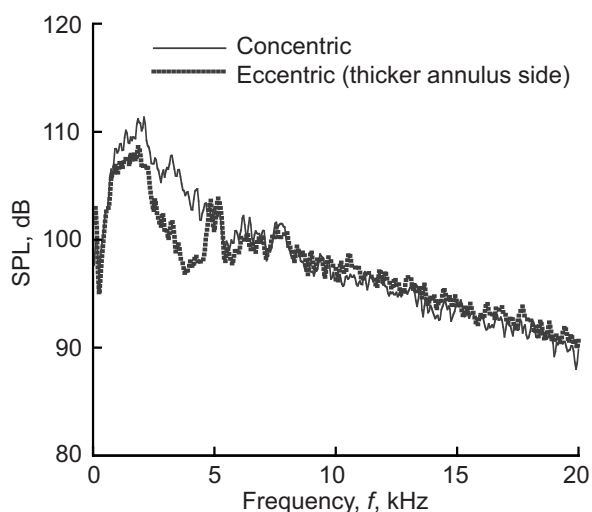
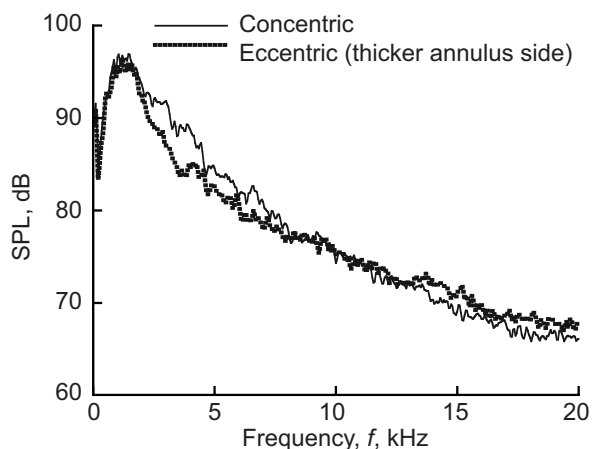
Dr. Khairul B. Zaman

Headquarters program office:

OAT

Programs/Projects:

UEET, QAT



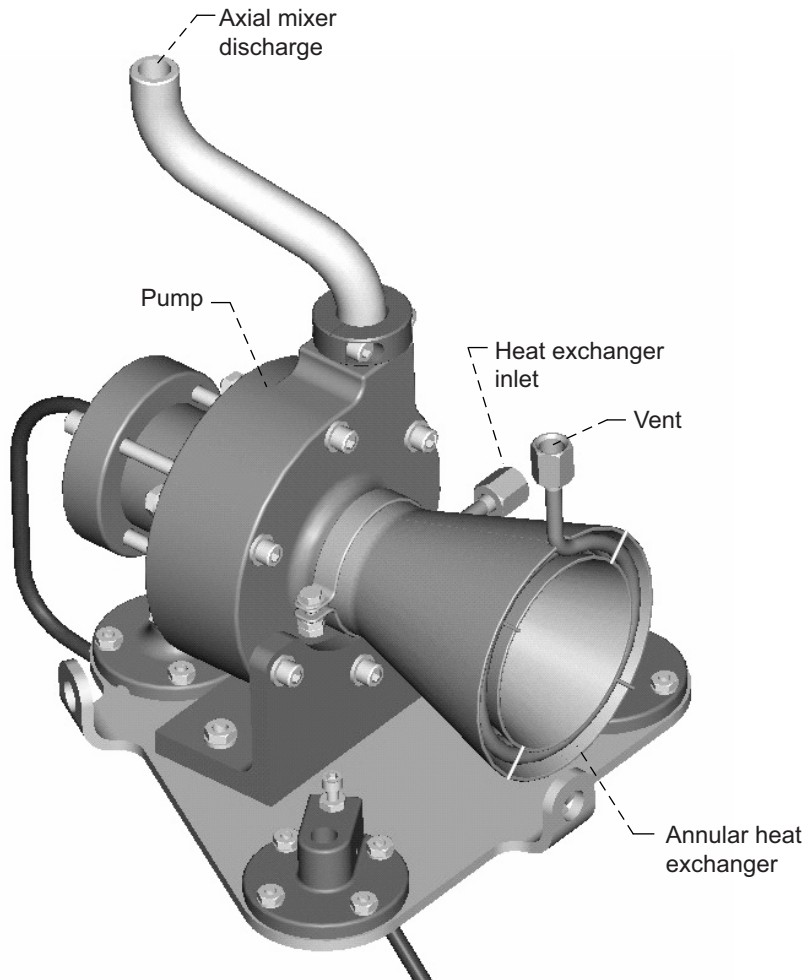
Sound-pressure-level (SPL) spectra at 25° relative to downstream jet axis. Δ OASPL, difference in overall sound pressure level between the concentric and eccentric cases. Top: $M_{ji} = 0.94$; Δ OASPL = -1.30 dB. Center: $M_{ji} = 1.30$; Δ OASPL = -2.00 dB. Bottom: $M_{ji} = 1.50$; Δ OASPL = -4.9 dB.

Pressure Control for Low Earth Orbit Investigated

There is renewed interest in cryogenic oxygen storage for an advanced second-generation orbital maneuvering system and reaction control systems in a low Earth orbit because cryogenic propellants are more energetic and environmentally friendly than current storable propellants. Unfortunately, heat transfer or heat leak into these storage systems increases tank pressure. On Earth, pressure is easily controlled by venting from the gaseous, or ullage,¹

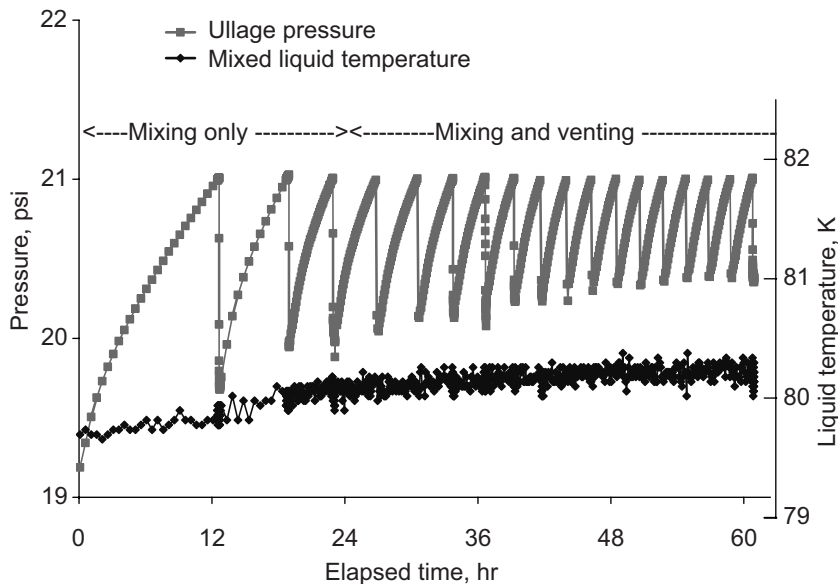
space above the liquid. In low gravity, the location of vapor is unknown and direct venting would expel liquid. Historically, upper stages have used auxiliary thrusters to resettle the tank contents and fix the location of the ullage space in orbit.

Thrusters, however, have weight penalties, and resettling may be required at inopportune times in the mission. An active thermodynamic vent system (TVS), which consists of a Joule-Thomson valve and a heat exchanger coupled with a mixer pump, has been proposed for low gravity. The combination is used to extract thermal energy from the tank fluid, reducing temperature, thus inducing condensation and reducing pressure. At the NASA Glenn Research Center, a pressure-control test was conducted to characterize the TVS concept for orbital cryogenic oxygen storage (ref. 1). A previous TVS test was much simpler and at ambient pressure (ref. 2). A 50-ft³ flight-weight tank was used. It was almost completely surrounded by a cryoshroud in a large vacuum tank. The cryoshroud was used to simulate low-Earth-orbit temperatures. Because mixer operation also caused tank heating, the TVS was sized so that the mixer only operated a small fraction of the time. Initially, the mixer used subcooled liquid to control pressure. After the mixed liquid temperature had risen, venting had to be used to limit further tank temperature increase. Pressure cycles were performed until steady-state operation was demonstrated. The graph on the next page shows the ullage pressure



Centrifugal mixer pump with TVS heat exchanger.

¹The ullage space is the vapor space—the portion of the tank that is not filled with liquid.



Ullage pressure and liquid temperature versus time for the first test run.

and liquid temperature in the middle of the tank for the first test run. Three successful pressure control runs were conducted. Two lower fills had time-averaged vent rates very close to steady-state boiloff rates. Thus, the TVS venting was almost as efficient as the traditional Earth-gravity (1g) vent system for lower tank

fills, and the vent fluid was completely vaporized within the test tank.

References

1. VanOverbeke, Thomas: Thermodynamic Vent System Test in a Low Earth Orbit Simulation. AIAA-2004-3838 (NASA/TM-2004-213193), 2004. <http://gltrs.grc.nasa.gov/cgi-bin/GLTRS/browse.pl?2004/TM-2004-213193.html>
2. Seigneur, Alban D.: Design, Analysis, Fabrication, and Testing of an Active Heat Exchanger for Use in Cryogenic Fluids. MS. Thesis, Cleveland State University, Mar. 1994.

Glenn contact:

Dr. Thomas J. VanOverbeke, 216-433-5867, Thomas.J.VanOverbeke@nasa.gov

Author:

Dr. Thomas J. VanOverbeke

Headquarters program office:

Exploration Systems

Programs/Projects:

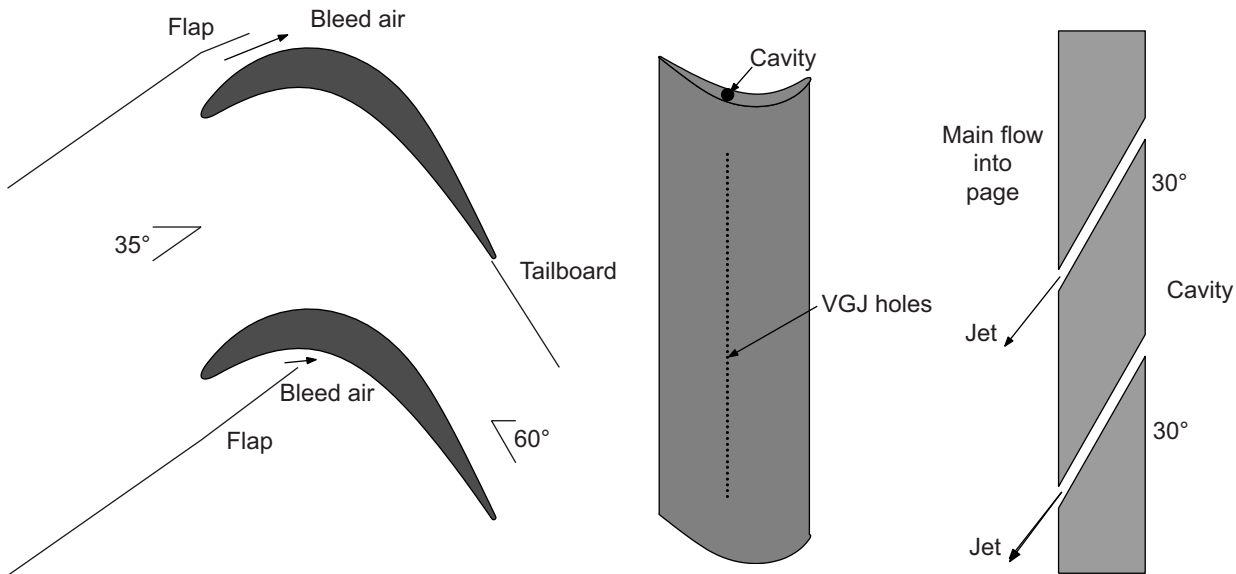
Microgravity Science, In-Space Propulsion, Auxiliary Propulsion

Synthetic Vortex Generator Jets Used to Control Separation on Low-Pressure Turbine Airfoils

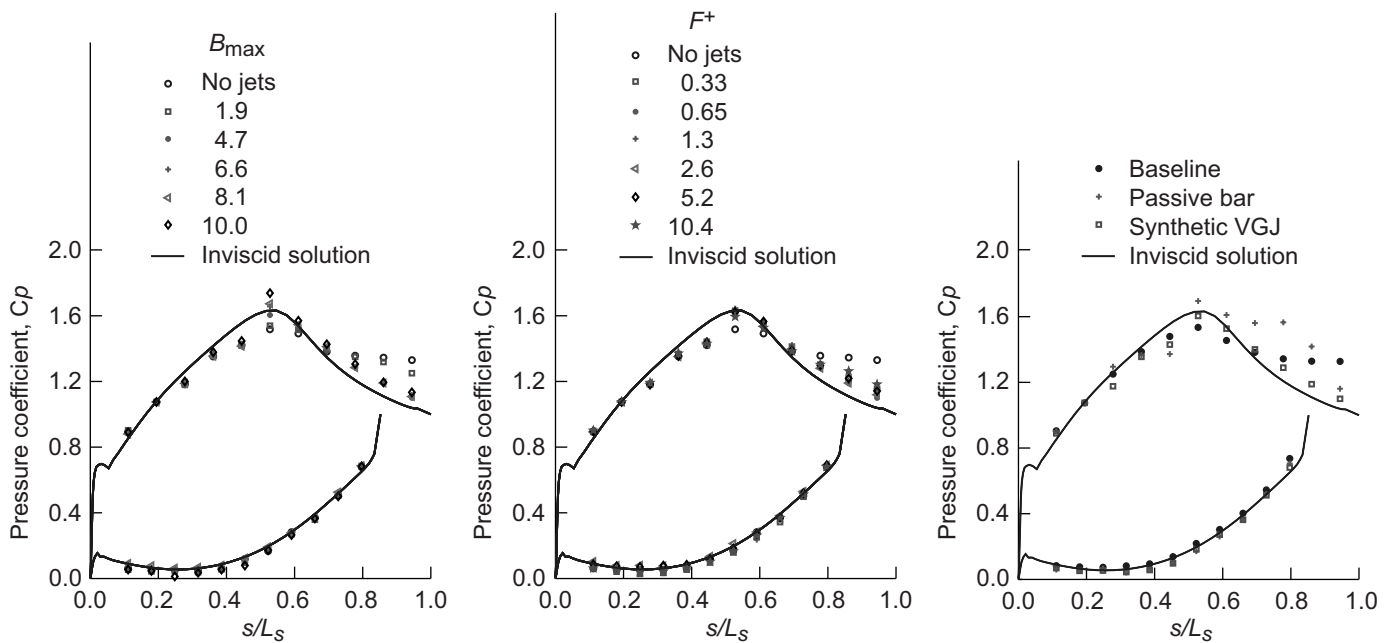
Low-pressure turbine (LPT) airfoils are subject to increasingly stronger pressure gradients as designers impose higher loading in an effort to improve efficiency and lower cost by reducing the number of airfoils in an engine. When the adverse pressure gradient on the suction side of these airfoils becomes strong enough, the boundary layer will separate. Separation bubbles, particularly those that fail to reattach, can result in a significant loss of lift and a subsequent degradation of engine efficiency. The problem is particularly relevant in aircraft engines. Airfoils optimized to produce maximum power under takeoff conditions may still experience boundary layer separation at cruise conditions because of the thinner air and lower Reynolds numbers at altitude. Component efficiency can drop significantly between takeoff and cruise conditions. The

decrease is about 2 percent in large commercial transport engines, and it could be as large as 7 percent in smaller engines operating at higher altitudes. Therefore, it is very beneficial to eliminate, or at least reduce, the separation bubble.

The focus of this research project was the development and experimental study of active separation control



Test setup. Left: Test section. Center and right: Suction-side airfoil with cavity and VGJ's showing full airfoils (center) and cross section of VGJ holes (right).



Pressure coefficient profiles. In each graph, the top line and data points are for the suction surface, and the lower line and data points are for the pressure surface; s , streamwise distance along the suction surface; L_s , wetted surface length of the suction surface. The closer the points are to the inviscid line on the downstream portion of the suction surface, the more effective the flow control is and the smaller the separation bubble is. Left: Effect of blowing ratio, B_{max} , at constant nondimensional frequency, $F^+ = 0.65$. Center: Effect of nondimensional frequency, F^+ , at constant blowing ratio, $B_{max} = 5$. Right: Comparison of baseline (no control), passive bar tripping, and synthetic VGJ with $B_{max} = 4.7$ and $F^+ = 0.65$.

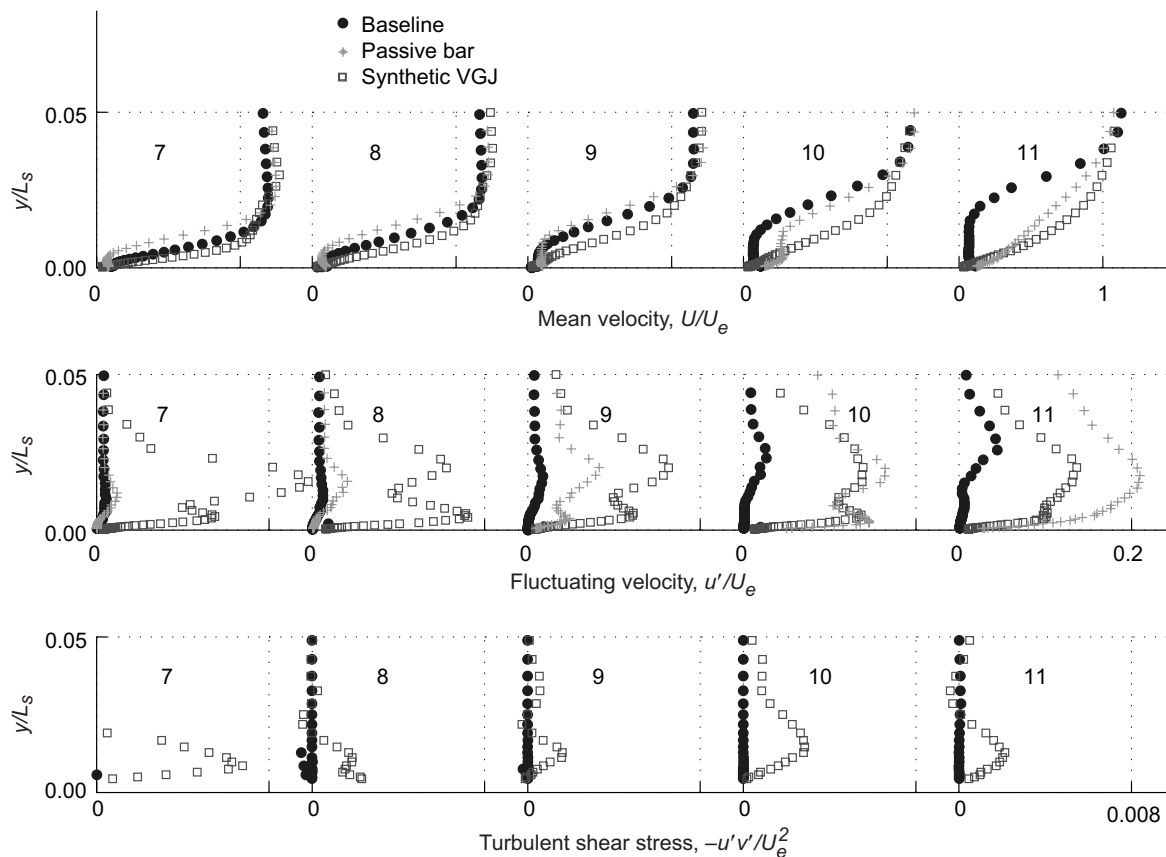
using synthetic vortex generator jets (VGJs). The results demonstrated successful significant reduction of the separation in simulated LPT flow conditions in a wind tunnel, laying the foundation for further development of the technology.

In a fluid-mechanics context, “flow control” means a technology by which a very small input has a very large effect on the flow. In this project, researchers wanted to eliminate or delay flow separation on LPT airfoils by using an active flow-control approach, in which disturbances were dynamically inserted into the flow, interacted with the flow, and led to separation delay. A variety of flow-control devices relevant to flows on aircraft wings and airframes were demonstrated in recent years in the context of external aerodynamics. However, the flow conditions in the LPT are significantly different because there are high levels of free-stream turbulence intensity and very low Reynolds numbers.

The focus of this project was on using a synthetic VGJ for separation control. A VGJ is a small jet that is injected from the surface through a small hole that is slanted relative to the streamwise and spanwise flow direction. It creates a streamwise vortex pair in the flow. The generation of VGJ involves the consumption of supply high-pressure air. In the research described here, a new type of oscillatory VGJ, called a synthetic VGJ, was developed and tested.

The synthetic VGJ is a combination of a device known as a synthetic jet and a steady-flow VGJ; it has the advantage of being a zero-net-mass device that does not consume any supply air.

The experiments were conducted in a wind tunnel that simulates the Reynolds number range of a typical LPT. A spanwise row of synthetic VGJs were incorporated in the surface and powered by a speaker. The measurements included surface pressure measurements using pressure taps and boundary layer velocity and shear stress measurements using hot-wire anemometry along streamwise stations on the suction surface. A range of VGJ oscillation frequencies and blowing velocities was tested.



Dimensionless time-averaged profiles as a function of normalized distance normal to surface, Y/L_s ; comparison of baseline, passive bar, and synthetic VGJ. The inflected profiles in the top graph indicate separation. The fuller profiles with control indicate attached or almost-attached flow.

The results show that the separation bubble was reduced significantly and remained very thin. The losses associated with the separation were substantially reduced in comparison to the baseline case without any flow control and to a passive flow-control device based on tripping with a rectangular bar strip.

This work was performed by Professor Ralph Volino at the U.S. Naval Academy under a contract from the NASA Glenn Research Center. The research is described in detail in reference 1. It is part of an ongoing sponsored and in-house Glenn research activity in the active and passive flow control of LPT flows (refs. 2 to 6).

References

1. Volino, Ralph, J.: Separation Control on Low-Pressure Turbine Airfoils Using Synthetic Vortex Generator Jets. *J. Turbomachinery*, vol. 125, 2003, pp. 765–777.
2. Volino, Ralph, J.: Passive Flow Control on Low-Pressure Turbine Airfoils. *J. Turbomachinery*, vol. 125, no. 4, 2003, pp. 754–764.
3. Tumin, Anatoli; and Ashpis, David E.: Transient Growth Theory Prediction of Optimal Placing of Passive and Active Flow Control Devices for Separation Delay in LPT Airfoils. NASA/TM—2003-212228, 2003. <http://gltrs.grc.nasa.gov/cgi-bin/GLTRS/browse.pl?2003/TM-2003-212228.html>
4. Tumin, Anatoli; and Ashpis, David E.: Optimal Disturbances in Boundary Layers Subject to Streamwise Pressure Gradient. *AIAA J.*, vol. 41, no. 11, 2003, pp. 2297–2299 (also NASA/TM—2003-212288, AIAA–2003–4242). <http://gltrs.grc.nasa.gov/cgi-bin/GLTRS/browse.pl?2003/TM-2003-212288.html>

5. Hultgren, Lennart S.; and Ashpis, David S.: Demonstration of Separation Delay With Glow Discharge Plasma Actuators. AIAA–2003–1025, 2003.
6. Huang, Juang; Corke, Thomas C.; and Thomas, Flint O.: Plasma Actuators for Separation Control of Low Pressure Turbine Blades. AIAA–2003–1027, 2003.

United States Naval Academy contact:

Dr. Ralph J. Volino, 410–293–6520,
volino@usna.edu

Glenn contact:

Dr. David E. Ashpis, 216–433–8317,
Ashpis@nasa.gov

Authors:

Dr. David E. Ashpis and
Dr. Ralph J. Volino

Headquarters program office:

Aeronautics Research

Programs/Projects:

PR&T, UEET

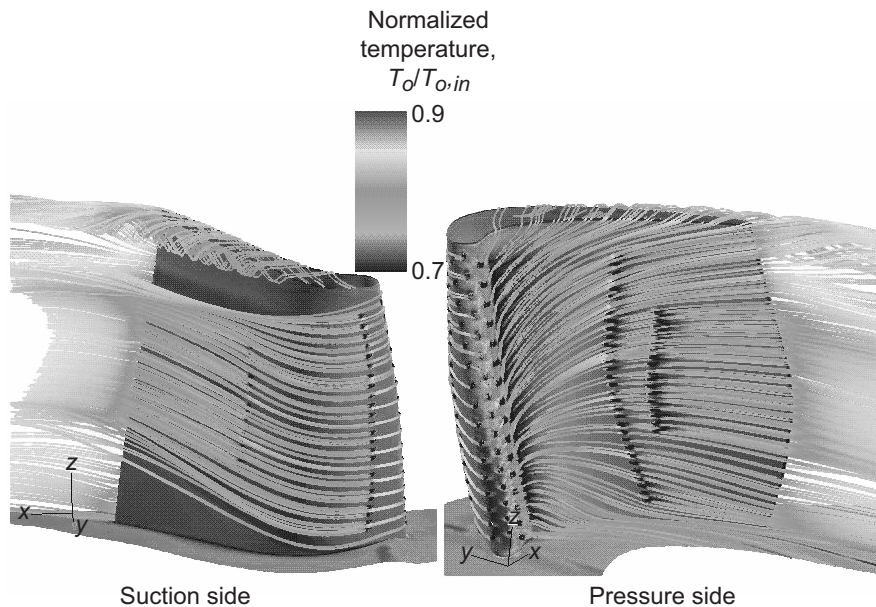
Object-Oriented Version of Glenn-HT Code Released: Glenn-HT2000

NASA Glenn Research Center's General Multi-Block Navier-Stokes Convective Heat Transfer Code (Glenn-HT) has been used extensively to predict heat transfer and fluid flow for a variety of steady gas turbine engine problems. Efforts have focused on turbine heat transfer, where computations have modeled tip clearance, internal coolant, and film cooling flows. Excellent agreement has been achieved for a variety of experimental test cases, and results have been published in over 40 technical publications. The code is available to U.S. industry and has been used by several domestic gas turbine engine companies. The top figure on the next page shows a typical flow solution from the Glenn-HT code for a film-cooled turbine blade.

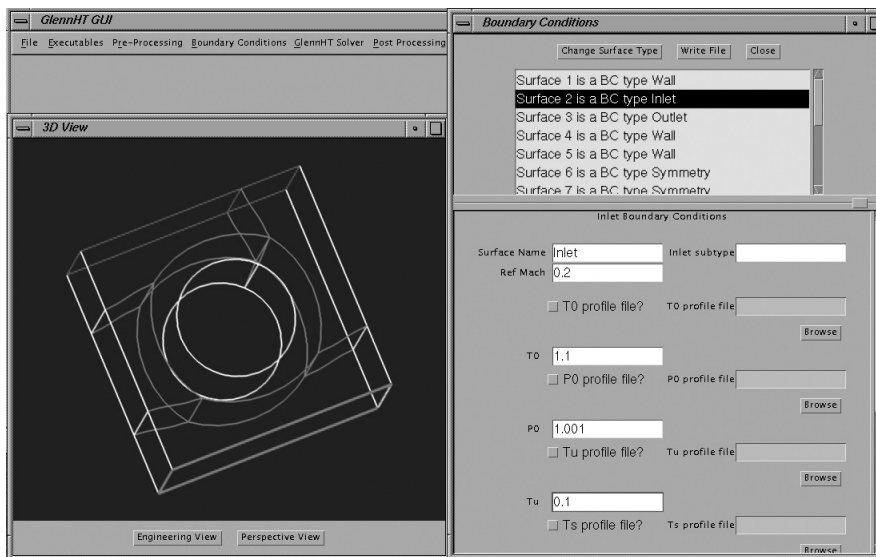
Originally, the Glenn-HT code was written in the Fortran 77 programming language. However, limitations in Fortran 77 restrict the generality of the code. Fortran 90/95 is a more object-oriented language and allows programmers to create code that is more modular and that makes more efficient use of data structures. Recently, the Glenn-HT code was completely rewritten using all the capabilities of the Fortran 90/95 programming language. The result,

Glenn-HT2000, provides dynamic memory allocation, a modular design, unsteady flow capability, and the ability to more easily implement new models and equations into the code.

In an effort to improve computational turnaround time and cost, Glenn's Turbine Branch purchased a 96-processor Linux-based personal-computer cluster to run the Glenn-HT2000 code. As a part of this effort, the Message Passing Interface (MPI) will have to be implemented in the code. MPI will allow the code to run on multiple processors on a distributed memory system, such as the Turbine



Glenn-HT solution for a film-cooled turbine blade. Streamlines, colored by temperature, emanate from holes over the cooled blade surface with a distribution of heat transfer coefficient, h . This figure is shown in color in the online version of this article (<http://www.grc.nasa.gov/WWW/RT/2004/RT/RTT-heidman.html>).



Screen shot from the Glenn-HT graphical user interface.

Branch cluster. Since the trend is toward larger computational problems, the use of many processors, and thus MPI, is very important. The MPI implementation effort is underway, and testing has begun.

In addition to the object-oriented capabilities in the Glenn-HT2000 code, a graphical user interface (GUI) has been produced that allows a user to more easily set up a case. Previously, users had to manually create and edit the various input files necessary for code execution. Although this is generally

sufficient for an expert user, it makes the process somewhat susceptible to errors. Furthermore, it is quite intimidating to new users of the code. The GUI allows users to set up a case by entering information about the case as prompted by the GUI, and it allows some graphical manipulation of the input information. In addition, a saved case can very easily be modified and rerun. The GUI also provides runtime convergence histories and comes packaged with the Java Runtime Environment for Linux and Unix systems. The bottom figure shows a screen shot from the GUI.

Future plans call for the application of the new Glenn-HT2000 code to a range of gas turbine engine problems of current interest to the heat transfer community. The new unsteady flow capability will allow researchers to predict the effect of unsteady flow phenomena on the convective heat transfer of turbine blades and vanes. Work also will continue on the development of conjugate heat transfer capability in the code, where convective and conductive heat transfer domains can be solved simultaneously. Finally, advanced turbulence and fluid flow models and automatic gridding techniques being developed within Glenn's Turbine Branch will be applied to the Glenn-HT2000 code and solution process.

Find out more about this research:
<http://www.grc.nasa.gov/WWW/TURBINE/Turbine.htm>

Glenn contact:
 Dr. James D. Heidmann, 216-433-3604,
 James.D.Heidmann@nasa.gov

Authors:
 Dr. James D. Heidmann, Dr. Ali A. Ameri,
 Dr. David L. Rigby, Dr. Vijay K. Garg,
 John C. Fabian, Barbara L. Lucci, and
 Dr. Erlendur Steinthorsson

Headquarters program office:
 Aeronautics Research

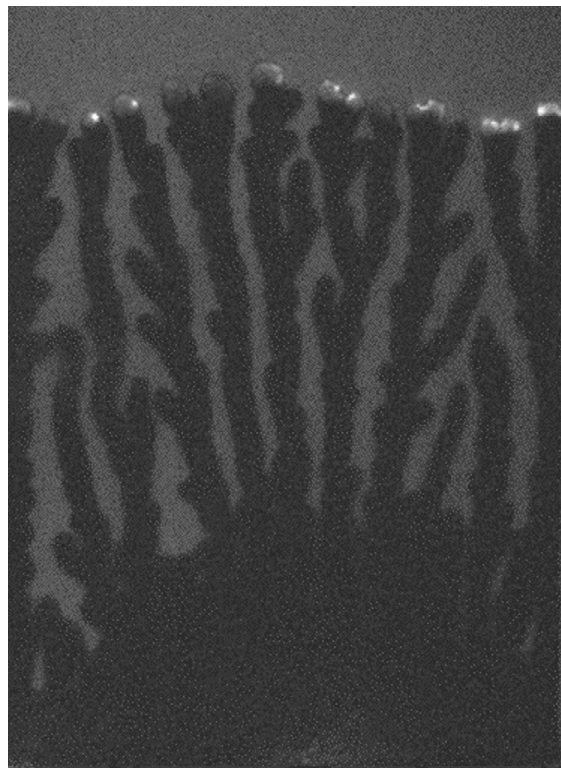
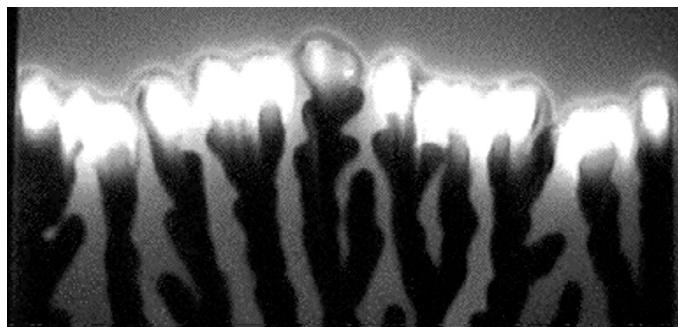
Programs/Projects:
 PR&T, UEET, RTA

Microgravity

New Species of Fire Discovered: Fingering Flamelets Form a Dynamic Population

“To me the fire is a splendid metaphor for life. Sometimes raging and fervent, sometimes glowing softly and evenly, other times reduced to struggling embers.”

—Jean Carnahan



Left: At the end of the test, the airflow is increased to see if the flamelets can be blown out. Instead, they flare up and remerge into a full flame front. Right: Green light illuminates the end of a fingering flame spread test, revealing the black char fingering patterns left behind on the paper once the flame breaks into flamelets. The black (bottom) section of the sample was entirely consumed during flame spread prior to airflow ramp down. As the airflow was reduced (air came from the top to the bottom of the image), the flame became starved for oxygen and broke into flamelets that survived by drawing oxygen from the sides as well as the front. The blue flamelets at the tips of the “fingers” formed a dynamic population that reproduced through bifurcation (branches in the black fingers) and died through quenching extinction (end of black fingers). The steady-state size that the population reached depended on how much oxygen was provided. In this case, the airflow was 2 cm/sec past the sample and the population was about 13. This figure is shown in color in the online version of this article (<http://www.grc.nasa.gov/WWW/RT/2004/RU/RUC-olson.html>).

Poets and artists have long used fire as a metaphor for life. At the NASA Glenn Research Center, recent experiments in a subcritical Rayleigh number flow channel demonstrated that this analogy holds up surprisingly well when tools developed to characterize a biological population are applied to a class of fire that occurs in near-extinction, weakly convective environments (such as microgravity) or in vertically confined spaces (such as our apparatus). Under these conditions, the flame breaks into numerous “flamelets” that form a Turing-type reaction-diffusion fingering pattern as they spread across the fuel.

It is standard practice on U.S. spacecraft for the astronaut crew to turn off the ventilation to help extinguish a fire, both to eliminate the fresh oxygen supply and to reduce the distribution of the smoke. When crew members think that the fire is fully extinguished, they reactivate the ventilation system

to clear the smoke. However, some flamelets can survive, and our experiments have demonstrated that flamelets quickly grow into a large fire when ventilation increases.

A similar event already happened aboard Russia's Mir space station on October 15, 1994. Cosmonaut Valery Polyakov was the first to reach a small fire and put it out using a jumpsuit belonging to crewmate Yuri Malenchenko. Later, however, the cosmonauts discovered that the jumpsuit was still burning and the flames had burned a hole through the chest area of the suit. Had the crew not noticed this fire, it could have grown undetected into a large damaging fire.

Because of the apparently fractal nature of this phenomenon, enhanced understanding of centimeter-scale fingering flame spread may be relevant not only to spacecraft fire safety, but to kilometer-scale fingering wildfire spread on Earth. The fractal nature of wildfire burn patterns has been noted. It also has been noted that the least damaging wildfires are those that burn in a mosaic pattern that leaves many random, irregular unburned fingers and islands. A better understanding of the dynamics of these kinds of fires could help control prescribed burns to achieve the desired mosaic burn patterns that appear to benefit both flora and fauna.

Flamelets form a dynamic population whose members interact competitively for the limited available oxygen. They reproduce through bifurcation and die either at the birth of the next generation or through extinction without bifurcation. Flamelets show many of the characteristics found in biological populations, such as a Type II age structure and a uniform pattern of dispersion. We utilized the continuous logistic model with a time lag to describe the flamelet population growth and fluctuation around a stable population characterized by the carrying capacity based on environmental limitations. This flame "adaptation" to adverse environmental conditions extends the flammability range to lower opposed flow velocities, lower oxygen concentrations, or higher heat loss by increasing the multidimensionality of the flame and, thus, enhancing oxygen transport to the flame zone.

Soldering Tested in Reduced Gravity

Whether used occasionally for contingency repair or routinely in nominal repair operations, soldering will become increasingly important to the success of future long-duration human space missions. As a result, it will be critical to have a thorough understanding of the service characteristics of solder joints produced in reduced-gravity environments. The National Center for Space Exploration Research (via the Research for Design program), the NASA Glenn Research Center, and the NASA Johnson Space Center are conducting an experimental program to explore the influence of reduced-gravity environments

Bibliography

Olson, Sandra; Miller, Fletcher; and Wichman, Indrek: Characteristics of the Flamelet Regime of Flame Spread. Presented at the 2005 Joint Meeting of the U.S. Sections of the Combustion Institute, Philadelphia, PA, Mar. 2005.

Olson, S.L.; Miller, F.J.; and Wichman, I.S.: Describing Near-Limit Flamelet Fingering Behavior Using Bio-Mathematical Population Models. Presented at the Fourth International Symposium on Scale Modeling, Cleveland, OH, Sept. 2003.

Find out more about this research:

Analysis of Thermal and Hydrodynamic Instabilities in Near-limit Atmospheres (ATHINA):

http://microgravity.grc.nasa.gov/combustion/athina/athina_index.htm

Exploring Limits in Microgravity—ATHINA videos:

http://exploration.grc.nasa.gov/combustion/web/vid_athina.htm

Glenn contact:

Dr. Sandra L. Olson, 216-433-2859, Sandra.L.Olson@nasa.gov

Authors:

Dr. Sandra L. Olson, Fletcher J. Miller, and Indrek S. Wichman

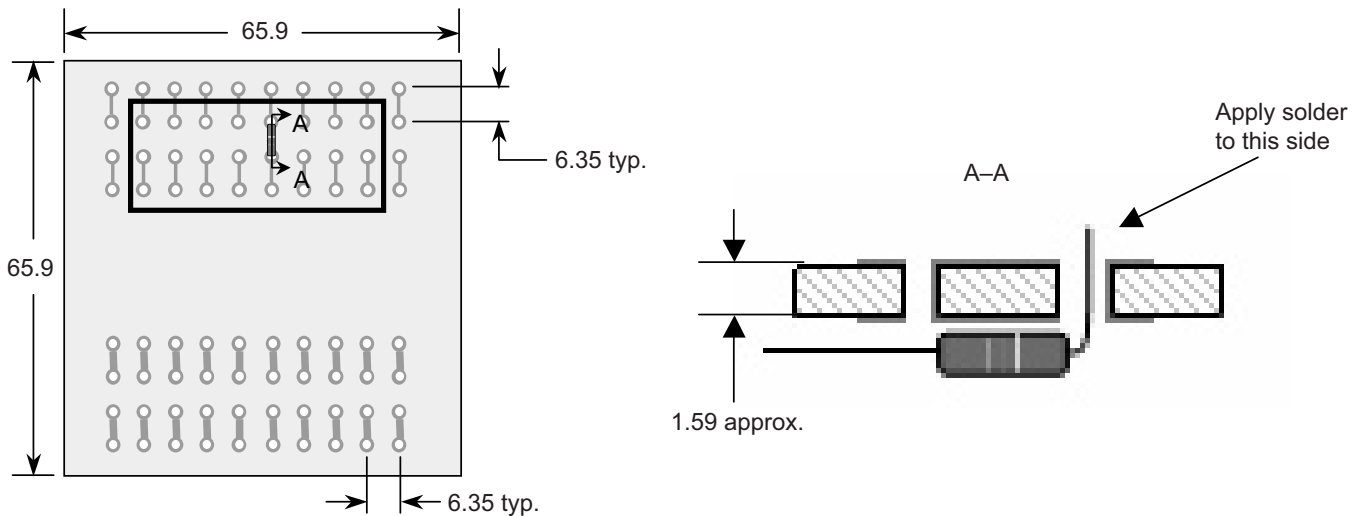
Headquarters program office:

Exploration Systems

Programs/Projects:

Microgravity Science

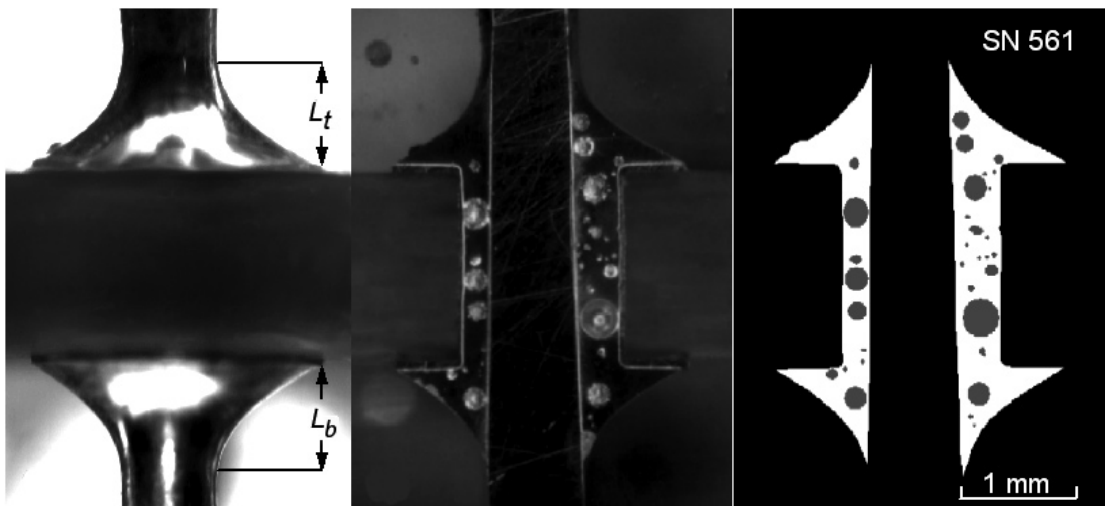
on the soldering process. Solder joint characteristics that are being considered include solder fillet geometry, porosity, and microstructural features. Both through-hole (see the drawing and image on the top figure on the next page) and surface-mounted devices are being investigated. This



Plated through-hole sample configuration used during reduced-gravity testing. All dimensions are given in millimeters.

effort (the low-gravity portion being conducted on NASA's KC-135 research aircraft) uses the soldering hardware currently available on the International Space Station. The experiment involves manual soldering by a contingent of test operators, including both highly skilled technicians and less skilled individuals to provide a skill mix that might be encountered in space mission crews. The experiment uses both flux-cored solder and solid-core solder with an externally applied flux. Other experimental parameters include the type of flux, gravitational level (nominally zero, lunar, or Martian gravity), and circuit-board moisture. Postflight analysis done jointly at Glenn and Johnson consists

of a visual inspection, photography, and leg-length measurements (L_t and L_b in the left image below) of the soldered joints. The cross sections of the joints are prepared and examined using standard metallographic techniques to obtain porosity measurements (see the center image below). A custom computer program



Images of joints after soldering in reduced gravity. Solder was applied to the top of the solder joint as oriented in the images. Left: Prior to cross sectioning. Center: After cross sectioning. Right: After computer analysis. This joint shows significant subsurface voids (18.8-percent porosity).

developed at Glenn assisted in a manual measurement of the pore area as seen in the right image at the bottom of the preceding page. Using these data, Glenn researchers calculated the percentage of porosity exposed by dividing the voided (porous) areas by the total two-dimensional area of the joint cross section. For example, the right image has a porosity of 18.8 percent.

To date, this experiment has generated 1347 solder samples in the through-hole configuration, including 938 low-gravity samples (including some partial-gravity samples) and 409 normal-gravity samples. Testing was performed during 8 flight-weeks of the KC-135 at Glenn and used seven test operators. Findings to date (refs. 1 to 4) indicate significant increases in joint porosity and changes in joint geometry in reduced-gravity environments. These changes may reduce the joint service life. Techniques are being considered to mitigate these increases in porosity. Also, a Space-station Detailed Test Objective (SDTO) has been accepted for flight aboard the space station to verify these effects on orbit.

References

1. Pettegrew, Richard D., et al.: Experimental Methods in Reduced-Gravity Research. NASA/TM—2002-211993, 2002. <http://gltrs.grc.nasa.gov/cgi-bin/GLTRS/browse.pl?2002/TM-2002-211993.html>
2. Pettegrew, R.D., et al.: Gravitational Effects on Solder Joints. *Welding J.*, vol. 82, no. 10, 2003, pp. 44–48. <https://www.aws.org/wj/oct03/feature.html>
3. Struk, Peter M., et al.: The Effects of an Unsteady Reduced Gravity Environment on the Soldering Process. NASA/TM—2004-212946 (AIAA-2004-1311), 2004. <http://gltrs.grc.nasa.gov/cgi-bin/GLTRS/browse.pl?2004/TM-2004-212946.html>
4. Struk, Peter M., et al.: The Influence of Gravity on Joint Shape for Through-Hole Soldering. NASA/TM—2005-213589 (AIAA-2005-0541), 2005. <http://gltrs.grc.nasa.gov/cgi-bin/GLTRS/browse.pl?2005/TM-2005-213589.html>

Find out more about this research:
<http://www.ncmr.org/r4d/>

Glenn contact:
Peter M. Struk, 216-433-5948,
Peter.M.Struk@nasa.gov

National Center for Space Exploration Research (NCSER) contact:
Richard D. Pettegrew, 216-433-8321,
Richard.D.Pettegrew@grc.nasa.gov

Authors:
Peter M. Struk, Richard D. Pettegrew,
J. Kevin Watson, Robert S. Down, and
Daniel R. Haylett

Headquarters program office:
Exploration Systems

Programs/Projects:
Microgravity Science

Special recognition:
An article featured in *Welding Journal* (Oct. 2003), "Gravitational Effects of Solder Joints," was based on our paper (Richard Pettegrew, Dan Haylett, Robert Downs, Peter Struk, and Kevin Watson) presented at the 2003 International Brazing and Soldering Conference. That paper was selected for one of two Outstanding Paper awards. The *Welding Journal* article reviews our recent effort to understand how the traditional manual soldering process is affected by reduced gravity.

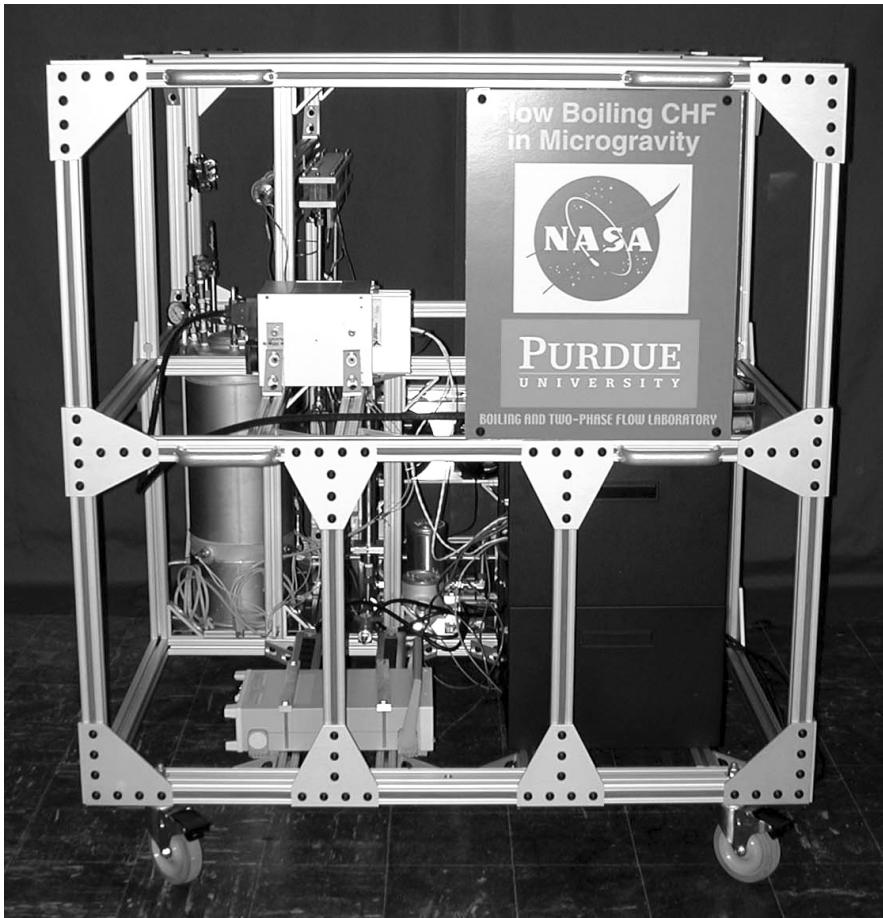
Flow-Boiling Critical Heat Flux Experiments Performed in Reduced Gravity

Poor understanding of flow boiling in microgravity has recently emerged as a key obstacle to the development of many types of power generation and advanced life-support systems intended for space exploration. The critical heat flux (CHF) is perhaps the most important thermal design parameter for boiling systems involving both heat-flux-controlled devices and intense heat removal. Exceeding the CHF limit can lead to permanent damage, including physical burnout of the heat-dissipating device. The importance of the CHF limit creates an urgent need to develop predictive design tools to ensure both the safe and reliable operation of a two-phase thermal management system under the reduced-gravity (like that on the Moon and Mars) and microgravity environments of space. At

present, very limited information is available on flow-boiling heat transfer and the CHF under these conditions.

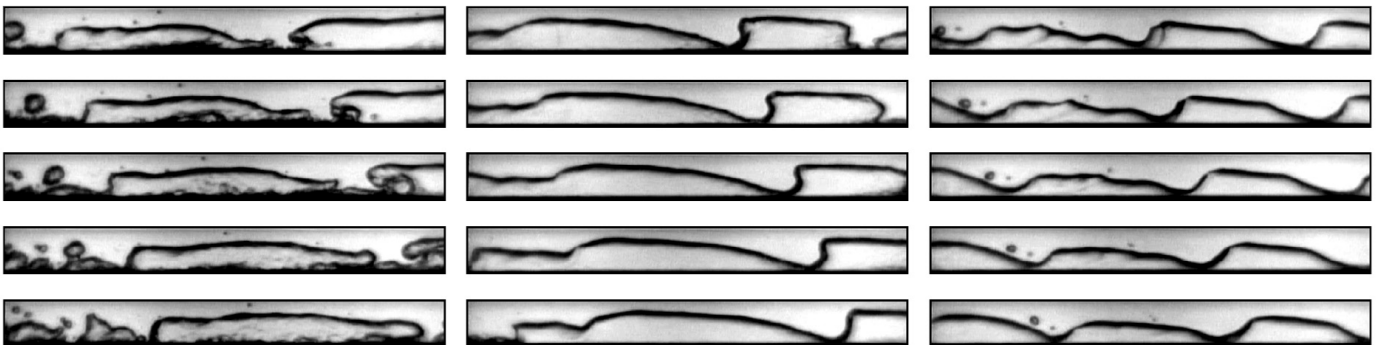
The goal of this project of the NASA Glenn Research Center and Purdue University is to develop a comprehensive understanding of and a predictive model for flow-boiling CHF in reduced gravity. This project is a continuation of

a recently concluded NASA project at Purdue University to explore flow-boiling CHF at different angles of orientation with respect to Earth's gravity. The findings of this research work are reported in several publications by Zhang et al. (refs. 1 and 2). The flow-boiling apparatus for that project was modified to perform experiments in parabolic flights. This apparatus is shown in the top figure.

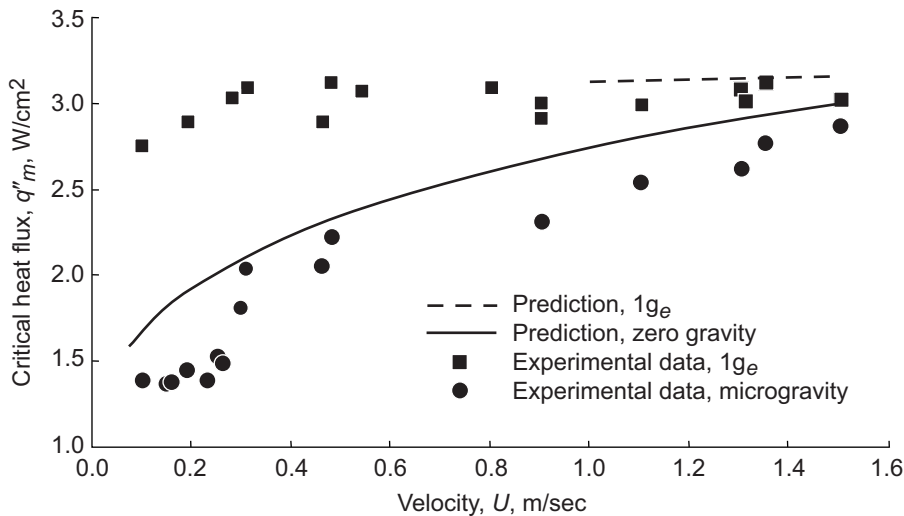


Flow-boiling apparatus flown onboard NASA's KC-135.

A limited number of experiments to determine the flow-boiling CHF in reduced gravity, including lunar and Martian gravitational levels, were performed in parabolic flight with a fluorinert liquid onboard NASA's KC-135. At high heat fluxes, bubbles quickly coalesced into fairly large vapor patches along the heated wall. As the CHF was approached, these patches grew in length and formed a wavy vapor layer that propagated along the wall, permitting liquid access only in the wave troughs. These phenomena, captured during the flight experiment, is shown in the bottom figure. The CHF was triggered by separation of the liquid-vapor interface from the wall because of intense vapor effusion in the troughs. This behavior is consistent with, and accurately predicted by, the interfacial liftoff CHF model. The graph on the next page shows that at low velocities the CHFs are significantly smaller in reduced gravity than they are in horizontal flow on Earth. However, the CHF differences between the two environments decreased with increasing velocity, culminating in virtual convergence at about 1.5 m/sec. This proves that it is possible to design inertia-dominated systems by maintaining flow velocities above the convergence limit. Such systems allow data, correlations, or models developed on Earth to be safely implemented in space systems.



CHF transient in microgravity for flow velocity, $U = 0.15$ m/sec, and subcooling, $\Delta T_{sub,o} = 3.0$ °C. Left: Below CHF. Center: CHF transient. Right: Above CHF.



Comparison of CHF data and interfacial liftoff model predictions for microgravity and horizontal Earth gravity ($1g_e$) flow boiling. Subcooling, $\Delta T_{sub,or}$ 2 to 8 °C.

References

1. Zhang, Hui; Mudawar, Issam; and Hasan, Mohammad M.: Experimental and Theoretical Study of Orientation Effects on Flow Boiling CHF. *Int. J. Heat Mass Transfer*, vol. 45, no. 22, 2002, pp. 4463–4477.
2. Zhang, Hui; Mudawar, Issam; and Hasan, Mohammad M.: A Method for Assessing the Importance of Body Force on Flow Boiling CHF. *J. Heat Tran.*, vol. 126, no. 2, 2004, pp. 161–168.

Find out more about this research:

Glenn's Microgravity Fluid Physics Research:

<http://microgravity.grc.nasa.gov/6712/research.htm>

Professor Mudawar's Research:

<http://www.ecn.purdue.edu/BTPFL/>

Glenn contact:

Dr. Mohammad M. Hasan, 216–977–7494, Mohammad.M.Hasan@nasa.gov

Purdue University contact:

Prof. Issam Mudawar, 765–494–5705, mudawar@ecn.purdue.edu

Authors:

Dr. Mohammad M. Hasan and Prof. Issam Mudawar

Headquarters program office:

Exploration Systems

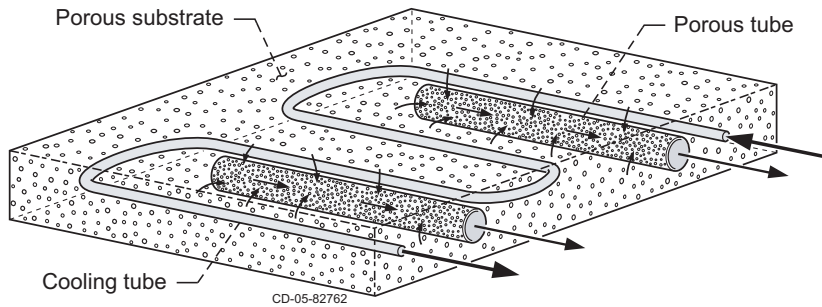
Programs/Projects:

Advanced Life Support Systems, Space Power and Propulsion Systems, Two-Phase Thermal Management, Microgravity Science

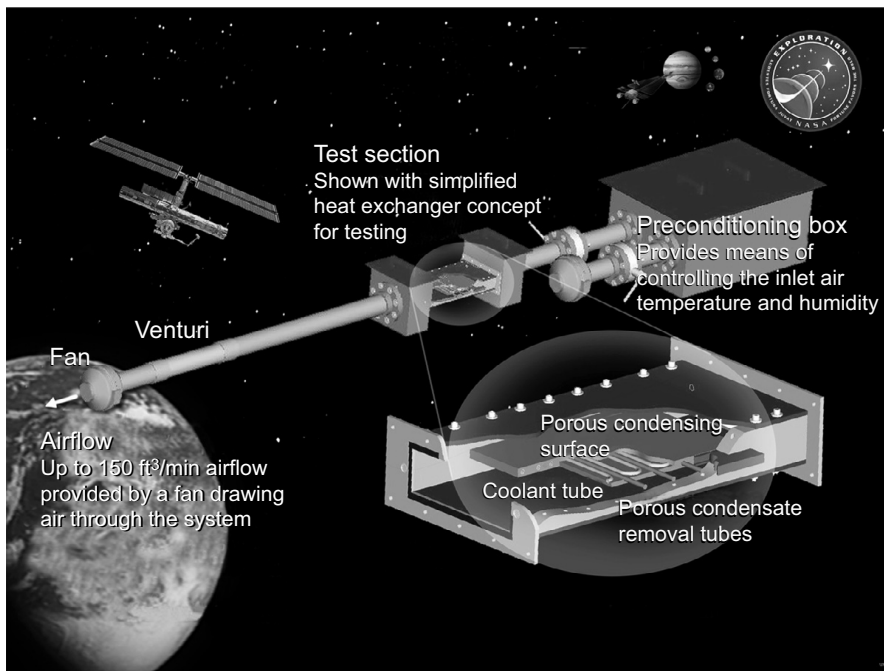
Condensing Heat Exchanger Concept Developed for Space Systems

The current system for moisture removal and humidity control for the space shuttles and the International Space Station uses a two-stage process. Water first condenses onto fins and is pulled through “slurper bars.” These bars take in a two-phase mixture of air and water that is then separated by the rotary separator. A more efficient design would remove the water directly from the air without the need of an additional water separator downstream. For the Condensing Heat Exchanger for Space Systems (CHESS) project, researchers at the NASA Glenn Research Center in collaboration with NASA Johnson Space Center are designing a condensing heat exchanger that utilizes capillary forces to collect and remove water and that can operate in varying gravitational conditions including microgravity, lunar gravity, and Martian gravity.

The CHESS concept for a condensing heat exchanger involves the use of a highly conductive porous substrate as the cold surface over which moisture condensation occurs. The condensed water vapor is removed through another embedded porous tube insert via a suction device. The thermal properties, porosity, and wetting characteristics of the porous materials are judiciously chosen so that efficient



Condensing heat exchanger design concept based on composite porous media.



Ground-based integrated testbed for the CHES Project, including advanced life support with temperature and humidity control and moisture removal.

condensation is promoted and, at the same time, air penetration into the suction tubes is avoided. Other engineering concerns, such as priming and the startup and shutdown transients, also influence the selection of the porous media used in the design. The top figure illustrates the CHES condenser design concept.

To test this concept and develop empirical heat- and mass-transfer correlations, NASA is building a ground-based test facility at Glenn. The bottom figure shows the integrated testbed. This testbed can provide a conditioned moist airstream over the wide range of conditions anticipated for future space missions. In addition, the test section can be rotated with respect to the gravity

vector to simulate, in a simple way, the effects of varying gravity on the condenser performance. The test article and the testbed are instrumented to acquire relevant data during the experiments. These data are being used to develop correlations and to validate the theoretical and numerical modeling studies currently underway. In addition, future space-based flight experiments are planned to evaluate the performance of the condensing heat exchanger in a microgravity environment.

The proposed method will provide a robust, lightweight passive condenser and liquid separator with no moving parts, and it will be operationally simple. It could be used for temperature and humidity control on the International Space Station and all advanced manned missions, a lunar habitat, a Martian habitat, and a Mars transit vehicle.

Find out more about this research:

Glenn's Microgravity Fluid Physics Research:

<http://microgravity.grc.nasa.gov/6712/research.htm>

Thermal Control Element:

<http://advlifesupport.jsc.nasa.gov/thermal/>

Glenn contact:

Dr. Mohammad M. Hasan,
216-977-7494,
Mohammad.M.Hasan@nasa.gov

National Center for Space Exploration Research (NCSER) contact:

Dr. Vedha Nayagam, 216-433-8702,
Vedha.Nayagam@grc.nasa.gov

Authors:

Dr. Mohammad M. Hasan and
Dr. Vedha Nayagam

Headquarters program office:
Exploration Systems

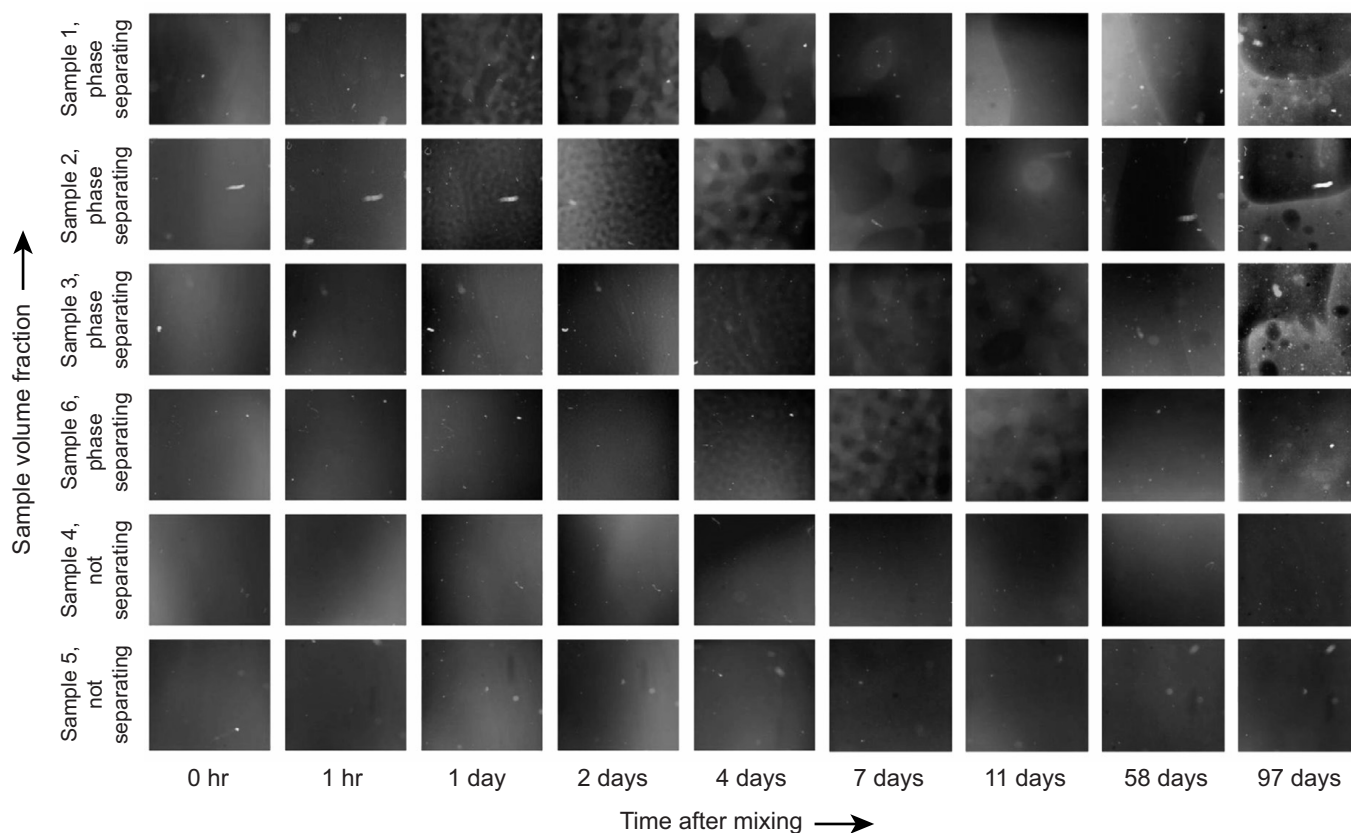
Programs/Projects:

Advanced Life Support Systems,
Humidity and Temperature Control
for ISS, CEV, Lunar and Martian
Missions, EVA

Binary Colloidal Alloy Test-3 (BCAT–3) Tabletop Space Station Experiment Continues

“As above, so below,” thus begins the Emerald Tablet that was inscribed in 300 B.C., long before we could look into the heavens and see a space station that might serve as a platform for exploring other worlds and for exploring the natural ways that order arises out of chaos. To raze the ancient intent of this quote (and lift it out of context), we note that the effects of gravity would be balanced (removed) at the center of the Earth (below) and that this is also the case aboard the International Space Station (above). Yet, those of us on Earth are caught in the middle, where the effects of gravity are profound and disturbing for observers wanting to study nature’s self-organizing tendencies, tendencies that are masked by sedimentation and convection on Earth.

For NASA principal investigators from Harvard (David Weitz and Peter Lu) and the University of Pennsylvania (Arjun Yodh and Jian Zhang), an orbiting space experiment (launched Jan. 2004) using small colloidal particles in a fluid revealed the progress of these organizing tendencies at a pace that can be captured by astronauts with a camera. Once colloidal particles are



BCAT–3 critical point samples 1 through 6 evolving in microgravity. Colloidal/polymer mixtures that are near the critical point are already starting to phase separate into two components: a colloid-rich phase (light areas) and a colloid-poor phase (dark areas). The quickly changing dynamic data captured in these photographs will help determine the boundary conditions for future models of critical behavior. The present observations include a determination of the shape of the interface and reveal which part of each sample wets the cell. The long-term observation of which samples phase separate will allow us to precisely determine the critical point of this colloidal mixture. This figure is shown in color in the online version of this article (<http://www.grc.nasa.gov/WWW/RT/2004/RU/RUF-meyer.html>).

mixed in a fluid (randomized) and begin to order themselves, photographs can capture the knowledge we are after in the form of beautiful blue and dark brown images of the Binary Colloidal Alloy Test-3 (BCAT-3) experiment (see the first 6 of 10 test tube images in the figure on the preceding page). Samples 1 through 6 for this experiment were created to cover a range of concentrations that allow David Weitz and Peter Lu to determine where the critical point is for these mixtures. This is akin to the critical point for a liquid-gas mixture: where the liquid and gas phases are no longer distinguishable. Knowledge about critical points has engineering applications (e.g., in extracting caffeine from coffee beans or magnesium from rocks on Mars to make rocket fuel) and also provides fundamental knowledge that helps us to understand how the material world operates.

Other samples in the BCAT-3 experiment use weak concentrations of similar particles that also are only about 1/100 the diameter of a fine human hair. Arjun Yodh and Jian Zhang use these samples to grow surface crystals composed of particles with sizes comparable to the wavelength of light. Ordered arrays of such particles might be ideal for switching and controlling light. Early results from this ongoing experiment are modifying our understanding of the theory used to predict when surface crystals will grow in an ideal environment where gravity is absent. The BCAT-3 experiment is finding that nature can reveal much more in the heavens than on Earth.

Find out more about this research:

BCAT-3:

<http://microgravity.grc.nasa.gov/6712/comflu/bcat3.html>

Experimental Soft Condensed Matter

Group:

<http://www.deas.harvard.edu/projects/weitzlab/>

Experimental Condensed-Matter

Physics:

<http://dept.physics.upenn.edu/faculty-info/yodh.html> (link to lab page)

National Center for Space Exploration Research (NCSER) contact:

Dr. William V. Meyer, NASA project scientist, 216-433-5011, William.V.Meyer@grc.nasa.gov

Glenn contact:

Monica I. Hoffmann, NASA project manager, 216-433-6765, Monica.I.Hoffmann@nasa.gov

Author:

Dr. William V. Meyer

Headquarters program office:

Life Support & Habitation

Programs/Projects:

Microgravity Science

Two-Phase Flow Technology Developed and Demonstrated for the Vision for Exploration

NASA's vision for exploration will once again expand the bounds of human presence in the universe with planned missions to the Moon and Mars. To attain the numerous goals of this vision, NASA will need to develop technologies in several areas, including advanced power-generation and thermal-control systems for spacecraft and life support. The development of these systems will have to be demonstrated prior to implementation to ensure safe and reliable operation in reduced-gravity environments. The Two-Phase Flow Facility (T Φ FFy) Project will provide the path to these enabling technologies for critical multiphase fluid products (refs. 1 and 2). The safety and reliability of future systems will be enhanced by addressing focused microgravity fluid physics issues associated with flow boiling, condensation, phase separation, and system stability, all of which are essential to exploration technology. The project—a multiyear effort initiated in 2004—will include concept development, normal-gravity testing (laboratories), reduced-gravity aircraft flight campaigns (NASA's KC-135 and C-9 aircraft), space-flight experimentation (International Space Station), and model development. This project will be implemented by a team from the NASA Glenn Research Center, QSS Group, Inc., ZIN Technologies, Inc., and the Extramural Strategic Research Team composed of experts from academia.

Two-phase systems (i.e., liquid and gas) for thermal-control and power-conversion systems rely on using the latent heat of vaporization of a working fluid to absorb and reject heat from the cycle. Typical components of two-phase thermal-control and power-conversion systems are a boiler-evaporator, phase separator(s), accumulator(s), a condenser, and a pump. Both the boiling and condensing processes can be affected by low-gravity conditions. The effects of gravity can alter such phenomena as bubble formation, liquid bridging, and carryover in the boiler. Conditions in the condenser that can be affected by the

gravity level include the maintenance of interface control during the condensation process and the prevention of vapor carryover into the pump.

The T Φ FFy project was conceived and initiated in 2004 to address two-phase issues in a reduced-gravity environment. During the first year, a project team was formed, experiment requirements were developed, and some reduced-gravity experiments were performed on NASA's KC-135 aircraft.

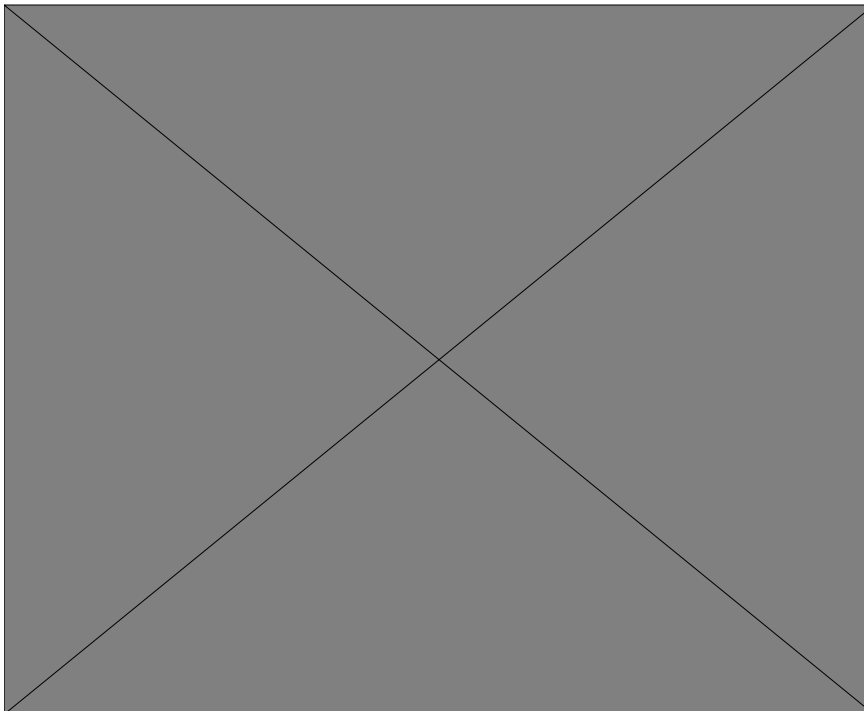
A space-flight experiment is being planned for future operations on the International Space Station. This experiment will include the operation of a single-fluid, two-phase closed thermodynamic loop testbed. A conceptual three-dimensional diagram of the T Φ FFy experiment mounted in the Fluids Integrated Rack (a Glenn facility that will be launched to the International Space Station) is shown in the illustration. A low-boiling-point surrogate fluid will be selected on the basis of scaling analyses using preliminary designs for operational systems. Time scales on the order of minutes or hours will be required to bring a system such as this to a steady-state condition, and to run a series of experiments.

In addition to the multiphase component space-operation demonstration, key measurements will include the flow regime, pressure drop, velocities, and quality. The data will be used to develop operational prototype components and to validate engineering correlations and new computational models. Three key products will result: (1) passive vortex-type phase separator technology will increase from technology readiness level 4 (TRL 4) to TRL 6, (2) flow boiler

tube technology will increase from TRL 3 to 6, (3) high-flow-rate, multiphase thermodynamic cycle stable operation demonstration in reduced gravity will increase from TRL 4 to 6. The project will increase exploration-enabling multiphase technology from TRL 4 to 6, will increase system safety, and will decrease development risks.

References

1. Viskanta, Raymond, et al.: Microgravity Research in Support of Technologies for the Human Exploration and Development of Space and Planetary Bodies. Proceedings of the Fifth Microgravity Fluid Physics and Transport Phenomena Conference, 2000.
2. Lahey, Richard T.; and Dhir, Vijay: Research in Support of the Use of Rankine Cycle Energy Conversion Systems for Space Power and Propulsion. NASA/CR—2004-213142, 2004. <http://gltrs.grc.nasa.gov/cgi-bin/GLTRS/browse.pl?2004/CR-2004-213142.html>



Three-dimensional conceptual model of the T Φ FFy experiment mounted to the optics bench of the Fluids Integrated Rack in the International Space Station. The major components of the experiment are identified.

Find out more about this research:

Exploration Systems at Glenn:

<http://exploration.grc.nasa.gov>

Microgravity Fluid Physics:

<http://exploration.grc.nasa.gov/6712/multiph.html>

NASA's Vision for Space Exploration:

http://www.nasa.gov/missions/solarsystem/explore_main.html

Glenn contacts:

John M. Sankovic, 216-977-7429, John.M.Sankovic@nasa.gov;
John B. McQuillen, 216-433-2876, John.B.McQuillen@nasa.gov; and
Jack F. Lekan, 216-433-3459, John.F.Lekan@nasa.gov

Authors:

John M. Sankovic, John B. McQuillen, and Jack F. Lekan

Headquarters program office:

Exploration Systems

Programs/Projects:

Project Prometheus, Life Support & Habitation

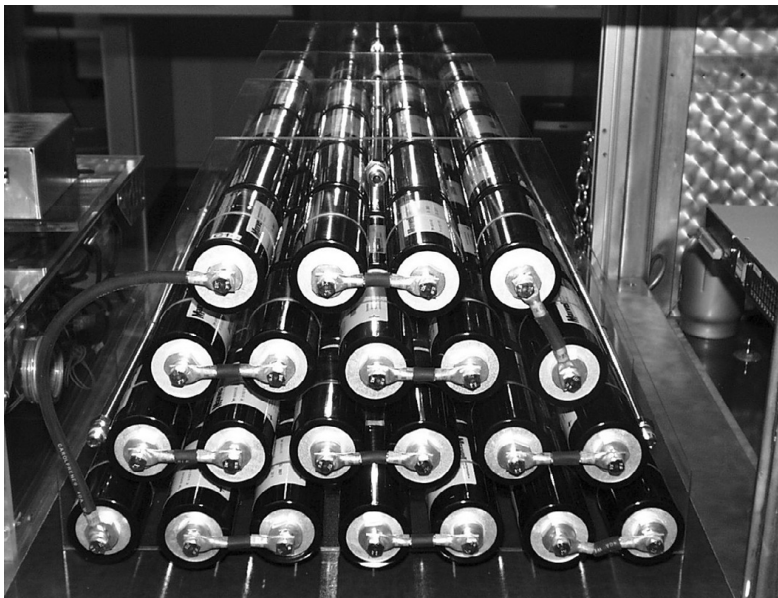
2004

ENGINEERING AND TECHNICAL SERVICES

ENGINEERING DEVELOPMENT

Engineering Development

Hybrid Power Management Program Evaluated Ultracapacitors for the Next Generation Launch Transportation Project



The Hybrid Power Management (HPM) Program applied to the Next Generation Launch Transportation (NGLT) Project. Top: Fuel cell laboratory with PEM fuel cells and a bank of ultracapacitors. Bottom: Bank of 110 ultracapacitors connected in a series configuration.

The NASA Glenn Research Center initiated baseline testing of ultracapacitors to obtain empirical data in determining the feasibility of using ultracapacitors for the Next Generation Launch Transportation (NGLT) Project. There are large transient loads associated with NGLT that require a very large primary energy source or an energy storage system. The primary power source used for this test was a proton-exchange-membrane (PEM) fuel cell. The energy storage system can consist of batteries, flywheels, or ultracapacitors. Ultracapacitors were used for these tests.

NASA Glenn has a wealth of experience in ultracapacitor technology through the Hybrid Power Management (HPM) Program, which the Avionics, Power and Communications Branch of Glenn's Engineering Development Division initiated for the Technology Transfer and Partnership Office. HPM is the innovative integration of diverse, state-of-the-art power devices in optimal configurations for space and terrestrial applications. The appropriate application and control of the various advanced power devices (such as ultracapacitors and fuel cells) significantly improves overall system performance and efficiency. HPM has extremely wide potential. Applications include power generation, transportation systems, biotechnology systems, and space power systems. HPM has the potential to significantly alleviate global energy concerns, improve the environment, and stimulate the economy.

Ultracapacitors are ideal for applications such as NGLT, where long life, maintenance-free operation, and excellent low-temperature performance are essential. For these tests, state-of-the-art symmetric ultracapacitors were interconnected in an innovative configuration to minimize interconnection impedance. PEM fuel cells provide excellent energy density but not good power density. Ultracapacitors not only have excellent power density, but virtually unlimited cycle life. The combination of PEM fuel cells and ultracapacitors provides a power source with excellent energy and power density. In addition, the life of PEM fuel cells is shortened significantly by large transient loads. Using ultracapacitors in conjunction with PEM fuel cells reduces the transients applied to the fuel cell, and thus appreciably improves the life of the power system. PEM fuel cells were tested with and without ultracapacitors to determine the benefits of ultracapacitors. Neither the fuel cell nor the energy storage system exhibited any problems under the rigorous test conditions it was exposed to. The performance of the fuel cell and the ultracapacitor bank proved to be excellent. In addition, a bank of ultracapacitors was assembled and tested at 275 V, which is the nominal voltage rating of the NGLT power system. The performance of the 275-V ultracapacitor bank was excellent, and there were no failures. Results showed that using ultracapacitors in the NGLT power system can improve space power system performance and reliability significantly.

Bibliography

Eichenberg, Dennis J.: Baseline Testing of Ultracapacitors for the Next Generation Launch Transportation (NGLT) Project. NASA/TM—2004-213344, 2004. <http://gltrs.grc.nasa.gov/cgi-bin/GLTRS/browse.pl?2004/TM-2004-213344.html>

Glenn contact:

Dennis J. Eichenberg, 216-433-8360, Dennis.J.Eichenberg@nasa.gov

Author:

Dennis J. Eichenberg

Headquarters program office:

Aeronautics Research

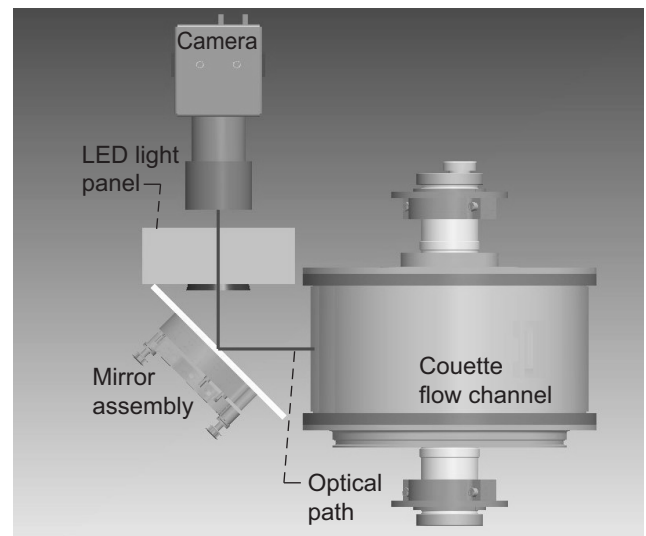
Programs/Projects:

NGLT

System Developed for Bulk Flow Imaging of a Two-Phase Fluid in a Cylindrical Couette

The Microgravity Observation of Bubble Interactions (MOBI) experiment is working to better understand the physics of gas-liquid suspensions. To study such suspensions, researchers generate bubbles in a large cylindrical flow channel. Then, they use various types of instrumentation, including video imaging, to study the bubbly suspension.

Scientists will need a camera view of the majority of the gas-liquid suspension inside of the couette in order to gather the information needed from the MOBI experiment. This will provide the scientists with a qualitative picture of the flow that may indicate flow instabilities or imperfect axial mixing inside the couette. These requirements pose a significant challenge because the imaging and lighting system must be confined to a very tight space since the space available on the International Space Station experiment racks is very limited. In addition, because of the large field of view needed and the detail needed to see the gas-liquid suspension behavior in the image, a digital video camera with high resolution (1024 by 1024 pixels) had to be used. Although the high-resolution camera will provide scientists with the image quality they need, it left little space on the experiment rack for the lighting system. Many configurations were considered for the lighting system, including frontlighting and backlighting, but because of mechanical design limitations with the couette, backlighting was not an option.



MOBI bulk-flow imaging layout. LED, light-emitting diode.

The next aspect of the design to be considered was the light source. Heat production had to be kept to a minimum, so light-emitting diodes (LEDs) were the most viable option because

of their efficiency and low heat production. The lighting system developed consisted of a light panel populated with 615 LEDs on a 140-mm square. The light panel was designed with a hole in the center for the camera to view through. The panel produced enough light, but it produced severe glare on the front of the couette, so a linear polarizer was mounted on the front of the LED panel and on the camera lens to eliminate the glare. Then, the polarizer on the camera was adjusted to remove the glare from the front surface of the couette.

This imaging hardware has been tested in the lab and produces good quality images of the bubbles in a mockup of the flow channel. However, because fast-moving bubbles will have to be imaged, the light panel design may be updated to include more LEDs. This experiment is currently scheduled to fly on the International Space Station in 2008.

Find out more about this research:
<http://microgravity.grc.nasa.gov/6712/overviews/MOBlover.html>

Glenn contacts:
Jeffrey R. Juergens, 216-433-5460, Jeffrey.R.Juergens@nasa.gov; and James D. Wagner, 216-433-5575, James.D.Wagner@nasa.gov

Authors:
Jeffrey R. Juergens and James D. Wagner

Headquarters program office:
Aeronautics Research

Programs/Projects:
MOBI, Microgravity Science

Acoustic Liquid Manipulation Used to Enhance Electrochemical Processes

Working in concert with the NASA Technology Transfer and Partnership Office, the Great Lakes Industrial Technology Center, and Alchemitron Corporation of Elgin, Illinois, the NASA Glenn Research Center has applied nonlinear acoustic principles to industrial applications.

High-intensity ultrasonic beam techniques employ the effects of acoustic radiation pressure and acoustic streaming to manipulate the behavior of liquids. This includes propelling liquids, moving bubbles, and ejecting liquids as droplets and fountains. Since these effects can be accomplished without mechanical pumps or moving parts, we are exploring how these techniques could be used to manipulate liquids in space applications. Some of these acoustic techniques could be used both in normal Earth gravity and in the microgravity of space.

The electroplating process is one Earth-based industry that benefits from the manipulation of liquids. Collaborating with Alchemitron Corporation, we adapted an acoustic transducer to create acoustic streaming in a tank of gold electroplating electrolyte typically used in the manufacture of electronic circuit boards.

Normally, the selective plating process uses masking tapes or coatings to distinguish the surface areas selected to be plated and to protect nonselected areas. Masking is the most labor- and tooling-intensive aspect of the plating process, and the subsequent removal and disposal of masking materials often becomes a source of toxic waste. The substantial cost, health, and environmental issues motivate us to eliminate the masking process.

In a normal electroplating process, the depletion of the electrolyte in the immediate vicinity of the part impedes the process, so agitation is typically used to keep fresh electrolyte in contact with the part. In contrast, the acoustically enhanced process treats this depleted electrolyte envelope as a virtual mask

and uses an acoustically driven liquid jet to penetrate the envelope with fresh electrolyte. The plating rate in the area defined by the acoustic beam is dramatically higher, and it appears that further refinement of the process may yield a mask-free process.

In our most recent work, we sought to improve the efficiency of acoustic streaming, which was believed to be the main mechanism for the enhanced plating. This was done by increasing the acoustic frequency from 2 to 45 MHz. In addition, we employed a Schlieren imaging system to observe the streaming process. As shown in the photograph on the next page, acoustic streaming can form a distinct and unusually long laminar flow. Surprisingly, the enhanced streaming did not improve the deposition. Further study revealed that the beam reflection observed at lower frequencies contributes to defining a distinct plating area. This finding also implies that acoustic phased arrays (common in medical ultrasound) could now be employed to dramatically improve the process by providing dynamic

beam steering and focusing. Future development will involve flexible beam control to perform selective plating by scanning the acoustic beam and “painting” preprogrammed plating patterns without masks. This development is covered by U.S. Patent 6,368,982 and is available for licensing by commercial users.

Glenn contact:

Richard C. Oeftering, 216-433-2285,
Richard.C.Oeftering@nasa.gov

Author:

Richard C. Oeftering

Headquarters program office:

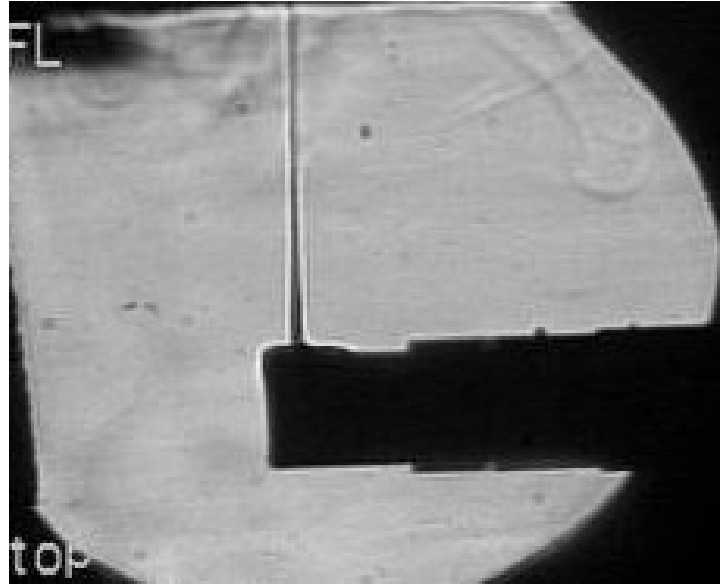
TTPO

Programs/Projects:

TTPO, Microgravity Science, PR&T, Space Power Systems R&T

Special recognition:

Awarded U.S. Patent 6,368,982



Schlieren image of an acoustic transducer producing acoustic streaming.

Theoretical and Experimental Unsteady Aerodynamics Compared for a Linear Oscillating Cascade With a Supersonic Leading-Edge Locus

Experimental data were obtained to help validate analytical and computational fluid dynamics (CFD) codes used to compute unsteady cascade aerodynamics in a supersonic-axial-flow regime. Results from two analytical codes and one CFD code were compared with experimental data. One analytical code did not account for airfoil thickness or camber; another, using piston theory (piston code), accounted for thickness and camber upstream of the first shockwave/airfoil impingement locations. The Euler CFD code accounted fully for airfoil shape.

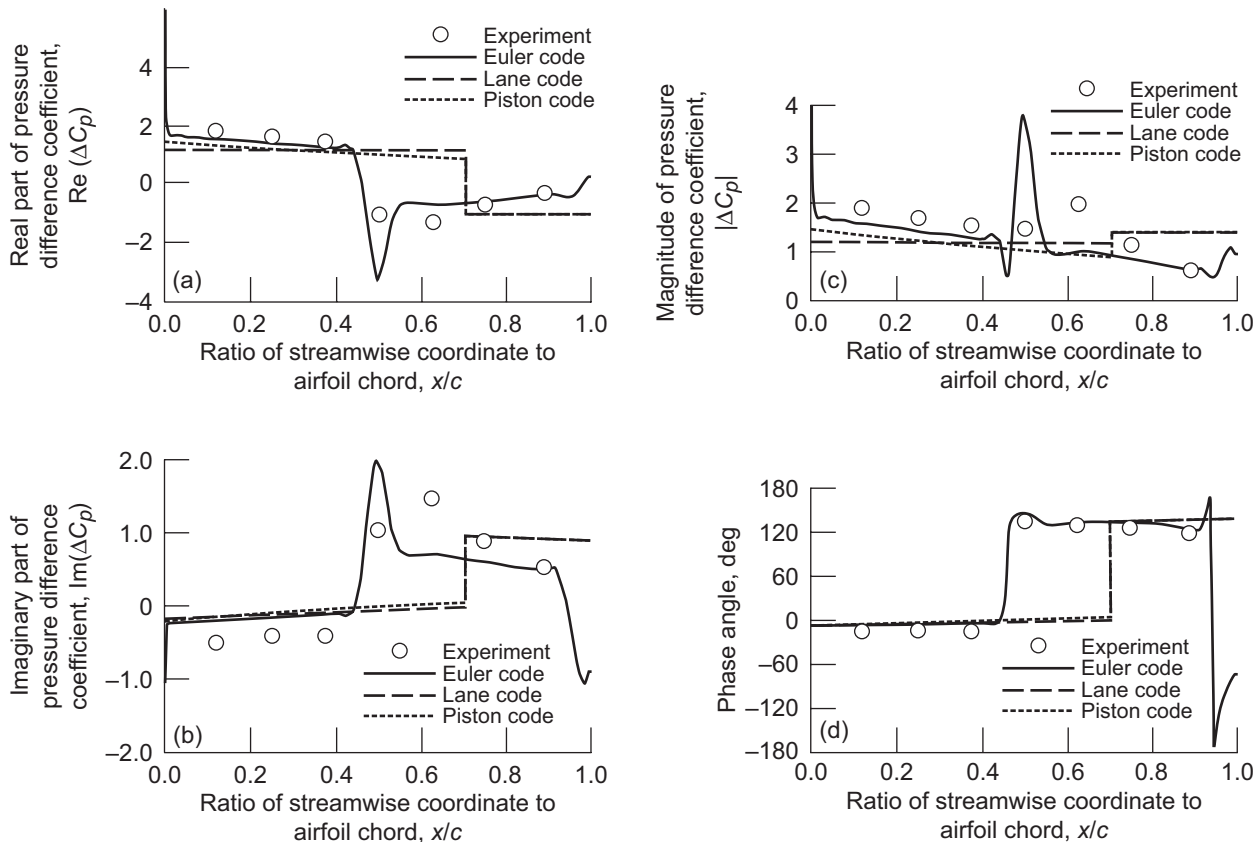
This effort was accomplished through a cooperative agreement with the Ohio State University and was supported by NASA Glenn Research Center’s Director’s Discretionary Fund. The experimental work was carried out at the Ohio State’s Aeronautical and Astronautical Research Laboratory.

An experimental influence coefficient technique was used to obtain unsteady pressures for a cascade of symmetric airfoils oscillating in pitch about mid-chord. Stagger angles of 0° and 10° were investigated for a cascade with a gap-to-chord ratio of 0.417 operating at an axial Mach number of 1.9, resulting in a supersonic leading-edge locus. Reduced frequencies ranged from 0.056

to 0.2. The influence coefficients obtained can be used to determine the unsteady pressures for any interblade phase angle. The unsteady pressures were compared with those predicted by two analytical and one CFD code for interblade phase angles of 0° and 180° .

This experimental program has laid the foundation for future unsteady aerodynamic cascade testing in the supersonic leading-edge-locus flow regime. The findings indicate that

- (1) Piston theory does reflect the general effects of the airfoil thickness distribution on unsteady pressures.



Unsteady pressure difference with interblade phase angle $\beta = 0^\circ$ (reduced frequency, k , 0.14577; stagger angle, θ , 0° ; free-stream Mach number, M_∞ , 1.9617; ratio of blade spacing to airfoil chord, s/c , 0.417). (a) Real part. (b) Imaginary part. (c) Magnitude of pressure difference coefficient. (d) Phase angle.

- (2) When the differences in shock wave/airfoil impingement locations predicted by the analytical and Euler CFD codes are accounted for, all of the codes predict similar phase angles between the airfoil motion and the unsteady pressure. Thus, the airfoil thickness distribution does not have a large effect on the unsteady-pressure phase angle.
- (3) The analytical codes do not accurately locate the shock wave/airfoil impingement locations, partly because of flat-plate airfoil assumptions. Even though the piston code accounts for airfoil geometry in the isolated airfoil regions, the shock wave/airfoil impingement locations were still based on flat-plate geometry.
- (4) The unsteady pressures predicted by the analytical codes could be greatly improved by repositioning the shock wave/airfoil impingement locations by using a steady-flow theory (e.g., the method of characteristics or a steady CFD flow solver) that accounts for airfoil geometry.
- (5) The accuracy of the experimental data can easily be improved by reducing oscillating system wear. This can be accomplished if the airfoil moment of inertia is decreased through an alternate design, the use of different materials, and the resizing of some oscillating system components.

Bibliography

Ramsey, John K.; and Erwin, Dan: Comparison of Theoretical and Experimental Unsteady Aerodynamics of Linear Oscillating Cascade With Supersonic Leading-Edge Locus. NASA/TM—2004-211820, 2004. <http://gltrs.grc.nasa.gov/cgi-bin/GLTRS/browse.pl?2004/TM-2004-211820.html>

Glenn contact:

Dr. John K. Ramsey, 216-433-6032, John.K.Ramsey@nasa.gov

Authors:

Dr. John K. Ramsey and Dr. Dan Erwin

Headquarters program office:

Aeronautics Research

Programs/Projects:

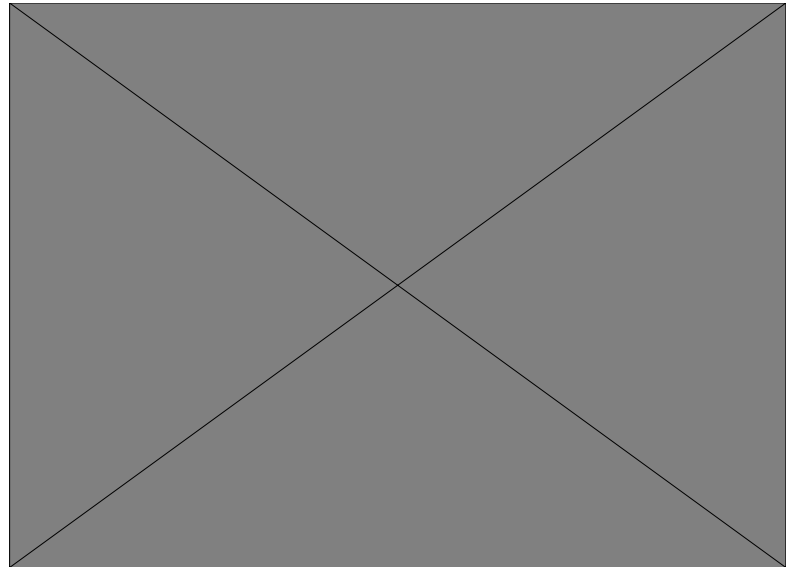
DDF

Model-Based, Multiscale Self-Tuning Controller Developed for Active Combustion Control

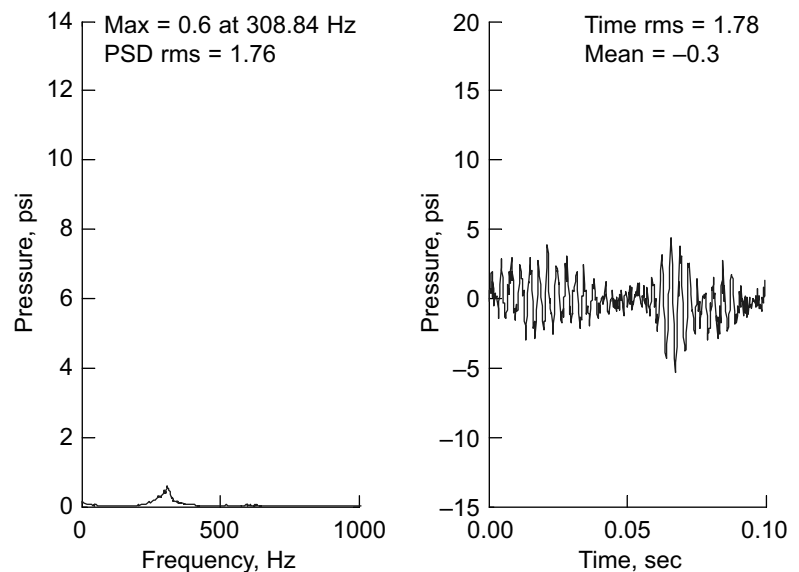
New challenges concerning system health-monitoring and life-extending robust controls for the Ultra-Efficient Engine Technology Project, as well as other advanced engine and power system concepts at NASA and elsewhere, have renewed the control community's interest in smart, model-based methods. In particular, these challenges have further motivated efforts at the NASA Glenn Research Center to exploit the versatility and superiority of the dynamic features extraction of multiscale analysis for controls—such as with “wavelets” and “wavelet filter-banks.” The accomplishments reported herein pertain to the active suppression of combustion instabilities in liquid-fuel combustors via fuel modulation. The fundamentals and initial success of this innovation were reported (ref. 1) for a unique demonstration of active combustion control (a research collaboration of NASA Glenn with Pratt & Whitney and the United Technologies Research Center, UTRC). This demonstration, conducted in 2002 at UTRC on the NASA single nozzle rig (SNR) combustor, was the first known suppression of high-frequency instability with a liquid-fueled combustor. The SNR is based on a high-powered military engine combustor that exhibited well-known instabilities.

Continuing studies of combustion instabilities and control were conducted during 2004 with the SNR installed at NASA. This latest research included a significant extension of this model-based, multiscale method to create a (autonomous) self-tuning controller. The controller showed much improvement in performance and robustness for different test rig configurations. This approach involves integrating suitable multiscale representations of system responses within the control dynamics model. The multiscale-enhanced (or scale-selective) model and associated performance metrics are used to automatically adjust and fine-tune control and model sensitive parameters to improve robustness and performance.

During the summer of 2004, this model-based self-tuning controller was demonstrated with great success for three vastly different configurations on the SNR by changing the plenum size upstream of the fuel nozzle: a high-frequency configuration (with an instability frequency greater than 500 Hz), a middle-frequency configuration, and a low-frequency configuration (with



Low-frequency instability (314 Hz) created in the NASA Single Nozzle Combustion Rig (June 4, 2004). PSD, power spectral density. (PLA1C1psi, run 425, 040602, point pt016.)



Low-frequency instability (314 Hz) suppressed by the multiscale extended Kalman controller (June 4, 2004). PSD, power spectral density. (PLA1C1psi, run 425, 040602, point pt080.)

a dominant instability frequency around 300 Hz). The most dramatic results were achieved for the low-frequency case (which had a high signal-to-noise ratio). The instability

was reduced by more than 90 percent rms as well as at the amplitude-spectrum peak (see the graphs on the preceding page). Even for the more challenging high-frequency and middle-frequency configurations (where the signal-to-noise ratio was very low and the instability weaker), the controller consistently reduced the instability amplitude at the amplitude-spectrum peak by 50 percent without peak splitting. This was a notable improvement in comparison to the initial 30-percent reduction achieved in 2002 for the high-frequency configuration. The controller converged fairly quickly toward its optimal points despite having very little a priori information on system parameters. Its good performance and robustness indicated that it could be applied to the lean-direct-injection combustors being developed at NASA.

Reference

1. Le, Dzu K.; Delaat, John C.; and Chang, Clarence T.: Control of Thermo-Acoustics Instabilities: The Multi-Scale Extended Kalman Approach. NASA/TM—2003-212536-REV1 (AIAA-2003-4934), 2003. <http://gltrs.grc.nasa.gov/cgi-bin/GLTRS/browse.pl?2003/TM-2003-212536-REV1.html>

Find out more about this research:
<http://www.grc.nasa.gov/WWW/cdtb/projects/combustor/>

Glenn contacts:

Dr. Dzu K. Le, 216-433-5640,
Dzu.K.Le@nasa.gov; and
John C. DeLaat, 216-433-3744,
John.C.DeLaat@nasa.gov

Author:

Dr. Dzu K. Le

Headquarters program office:

Aeronautics Research

Programs/Projects:

UEET

NASA Headquarters Program Offices

Aeronautics Mission
Aeronautics Research
Aerospace Technology
Earth Science
Energetics
Exploration Systems
Life Support & Habitation
NESC—NASA Engineering Safety Center
NGLT—Next Generation Launch Technology
OAT—Office of Aerospace Technology
OSF—Office of Space Flight
OSS—Office of Space Science
Science
Space Exploration
Space Flight
Space Operations Mission Directorate
Space Science
TTPO—Technology Transfer and Partnership Office
Vehicle Systems

Programs and Projects

Access to Space

Advanced Life Support Systems

Advanced Stirling Technology

AEFT—Alternate Energy Foundation Technologies

Aerospace Propulsion and Power R&T

Aerospace and Power Base

AFFT—Alternate Fuels Foundation Technologies

Alternate Fuel Propulsion System Tech Development program

Auxiliary Propulsion

AvSSP—Aviation Safety and Security Program

Base R&T

BPP—Breakthrough Propulsion Physics

CEV—Crew Exploration Vehicle

CICT—Computing Information and Communications Technology Program

DDF—Director's Discretionary Fund (NASA Glenn)

Earth Science

Enabling Concepts & Technologies

Energetics

Engineering for Complex Systems

Environmentally durable spacecraft

EOS—Earth-Observing Systems

ESR&T—Exploration Systems Research and Technology

Europa Lander

EVA—Extravehicular Activities

Exploration Systems

Exposure of components and materials for durability testing for high-altitude airship testing

Future spacecraft

High-conductivity, low-weight applications

HLLWCT—Highly Loaded Light Weight Compressors and Turbines

HOTPC—High Operating Temperature Propulsion Components

HPCCP—High-Performance Computing and Communications Program

Human & Robotic Technology

Human Lunar Return

Human System Research and Technology

Humidity and Temperature Control for ISS
In-Space Propulsion
In-Space Systems
In-Space Technology
Intelligent Engines Foundation Technology
IPSFT—Intelligent Propulsion Systems Foundation Technology
IR&D—Individual Research & Development
ISS—International Space Station
JIMO—Jupiter Icy Moons Orbiter
JWST—James Webb Space Telescope
LEAP—Low Emissions, Alternative Power Project
Life Support & Habitation
Low-Gravity and Exploration Research
Lunar and Martian Missions
Mars 07
Microgravity Science
MOBI—Microgravity Observations of Bubble Interactions
Multiphase Flow Technologies
Nanotechnology
NEPAG—NASA Electronic Parts Assurance Group
NEPP—NASA Electronic Parts and Packaging
NESC—NASA Engineering Safety Center
NGLT—Next Generation Launch Technology
PERS—Polymer Rechargeable System program
Power Systems R&T
Project Prometheus
Propulsion and Power
PR&T—Propulsion Systems Research and Technology
Propulsion Research and Technology
Propulsion Technology and Integration
QAT—Quiet Aircraft Technology
RAC—Revolutionary Aeropropulsion Concepts
RLV—Reusable Launch Vehicles
RTA—Revolutionary Turbine Accelerator
RTF—Return To Flight
Science and Exploration Orbiters

Science Mission
Space Launch Initiative
Space Operations
Space Power and Propulsion Systems
Space Power Systems R&T
Space Science
Space Shuttle
Spacecraft Power Systems
SRG110—110-W Stirling Radioisotope Generator
System Wide Accident Prevention Project
TBCC—Turbine-Based Combined Cycle
TTPO—Technology Transfer and Partnership Office
Two-Phase Thermal Management
UEET—Ultra-Efficient Engine Technology
Ultra Safe—Ultra Safe Propulsion
U.S. Army Research Laboratory, Vehicle Technology Directorate
VSP—Vehicle Systems Program

Index of Authors and Contacts

Both authors and contacts are listed in this index. Articles start on the page numbers following the names.

- A**
- Aadlund, Randall 5
 Abbott, John M. 177
 Abel, Dr. Phillip B. 161
 Ameri, Dr. Ali A. 187
 Andrews, Michael 5
 Arrington, Lynn A. 96
 Ashpis, Dr. David E. 184
- B**
- Baaklini, Dr. George Y. 41
 Bakhle, Dr. Milind A. 146
 Bangar, Dr. Kulbinder K. 108
 Banks, Bruce A. 110, 112, 116
 Bansal, Dr. Narottam P. 77, 78
 Barrett, Michael J. 101
 Bauman, Steven W. 157
 Beach, Raymond F. 95
 Beheim, Dr. Glenn M. 44
 Bencic, Timothy J. 31
 Bennett, William R. 60
 Berger, Dr. M.H. 89
 Bhatt, Dr. Ramakrishna T. 85
 Biles, Tiffany A. 67, 68
 Blaha, Charles A. 46
 Bodis, James R. 36
 Bond, Thomas H. 176
 Borowski, Dr. Stanley K. 2
 Bowman, Dr. Cheryl L. 135
 Bowman, Dr. Randy R. 69, 121
 Brewe, David E. 161
 Bridges, Dr. James E. 181
 Bright, Dr. Michelle M. 22
 Brown, Dr. Gerald V. 130, 131a, 133, 137, 144
 Bunnell, Charles T. 126
 Button, Robert M. 94
- C**
- Cable, Dr. Thomas L. 80
 Calomino, Dr. Anthony M. 49
 Campbell, Sandi G. 54
 Cardin, Joseph 5
- Choi, Dr. Benjamin B. 133
 Choi, Dr. Sung R. 78
 Choo, Dr. Yung K. 175
 Clark, David A. 161
 Copland, Dr. Evan H. 74
 Cosgriff, Laura M. 40, 124
 Culley, Dennis E. 22
 Cytron, Dr. Sheldon J. 156
- D**
- Dahl, Dr. Milo D. 164
 Davis, Dr. David O. 178
 Decker, Dr. Arthur J. 43
 de Groh, Kim K. 110
 DeLaat, John C. 205
 DellaCorte, Dr. Christopher 157
 Delleur, Ann M. 7
 DeMange, Jeffrey J. 151, 153
 Dever, Joyce A. 112
 Dhadwal, Harbans S. 143
 DiCarlo, Dr. James A. 85
 Dickens, Kevin W. 82
 Dickman, Dr. John E. 108
 Down, Robert S. 190
 Draper, Susan L. 68, 123
 Dudzinski, Leonard A. 2
 Dunlap, Patrick H., Jr. 151, 153
 Dynys, Dr. Frederick W. 87, 88, 89
- E**
- Eckel, Dr. Andrew J. 53
 Eichenberg, Dennis J. 200
 Elam, Kristie A. 37
 Ellis, Dr. David L. 71
 Envia, Dr. Edmane 164
 Evans, Laura J. 44
 Ercegovic, David B. 114
 Erwin, Dr. Dan 203
- F**
- Fabian, John C. 187
 Farmer, Dr. Serene C. 46, 80, 86
 Fink, Jeffrey E. 61
- Flatico, Joseph M. 33
 Fleming, Dr. David P. 154
 Fralick, Gustave C. 46, 47
 Freedman, Marc R. 84
- G**
- Gabb, Dr. Tim P. 65
 Gaier, Dr. James R. 113
 Garg, Dr. Anita 67
 Garg, Dr. Vijay K. 187
 Gati, Frank G. 14
 Gaydosh, Darrell J. 67
 Gemeiner, Russel 94
 Georgiadis, Dr. Nicholas J. 180
 Gerber, Scott S. 98
 Ghosn, Dr. Louis J. 73, 124
 Gilland, James H. 96
 Goldsby, Dr. Jon C. 79
 Gonzalez, José M. 46
 Goudy, Rick 71
 Green, Robert D. 10
 Greer, Lawrence C. 33
 Griffin, Dr. Jerry H. 147a
 Guo, Dr. Ten-Huei 23
 Gustafson, Kenneth 114
 Gyekenyesi, Dr. Andrew L. 41
- H**
- Halford, Dr. Gary R. 121
 Hammoud, Ahmad 119
 Hasan, Dr. Mohammad M. 192, 194
 Hathaway, Dr. Michael D. 173
 Haylett, Daniel R. 190
 Hebsur, Dr. Mohan G. 124
 Heidmann, Dr. James D. 187
 Hepp, Dr. Aloysius F. 108
 Hervol, David S. 100
 Hickman, J. Mark 10
 Hill, Myron E. 14
 Hoberecht, Mark A. 92
 Hoffmann, Monica I. 196
 Hojnicky, Jeffrey S. 9
 Holland, Frederic A., Jr. 124

Hopkins, Dale A. 135, 140
Hughes, Christopher E. 166

I

Iannetti, Anthony C. 167
Ilhan, Dr. Faysal 57

J

Jacobson, David T. 5
Jacobson, Dr. Nathan S. 49, 50, 74
Jamison, Mike 98
Jansen, Ralph H. 95, 132
Jaskowiak, Martha H. 82
Jenkins, Phillip P. 33
Jin, Dr. Michael H.-C. 108
Johnson, Dr. Dexter 144
Johnson, Paul K. 101
Juergens, Jeffrey R. 201

K

Kamhawi, Dr. Hani 96
Kantzios, Dr. Pete T. 65
Kascak, Albert F. 130, 131a
Kay, Robert 5
Kerslake, Thomas W. 7
Kielb, Dr. Robert E. 147b
Kilgore, Kevin 114
Kinder, Dr. James D. 56, 60
Kiser, J. Douglas 85
Kobayashi, Takahisa 25
Kojima, Dr. Jun 34, 170
Kopasakis, George 26
Krantz, Dr. Timothy L. 149
Krasowski, Michael J. 33
Krause, David L. 120, 121, 123
Kurta, Carol E. 126
Kurkov, Dr. Anatole P. 143

L

Le, Dr. Dzu K. 205
Lebron, Marisabel 58
Lee, Prof. Andre 54
Lee, Dr. Ho-Jun 136
Lekan, Jack F. 197
Lekki, John D. 34
Leonhardt, Todd 68
Lerch, Dr. Bradley A. 124, 126
Leventis, Dr. Nicholas 63

Levy, Robert K. 7
Lewandowski, Beth 114
Lewandowski, Edward J. 102
Litt, Jonathan S. 28, 29
Lucci, Barbara L. 187
Lukco, Dr. Dorothy 156

M

Ma, David 110
Malarik, Diane C. 15
Manzo, Michelle A. 94
Marchetti, Mario 159
Martin, Richard E. 36, 40, 41
Mason, Lee S. 100
McGuire, Melissa L. 2
McKissock, Barbara I. 93
McLallin, Kerry L. 132
McNatt, Jeremiah S. 108
McQuillen, John B. 197
Meador, Dr. Maryann B. 60
Meador, Dr. Michael A. 56, 57, 58
Meyer, Dr. William V. 196
Mielke, Amy F. 37
Miller, Fletcher J. 189
Miller, Dr. Robert A. 75
Miller, Sharon K. 116
Miller, Thomas B. 93
Min, Dr. James B. 124, 139, 142
Miyoshi, Dr. Kazuhisa 156
Montague, Gerald T. 131b
Moran, Matthew E. 117
Morscher, Dr. Gregory N. 85
Mudawar, Prof. Issam 192
Mueller, Juergen 5
Myers, Dr. Dwight 74

N

Nayagam, Dr. Vedha 194
Nemeth, Noel N. 127
Nesbitt, Dr. James A. 51
Nguyen, Binh V. 34
Nguyen, Dr. Quang-Viet 34, 170
Noebe, Dr. Ronald D. 67, 68
Norris, Andrew T. 167

O

Oeftering, Richard C. 202
Olson, Dr. Sandra L. 189

O'Malley, Terence F. 17
Opalski, Dr. Anthony B. 38
Opila, Dr. Elizabeth J. 50, 74
Oswald, Fred B. 149
Otsap, Ben 5

P

Pai, Dr. Shantaram S. 147a,
147b, 148
Palfi, Tamas 127
Panda, Dr. Jayanta 37
Patnaik, Dr. Surya N. 140, 148
Patterson, Richard L. 119
Pencil, Eric J. 96
Penko, Paul F. 172
Pereira, Dr. J. Michael 135
Petko, Jeanne F. 85
Pettegrew, Richard D. 190
Pham, Nang T. 92
Poplawski, J.V. 154
Provenza, Andrew J. 131b

R

Radzikowski, Mark 143
Raj, Dr. Sai V. 73, 124
Ramsey, Dr. John K. 203
Ratvasky, Thomas P. 176
Rawlin, Vincent K. 5
Regan, Timothy F. 102
Reh, Stefan 127
Reid, Concha M. 94
Riehl, John P. 3
Rigby, Dr. David L. 187
Ritzert, Frank J. 51, 69
Roberts, Dr. Gary D. 135
Robinson, Raymond C. 73
Roth, Dr. Don J. 36, 40
Roth, Mary Ellen 98
Ruff, Dr. Gary A. 12
Rusick, Jeffrey J. 9
Russell, Carolyn K. 71

S

Salamone, Dr. Sam 80
Sanders, Terry M. 34
Sankovic, John M. 197
Sawicki, Prof. Jerzy T. 41
Sayir, Dr. Ali 46, 87, 88, 89

Schreiber, Jeffrey G. 102, 104, 105
 Seasholtz, Dr. Richard G. 37
 Seibert, Marc A. 34
 Shah, Aswin R. 105
 Shah, Neerav 28
 Sheredy, William A. 12
 Shih, Tsan-Hsing 167
 Shin, Dr. E. Eugene 61, 120
 Shpargel, Tarah P. 53
 Siebert, Mark W. 137
 Simon, Donald L. 25
 Singh, Dr. Mrityunjay 53, 84
 Sjauw, Waldy K. 3
 Slater, Dr. John W. 178
 Smith, James W. 65
 Soeder, James F. 95, 132
 Sofie, Dr. Stephen W. 80
 Solano, Paul A. 178
 Song, Prof. Gangbing 136
 Srivastava, Dr. Rakesh 146
 St. Onge, Thomas H. 15
 Steinetz, Dr. Bruce M. 151, 153
 Steinthorsson, Dr. Erlendur 187
 Strazisar, Dr. Anthony J. 173
 Street, Dr. Kenneth W. 156, 159
 Struk, Peter M. 190
 Strukov, Dmitri 143
 Sutter, Dr. James K. 61, 120
 Sydenstricker, Mike 126

T

Tallant, David 50
 Taylor, Shawn C. 151
 Telesman, Dr. Jack 65
 Thesken, Dr. John C. 61, 120, 126
 Tigelaar, Dr. Dean M. 60
 Tomasek, Aaron J. 159
 Towne, Dr. Charles E. 180
 Trudell, Jeffrey J. 130, 131a
 Tyson, Dr. Daniel S. 57

U

Urban, Dr. David L. 12

V

Vander Wal, Dr. Randall L. 31, 159
 VanOverbeke, Dr. Thomas J. 183

Verhey, Timothy R. 5
 Verrilli, Michael J. 40
 Vickerman, Mary B. 175
 Volino, Dr. Ralph J. 184

W

Wagner, James D. 201
 Watson, J. Kevin 190
 Webster, Neal 49
 Weiland, Dr. Karen J. 17
 Weiland, Kenneth E. 34, 47
 Wernet, Dr. Mark P. 38
 Wey, Changlie 172
 Wichman, Indrek S. 189
 Wilt, David M. 33
 Wong, Edmond 29
 Wong, Wayne A. 106
 Woodward, Richard P. 166
 Wrbanek, John D. 46, 47
 Wrbanek, Susan Y. 43, 47

Y

Yan, Li 112
 Yun, Dr. Hee Mann 85

Z

Zaman, Dr. Khairul B. 181
 Zhong, Zhimin 79
 Zhu, Dr. Dongming 75, 77

REPORT DOCUMENTATION PAGE

Form Approved
OMB No. 0704-0188

Public reporting burden for this collection of information is estimated to average 1 hour per response, including the time for reviewing instructions, searching existing data sources, gathering and maintaining the data needed, and completing and reviewing the collection of information. Send comments regarding this burden estimate or any other aspect of this collection of information, including suggestions for reducing this burden, to Washington Headquarters Services, Directorate for Information Operations and Reports, 1215 Jefferson Davis Highway, Suite 1204, Arlington, VA 22202-4302, and to the Office of Management and Budget, Paperwork Reduction Project (0704-0188), Washington, DC 20503.

1. AGENCY USE ONLY (<i>Leave blank</i>)		2. REPORT DATE June 2005	3. REPORT TYPE AND DATES COVERED Technical Memorandum	
4. TITLE AND SUBTITLE Research & Technology 2004			5. FUNDING NUMBERS None	
6. AUTHOR(S)				
7. PERFORMING ORGANIZATION NAME(S) AND ADDRESS(ES) National Aeronautics and Space Administration John H. Glenn Research Center at Lewis Field Cleveland, Ohio 44135-3191			8. PERFORMING ORGANIZATION REPORT NUMBER E-14945	
9. SPONSORING/MONITORING AGENCY NAME(S) AND ADDRESS(ES) National Aeronautics and Space Administration Washington, DC 20546-0001			10. SPONSORING/MONITORING AGENCY REPORT NUMBER NASA TM-2005-213419	
11. SUPPLEMENTARY NOTES Responsible person, Dean W. Bitler, organization code XT, 216-433-2226.				
12a. DISTRIBUTION/AVAILABILITY STATEMENT Unclassified - Unlimited Subject Categories: 01 and 31 Available electronically at http://www.grc.nasa.gov/WWW/RT/ This publication is available from the NASA Center for AeroSpace Information, 301-621-0390.			12b. DISTRIBUTION CODE	
13. ABSTRACT (<i>Maximum 200 words</i>) This report selectively summarizes NASA Glenn Research Center's research and technology accomplishments for fiscal year 2004. It comprises 133 short articles submitted by the staff scientists and engineers. The report is organized into three major sections: Programs and Projects, Research and Technology, and Engineering and Technical Services. A table of contents and an author index have been developed to assist readers in finding articles of special interest. This report is not intended to be a comprehensive summary of all the research and technology work done over the past fiscal year. Most of the work is reported in Glenn-published technical reports, journal articles, and presentations prepared by Glenn staff and contractors. In addition, university grants have enabled faculty members and graduate students to engage in sponsored research that is reported at technical meetings or in journal articles. For each article in this report, a Glenn contact person has been identified, and where possible, a reference document is listed so that additional information can be easily obtained. The diversity of topics attests to the breadth of research and technology being pursued and to the skill mix of the staff that makes it possible. For more information, visit Glenn's Web site at http://www.nasa.gov/glenn/ . This document is available online (http://www.grc.nasa.gov/WWW/RT/). For publicly available reports, visit the Glenn Technical Report Server (http://gltrs.grc.nasa.gov).				
14. SUBJECT TERMS Aeronautics; Aerospace engineering; Space flight; Space power; Materials; Structures; Electronics; Space experiments			15. NUMBER OF PAGES 224	
			16. PRICE CODE	
17. SECURITY CLASSIFICATION OF REPORT Unclassified	18. SECURITY CLASSIFICATION OF THIS PAGE Unclassified	19. SECURITY CLASSIFICATION OF ABSTRACT Unclassified	20. LIMITATION OF ABSTRACT	